Image Processing Systems Institute, Russian Academy of Sciences

Samara State Aerospace University

ITNT-2015

International Conference Information Technology and Nanotechnology

June 2015, Samara, Russia

Proceedings of International conference *Information Technology and Nanotechnology (ITNT-2015).*

Preface

International conference Information Technology and Nanotechnology (ITNT-2015) held in Samara at the Samara State Aerospace University.

Languages of the ITNT-2015 Conference: Russian and English.

The goals of the ITNT-2015 Conference are:
- to discuss problems of fundamental and applied researches, computer modeling, development and implementation of information telecommunication systems with leading scientists from Russia, the UK, Germany, Austria, China and India;
- to promote academic and research activities in that direction and to share experiences in teaching IT professionals using innovative educational technology and facilities.

The ITNT-2015 Conference covers a variety of topics related to applications of information technology to aeronautics and astronautics and other branches of high-technology industry.

The major topics of the ITNT-2015 Conference include the following:
- Computer Optics and Nanophotonics
- Mathematical Modeling
- Image Processing and Geoinformatics
- Data Mining and Big Data

The ITNT-2015 Conference has been focused on the educational problems providing opportunities to students and young scientists to become familiar with unique scientific equipment and laboratory facilities in order to achieve scientific results in theory, practice and innovation management according to the major topics of the ITNT-2015 Conference.

Over 200 persons from 7 countries, 15 cities and 27 educational institutions have been participated in the ITNT-2015 Conference. Over 120 reports have been presented.

Proceedings include scientific papers selected by editors on the base of recommendation of Program Committee. The editors accepted 51 articles for publication after the review of the Conference papers.

Official website of the ITNT-2015 Conference: http://agora.guru.ru/itnt-2015.

Organisation

Organizers

Samara Region Government (http://www.samregion.ru)

Samara State Aerospace University (http://www.ssau.ru)

Image Processing Systems Institute, Russian Academy of Sciences
(http://www.ipsi.smr.ru/)

Organizing Committee

Shakhmatov E.V. (Chairman) Samara State Aerospace University, Samara, Russia

Co-Chairpersons

Kazarin S.V. Samara Region Government, Samara, Russia

Kazanskiy N.L. Image Processing Systems Institute, Russian Academy of Sciences, Samara, Russia

Kolomiets E.I. Samara State Aerospace University, Samara, Russia

Executive secretary

Dodonova N.L. Samara State Aerospace University, Samara, Russia

Organizing Committee (Samara State Aerospace University)

Kovartsev A.N.	*Prokhorov S.A.*
Kudryashov D.V.	*Sergeev V.V.*
Kupriyanov A.V.	*Fursov V.A.*
Privalov A.Yu.	*Shchepakina E.A.*

Program Committee

Soifer V.A. (Chairman) Samara State Aerospace University, Samara, Russia

Anshakov G.P. Joint Stock Company Space Rocket Centre "Progress", Samara, Russia

Vasin Y.G. Lobachevsky State University of Nizhni Novgorod, Nizhny Novgorod, Russia

Kazanskiy N.L. Image Processing Systems Institute, Russian Academy of Sciences, Samara, Russia

Konov V.I. Natural Sciences Center, Prokhorov General Physics Institute of RAS, Moscow, Russia

Kotlyar V.V. Image Processing Systems Institute, Russian Academy of Sciences, Samara, Russia

Labunets V.G. Ural Federal University, Ekaterinburg, Russia

Rudakov K.V. Dorodnicyn Computing Centre of the Russian Academy of Sciences, Moscow, Russia

Ryazhskih V.I. Voronezh State Technical University, Voronezh, Russia

Sergeev V.V. Samara State Aerospace University, Samara, Russia

Skidanov R.V. Image Processing Systems Institute, Russian Academy of Sciences, Samara, Russia

Sobolev V.A. Samara State Aerospace University, Samara, Russia

Sokolov B.V. St. Petersburg Institute for Informatics and Automation of RAS, St. Petersburg, Russia

Sokolov I.A. Federal Research Center "Informatics and Control", Russian Academy of Sciences, Moscow, Russia

Mau Jochen. Heinrich-Heine-University, Dusseldorf, Germany

O'Faolain Liam. University of St. Andrews, St Andrews, Scotland, United Kingdom

Sazhin Sergei. University of Brighton, Brighton, United Kingdom

Sverdlov Victor. Vienna University of Technology, Vienna, Austria

Editors

Kazanskiy N.L.   *Skidanov R.V.*

Popov S.B.   *Sobolev V.A.*

Sergeev V.V.

Editor release

Kudryashov D.V.

Table of Contents

Computer Optics and Nanophotonics

Mathematical Modeling

Image Processing and Geoinformatics

Data Mining and Big Data

On the 70th Birthday of corresponding member of the Russian Academy of Sciences Victor A. Soifer

Sokolov V.O.

Samara Scientific Center of the Russian Academy of Sciences

Abstract. The article briefly tells about the life and scientific work of professor, doctor of Technics, corresponding member of Russian Academy of Sciences Victor Aleksandrovich Soifer - an outstanding scientist in the field of diffractive optics and computer image processing. I analyze the jubilee contribution to the development of photonics, computer optics and image analysis systems.

Keywords: computer optics, diffractive nanophotonics, analysis and understanding of images, nanoscale images processing, optical computing.

Introduction

June 18, 2015 we celebrated 70 years since the birth of the outstanding scientist, teacher, public figure, scientific director of the Image Processing Systems Institute of the Russian Academy of Sciences (IPSI RAS), the president of the Samara State Aerospace University (National Research University) (SSAU), head of the Technical Cybernetics Department of SSAU, doctor of Technics, of the professor, corresponding member of Russian Academy of Sciences Viktor Aleksandrovich Soifer.

I talk in the article about the life and scientific results of the jubilee, analyzing V.A. Soifer's contribution to the creation of a new direction in science – computer optics.

Milestones

Victor Soifer graduated in 1962 with honors from school and enrolled at the Radio Engineering Department of the Kuibyshev Aviation Institute (KuAI, now - Samara State Aerospace University). He graduated with honors studies in KuAI in 1968. In 1968-1971 years he was trained in postgraduate KuAI on specialty "Theoretical radio engineering" and in 1971 in St. Petersburg Electrotechnical Institute of Communications defended his thesis "Modeling of the generalized Gaussian channel for analysis and synthesis of information transfer" for the degree of candidate of Technics. At the same time, from 1968 to 1971 he worked part-time as a junior

researcher KuAI. The results of the thesis formed the basis of the monograph [1]. After defending his thesis in 1971, V.A. Soifer worked in KuAI as senior researcher, from 1971 to 1973 he was an assistant, from 1973 to 1974 he was senior lecturer, in 1974-1981 he was assistant professor. In 1975, he received a certificate of associate professor of Automated Control Systems (ACS) department, and worked as the dean of the Faculty of Computer Science KuAI from 1975 to 1983.

Fig. 1. – Doctor of Technics, Professor, corresponding member of the Russian Academy of Sciences, Victor A. Soifer

In 1979, V.A. Soifer defended his doctoral thesis on "Restoring the fields parameters of automation systems for experimental studies" at the St. Petersburg Electrotechnical Institute. V.A. Soifer included some of the dissertation results in the monograph [2]. In 1981 he received a degree of Doctor of Technical Sciences, and in 1982 - a certificate of professor of ACS department. In 1982 he organized the Department of Technical Cybernetics in KuAI, headed it up to the present time. In 1988, V.A. Soifer organized and became the director of the Samara branch of the Central Design Bureau for Unique Instrumentation (CDB UI) of the USSR Academy of Sciences. In 1993, Samara Branch of CDB UI was reorganized into the Image Processing Systems Institute of the Russian Academy of Sciences (IPSI RAS). Until January 2015, V.A. Soifer superbly worked as director of IPSI RAS. In January 2015, V.A. Soifer was elected as the scientific head of IPSI RAS. From 1990 to 2010 he worked as the rector of Samara State Aerospace University [3]. From 2010 to the present time he is working SSAU president. Under the leadership of V.A. Soifer SSAU got the status of the national research university.

Scientific direction
V.A. Soifer created the theoretical foundations of computer optics – a new trend in information technology and optical system having a global priority. He and his disciples decided inverse problems of diffraction theory, developed iterative methods of optimization and synthesis, by computer based on the use of micro and

2

nanotechnologies created diffractive optical elements for transformation of laser light: the focus given geometric area, selection of transverse modes, the forming self-replicating beams. Together with his team, he studied the fundamental problems in the analysis and understanding of optical images, opto-information technology with practical applications in aerospace technology, medical diagnostics and geographic information systems. He prepared 16 doctors and 25 candidates of sciences. From 1996 to the present scientific school headed by V.A. Soifer received state support as the leading scientific schools of Russia in the field of computer optics and image processing.

Scientific results

The first scientific article by the student V.A. Soifer in collaboration with the student B.A. Esipov was published in 1967 in a collection of student research papers KuAI. It was called "The accumulation of information by repeating" [4]. It presents a method of reducing the loss of information that is transmitted in discrete binary Gaussian channel with losses.

In 1973, V.A. Soifer introduced spatial variable in the description of the generalized channel [5]. In this article, radio communication was treated as a multipath propagation environment. Even more clearly the analogy between the time radio channel and a coherent optical system, he wrote with D.D. Klovsky [6]. In this article, the authors used the optimum Karhunen-Loeve decomposition and the finite size of the antenna (this is the ultimate in optics as aperture) is considered an expansion in prolate spheroidal functions.

In August 1980, V.A. Soifer and colleagues published the first work on the synthesis of the optical element, which solves a specific task. Therefore, in 2015 we celebrate 35 years since the birth of a new scientific direction - computer optics. In this first paper [6] Academician A.M. Prokhorov and Professor I.N. Sisakyan were coauthors of Prof. V.A. Soifer. Article [7] has been devoted to the geometrical optics calculation of compensators. Compensator is the optical element forming the given wavefront (wavefront of desired shape). The main thing in this work is that the calculation of the compensator was regarded as the inverse problem of the diffraction theory.

The first work on the calculation and synthesis of focusator in longitudinal segment was published in 1981 [8]. The title of this paper was sufficiently general and set the direction of research - "Focusing of radiation into a proper space domain with computer-generated holograms." In 1982 he published a work [9], which was synthesized by reflecting focusator in the ring for the CO2 laser. The shape of the reflecting surface of the focusator was a combination of a spherical lens and axicon.

The first work on the synthesis of spatial filters for the study of transverse mode composition of laser radiation was published in 1982 [10]. In this paper authors presented the amplitude mask for creating Laguerre-Gaussian and Gauss-Hermite modes. The next (1983) filters have already been synthesized in the form of two amplitude masks for Hermite-Gaussian modes (0,0) and (0,1) [11]. Experimental studies on the measurement of the power distribution over transverse modes in an optical fiber using the spatial filters have been carried out in [12].

In 1984 V.A. Soifer with co-authors published the key article [13], devoted to Bessel-optics. This work stands alone in the scientific heritage of V.A. Soifer, it has

3

great importance for optics. The authors proposed an optical element with a complex phase function and the argument of this phase function was a linear function of the polar angle (angular harmonic). The authors proposed the optical implementation of Hankel transform for the n-th order with the help of such diffractive optical element (DOE).

 The above several papers [7 – 13] are the pioneer and define the main directions in the development of diffractive optics. Many other scientific papers on calculation and creation of diffractive optical elements and photonic devices [14 – 65] emerged based on these pioneering publications. Applying these elements and devices is relevant to solving the problems of advanced information technology and micromanipulation [66].

Community involvement and recognition

 Teaching, research and administrative activities of V.A. Soifer combines with social work. He is a member of the editorial boards of scientific journals "Optoelectronics, Instrumentation and Data Processing", "Computational Technologies", "Pattern Recognition and Image Analysis (Advances in Mathematical Theory and Applications)", "Optical Memory & Neural Networks (Information Optics)", "Computer Optics" (Editor-in-Chief defining the main directions and development strategy [67]), "SPIIRAS Proceedings", "Bulletin of Samara Scientific Center of the Russian Academy of Sciences", "Bulletin of SSAU", "Mechatronics, Automation, Control", "Information and Communication Technologies". Victor A. Soifer is a member of the Interagency Council on award Prizes of the Government of the Russian Federation, the chairman of the three dissertation councils, a member of the expert group of the International Prize in Nanotechnology "RUSNANOPRIZE", a board member of the International Association for Pattern Recognition (IAPR), a member of the International Association of University Presidents (IAUP), an expert of the Russian Foundation for Basic Research and Skolkovo. V.A. Soifer is a member of the Academy of Engineering Sciences, member of the Academy of Quality Problems. He is the chairman of the Public Chamber of the Samara Region.

 The country's leadership noted labor achievements of V.A. Soifer by several awards: the Order of Merit; "Order of Merit for the Fatherland» IV degree and III degree; medal "For merits in the All-Russia population census", and by titles: Honored Scientist of the Russian Federation; Corresponding Member of the Russian Academy of Sciences; winner of the State Prize of Russia in the field of science and technology for 1992; winner of the RF Government in the field of science and technology in 2007; winner of the RF Government in the field of education in 2010; winner of the first prize of the German Society for the Promotion of Applied Computer Science; winner of the Provincial Prize for Science and Technology; winner of the Governor of the Samara region for excellence in solving technical problems; Honorary Citizen of Samara Region.

Conclusion

 In conclusion, I wish Victor A. Soifer good health, inexhaustible energy, ongoing scientific curiosity, outstanding disciples and new creative achievements for the benefit of our country and science!

References

1. **Klovsky DD, Soifer VA.** Processing spatiotemporal signals (information channels). Moscow: "Svyaz'" Publisher, 1976. 207 p. [in Russian]
2. **Wittich VA, Sergeev VV, Soifer VA.** Image processing in automated systems for scientific research. Moscow: "Nauka" Publisher, 1982. 214 p. [in Russian]
3. **Soifer VA.** Samara Aerospace University - Step into the Future. Accreditation in Education, 2008; 25: 74-76. [in Russian]
4. **Esipov BA, Soifer VA.** Collect information by repetition. Collection of students' scientific works of KuAI, 1967; 28: 121-129. [in Russian]
5. **Soifer VA.** Measurement of spatial and temporal characteristics of linear channels with scattering. Radioengineering, 1973; 28 (10): 12-17. [in Russian]
6. **Klovsky DD, Soifer VA.** Optimal processing of spatiotemporal fields in channels with selective fading. Problems of Information Transmission, 1974; 10 (1): 73-79. [in Russian]
7. **Golub MA, Zhivopistsev ES, Karpeev SV, Prokhorov AM, Sisakyan IN, Soifer VA.** Creating aspherical wavefronts using computer-generated holograms. Dokl. Akad. Nauk USSR, 1980; 253 (5). 1104-1108. [in Russian]
8. **Golub MA, Karpeev SV, Prokhorov AM, Sisakyan IN, Soifer VA.** Focusing of radiation into a proper space domain with computer-generated holograms. Soviet Technical Physics Letters, 1981; 7(10): 618-623.
9. **Golub MA, Degtyarova VP, Klimov AN, Popov VV, Prokhorov AM, Sisakyan IN, Soifer VA.** Machine synthesis of focusing elements for CO_2-laser. Soviet Technical Physics Letters, 1982; 8(13): 449-451.
10. **Golub MA, Prokhorov AM, Sisakyan IN, Soifer VA.** Synthesis of spatial filters for investigation of the transverse mode composition of coherent radiation. Soviet Journal of Quantum Electronics, 1982; 12(9): 1208-1209.
11. **Golub MA, Karpeev SV, Krivoshlykov SG, Prokhorov AM, Sisakyan IN, Soifer VA.** Experimental investigation of spatial filters separating transverse modes of optical fields. Soviet Journal of Quantum Electronics, 1983; 13 (8). 1123-1124.
12. **Golub MA, Karpeev SV, Krivoshlykov SG, Prokhorov AM, Sisakyan IN, Soifer VA.** Spatial filter investigation of the distribution of power between transverse modes in a fiber waveguide. Soviet Journal of Quantum Electronics, 1984; 14(9): 1255-1256.
13. **Bereznyi AE, Prokhorov AM, Sisakyan IN, Soifer VA.** Bessel-optics. Dokl. Akad. Nauk USSR, 1984; 274(3): 605-608. [in Russian]
14. **Golub MA, Kazanskii NL, Sisakyan IN, Soifer VA, Kharitonov SI.** Diffraction calculation for an optical element which focuses into a ring. Optoelectronics, Instrumentation and Data Processing, 1987; 6: 7-14.
15. **Sisakyan IN, Soifer VA.** Computer Optics: achievements and problems. Computer Optics, 1989; 1(1): 3-12.
16. **Golub MA, Kazanskii NL, Prokhorov AM, Sisakyan IN, Soifer VA.** Synthesis of optical antennae. Computer Optics, 1989; 1(1): 25-28.
17. **Golub MA, Kazanskii NL, Sisakyan IN, Soifer VA.** Computational experiment with plane optical elements. Optoelectronics, Instrumentation and Data Processing, 1988; 1: 78-89.
18. **Golub MA, Karpeev SV, Kazanskii NL, Mirzov AV, Sisakyan IN, Soifer VA, Uvarov GV.** Spatial phase filters matched to transverse modes. Soviet Journal of Quantum Electronics, 1988; 18 (3): 392–393.
19. **Golub MA, Kazanskiy NL Sisakyan IN, Soifer VA.** Formation of reference wavefronts by computer optics elements. Computer Optics, 1990; 7: 3-26. [in Russian]

20. **Golub MA, Sisakian IN, Soifer VA.** Infra-red Radiation Focusators. Optics and Lasers in Engineering, 1991; 15(5): 297–309.
21. **Khonina SN, Kotlyar VV, Uspleniev GV, Shinkarev MV, Soifer VA.** The phase rotor filter. Journal of Modern Optics, 1992; 39(5): 1147-1154.
22. **Khonina SN, Kotlyar VV, Soifer VA, Shinkaryev MV, Uspleniev GV.** Trochoson. Optics Communications, 1992; 91(3, 4): 158-162.
23. **Golub MA, Doskolovich LL, Kazanskiy NL, Kharitonov SI, Soifer VA.** Computer generated diffractive multi-focal lens. Journal of Modern Optics, 1992; 39(6): 1245-1251.
24. **Soifer VA, Doskolovich LL, Kazanskiy NL.** Multifocal diffractive elements. Optical Engineering, 1994; 33(11): 3610-3615.
25. **Kazanskiy NL, Kotlyar VV, Soifer VA.** Computer-aided design of diffractive optical elements. Optical Engineering, 1994; 33(10): 3156–3166.
26. **Kazanskiy NL, Soifer VA.** Diffraction investigation of geometric-optical focusators into a segment. Optik – International Journal for Light and Electron Optics, 1994; 96(4): 158-162.
27. **Doskolovich LL, Kazanskiy NL, Soifer VA.** Comparative analysis of different focusators into segment. Optics and Laser Technology. 1995; 27(4): 207-213.
28. **Volkov AV, Volotovsky SG Granchak VM, Kazanskiy NL, Moiseev OYu, Soifer VA, Solovyov VS, Yakunenkova DM.** Experimental study of heat transfer in a liquid photopolymerisable compositions. Technical Physics, 1995; 65(9): 181-5. [In Russian]
29. **Doskolovich LL, Kazanskiy NL, Soifer VA, Tzaregorodtzev AYe.** Analysis of quasiperiodic and geometric optical solutions of the problem of focusing into an axial segment. Optik – International Journal for Light and Electron Optics, 1995; 101(2): 37-41.
30. **Doskolovich LL, Golub MA, Kazanskiy NL, Khramov AG, Pavelyev VS, Seraphimovich PG, Soifer VA, Volotovskiy SG.** Software on diffractive optics and computer generated holograms. Proceedings of SPIE, 1995; 2363: 278-284.
31. **Kazanskiy NL, Kharitonov SI, Soifer VA.** Application of a pseudogeometrical optical approach for calculation of the field formed by a focusator. Optics & Laser Technology, 1996; 28(4): 297-300.
32. **Doskolovich LL, Kazanskii NL, Kharitonov SI, Soifer VA.** A method of designing diffractive optical elements focusing into plane areas. Journal of Modern Optics, 1996; 43(7): 1423-1433.
33. **Volkov AV, Kazanskiy NL, Soifer VA, Soloviev VS**. Technology for forming continuous microrelief of diffractive optical elements. Computer Optics, 1997; 17: 91-93. [In Russian]
34. **Volkov AV, Kazanskiy NL, Moiseev OJu, Soifer VA.** A Method for the Diffractive Microrelief Forming Using the Layered Photoresist Growth. Optics and Lasers in Engineering, 1998; 29(4-5): 281–288.
35. **Soifer VA, Kazanskiy NL, Kharitonov SI.** Synthesis of a Binary DOE Focusing into an Arbitrary Curve, Using the Electromagnetic Approximation. Optics and Lasers in Engineering, 1998; 29(4-5): 237-247.
36. **Volkov AV, Kotlyar VV, Moiseev OYu, Rybakov OE, Skidanov RV, Soifer VA, Khonina SN.** Binary diffraction optical element focusing a Gaussian beam to a longitudinal segment. Optics and Spectroscopy. 2000; 89(2): 318-323.
37. **Doskolovich LL, Golovashkin DL, Kazanskiy NL, Khonina SN, Kotlyar VV, Pavelyev VS, Skidanov RV, Soifer VA, Solovyev VS, Usplenyev GV, Volkov AV.** Methods for Computer Design of Diffractive Optical Elements. Edited by V.A. Soifer. John Wiley & Sons, Inc, 2002: 765 p.
38. **Doskolovich LL, Kazanskiy NL, Soifer VA, Kharitonov SI, Perlo P.** A DOE to form a line-shaped directivity diagram. Journal of Modern Optics, 2004; 51(13): 1999-2005.

39. **Doskolovich LL, Kazanskiy NL, Soifer VA, Perlo P, Repetto P.** Design of DOEs for wavelength division and focusing. Journal of Modern Optics, 2005; 52(6): 917-926.
40. **Soifer VA.** Nanophotonics and diffractive optics. Computer Optics, 2008; 32(2): 110-118. [in Russian]
41. **Nalimov AG, Kovalev AA, Kotlyar VV, Soifer VA.** Simulation of 3d nanophotonics device for coupling light into planar waveguide. Computer Optics, 2009; 33(1): 4-9. [in Russian]
42. **Bezus EA, Doskolovich LL, Kazanskiy NL, Soifer VA, Kharitonov SI, Pizzi M, Perlo P.** The design of the diffractive optical elements to focus surface plasmons. Computer Optics, 2009; 33(2): 185-192. [in Russian]
43. **Soifer VA, Kotlyar VV, Doskolovich LL.** Diffractive optical elements in nanofotonics devices. Computer Optics, 2009; 33(4): 352-368. [in Russian]
44. **Kotlyar VV, Kovalev AA, Soifer VA.** Subwavelength Focusing with a Mikaelian Planar Lens. Optical Memory and Neural Networks (Information Optics), 2010; 19(4): 273-278.
45. **Bykov DA, Doskolovich LL, Soifer VA, Kazanskiy NL.** Extraordinary Magneto-Optical Effect of a Change in the Phase of Diffraction Orders in Dielectric Diffraction Gratings. Journal of Experimental and Theoretical Physics, 2010; 111(6): 967-974. doi:10.1134/S1063776110120095.
46. **Bezus EA, Doskolovich LL, Kazanskiy NL, Soifer VA, Kharitonov SI.** Design of diffractive lenses for focusing surface plasmons. Journal of Optics, 2010; 12(1): 015001.
47. **Kotlyar VV, Nalimov AG, Shanina MI, Soifer VA, O'Faolein L.** Zone plate on a film for hard x-ray radiation. Computer Optics, 2011; 35(1): 36-41. [in Russian]
48. **Soifer VA, Kupriyanov A.V.** Analysis and recognition of the nanoscale images: conventional approach and novel problem statement. Computer Optics, 2011; 35(2): 136-144. [in Russian]
49. **Nalimov AG, Kotlyar VV, Soifer VA.** Modeling of an image forming by a zone plate in x-ray. Computer Optics, 2011; 35(3): 290-296. [in Russian]
50. **Stafeev SS, O'Faolain L, Shanina MI, Kotlyar VV, Soifer VA.** Subwavelength focusing using fresnel zone plate with focal length of 532nm. Computer Optics, 2011; 35(4): 460-461. [in Russian]
51. **Bezus EA, Doskolovich LL, Kazanskiy NL, Soifer VA.** Scattering in elements of plasmon optics suppressed by two-layer dielectric structures. Technical Physics Letters, 2011; 37(12): 1091-1095. doi: 10.1134/S1063785011120030.
52. **Gavrilov AV, Soifer VA.** Prospects of optical analog computer development. Computer Optics, 2012; 36(2): 149-150.
53. **Kovalev AA, Kotlyar VV, Stafeev SS, Soifer VA.** Diffraction of light by a spiral phase plate with piecewise-continuous microrelief. Computer Optics, 2012; 36(2): 205-210. [in Russian]
54. **Kupriyanov AV, Soifer VA.** On the observability of the crystal lattice with the images of their projections. Computer Optics, 2012; 36(2): 249-256. [in Russian]
55. **Golovastikov NV, Bykov DA, Doskolovich LL, Soifer VA.** Temporal differentiation of optical signals in reflection using resonant gratings. Computer Optics, 2012; 36(2): 151-157. [in Russian]
56. **Golovastikov NV, Bykov DA, Doskolovich LL, Soifer VA.** Resonant diffraction gratings for differentiation of optical signals in reflection and transmission. Computer Optics, 2013; 37(2): 138-145. [in Russian]
57. **Golovastikov NV, Bykov DA, Doskolovich LL.** Spatial integration of optical beams using phase-shifted Bragg grating. Computer Optics, 2014; 38(3): 372-376. [in Russian]

58. **Kotlyar VV, Kovalev AA, Soifer VA.** Diffraction-free asymmetric elegant bessel beams with fractional orbital angular momentum. Computer Optics, 2014; 38(1): 4-10. [in Russian]

59. **Kotlyar VV, Kovalev AA, Skidanov RV, Soifer VA.** Rotating elegant Bessel-Gaussian beams. Computer Optics, 2014; 38(2): 162-170. [in Russian]

60. **Soifer VA, Golovashkin DL, Doskolovich LL, Kazansky NL, Kotlyar VV, Pavelev VS, Skidanov RV, Khonina SN.** Computer design of diffractive optics. Edited by V.A. Soifer. Cambridge Inter. Scien. Pub. Ltd. & Woodhead Pub. Ltd, 2012: 896 p.

61. **Soifer VA, Kovalev AA, Kotlyar VV, Doskolovich LL, Nalimov AG, Gavrilov AV, Golovashkin DL, Dyachenko PN, Khonina SN, Nesterenko DV, Pavelev VS, Shuyupova YaO, Skidanov RV.** Diffractive nanophotonics. Edited by V.A. Soifer. London: CRC Press, 2014: 704 p.

62. **Bykov DA, Doskolovich LL, Bezus EA, Soifer VA.** Optical computation of the Laplace operator using phase-shifted Bragg grating. Optics Express, 2014; 22(21): 25084-25092.

63. **Doskolovich LL, Bykov DA, Bezus EA, Soifer VA.** Spatial differentiation of optical beams using phase-shifted Bragg grating. Optics Letters, 2014; 39(5): 1278-1281.

64. **Khonina SN, Karpeev SV, Alferov SV, Soifer VA.** Generation of cylindrical vector beams of high orders using uniaxial crystals. Journal of Optics, 2015; 17(6): 065001.

65. **Kotlyar VV, Kovalev AA, Soifer VA.** Nonparaxial Hankel vortex beams of the first and second types. Computer Optics, 2015; 39(3): 299-304. [in Russian]

66. **Soifer VA.** Diffractive Nanophotonics and Advanced Information Technologies. Herald of the Russian Academy of Sciences, 2014; 84(1): 9-18.

67. **Soifer VA.** Quo vadis. Computer Optics, 2014; 38(4): 589.

Optical trapping of air-borne light-absorbing particles with various laser beams

Porfirev A.P.

Samara State Aerospace University
Image Processing Systems Institute, Russian Academy of Sciences

Abstract. We demonstrate optical trapping carbon nanoparticle agglomerations in the air employing photophoretic forces. Three types of laser beams were used for optical trapping: a focused Hermite-Gaussian laser beam (TEM_{10}), an optical bottle beam and a hollow optical beam generated by Bessel beams superposition. The experimental results for each of the laser beams types are shown. Description of trapping features in each case is shown. Perspectives of application for each type of laser beams for three-dimensional optical manipulation are discussed.

Keywords: optical trapping, light-absorbing particles, Hermite-Gaussian beam, optical bottle beam, hollow optical beam

Introduction

The optical manipulation of micro- and nanoscale objects with a laser beam was first demonstrated by A. Ashkin [1]. To date, this technique is widely used in the area of biophotonics and micromechanics for the manipulation of micro- and nano-objects [2-8]. Implementation of optical manipulation is possible in various environments such as in liquids or air. The causes of trapping are different depending on the medium and parameters of trapped objects. Therefore, the trapping of transparent micro-objects in liquids is typically carried out due to the action of the gradient force of a focused laser beam [9]. The trapping of light-absorbing micro-objects in air occurs through the action of photophoretic forces [10]. In the latter case, there are two phenomena present: positive photophoresis (particles move in a direction from the light source) and negative photophoresis (particles move towards the light source) [11].

This paper presents a comparison of the optical manipulation of light-absorbing carbon nanoparticle agglomerations using laser beams of three types: 1) a focused Hermite-Gaussian (HG) laser beam (TEM_{10}); 2) an optical bottle beam (a beam with dark regions of exactly zero intensity surrounded by regions of higher intensity) [12];

and 3) a hollow optical beam that has zero intensity on the optical axis. Each of these beams has certain features that allows one to perform various types of manipulation.

Optical manipulation with a Hermite-Gaussian laser beam (TEM10)

In [13], it was shown that it is possible to carry out the three-dimensional trapping of non-spherical light-absorbing particles with a single focused Gaussian beam. This is possible through the action of the photophoretic force resulting from a different thermal accommodation coefficient that depends strongly on the surface state. In fact, the trapping of particles occurs in a region near the laser beam focus. Thus, it is possible to carry out independent multiple manipulation of light-absorbing particles by forming a plurality of intensity peaks in the focal plane.

The Hermite-Gaussian mode is described by the following well known expression [11]:

$$
E_{nm}\left(x,y,z\right) = i^{n+m}\left[\frac{w}{w(z)}\right]^2 H_n\left[\frac{\sqrt{2}x}{w(z)}\right] H_n\left[\frac{\sqrt{2}y}{w(z)}\right] \times
$$
$$
\exp\left[-\frac{x^2+y^2}{w^2(z)} + \frac{ik\left(x^2+y^2\right)}{2R(z)}\right] \times \tag{1}
$$
$$
\exp\left[-i\left(n+m+1\right)arctg\,\frac{z}{z_0}\right],
$$
$$
\text{where } z_0 = \frac{kw^2}{2},\, w(z) = w\left[1+\left(\frac{z}{z_0}\right)^2\right]^{1/2},\, R(z) = z\left[1+\left(\frac{z}{z_0}\right)^2\right],
$$

w is the Gaussian beam waist, $R(z)$ is the Gaussian beam's wavefront curvature radius, z_0 is the Rayleigh range, k is the wavenumber of light, $Hn(x)$ is the Hermite polynomial.

Such beams are propagation-invariant (up to scale); that is, they keep structure of the transverse intensity distribution. Figure 1 shows the cross-section profiles of the intensity distribution for the different orders Hermite-Gaussian beams. We see that the order of a HG beam determines the number of generated intensity peaks, each of which can be used as an optical trap to capture light-absorbing particles in gaseous media.
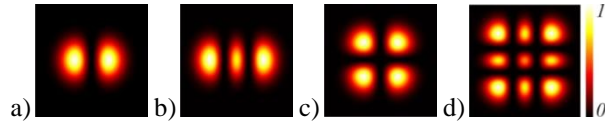
Fig. 1. – Cross-section profiles of the intensity distribution for Hermite-Gaussian laser beams: (a) TEM10, (b) TEM20, (c) TEM11, (d) TEM22

In optical trapping and optical guiding experiments, we use a laser TEM_{10} ($\lambda = 457$ nm, with a maximum output power of 2000 mW) (Fig. 8). An optical scheme of the experimental setup shown in Figure 2a. A generated beam is focused horizontally by a micro-objective *MO* (3.7×, NA=0.1) in the area inside the glass cuvette *C*

10

containing a suspension of micro-particles. Observation of the particle trapping is possible due to the scattered light recorded by the video camera *Cam* (Panasonic HDC-SD800, 1920 × 1080 pixels). A neutral density filter *F* has been used to adjust the power of the laser beam.
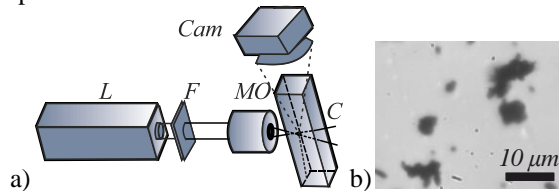
Fig. 2. – Optical manipulation experiment: (a) an experimental setup: L is a laser TEM_{10} (λ=457 nm), F is a neutral density filter, MO is a micro-objective (3.7×, NA=0.1), C is a glass cuvette, Cam is a video camera Panasonic HDC-SD800 (1920 × 1080 pixels); (b) carbon nanoparticle agglomerations used in experiment

To demonstrate the optical trapping and holding of absorbing particles, we used carbon nanoparticle agglomeration. The typical size of the agglomerations ranged to up to tens of micrometers (Figure 2b). The particles were sprayed with a syringe pump. Therefore, the particles initially had a significant acceleration directed to the bottom of the cuvette. The particles settled in the bottom of the cuvette under the influence of gravity. Some of them were trapped in the area of the laser beam. The guiding of the trapped particles was carried out by moving the micro-objective, which can be moved in three mutually perpendicular directions. As a result, movement of the focused laser beam results in movement of the trapped micro-particles.

Figure 3 shows the movement stage of two carbon nanoparticle agglomerations, each of which was trapped in the various intensity peaks of the HG TEM_{10} laser beam. In this case, we carried out a controlled movement of the optically trapped micro-objects.
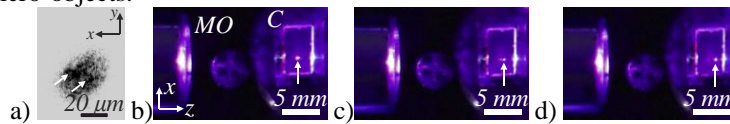
Fig. 3. – Optical trapping and guiding two carbon nanoparticle agglomerations with a Hermite-Gaussian TEM_{10} laser beam: (a) trapped particles (denoted by white arrows); (b)-(d) movement stages of particles in plane xz

Thus, the structure of the HG beams allows simultaneous, parallel three-dimensional movement of several trapped light-absorbing micro-particles. The particles retain their relative position when moving in the space. These beams offer new opportunities for the controlled, multiple simultaneous manipulation of light-absorbing non-spherical micro-objects. For example, it is possible to transport an array of light-absorbing particles, while their original location relative to each other will remain. Furthermore, this technique does not require the additional modulators to create multiple optical traps.

Optical manipulation with optical bottle beams

Photophoresis phenomenon causes a light-absorbing object to move in a direction from the more heated to the less heated side of object. This makes it impossible to trap spherical micro-objects with a single Gaussian beam. The so-called optical bottle beams allow stable three-dimensional trapping of light-absorbing micro-particles to be carried out in gaseous media. An optical bottle beam is a beam with dark regions of exactly zero intensity surrounded by regions of higher intensity. For generation optical bottle beams, we used the method based on the formation of Bessel beams superposition [15]. This method enabled an optical bottle beam to be formed with a predetermined shape, such as a double optical bottle or optical bottle with a triangular profile of the intensity distribution.

For the experiments with optical bottle beams, we used the particles presented in Figure 2b. Figure 4 shows the optical scheme of the experimental setup. The laser beam is transformed by the diffractive optical element *DOE* focused in the area inside glass cuvette by the micro-objective *MO* (3.7×, NA = 0.1). Observation was carried out by a lens L_3. Adjustment of the output power of the laser beam allows us to vary intensity of formed traps and, therefore, change the values of the photophoretic forces acting on the trapped particles.
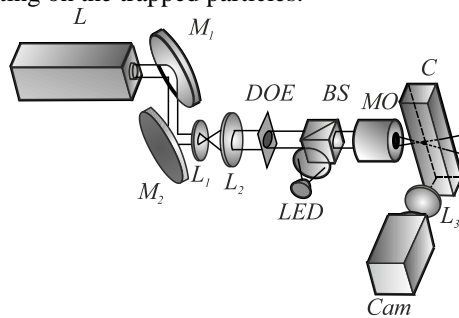
Fig. 4. – Experimental setup: L is a solid-state laser (λ=532 nm), M_1, M_2 are mirrors, L_1, L_2, L_3 are lenses, DOE is a diffractive optical elements that forms an optical bottle beam, BS is a beam splitter, LED is illuminating light-emitted diode, MO is a micro-objective (3.7×, NA = 0.1), C is glass cuvette, Cam is a CCD video camera

Figure 5 illustrates a typical trapping single carbon nanoparticle agglomeration with a single optical bottle. It can be seen that the trapped agglomeration remains in the optical trap during its transfer. We moved the optical trap by moving the focusing micro-objective *MO*, similar to experiments with a Hermite-Gaussian TEM_{10} laser beam. For this experiment, we have managed to move the agglomeration along the beam axis at distance of about 340 μm. The estimated value of the power within the boundaries of the optical bottle is about 16 mW.

The methods described in [16], allow optical bottle arrays to form. The use of optical bottle arrays enables the boundary of trapping to be increased without changing the size of the traps themselves. As shown in [17], if the dimensions of the

formed light traps and trapped micro-objects do not match, it is impossible to achieve stable trapping of micro-objects because they move uncontrollably inside the trap.
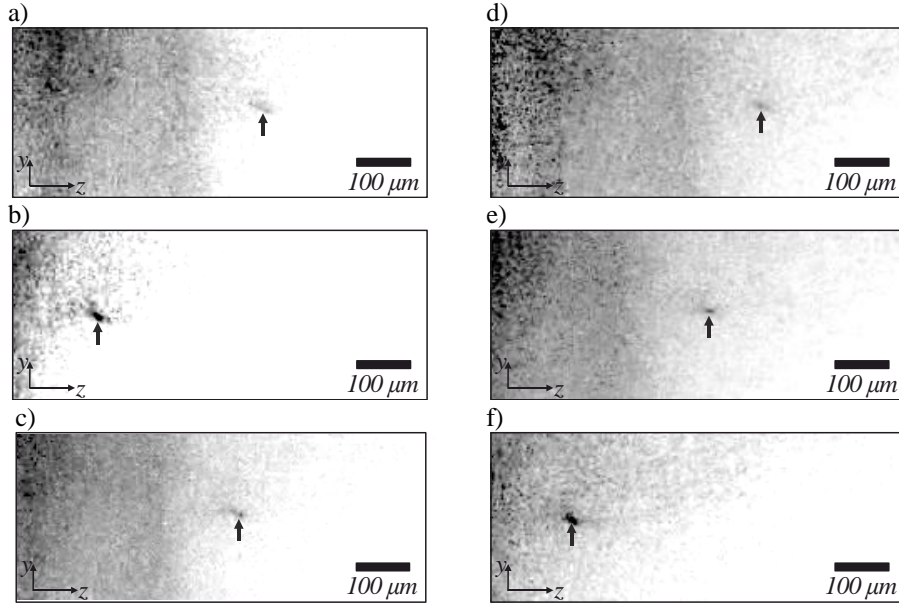
Fig. 5. – Experimental demonstration of trapping and guiding the carbon nanoparticles agglomeration with a single optical bottle. The black arrow points to the agglomeration

Optical manipulation with hollow optical beams

Hollow optical beams (HOBs) are optical beams with zero axial intensity along the propagation axis. These beams have diffraction-free properties on a limited interval along the optical axis. Due to such a configuration, the HOBs are universal optical traps to trapping both transparent and opaque micro-particles [18, 19].

There are various methods of forming such HOBs that have a predetermined cross-sectional shape [20-24]. Changing the cross-sectional shape of the beams can change the shape of the region in which trapped particles will be moved.

In optical trapping experiments with HOBs, we used a solid-state laser L ($\lambda = 532$ nm, with a maximum output power of 500 mW) (Figure 6). The laser beam was expanded with a telescope (L_1 with $f_1 = 15$ mm and L_2 with $f_2 = 35$ mm) to illuminate the DOE formed HOB. An airborne absorbing particle in a cuvette is trapped in the area of minimum intensity of the generated HOB. Observation of the particle trapping was possible due to the scattered light recorded by the video camera *Cam* (MDCE-5, 1280×1024 pixels). The particles were imaged through a micro-objective *MO* (8×, NA=0.2).

To demonstrate the optical trapping and holding of absorbing particles, we used carbon nanoparticle agglomeration as in the experiments described above (Figure 2b). Figure 7 shows the motion stages of a carbon nanoparticle agglomeration trapped by the HOB with an intensity distribution in the form of a regular pentagon contour. It

13

can be clearly seen that the particle is also moved in a limited volume. At the time when the trapped particles remain inside the region of minimum intensity of the formed HOB, other particles settle on the bottom of the cuvette under the influence of gravity. Trapped particles do not leave the boundaries of the HOB because photophoretic force push them away from the region of maximum intensity in the region on the optical axis of the beam.
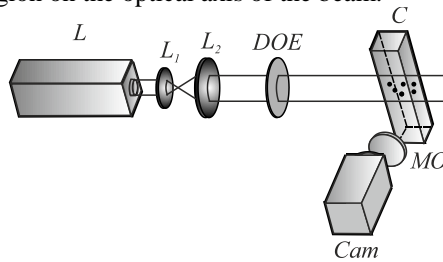
Fig. 6. – Experimental setup: L is a solid-state laser (λ=532 nm), L_1, L_2 are lenses, DOE is a diffractive optical elements that forms a hollow optical beam, MO is a micro-objective (8×, NA=0.2), C is glass cuvette, Cam is a CCD video camera MDCE-5 (1280 × 1024 pixels)
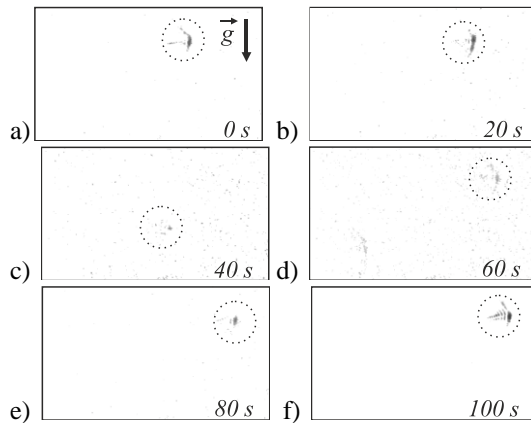
Fig. 7. – Optical trapping and holding of light-absorbing particles with HOB formed by DOE

The use of additional focusing optics enables the generation of converging HOBs, which have predetermined intensity distribution. It is therefore possible to form a complex spatial configuration of the optical beams. Each of these beams can be used to hold the particles in the region of desired size and shape. This 'storage' of micro-particles can be used for contactless transport of microscopic objects. Furthermore, they can be used to study the interaction of various micro-objects trapped in a limited volume.

Conclusion

The paper describes the various ways to manipulate air-borne light-absorbing microscopic objects in air with laser beams of different types. The results of trapping

and manipulation experiments for each of laser beam types are shown. It is shown that:

1) With the use of Hermite-Gaussian beams, it is possible to achieve stable multiple trapping and guiding of light-absorbing non-spherical particles in generated separate intensity peaks;

2) With the use of optical bottle beams, it is possible to achieve stable trapping and guiding of the same particles at distances of hundreds of times their own dimensions;

3) With the use of hollow optical beams with a predetermined shape, trapping and holding light-absorbing particles can be carried out inside an area of predetermined shape within the area given shape, the dimensions of which exceed by ten times the particles' size.

None of these cases d require high-power lasers (enough power about 10-20 mW), due to the fact that photophoretic forces exceed the radiation pressure forces at the order of atmospheric pressure. [20].

References
 1. **Ashkin A.** Acceleration and trapping of particles by radiation pressure. Phys Rev Lett, 1970; 24(4): 156-159. doi: 10.1103/PhysRevLett.24.156
 2. **Grier DG.** A revolution in optical manipulation. Nature, 2003; 424: 810-816. doi: 10.1038/nature01935
 3. **Dholakia K, Cizmar T.** Shaping the future of manipulation. Nat Photonics, 2011; 5: 335-342. doi: 10.1038/nphoton.2011.80
 4. **Kim K, Yoon J, Park YK.** Simultaneous 3D visualization and position tracking of optically trapped particles using optical diffraction tomography. Optica, 2015; 2(4): 343-346. doi: 10.1364/OPTICA.2.000343
 5. **Korobtsov A, Kotova S, Losevsky N, Mayorova A, Patlan V, Timchenko E, Lysov N, Zarubina E.** Optical tweezers technique for the study of red blood cells deformation ability. Laser Phys, 2012; 22(7): 1265-1270. doi: 10.1134/S1054660X12070067
 6. **Morozov AA, Skidanov RV.** Rotation of microturbine in compex vortex beams. Computer Optics, 2013; 37(2): 203-207. [in Russian]
 7. **Morozov AA, Skidanov RV.** Complex vortex beams for of rotation of micromechanical elements. Computer Optics, 2013; 37(1): 68-75. [in Russian]
 8. **Skidanov RV, Rykov MA.** The modificaction of laser beam for optimization of optical trap force characteristics. Computer Optics, 2013; 37(4): 431-435. [in Russian]
 9. **Ashkin A, Dziedzic JM, Bjorkholm JE, Chu S.** Observation of a single-beam gradient force optical trap for dielectric particles. Opt Lett, 1986; 11(5): 288–290. doi: 10.1364/OL.11.000288
10. **Shvedov VG, Desyatnikov AS, Rode AV, Krolikowski W, Kivshar YuS.** Optical guiding of absorbing nanoclusters in air. Opt Express, 2009; 17(7): 5743-5757. doi: 10.1364/OE.17.005743

11. **Keh HJ.** Photophoresis of an aerosol sphere in a spherical cavity. Aerosol Air Qual Res, 2001; 1(1): 21-30.
12. **Arlt J, Padgett MJ.** Generation of a beam with a dark focus surrounded by regions of higher intensity: the optical bottle beam. Opt Lett, 2000; 25(4): 191-193. doi: 10.1364/OL.25.000191
13. **Zhang Z, Cannan D, Liu J, Zhang P, Christodoulides DN, Chen Z.** Observation of trapping and transporting airborne absorbing particles with a single optical beam. Opt Express, 2012; 20(15): 16212-16217. doi: 10.1364/OE.20.016212
14. **Kogelnik H, Li T.** Laser Beams and Resonators. Appl Optics, 1966; 5(10): 1550-1567. doi: 10.1364/AO.5.001550
15. **Porfirev AP, Skidanov RV.** Generation of optical bottle beams array by superposition Bessel beams. Computer Optics, 2012; 36(1): 80-90. [in Russian]
16. **Porfirev AP, Skidanov RV.** Generation of an array of optical bottle beams using a superposition of Bessel beams. Appl Optics, 2013; 52(25): 6230-6238. doi: 10.1364/AO.52.006230
17. **Zhang P, Zhang Z, Prakash J, Huang S, Hernandez D, Salazar M, Christodoulides DN, Chen Z.** Trapping and transporting aerosols with a single optical bottle beam generated by moiré techniques. Opt Lett, 2011; 36(8): 1491-1493. doi: 10.1364/OL.36.001491
18. **Porfirev AP, Skidanov RV.** Optical capture of microparticles in special traps. Computer Optics, 2012; 36(2): 211-218. [in Russian]
19. **Kachalov DG, Pavelyev VS, Khonina SN, Skidanov RV, Porfirev AP.** Experimental realisation of microparticle's optical trapping by use of binary radial DOE. Computer Optics, 2012; 36(1): 91-95. [in Russian]
20. **Porfirev AP, Skidanov RV.** A simple method of the formation nondiffracting hollow optical beams with intensity distribution in form of a regular polygon contour. Computer Optics, 2014; 38(2): 243-248. [in Russian]
21. **Skidanov RV, Porfirev AP.** Formation of optical beams with given intensity distribution in transverse plane for deposition and positioning of microscopic objects. Opt Mem Neural Net, 2014; 23(4): 233-239. doi: 10.3103/S1060992X14040080
22. **Kovalev AA, Kotlyar VV, Porfirev AP, Kalinkina DS.** Analysis of the orbital angular momentum of superposition of diffraction-free Bessel beams with a complex shift. Computer Optics, 2015; 39(2): 172-180. [in Russian]
23. **Abramochkin EG, Kotova SP, Korobtsov AV, Losevsky NN, Mayorova AM, Rakhmatulin MA, Volostnikov VG.** Microobject manipulation using laser beam with nonzero orbital angular momentum. Laser Phys, 2006; 16(5): 1. doi: 10.1134/S1054660X06050161
24. **Porfirev AP, Skidanov RV.** Formation of the massif of hollow beams for sedimentation and positioning of microparticles. Computer Optics, 2012; 36(3): 387-394. [in Russian]

Diffraction lens in imaging spectrometer

Blank V.A., Skidanov R.V.

Image Processing Systems Institute, Russian Academy of Sciences,
Samara State Aerospace University

Abstract. A possibility of using a diffractive lens as the simplest imaging spectrometer was considered. An experimental construction of the spectral imaging for white, red and green LEDs was conducted. When processing the images the influence of the scattered components of the initial point and nearly points of the image was taken into consideration. There was made a comparison of the received spectral distribution with the spectra of these LEDs, received by means of spectrometer. Root-mean-square error (RMSE) from 8 to 13%.

Keywords: diffraction lens, imaging spectrometer, spectral image.

Introduction

In the past decade, in applied spectroscopy there have been intensively developing the new methods, which allow getting and analyzing the spectroscopic information about an object with a spatial resolution, providing the reception for each small area (point) the two-dimensional image of the object on the input aperture of the optical spectrum instrument. In scientific literature such methods are called imaging spectroscopy, three-dimensional matrix containing the dependence of intensity of light from the two spatial and spectral coordinates are called spectral images [1].

In most modern imaging spectrometers optical system forming that imaging and dispersive element are clearly separated. As a dispersive element in imaging spectrometer can be used a prism as well as diffraction grating [2,3]. However, there is a diffractive optical element that can combine these two functions. For quite a long time the attempts have been made to use a diffractive lens in various applications [4-9]. Including the works dedicated to the spectral properties of the diffractive lens [9]. However, high chromatic aberration does not allow the use of the diffraction lens in the imaging systems [6]. The diffraction lens builds images for different wavelengths at different distances. However, this disadvantage of the diffractive lens is more likely to be an advantage, when using the diffraction lens as a basis for the spectrometer [10-12]. In this paper [10,11] a spectrometer using a diffractive lens as a dispersive element is regarded. The light focalized by the diffractive lens passes through the

17

diaphragm and falls on the photodiode, i.e. the spectrometer observed in the papers [10, 11] is not imaging. In the papers [12, 13] the spectrometer based on a combination of diffraction lens and diffraction grating is observed, due to which, a really compact construction is obtained. However, this spectrometer is not an imaging one as well. In the paper [14] there is a simple research on the possibility of using the diffractive lens as a basis for the imaging spectrometer. However, in the paper [14] the authors reviewed rather simple work situation of such spectrometer when the initial object is several multicolored characters on the screen, each of which radiates in a relatively narrow spectral range. Besides, for convenience the symbols are spatially separated which only facilitates the task. In addition, no spectrum was given. In the paper [15] was presented an extended research and was given measured spectra for the laser beams (lasers He-Ne and Cr-Ne). On the imaging spectrometer a spectrum of a point object was measured, consisting of one spectral line. I.e. it is possible to draw a conclusion from the papers [14, 15] that the diffraction lens actually allows getting a spectral image. To confirm the efficiency of such configuration it is necessary to conduct a research on the magnitude of error starting from which is built a spectral image in the spectrometer based on the diffraction lens. In the given article the constructions errors of the spectral image of the white LED by means of the diffraction lens are examined. In addition, a spectral image for the structure of several LEDs with different spectral characteristics is built.

1. Experimental reception of a series of images by means of diffraction lens

To test the possibility of restoring the spectral distribution for every dot of the image for the objects with a wide spectrum there was conducted an experiment in which was built a series of white LED images by means of diffraction lens with a focal length of 50 mm for a wavelength of 500 nm. For the experiment, a four-leveled diffraction lens was used, described in [6]. The lens diameter was 8 mm.

Fig. 1 Shows the optical scheme of the experiment.
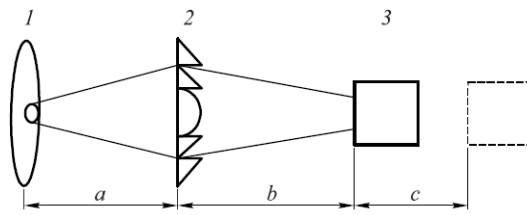
Fig. 1. – Installation diagram. 1 - diode disposed at a distance from the diffraction lens 2, 3 – CCD camera disposed at a distance $b = 40$ mm from the diffraction lens. CCD camera is installed on a moving table with an approach increment of 0.5 mm, $c = 20$ mm

Whilst the distance from the LED to the diffraction lens a = 2000 mm was less than the distance from the diffraction lens to a CCD camera (VIDEOSCAN-2-205) with a resolution of 1390*1040. In the experiment, the camera moved from 40 mm to 60 mm with a step of 0.5 mm. Each image corresponds to its own wavelength. For convenience, the diode was located close to the optical axis.

18

Fig. 2 shows a part of white LED spectrum, obtained by the spectrometer MS7501 (fig. 2). A relative error of spectrum measurement on this spectrometer is not more than 2%.
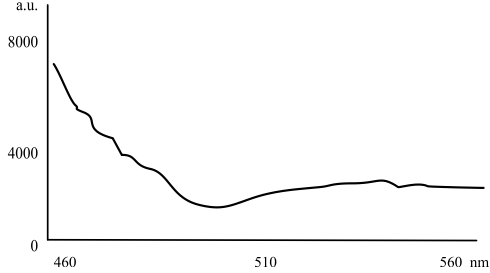
Fig. 2. - A segment of white LED spectrum (standard)

The spectral distribution in Fig. 2 hereinafter to be used as a standard spectrum for comparison of the spectra of individual image points of the LED obtained by means of diffractive lens.

Fig. 3 shows the examples of the LED images at several distances, which correspond to the wavelengths of 481 nm, 505 nm and 550 nm. The image size of the LED in fig. 3 was nearly 100 micrometer (22 pixels on CCD array).
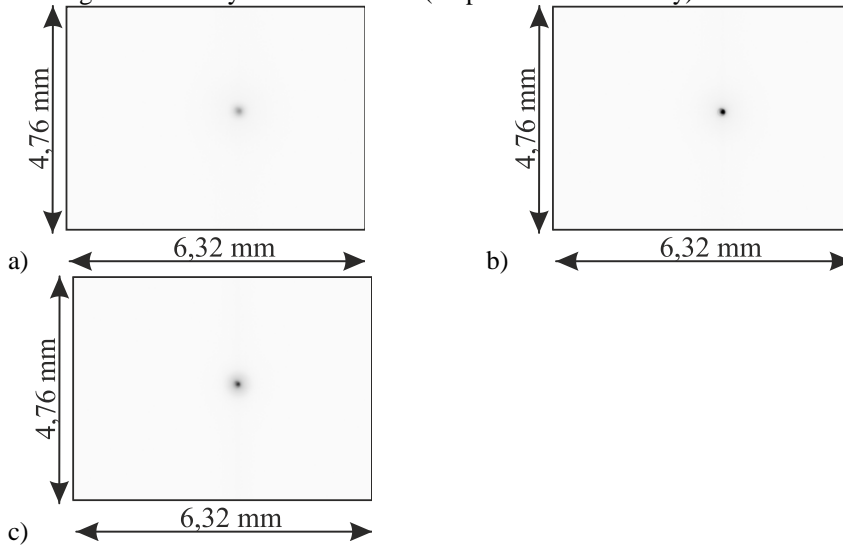
Fig. 3. - Experimental images: 481nm (a), 505nm (b), 550nm (c)

2. Processing of the experimental images to obtain a spectral image

However, it is not allowed to use the experimental images directly without complementary processing. The matter is that due to the change of distance from lens to image changes the scale. I.e. the LED image shifts in relation to the center of the image pattern and additionally changes its size. It cannot be avoided even if the LED image is positioned at the exact center. In this case what is left is a change if the

19

image's scale. To overcome this effect, the experimental images were subjected to geometric transformation of tension / compression relative to the center of the picture with a coefficient equal to the ratio of the distances. Fig. 4 shows the LED images at several distances corresponding to different wavelengths (481 nm, 505 nm, 550 nm) after the geometric transformation. After this transformation, the image of any size keeps the size and position for any wavelength.
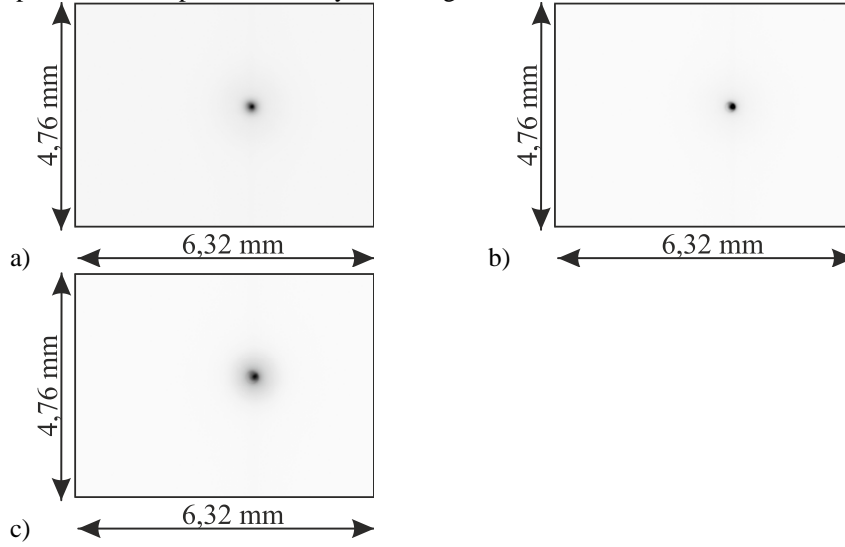
Fig. 4. – Experimental images after geometric transformation: 481 nm (a), 505 nm (b), 550 nm (c)

For non-imaging spectrometer with a diffraction lens [10], the procedure of the spectrum recovery according to the measurement sequence is quite simple. In the paper [10] itself the authors do not make an additional processing to remove the scattered components. But having obtained the sequence of the intensity distributions at different distances $I_j(x,y)$ it is necessary to solve a system of linear equations.

$$I_j(x,y) = \sum_{i=1}^{N} I(x,y,\lambda_i) \frac{A}{A + (b_j - b_i)^2 k_i^{-2}\pi/4}, j = \overline{1,N},$$ (1)

where $I(x,y,\lambda_i)$ are the elements of spectral image, b_i, b_j are distances corresponding to the wavelengths, k_i – f-number of the diffractive lens, $I_j(x,y)$ – intensity distributions taken at distances b_j, A – square of pixel in CCD array. F-number for the diffractive lens is determined by the formula $k_i = d/b_i$, where d is lens diameter. The formula (1) was derived from geometrical considerations. For a precise focus, when the distance b_j corresponds to the wavelength we supposed that the size of aberration image is smaller than the size of pixel of the CCD array (4.65 micrometer*4.65 micrometer). It is actually so, the lens diameter is 8 mm at a focal length of 50 mm, i.e. the size of the diffraction aberration image will be about 4

20

micrometers. At displacement of over a certain distance, we calculated the size of the spot based on the geometrical considerations. For the imaging spectrometer, this system of equations becomes more complicated because it is necessary to take into account the contribution of neighboring dots to the diffuse component on the object

$$I_j(x,y) = \sum_{i=1}^{N} \int_{u^2+v^2<R^2} \frac{I(x+u,y+v,\lambda_i)A}{A+(b_j-b_i)^2 k_i^{-2}\pi/4} \, du dv, \; j=\overline{1,N} \; , \tag{2}$$

where $R=(b_j-b_i)k^{-1}$ is the blur size of a dot at focus displacement, when j=i, in the calculations we shall assume that aberration image coincides in radius with pixel. In the discrete case, the integral in formula (2) degenerates into a sum over the aberration image's dot for the appropriate wavelength. The system of equations (2) for a wide spectral range has a high computational complexity. The number of dots in a discrete variant according to which the summation is performed can reach several thousands.
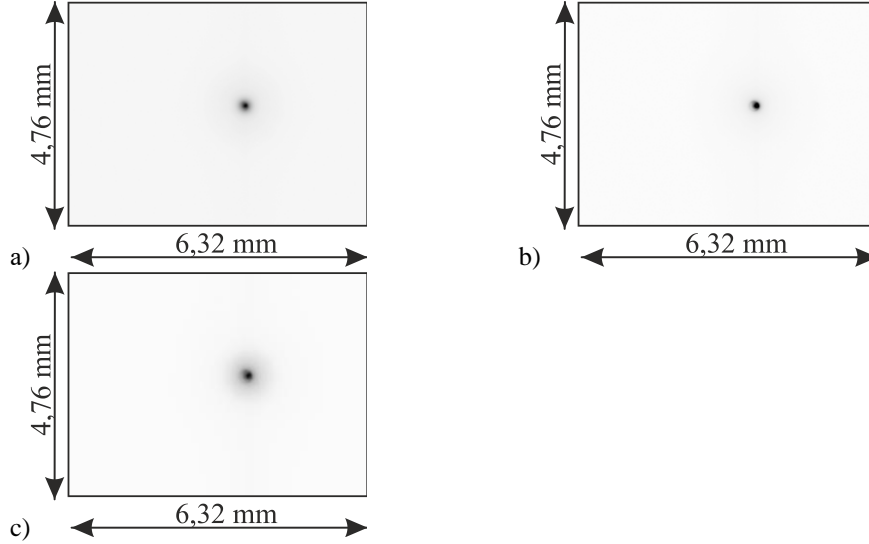
Fig. 5. – Processed images: 481 nm (a), 505 nm (b), 550 nm (c)

For the case where the object for which the spectral image is formed is relatively compact, the computational complexity reduces. Thus, for the LED (fig. 3) it is necessary to take into account just a few tens of dots. Besides, for the spectrum recovery process there was considered a different diffractive effectiveness of the diffractive lens for different wavelengths, which is calculated according to the formula [15]

$$\eta = \frac{\sin^2\left[(n-1)h\frac{\pi}{\lambda}-\pi\right]}{\left((n-1)h\frac{\pi}{\lambda}-\pi\right)^2} \frac{\sin^2\left[(n-1)h\frac{\pi}{4\lambda}\right]}{\left((n-1)h\frac{\pi}{4\lambda}\right)^2} ,$$

where η is spectral sensitivity, h is relief depth, n is a refractive index of the lens material.

The spectral sensitivity of CCD array [16] was also taken into consideration. Thus, fig. 5 shows the processed images.

As a result of the solution of equations (2), the following spectral distribution was obtained for one of the dots for the diode image (fig. 6).
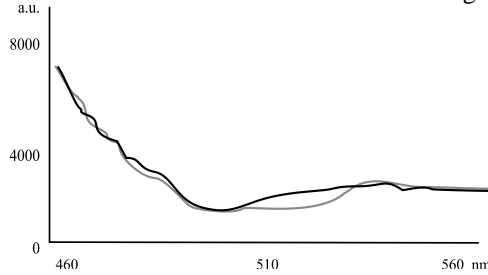
Fig. 6. – Diode spectrum obtained by means of spectrometer and by the results of processing a set of experimental images according to the formula (2)

RMSE of recovery range was 11%. However, for such compact objects as LED it is possible to use a simpler means of obtaining a spectral image with an insignificant loss of accuracy. After obtaining a geometrically correct image (fig. 4), a scattered component can be removed from all images. To do that, there was determined an average number of the intensity of the scattered light outside the LED image for each image individually, then this number was subtracted from every experimental image. Fig. 5 shows an example of the thus processed images for the wavelengths: 481 nm, 505 nm, 550 nm.
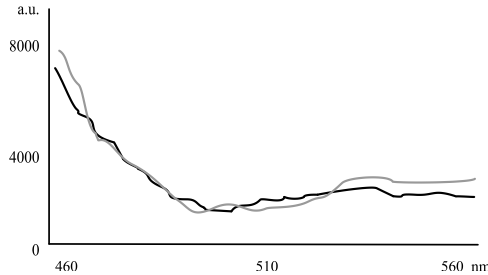
Fig. 7. – Diode spectrum obtained by means of spectrometer and by the results of processing a set of experimental images according to the simplified method

Based on the obtained images, a spectral distribution for each dot of the image can be obtained (fig. 7).

Fig. 7 shows a certain deterioration (in comparison with fig. 6) of the correspondence of a spectrum obtained on the spectrometer (dark line) and a spectrum obtained after processing the image sequence, formed by the diffraction lens. RMSE in this case was 13%. Which is 2% more than RMSE of the exact solution. However,

22

the processing time here significantly reduces and in certain cases, it is possible to use a simplified algorithm to obtain spectral images of compact objects.

Spectra obtained for the different LED dots are a little bit different (fig. 8). Various dots at which the spectrum was measured were marked in fig. 8a. The spectrum for a point marked with an arrow is shown in Fig. 7. The spectra for the points marked with a triangle and square, are shown in Fig. 6bc, respectively.

For fig. 8b and 8c graphics differ slightly from the graphic in Fig. 7, and RMSE value is about 13%.
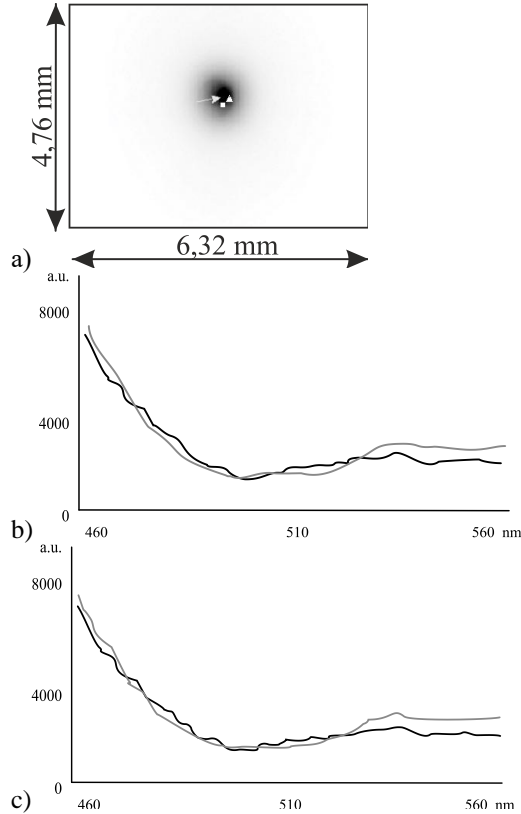
Fig. 8. - The diode spectrum obtained using a spectrometer and by the results of processing a set of experimental images by simplified method

Let us also consider the spectral image of the structure of the green, red and white LEDs in a cross shape, a white diode is situated in the center, green diodes are in vertical direction, and red diodes are in horizontal direction (Fig. 9). The spectra of these diodes are quite different from each other, and obtaining the spectral image of such object, we hereby confirm that the spectrometer based on diffractive lens is indeed imaging.
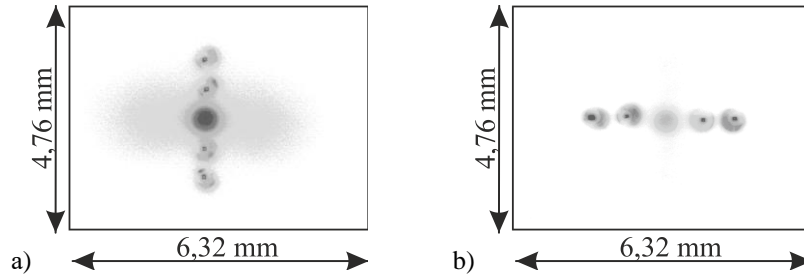
Fig. 9. – Image of patterns of green, red and white diode (in the center). (a) position of the matrix, wherein the green diodes are visible, (b) the position of the matrix, wherein the red diodes are visible

In Fig. 9, it is clearly seen that images of the red and green diodes are formed at different distances from the lens. Fig. 10 shows the spectra obtained for red and green diodes in comparison with their spectra measured on MS7501.
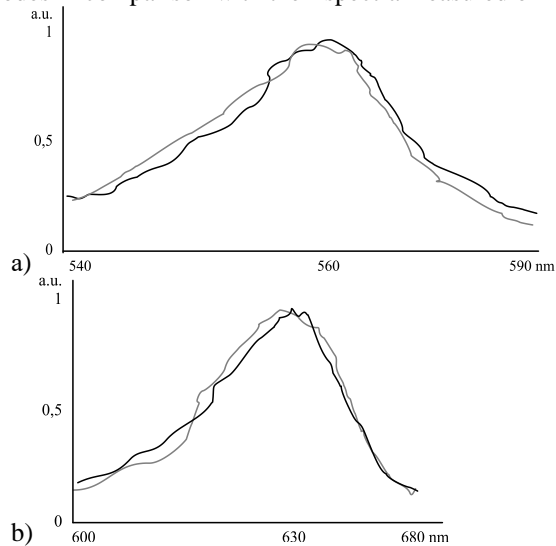
Fig. 10. – Spectrum of the green diode obtained in the experiment in comparison with its spectrum measured on MS7501 (a), the spectrum of the red diode obtained in the experiment in comparison with its spectrum measured on MS7501 (b)

The value of RMSE in fig.10a - 8%, in fig. 10b – 11%. The RMSE value obtained in the experiment is rather large 8-13%, but we must consider three things:

1. spectrum of a single dot on the spectral image should not be identical with the spectrum of the entire diode (fig. 8b and 8c) (spectrometer measures the integral characteristics);
2. only a part of the spectrum was studied, but CCD array is also sensitive to components outside the measured range, therefore, they also introduce distortions

24

in the spectrum reconstruction. In the future this can be avoided by installing the cutoff light filters;
3. the usual error level of imaging spectrometers is quite large compared to the errors of non-imaging spectrometers (1-2%). As a rule, manufacturers of hyperspectral cameras indicate an error in the measurement of the spectrum in the range of 5-10% [17]. I.e. in our experiment, results that can be compared in accuracy are obtained with the obviously more simple design.

When working with more complex images in the future, a precise method based on system should be used (2).

However, based on the obtained results, we can talk about the working efficiency of this simple imaging spectrometer, consisting of a single diffractive lens.

Conclusion

The error in operation of the simplest imaging spectrometer, where the imaging system and the dispersion element are integrated, is investigated – spectrometer is based on diffractive lens.

The experimental results on the formation of the spectral image from the series of images formed by the diffraction lens, allow us to speak about the error of forming spectral images using diffractive lens with an error of 8-13%, which roughly corresponds to the error of the existing samples of hyperspectral cameras.

Funding Information

Reference

1. **Voropay ES, Gulis IM, Kupreev AG.** The dispersion hyperspectrometer with reconfigurable input aperture on the basis of the micro-mirror matrix. Herald BSU, 2009; 1(3): 31-35.
2. **Kazanskiy NL, Kharitonov SI, Khonina SN, Volotovskiy SG, Strelkov YuS.** Simulation of hyperspectrometer on spectral linear variable filters. Computer Optics, 2014; 38(2): 256-270.
3. **Kazanskiy NL, Kharitonov SI, Karsakov AV, Khonina SN.** Modeling action of a hyperspectrometer based on the Offner scheme within geometric optics. Computer Optics, 2014; 38 (2): 271-280.
4. **Khonina SN, Ustinov AV, Skidanov RV**. Binary lens: investigation of local focuses. Computer Optics, 2011; 35(3): 339-346.
5. **Buralli DA, Morris GM.** Design of diffractive singlets for monochromatic imaging. Applied optics, 1991; 30(16): 2151-2158.
6. **Kazanskiy NL, Khonina SN, Skidanov RV, Morozov AA, Kharitonov SI, Volotovskiy SG.** Formation of images using multilevel diffractive lens. Computer Optics, 2014; 38(3): 425-434.
7. **Motogaito A, Hiramatsu K.** Fabrication of Binary Diffractive Lenses and the Application to LED Lighting for Controlling Luminosity Distribution. Optical and Photonics Journal, 2013; 3(1): 67-73.

8. **Miyamoto K.** The phase Fresnel lens. Journal of the Optical Society of America, 1961; 51(1): 17-20.

9. **Faklis D, Morris GM.** Spectral properties of multiorder diffractive lenses. Applied Optics, 1995; 34(14): 2462-2468.

10. **Kitaura N, Ogata S, Mori Y.** Spectrometer employing a micro-Fresnel lens. Optical Engineering, 1995; 34: 584-588.

11. **Park Y.** Miniaturization of a Fresnel spectrometer. Journal of Optics A: Pure and Applied Optics, 2008; 10: 095301.

12. **Yang C, Edwards P, Shi K, Liu Z.** Proposal and demonstration of a spectrometer using a diffractive optical element with dual dispersion and focusing functionality. Optical Letters, 2011; 36: 2023-2025.

13. **Yang C, Shi K, Edwards P, Liu Z.** Demonstration of a PDMS based hybrid grating and Fresnel lens (G-Fresnel) device. Optics Express, 2010; 18(23): 23529-23534.

14. **Lyons D.** Image spectrometry with a diffractive optic. Proceedings of SPIE, 1995; 2480: 123-131.

15. **Lyons D, Whitcomb K.** The DOE in "DOIS" a diffractive optic image spectrometer. Proceedings of SPIE, 1996; 2689: 274-283.

16. **Petropavlovskiy U.** The application features CCD interline transfer. Components and technologies, 2009; 5: 17-24.

17. Special Design Bureau of Instrument. Source: <http://www.kbsp.ru/ projects/detail.php? ELEMENT_ID=12>.

Diffraction by an axicon with taking into consideration multiple internal reflections

Degtyarev S.A., Ustinov A.V., Khonina S.N.

Samara State Aerospace University,
Image Processing Systems Institute, Russian Academy of Sciences

Abstract. In this work we consider laser beam diffraction by narrow elongated axicon with conical angle, which is small enough for multiple internal reflection arising. Those sorts of tapers are widely used in micro and nanooptics. We have to take into account more than one internal reflection for correct description of beam propagation through the axicon. The diffraction is simulated with two approaches: pure "geometrical optics" and Helmholtz equation solving with "Finite Elements Method". Based on ray optics we derive analytic formulas for conical angles meanings, which provide maximums and minimums of intensity on optical axis. Derived numerical simulation verifies theoretically obtained results.

Keywords: tapers, conical angle, geometrical optics, internal reflection, Finite Elements Method

Introduction

Axicons [1, 2] can be used to create nondiffraction Bessel beams in classical Optics [3, 4]. Metalized axicons with small cone angles are also utilised as near-field probes and tapers for sharp focusing in Nanophotonics [5, 6] and especially in near-field microscopy [7-9] and spectroscopy [10]. To determine the optimum parameters of such tapers we need to provide simulation in accordance with the assumptions of the rigorous vectorial diffraction theory [11-14].

Working of metal conical structure is explained by the lightning-rod effect [15] which can be observed near dielectric structures [16]. The lightning-rod effect lies in the fact that longitudinal electric field component are enhanced near sharp structures. It can be observed, for example, in cases where radially polarized beams [17-19] or linearly polarized beams [20-22] are focused.

The dielectric characteristics of axicons can be approximately estimated with ray and scalar optical theory [23, 24], and then defined more accurately with more rigorous methods.

In this work the ray optics approach was used as a rough calculation method. Using ray optics we derived analytic formulas for beam diffraction by the axicon with high numerical aperture (NA) including NAs that were over than the limiting value. Overcoming the limiting value of NA in ray optics means the axicon angle is small enough for total internal reflection arising. Consequently, we have to take into consideration more than one total internal reflection with further decrease of axicon's angle. We obtained axicon's angles which provide maximum and minimum values of intensity on the optical axis. Finite element method of solving Helmholtz equation was used to provide a more rigorous approach for verification of results of the analytical estimations.

1. Theoretical analysis with ray optics approach

Ray paths are described in detail in works [23]. But authors are not have deal with the case that axicon angle is much less than limited value.

Let us quote few results from [23] without any proofs. Notice that every ray impinges to the plain base of the axicon (left side in figure 1). α_0 is a half angle of axicon's top. We call α_0 axicon's angle. If α_0 is large enough, total internal reflection is absent. In addition, rays pass through the right side and converge into the focal straight line segment.
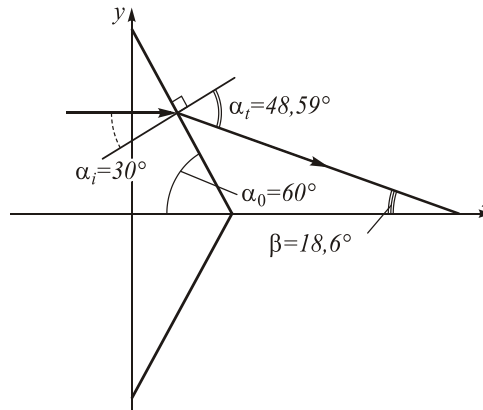
Fig. 1. – Rays paths in axicon in case of absence of total internal reflection

Such configuration remains as long as axicons angle satisfies inequality:

$$\alpha_0 \geq \arccos(1/n), \tag{1}$$

Where n is refractive index of the axicon's material.

If refractive index of $n = 1.5$ the maximum angle is 48.19°. If the angle is less, total internal reflection occurs at the upside of the axicon (see figure 2). In this diagram it is apparent that the angle α_0 is greater than

$$\alpha_0 > 30° + \frac{1}{3}\arcsin\frac{1}{n}, \tag{2}$$

therefore, total internal reflection takes place at bottom side of the axicon. Consequently, the rays turn back and leave the axicon and travel back to the left side.

If $n = 1.5$ we can derive from Eq. (2) that $\alpha_0 > 43.94°$. Ray paths for different angles $\alpha_0 = 44°, 45°, 47°$ are also shown in figure 2 and it is obvious from the symmetry that rays travel back if $\alpha_0 = 45°$.
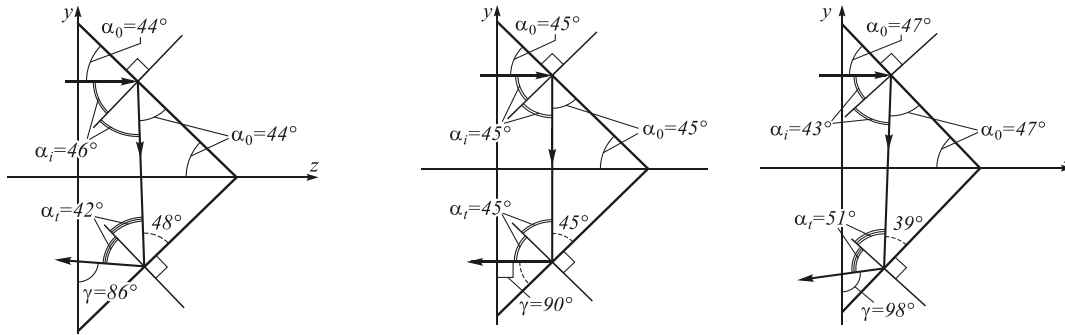
Fig. 2. – Rays paths in axicon in case of double total internal reflections from top and bottom sides $\alpha_0 = 44°, 45°, 47°$

If the angle is less than this expression (2), full internal reflection from the bottom side does not occur; therefore rays leave the axicon through the bottom side and travel down. Nevertheless, if the angle is not much less than (2), the ray travels to the bottom-left direction. Thus, we can call this axicon opaque (figure 3).
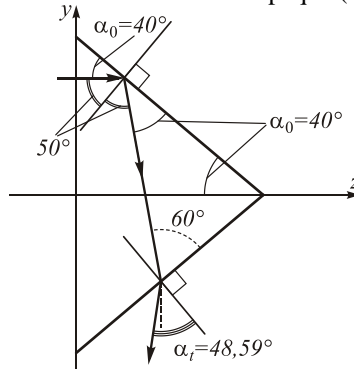
Fig. 3. – Rays paths in axicon in case of $\alpha_0 = 40°$

In figure 3, the horizontal projection of the ray is decreasing with a decrease of the angle. Therefore, if the angle $\alpha_0 = \alpha_{ver}$ horizontal projection becomes zero, hence the ray travels vertically down (figure 4). This angle is defined from the equation:

$$\sin\alpha_{ver} + n(4\cos^3\alpha_{ver} - 3\cos\alpha_{ver}) = 0. \tag{3}$$

29

If $n = 1.5$, $\alpha_{ver} \approx 38°$.
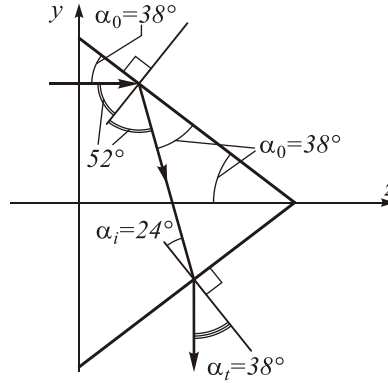
Fig. 4. – Rays paths in axicon in case of $\alpha_0 = \alpha_{ver}$
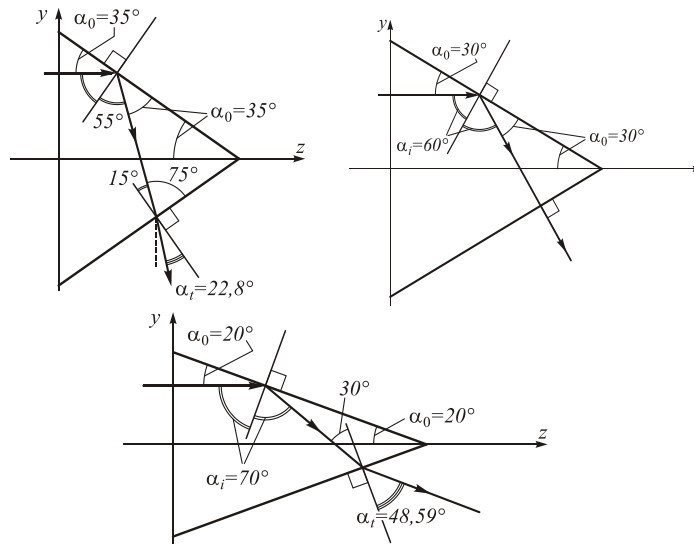
Fig. 5. – Rays paths in axicon in case of $\alpha_0 = 35°; 30°; 20°$

For smaller meanings of the angle α_0 horizontal projection of leaving ray is directed to the right. Although, rays do not intersect optical axis, thus focus is apparent (figure 5).

In [23] the authors consider only those configurations of axicon which are described above. However, it is noticed that by decreasing the axicon's angle right-directed horizontal projection of leaving ray are increasing. If $\alpha_0 = 30°$ this presents a special case. The rays pass through the bottom side without any refraction because the ray is perpendicular to the side, which happens if the refractive index lies in the range:

30

$2/\sqrt{3} < n < 2$. If we continue decreasing α_0, the vertical projection is also decreasing and once it reaches zero, the rays travel horizontally to the right side.

Let us have a look to the last scheme in figure 5. We can make sure that horizontally leaving ray can appears if following equation takes place: $\alpha_0 + \alpha_t = 90°$ (α_t is the refracting angle). If we take into account previous equation, refraction law and the fact that the angle of incidence to the bottom side is $90° - 3\alpha_0$, if a single reflection is from the top side and $\alpha_0 < 30°$, we can see that α_0 has to satisfy following equation if the leaving ray is horizontally-oriented.

$$n\cos 3\alpha_0 = \cos\alpha_0 . \tag{4}$$

If $n = 1.5$, $\alpha_0 = 16.78°$.
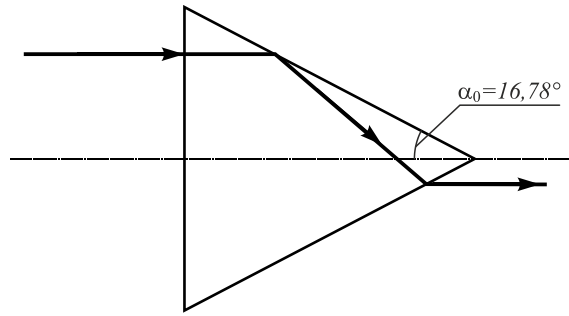
Fig. 6. – Horizontal ray path in axicon in case of $\alpha_0 = 16.78°$

If the angle does not satisfy the equation (4), vertical projection of the leaving ray becomes directed upwards. Therefore, rays intersect with optical axis and form real focus (figure 7). In contrast to the results presented in the figure 1, in this situation leaving ray intersects the optical axis from the bottom to the top. Once more distinguishing feature is that the entrance pupil diameter is much greater than exit pupil diameter.

However, from the equation (4) we can determine that the angle's interval which provides real focuses of the axicon with single total internal reflection is very small. The condition for the second total internal reflection from the bottom side is therefore as follows:

$$n\cos 3\alpha_0 = 1 \quad \Rightarrow \quad \alpha_0 = \frac{1}{3}\arccos\frac{1}{n} \tag{5}$$
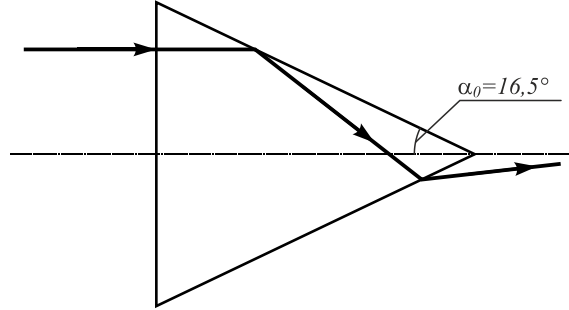
Fig. 7. – Real focus with single total internal reflection in the axicon

This is three times less than the angle which is satisfying inequality in (1). In this case $\alpha_0 = 16.06°$, if $n = 1.5$. Varying the angle from (4) to (5) we can achieve focal segment theoretically with any length. As we can see the angles interval which provides real axicon's focus, is very small and equals just 0.72 degree.

If the angle is smaller than (5), second full internal reflection occurs at the bottom side, the ray falls into the top side. Here ray is refracted and travels to the up-right direction. Thus, we have an apparent focus again. As it is shown in figure 6, the leaving ray is oriented horizontally if the same equation $\alpha_0 + \alpha_t = 90°$ is satisfied. But where the angle of incidence equals $90° - 5\alpha_0$ at the top side in case of double total internal reflection from the top and then the bottom sides. Hence, the leaving ray will be oriented horizontally (figure 8) if the angle satisfies the equation:

$$n\cos 5\alpha_0 = \cos\alpha_0 . \tag{6}$$

If $n = 1.5$ this angle equals $9.785°$.
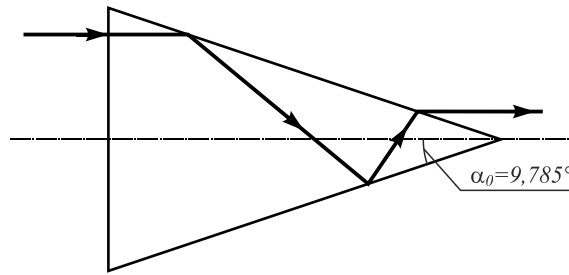
Fig. 8. – Horizontal ray path in axicon in case of $\alpha_0 = 9.785°$

If the angle even smaller than is defined from equation (6), the vertical projection of the ray becomes oriented downward. Rays intersect the optical axis and form the real focus as indicated in figure 9. The leaving ray intersects the optical axis from up to down (as in figure 1), but only after two total internal refractions.
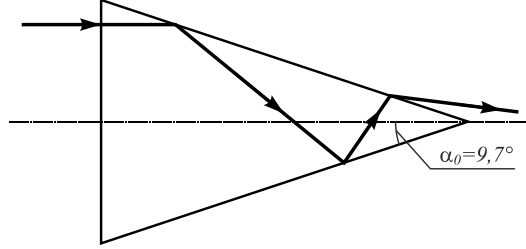
Fig. 9. – Real focus with double total internal reflection in the axicon

In the same way as in figure 7 we can therefore surmise derive that another total internal reflection occurs if following equation is satisfied:

$$n\cos 5\alpha_0 = 1 \quad \Rightarrow \quad \alpha_0 = \frac{1}{5}\arccos\frac{1}{n}. \tag{7}$$

That is five time less than it is derived from (1). If $n = 1.5$, $\alpha_0 = 9.64°$. Thus, angle interval which provides real focus with two total internal reflections is much smaller and equals 0.145 degree.

It is also possible to make sure that with the continuing decreasing of the angle we have infinite exchanging of real and apparent focuses. Boundaries of intervals of real and apparent focuses were defined by situations of total internal reflections (as in (5) and (7)) and the situations of leaving ray horizontality (as in (4) and (6)).

Real focus will be observed in narrow ranges of axicon's angles which are defined by the following inequalities:

$$\alpha_{min}^{real} < \alpha_0 < \alpha_{max}^{real}, \tag{8}$$

here α_{min}^{real} is achieved from equation:

$$n\cos\left[(2p+1)\alpha_{min}^{real}\right] = \cos\left(\alpha_{min}^{real}\right), \tag{8a}$$

and α_{max}^{real} from the equation:

$$n\cos\left[(2p+1)\alpha_{max}^{real}\right] = 1. \tag{8b}$$

Equations (8a) and (8b) give boundaries for p-fold total internal reflection, $p \geq 1$. If p is even, the ray intersects the optical axis from up to down as it is shown in figure 9. If p is odd, the ray intersects the optical axis from down to up as in figure 7.

Apparent focus is observed with p-fold total internal reflection in larger ranges, which are further defined by adding the following inequalities:

$$\alpha_{min}^{app} < \alpha_0 < \alpha_{max}^{app}. \tag{9}$$

here

$$n\cos\left[(2p-1)\alpha_{min}^{app}\right] = 1, \quad p \geq 2, \tag{9a}$$

$$n\cos\left[(2p+1)\alpha_{max}^{app}\right] = \cos\left(\alpha_{max}^{app}\right), \quad p \geq 1 \tag{9b}$$

The bottom boundary for single total internal reflection is not defined by formula (9a). It is equals the α_{ver}, which is derived from (3). From this it is evident that the range of the intervals is becoming increasingly smaller. That has explicitly resulted from the meaning of the boundary of new total internal reflection, which can be easily

33

obtained analytically: $\dfrac{1}{2p+1}\arccos\dfrac{1}{n}$. This indicates the boundary is decreasing if p is increasing. Thus, the received width of the 'real focus gap' is the largest and equals 0.72 degree for $p=1$. As noted, other gaps are becoming increasingly narrower.

Because of narrowness of angle ranges for real focuses, we should discuss the resonant phenomena. The same problems with polychromatic light can occur, because of dispersion transmission ranges can be different for different wavelengths. Furthermore, for one part of the spectrum the axicon can provide real focus and for another part of spectrum focus can be apparent. It is evident, therefore, that the axicon makes spectral redistribution as a prism.

Thus, from the finding we can see that ray optical approach has become useful for understanding of rays paths and intensity distribution in an axicon. However, it is problematic to receive total intensity distribution and estimations of beams sizes. For these reasons we have to apply a more rigorous theory.

2. Numerical simulation by means of solving Helmholtz equation with finite element method

In this work we provide numerical simulation of Gaussian beam diffraction by flat axicon with finite element method which is realized in Comsol.
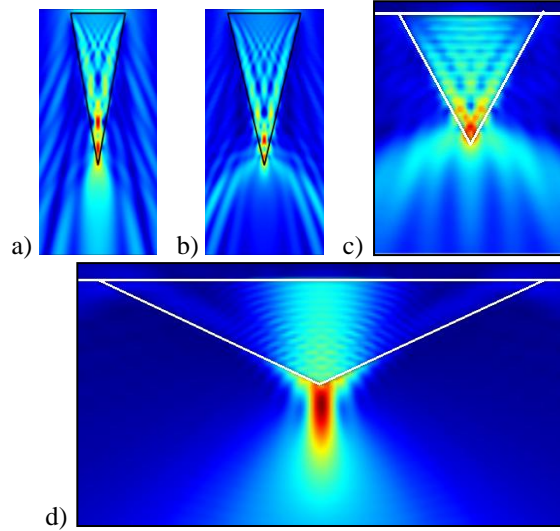
Fig. 10. – Simulation results of Gaussian beam diffraction by axicons with different cone angles: a) $\alpha_0 = 10.5°$, b) $\alpha_0 = 11°$, c) $\alpha_0 = 30°$, d) $\alpha_0 = 61°$

In the figure 10 we show the simulation results of TE-polarized Gaussian beam diffraction by 2D axicons with different axicon's angle α_0. Wavelength is $\lambda = 532$ nm, and refraction index is $n = 1.5$.

As we can see in figure 10, whereas we increase axicon angle from $10.5°$ to $11°$, the internal reflection arises and the main part of energy scatters at a high angle to the

optical axis. Ray optics predicts that this beam splitting is in contrast to wave optics which takes into evanescent field. An axicon works as a refractive element and produces a strong light segment where the axicon angle is more $49°$.

Conclusions

In this work we considered diffraction of Gaussian beams by the refractive axicon in case of numerical aperture of the axicon is much greater than limited value which corresponds to total internal reflection. This situation did not take into account because it was reckoned that axicon did not transmit light in case of out-the-limited.

Diffraction was considered using two approaches: ray optics and numerical solving of the Helmholtz equation with finite elements method. In the first case analytical estimations are derived for high numerical aperture including the case of out-of-limited numerical aperture.

However, out-of-limited numerical aperture in ray optics corresponds to total internal reflection arising, careful analysis of ray paths reveals that with increasing numerical aperture (decreasing axicon's angle) part of incident energy passes through the axicon though and the transmitted rays form either real or apparent focus.

Finally, the rigorous wave approach allowed us to verify the perceived analytical results.

Acknowledgements

References

1. **McLeod JH.** The axicon: a new type of optical element. Journal of the Optical Society of America, 1954; 44: 592-597.
2. **Jaroszewicz Z, Burvall A, Friberg AT.** Axicon – the most important optical element. Optics & Photonics News, 2005; April.
3. **Durnin J, Miceli JJ, Eberly JH.** Diffraction-free beams. Physical Review Letters, 1987; 58: 1499-1501.
4. **McGloin D, Dholakia K.** Bessel beams: diffraction in a new light. Contemporary Physics, 2005; 46(1): 15-28.
5. **Babadjanyan AJ, Margaryan NL, Nerkararyana KhV.** Superfocusing of surface polaritons in the conical structure. Journal Applied Physics, 2000; 87(8): 3785-3788.
6. **Novotny L, Hecht D.** Principles of Nano-Optics. Cambridge: New York, 2006.
7. **Goncharenko AV, Chang H-C, Wang J-K.** Electric near-field enhancing properties of a finite-size metal conical nano-tip. Ultramicroscopy, 2007; 107: 151-157.
8. **Antosiewicz TJ, Wróbel P, Szoplik T.** Nanofocusing of radially polarized light with dielectric-metal-dielectric probe. Optics Express, 2009; 17(11): 9191-9196.
9. **Choo H, Kim M-K, Staffaroni M, Seok TJ, Bokor J, Cabrini S, Schuck PJ, Wu MC, Yablonovitch E.** Nanofocusing in a metal–insulator–metal gap plasmon waveguide with a three-dimensional linear taper. Nature Photonics, 2012; 6: 838-844.
10. **Berweger S, Atkin JM, Olmon RL, Raschke MB.** Light on the tip of a needle: plasmonic nanofocusing for spectroscopy on the nanoscale. The Journal of Physical Chemistry Letters, 2012; 3: 945-952.

11. **Gramotnev DK, Vogel MW, Stockman MI.** Optimized nonadiabatic nanofocusing of plasmons by tapered metal rods. Journal Applied Physics, 2008, 104: 034311-034318.
12. **Davoyan AR, Shadrivov IV, Kivshar YS.** Gramotnev DK. Optimal tapers for compensating losses in plasmonic waveguides. Physica Status Solidi – Rapid Research Letters, 2010; 4(10): 277- 279.
13. **Degtyarev SA, Khonina SN, Alferov SV, Karpeev SV.** Theoretical and experimental study of aperture size effects on the polarization sensitivity of near-field microscopy fiber-optic probes. Proceedings of SPIE, 2014; 9156: 915608; doi:10.1117/12.2054204.
14. **Degtyarev SA, Khonina SN.** Transmission of focused light signal through an apertured probe of a near-field scanning microscope. Pattern Recognition and Image Analysis, 2015; 25(2): 306-313.
15. **Gramotnev DK, Bozhevolnyi SI.** Nanofocusing of electromagnetic radiation. Nature Photonics, 2014; 8: 14-23.
16. **Degtyarev SA, Khonina SN, Ustinov AV, Kazanskiy NL.** Lightning-rod effect near sharp dielectric structures. Proceedings of SPIE, 2015; 9533: 95330A; doi: 10.1117/12.2180353.
17. **Zhang Y, Wang L, Zheng C.** Vector propagation of radially polarized Gaussian beams diffracted by an axicon. Journal of the Optical Society of America A, 2005; 22(11): 2542-2546.
18. **Kotlyar VV, Stafeev SS.** Modeling sharp focusing of a radially polarized laser mode with a conic and binary microaxicons. Computer Optics, 2009; 33(1): 52-60.
19. **Khonina SN, Degtyarev SA.** A longitudinally polarized beam generated by a binary axicon. Journal of Russian Laser Research, 2015; 36(2): 151-161.
20. **Khonina SN, Nesterenko DV, Morozov AA, Skidanov RV, Soifer VA.** Narrowing of a light spot at diffraction of linearly-polarized beam on binary asymmetric axicons. Optical Memory and Neural Networks (Information Optics), 2012; 21(1): 17-26.
21. **Khonina SN, Karpeev SV, Alferov SV, Savelyev DA, Laukkanen J, Turunen J.** Experimental demonstration of the generation of the longitudinal E-field component on the optical axis with high-numerical-aperture binary axicons illuminated by linearly and circularly polarized beams. Journal of Optics, 2013; 15: 085704-085712.
22. **Khonina SN, Savelyev DA.** High-aperture binary axicons for the formation of the longitudinal electric field component on the optical axis for linear and circular polarizations of the illuminating beam. Journal of Experimental and Theoretical Physics, 2013; 117(4): 623-630.
23. **Ustinov AV, Khonina SN.** Calculating the complex transmission function of refractive axicons. Optical Memory and Neural Networks (Information Optics), 2012, 21(3): 133-144.
24. **Ustinov AV, Khonina SN.** Analysis of laser beam diffraction by axicon with the numerical aperture above limiting. Computer Optics, 2014; 38(2): 213-222.

Calculation of a mode set in weakly guiding fibers

Aleksandrova A.V.

Samara State Aerospace University

Abstract. The aim of the paper is to calculate the mode set in weakly guiding fibers using a calculation of the eigenmodes of the optical fiber with a step index of refraction. The superposition of modes with various properties of self-reproduction for a given set of physical characteristics was determined. The propagation of light signals in the non-ideal optical waveguides has been studied by computer simulation using the commercial software BeamProp.

Introduction

The optical fiber is considered now to be the perfect physical environment for information transfer as well as the most preferable environment for significant data flows over considerable distances. Optical fibers have wider applications in computer networking and telecommunications thanks to a number of the features inherent in optical waveguides.

Success achieved in the production of optical fibers allows information to be transferred at high speeds over hundreds of kilometres without regeneration of a signal. High-noise immunity, safety of the transmitted data and electromagnetic compatibility of communication channels are serious arguments in favour of fiber-optical systems.

There are two types of optical fibers: single-mode and multi-mode. Fibers with various refractive index profiles (step-index profile or gradient-index profile) are used, depending on the field of application. For step-index optical fiber, a refractive index profile characterized by a uniform refractive index within the core and a sharp decrease in the refractive index at the core-cladding interface is used so that the cladding is of a lower refractive index. Gradient-index fiber is an fiber whose core has a refractive index that decreases with increasing radial distance from the optical axis of the fiber. In this investigation, we have looked at fibers with a step profile index of refraction because of their wide extension.

The term "mode division multiplexing" (MDM) is used for multimodal optical fibers when describing methods for data transmission channel multiplexing, with each

spatial fiber mode being treated as a separate channel that carries its own signal [1,2]. The essence of mode division multiplexing is as follows: as a linear superposition of fiber modes, laser beams can be used to generate signals that will effectively transmit data in a physical carrier - a multimodal fiber; the data transmitted can be contained both in the modal composition and in the energy portion associated with each laser mode [3-13]. In addition, the division of the vortex basis connected with orbital angular momentum is especially perspective [7-14].

Recent years have witnessed a number of research activities in the field of singular optics [15, 16, 25-27]. In terms of quantum theory vortex modes they are characterized as spin-orbital states that the current speed of transfer on one fiber allows to increase repeatedly without additional polarizing multiplexing.

1. Mode set in weakly guiding stepped-index fibers

Use of the diffraction optical elements is the most popular method for devices of generation and selection of vortex modes [8, 10, 17-21]. For most popular commercial fibers, the core-cladding index contrast, $\Delta n = n_1 - n_2$, is less than 1%. For such fibers, termed weakly guiding fibers, assuming $n_1 \cong n_2$, in place of the hybrid modes of the propagating electromagnetic field we can consider their linearly polarized superpositions. Considering that for the LP-mode the transverse field is essentially linearly polarized, a complete set of modes takes place when only one electric and one magnetic component are predominant.

The aim of this study is to simulate an ideal optical fiber with a superposition of linearly polarized modes determined by the given physical characteristics of a possible set of modes and their superpositions, with various properties of self-reproduction.

Moreover, the intention is to study the propagation of light signals in non-ideal optical waveguides with a Beam PROP simulation tool (RSoft Design, USA), which implements the well-known Beam Propagation Method (BPM).

To research a set of modes, we considered the weakly guiding cylindrical optical fiber with a step profile of index of refraction. The core radius is a, the cladding radius is b and the respective refractive indices of the core and cladding are n_1 and n_2 (Fig.1). The electromagnetic field extending in such a waveguide is conveniently described using the Bessel functions [22-24].
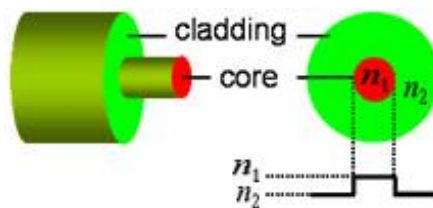
Fig. 1. – The structure of a typical single-mode fiber

Approximation LP-modes are applicable for weakly guiding fibers:

$$LP_{pq}(r,\phi) = \begin{Bmatrix} \cos(p\phi) \\ \sin(p\phi) \end{Bmatrix} \begin{cases} \dfrac{J_p(u_{pq}r/a)}{J_p(u_{pq})}, & 0 \le r \le a \\[2ex] \dfrac{K_p(w_{pq}r/a)}{K_p(w_{pq})}, & a \le r \le b \end{cases}. \qquad (1)$$

In Eq. (1), the first-kind Bessel functions $J_p(x)$ describe the field in the fiber core, whereas the modified Bessel functions $K_p(x)$ are used for the cladding.

$$\frac{uJ_m(u)}{J_{m+1}(u)} + \frac{wK_m(w)}{K_{m+1}(w)} = 0, \qquad (2)$$

where the parameters $u^2 + w^2 = V^2$, $V = \dfrac{2\pi}{\lambda}a\sqrt{n_1^2 + n_2^2}$ form the cut-off number and λ is the wavelength of laser light in air. The cut-off number V, which includes the main parameters of fibers and laser radiation, is the number of modes propagating in the fiber. The numerical simulation parameters are as follows: the core radius is a=5μm, the cladding radius is b=62.5 μm, and the respective refractive indices of the core and cladding are n_1=1.45 and n_2=1.44. For example, when λ=0.633 μm and V≈8,4398, fiber with the above parameters in addition to the fundamental mode LP01 will behave as LP02, LP03, LP11, LP12, LP21, LP41. Figure 2 shows cross-section distributions for some modes for a stepped-index fiber with the cut-off number V=8.4398.
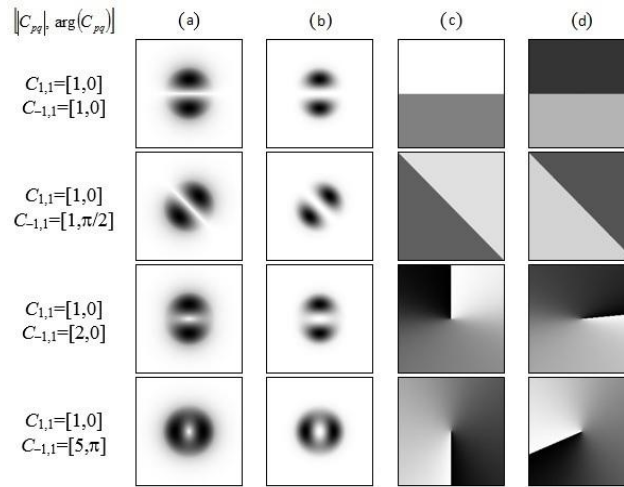
Fig. 2. – Superposition of the (p,q) modes: $(1,1)+(-1,1)$ with different complex coefficients: (a) transverse amplitude distribution, (b) transverse intensity distribution, and (c) phase in the plane z=0, and (d) phase distribution at distance z=200 μm

We consider the propagation of a linear superposition of LP-modes in an ideal stepped index optical fiber:

$$U_0(r,\phi) = \sum_{p,q\in\Omega} C_{pq}\Psi_{pq}(r,\phi) \qquad (3)$$

where C_{pq} are the complex coefficients and $\Psi_{pq}(r,\phi)$ are the modes at $z=0$, whose angular component is represented in a different way without a loss of generality:

$$\Psi_{pq}(r,\phi,z) = \exp\left(-i\beta_{pq}z\right)T_p(\phi)R_{pq}(r) =$$

$$= \exp\left(-i\beta_{pq}z\right)\exp\left(ip\phi\right)\begin{cases} \dfrac{J_p(u_{pq}r/a)}{J_p(u_{pq})}, & 0\le r\le a \\[2mm] \dfrac{K_p(w_{pq}r/a)}{K_p(w_{pq})}, & a\le r\le b \end{cases} \qquad (4)$$
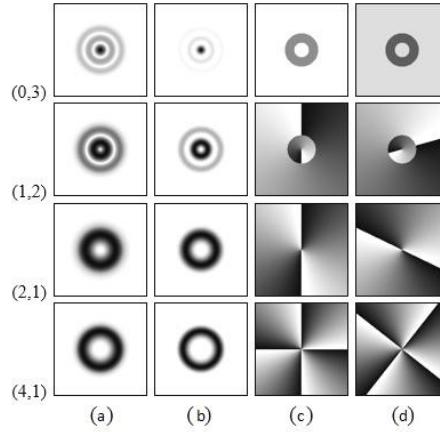
Fig. 3. – The (p,q) modes: (0,3), (1,2), (2,1), (4,1): (a) transverse amplitude distribution (negative), (b) transverse intensity distribution (negative) in the plane $z=0$; transverse phase distribution (white: zero phase, black: 2π) in the planes (c) $z=0$ and (d) $z=100$ μm

Models of optical fibers with the different parameters, structures and shapes have been established in the software BeamProp in order to research, analyse and compare non-ideal optical waveguides (Fig. 4).
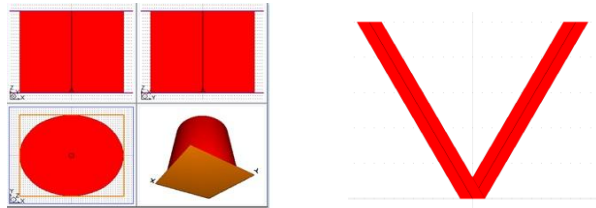
Fig. 4. – Various models of waveguides

The main characteristic of optical fiber is the set of modes extending within it (Fig. 5).

40
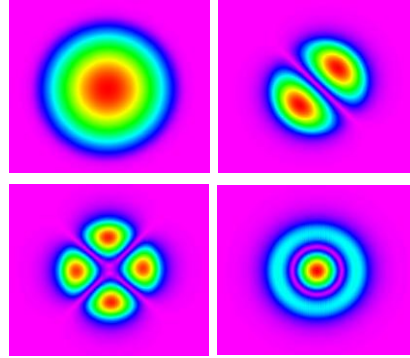
Fig. 5. – Some of the modes supported by a simple 3D fiber structure

Figure 6 shows the distribution of radiation *S*-shaped optical fiber and power of the propagating radiation.
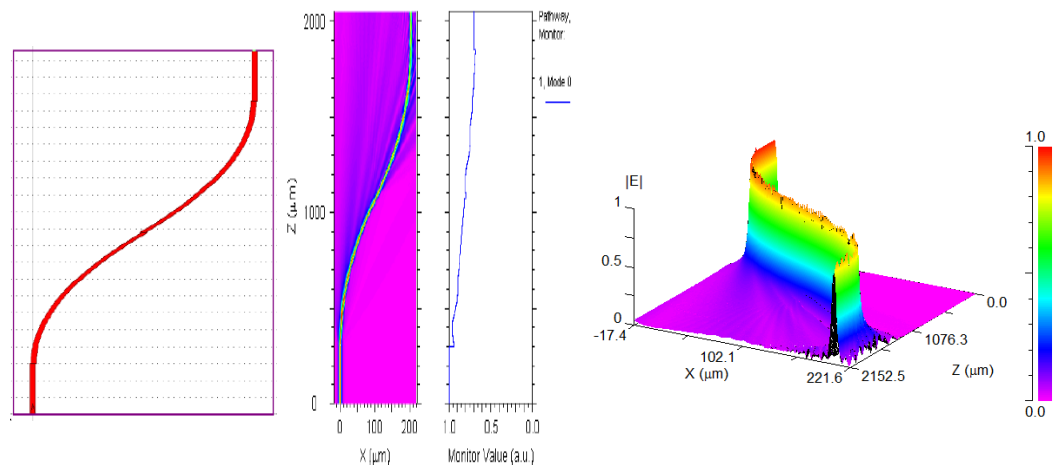
Fig. 6. – The completed s-bend circuit in the CAD window; the simulation results found using the arc waveguides

Figure 7 shows the distribution of radiation of *X*-shaped coupler and the power of the propagating radiation zero and first modes.

By modelling the propagation of radiation in optical fibers, it is possible to determine their output values and make sure the elements have the given parameters, and to predict their behaviour depending on external influences.

41
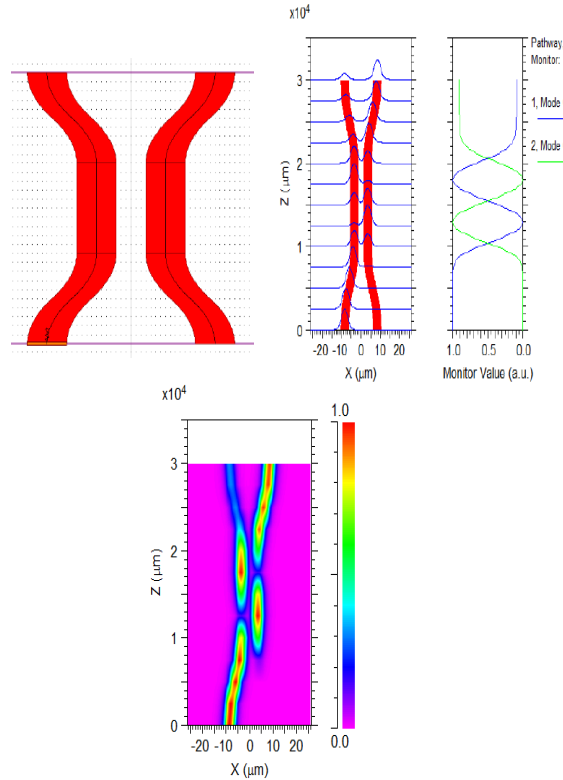
Fig. 7. – X-shaped coupler

Conclusions

Using the BeamProp program it is possible to investigate various samples of non-ideal optical fibers with a step profile of index of refraction, according to following characteristics:

— profile and index of refraction;
— difference of indices of refraction;
— waveguide length;
— a type of function on which the index of refraction changes;
— etc.

Studying the resistance of vortex modes to fiber bends under various characteristics of a core and cover of optical fiber is of great interest for the researchers.

Acknowledgements

References

1. **Berdague S, Fasq P.** Mode division multiplexing in optical. Applied Optics, 1982; 21: 1950-1955.
2. **Levi L.** Applied optics. John Wiley & Sons Inc, 1980.
3. **Amin AA, Li A, Chen S, Chen X, Gao G, Shieh W.** LP11mode 4×4 MIMO-OFDM transmission over a two-mode fiber. Optics Express, 2011; 19(17): 16672-16679.
4. **Randel S.** 6×56-Gb/s mode-division multiplexed transmission over 33-km few-mode fiber enabled by 6×6 MIMO equalization. Optics Express, 2011, 19(17): 16697-16707.
5. **Hanzawa N, Saitoh K, Sakamoto T, Matsui T, Tomita S, Koshiba M.** Demonstration of mode-division multiplexing transmission over 10 km two-mode fiber with mode coupler. Optical Fiber Communication Conference and Exposition (OFC/NFOEC), 2011.
6. **Chen Xi, Jia Ye, Yue Xiao, An Li, Jiayuan He, Qian Hu, William Shien.** Equalization of two-mode fiber based MIMO signals with larger receiver sets. Optics Express, 2012; 20(26): B413-B418.
7. **Wang Z, Zhang N, Yuan XC.** High-volume optical vortex multiplexing and de-multiplexing for free-space optical communication. Optics Express, 2011; 19: 482-492.
8. **Khonina SN, Kazanskiy NL, Soifer VA.** Optical Vortices in a Fiber: Mode Division Multiplexing and Multimode Self-Imaging. Recent Progress in Optical Fiber Research, 2012.
9. **Sakaguchi J.** Space Division Multiplexed Transmission of 109-Tb/s Data Signals Using Homogeneous Seven-Core Fiber. Journal of Lightwave Technology, 2012; 30(4): 658-665.
10. **Kirilenko MS, Khonina SN.** Information Transmission Using Optical Vortices. Optical Memory and Neural Networks (Information Optics), 2013; 22(2): 81-89.
11. **Bozinovic N, Yue Y, Ren Y, Tur M, Kristensen P, Huang H, Willner AE, Ramachandran S.** Terabit-scale orbital angular momentum mode division multiplexing in fibers. Science, 2013; 340: 1545-1548.
12. **Lyubopytov VS, Tlyavlin AZ, Sultanov AKh, Bagmanov VKh, Khonina SN, Karpeev SV, Kazanskiy NL.** Mathematical model of completely optical system for detection of mode propagation parameters in an optical fiber with few-mode operation for adaptive compensation of mode coupling. Computer Optics, 2013; 37(3): 352-359.
13. **Huang H, Xie G, Yan Y, Ahmed N, Ren Y, Yue Y, Rogawski D, Willner MJ, Erkmen BI, Bimbaum KM, Dolinar SJ, Lavery MPJ, Padgett MJ, Tur M, Willner AE.** 100 Tbit/s free-space data link enabled by three-dimensional multiplexing of orbital angular momentum, polarization, and wavelength. Optics Letters, 2014; 39(2): 197-200.
14. **Willner AE.** Optical communications using orbital angular momentum beams. Advances in Optics and Photonics, 2015; 7(1): 6-106.
15. **Soskin MS, Vasnetsov VM.** Singular Optics. Progress in Optics, 2001; 219-276.
16. **Padgett MJ, Courtial J, Allen L.** Light's Orbital Angular Momentum. Physics Today, 2004; 35-40.
17. **Khonina SN, Skidanov RV, Kotlyar VV, Jefimovs K, Turunen J.** Phase diffractive filter to analyze an output step-index fiber beam. Optical Memory and Neural Networks, Allerton Press, 2003; 12(4): 317-324.
18. **Almazov AA, Khonina SN.** Periodic self-reproduction of multi-mode laser beams in graded-index optical fibers. Optical Memory and Neural Networks, 2004; 13(1): 63-70.
19. **Karpeev SV, Pavelyev VS, Khonina SN, Kazanskiy NL.** High-effective fiber sensors based on transversal mode selection. Proceedings SPIE, 2005; 5854: 163-169.
20. **Karpeev SV, Pavelyev VS, Khonina SN, Kazanskiy NL, Gavrilov AV, Eropolov VA.** Fibre sensors based on transverse mode selection. Journal of Modern Optics, 2007; 54(6): 833-844.

21. **Karpeev SV, Khonina SN.** Experimental excitation and detection of angular harmonics in a step-index optical fiber. Optical Memory & Neural Networks (Information Optics), 2007; 16(4): 295-300.
22. **Koshiba M.** Optical waveguide analysis. McGraw-Hill Inc, 1948.
23. **Snyder AW, Love JD.** Optical waveguide theory. Chapman and Hall, 1983.
24. **Cherin AH.** An introduction to optical fiber. McGraw-Hill Inc, 1987.
25. **Kotlyar VV, Soifer VA, Khonina SN.** Rotation of multimodal Gauss-Laguerre light beams in free space and in a fiber. Optics and Lasers in Engineering, 1998; 29(4-5): 343-350.
26. **Khonina SN, Volotovsky SG.** Self-reproduction of multimode laser fields in weakly guiding stepped-index fibers. Optical Memory & Neural Networks (Information Optics), Allerton Press, 2007; 16(3): 167-177.
27. **Khonina SN, Striletz AS, Kovalev AA, Kotlyar VV.** Propagation of laser vortex beams in a parabolic optical fiber. Proceedings SPIE, 2010; 7523:75230B.

Modeling superlattice patterns using the interference of sharp focused spherical waves

Fidirko N.S.

Samara State Aerospace University

Abstract. In this paper, modelling of pseudonondiffrational beams forming superlattice structures in a cross section has been performed. To create such distributions we suggest using superposition of sharp focused spherical waves. Thus, we have done simulations for several spherical waves generated by coherent light sources located on a ring with a certain radius. It is shown that depending on the configuration of the source field we can achieve different superlattice patterns in a cross section with a small amount of waves in the input field. Using more waves, we can obtain Bessel-like beams in the cross section.

Keywords: interference, optical vortices, sharp focusing, polarization

Introduction

A nondiffracting wave field is comprehended as a monochromatic optical field whose transverse shape remains invariant in free-space propagation. In 1987, Durnin proposed that nondiffracting wave fields are exact solutions to the homogeneous Helmholtz equation [1]; such particular solutions can be described as Bessel functions and are called nondiffracting Bessel beams. The realizable beams that propagate with relatively small divergence angles up to a certain range have finite energy and are known as pseudonondiffracting optical beams. Along with his co-authors, Durnin first experimentally realized a pseudonondiffracting Bessel beam in a cylindrical coordinates system [2]. Since then, nondiffracting Bessel beams have been extensively studied and applied in diverse fields, for example optical manipulation, the capture of micro particles and optical coherence tomography [3-7].

In recent years, the attention of physicists and mathematicians has been drawn to two-dimensional nondiffractive superlattice patterns [8]. Besides, realization of such distributions related to crystals, quasicrystals and other periodic structures has been actively researched [9-12].

A two dimensional distribution made by superposition of several plain lattices is called a superlattice [8, 12]. In this work, we show an approach to create superlattice distributions using the interference of sharp focused spherical waves.

Model of sharp focusing

A sharp focused electromagnetic field in the focal area in Cartesian coordinates can be described with the following equation:

$$
\begin{pmatrix} \mathbf{E}(\rho,\varphi,z) \\ \mathbf{H}(\rho,\varphi,z) \end{pmatrix} = -\frac{if}{\lambda} \int_0^\alpha \int_0^{2\pi} B(\theta,\phi)T(\theta) \begin{pmatrix} \mathbf{P}_E(\theta,\phi) \\ \dfrac{1}{\mu}\mathbf{P}_H(\theta,\phi) \end{pmatrix} \times
\tag{1}
$$

$$
\times \exp\left[ik\left(\rho\sin\theta\cos(\phi-\varphi)+z\cos\theta\right)\right]\sin\theta\, d\theta\, d\phi,
$$

where (ρ,φ,z) – cylindrical coordinates in the focal area, (θ,ϕ) – spherical angular coordinates of the output pupil of the focusing system, α - maximal value of the azimuth angle, related to the numerical aperture, $B(\theta,\phi)$ – transmission function, $T(\theta)$ – apodization function (for aplanatic systems it is $T(\theta)=\sqrt{\cos\theta}$), $k=2\pi/\lambda$ – wavenumber, λ – wavelength, f – focal distance. $\mathbf{P}_E(\theta,\phi)$ и $\mathbf{P}_H(\theta,\phi)$ – polarization matrixes for electric and magnetic fields respectively:

$$
\mathbf{P}_E(\theta,\phi) = \begin{bmatrix} 1+\cos^2\phi(\cos\theta-1) & \sin\phi\cos\phi(\cos\theta-1) \\ \sin\phi\cos\phi(\cos\theta-1) & 1+\sin^2\phi(\cos\theta-1) \\ -\sin\theta\cos\phi & -\sin\theta\sin\phi \end{bmatrix} \begin{pmatrix} c_x(\phi) \\ c_y(\phi) \end{pmatrix};
\tag{2}
$$

$$
\mathbf{P}_H(\theta,\phi) = \begin{bmatrix} \sin\phi\cos\phi(\cos\theta-1) & -\left(1+\cos^2\phi\left(\cos\theta-1\right)\right) \\ 1+\sin^2\phi\left(\cos\theta-1\right) & -\sin\phi\cos\phi(\cos\theta-1) \\ -\sin\theta\sin\phi & \sin\theta\cos\phi \end{bmatrix} \begin{pmatrix} c_x(\phi) \\ c_y(\phi) \end{pmatrix}.
\tag{3}
$$

where $c_x(\phi), c_y(\phi)$ is the polarization coefficients of the source field.

For vortex fields $B(\theta,\phi)=R(\theta)\exp(im\phi)$, so formula (1) can be reduced to an equation with one-time integration:

$$
\begin{pmatrix} \mathbf{E}(\rho,\varphi,z) \\ \mathbf{H}(\rho,\varphi,z) \end{pmatrix} = -ikf\int_0^\alpha R(\theta)T(\theta)\begin{pmatrix} \mathbf{Q}_E(\rho,\varphi,\theta) \\ \dfrac{1}{\mu}\mathbf{Q}_H(\rho,\varphi,\theta) \end{pmatrix}\sin\theta\exp(ikz\cos\theta)d\theta.
\tag{4}
$$

where $\mathbf{Q}_{E,H}(\rho,\varphi,\theta)$ matrices can be explicitly written for certain types of polarizations and consist of superposition of Bessel functions of different orders [13-14].
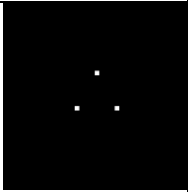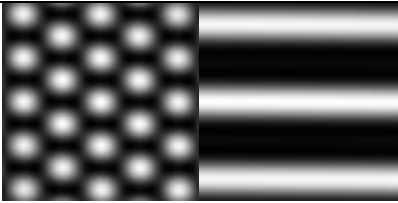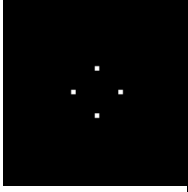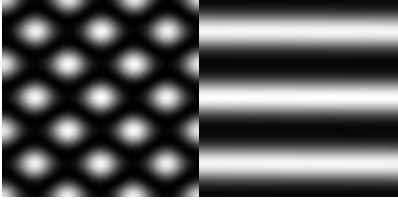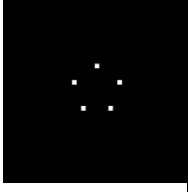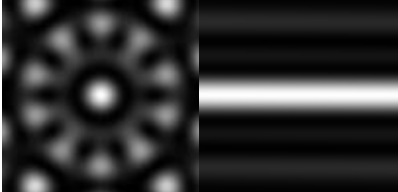
If all beams are generated by different zones of the optical element supplementing a lens with a high numerical aperture, the resulting field in the focal area will be a superposition of the fields established by different zones of the optical element:

$$\mathbf{E}(\rho,\varphi,z) = \sum_i \mathbf{E}_i(\rho,\varphi,z). \tag{5}$$

The interference of spherical waves

The next step is to review an opaque diaphragm, imposed on the pupil of a focusing system with a high numerical aperture. The diaphragm has several small holes, located evenly on a certain radius from the centre of the diaphragm.

Table 1. – The resulting electric field for the central radius $r_c = 25\lambda$

N	Source field	$\|\mathbf{E}\|^2$ (latitudinal and longitudinal sections)
3		
4		
5		
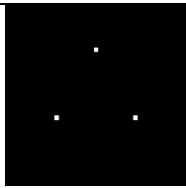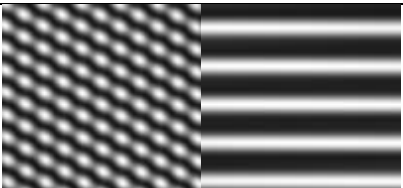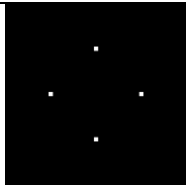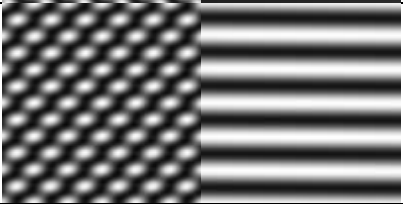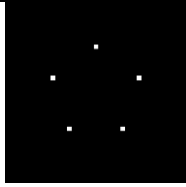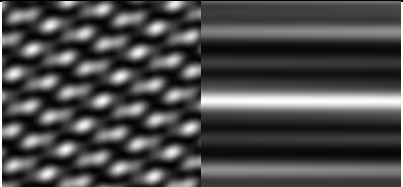
Thereby, we gain a system of point light sources. Every source generates a spherical wave that is being focused on and interferes with waves from other point sources. Herewith, we can vary the number of point sources and their distance from the centre of the aperture.

In figure 1, the shapes of the diaphragms generating different number of waves is evident. In tables 1-5 results of modelling with different parameters are listed.

From the tables above, with the interference of three and four spherical waves in the cross section of the focal area there are bright light spots located in the lattice sites; furthermore, the configurations of the lattices can be different. In addition, longitudinal plane long light channels are formed. The nondiffractional nature of the beams, the spectrum of which is localized on the ring, has been evident for a long time. It has been successfully used to create different structures that remain invariant

47

in the longitudinal direction [16-18]. The obtained distributions can be used to create photonic crystals and plasma channels.

Table 2. – The resulting electric field for the central radius $r_c = 50\lambda$

N	Source field	$|\mathbf{E}|^2$ (latitudinal and longitudinal sections)
3		
4		
5		

With the interference of five or more waves in the cross section, we can see a superlattice pattern. If the radius of the ring is increased (for comparison see tables 3 and 4) the central spot is decreased, which corresponds to the increase in the numerical aperture. With the increase in the numerical aperture (radius of the ring), the interference pattern becomes more complex and different symmetries appear.
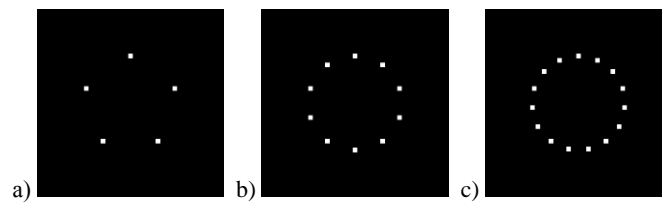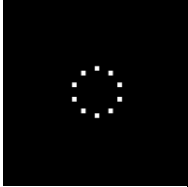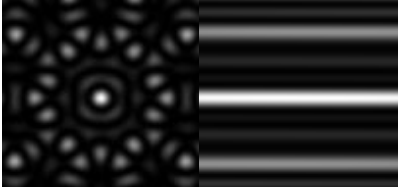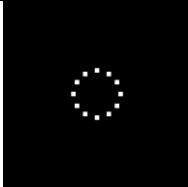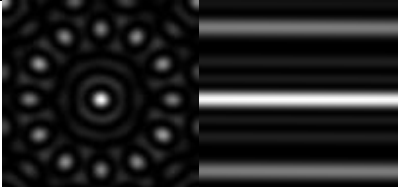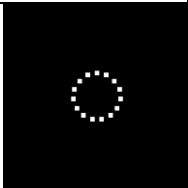
Fig. 1. – Shape of the diaphragm for a) 5 point sources, b) 10 point sources, c) 15 point sources with a central radius $r_c = 50\lambda$, the radius of every point is - $r_d = 2\lambda$

Table 3. – The resulting electric field for the central radius $r_c = 25\lambda$

N	Source field	$\|\mathbf{E}\|^2$ (latitudinal and longitudinal sections)
10		
12		
15		

If we use many point sources so that the ring aperture is tightly filled, Bessel-like beams begin to form in the cross section. In these situations, the size of the central spot of the Bessel beam depends on the radius of the ring aperture. It is worth noting that this approach to generating a Bessel beam is more convenient than creating the ring aperture.

Conslusion
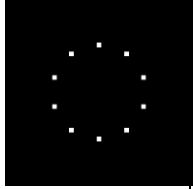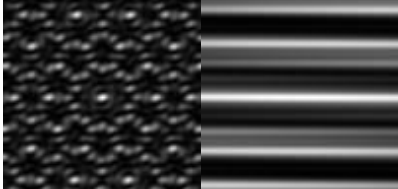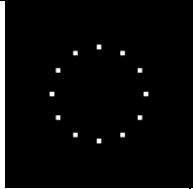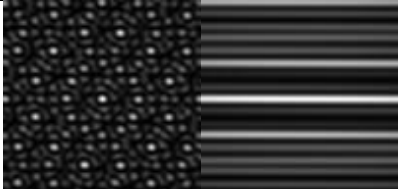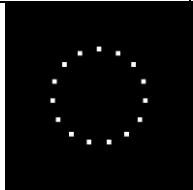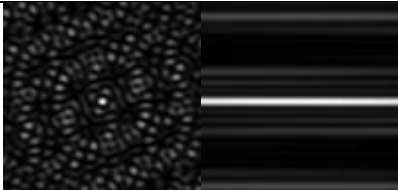
By varying the number of waves and distance between them one can therefore obtain a wide range of superlattice patterns in the cross section, which will keep their structure at a long distance. In this case, the radius of the holes in the diaphragm and the radius of the ring determine the length of the longitudinal section. Increasing the size of the holes and the numerical aperture leads to a reduction of the focus depth.

More complex superlattice patterns can be added by increasing the number of phases of the point sources with special phase elements and by adding polarization to the focused beam [13, 19-21].
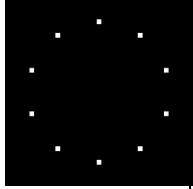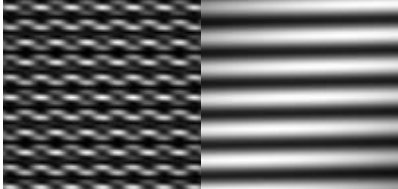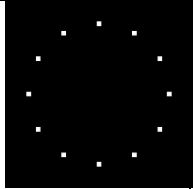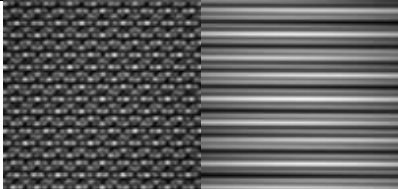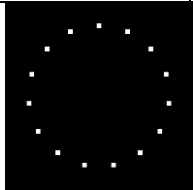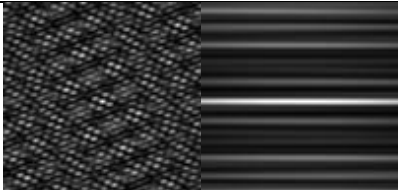
Table 4. – The resulting electric field for the central radius $r_c = 50\lambda$

N	Source field	$\lvert\mathbf{E}\rvert^2$ (latitudinal and longitudinal sections)
10		
12		
15		

References
1. **Durnin J.** Exact solutions for nondiffracting beams. I. The scalar theory. Journal of the Optical Society of America A, 1987; 4(4): 651-654.
2. **Durnin J, Miceli JJ Jr, Eberly JH.** Diffraction-free beams. Physical Review Letters, 1987; 58(15): 1499-1501.
3. **Garcés-Chávez V, McGloin D, Melville H, Sibbett W, Dholakia K.** Simultaneous micromanipulation in multiple planes using a self-reconstructing light beam. Nature, 2002; 419(6903): 145-147.
4. **McGloin D, Garcés-Chávez V, Dholakia K.** Interfering Bessel beams for optical micromanipulation. Optics Letters, 2003; 28(8): 657-659.
5. **Arlt J, Garcés-Chávez V, Sibbett W, Dholakia K.** Optical micromanipulation using a Bessel light beam. Optics Communications, 2001; 197(4-6): 239-245.
6. **Ding Z, Ren H, Zhao Y, Nelson JS, Chen Z.** High-resolution optical coherence tomography over a large depth range with an axicon lens. Optics Letters, 2002; 27(4): 243-245.
7. **Yu C, Wang MR, Varela AJ, Chen B.** High-density non-diffracting beam array for optical interconnection. Optics Letters, 2000; 177(1-6): 369-376.
8. **Bouchal Z.** Nondiffracting optical beams: physical properties, experiments, and applications. Czechoslovak Journal of Physics, 2003; 53(7): 537-624.
9. **Boguslawski M, Rose P, Denz C.** Increasing the structural variety of discrete nondiffracting wave fields. Physical Review A, 2011; 84(1): 013832.

Table 5. – The resulting electric field for the central radius $r_c = 75\lambda$

N	Source field	$\|\mathbf{E}\|^2$ (latitudinal and longitudinal sections)
10		
12		
15		

10. **Boguslawski M, Rose P, Denz C.** Nondiffracting kagome lattice. Applied Physics Letters, 2011; 98(6): 061111.
11. **Chen YF, Liang HC, Lin YC, Tzeng YS, Su KW, Huang KF.** Generation of optical crystals and quasicrystal beams: Kaleidoscopic patterns and phase singularity. Physical Review A, 2011; 83(5): 053813.
12. **Tsou CH, Wu TW, Tung JC, Liang HC, Tuan PH, Chen YF.** Generation of pseudonondiffracting optical beams with superlattice structures. Optics Express, 2013; 21(20): 23441-23449.
13. **Khonina SN, Volotovsky SG.** Managing the contribution of various vector field components in the focal area of a high-aperture lens with binary phase structures. Computer Optics, 2010; 34(1): 58-68. [in Russian]
14. **Khonina SN, Kazanskiy NL, Volotovsky SG.** Vortex phase transmission function as a factor to reduce the focal spot of high-aperture focusing system. Journal of Modern Optics, 2011; 58(9): 748-760.
15. **Khonina SN, Kazanskiy NL, Volotovsky SG.** Influence of vortex transmission phase function on intensity distribution in the focal area of high-aperture focusing system. Optical Memory and Neural Networks (Information Optics), 2011; 20(1): 23-42.
16. **Ziolkowski RW, Besieris IM, Shaarawi AM.** Aperture realizations of exact solutions to homogeneous-wave equations. Journal of the Optical Society of America A, 1993; 10(1): 75-87.
17. **Gutierrez-Vega JC, Iturbe-Castillo MD, Chavez-Cerda S.** Alternative formulation for invariant optical fields: Mathieu beams. Optics Letters, 2000; 25(20): 1493-1495.

18. **Khonina SN.** An easy and efficient way to create different nondiffractional laser beams. Computer Optics, 2009; 33(1): 70-78. [in Russian]
19. **Gao X, Wang J, Gu H, Xu W.** Focusing properties of concentric piecewise cylindrical vector beam. Optik, 2007; 118: 257-265.
20. **Khonina SN, Golub I.** Optimization of focusing of linearly polarized light. Optics Letters, 2011; 36(3): 352-354.
21. **Khonina SN, Fidirko NS.** Research of the interference of counterpropagating sharp focused beams with different polarizations. News of the Samara Science Center of the RAS, 2014; 16(4): 27-33. [in Russian]
22. **Khonina SN, Ustinov AV.** Analysis of interference of cylindrical laser beams generated by ring optical elements with a vortex phase at sharp focusing. Computer Optics, 2015; 39(1): 12-25. [in Russian]

Diffractive optical elements for capturing and controlled rotation of micro-objects

Ganchevskaya S.V., Skidanov R.V.

Image Processing Systems Institute, Russian Academy of Sciences,
Samara State Aerospace University

Abstract. A method is proposed for the controlled rotation of microobjects in non-ring vortex light fields generated by vortex axicons. In the real experiment, the rotation of the group of polystyrene microparticles with a diameter of 5 μm is carried out.

Keywords: light beams, vortex axicon, optical micromanipulation, rotation of particles.

Introduction

Vortex light beams are used for transmission of information [1], in optical inspection systems [2], in optical micromanipulation [3, 4]. The presence of orbital angular momentum is determined by the use of optical vortex beams, especially for the rotation of microobjects. Most of the used vortex beams have a distinct ring structure. But there are light beams that have a more complex structure [5, 6], in the form of closed light lines. Optical actuator for micromechanical systems [7 – 12] is typically considered as the practical use of such light beams, but there are many other practical issues in the field of micromanipulation using vortex beams [13, 14].

1. Formation of the superposition of light fields by vortex axicons.

Diffractive helically-formed axicon is described by a function of complex transmission of the following form:

$$\tau(r,\phi) = \exp\left(i2\pi\nu r\right)\exp\left(in\phi\right), \tag{1}$$

where r, φ are polar coordinates in the plane of the DOE, υ is the spatial frequency of the lines of the axicon, n is the number of the helical component. When light passes through the axicon, a Bessel beam of the n-power is formed, $J_n(\alpha r)$, where $\alpha = k\cos(\upsilon\lambda)$ (k – wave number).

53

In accordance with one work [15], it is provided to generate Bessel beams using the DOE with a transmission function

$$\tau(r,\phi) = \text{sgn}\big(J_n\big(\alpha r\big)\big)\exp\big(in\phi\big). \tag{2}$$

Helical DOE with the transmission (1) effectively forms a light field, the amplitude of which is proportional to the Bessel function $J_n(\alpha r)\exp(in\varphi)$, near the optical axis on the interval $0 < z < Rk/\alpha$, where R is the radius of the axicon.

If we consider the structure of the DOE with the function of the transmission (2) with regard to the geometrical arrangement of the zones, we can say that the DOE is a set of ring zones of approximately equal width in which the phase function is rotated by a azimuthal angle of $\phi_0 = \pi/n$, if the sign of the function $J_n(\alpha r)$ is negative.

Consider a diffractive optical element with the function of the transmission

$$\tau\big(r,\phi\big) = \frac{1}{2}\Big[\exp\big(im_1\phi\big) + \exp\big(im_2\phi\big)\Big] +$$

$$+ \frac{1}{2}\Big[\exp\big(im_2\phi\big) - \exp\big(im_1\phi\big)\Big]\text{sgn}\Big[\cos\big(2\pi v r + n\phi\big)\Big], \tag{3}$$

where m_1, m_2 – numbers of additional vortex components, r, φ – polar coordinates, v – spatial carrier frequency, n – topological charge of binary diffractive axicon, which is the basis of the structure of this DOE. In terms of the geometry, the DOE with such a function of the transmission looks like a binary diffractive axicon, in the ridges of which the vortex component of m_1 is recorded, and in the hollows – the vortex component of m_2, while the location of these zones is that a light field with topological charge n can also be formed in the near zone. Hereinafter the topological charge n will be called the topological charge of structure. In addition, if topological charge is the same in neighboring areas, some constant can be added to the phase in the whole area for the structural separation of these zones. It will look as rotation of the vortex phase at a certain angle. Let is say, for instance, about the phase shift of semiperiod, if this angle is π. The light fields formed in this DOE are notable for a great variety of intensity and phase distributions, that allows to say about their possible use in optical micromanipulation for a very wide range of tasks.

One of such tasks is the rotation of microobjects. In the present paper, a superposition of vortex beams with topological charges $n = 6$, $m_1 = 2$, (figure 1, a-c) and $n = 0$, $m_1 = 7$, $m_2 = -5$, (figure 1, d-f) is formed for this task.

Despite the complex shape of the beam in figure 1e, the motion of the particles takes place on the outer ring. However, light traps in figures 1b, e have many ways of application – the rotation of not only microparticles and bacteria, but more complex objects, for example, microturbines [16].

54
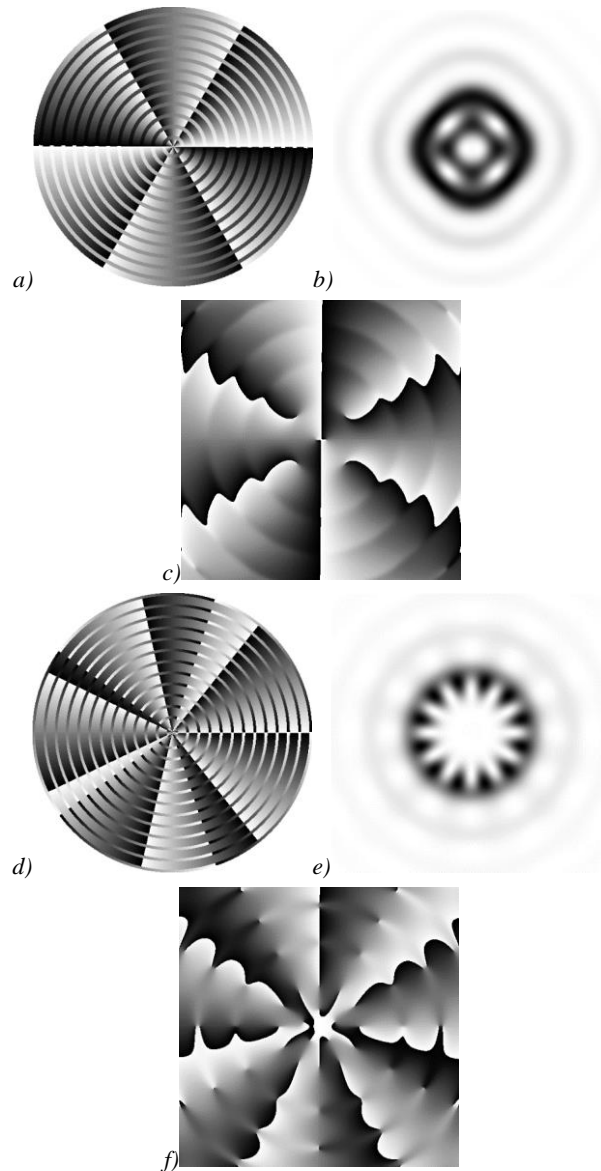
Fig. 1. − Phase function of the DOE (a, d), the intensity distribution in the far field of diffraction (b, e), the phase of the beam (c, f)

2. The experiments on the rotation of the agglomeration of the microparticles in the complex vortex beams

A series of experiments was conducted to check the possibility of rotation of microobjects in complex vortex beams. Figure 2 presents the scheme of the experimental setup. The beam was focused on the polystyrene microparticles with a

55

diameter of 5µm located inside a drop of distilled water on the surface of the glass substrate. Two stepper motor system was used to move the platform with the installed cuvette, which allowed to move the platform with a step of 0.5 µm.
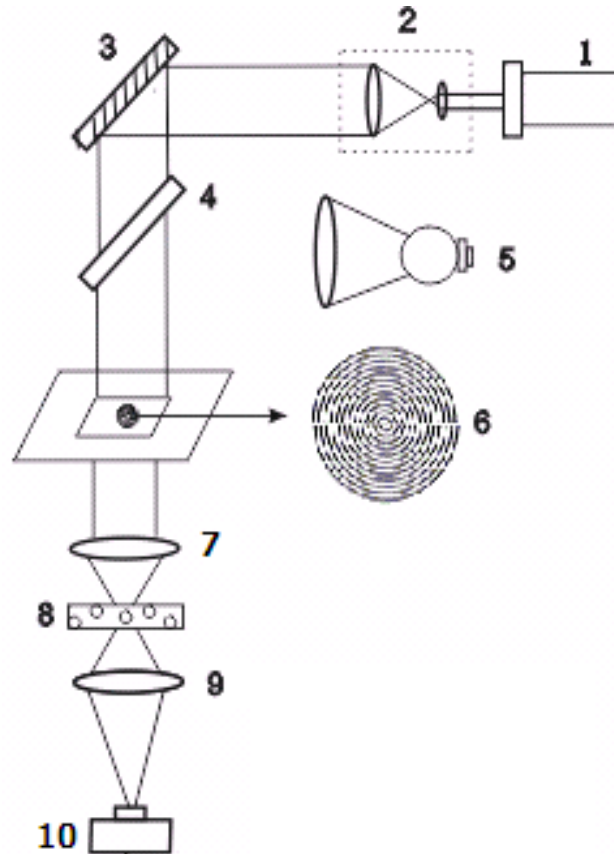
Fig. 2. – Optical scheme of the experiment on the capture of polystyrene microobjects in the beam: 1 – laser; 2 - collimator; 3, 4 – rotary mirrors; 5 – backlight; 6 – axicon; 7 – focusing microlens; 8 – substrate with microparticles; 9 – depicting microlens; 10 – CCD-camera

Figure 3 shows different stages of the movement process of the polystyrene particles in the beam, presented in figure 1b. At different focusing, microparticles get into the area corresponding to the different sign of the orbital angular momentum of the beam and rotate by a fixed angle before reaching the nearest maximum.

As a result of real experiment, capture of polystyrene particles was carried out and the rotation of the group of particles was initiated at the expense of focusing and defocusing of the light beam.
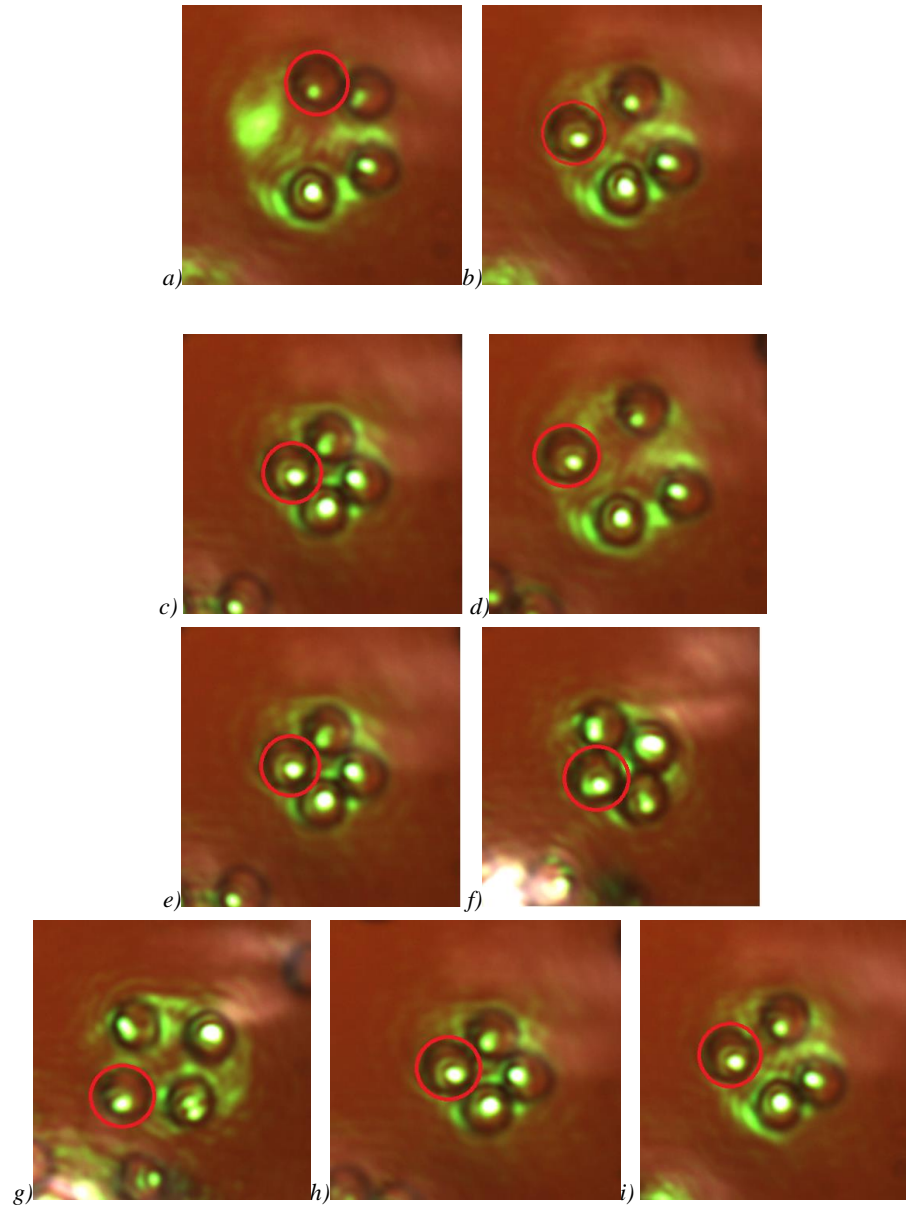
Fig. 3. – Stages of polystyrene microparticles rotation, taken with an interval of 2 seconds

Figure 4 shows the different stages of the movement process of polystyrene particles on a ring, taken with an interval of 2 sec.
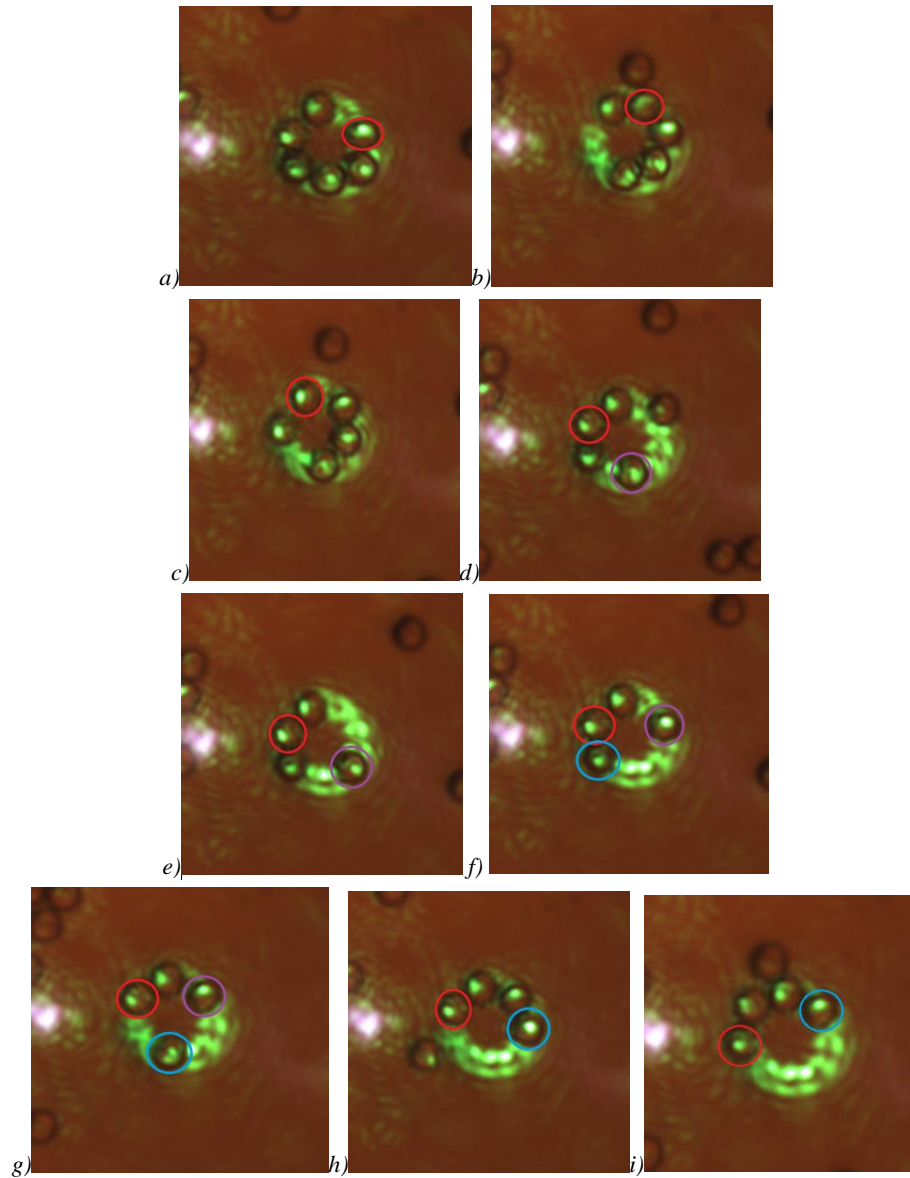
Fig. 4. – Stages of the micromanipulation process of polystyrene microparticles, taken with an interval of 2 seconds

As seen from figures 3, 4, there is rotation of microparticle group in the beams having substantially non-ring structure. Thus in figure 4, the rotation is performed in different directions, depending on the focus.

58

Conclusion

The light beams are described based on the superposition of vortex light beams with different topological charges. The presented results of experiments prove the possibility of controlled rotation of the group of microparticles in such light beams. It is shown that multidirectional rotation of the group of microparticles is possible with the superposition of vortex beams with a different sign of the topological charge, depending on the focus.

Funding Information

References

1. **Bai N, Ezra Ip, Hang Y, Mateo E, Yaman F, Li M, Bickham S, Ten S, Liñares J, Montero C, Moreno V, Prieto X, Tse V, Chung K, Lau APT, Tam H, Lu C, Luo Y, Peng G, Li G, Wang T.** Mode-division multiplexed transmission with inline few-mode fiber amplifier. Optics Express, 2012; 20(3): 2668-2680.

2. **Kotlyar VV, Skidanov RV, Khonina SN.** Non-contact precision measurement of linear displacement with DOE forming fashion Bessel. Computer Optics, 2001; 21: 102-104. [in Russian]

3. **Skidanov RV, Khonina SN, Kotlyar VV, Soifer VA.** Experimental research of movement of dielectric spheres in light beams with angular harmonics of high orders. Computer Optics, 2007; 31(1): 14-21. [in Russian]

4. **Kotlyar VV, Kovalev AA, Skidanov RV, Moiseev OYu, Soifer VA.** Diffraction of a finite-radius plane wave and a gaussian beam by a helical axicon and a spiral phase. Journal of the Optical Society of America A: Optics and Image Science, and Vision, 2007; 24(7): 1955-1964.

5. **Abramochkin EG, Kotova S, Korobtsov A, Losevsky N, Mayorova A, Rakhmatulin M, Volostnikov V.** Microobject manipulations using laser beams with nonzero orbital angular momentum. Laser Physics, 2006; 16: 842-848.

6. **Abramochkin EG, Volostnikov VG.** Spiral light beams. Physics-Uspekhi, 2004; 47: 1177.

7. **Ladavac K, Grier D.** Microoptomechanical pumps assembled and driven by holographic optical vortex arrays. Optics Express, 2004; 12: 1144-1149.

8. **Lin X-F, Hu G-Q, Chen Q-D, Niu L-G, Li Q-S, Ostendorf A, Sun H-B.** A light-driven turbine-like micro-rotor and study on its light-to-mechanical power conversion efficiency. Applied Physics Letters, 2012; 101(11): 113901.

9. **Ukita H.** Rotation rate of a three-wing rotor illuminated by upward-directed focused beam in optical tweezers. Optical Review, 2008; 15: 97-104.

10. **Chaumet PC.** Coupled dipole method to compute optical torque: Application to a micropropeller. Journal Applied Physics, 2007; 101: 0231106.

11. **Maruo S.** Force-controllable, optically driven micromachines fabricated by single-step two-photon microstereolithography. Journal of Microelectromechanical Systems, 2003; 12: 533-539.

12. **Morozov AA, Skidanov RV.** Complex vortex beams for of rotation of micromechanical elements. Computer Optics. 2013; 37(1): 68-75. [in Russian]

13. **Burrow GM, Gaylord TK.** Multi-Beam Interference Advances and Applications: Nano-Electronics, Photonic Crystals, Metamaterials, Subwavelength Structures, Optical Trapping, and Biomedical Structures. Micromachines, 2011; 2: 221-257.
14. **McGloin D, Reid JP.** 40 years of optical manipulation. Optics & Photonics News, 2010; 21(3): 20-26.
15. **Fedotowsky A, Lehovec K.** Optimal filter design for annular imaging. Applies Optics, 1974; 13(12): 2919-2923.
16. **Morozov AA, Skidanov RV.** Rotation of microturbine in complex vortex beams. Computer Optics, 2013; 37(2): 203-207.

Study of the chromatic properties of harmonic diffractive lens

Kovalenko A.I.

Samara State Aerospace University

Abstract. This work is devoted to the study of the axial image point formed by a layered diffractive lens illuminated by laser light of different wavelengths. The influence of chromaticity can be identified when there is a change of quantisation levels and harmonic interval (bringing the phase to the level $2\pi n$). The influence of aberrations introduced in the form of converging or diverging conical and cubic wavefronts will also be considered in this study.

Introduction

Diffractive optical elements (DOE) are used for the miniaturisation and weight saving of optical systems. Furthermore, they enable the formation of light beams with properties that can not otherwise be obtained by classical optical refractive elements. However, DOE are characterised by significant chromatic aberration, which can have both negative and positive impacts upon the imaging system [1-10].

Traditional lenses and mirrors are designed on the basis of geometrical optics. Due to their large size there are not suitable for use in optical and optoelectronic microsystems. Furthermore, the formation of difficult complex distributions of the laser fields can not be performed by classical refractive elements. However, this problem is solved effectively by means of diffractive optics. DOE are able to take into account the wave nature of light, so as to successfully carry out the conversion of laser radiation in practically any amplitude-phase distribution [11, 12].

The main property of DOE is the use of the diffraction phenomenon to change the propagation direction of light beams. The diffraction elements split the light beam into multiple beams, each of which is redirected from different angles. Diffraction angles are different for different wavelengths: longer wavelengths are diffracted at higher angles than shorter wavelengths. Thus, a chromatic dispersion effect manifests itself in this case [13, 14]. The negative impact of this case affects both the imaging [1, 6, 9], and focusing [15, 16] systems containing DOE. To compensate for the

chromaticity DOE, the use of a hybrid system is often suggested – i.e., a combination of refractive and diffractive elements having opposite chromatism [13, 14, 17, 18].

Several DOE can combine the properties of both diffractive and refractive lenses. An example of this is the so-called harmonic diffractive elements, whereby the diffractive and refractive properties of the lens depends on the phase of bringing the different intervals [19-21]. Harmonic intervals, as they are known, bring the phase to the level $2\pi n$. Obviously, the larger the n, the closer it is to the properties of harmonic DOE refractive element. However, the manufacture of such elements faces technological difficulties, since in this case deep etching is required. It is therefore desirable to find a compromise between the need to increase the harmonic interval to overcome the chromaticity and opportunities for the process of manufacturing the optical element.

1. Theoretical bases and study chromatic properties

In this work the optical system is shown in Figure 1, where z_1 is the distance from the radiation source to the DOE, and z_2 is the distance from the DOE to the image plane. Diverging spherical waves are assumed, for which a high z_1 obtains parallel beams of light coming from the source of radiation.
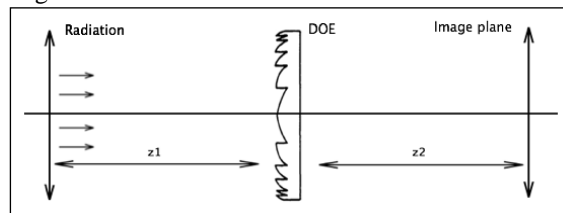
Fig. 1. – Optical system with DOE

The main stages of the formation of the DOE are as follows:

1. Continuous phase transmission function $\varphi(r)$ is reduced to the interval $[0, 2\pi n)$, where n - number of periodicity;
2. Resulting n – periodic phase $\varphi_t(r) = \mod_{2\pi n} \varphi(r)$ are quantised with a similar step height, forming m levels.

The greater the number of quantisation levels in phase m, the more accurate the resulting phase repeats will be for the relief of the continuous case. An increase in the periodicity n allows relief to be brought to the refractive diffraction.

In this work the focus of study was the intensity of light passing through the multi-level DOE when changes were made to the quantisation levels of the element. Figures 2, 3 and 4 are graphs of the intensities obtained for the refractive, binary and sixteen-level lens respectively.

For multi-level DOE we see the difference in foci for different wavelengths and a reduction in intensity with decreasing quantisation levels in comparison with the refractive lens. This reduction in intensity is due to the fact that part of the energy for the quantised DOE is redistributed along the optical axis, closer to the optical element.
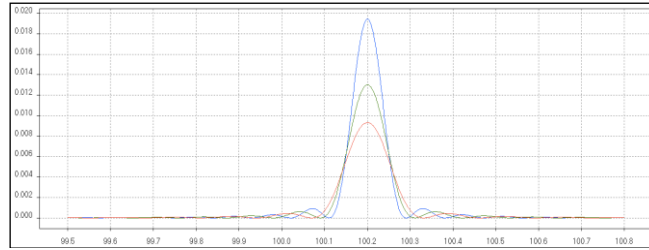
Fig. 2. – The intensity on the optical axis obtained for the refractive element
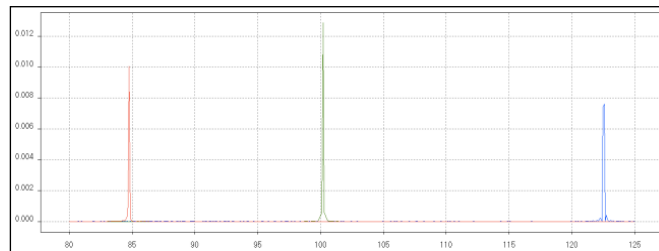
Fig. 3. – The intensity on the optical axis obtained for the sixteen-level element
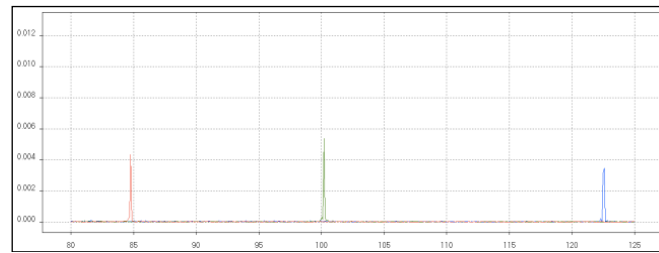
Fig. 4. – The intensity on the optical axis obtained for the binary element

In addition, a study was conducted of the intensity obtained by introducing a phase transmission function of various kinds of aberrations – namely, the introduction of a wavefront with a radial phase function of the first or third degree. It is known that such changes of wavefront lead to a deepening focus of the imaging system [22, 23], which may also help to compensate for chromatic effects. A conical wavefront can be implemented using an additional axicon, while a cubic wavefront can be implemented using the appropriate DOE.

In general, the phase transmission function of the DOE is:

$$\tau(r) = \exp\left[ik\left(c_0 + c_1 r + c_2 r^2 + \ldots + c_9 r^9 + \frac{c_{-1}}{r} + \frac{c_{-2}}{r^2} \right) \right]$$

If the lens is parabolic: $\tau(r) = \exp\left(-ik\frac{r^2}{2f} \right)$, then $c_2 = -\frac{1}{2f}$, and the other factors set the aberration changing point, thus spreading the function of the imaging

63

system. Tables 1, 2 and 3 are graphs of the intensities depending on changes in factors which are responsible for conical and cubic wavefronts.

Table 1. Graphs of the intensity at the optical axis caused by the addition of a divergent conical wavefront.

c1=0.00001	c1=0.0001
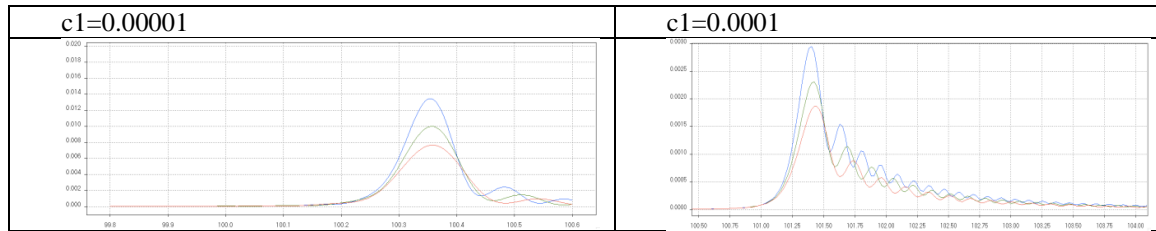
Table 2. Graphs of the intensity at the optical axis caused by the addition of a convergent conical wavefront.

$c_1=-0.00001$	$c_1=-0.0001$
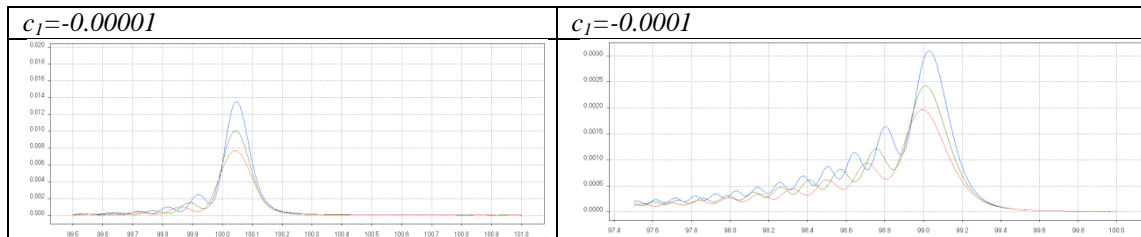
Table 3. Graphs of the intensity at the optical axis caused by the addition of a cubic diverging wavefront.

$c_3=0.000001$	$c_3=0.0000015$
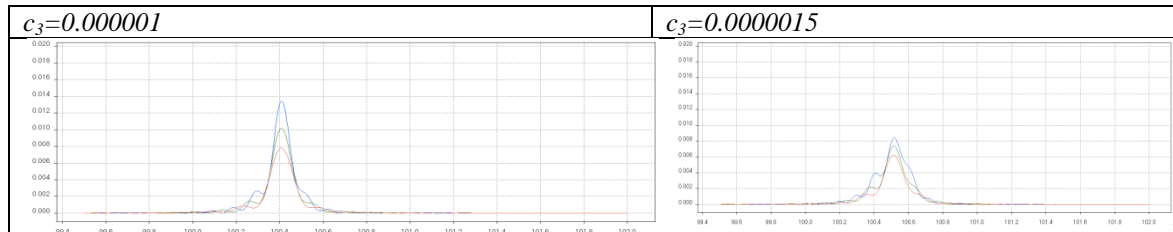
Tables 1, 2 and 3 show that when a conical or cubic aberration occurs, there is a drop in intensity at the focal point and an increased depth of focus. The point of maximum intensity is displaced along the optical axis. Note that the introduction of such wave aberrations may help to compensate for chromatic aberrations associated with different focal lengths for different wavelengths.

In addition, a study was carried out of the formation of an image depending on the change of quantisation levels of the element, bringing the phase to the interval $[0, 2\pi n)$, where $n = 1, 2, ..., 10$. The study was conducted for the elements with different radii and illustrates the dependence of M and N on the radius of the lens.

A number of factors were found to affect the intensity of light obtained by passing through the radiation element; not only the number of quantisation levels and relief depth, but also the number of zones of the element. Figure 5 shows the DOE with

64

radius $R = 1$ mm, the number of quantisation levels of $M = 16$, the periodicity $N = 1$, for which the number of zones is 10 (the peaks in the image). The intensity on the optical axis to such an element is shown in Figure 6.
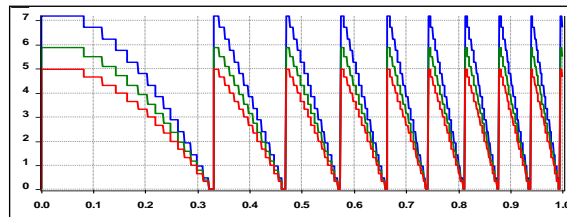
Fig. 5. – 16-level DOE with periodicity $N = 1$
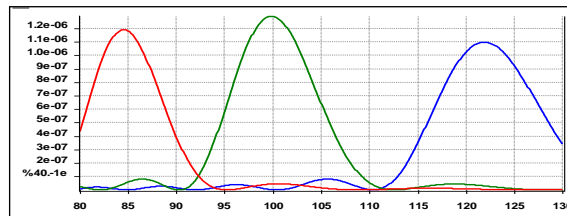
Fig. 6. – The intensity on the optical axis for 16-level DOE with periodicity $N = 1$

In Figure 6 we see the divergence of foci for different wavelengths. The convergence of points of focus is necessary to reduce the number of zones to one element by increasing the periodicity of interval (increasing the depth of the relief elements). Thus, DOE will tend to refract when the number of zones is reduced, but will never reach this point.

Figures 7 and 8 demonstrate the above effect. Elements with one zone of periodicity $N = 9$, and the intensity obtained when the radiation passes through the DOE are shown respectively.
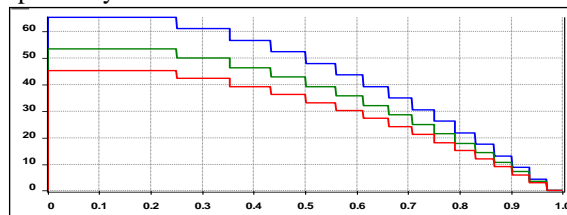
Fig. 7. – 16-level DOE with periodicity $N = 9$

Graphs of the intensity of light at changing radii of the lens and the quantisation levels M are shown in Table 4. The periodicity N for each element was chosen so that the number of zones of the lens is equal to one.

65
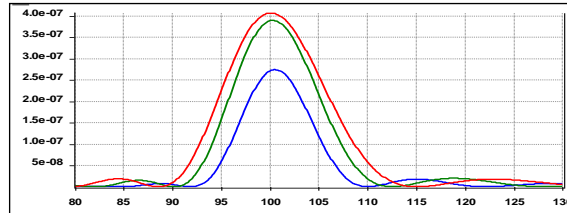
Fig. 8. – The intensity on the optical axis for a 16-layer DOE with periodicity $N = 9$

From the table above it is clear that increasing the radius of the lens to shift the focus is necessary to increase the number of quantisation levels (a lens radius of 1 mm is sufficient at 32 level quantisation for a lens with a radius of 10 mm - 2048 levels). Thus, the lenses of one zone with a larger radius can be achieved through relief depth increases (lens radius 1 mm $N = 9$ to 10 mm radius $N = 910$).

Conclusions

The study results are as follows:

- If you reduce the level of quantisation of elements for different wavelengths, different focal lengths can be observed, along with a drop in intensity and the redistribution of available energy along the optical axis;
- In the case of entering divergent or convergent conical and cubic wavefronts, a drop in intensity at the focal point while increasing the depth of focus could be observed. The point of maximum intensity is displaced along the optical axis;
- By increasing the radius of the DOE to achieve the shift in focus for different wavelengths at one point necessary to increase the number of quantisation levels of the lens, and choose a value of the periodicity N, the number of zones are required to be equal to one element.

The problems associated with chromatic aberration of DOE for some applications can be solved by entering different aberrations into the wavefront and increasing the depth of focus.

Acknowledgements

Table 4. Graphs showing intensities, obtained by varying the quantisation levels *M* for elements with different radii *R*
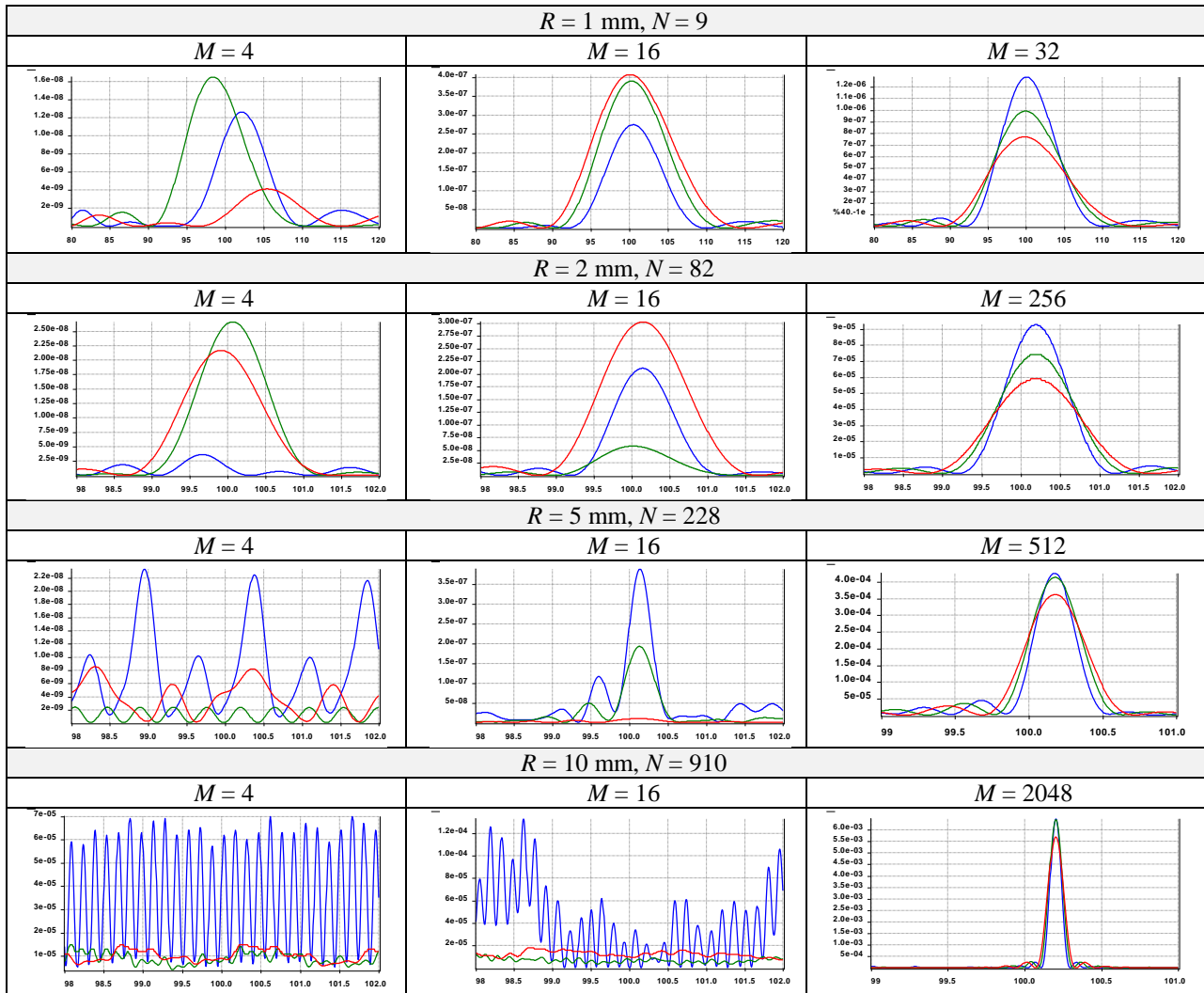
References

1. **Bobrov ST, Greisukh GI, Turkevich YG.** Diffractive optics elements and systems. Leningrad: "Mashinostroenje" Publisher, 1986. 223 p. [in Russian]
2. **Falkis D, Morris GM.** Broadband imaging with holographic lenses. Optical Engineering. 1989; 28: 592-598.
3. **Buralli DA, Morris GM.** Design of diffractive singlets for monochromatic imaging. Applied Optics, 1991; 30: 2151-2158.
4. **Dobson SL, Sun P, Fainman Y.** Diffractive lenses for chromatic confocal imaging. Applied Optics, 1997; 36: 4744-4748.

5. **Greisukh GI, Ezhov EG, Stepanov SA.** Aberration properties and performance of a new diffractive-gradient-index high-resolution objective. Applied Optics, 2001; 40: 2730-2735.

6. **Greisukh GI, Ezhov EG, Stepanov SA.** Comparative analysis of chromaticity diffractive and refractive lenses. Computer Optics, 2005; 28: 60-65. [in Russian]

7. **Kazanskiy NL, Kharitonov SI, Karsakov AV, Khonina SN.** Modeling action of a hyperspectrometer based on the Offner scheme within geometric optics. Computer Optics, 2014; 38(2): 271-280. [in Russian]

8. **Kazanskiy NL, Khonina SN, Skidanov RV, Morozov AA, Kharitonov SI, Volotovskiy SG.** Formation of images using multilevel diffractive lens. Computer Optics, 2014; 38(3): 425-434. [in Russian]

9. **Karpeev SV, Khonina SN, Kharitonov SI.** Study of the diffraction grating on a convex surface as a dispersive element. Computer Optics, 2015; 39(2): 211-217. [in Russian]

10. **Khonina SN, Ustinov AV, Skidanov RV, Morozov AA.** Comparative study of the spectral characteristics of aspheric lenses. Computer Optics, 2015; 39(3): 363-369. [in Russian]

11. **Golovashkin DL, Kotlyar VV, Soifer VA, Doskolovich LL, Kazanskiy NL, Pavelyev VS, Khonina SN, Skidanov RV.** Computer Design of Diffractive Optics. Edited by V.A. Soifer**.** Cambridge Inter. Scien. Pub. Ltd.& Woodhead Pub. Ltd, 2012: 896 p.

12. **Gavrilov AV, Golovashkin DL, Doskolovich LL, Dyachenko PN, Khonina SN, Kotlyar VV, Kovalev AA, Nalimov AG, Nesterenko DV, Pavelyev VS, Shuyupova YO, Skidanov RV, Soifer VA.** Diffracrive Nanophotonics. Edited by V.A. Soifer**.** CRC Press, Taylor & Francis Group, CISP, Boca Raton, 2014: 679 p.

13. **Aieta F, Kats MA, Genevet P, Capasso F.** Multiwavelength achromatic metasurfaces by dispersive phase compensation. Science Express, 2015; 2494-2498.

14. **Swanson G J.** Binary optics technology: the theory and design of multi-level diffractive optical elements. Technical Report, 1989; 1-47.

15. **Alferov SV, Karpeev SV, Khonina SN, Tukmakov KN, Moiseev OYu, Shulyapov SA, Ivanov KA, Savel'ev-Trofimov AB.** On the possibility of controlling laser ablation by tightly focused femtosecond radiation. Quantum Electronics, 2014; 44(11): 1061-1065.

16. **Karpeev SV, Alferov SV, Khonina SN, Kudryashov SI.** Study of the broadband radiation intensity distribution formed by diffractive optical elements. Computer Optics, 2014; 38(4): 689-694. [in Russian]

17. **Davidson N, Friesem AA, Hasman E.** Analytic design of hybrid diffractive-refractive achromats. Applied Optics, 1993; 32(25): 4770-4774.

18. **Fang YC, Liu TK, Tsai CM, Chou JH, Lin HC, Lin WT.** Extended optimization of chromatic aberrations via a hybrid Taguchi–genetic algorithm for zoom optics with a diffractive optical element. Journal of Optics A: Pure Applied Optics, 2009; 11: 045706.

19. **Sweeney DW, Sommargen GE.** Harmonic diffractive lenses. Applied Optics, 1995; 34(14): 2469-2475.

20. **Rossi M, Kunz RE, Herzig HP.** Refractive and diffractive properties of planar micro-optical. Applied Optics, 1995; 34(26): 5996-6007.

21. **Sales TRM, Morris GM.** Diffractive-refractive behavior of kinoform lenses. Applied Optics, 1997; 36(1): 253-257.

22. **Khonina SN, Volotovsky SG.** Fracxicon – diffractive optical element with conical focal domain. Computer Optics, 2009; 33(4): 401-411. [in Russian]

23. **Khonina SN.** Phase apodization of imaging system to increase the focal depth in coherent and incoherent cases. Computer Optics, 2012; 36(3): 357-364. [in Russian]

Modeling of the propagation of Bessel beams in a uniaxial crystal at different positions of the crystal axis

Krasnov A.P.

Samara State Aerospace University

Abstract. The numerical study of the propagation of the Bessel beams in anisotropic media with different orientations of the crystal axis and different polarizations of the input beams has been carried out using distributed computing on supercomputers. The analysis is based on two models: the geometric optics model based on ray tracing and implemented using the ZEMAX software, and the wave model in the approximation of thin optical elements based on plane waves expansion and implemented using the VectorAnisotropicPropagators package. High-performance computing resources have been necessary to implement the wave model. The results obtained can be used in various fields of optical design, for example to determine the position of the crystal axis and for the development of devices that perform polarization conversion.

Keywords: Bessel beams, axicon, astigmatic transformations, uniaxial crystal, polarization

Introduction

One of the major challenges for optical information science is the calculation of the propagation of electromagnetic waves in different media. Thus, optical devices that allow certain properties of electromagnetic radiation to be converted have acquired growing interest and practical use. Most often, mode and polarization conversions are needed. One tool for such transformations are anisotropic crystals [1-20]. One method of modelling the propagation of electromagnetic waves in anisotropic media is the method of plane waves expansion [21-26]. As a rule, the use of this method causes large computational problems due to the need to calculate the direct and inverse Fourier transforms for all electromagnetic field components. One solution is the use of various fast algorithms, including FFT, which significantly reduces computation time. However, the use of the FFT algorithm has drawbacks associated with the fixed discreteness of input and output signals and the ability to calculate only the transverse distribution. Another option is the use of parallel algorithms using high performance computing resources (supercomputers).

In this work, a comparative modeling of the propagation of the Bessel and Gaussian beams with different polarization in a uniaxial crystal along and perpendicular to the axis of the crystal is carried out. It is shown that in this case there are different effects: one is the astigmatic distortion and the second is the interference interaction of ordinary and extraordinary rays. Furthermore, the influence of the anisotropic medium in the different types of modes has been varied and is dependent on the distribution of the spatial spectrum of the beam.

The simulation has been carried out in three different ways – ray tracing, plane waves expansion and the finite-difference time-domain method. In the last two cases parallel execution of programs on supercomputers is used. A comparison of methods for speed, efficiency, scalability and the nature of the results has been performed.

The theoretical part

The laser beam with a super-Gaussian amplitude is determined by the formula:

$$\Psi_m(r,\varphi) = \exp\left(-\left(\frac{r}{\sigma}\right)^p\right)\exp(im\varphi),$$

where σ is the radius of the beam waist.

Selecting $p = 2$ and $\varphi = 0$ we get the usual Gaussian beam, which will be modelled in the future:

$$F_\sigma(r) = \exp\left(-\frac{r^2}{\sigma^2}\right).$$

In order to observe the paraxial effects, the beam is focused through the converging lens. Instead of lenses, it is possible to use the multiplication of the input beam amplitude with the corresponding converging wave front:

$$\exp\left(-\frac{ikr^2}{2f}\right),$$

where f is the focal length of the lens.

Another laser beam selected for modelling is the Bessel mode:

$$F_{m,\alpha}(r,\varphi,z) =$$

$$= A \cdot J_m(\alpha r) \cdot \exp(im\varphi) \cdot \exp\left(iz\sqrt{k^2 - \alpha^2}\right),$$

where α is the large-scale radial index of a Bessel beam and m is the angular index.

Instead of the Bessel beam, it is acceptable to simulate the passage of a flat beam through a linear axicon:

$$\exp(-ikpr),$$

where $k = 2\pi/\lambda$ is the wave number and $p = NA$ is the numerical aperture of the axicon.

The complex function of the axicon means that its structure is kept at a certain distance, but it has similar properties and does not require infinite energy.

Implementation

The geometric optics approach is implemented in various commercial software products (e.g., ZEMAX, LightTrans) and is used to obtain a visual representation of the investigated phenomena.

The ZEMAX program has been used for optical simulation. A detailed description of the software used is given in the manual [27]. The important advantage of this software is the ability to examine the distribution of ordinary and extraordinary rays separately.

Submit the input Gaussian beam and place in front of the crystal thin converging lens. Then the ordinary and extraordinary rays will have different angles of refraction at the interface of two media, which will give rise to different effects.

Figures 1-2 show that when the crystal axis is parallel to the z axis, the ordinary and extraordinary rays will focus at two different points on the z axis. Thus in the general case the output beam has elliptical polarization, the shape of which at any given point depends on the transverse coordinates and is different for these rays.
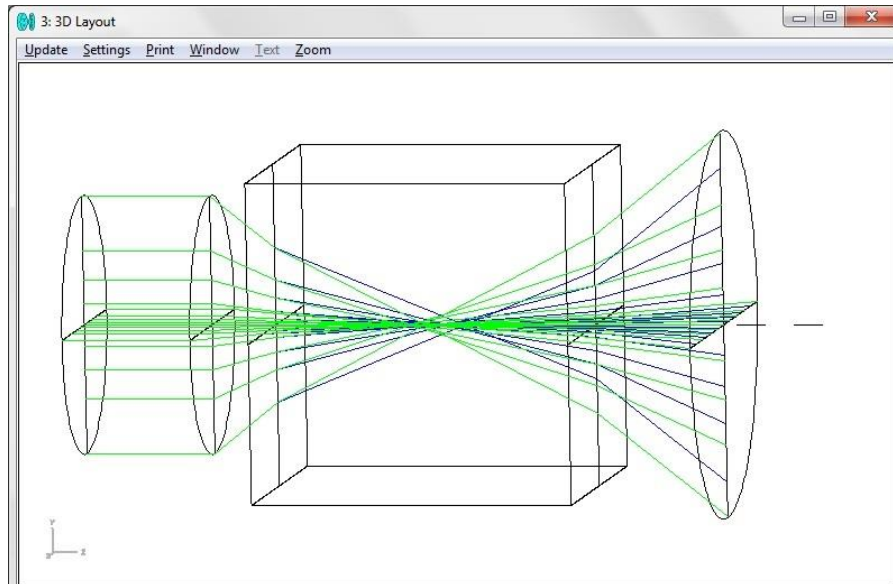
Fig. 1. – The focusing of the Gaussian beam transmitted through a lens in the crystal of an Icelandic spar at the location of the crystal axis parallel to the z axis

We have applied a flat beam for the entrance and put the axicon in its way to simulate the Bessel beam as in the ZEMAX program it is not possible to specify an arbitrary type of input beam.
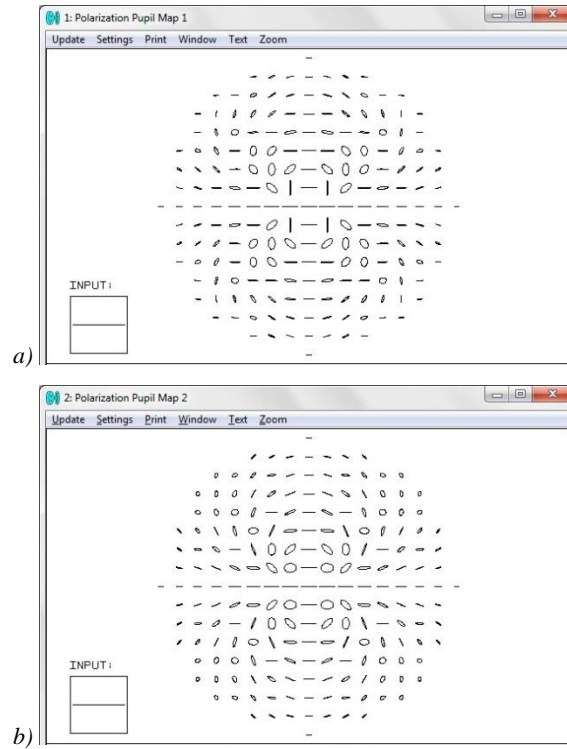
Fig. 2. – The polarization of the Gaussian beam transmitted through a lens at the exit of the crystal of an Icelandic spar: a – the ordinary ray, b – the extraordinary ray

Figures 3-4 show the simulation results of beam propagation in the crystal of an Icelandic spar along the axis of the crystal. It is evident that the ordinary and extraordinary rays are focused in different ways, however the result of their interaction remains unclear. During propagation along the crystal axis, the beam is elliptically polarized. For ordinary ray, polarization is close to linear and varies in a complicated way depending on the transverse coordinates, whereas for extraordinary ray polarization ellipses in an elongated fashion along the initial polarization of the beam.

The use of ray tracing does not require considerable investment of time and allows for the focus in the crystal at different positions of the axis to be explored and for the beam polarization to be changed. However, it is difficult to define wave characteristics of generated fields in this case. Therefore, we have considered the focusing of radiation in an anisotropic medium on the basis of the wave theory of diffraction [21-26].
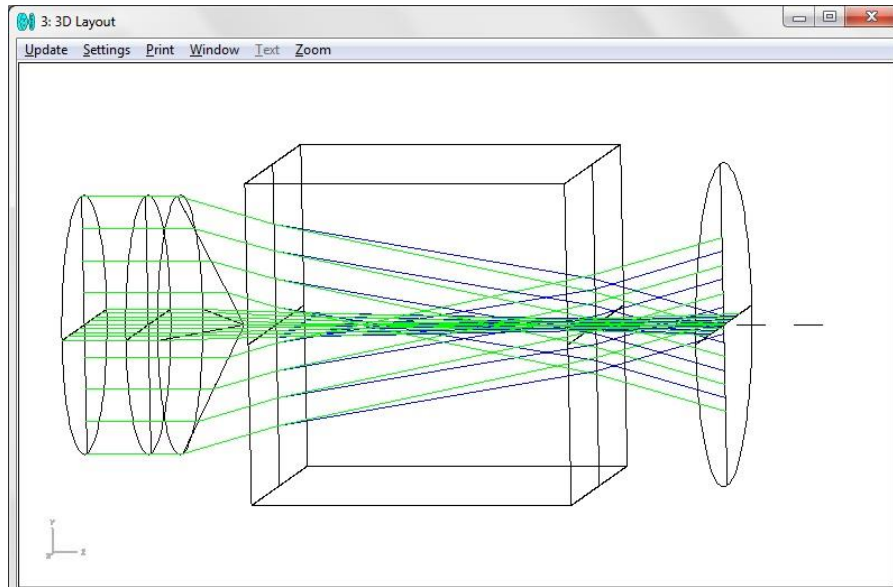
Fig. 3. – The focusing of the flat beam having passed through an axicon in the crystal of an Icelandic spar at the location of the crystal axis parallel to the z axis

a)

b)
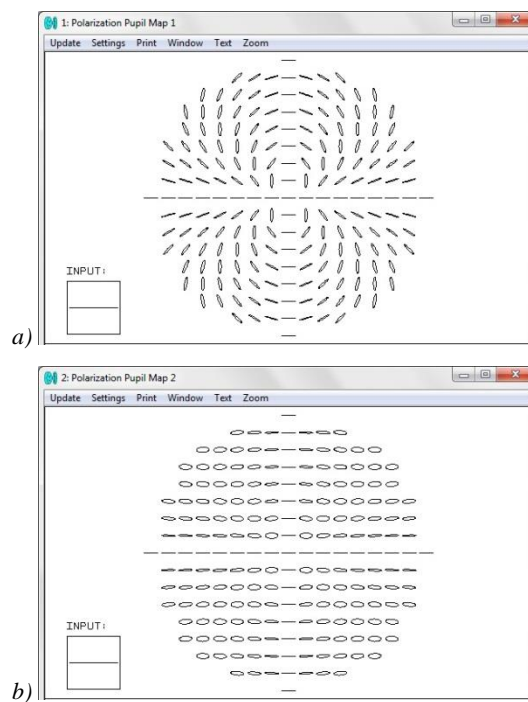
Fig. 4. – The polarization of the flat beam having passed through an axicon, at the exit of the crystal of an Icelandic spar: a – the ordinary ray, b – the extraordinary ray

Fig. 5. – The longitudinal section of the amplitude of the electric field during *x*-polarization of the beam in the axial plane, $z = \overline{0,1500}\ \mu m$, the axis of the crystal is oriented along the *y* axis
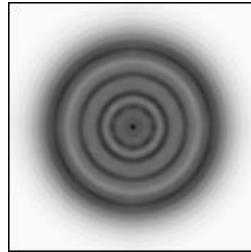
Fig. 6. – The cross section of the amplitude of the electric field during x-polarization of the beam in the plane $z = 750\ \mu m$, the axis of the crystal is oriented along the *y* axis

The input Gaussian beam is submitted with a converging wave front corresponding to the thin lens in the path of the beam.

The passage of the beam in an Icelandic spar is considered.

The first case is the axis of the crystal is oriented along the y axis.

Following this, the passage of the x-polarized beam is simulated. Figure 5 shows a longitudinal section of the amplitude, and figure 6 is the cross section of the amplitude near the area of focus of the beam. It is evident that the beam is distributed identically to an isotropic medium that is without a division into ordinary and extraordinary rays and without distortion.

Polarization is defined at the angle of 45 degrees to the *x* axis. At this point, the split of the beam into ordinary and extraordinary rays appears: the former is unchanged while the second undergoes a distortion, stretching itself along the axis of the crystal. Figures 7 and 8 confirm this by showing the longitudinal and cross section of the beam as a whole and for each of the rays.

Fig. 7. – The longitudinal section of the amplitude of the electric field during *xy*-polarization of the beam in the axial plane, $z = \overline{0,1500}\ \mu m$, the axis of the crystal is oriented along the *y* axis
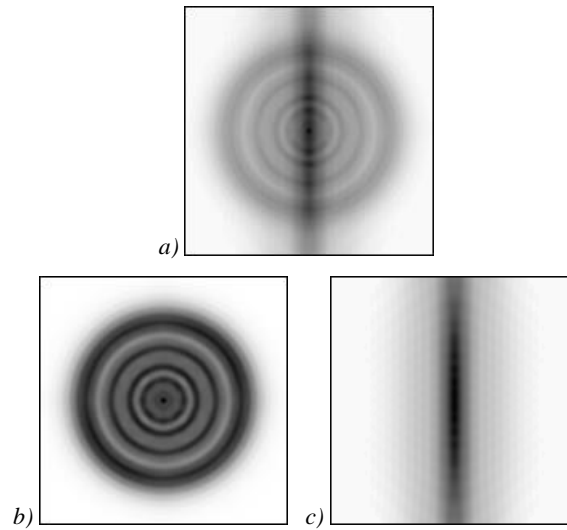
Fig. 8. – The cross section of the amplitude of the electric field during *xy*-polarization of the beam in the plane $z = 750\ \mu m$, the axis of the crystal is oriented along the *y* axis: a – the total amplitude, b – the ordinary ray, c – the extraordinary ray

Fig. 9. – The longitudinal section of the amplitude of the electric field during *y*-polarization of the beam in the axial plane, $z = \overline{0,1500}\ \mu m$, the axis of the crystal is oriented along the *y* axis
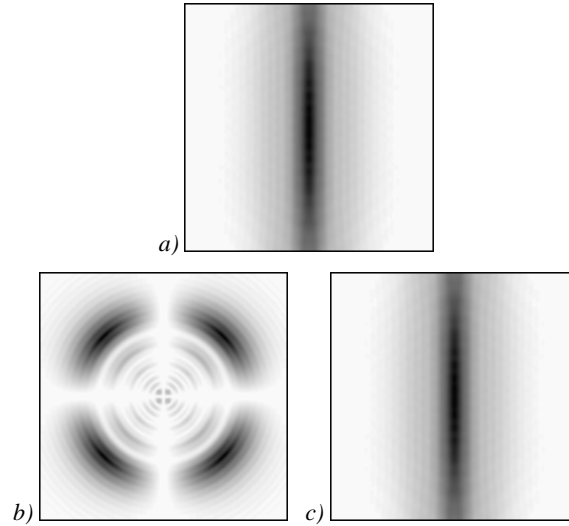
Fig. 10. – The cross section of the amplitude of the electric field during *y*-polarization of the beam in the plane $z = 750\ \mu m$, the axis of the crystal is oriented along the *y* axis: a – the total amplitude, b – the ordinary ray, c – the extraordinary ray

The input beam is defined as y-polarized. Here, the electric field is formed mainly by the extraordinary ray, which is elongated as in the previous case, and the contribution of the ordinary ray is negligible (figures 9-10).

The second case is where the crystal axis is oriented along the z axis.

Where the linear polarization of the beam is defined the two focuses are formed on the optical axis, the near focus is formed by the extraordinary ray and the far focus is formed by the ordinary ray. This is well illustrated in figures 11-12.
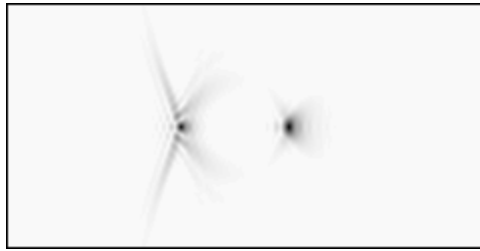
Fig. 11. – The longitudinal section of the amplitude of the electric field in the axial plane, $z = \overline{0,1500}\ \mu m$, the axis of the crystal is oriented along the *z* axis

a)

b)   *c)*
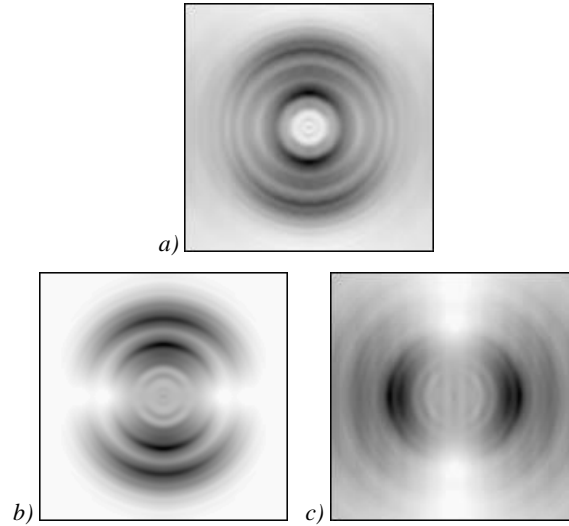
Fig. 12. – The cross section of the amplitude of the electric field in the plane $z = 750 \, \mu m$, the axis of the crystal is oriented along the z axis: a – the total amplitude, b – the ordinary ray, c – the extraordinary ray

The Bessel beam has also been considered.

In the case where the crystal axis is oriented along the y axis and the beam has an y-polarization, the electric field is almost completely formed by the extraordinary ray, which is astigmatically distorted (figures 13-14).

Fig. 13. – The longitudinal section of the amplitude of the electric field during y-polarization of the beam in the axial plane, $z = \overline{0,1500} \, \mu m$, the axis of the crystal is oriented along the y axis

a)

b)   *c)*
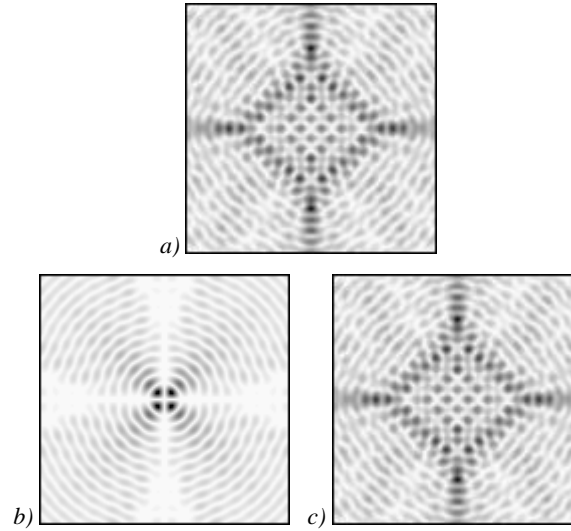
Fig. 14. – The cross section of the amplitude of the electric field during *y*-polarization of the beam in the plane $z = 250\,\mu m$, the axis of the crystal oriented along the *y* axis: a – the total amplitude, b – the ordinary ray, c – the extraordinary ray

At the x-polarization the beam is distributed as an isotropic medium, which means there is no distortion and the structure is preserved to certain distance.

The most interesting results have been obtained when modelling the propagation of the Bessel beam along the crystal axis. Due to the interference of the ordinary and extraordinary rays, there are periodic oscillations of the axial intensity that persisted until the collapse of the beam that is clearly visible in figures 15-16.
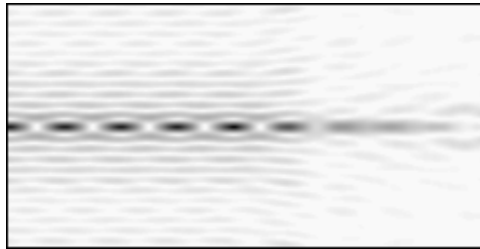
Fig. 15. – The longitudinal section of the amplitude of the electric field in the axial plane, $z = \overline{0,1500}\,\mu m$, the axis of the crystal is oriented along the *z* axis
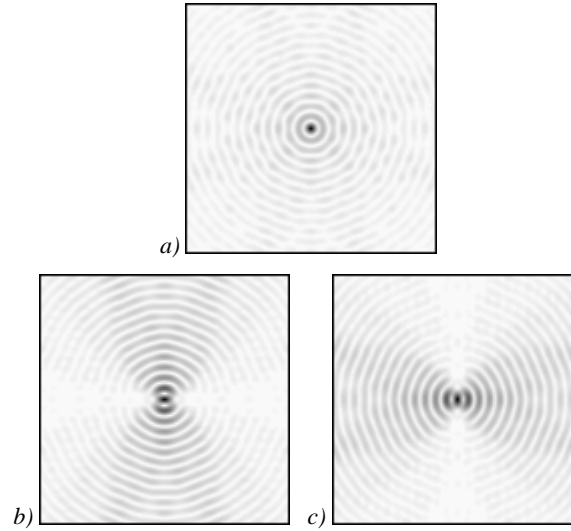
Fig. 16. – The cross section of the amplitude of the electric field in the plane $z = 500 \ \mu m$, the axis of the crystal is oriented along the z axis: a – the total amplitude, b – the ordinary ray, c – the extraordinary ray

Conclusion

The following results have been obtained in the course of work.

Numerical simulations of the propagation of Gaussian and Bessel beams in a birefringent medium have been conducted. It has been shown that under certain conditions there is spatial separation of the ordinary and extraordinary rays; the more extensive the path the beam passes in the crystal, the stronger the discrepancy.

The two beams are formed through the focusing of a Gaussian beam in the crystal having a different wave front curvature due to the variation in the refractive indices of the ordinary and extraordinary rays.

At the propagation in the crystal, the axis of which is perpendicular to the propagation direction and the polarization direction, the Bessel beam behaves identically as in a homogeneous medium maintaining the mode properties. Otherwise, the Bessel beam experiences an astigmatic distortion. At the propagation of a Bessel beam along the axis of the crystal, in addition to the astigmatic transformation, there is also a periodic variation in the intensity on the axis of propagation; this is associated with the interference of the ordinary and extraordinary rays.

The study was carried out in several ways, including using high-performance computing facilities, which allows physical processes to be visualized. The dependence of the time of the programs work on different parameters is demonstrated. It is easy to verify that the various simulation methods give qualitatively consistent results.

Geometric optics modelling does not require considerable investment of time and allows the visualization of the polarization transformation to be implemented conveniently as the focusing in the crystal well at different positions of the axis and

the changes in the beam polarization are tracked. However, it is difficult to define the wave characteristics of the generated fields in this case.

Wave simulation based on the decomposition of flat waves makes it possible to quantify the characteristics of the generated electromagnetic fields, but does not take into account the physical properties of the elements making up the bundles and requires a lot of time for the calculation.

A numerical simulation with a different type of beam polarization and different positions of the crystal axis allows the conditions under which there is the greatest astigmatic distortion of the beams to be determined. The analysis can be useful in practice for ascertaining the position of the crystal axis.

Acknowledgements

References

1. **Fedorov FI.** Optics of anisotropic media. Minsk: Publishing House of the Academy of Sciences of the BSSR, 1958. 381 p. [in Russian]
2. **Yariv A, Yeh P.** Optical waves in crystals. New York: Wiley, 1984. 589 p.
3. **Khilo NA, Petrova ES, Ryzevich AA.** Conversion order Bessel beams in uniaxial crystals. Quantum Electronics, 2001, 31(1): 85-89.
4. **Ciattoni A, Cincotti G, Palma C.** Propagation of cylindrically symmetric fields in uniaxial crystals. Journal of the Optical Society of America A, 2002; 19(4): 792-796.
5. **Hacyan S, Jáuregui R.** Evolution of optical phase and polarization vortices in birefringent media. Journal of Optics A: Pure and Applied Optics, 2009; 11(8): 085204-085208.
6. **Zusin DH, Maksimenka R, Filippov VV, Chulkov RV, Perdrix M, Gobert O, Grabtchikov AS.** Bessel beam transformation by anisotropic crystals. Journal of the Optical Society of America A, 2010; 27(8): 1828-1833.
7. **Fadeyeva TA, Shvedov VG, Izdebskaya YV, Volyar AV, Brasselet E, Neshev DN, Desyatnikov AS, Krolikowski W, Kivshar YS.** Spatially engineered polarization states and optical vortices in uniaxial crystals. Optics Express, 2010; 18(10): 10848-10863.
8. **Khonina SN, Volotovsky SG, Kharitonov SI.** Periodic intensity change for laser mode beams propagating in anisotropic uniaxial crystals. News of the Samara Scientific Center of RAS, 2012; 14(4): 18-27.
9. **Khonina SN, Zoteeva OV, Kharitonov SI.** Nonparaxial propagation of Gaussian beams at an angle to the axis of an anisotropic crystal. Computer Optics, 2012; 36(3): 346-356.
10. **Khilo NA.** Diffraction and order conversion of Bessel beams in uniaxial crystals. Optics Communications, 2012; 285(5): 503-509.
11. **Zhou G, Chen R, Chu X.** Propagation of Airy beams in uniaxial crystals orthogonal to the optical axis. Optics Express, 2012; 20(3): 2196-2205.
12. **Zhou Y, Wang X, Dai C, Chu X, Zhou G.** Nonparaxial analysis in the propagation of a cylindrical vector Laguerre-Gaussian beam in a uniaxial crystal orthogonal to the optical axis. Optics Communications, 2013; 305: 113-125.
13. **Zoteeva OV, Khonina SN.** Diffraction of Bessel laser beams on a birefringent object. Proc of SPIE, 2013; 9156: 91560D-8.

14. **Khonina SN, Volotovsky SG, Kharitonov SI.** Features of nonparaxial propagation of Gaussian and Bessel beams along the axis of the crystal. Computer Optics, 2013; 37(3): 297-306.

15. **Li J, Chen Y, Cao Q.** Propagation properties of cylindrically polarized vector beam through uniaxial crystals along the optical axis. Optics & Laser Technology, 2013; 45: 364-372.

16. **Khonina SN, Morozov AA, Karpeev SV.** Effective transformation of a zero-order Bessel beam into a second-order vortex beam using a uniaxial crystal. Laser Physics, 2014; 24(5): 056101-056105.

17. **Krasnov AP, Khonina SN.** Comparative modelling of laser beam propagation in a uniaxial crystal based on integral operators. Bulletin of Samara State Aerospace University, 2014; 43(1): 238-252.

18. **Khonina SN, Kharitonov SI.** Comparative investigation of nonparaxial mode propagation along the axis of uniaxial crystal. Journal of Modern Optics, 2015; 62(2): 125-134.

19. **Turpin A, Loiko YV, Kalkandjiev TK, Mompart J.** Light propagation in biaxial crystals. Journal of Optics, 2015; 17: 065603-065606.

20. **Khonina SN, Karpeev SV, Alferov SV, Soifer VA.** Generation of cylindrical vector beams of high orders using uniaxial crystals. Journal of Optics, 2015; 17: 065001-065011.

21. **Born M, Wolf E.** Principles of optics. Cambridge: Cambridge University Press, 1999. 986 p.

22. **Luneburg RK.** Mathematical Theory of Optics. Berkeley. California: University of California Press, 1964. 440 p.

23. **Fleck JA Jr, Feit MD.** Beam propagation in uniaxial anisotropic media. Journal of the Optical Society of America, 1983; 73(7): 920-926.

24. **Ciattoni A, Crosignani B, Di Porto P.** Vectorial theory of propagation in uniaxially anisotropic media. Journal of the Optical Society of America A, 2001; 18(7): 1656-1661.

25. **Doskolovich LL, Kazanskiy NL, Kharitonov SI.** Integral representations of solutions of a system of Maxwell's equations for anisotropic media. Computer Optics, 2010; 34(1): 52-57.

26. **Khonina SN, Kharitonov SI.** An analog of the Rayleigh-Sommerfeld integral for anisotropic and gyrotropic media. Journal of Modern Optics, 2013; 60(10): 814-822.

27. ZEMAX. Optical Design Program. User's Guide. ZEMAX Development Corporation 2009. 766 p.

Laser ablation of thin films of molybdenum for the fabrication of contact masks elements of diffractive optics with high resolution

Poletaev S.D.

Image Processing Systems Institute, Russian Academy of Sciences,
Samara State Aerospace University

Abstract. Considered the task of reducing the thickness of the contact lines of the pattern masks used in the formation of the microrelief of diffractive optical elements (DOE) and produced by laser ablation of thin films of refractory metals. For contact mask of DOEs on molybdenum films with thickness of 40 nm using a laser ablation patterns recorded with elements of the picture width 0.25–0.3 μm. This is approximately 3 times smaller than the characteristic dimensions, obtained by thermochemical recording chromium films of the same thickness in the standard process. Reactive ion etching in an inductively coupled plasma through a mask was formed micro-relief height up to 300 nm in a quartz substrate. We have shown promising applications of thin films of molybdenum as a metallic mask in the formation of microrelief of DOEs.

Keywords: diffractive microrelief, metallic mask, laser ablation, thermochemical recording, film molybdenum, reactive ion etching

Introduction

Thermochemical laser writing [1, 2], the contact masks plays a decisive role for a wide range of [3-9] The methods of forming the microrelief diffractive optical elements. Currently, the widely used form metalized microrelief mask thin films of metals [1-2, 5], in which during exposure to laser radiation is focused thermochemical conversion of the surface layer of the working material. The starting material is widely used chromium [1-2, 5]. The sequence of formation of micro-relief in a quartz substrate, in this case, following [5, 7]:

— Chromium plating film of a given thickness on a substrate;
— The formation of topological pattern of the future impact of the laser element in the film;

— The creation of metallic liquid etching mask film of chromium areas not exposed to laser radiation;
— Plasma etching the substrate through the resulting metallic mask (the formation of microrelief in the substrate).

The disadvantage of this technology is pretty low resolution. Standard achievable feature size structures in this case - the order of the wavelength, i.e. about 0.8 μm [10]. In this regard, the actual task is the development of technological methods for creating elements with high spatial resolution.

On the basis of the above-described process sequence, for example, in [11], there has been an element size of 0.5 μm on the structure of the chromium films 50 nm thick inflicted thermal vacuum process substrates of optical glass.

Patent [12] describes how to increase the resolution of the method of laser thermochemical oxidation film of titanium thickness of 3 - 60 nm, deposited on the glass substrate.

A characteristic feature of the studies described in [1-11], is that the resistance to the subsequent chemical resistance increases for portions of film exposed to the laser radiation. In contrast to [1-11], we propose an approach based on evaporation (ablation) portions of the film exposed to laser radiation.

The purpose of this paper is the experimental investigation of the possibility of further increasing the spatial resolution diffraction microrelief formed by using the contact masks using laser recording. It is proposed to achieve this total rejection of liquid chemical processes of lithography through the use of new materials and other physical effects of producing binary microstructures.

1. Problem statement and proposed approach

In [13] have demonstrated the possibility of ablation of molybdenum films picosecond laser beam with a wavelength of 1064 nm, deposited on a sublayer of silicon nitride thickness of about 140 nm. The grounds were glass substrate of a thickness of 3 mm. Ablation of the films of molybdenum with a thickness of about 0.5 μm was carried out by laser beam with a maximum energy flux density of 260 W/cm^2, and it was suggested that the molybdenum is removed from the substrate surface without chemical transformations. In our case, a contact mask on the basis of thin films of molybdenum was used for forming a diffraction microrelief in the following sequence of operations:

— sputtering thin films of molybdenum on a substrate;
— the formation of metal mask element, the influence of laser radiation on the film of molybdenum;
— reactive-ion etching in inductively coupled plasma substrate through a metallic mask (formation of microrelief in the substrate).

The microrelief formed on substrates of fused quartz brand KV of size 50×50 mm, thickness 3 mm and 14 class of surface cleanliness. Film of molybdenum was deposited by magnetron sputtering method on the "Caroline D-12A" [14] a thickness

83

of 40 nm. The formation of topological drawing of patterns in the molybdenum film (metal mask) was performed on the laser writing station CLWS200 [5, 13] with the following parameters: operating wavelength of the laser radiation is 488 nm; the power supplied to the recording head, is about 100 mW; record structure – concentric rings with a pitch of 3 μm and the outer radius of 2 mm; the magnitude of the power for each ring was reduced from 100% to 0 from the maximum power in 0.5% increments. On the outer rings with the capacity of about 80 to 40 mW, the laser radiation would result in a localized evaporation of thin films of molybdenum for all thickness down to the quartz substrate.

2. Analysis of the results

The results of the research profile of microstructur-ture formed in the molybdenum film when exposed to a laser beam of various capacities, represented in Fig. 1. Measurement of the profile of the microstructure was carried out on a scanning probe microscope (SPM) "Solver-Pro". On the profile visible area of complete removal of molybdenum (complete ablation). The boundary of the critical power at which ablation stops, well marked (the power decreases from left to right, Fig. 1a). On the edges of the formed structures have shown that the characteristic outbursts, which can be explained by the release of material during exposure to the beam.

In Fig. 2 shows the same image of microstructures, but obtained by scanning electron microscope (SEM) "Supra 25". The picture shows a clear band width 253-256 nm (Fig. 2a, b). On these pictures it can be seen that the edges of the grooves are damage to the film or the formation of the projecting profile, which is confirmed by the data obtained with SPM.

The width of the line of the laser beam (the portions of the substrate, free from films of molybdenum) is 220...300 nm (Fig. 1b) and depends on the magnitude of power greater than that required for ablation, which is confirmed by Fig. 2b.

For the formation of diffractive microrelief was used for reactive-ion etching of quartz substrates at the "Caroline PE-15" induction plasma excitation from the generator of radio-frequency voltage of 13.56 MHz. Working chamber cylindrical shape of the planar type. The etching was conducted in an environment hexafluoride SF_6 [15]. To stabilize the discharge in the plasma mixture was added in argon [16 – 18]. Power from the RF source is supplied to the inductor that is installed at the top inside the chamber. Etching of the sample 1 was carried out in the following mode: power inductor – 400 W; power stage – 200 W; the flow rate hexafluoride SF_6 – 60 cm^3/min; flow rate of argon Ar – 50 cm^3/min; the pressure of a gas is $5.0 \cdot 10^{-1}$ Pa; the etching time of 10 min.

The mode of etching of the sample 2 from the mode of etching of the sample 1 differs only in the time of etching, is accounted to him for 15 min.

After reactive-ion etching of the substrate remnants of the mask was removed.
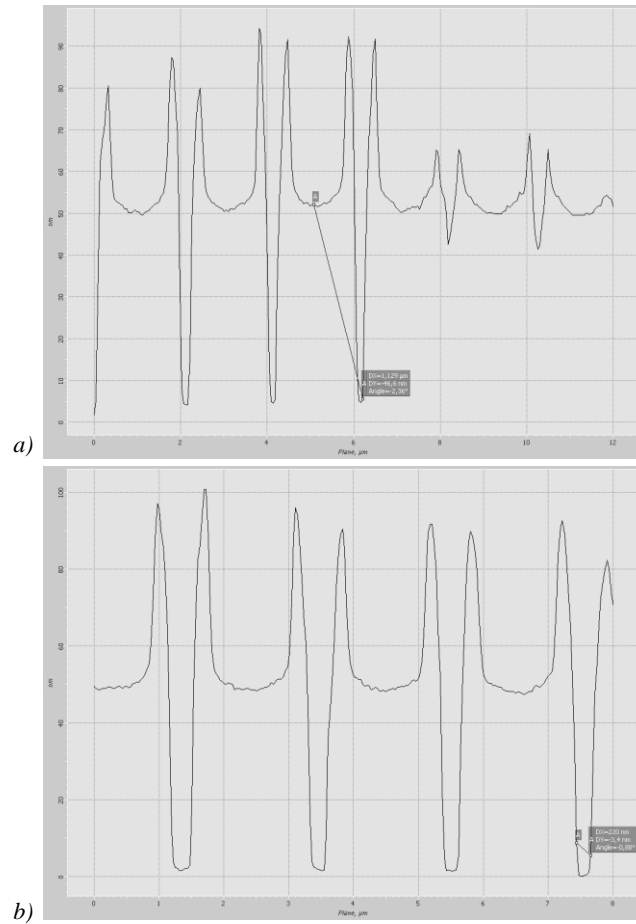
Fig. 1. – SPM results profile molybdenum film after laser writing: the border at the beginning of the burn process when the critical power (a), the recorded patterns with a line width of 220 nm (b)

The resulting SPM profile of the samples is shown in Fig. 3a, b. The images show that the quality of the surface microrelief of the sample 1 is higher than sample 2, which is probably due to the long time of etching, resulting in the masking film of the sample 2 is completely degraded in the plasma, which led to the destruction of the surface microrelief. In addition to increasing the rate of etching in these areas can be explained by changes in the chemical composition of the masking layer during laser recording, the more the height of the mask at the edges of the grooves is higher than in other areas. On the submitted drawings the width of the lines for samples 1 and 2 – 294 and 353 nm, respectively.
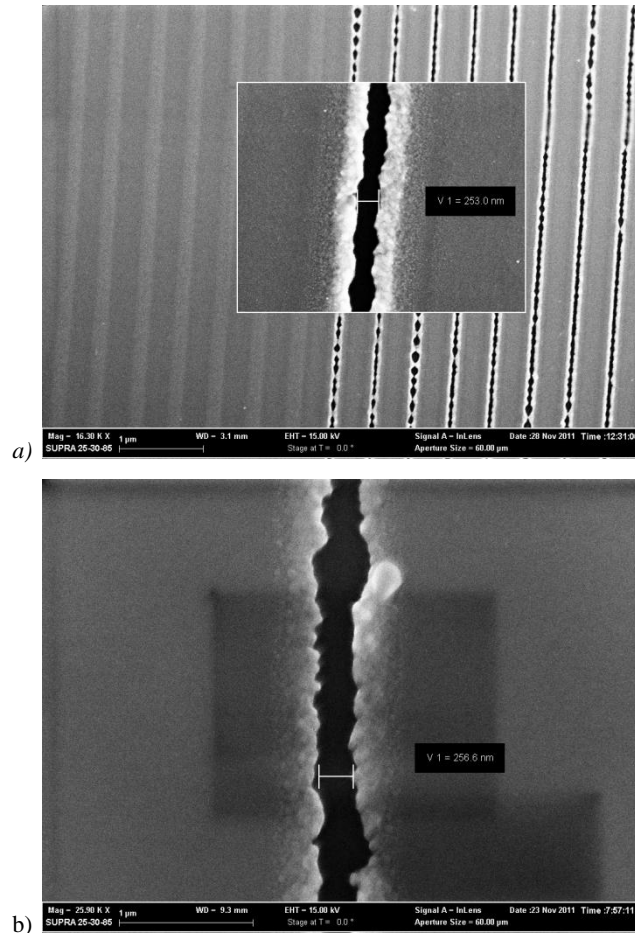
Fig. 2. – SEM image of the sample after laser writing: the border at the beginning of the burn process when reaching the critical power (a), the enlarged part of image (b)

Conclusion

In our experiments, the possibility of creating optical structures of submicron resolution, including with elements smaller than the diffraction limit (0.25 μm), based on the dry etching of quartz using a contact mask obtained by the method of laser ablation of molybdenum film. Reduction of the characteristic dimensions of the diffractive microrelief [19–22] to create a DOE with a smaller focal lengths, with a larger aperture, or DOE, is designed to lower the working wavelength. Of course, the proposed improvements are not suitable for everyone [23–25] technological approaches, but can be effectively used for a wide range [3–11] methods for forming diffractive microrelief. Further research is planned and on the way of formation and

86

use of thinner films (25 nm or less), which should lead to a further increase in the resolution of laser writing.

a)

b)
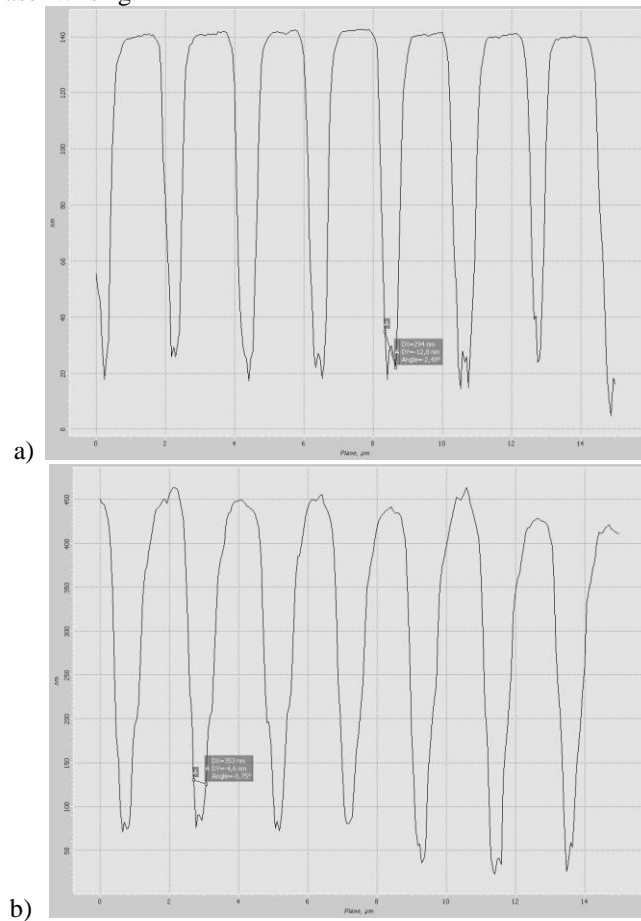
Fig. 3. – SPM microrelief formed by etching in inductively coupled plasmas: profile of sample 1 (a) profile of sample 2 (b); the line width of 294 nm and 353 nm, respectively

Acknowledgements

References

1. **Veiko VP, Korol'kov VI, Poleshchuk AG, Sametov AR, Shakhno EA, Yarchuk MV.** Study of the spatial resolution of laser thermochemical technology for recording diffraction microstructures. Quantum Electronics, 2011; 41(7): 631-636.

2. **Veiko VP, Sinev DA, Shakhno EA, Poleshchuk AG, Sametov AR, Sedukhin AG.** Researching the features of multibeam laser thermochemical recording of diffractive microstructures. Computer Optics, 2012; 36(4): 562-571. [in Russian]

3. **Volkov AV, Kazanskiy NL, Rybakov OYe.** The study of plasma etching technology for creation of multi-level diffractive optical elements. Computer Optics, 1998; 18: 127-130. [in Russian]

4. **Volkov AV, Kazanskiy NL, Rybakov OYe.** Development of technology for creation of diffractive optical elements with submicron dimensions of the relief in the silicon wafer. Computer Optics, 1998; 18: 130-133. [in Russian]

5. **Poleshchuk AG, Churin EG, Koronkevich VP, Korolkov VP, Kharissov AA, Cherkashin VV, Kiryanov VP, Kiryanov AV, Kokarev SA, Verhoglyad AG.** Polar coordinate laser pattern generator for fabrication of diffractive optical elements with arbitrary structure. Applied Optics, 1999; 38(8): 1295-1301.

6. **Kazanskii NL, Kolpakov VA, Kolpakov AI.** Anisotropic etching of SiO_2 in high-voltage gas-discharge plasmas. Russian Microelectronics, 2004; 33(3): 169-182.

7. **Kazanskiy NL.** A research complex for solving computer optics problems. Computer Optics, 2006; 29: 58-77. [in Russian]

8. **Pavelyev VS, Borodin SA, Kazanskiy NL, Kostyuk GF, Volkov AV.** Formation of diffractive microrelief on diamond film surface. Optics & Laser Technology, 2007; 39(6): 1234-1238.

9. **Bezus EA, Doskolovich LL, Kazanskiy NL.** Evanescent-wave interferometric nanoscale photolithography using guided-mode resonant gratings. Microelectronic Engineering, 2011; 88(2): 170-174.

10. **Kazanskiy NL.** Research and technological center of diffraction optics. Bulletin of Samara Scientific Center of the Russian Academy of Sciences, 2011; 13(4-1): 54-62. [in Russian]

11. **Agafonov AN, Moiseyev OYu, Korlyukov AA.** The analysis of dependence of resolution of technology of local thermochemical oxidation from parameters of structure of a photosensitive film of chrome. Computer Optics, 2010; 34(1): 101-108. [in Russian]

12. **Jörgens R, Gorbunov A, Pompe W.** Verfahren und Anordnung zur Erzeugung von Strukturen im Submikrometerbereich. Patent DE19544295A1 – 05.06.1997. G02B 5/18, 21/00.

13. **Heise G, Englmaier M, Hellwig C, Kuznicki T, Sarrach S, Heinz P.** Huber Laser ablation of thin molybdenum films on transparent substrates at low fluences. Applied Physics A: Materials Science & Processing, 2011; 102(1): 173-178.

14. **Kazanskiy NL.** Research and Education Center of Diffractive Optics. Proceedings of SPIE, 2012; 8410: 84100R. doi: 10.1117/12.923233.

15. **Zeze DA, Forrest RD, Carey JD, Cox DC, Robertson ID, Weiss BL, Silva SRP.** Reactive ion etching of quartz and Pyrex for microelectronic application. Journal of Applied Physics, 2002; 92(7): 3624-3629.

16. **Xuming W, Changhe Z, Peng X, Enven D, Huayi R, Liren L.** Etching quartz with inductively coupled plasma etching equipment. Proceedings of SPIE, 2003; 5183: 192-198.

17. **Volkov AV, Kazanskiy NL, Kostyuk GF, Pavelyev VS.** Dry Etching of Polycrystalline Diamond Films. Optical Memory And Neural Networks (Information Optics), 2002; 11(2): 135-137.

18. **Nesterenko DV, Poletaev SD, Moiseev OYu, Yakunenkova DM, Volkov AV, Skidanov RV.** Creating a curved diffraction gratings for ultraviolet. Bulletin of Samara Scientific Center of the Russian Academy of Sciences, 2011; 13(4): 66-71. [in Russian]

19. **Golub MA, Kazanskii NL, Sisakyan IN, Soifer VA.** Computational experiment with plane optical elements. Optoelectronics, Instrumentation and Data Processing, 1988; 1: 78-89.

20. **Kazanskiy NL.** The study of the diffraction characteristics of focusators into the ring by computational experiment. Computer Optics, 1992; 10-11: 128-144. [in Russian]

21. **Kazanskiy NL, Soifer VA.** Diffraction investigation of geometric-optical focusators into segment. Optik, 1994; 96(4): 158-162.

22. **Doskolovich LL, Kazanskiy NL, Soifer VA.** Comparative analysis of different focusators focusing into segment. Optics and Laser Technology, 1995; 27(4): 207-213.

23. **Kazanskiy NL, Murzin SP, Osetrov YeL, Tregub VI.** Synthesis of nanoporous structures in metallic materials under laser action. Optics and Lasers in Engineering, 2011; 49(11): 1264-1267. doi: 10.1016/j.optlaseng.2011.07.001.

24. **Volkov AV, Kazanskiy NL, Moiseev OYu, Soifer VA.** A Method for the Diffractive Microrelief Formation Using the Layered Photoresist Growth. Optics and Lasers in Engineering, 1998; 29(4-5): 281-288.

25. **Abul'khanov SR, Kazanskii NL, Doskolovich LL, Kazakova OY.** Manufacture of diffractive optical elements by cutting on numerically controlled machine tools. Russian Engineering Research, 2011; 31(12): 1268-1272.

The research of the properties of thin films of molybdenum to form the contact masks for diffractive optics elements

Poletaev S.D.

Image Processing Systems Institute, Russian Academy of Sciences,
Samara State Aerospace University

Abstract. Researched the parameters of the microstructures, obtained by laser termochemical space recording in films of molybdenum with a thickness of 17, 35 and 70 nm, deposited on a glass and quartz substrates. Graphs of the spatial resolution of the microstructures as a function of the laser power are plotted for different substrate materials. It is shown that a higher spatial resolution of the microstructures can be achieved in the molybdenum films with a 17 nm thickness.

Keywords: microstructure, laser ablation, thermal recording of a molybdenum film, glass and quartz substrates

Introduction

It seems promising to use in various fields of science and technology of diffractive optical elements (DOE), which are plates formed on their surface microstructure [1, 2]. The most important stage of manufacture of the microreliefs is get contact mask resistant to plasma-chemical processes necessary to transmit the calculated microstructure of the DOE in the substrate. Previously this had been circulated lithographic (wet) technology [3–8].

At the present time to reduce the dimensions of the microstructures, the widely used method of formation of topological drawing directly in the source layer of the material of the contact mask without the use of photoresists. It is based on local processing of thin films of chromium focused laser radiation [9, 10], under the influence of which is thermochemical conversion of the surface layer of the work material.

The disadvantage of this technology is the low resolution of about 0.8 μm. Therefore urgency to the task of developing techniques that allow to overcome this barrier. This result is possible through search and application of materials with

contrasting characteristics to selectively use a maximum of activating radiation. In this respect, a well-known series of works, where instead of chrome offers a variety of alternative materials, such as silicon, indium phosphide and the oxides of various metals [11–13]. Unlike standard technologies they propose to form a microstructure by evaporation (ablation) of material.

In [14] have demonstrated the possibility of ablation of molybdenum films with a thickness of about 0.5 μm picosecond laser beam with a wavelength of 1064 nm, deposited on a sublayer of silicon nitride thickness of about 140 nm. The grounds were glass substrate of a thickness of 3 mm.

Based on [14], we proposed an approach based on the ablation areas of the film of molybdenum exposed to laser radiation [15].

The purpose of this work is to study the feature of the contact mask, obtained by laser ablation of films of molybdenum, depending on the thickness of the films, which will produce the optimum conditions of carrying out the process.

1. Methods and materials

The base served as an optically smooth substrate made of glass and fused quartz brand KV of size 50×50 mm, thickness 3 mm. Film of molybdenum with a thickness of 17, 35 and 70 nm were deposited by magnetron sputtering method on the "Caroline D-12A" under the following conditions: the power of the magnetron is 700 W, the temperature of the substrate is 200°C, a pressure of argon to 2.0·10-1 Pa. The time of deposition was determined by the finite thickness of the films and ranged from 2 to 8 min.

Patterns in the films formed on the laser writing station CLWS-200 [16–18].

Recording was conducted under the following conditions: operating wavelength of the laser radiation is 488 nm; maximum power supplied to the recording head 100 mW; record structure – concentric rings with a pitch of 3 μm and an outer radius of 3 mm; the magnitude of the power for each ring decreased from 100 % at the point of greatest radius to 0 in the centre with a step of 0.5 %. The speed of rotation of the sample – about 10 s^{-1}. the Specified parameters of the process corresponded to the maximum power density of laser radiation $E_{max} = 2·10^7$ W/cm^2. The effect of laser radiation led to local evaporation thin film of molybdenum over the entire thickness.

The morphology and elemental composition of the surface of the nanostructures were studied using scanning electron microscope (SEM) Hitachi TM3030 with integrated EDS spectrometer.

2. Analysis of the results

In Fig. 1 shows the dependence of the width of the lanes from the laser output power for a radius record of 3 mm. Dependence obtained for quartz and glass substrates. The width of the recorded tracks in the first place, depends linearly on the laser power. When they are the same width for quartz substrates requires approximately 20% more power, due to the difference in the thermophysical properties of quartz and glass. Quartz, having a larger thermal conductivity, assigns laser energy from the field of film. Film thickness of 17 nm show higher spatial resolution, 2500 mm^{-1}, against 1500 mm^{-1} for films with a thickness of 35 nm. The permissions that are close to the maximum was reached in the power density in the

91

range $(0,7...1,2) \cdot 10^7$ W/cm^2. Note that this is significantly less than the theoretical values obtained, for instance, in [11].
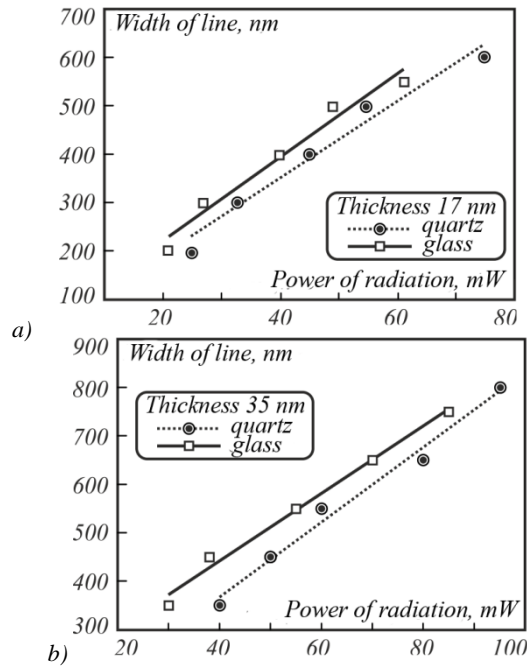
Fig. 1. – The dependence of the line width of the nanostructure on the power of laser radiation for films with a thickness of 17 nm (a) and for films with a thickness of 35 nm (b)

Presented on Fig. 2 pictures of SAM films with a thickness of 35 nm, exposed to the laser beam, allow the edges of the tracks to watch the products of destruction as representing a zone of thermal influence. Most likely, their emergence with the removal of a significant portion of the substance from the area of reactive ablation recoil pressure PA-world jet [19]. As shown earlier, their height does not exceed the thickness of the film [15].

For films with a thickness of 17 nm, the formation of degradation products is not typical (Fig. 3). This can be explained by the fact that the energy of laser radiation is enough for a quick and complete evaporation of the material at the point of impact. For these two cases are well for-markedly boundary of the critical power at which the evaporation of the metal stops. Also around tracks observed subtle trace of a width equal to the diameter of the laser spot. Probably, this area needs to impose restrictions on the minimum recording period. For films with a thickness of 70 nm of the radiation energy is insufficient for the formation of tracks even in areas with a minimum radius of recording (Fig. 4). It is important to note the following. For systems with circular scanning absorbed by the material energy (dose) of laser radiation at a constant power density varies with the radius record, since the radius of the record specifies an effective time of exposure. The decrease of power density from the edge to the center with simultaneous increase of exposure time to have an opposite effect on the magnitude of the radiation energy. However, in our case a

92

decrease in the size of the track as you approach the center, that allows claim about the decrease of the absorbed energy.
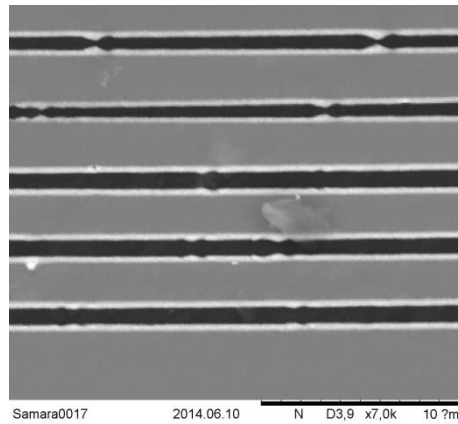
Fig. 2. – The SEM picture of the surface nanostructures on film of molybdenum with a thickness of 35 nm
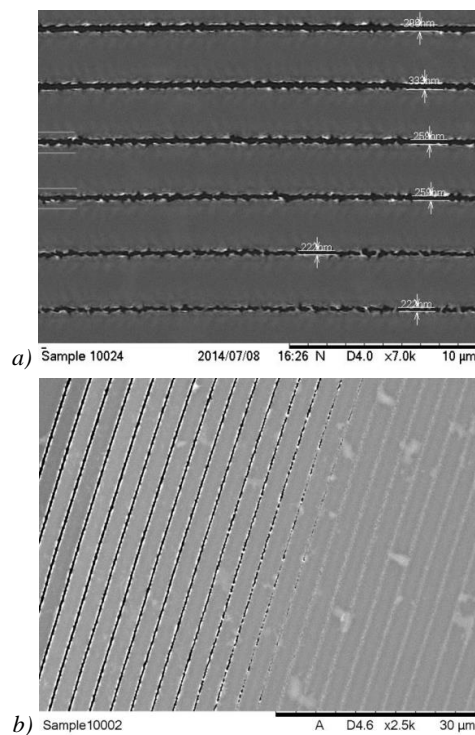
Fig. 3. – The SEM picture of the surface nanostructures on film of molybdenum with a thickness of 17 nm: the shape and the characteristic sizes of tracks (a) General view (b)

Conclusion

The study of microstructures of metallic patterns of the DOE showed that the best spatial resolution and minimum defects in the figure of the mask is achieved at a film thickness of molybdenum 17 nm.

Minimum attainable period of record limit width trace of the laser spot and is in our case 0.8 μm. Spatial resolution will be limited to this value and can be increased by reducing the wavelength and, correspondingly, the diameter of the laser spot.

Given the fact that the selectivity of the plasma etching films of molybdenum relative to quartz can reach several hundred, the result opens the way for the creation of structures with submicron resolution, in particular, short-focus of the DOE, and also allows you to create patterns with a minimum number of manufacturing operations. In addition, as described in the article, the research is also relevant for the development of certain laser technology [20 – 22].
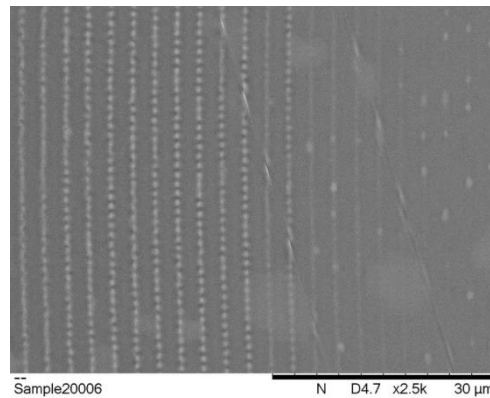
Fig. 4. – The SEM picture of the surface nanostructures on film of molybdenum with a thickness of 70 nm

References

1. **Soifer VA, Kotlyar VV, Kazanskiy NL, Doskolovich LL, Kharitonov SI, Khonina SN, Pavelyev VS, Skidanov RV, Volkov AV, Golovashkin DL, Solovyev VS, Usplenyev GV.** Methods for Computer Design of Diffractive Optical Elements. Edited by V.A. Soifer. New York: John Wiley & Sons. Inc., 2002. 765 p.
2. **Golovashkin DL, Doskolovich LL, Kazanskiy NL, Kotlyar VV, Pavelyev VS, Skidanov RV, Soifer VA, Khonina SN.** Diffractive computers optics. Edited by V.A. Soifer. Moscow: FIZMATLIT Publisher, 2007. 736 p. [in Russian]
3. **Volkov AV, Kazanskiy NL, Rybakov OYe.** The study of plasma etching technology for creation of multi-level diffractive optical elements. Computer Optics, 1998; 18: 127-130. [in Russian]

4. **Volkov AV, Kazanskiy NL, Rybakov OYe.** Development of technology for creation of diffractive optical elements with submicron dimensions of the relief in the silicon wafer. Computer Optics, 1998; 18: 130-133. [in Russian]

5. **Kazanskii NL, Kolpakov VA, Kolpakov AI.** Anisotropic etching of SiO_2 in high-voltage gas-discharge plasmas. Russian Microelectronics, 2004; 33(3): 169-182.

6. **Pavelyev VS, Borodin SA, Kazanskiy NL, Kostyuk GF, Volkov AV.** Formation of diffractive microrelief on diamond film. Optics & Laser Technology, 2007; 39(6): 1234-1238.

7. **Bezus EA, Doskolovich LL, Kazanskiy NL.** Evanescent-wave interferometric nanoscale photolithography using guided-mode resonant gratings. Microelectronic Engineering, 2011; 88(2): 170-174.

8. **Bezus EA, Doskolovich LL, Kazanskiy NL.** Interference pattern formation in evanescent electromagnetic waves using waveguide diffraction gratings. Quantum Electronics, 2011; 41(8): 759-764. doi: 10.1070/QE2011v041n08ABEH014500.

9. **Veiko VP, Korol'kov VI, Poleshchuk AG, Sametov AR, Shakhno EA, Yarchuk MV.** Study of the spatial resolution of laser thermochemical technology for recording diffraction microstructures. Quantum Electronics, 2011; 41(7): 631-636. [in Russian]

10. **Veiko VP, Sinev DA, Shakhno EA, Poleshchuk AG, Sametov AR, Sedukhin AG.** Researching the features of multibeam laser thermochemical recording of diffractive microstructures. Computer Optics, 2012; 36(4): 562-571.

11. **Krause S, Miclea T, Steudel F, Schweizer S, Seifert G.** Precise microstructuring of indium-tin oxide thin films on glass by selective femtosecond laser ablation. EPJ Photovoltaics, 2013; 4(40601): p1-p5.

12. **Zoppel S, Huber H, Reider GA.** Selective ablation of thin Mo and TCO films with femtosecond laser pulses for structuring thin film solar cells. Applied Physics, 2007; A 89: 161-163.

13. **Tan B, Dalili A, Venkatakrishnan K.** High repetition rate femtosecond laser nano-machining of thin films. Applied Physics A, 2009; 95: 537-545.

14. **Heise G, Englmaier M, Hellwig C, Kuznicki T, Sarrach S, Huber Heinz P.** Laser ablation of thin molybdenum films on transparent substrates at low fluences. Applied Physics A: Materials Science & Processing, 2011; 102(1): 173-178.

15. **Volkov AV, Moiseev OYu, Poletayev SD.** Precision laser recording on a molybdenum films for diffractive microrelief formation. Computer Optics, 2013; 37(2): 220-225.

16. **Poleshchuk AG, Churin EG, Koronkevich VP, Korolkov VP, Kharissov AA, Cherkashin VV, Kiryanov VP, Kiryanov AV, Kokarev SA, Verhoglyad AG.** Polar coordinate laser pattern generator for fabrication of diffractive optical elements with arbitrary structure. Applied Optics, 1999; 38(8): 1295-1301.

17. **Kazanskiy NL.** Research and technological center of diffraction optics. Bulletin of Samara Scientific Center of the Russian Academy of Sciences, 2011; 13(4-1): 54-62. [in Russian]

18. **Kazanskiy NL.** Research and Education Center of Diffractive Optics. Proceedings of SPIE, 2012; 8410: 84100R, doi: 10.1117/12.923233.

19. **Grigoryanc AG, Shiganov IN.** Laser welding of metals. Moscow: High school Publisher, 1988. 207 p. [in Russian]

20. **Kazanskiy NL, Murzin SP, Tregub VI.** Optical system for realization selective laser sublimation of metal alloys components. Computer Optics, 2010; 34(4): 481-486. [in Russian]

21. **Kazanskiy NL, Murzin SP, Osetrov YeL, Tregub VI.** Synthesis of nanoporous structures in metallic materials under laser action. Optics and Lasers in Engineering, 2011; 49(11): 1264-1267.

22. **Doskolovich LL, Kazanskiy NL, Kharitonov SI, Usplenjev GV.** Focusators for laser-branding. Optics and Lasers in Engineering, 1991; 15(5): 311-322.

Simulation of linear gradient lenses for subwavelength focusing of Gaussian beams

Savelyev D.A.

Samara State Aerospace University,
Image Processing Systems Institute, Russian Academy of Sciences

Abstract. This paper demonstrates the use of linear gradient lenses (a diverging lens and a converging lens) for subwavelength focusing of Gaussian beams. Numerical simulations have shown that increasing the length lens provides a more compact focal region in both the transverse and longitudinal directions.

Introduction

The subject of the study gradient optics is phenomena associated with optical effects in media with a gradual change of the refractive index [1]. Medium consisting of materials which are of the type GRIN (GRadient INdex), have distributed on the gradient refractive index material [2]. Thus, light rays are bent in a curve passing through them, which allows using them for the best focus [3-6]. In [3] used hyperbolic planar lens, which allowed to focus the light in the focal spot with a diameter of the half-width at half intensity (FWHM) equal $0,131\lambda$, in [4] dealt with a 2-D gradient microlenses Mikaelian, in [5-6] - two-dimensional photonic crystals. Photonic crystals due to their properties are used for several applications [7], among which their application to optical waveguides [8-9].

Currently in the integrated and fiber optics there is a large variety of optical waveguides with different properties. Planar waveguides and fibers along the profile of the spatial distribution of the refractive index can be divided into two groups: with step refractive index profile and with gradient profile [10-11]. In the case of a gradient profile refractive index varies smoothly from the center of the waveguide to the boundary defined by the law [11].

One of the major advantages of the lenses belonging to the gradient optics is that the optical surfaces of gradient lenses may be flat, which is important for the input-output of radiation of the fiber.

It is known that high-order mode exhibit greater divergence, however, the use of multimode method is one of the possible ways to increase the capacity of modern

communication systems [12]. And the most promising is the multiplexing of modes with different orders of the vortex phase singularity [13-14].

Distribution and generation of free-space laser vortices studied quite well [15-18], in [19-21] shows how to use them to focus the simple micro-elements of square and cylindrical shape. However, obtaining an optical fiber separate vortex modes and their superpositions is a big problem [14, 22-26]. In contrast to the classic LP-mode (mode optical fibers), angular harmonics are invariant to the scale at the input and output of fiber with the help of diffraction microstructures. This gives greater freedom in choosing the parameters of the optical circuit. In [27] have been identified application features sharp focusing of laser modes for introduction into a fiber of smaller diameter with using the binary micro-relief applied at the output end of the optical fiber. Overlaying certain conditions can generate laser light having a property of reproducible [28], while the phase shift between the modes at certain distances to approximate the desired cross-sectional intensity distribution of the laser beam [29].

In this paper, numerically investigate the diffraction of Gaussian beams on a linear gradient lens with different length. For the numerical simulation of diffraction of the considered laser beams using finite-difference time-domain method (FDTD), implemented in the software package Meep [30]. Numerical simulations were performed using the computing power of a cluster 775 GFlops. Features a cluster: the number of cores – 116, computes nodes: 7 twin servers HP ProLiant 2xBL220c, the amount of RAM 112 GB.
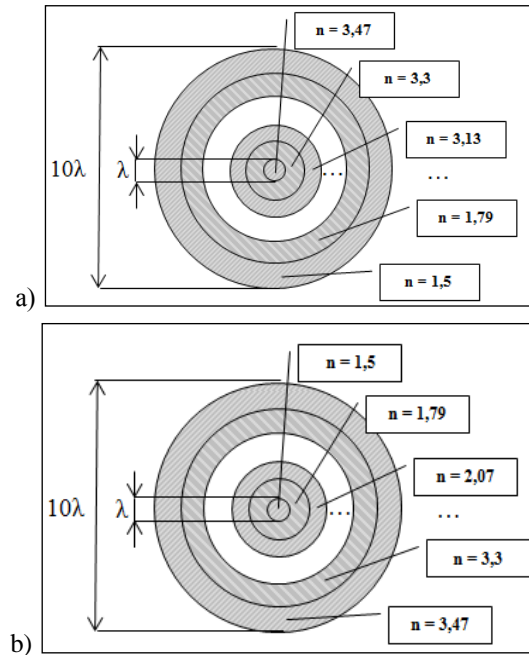
Fig. 1. – The transverse structure of the considered optical element: a) converging lens, b) diverging lens

Investigation of diffraction of Gaussian beams

In the paper considers two types of laser beams, which retain their structure during propagation in the free space in the circular polarization: a fundamental Gaussian mode, mode Gauss-Laguerre (0,1).

Figure 1 shows the transverse structure of the considered optical trace element (diverging lens and the converging lens). Later in the linear gradient lenses, in which the refractive index decreases from the central part to the edges of the lens will be called converging lens. The refractive index gradient lenses varies linearly as: all considered 10 rings (width λ), each of which had a their refractive index (from $n = 3.47$ on the center, until $n = 1.5$ on the edge of the lens).

a)　　　　　　　　b)　　　　　　　　c)

d)
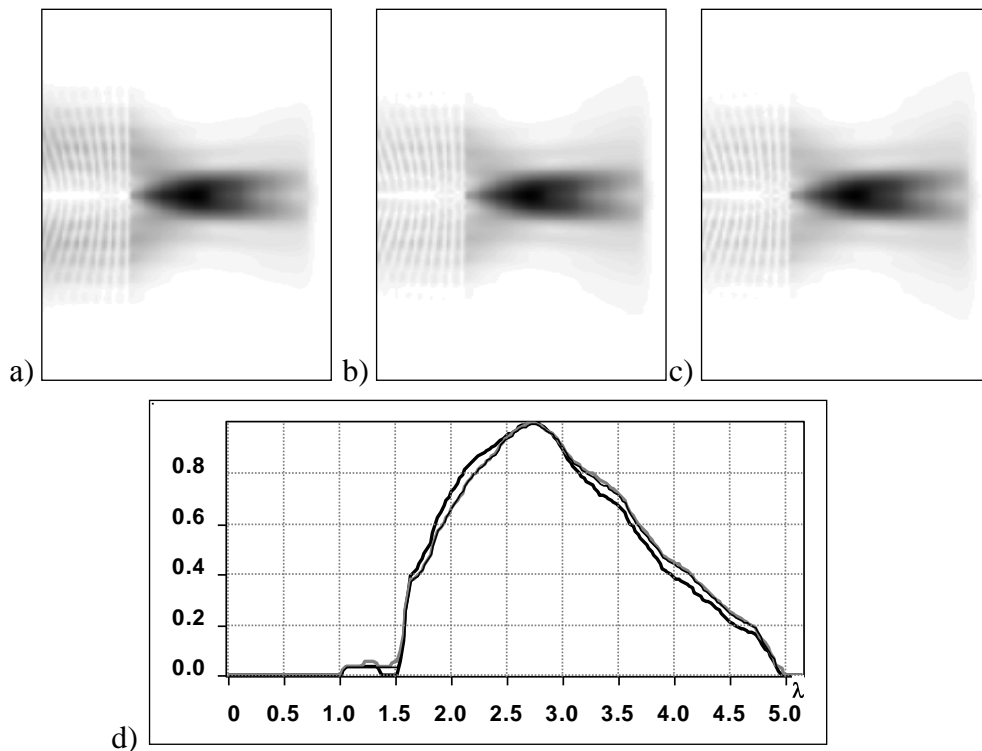
Fig. 2. – Diffraction mode Gauss - Laguerre (0,1) on the converging linear gradient lens, the overall intensity of the: a) 40 tacts, b) 60 tacts, c) 80 tacts, d) the schedule of general axial intensity, thick black lines - 40 tacts black fine line - 60 tacts, gray line - 80 tacts

Simulation parameters: the wavelength $\lambda = 1.55$ microns, the size of the computational domain $x, y, z \in [-4.5\lambda; 4.5\lambda]$. The thickness of the absorbing layer PML $\sim 0.65\lambda$ (1 micron), the sampling step of space $- \lambda/31$, the sampling step of time $- \lambda/(62c)$, where c is the velocity of light. Simulation time - 40 tacts (one for that meant the propagation time over a single wavelength), and was chosen so that the kind of laser radiation did not change with increasing simulation time (Figure 2).

The size of the focal spot on the FWHM considered a global maximum (maximum intensity). Table 1 shows the diffraction of a fundamental Gaussian mode and mode

Gauss-Laguerre (0,1) on the converging lens when you change the length L. Considered the overall intensity.

The table shows both the diffraction pattern and the size of the focal spot, that with increasing length of the focusing lens has been increasing. If $L = 0.25\lambda$ presence lens has almost no effect, then $L = 2\lambda$ diffraction pattern has changed significantly: the size of the focal spot on the half-width at half intensity decreased by 2.67 times (from $FWHM_{max} = 1.95\lambda$ for $L = 0.25\lambda$, to $FWHM_{max} = 0.73\lambda$ for $L = 2\lambda$). Comparing 4 and 5 columns of Table 1, it can be seen that the depth of focus, decreased significantly with a slight reduction of the transverse dimension of the focal spot in both these cases. Increasing the length of the lens results in better focus, it is clearly seen when comparing the first and last column of Table 1 for the case of fashion Gauss - Laguerre (0.1). Note that $FWHM_{max}$ also decreases with increasing length of the lens. Also the global maximum (max) also considered at the edge section of the optical element (out).

Table 1. Diffraction of Gaussian beams on the converging linear gradient lens, the overall intensity
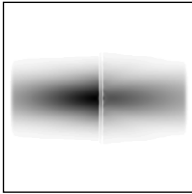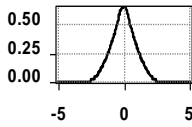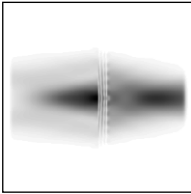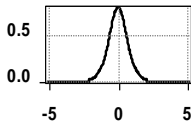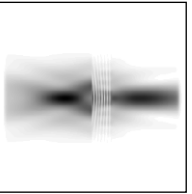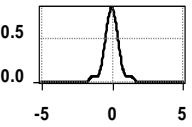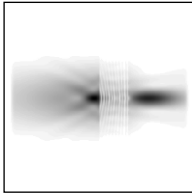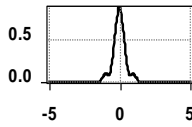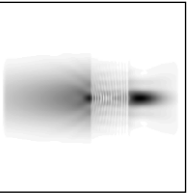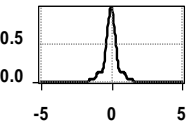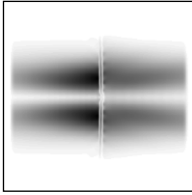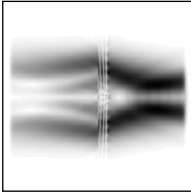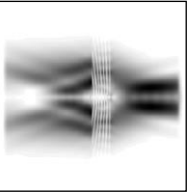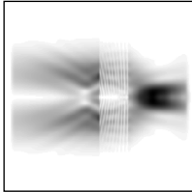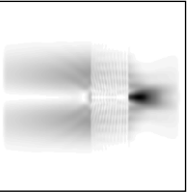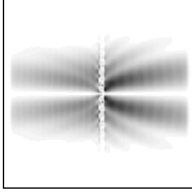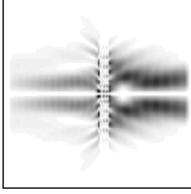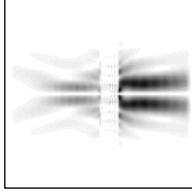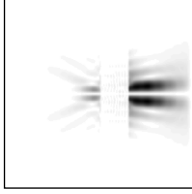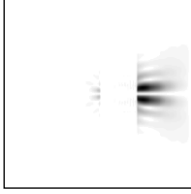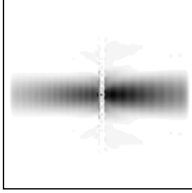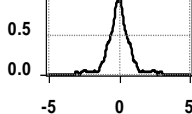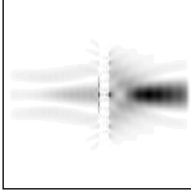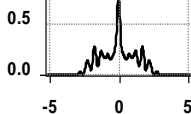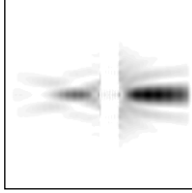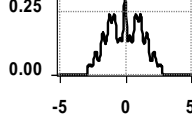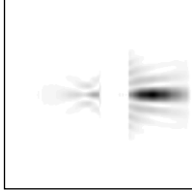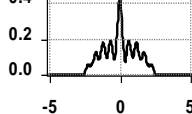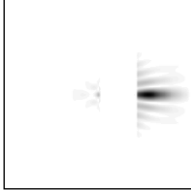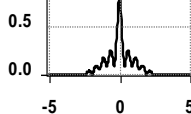
	$L = 0.25\lambda$	$L = 0.5\lambda$	$L = \lambda$	$L = 1.55\lambda$	$L = 2\lambda$
The fundamental Gaussian mode	$FWHM_{max} = 1.95\lambda$	$FWHM_{max} = 1.45\lambda$	$FWHM_{max} = \lambda$	$FWHM_{max} = 0.79\lambda$	$FWHM_{max} = 0.73\lambda$
Mode Gauss - Laguerre (0,1)				$FWHM_{out} = 3.92\lambda$ $FWHM_{max} = 1.41\lambda$	$FWHM_{out}=0.48\lambda$ $FWHM_{max} = 0.76\lambda$

Table 2 shows research of changes in the length L of the converging linear gradient lenses separately dedicated to the longitudinal component of the electric field. In addition to the global maximum (max) is considered the first maximum of the optical element (fmx).

Table 2. Diffraction of Gaussian beams on the converging linear gradient lens, the intensity of longitudinal component

	L = 0.25λ	L = 0.5λ	L = λ	L = 1.55λ	L = 2λ
The fundamental Gaussian mode					
Mode Gauss - Laguerre (0,1)					
	FWHM$_{fmx}$ = 1.22λ	FWHM$_{fmx}$ = 0.33λ	FWHM$_{fmx}$ = 0.36λ	FWHM$_{out}$ = 0.44λ	FWHM$_{out}$ = 0.4λ
	FWHM$_{max}$ = 1.16λ	FWHM$_{max}$ = 0.9λ	FWHM$_{max}$ = 0.77λ	FWHM$_{max}$ = 0.58λ	FWHM$_{max}$ = 0.46λ
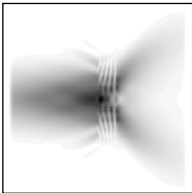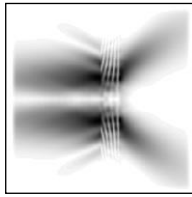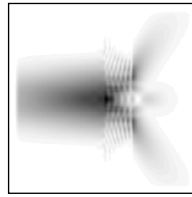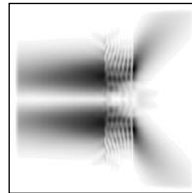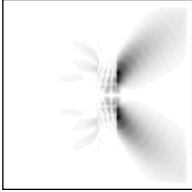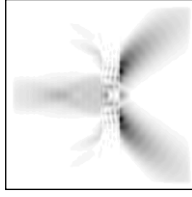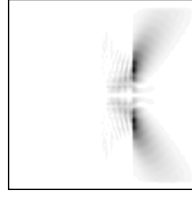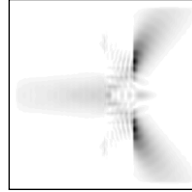
The longitudinal electric field component (component z) in the case of the fundamental Gaussian mode also becomes smaller with increasing length of the lens. Comparing Tables 1 and 2 for the case of mode Laguerre - (0,1), it should be noted that increasing the length of the lens, there is a significant enhancement z components, and the size of the focal spot begins to form mainly due to the longitudinal component of the electric field. This is particularly noticeable when analyzing the last column of table 1 and 2: for mode Gauss - Laguerre (0,1) size of the focal spot next to the central part of which contains the longitudinal component of the electric field is FWHM$_{out}$ = 0.4λ, while the total intensity of the light Spot contains a cross-polarized side lobes that broadens the spot size to FWHM = 0.48λ. In the plane of maximum intensity, the effect of cross-polarized components of the electric field is more significant (broadened to 0.76λ). Of special note is the case of $L = 0.5λ$, when the longitudinal component of the electric field near the plane of the first element in the maximum was obtained by the minimum size of the focal spot: FWHM$_{fm}$ = 0.33λ, but as you can see on the the graphs - by increasing the intensity of the side lobes.

Table 3 shows the result of diffraction of Gaussian beams at the diverging linear gradient lens when changing the length L, that is, on the lens, whose refractive index increases from the center to the edges. Such a lens can be used for the introduction of laser radiation into a hollow (annular) optical waveguide. The refractive index in this case, i have a similar case considered earlier: also examined 10 rings (width λ), each

of which had a their refractive index. But they are changed in the reverse order of $n = 1.5$ in the middle, to $n = 3.47$ at the edge of the lens (Figure 1b).

Table 3 shows that the longitudinal component of the electric field using Gauss-Laguerre modes (0.1) in the plane of maximum intensity able to obtain a focal spot size smaller than the collecting lens, and in the case of $L = 1.55\lambda$ size of the focal spot is the focal spot in the case of $L = 2\lambda$ in Table 2. However, the intensity of the spots materially ~ 5 times less.

Table 3. Diffraction of Gaussian beams on the diverging linear gradient lens

	$L = \lambda$		$L = 1.55\lambda$	
	Gauss	Mode G-L (0,1)	Gauss	Mode G-L (0,1)
The overall intensity				
			$\text{FWHM}_{max} = 0.8\lambda$	
The intensity of longitudinal component				
		$\text{FWHM}_{max} = 0.63\lambda$		$\text{FWHM}_{max} = 0.46\lambda$

Fig. 3. – Graphics cross-section of the intensity of the longitudinal component for modes Gauss - Laguerre (0,1) on the diverging linear gradient lens, black thick line - $h = 1.55\lambda$, black thin line - $h = \lambda$

Figure 3 is a graph showing the cross section of the components of z to Laguerre-Gaussian modes (0,1) (bottom row of Table 3). As seen from the graph, a reduction intensity of the focal spot accompanied by decrease intensity of side lobes.

Conclusion

In this paper using the FDTD method, was numerically research of circularly polarized Gaussian beams passing through a linear gradient lens, considered two options of lenses - converging and diverging.

It has been shown that increasing the length lens provides a more compact size of the focal region in all directions, both for total intensity and the longitudinal electric field component.

The minimum size of the focal spot was not obtained at the maximum intensity, but at the first maximum out of optical element. For modes Gauss-Laguerre (0,1) the minimum size of the focal spot on the FWHM for the longitudinal electric field component was 0.33 wavelength for $L = 0.5\lambda$; in the plane of maximum intensity using a diverging lens for z components able to obtain a focal spot size less than when using a converging lens (at falling intensity ~ 5 times).

Acknowledgements

References

1. **Tomlinson WJ.** Applications of GRIN-rod lenses in optical fiber communication systems. Applied Optics, 1980; 19(7): 1127-1138.
2. **Emkey W, Jack C.** Analysis and evaluation of graded-index fiber lenses. Journal of Lightwave Technology, 1987; 5(9): 1156-1164.
3. **Kotlyar VV, Kovalev AA, Triandafilov YaR, Nalimov AG.** Modes of planar gradient-index hyperbolic secant waveguide. Computer optics, 2010; 34(2): 146-154.
4. **Kotlyar VV, Kovalev AA, Nalimov AG.** Gradient-index element of micro-optics for super-resolution. Computer Optics, 2009; 33(4): 369-378.
5. **Matsumoto T.** Focusing of light by negative refraction in a photonic crystal slab superlens on silicon-on-insulator substrate. Optics letters, 2006; 31(18): 2786-2788.
6. **Kurt H.** The focusing effect of graded index photonic crystals. Applied Physics Letters, 2008; 93(17): 171108.
7. **Zhu Q, Jin L, Fu Y.** Graded index photonic crystals: A review. Annalen der Physik, 2015; 527(3-4): 205-218.
8. **Xiong C.** Slow-light enhanced correlated photon pair generation in a silicon photonic crystal waveguide. Optics letters, 2011; 36(17): 3413-3415.
9. **Liang J.** Wideband ultraflat slow light with large group index in a W1 photonic crystal waveguide. Journal of Applied Physics, 2011; 110(6): 063103.
10. **Goncharenko A, Karpenko V, Goncharenko I.** Fundamentals of the theory of optical waveguides. Minsk: Belarusian science; 2009.
11. **Snyder AW, Love J.** Optical Waveguide Theory. Springer Science & Business Media, 1983.

12. **Bozinovic N.** Terabit-scale orbital angular momentum mode division multiplexing in fibers. Science, 2013; 340(6140): 1545-1548.
13. **Essiambre R.** Capacity limits of optical fiber networks. Journal of Lightwave Technology, 2010; 28(4): 662-701.
14. **Khonina SN, Kazanskiy NL, Soifer VA.** Optical vortices in a fiber: Mode division multiplexing and multimode self-imaging. Editer Dr Moh. Yasin. Recent Progress in Optical Fiber Research. InTech, 2012.
15. **Savelyev DA, Khonina SN.** Maximizing the longitudinal electric component at diffraction on a binary axicon linearly polarized radiation. Computer Optics, 2012; 36(4): 511-517.
16. **Khonina SN, Savelyev DA.** High-aperture binary axicons for the formation of the longitudinal electric field component on the optical axis for linear and circular polarizations of the illuminating beam. Journal of Experimental and Theoretical Physics, 2013; 117(4): 623-630.
17. **Khonina SN, Karpeev SV, Alferov SV, Savelyev DA, Laukkanen J, Turunen J.** Experimental demonstration of the generation of the longitudinal E-field component on the optical axis with high-numerical-aperture binary axicons illuminated by linearly and circularly polarized beams. Journal of Optics, 2013; 15: 085704.
18. **Khonina SN, Savelyev DA, Kazanskiy NL.** Vortex phase elements as detectors of polarization state. Optics Express, 2015; 23(14): 17845-17859.
19. **Khonina SN., Savelyev DA., Ustinov AV.** Diffraction of laser beam on a two-zone cylindrical microelement. Computer Optics, 2013; 37(2): 160-169.
20. **Kotlyar VV, Stafeev SS, Feldman AYu.** Photonic nanojets formed by square microsteps. Computer Optics, 2014; 38(1): 72-80.
21. **Savelyev DA, Khonina SN.** Numerical analysis of subwavelength focusing using a silicon cylinder. Computer Optics, 2014; 38(4): 638-642.
22. **Berdague S, Facq P.** Mode division multiplexing in optical fibers. Applied Optics, 1982; 21: 1950-1955.
23. **Mikaelian AL.** Optical Methods in Informatics. Moscow: Nauka (Science) Publishers, 1990.
24. **Soifer VA, Golub MA.** Laser beam mode selection by computer-generated holograms. Boca Raton, CRC Press, 1994.
25. **Karpeev SV, Khonina SN.** Experimental excitation and detection of angular harmonics in a step-index optical fiber. Optical Memory & Neural Networks (Information Optics), 2007; 16(4): 295-300.
26. **Khonina SN, Striletz AS, Kovalev AA, Kotlyar VV.** Propagation of laser vortex beams in a parabolic optical fiber. Proceedings SPIE, 2010; 7523: 75230B-1-12.
27. **Savelyev DA, Khonina SN.** Sharp focusing by means of binary relief at the end of the optical fiber. Proceedings SPIE, 2013; 9156: 915609-1-6.
28. **Khonina SN, Kotlyar VV, Soifer VA, Paakkonen P, Turunen J.** Measuring the light field orbital angular momentum using DOE. Optical Memory and Neural Networks (Allerton Press), 2001; 10(4): 241-255.
29. **Almazov AA, Khonina SN.** Periodic self-reproduction of multi-mode laser beams in graded-index optical fibers. Optical Memory and Neural Networks (Information Optics), 2004; 13(1): 63-70.
30. **Oskooi AF.** Meep: A flexible free-software package for electromagnetic simulations by the FDTD method. Computer Physics Communications, 2010; 181: 687-702.

Modeling of propagation of optical signals in gradient index media based on fractional Fourier transform

Zubtsov R.O.,

Samara State Aerospace University

Kirilenko M.S.

Samara State Aerospace University,
Image Processing Systems Institute, Russian Academy of Sciences

Abstract. This research has simulated the propagation of the light beams through the quadratic index media. Five methods of simulation were considered and the propagating beams corresponding to different input signals such as Airy-Gaussian beams, rectangular function pulses, triangular function pulses, cosine function signals and finite eigenfunctions were demonstrated.

Introduction

Fractional Fourier transform (FrFT) is a set of linear transformations that generalize Fourier transform. Fourier transform is generally interpreted as a convention of the time domain of the signal to its frequency domain.

The canonical FrFT was considered [1] as the Fourier transform of α-order, where α is the real value. We can likewise define the FrFT as the operation of the frequency-time distribution (Wigner distribution function) rotation at a certain angle [2].

Originally, FrFT was used in quantum mechanics; however, recently it has increasingly become a focus of opticists. As a result, extensive research involving its properties, optical realization and potentiality opportunities in optic applications has been performed. Thus, currently FrFT is actively used in optical image processing [3]. Moreover, the fractioning of some transformation provides a new degree of freedom (fraction order) that can be used for a more complete description of the object (signal) or as an additional encoding parameter.

FrFT is used in differential equation solving, in quantum mechanics and quantum optics, in optical theory of diffraction, in optical system and optical signal processing

descriptions including the application of frequency filters, time filtration and multiplexing, as well as in pattern recognition, in wavelet-transformations, in operations with chirp-functions, in encryption, for neural network creation and other applications. A more detailed review of FrFT can be found in the paper [3] produced by T. Alieva et al.

The modular lens system and the system of several spherical and/or cylindrical lenses are among the methods of FrFT optical realization [4-8]. Some of these systems (especially cylindrical lenses) are used for astigmatic transformation in order to form vortex beams [5, 8-10].

One of application of FrFT is the description of laser beam propagation in gradient index media [11, 12].

In this work, we use one-dimensional FrFT to model optical signal propagation in optical waveguides with parabolic dependence of the refractive index. The eigenfunctions of the transforms are Hermite-Gaussian modes [1].

During the modelling process special attention is given to Airy-Gaussian beams, which carry finite power and keep the properties of non-diffracted propagation in a partial area. They can be experimentally realized with a particularly good approximation [13-16].

1. General theory

The light beam propagation through the ABCD-system in one-dimensional cases is described by the Huygens integral:

$$U_2(x_2) = \sqrt{\frac{k}{i2\pi B}} \int_{-\infty}^{+\infty} U_1(x_1) \exp\left[\frac{ik}{2B}\left(Ax_1^2 - 2x_1 x_2 + Dx_2^2\right)\right] dx_1 .$$
(1)

where $k = 2\pi/\lambda$, $U_1(x_1)$ is input field, $U_2(x_2)$ is output field.

In gradient index media with the refraction index $n = n_0\left(1 - x^2/2a^2\right)$, the matrix of ABCD-system is (beam propagation from $z_1 = 0$ to $z_2 = z$) [13, 14, 17, 18]:

$$\begin{bmatrix} A & B \\ C & D \end{bmatrix} = \begin{bmatrix} \cos(z/a) & a\sin(z/a) \\ -\sin(z/a)/a & \cos(z/a) \end{bmatrix}.$$
(2)

With this type of matrix the integral (1) turns into FrFT.

The complete set of FrFT eigenfunctions is the following set of Hermite-Gaussian functions:

$$\Im^\alpha\left[\psi_n(x)\right] = e^{-i\alpha n\pi/2}\psi_n(x),$$

$$\psi_n(x) = \frac{2^{1/4}}{\sqrt{2^n n!}} H_n\left(\sqrt{2\pi}x\right)e^{-\pi x^2},$$
(3)

where $H_n(x)$ − a Hermite polynomial of order n:

$$H_n(x) = (-1)^n e^{x^2} \frac{d}{dx^n} e^{-x^2} .$$
(4)

If the FrFT has finite integration limits (in other words the input beam is limited), its eigenfunctions are somewhat different from the Hermite-Gaussian modes [19].

The propagation of a light beam through the gradient index media was modeled. The Airy-Gaussian beams are:

$$U_1(x_1; \kappa_1, \delta_1, S_1, q_1) =$$

$$= Ai\left(\frac{x_1 + \delta_1}{\kappa_1}\right) \exp\left[iS_1\left(\frac{x_1 + \delta_1}{\kappa_1}\right) + i\frac{S_1^2}{3} + \frac{ikx_1^2}{2q_1}\right], \tag{5}$$

$$\kappa_1, \delta_1, S_1, q_1 \in C.$$

Furthermore, the cosine distribution function is:

$$f(x) = A\cos(\omega x + \varphi), \tag{6}$$

$$A, \omega, \varphi \in R.$$

In addition, the rectangular function, triangle function and eigenfunctions have been simulated.

2. Simulation

Method 1: direct numerical calculation of FrFT by definition.

The integral (1) is rarely solved analytically, so we use numerical computations. If typical methods are use, the numerical calculations of quadratic exponents require a very large number of sampling points because of rapid oscillations in the kernel. The problem is especially pronounced if α is close to 0 or ±2. We assume that functions and their Fourier transformations are limited (they are not equal to zero in finite intervals) and this difficulty can be avoided. If $0.5 \leq \alpha \leq 1.5$ or $2.5 \leq \alpha \leq 3.5$, we can directly calculate the integral. If $-0.5 < \alpha < 0.5$ or $1.5 < \alpha < 2.5$, we can use the property of additivity: $\mathfrak{I}^\alpha = \mathfrak{I}^1 \mathfrak{I}^{\alpha-1}$, where in the transformation of α-1 order may be found immediately.

For the integration we use Simpson's rule (n is even):

$$\int_a^b f(x)dx \approx \frac{h}{3}\sum_{j=1}^{n/2}\left(f(x_{2j-2}) + 4f(x_{2j-1}) + f(x_{2j})\right), \tag{7}$$

$$x_j = a + jh, \ j = \overline{0, n-1}, \ h = (b-a)/n.$$

Although this method of FrFT calculation can produce accurate results, it operates slowly and has a computational complexity $O(N^2)$ [20].

Method 2: Fast FrFT.

FrFT is a special case of the more general transform class sometimes known as linear canonical transformations or quadratic-phase transformations. The elements of this class can be decomposed to a sequence of simple operations such as chirp-multiplication, chirp-convolution, scaling and typical Fourier transform. There are two different decompositions demonstrated here, leading to different algorithms.

Method 3: the decomposition into chirp-multiplication, chirp-convolution and another single chirp-multiplication sequence.

In this approach, we assume that $-1 \leq \alpha \leq 1$. The transformation (1) can be written as:

$$f_\alpha(x) = \exp\left[-\frac{i\pi}{\lambda a}x^2 \tan\left(\frac{\varphi}{2}\right)\right] g'(x), \tag{8}$$

107

$$g'(x) = A_\varphi \int_{-\infty}^{+\infty} \exp\left[\frac{i\pi}{\lambda a}\beta(x-x')^2\right]g(x')dx', \tag{9}$$

$$g(x) = \exp\left[-\frac{i\pi}{\lambda a}x^2\tan\left(\frac{\varphi}{2}\right)\right]f(x), \tag{10}$$

where $g(x), g'(x)$ represents an intermediate result, $\varphi = \dfrac{z}{a}$, $\beta = \csc\varphi$, $A_\varphi = \sqrt{\dfrac{\beta}{i\lambda a}}$.

Method 4: another decomposition involving the Whittaker-Shannon interpolation formula (sinc-interpolation). The defining expression of FrFT can be written as:

$$\left\{\Im^\alpha f\right\}(x) = A_\varphi \exp\left(\frac{i\pi}{\lambda a}\alpha x^2\right)\times$$
$$\times\int_{-\infty}^{+\infty}\exp\left(-\frac{i2\pi\beta}{\lambda a}xx'\right)\exp\left(\frac{i\pi}{\lambda a}\alpha x'^2\right)f(x')dx'. \tag{11}$$

The function $\exp\left(\dfrac{i\pi}{\lambda a}\alpha x'^2\right)f(x')$ can be represented by the Shannon interpolation formula:

$$\exp\left(i\pi\alpha x'^2\right)f(x') = \sum_{-N}^{N}\exp\left[\frac{i\pi}{\lambda a}\alpha\left(\frac{n}{2\Delta x}\right)^2\right]\times$$
$$\times f\left(\frac{n}{2\Delta x}\right)\mathrm{sinc}\left(2\Delta x\left(x'-\frac{n}{2\Delta x}\right)\right). \tag{12}$$

We substitute (12) in (11), change sequence of integration and summation and use certain algebraic manipulations to obtain the following expression:

$$\left\{\Im^\alpha f\right\}\left(\frac{m}{2\Delta x}\right) = \frac{A_\varphi}{2\Delta x}\exp\left[\frac{i\pi}{\lambda a}(\alpha-\beta)\left(\frac{m}{2\Delta x}\right)^2\right]\times$$
$$\times\sum_{-N}^{N}\exp\left[\frac{i\pi}{\lambda a}\beta\left(\frac{m-n}{2\Delta x}\right)^2 + \frac{i\pi}{\lambda a}(\alpha-\beta)\left(\frac{n}{2\Delta x}\right)^2\right]f\left(\frac{n}{2\Delta x}\right). \tag{13}$$

There are other methods, for example those described in [21], however they are not well suited for plotting images on a plane. The modeling results are demonstrated in Figures 1-6.
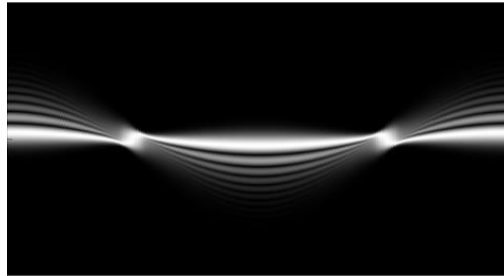
Fig. 1. – The propagation of Airy-Gaussian beams (version 1)
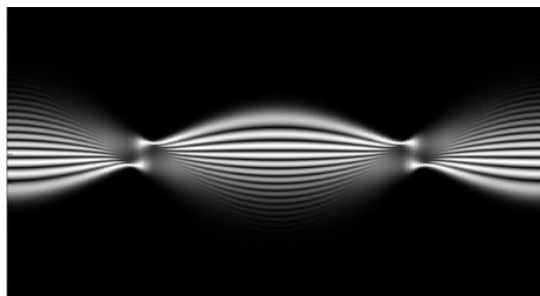
Fig. 2. – The propagation of Airy-Gaussian beams (version 2)
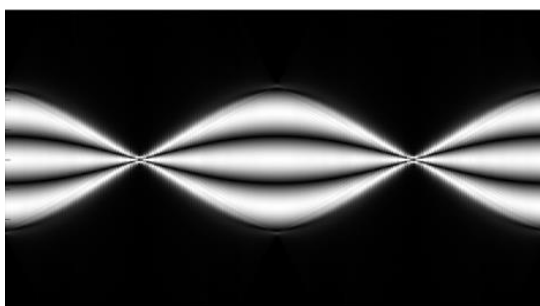
Fig. 3. – The propagation of cosine function signals
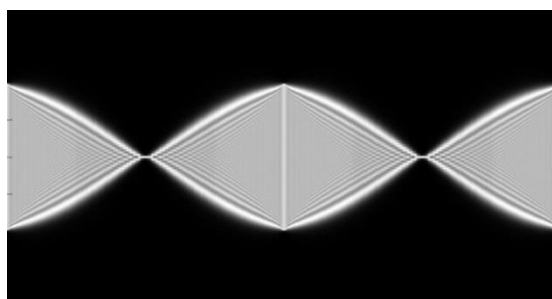
Fig. 4. – The propagation of rectangular pulses
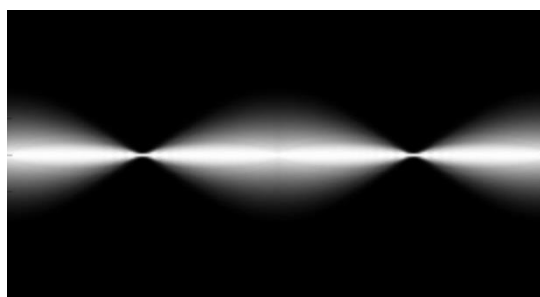
Fig. 5. – The propagation of triangular pulses

109
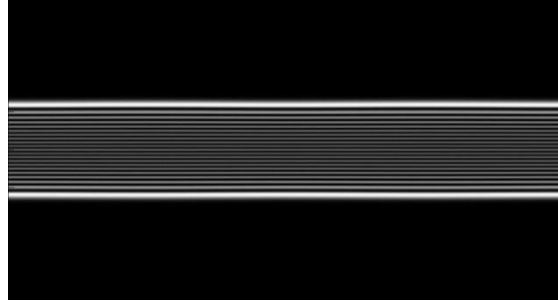
Fig. 6. – The propagation of eigenfunctions

Acknowledgments

References

1. **Namias V.** The fractional Fourier transform and its application in quantum mechanics. Journal of the Institute of Mathematics and Its Applications, 1980; 25: 241-265.
2. **Abet S, Sheridant JT.** Generalization of the fractional Fourier transformation to an arbitrary linear lossless transformation: an operator approach. Journal of Physics A: Mathematical and General, 1994; 27: 4179-4187.
3. **Alieva T, Bastiaans MJ, Calvo ML.** Fractional transforms in optical information processing. EURASIP Journal on Advances in Signal Processing, 2005; 10: 1-22.
4. **Dorsch RG, Lohmann AW.** Fractional Fourier transform used for a lens-design problem. Applied Optics, 1995; 34(20): 4111-4112.
5. **Cai LZ, Wang YQ.** Optical implementation of scale invariant fractional Fourier transform of continuously variable orders with a two-lens system. Optics & Laser Technology, 2002; 34: 249-252.
6. **Malutin AA.** Use of fractional Fourier-transformation in $\pi/2$-converters of laser modes. Quantum Electronics, 2004; 2: 165-171.
7. **Hahn J.** Optical implementation of iterative fractional Fourier transform algorithm. Optics Express, 2006; 14(23): 11103-11112.
8. **Khonina SN, Karpeev SV, Ustinov AV.** Functional enhancement of mode astigmatic converters on the basis of application of diffractive optical elements. News of the Samara Science Center of the RAS, 2009; 11(5): 13-23.
9. **Abramochkin E, Volostnikov V.** Beams transformations and nontransformed beams. Optics Communications, 1991; 83: 123-135.
10. **Beijersbergen MW, Allen L, van der Veen HELO, Woerdman JP.** Astigmatic laser mode converters and transfer of orbital angular momentum. Optics Communications, 1993; 96: 123-132.
11. **Ozaktas HM, Mendlovic D.** Fourier transforms of fractional order and their optical interpretation. Optics Communications, 1993; 101: 163-169.
12. **Mendlovic D, Ozaktas HM.** Fractional Fourier transforms and their optical implementation: I. Journal of the Optical Society of America A, 1993; 10(9): 1875-1881.
13. **Bandres MA, Gutiurrez-Vega JC**. Airy-Gauss beams and their transformation by paraxial optical systems. Optics Express, 2007; 15(25): 16719-16728.

14. **Khonina SN, Volotovsky SG.** Bounded 1D Airy beams: laser fan. Computer Optics, 2008; 32(2): 168-174. [in Russian]
15. **Khonina SN, Skidanov RV, Moiseev OY.** Airy laser beams generation by binary-coded diffractive optical elements for microparticles manipulation. Computer Optics, 2009; 33(2): 138-146. [in Russian]
16. **Khonina SN.** Specular and vortical Airy beams. Optics Communications, 2011; 284: 4263–4271
17. **McMullin JN.** The ABCD matrix in arbitrarily tapered quadratic-index waveguides. Applied Optics, 1986; 25: 2184.
18. **Striletz AS, Khonina SN.** Matching and investigation methods based on differential and integral operators of laser radiation propagation in a medium with small inhomogeneities. Computer Optics, 2008; 32(1): 33-38.
19. **Kirilenko MS, Zubtsov RO, Khonina SN.** Calculation of eigenfunctions of a bounded fractional Fourier transform. Computer Optics, 2015; 39(3): 332-338.
20. **Ozaktas HM, Ankan O, Kutay A, Bozdaki G.** Digital computation of the Fractional Fourier Transform. IEEE Transactions On Signal Processing, 1996; 44(9): 2141-2150.
21. **Marinho FJ, Bernardo LM.** Numerical calculation of fractional Fourier transforms with a single fast-Fourier-transform algorithm. Journal of the Optical Society of America A, 1998; 15(8): 2111-2116.

Vibration resistance of headlight design for electric locomotive

Abulkhanov S.R.

Samara State Aerospace University

Abstract. I determined the natural frequencies of the headlight design for electric locomotive VL by software system of the finite-element analysis ANSYS. The obtained values of the natural frequencies are compared with the frequencies of the periodic vibrations experienced by the railway rolling stock. The analysis reveals the vibration frequencies determining the period of the trouble-free operation of the headlight.

Keywords: headlight, electric locomotive, natural frequencies of design, trouble-free service life, periodic vibration, noise and re-emitted noise.

Introduction

The main sources of vibration for driving railway locomotive are just a vehicle, wheels, rails and railway track. According to the Resolutions of 15.07.2011, N 710 "On the adoption of the technical regulations of the Customs Union" ("On the safety of the railway rolling stock", "On the safety of the high-speed railway transport", and "On the safety of the railway infrastructure") [1], the range of vibration frequency causing the damage to structures (buildings) is from 1 to 500 Hz, and the greatest damage to structures is at the low-frequency vibrations (the frequencies from 1 to 150 Hz).

A railway locomotive undergoes periodic and random vibrations. The reasons of the excitation of the periodic vibrations are the deflection of the rail track moving along with the movement of the train and the support system; the discrete structure of the rail support (the distance between the axes of sleepers); the discreteness of the effect on the object due to the distance between the axes of wheel pairs and bogies; the breaks of the rail track (at the diverters, at the blind crossings of the railway track, at the junctions of the rails, and so on.
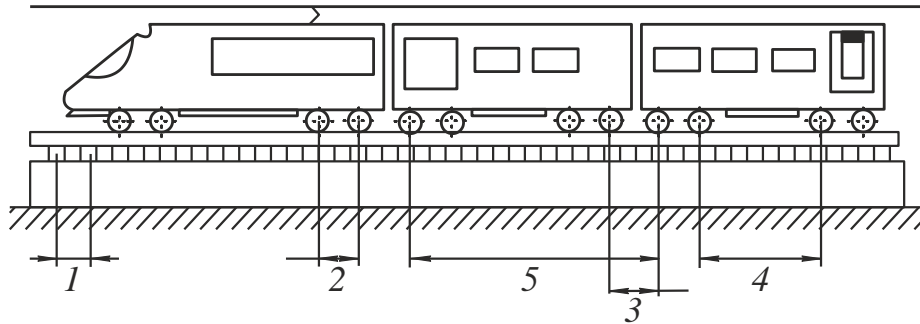
Fig. 1. – The causes of the excitation of periodic vibrations of a railway locomotive: 1 is the distance between the support elements of the railway track; 2 is the distance between the wheel pairs of the bogie; 3 is the distance between the adjacent bogies of adjacent railway cars; 4 is the distance between the bogies of a railway car; 5 is the distance between railway cars

The random vibrations are the noise emitted by the rattling objects (panes, lamps, conjugations of a shaft-hole with the loose fit and so on). The vibration is transmitted, being changed through the rail tracks on their support and further into the ground, the frame and the body of a locomotive, the surface roughness of a wheel rim and when riding the rail, causing at the same time the re-radiated noise. The re-radiated noise of the object of the exposure is observed in the frequency range from about 16 to 250 Hz in accordance with the Resolution. The description of the noises is quantitatively associated with certain difficulties, so they will not be considered.

When analyzing the vibration and the noise, it should be considered that the vibration sources, their pathways of the propagation and the objects of their effect depend on many factors, namely, according to the Resolution: the geometry of the rail track, the characteristics of the rolling stock (its length, a wheel profile, a wheel diameter, the roughness and surface defects when riding a wheel, the system of the wheel suspension, wheels with elastic elements and etc.), the characteristics of rails, elements of the rail track, and others. The vibration source, the pathway of the vibration propagation and the object of the effect are shown schematically in Fig. 2.

1. The definition of the boundaries of the range of possible fluctuations of a railway locomotive

The frequency of the periodic vibrations depends on the speed of a railway locomotive. Table 1 summarizes the possible oscillation frequencies depending on the speed of the movement (VM) applied to an electric locomotive VL series. The phenomena of interference, the vibration diffraction are not taken into account, i.e. the locomotive is considered as one rigid body.

A locomotive, ahead of the next train, experiences the vibrations generated not only by the train and by the railroad track, but the vibrations generated by the bogies of the driven railway cars. The vibration oscillation of each railway car is transmitted by the rails as through the waveguides with the velocity of the sound in metals ($\approx$22000 km/h). The vibration oscillation caused by the deflection of the rails in the intervals between the sleepers, results in the formation of a surface (Rayleigh) wave on the ground surface. These waves formed by the railway cars of the rolling stock,

113

provided the hard ground, can catch up and overtake a locomotive, that in turn can result in the change of the oscillation spectrum of the rolling stock as well as of the locomotive. If the high-speed train moves along the rail track, provided the soft ground, then, the velocity of its movement can exceed the speed of the propagation of a surface (Rayleigh) wave in the ground. This creates a high level of vibration, just as the flight of a supersonic aircraft is accompanied by the sonic boom (based on the Solution).
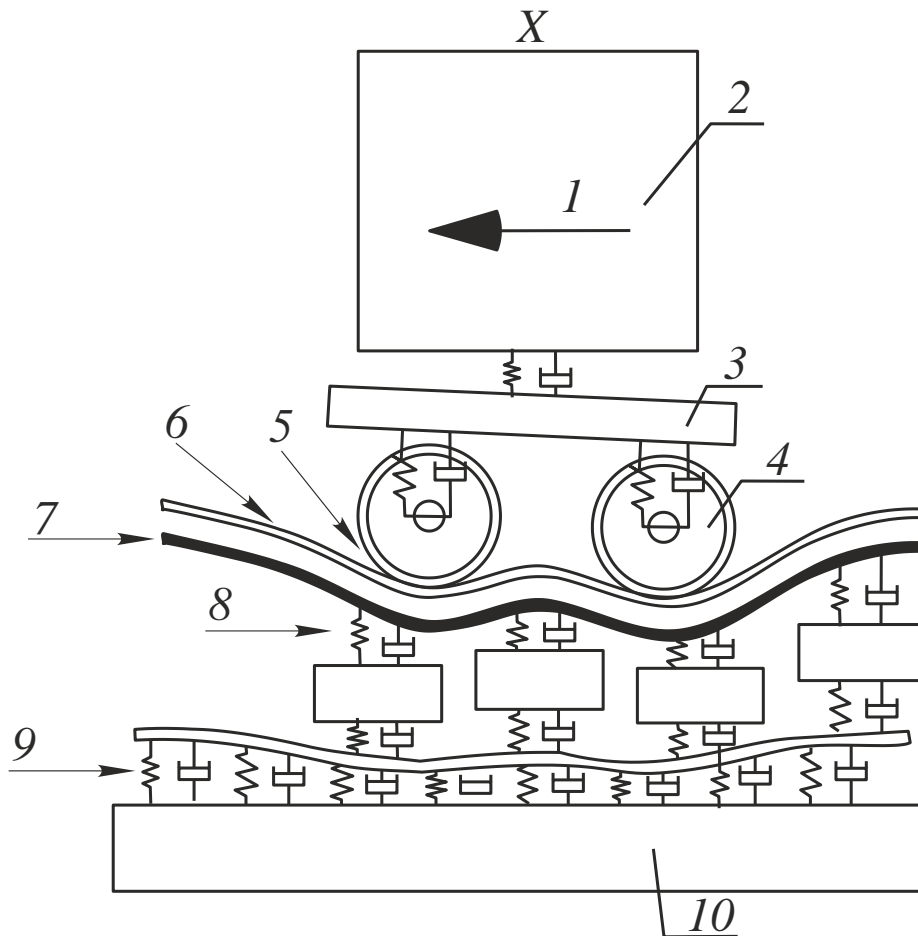
Fig. 2. – The description of the vibration source: 1 is the speed of movement; 2 is the part of the mass of the body; 3 is the part of the mass of the bogie; 4 is the unsprung weight; 5 is the roughness of the surface of the wheel rim; 6 is the roughness of the surface when riding the rail; 7 is the impedance of the rail; 8 is a model of the system "rail-wheel"; 9 is a model of the system "base - rail"; 10 is impedance of the ground

Thus, the vibrations of the entire rolling stock participate in the formation of the oscillation spectrum of the locomotive vibrations. The range of the locomotive

114

vibration spectrum in this case can only change as a result of the dispersion of various vibration sources formed by railway cars of the rolling stock. In the paper we assume that there is no dispersion of the oscillation vibration.

Table 1. The frequencies of the potential oscillation of an electric locomotive

Name of parameters of railway track and suspension of an electric locomotive	Geometric dimensions and sources of information	Speed of movement of an electric locomotive, km/hour (m/c)	Frequency oscillation f, Hz	fMAX / fMIN, Hz	[fMAX; fMIN], Hz
Distance between support elements of the track, m	0,501 -0,632 (GOST R 51248-99; GOST 78-2004; GOST 9238-83; GOST 10629-88, [1])	3* - 200** 103 (0.83 − 55.56)***	$\dfrac{V_M}{0,501-0,632}$	1.31 − 1.66 / 87.91 − 110.9	0.001 − 110.9
Distance between wheel pairs of the bogie, m	1,85 [2]		$V_M/1,85$	0.45 − 30.03	
	1,35 [2]		$V_M/1,35$	0,61 − 41.16	
Distance between adjacent bogies of adjacent railway cars, m	5,72 electric locomotive VL8 [2]		$V_M/5,72$	0,15 − 9.71	
Distance between bogies of a railway car, m	4,5 electric locomotive VL8 [2]		$V_M/4,5$	0.18 − 12.35	
Distance between railway cars, m	162,2 electric locomotive VL8 [2]		$V_M/162,2$	0,01 − 0,34	
Length of rails, m	12,5 [GOST R 51045-97; GOST R 51685-2000]		$V_M/12,5$	0,07 − 44.4	
	25 [GOST R 51045-97; GOST R 51685-2000]		$V_M/25$	0.03 − 2.22	
	800*** (welded)		$V_M/800$	0.001 − 0.07	

* Minimum speed of a shunting locomotive;

** Maximum speed of an electric locomotive on the railroads of RF (Ch. Speed 200 - 200 km / h of the high speed train 165/166 Petersburg-Moscow)

*** Technical instructions on design, installation, maintenance and repair of continuous welded railroad. March 31, 2000 M- Movement

2. The light requirements to a searchlight of a railway locomotive

A headlight of an electric locomotive VL series must meet certain requirements. A lamp should be installed along the longitudinal axis of the symmetry of a locomotive. The axial beam of the headlight should be directed parallel to the horizontal plane of the road. The nominal axial intensity of the lamp should be (6.4-9.6)·105 cd. The closed circuit of the lamp must provide the possibility of powering up the bright light, providing the nominal axial force of the light and the dim light, providing the power of the light within (0.7-1.2)·105 cd in accordance with GOST 12.2.056-81.

The test method for measuring the axial light intensity of the headlight is to determine the light intensity by measuring the light with simultaneous measuring the voltage of the light source in accordance with the regulations of 2000, agreed by the contact group 28/01/2010 V1.00, about the preservation of technical and interoperability of the rail system of the rail road of 1520 mm and 1435 mm at the border of the CIS and the EU, as well as in accordance with [3]. The measurement of the light intensity of the headlight is carried out when a photodetector is located along the axis of the pathway from the light at the distance that is greater than the distance

115

of the formation of the light flow of the lamp. For the headlight used currently on the rolling stock, the distance of forming the light flow is not less than 20 m in accordance with the paragraph A.19.1 GOST 12.2.056-81, and also in accordance with [3].

To achieve the nominal axial force of the light of the headlight and to achieve the angles of ray scattering [3] in the vertical and horizontal planes ~ 3°, it is necessary to focus the headlight in accordance with Annex 1 of the Rules of the technical operation of railways of RF. The light spot having the axial strength of 6.4-9.6 • 10 cd is formed on a flat screen perpendicular to the horizon by the headlight spaced apart from the screen at 10 m. The required orientation of the light spot on the screen is provided by the design of the headlight [4−7]. The operating experience of the headlight shows that the lamp SL (TU 16-87 IMFR 675000,003 W) 500 W and 50 V burns most frequently, and also a glass reflector with a diameter of 370 mm breaks, when installed behind the lamp SL. These failures could be caused by the vibration oscillations.

3. The conditions for the determination of the natural frequencies of a solid model of the design of the searchlight of a locomotive

To determine the natural frequencies of a headlight in the software environment ANSYS the 3D model is used that is obtained in [8]. In the solid model the screw connections (screws and bolts have been removed from the model) are not taken into account due to the lack of the computing power. The parameters of the finite element mesh on the surface of a solid model are selected automatically by the program (Fig. 3).
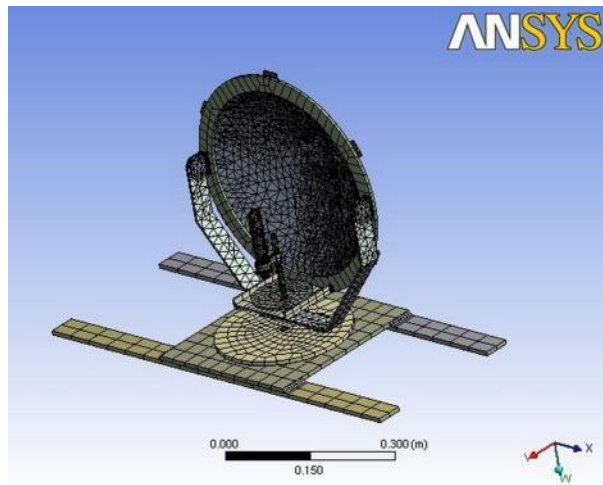
Fig. 3. – The finite element mesh on the surface of a solid model of a headlight

The requirements for modeling are defined by the rules of the computational experiments in the optics [9 – 17]. The conducted simulation shows that in the frequency range of the periodic vibrations (Table. 1), we have the greatest deformations of the glass reflector for the natural frequencies of 22.368 and 62.595 46.49 Hz. The oscillation frequency $f = 46.49$ Hz may correspond to the vibrations

caused by the length of the rails (25 m), the distance between the wheel pairs of a bogie and the distance between the support elements of the railroad (slippers). At the frequency $f = 95.998$ Hz occurs the deformation of a glass bulb of the lamp SL, and there is no deformation of the glass reflector of the headlight.

a)

b)

c)

d)
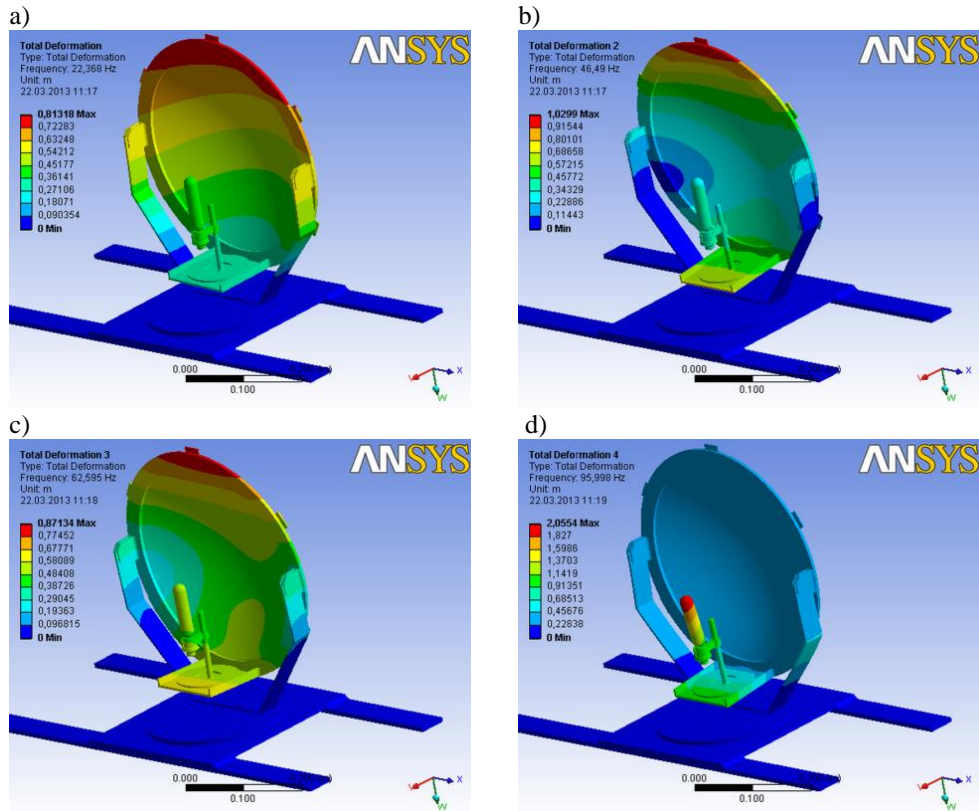
Fig. 4. – The oscillation of the design of a headlight at the natural frequencies: a) f = 22.368 Hz; b) f = 46.49 Hz; c) f = 62.595 Hz; d) f = 95.998 Hz

For the frequencies above the maximum frequency of the periodic vibrations ($f = 110.9$ Hz Tab. 1), the maximum deformations are at the end of the glass bulb of the lamp SL. A glass reflector in this case is deformed slightly (Fig. 4).

4. Conclusions

1. The destruction of a glass reflector is in the range of the frequencies of the vibration oscillation [22.368 – 62.595] Hz.
2. The destruction of a glass lamp SL is at the frequencies greater than 95.998 Hz.
3. The increase in the resource of the lamp SL can be achieved by changing the design of a headlight, namely by using the high-frequency dampers.

117
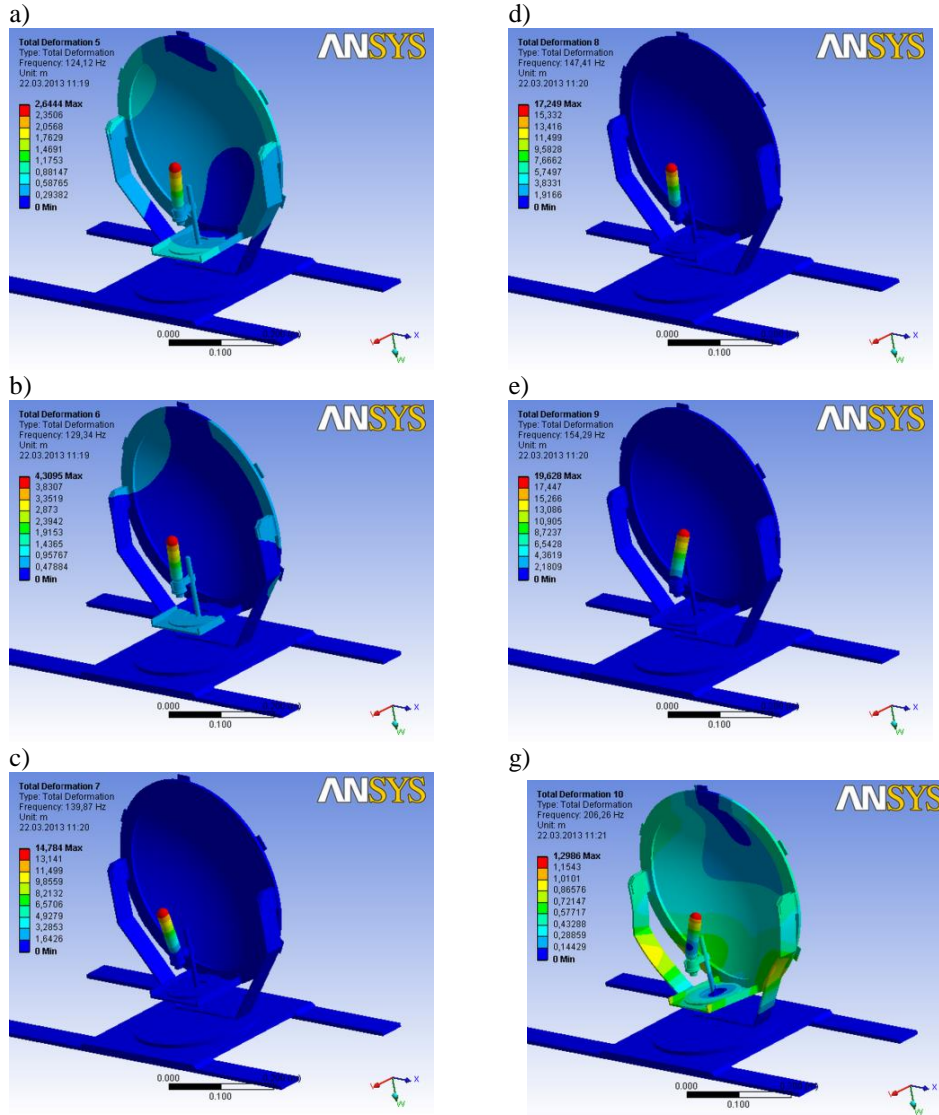
Fig. 5. – The oscillation of the design of a headlight at the natural frequencies: a - *f* = 22.368 Hz; b - *f* = 46.49 Hz; c - *f* = 62.595 Hz; d - *f* = 95.998 Hz; e - *f* = 154.29 Hz; g - *f* = 206.26 Hz.

4. The substantial increase in the resource of a headlight can also be achieved by replacing an incandescent lamp by the high power light emitting diodes (LEDs) using new methods and the necessary software for designing such a lighting device [18 – 24].

5. The presented results play an important role in the design [25 – 28] of hyperspectral remote sensing equipment feeling strong vibrations loads in the derivation of Earth's

118

orbit. Also, these results will be useful for creating transport systems of computer vision [29−32], optical devices [33−36], components, and devices of diffractive nanophotonics [37−44].

References

1. Methods of assessing the impact of the rolling stock on the railroad under the terms of ensuring its reliability. Ed. Zhelnin GG. Moscow: "VNIIJT" Publisher; 2000. 38 p. [in Russian]
2. **Pushkarev BA, Pozdnyakov LA, et al.** Electric locomotive VL85: Operation instruction. Moscow: "Transport" Publisher, 1992. 480 p. [in Russian]
3. **Kazanskiy NL, Kharitonov SI, Soifer VA, Volkov AV.** Investigation of Lighting Devices Based on Diffractive Optical Elements. Optical Memory & Neural Networks (Information Optics), 2000; 9(4): 301-312.
4. **Kazanskiy NL, Kotlyar VV, Soifer VA.** Computer-aided design of diffractive optical elements. Optical Engineering, 1994; 33(10): 3156-3166.
5. **Golovashkin DL, Kasanskiy NL.** Solving Diffractive Optics Problem using Graphics Processing Units. Optical Memory and Neural Networks (Information Optics), 2011; 20(2): 85-89.
6. **Doskolovich LL, Golub MA, Kazanskiy NL, Khramov AG, Pavelyev VS, Seraphimovich PG, Soifer VA, Volotovskiy SG.** Software on diffractive optics and computer generated holograms. Proceedings of SPIE, 1995; 2363: 278-284.
7. **Doskolovich LL, Kazansky NL, Kharitonov SI, Soifer VA.** A method of designing diffractive optical elements focusing into plane areas. Journal of Modern Optics, 1996; 43(7): 1423-1433.
8. **Abulkhanov SR.** The construction of an authentic 3-D model of a headlight of an electric locomotive. Bulletin SamGUPS, 2012; 3(17): 81-86.
9. **Golub MA, Kazanskii NL, Sisakyan IN, Soifer VA, Kharitonov SI.** Diffraction calculation for an optical element which focuses into a ring. Optoelectronics, Instrumentation and Data Processing, 1987; 6: 7-14.
10. **Golub MA, Kazanskii NL, Sisakyan IN, Soifer VA.** Computational experiment with plane optical elements. Optoelectronics, Instrumentation and Data Processing, 1988; 1: 78-89.
11. **Kazanskiy NL, Soifer VA.** Diffraction investigation of geometric-optical focusators into segment. Optik - International Journal for Light and Electron Optics, 1994; 96(4): 158-162.
12. **Doskolovich LL, Kazanskiy NL, Soifer VA, Tzaregorodtzev AYe.** Analysis of quasiperiodic and geometric optical solutions of the problem of focusing into an axial segment. Optik - International Journal for Light and Electron Optics, 1995; 101(2): 37-41.
13. **Doskolovich LL, Kazanskiy NL, Soifer VA, Perlo P, Repetto P.** Design of DOEs for wavelength division and focusing. Journal of Modern Optics, 2005; 52(6): 917-926. doi:10.1080/09500340512331313953.
14. **Golovashkin DL, Kazanskiy NL.** Mesh Domain Decomposition in the Finite-Difference Solution of Maxwell's Equations. Optical Memory & Neural Networks (Information Optics), 2009; 18(3): 203-211.
15. **Khonina SN, Kazanskii NL, Ustinov AV, Volotovskii SG.** The lensacon: nonparaxial effects. Journal of Optical Technology, 2011; 78(11): 724-729. doi: 10.1364/JOT.78.000724.

16. **Khonina SN, Kazanskiy NL, Volotovsky SG.** Influence of Vortex Transmission Phase Function on Intensity Distribution in the Focal Area of High-Aperture Focusing System. Optical Memory and Neural Networks (Information Optics), 2011; 20(1): 23-42. doi: 10.3103/S1060992X11010024.

17. **Kazanskiy NL.** Research & Education Center of Diffractive Optics. Proceedings of SPIE, 2012; 8410: 84100R. doi: 10.1117/12.923233.

18. **Doskolovich LL, Kazanskiy NL, Soifer VA, Kharitonov SI, Perlo P.** A DOE to form a line-shaped directivity diagram. Journal of Modern Optics, 2004; 51(13): 1999-2005.

19. **Doskolovich LL, Kazanskiy NL, Kharitonov SI, Perlo P, Bernard S.** Designing reflectors to generate a line-shaped directivity diagram. Journal of Modern Optics, 2005; 52(11): 1529-1536.

20. **Doskolovich LL, Kazanskiy NL, Bernard S.** Designing a mirror to form a line-shaped directivity diagram. Journal of Modern Optics, 2007; 54(4): 589-597.

21. **Kazanskiy N, Skidanov R.** Binary beam splitter. Applied Optics, 2012; 51(14): 2672-2677. doi: 10.1364/AO.51.002672.

22. **Aslanov ER, Doskolovich LL, Moiseev MA, Bezus EA, Kazanskiy NL.** Design of an optical element forming an axial line segment for efficient LED lighting systems. Optics Express, 2013; 21(23). 28651-28656.

23. **Doskolovich LL, Dmitriev AYu, Moiseev MA, Kazanskiy NL.** Analytical design of refractive optical elements generating one-parameter intensity distributions. J. Opt. Soc. Am. A, 2014; 31(11): 2538-2544. doi: 10.1364/JOSAA.31.002538.

24. **Doskolovich LL, Kazanskiy NL, Perlo P, Repetto P, Soifer VA.** Direct two-dimensional calculation of binary DOEs using a non-binary series expansion approach. International Journal of Optoelectronics, 1996; 10(4): 243-249.

25. **Kazanskiy NL, Kharitonov SI, Khonina SN, Volotovskiy SG, Strelkov YuS.** Simulation of hyperspectrometer on spectral linear variable filters. Computer Optics, 2014; 38(2): 256-270. [in Russian]

26. **Kazanskiy NL, Kharitonov SI, Karsakov AV, Khonina SN.** Modeling action of a hyperspectrometer based on the offner scheme within geometric optics. Computer Optics, 2014; 38(2); 271-280. [in Russian]

27. **Kazanskiy NL, Kharitonov SI, Khonina SN.** Simulation of a hyperspectrometer based on linear spectral filters using vector Bessel beams. Computer Optics, 2014; 38(4): 770-776. [in Russian]

28. **Kazanskiy NL, Kharitonov SI, Doskolovich LL, Pavelyev AV.** Modeling the performance of a spaceborne hyperspectrometer based on the Offner scheme. Computer Optics, 2015; 39(1): 70-76. [in Russian]

29. **Kazanskiy NL, Popov SB.** Machine Vision System for Singularity Detection in Monitoring the Long Process. Optical Memory and Neural Networks (Information Optics), 2010; 19(1): 23-30. doi:10.3103/S1060992X10010042.

30. **Kazanskiy NL, Popov SB.** The distributed vision system of the registration of the railway train. Computer Optics, 2012; 36(3): 419-428. [in Russian]

31. **Kazanskii NL, Khonina SN, Skidanov RV, Morozov AA, Kharitonov SI, Volotovskiy SG.** Formation of images using multilevel diffractive lens. Computer Optics, 2014; 38(3): 425-434. [in Russian]

32. **Kazanskiy NL, Popov SB.** Integrated Design Technology for Computer Vision Systems in Railway Transportation. Pattern Recognition and Image Analysis, 2015; 25(2): 215-219. doi: 10.1134/S1054661815020133.

33. **Karpeev SV, Pavelyev VS, Khonina SN, Kazanskiy NL, Gavrilov AV, Eropolov VA.** Fibre sensors based on transverse mode selection. Journal of Modern Optics, 2007; 54(6): 833-844. doi:10.1080/09500340601066125.

34. **Doskolovich LL, Kazanskiy NL, Khonina SN, Skidanov RV, Heikkila N, Siitonen S, Turunen J.** Design and investigation of color separation diffraction gratings. Applied Optics, 2007; 46(15): 2825-2830.

35. **Borodin SA, Volkov AV, Kazanski NL.** Device for analyzing nanoroughness and contamination on a substrate from the dynamic state of a liquid drop deposited on its surface. Journal of Optical Technology, 2009; 76(7): 408-412.

36. **Khonina SN, Savelyev DA, Kazanskiy NL.** Vortex phase elements as detectors of polarization state. Optics Express, 2015; 23(14): 17845-17859. doi: 10.1364/OE.23.017845.

37. **Kazanskiy NL, Serafimovich PG, Khonina SN.** Harnessing the Guided-Mode Resonance to Design Nanooptical Transmission Spectral Filters. Optical Memory and Neural Networks (Information Optics), 2010; 19(4): 318-324. doi: 10.3103/S1060992X10040090.

38. **Bezus EA, Doskolovich LLKazanskiy NL.** Scattering suppression in plasmonic optics using a simple two-layer dielectric structure. Applied Physics Letters, 2011; 98(22): 221108. 3 pp. doi: 10.1063/1.3597620.

39. **Bezus EA, Doskolovich LL, Kazanskiy NL, Soifer VA.** Scattering in elements of plasmon optics suppressed by two-layer dielectric structures. Technical Physics Letters, 2011; 37(12): 1091-1095.

40. **Kazanskiy NL, Serafimovich PG, Khonina SN.** Use of photonic crystal cavities for temporal differentiation of optical signals. Optics Letters, 2013; 38(7): 1149-1151.

41. **Kazanskiy NL, Serafimovich PG.** Cloud Computing for Nanophotonic Simulations. Lecture Notes in Computer Science, 2013; 7715: 54-67.

42. **Bezus EA, Doskolovich LL, Kazanskiy NL.** Low-scattering surface plasmon refraction with isotropic materials. Optics Express, 2014; 22(11): 13547–13554. doi: 10.1364/OE.22.013547.

43. **Kazanskiy NL, Serafimovich PG.** Coupled-resonator optical waveguides for temporal integration of optical signals. Optics Express, 2014; 22(11): 14004–14013. doi: 10.1364/OE.22.014004.

44. **Soifer VA.** Diffractive Nanophotonics and Advanced Information Technologies. Herald of the Russian Academy of Sciences, 2014; 84(1): 9-18. doi: 10.1134/S1019331614010067.

Vibration resistance of headlamp design with light emitting diodes for electric locomotive

Abulkhanov S.R., Skuratov D.L.

Samara State Aerospace University

Abstract. We determined the natural frequencies of the headlight structure with light emitting diodes (LEDs) for electric locomotive (VL series). We used the ANSYS software system of finite-element analysis for computations. The obtained values of the natural frequencies and the oscillation character of the design on every mode made it possible to determine the design activities that increase the vibration resistance of the design of a headlight.

Keywords: a headlight of a locomotive, the natural frequencies of the structure, trouble-free service life, periodic vibration, light-emitting diodes (LEDs).

Introduction

The light emitting diodes (LEDs) have several advantages over incandescent lamps, among them are the reliability (MTBF http://www.google.ru/url?source=transpromo&rs=rssf&q=//translate.google.com/community?source=all – mean time between failures to 1.4 million H). The service life (not less $50 - 103$ hours), the viewing angle ($\phi \subset \left[4^0 - 160^0 \right]$), the brightness (up to 15,000 mcd and above) and the energy efficiency (the energy consumption is reduced to 87 % compared to an incandescent lamp) $[1 - 2]$.

The lighting devices with the LED light sources have a number of disadvantages identified during the operation

[http://trainclub.ru/view_blog/svetodiody_na_zheleznodorozhnom_transporte/]:

— apparent signals appearing due to the reflection of the sunlight or light from a searchlight of a locomotive ("phantoms");
— signals with apparent white dots appearing due to the exposure to the direct sunlight ("washouts");
— to provide the desired light flow in industrial light lamps it is necessary to use a large number of the light-emitting diodes.

These factors indicate that it is impossible to realize all the advantages of the LEDs without considering the peculiarities of their application in a particular industry. So, the lighting devices of general industrial use on the LEDs are not applied, for example, in the rail transport.

For this reason, the research and designs aimed at optimizing the construction of lighting devices using the LED light sources are of great importance. At the same time it should be noted that the Russian railways would like to use the LED lamps as a substitute for the exploited ones, i.e. the existing rail lighting devices have to be modernized as the LED light sources with a minimum number of design changes [http://trainclub.ru/view_blog /svetodiody_na_zheleznodorozhnom_transporte/]. The Railways reflect a global world trend, associated with the modernization of signaling devices used on the railways. For example, the transport administration MTA in New York replaced the light sources in the outdoor traffic lights by the LED light sources, without changing the design of the traffic lights.

Several companies that produce searchlights for a locomotive with the LED light sources are known all over the world, among them are the LEDtronic (Canada), Translight Corp (USA), SBF Spezialleuchten GmbH (Germany) and others. In Russia, the front LED searchlight LPB-01 is designed by the Company SMU "RoSAT" (Armavir) and is produced by the plant-producer "Svetodiod ltd." (St. Petersburg). The powerful original LEDs with the white light serve as the light source. A searchlight LPB-01 has a greater board (the light emitting surface) than a frontal lamp with an incandescent lamp, so as a result, to install it, for example, on the electric locomotive EP1M it's necessary to reconstruct not only a bracket for placing a searchlight in the cab, but also the body of the locomotive cab. This fact increases the cost of modernizing a frontal lamp and does not meet the requirements of the Russian Railways - ensuring a minimum number of the design changes.

A set of regulations with the requirements for locomotive lighting devices is developed with the participation of the Russian Railways. A headlight must provide the nominal axial force of light when achieving the angles of scattering the light beam in the vertical and horizontal planes ~ $3°$ in accordance with Appendix 1 GOST 12.2.056-81. Focusing the searchlight is carried out in this case the following way: a searchlight spaced apart from the screen at 10 m forms a light spot with the diameter of 1000 mm on a flat screen perpendicular to the horizon. The nominal axial force of the light in the center of the light spot should be $6.4 - 9.6 \cdot 10^5$ cd. The light emitting surface of a circular board of the front lamp with LEDs replacing a reflector should have a diameter 370 mm.

When replacing an elliptical reflector and an incandescent lamp in the existing design of a headlight [3] with the board with the LEDs it is possible to preserve the lighting characteristics of a searchlight, without altering the body of a locomotive cab. Simultaneously, the work of a front lamp becomes more reliable, vibration-resistant and economical.

1. The analysis of the lighting characteristics of a searchlight and the LED light sources

A searchlight as a light-signal lighting device redistributes the light flow in a small solid angle.

Its diagram of the angular distribution of the light intensity may differ from its own diagram of the light source. In this connection, it is necessary to estimate the

number and type of the LEDs installed on the board, replacing an incandescent lamp and an elliptical reflector.

The area of a circle, lightened by a headlight, on the shield will be

$$S = \frac{\pi \cdot D^2}{4} = \frac{\pi \cdot (1000)^2}{4} = 785375 \, \text{mm}^2$$

Suppose that the design of a searchlight uses 56 LEDs. In this case, one LED has the area 14024.553 mm2 of the lightened circle on the shield. Since a LED generates the light flow in an axially symmetric solid angle (angle of lightening α), each of the 56 LEDs should lighten a circle of diameter

$$D = \sqrt{\frac{4 \cdot S}{\pi}} = \sqrt{\frac{4 \cdot 14024.553}{\pi}} = 133.63 \quad \text{mm}$$

The indicator LEDs of the brand RL50-WH744D, implemented by "DART Electronics» (http://www.dart.ru/), have a diameter of 5 mm and generate the white light of the brightness (the light intensity) 8000 mcd. We take an angle of lighting α of the LED, equal to 1600. In this case, the light intensity of 8000 mcd fits the light flow:

$$F = I \cdot 2\pi \left(1 - \cos\left(\frac{\alpha}{2}\right)\right) = 8 \cdot 2\pi \left(1 - \cos\left(\frac{160}{2}\right)\right) = 41.537 \quad \text{lm},$$

where F is the light flow (lm), I is the light intensity (cd), α is an angle of lightening (degrees).

For the LED diameter of 5 mm, the distance to the shield of 10 meters and the diameter of the circle lightened by one LED on the board 133 mm the angle of lightening will be α=2·θ 0,73 ^{0}. Here θ is an angle of half brightness.

The redistribution in the space of the light flow generated by a LED, is performed by the selection of elements of the secondary optics, which are intended to create a smooth spot of the exposure with the right diagram of dissipation. Thus, a collimator of the secondary optics is the required structural element of a headlight with the LED light sources. In the case of using the secondary optics for the LEDs developed at IPSI RAS [4 – 16], the generated light flow can be directed practically with no loss in the axial symmetric solid angle of 0.73 0. In this case, the light intensity will be of the amount:

$$I = \frac{F}{2\pi \left(1 - \cos\left(\frac{\alpha}{2}\right)\right)} = \frac{41.537}{2\pi \left(1 - \cos\left(\frac{0.73}{2}\right)\right)} = 325780.392 \quad \text{cd.}$$

For 56 LEDs the power of light on the lighted circle of the shield may be on the axis of symmetry (the interference is not taken into account)

I_Σ=325780 cd·56 = 18243680 cd ≈ 18.245·10^6 cd.

An incandescent lamp SL 5-500, of the power 500-watt used as a light source of a headlight with an elliptical reflector with a diameter of 370 mm [3], generates the light flow of 11100 lm according to the technical certificate.

From the requirements of Annex 1 it can be determined that the angle of lightening α on the shield of the circle with a diameter of 1000 mm is equal to α = 2·θ = 3.6°. The light intensity in this case is equal (for α = 3.6°)

$$I = \frac{F}{2\pi(1 - \cos(\frac{\alpha}{2}))} = \frac{11100}{2\pi(1 - \cos(\frac{3.6}{2}))} = 3533343.9 \quad \text{cd} \approx 3.5 \cdot 10^6 \text{ cd.}$$

The light parameters of an incandescent lamp and the LEDs, as well as the requirements to the light source, regulated by GOST 12.2.056-81 are summarized in Table 1.

Table 1. The lighting characteristics of different light sources

№	Type of light source	Power, W	Amount	Light without optics, lx	Used optics	Angle of light, formed by optics	Light intensity, cd
1	Incandescent lamp, SL 5-500	500	1	11100	Elliptical reflector with diameter 370 mm	0.73^0	$3.5 \cdot 10^6$
2	Signal LED, brand RL50-WH744D	0.06	56	41.537	Secondary optics (collimator) [4 − 16]	3.6^0	$18.245 \cdot 10^6$
3	The intensity of light recommended in Appendix GOST 12.2.056-81. «The System of standards of labor safety. Electric and diesel locomotives of track 1520 mm»					$6.4 − 9.6 \cdot 10^5$	

The table shows that in order to achieve the light intensity required by the regulatory documents it is possible to use a smaller number of the LEDs or (and) a collimator [4 − 16] of a greater angle of lighting, that is $\alpha = 2 \cdot \theta > 0.73°$.

The heat is produced in the semiconductor junction of the crystal LED, and the high-power LEDs have the magnitude of the heat, that is sufficient to change the characteristics of the LED light source. The installing armature of the LED made of materials with the high thermal conductivity (typically aluminum alloy) is made for the effective heat dissipation of the LED. The thermal deformation of the structure of the lighting device is capable of changing the diagram of the angular distribution of the light intensity generated by the LEDs. Using the design of a searchlight of a locomotive as light sources indicating LEDs, we can ignore the thermal deformation of the board with the LEDs.

To ensure the required diagram of the angular distribution of the light intensity, we use the matrix (block) system of the light sources arranged on the board (the light emitting surface) of a searchlight in accordance with the interstate standards "Occupational safety of labor standards system. Electric and diesel locomotives with the rail track of 1520 mm. Safety requirements." From the technological considerations the placement of the LEDs on the board evenly on the coaxial circles is most appropriate. The radii of the adjacent circles differ in one value.

As an original model of a headlight of a locomotive weighing 17.438 kg, a model of a searchlight with an incandescent lamp and an elliptical reflector is used [3], in which a reflector and the installing armature of an incandescent lamp have been removed, and instead, a disk, made of the aluminum alloy D16T of the thickness of 3 mm and a diameter 370 mm, is installed, on which the LEDs are installed (Fig. 1).

Two lugs made of aluminum alloy D16T are welded on the disk. As the LED light source a model of the LED SMD 3528-W produced by the firm CIVILIGHT (Taiwan) is used (Fig. 2), generating the white light and is analogous to the indicator LED of the brand RL50-WH744D, the characteristics of which are used in the calculations. An LED 1 is installed in the special armature, consisting of an aluminum base 2, which is installed in a ceramic conductor 3, centering the lens of the secondary optics 4 (Fig. 2).
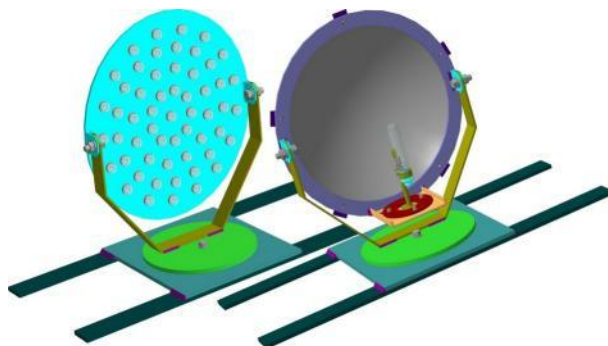
Fig. 1. – A headlight of a locomotive with the LED light sources and with an incandescent lamp.
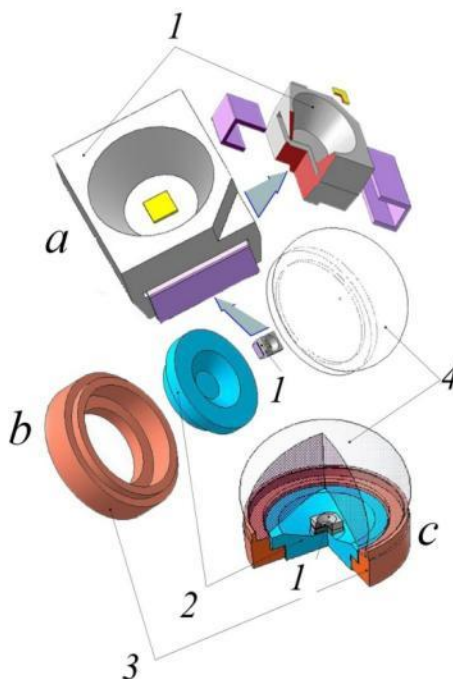
Fig. 2. – The LED light source: a - the design of the LED; b – the armature of the LED construction; c - the assembly of the structure of the LED light source.

2. The vibration resistance of the modernized design of a searchlight

The modification of the design of a searchlight results in changing the natural frequencies of the lighting device, the values of which can lead to the resonance of the whole structure during the operation of a railway locomotive [17 – 19]. For this reason, it is necessary first to determine the natural frequencies of the modified design

of a searchlight and, if necessary, to provide measures that increase the vibration resistance of the design of a locomotive frontal lamp.

Table 2 summarizes the weights and elastic characteristics of the elements of a searchlight, removed from the construction, and the elements included in the design. Table 2 shows that the weight of the structure of the modernized searchlight is 18.725 kg, i. e. it increased by 1.287 kg or 7.4 %. This fact indicates the possibility of optimizing the design of the board, that can be performed with the holes making it easier and optimizing the number of LEDs. The control of the weight of a searchlight allows you to change the natural frequency of its design, and thus to influence the vibration resistance of a headlight.

To determine the natural frequencies of the modernized design of a searchlight we use the software that runs on the platform of ANSYS Workbench.

The model does not take into account the threaded connections used in the actual design. Fig. 3 shows the layout of a model into finite elements.
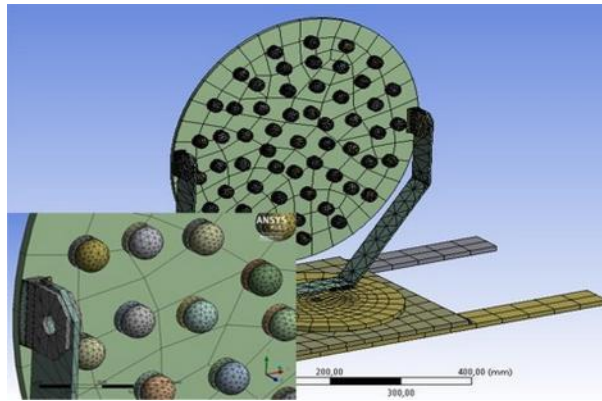
Fig. 3. – The layout of the model of a front lamp with the LED light sources.

Fig. 3 shows the deformation of the design of a searchlight on the first six natural frequencies of the design. Fig. 4 shows that the aluminum board experiences the significant deformation at different frequencies, which may occur during the movement of the locomotive [18]. In addition, the posts supporting the board, is also experiencing the considerable deformation. Both of these circumstances indicate that the design of the board and post should be reinforced with the gussets and rigidity edges, such as in Fig. 5. The weight of the design of a searchlight should not be increased in comparison with the front lamp with an incandescent lamp as the light source. In addition to the full range of vibration frequencies that can occur when operating a railway locomotive [18], a searchlight has to ensure the creation of a stable smooth spot of the exposure with the right diagram of scattering. Solving such complex problems is only possible in case of the construction of a parametric model of a head-lamp, establishing the criteria of the optimization of a model and its geometry parameters in the software environment of ANSYS.
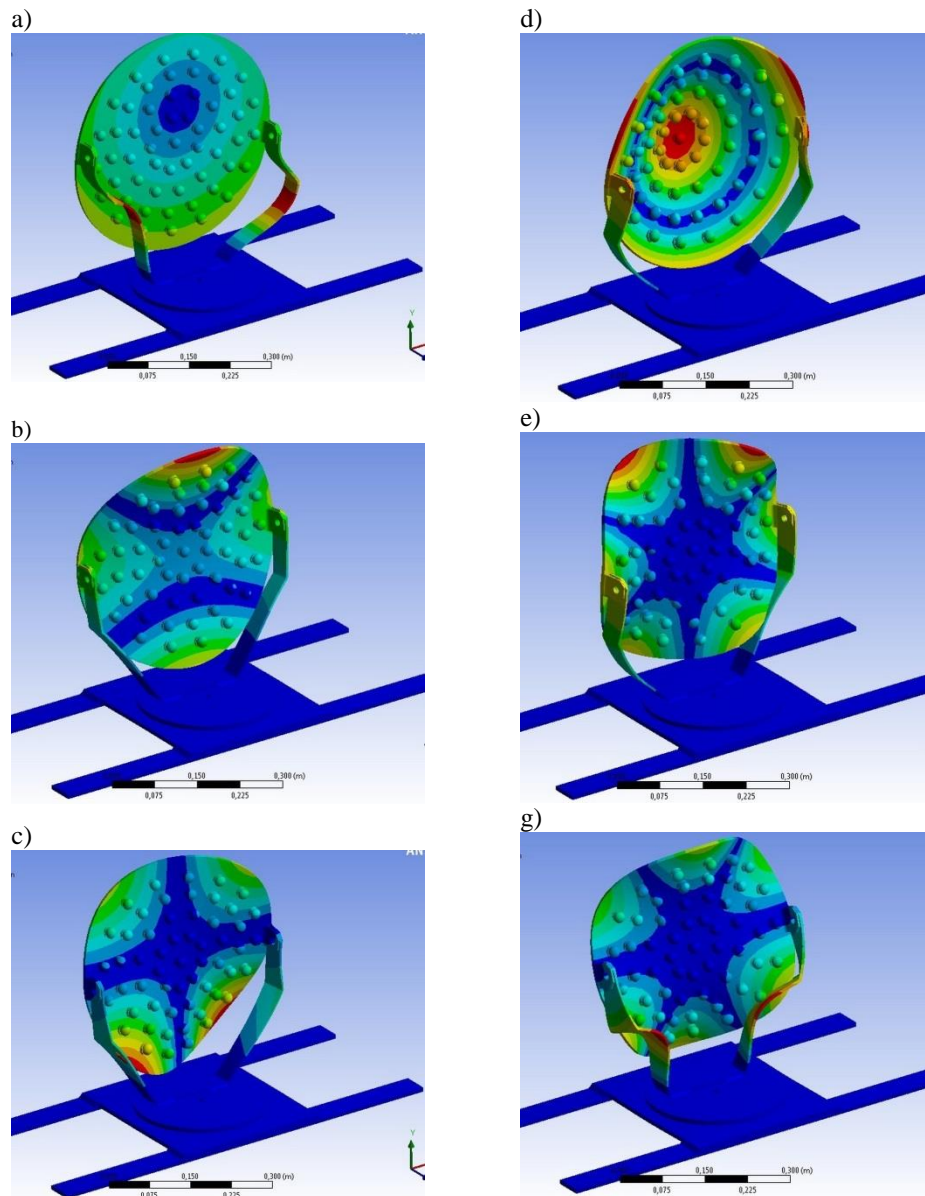
Fig. 4. – The deformations of the design of a headlight with the LED light sources in various modes: a) $f = 202.43$ Hz; b) $f = 231.22$ Hz; c) $f = 292.39$ Hz; d) $f = 202.43$ Hz; e) $f = 393.42$ Hz; g) $f = 439.08$ Hz
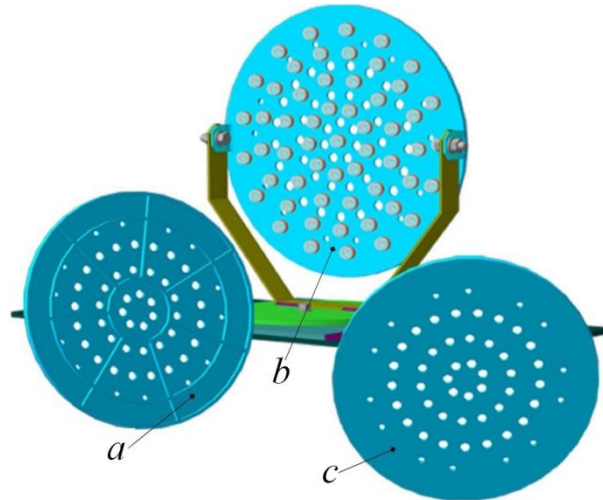
Fig. 5. – The design of the board for the LEDs: a - a rear view of the board; b – the assembly of a searchlight with the modernized board; c - full face of the board

Table 2. Weight and elastic characteristics of the elements of the headlight design

№	Part Name	Amount	Material	Weight of a unit, kg	volume of a unit, 10^{-6} m^3	Total Weight, kg
Components of a searchlight with an incandescent lamp, removed from the construction						
1	Reflector	1	glass	0.603	270.279	0.603
2	E / Lamp	1	-*	0.105	78.242	0.105
3	E / Lamp socket	1	Carbolite*	0.032	7.485	0.032
4	Post	1	St. 20G	0.969	123.967	0.969
5	Lug	2		0.077	9.869	0.154
6	Flange	1		0.172	219.757	0.172
7	Plank	1		0.552	70.646	0.552
8	Bolt shaped	1		0.178	22.711	0.178
9	Disk	1		0.212	27.148	0.212
10	Base	1		6.189	791.371	6.189
11	Strip	2		2.502	320.0	5.005
12	Holder	5		0.017	2.202	0.086
13	Brackets	2		0.019	2.372	0.037
14	Rubber gasket	5	C/rubber	≤ 0.005	4.058	≤ 0.026
15	Weld	-	St. 60C2A; 65C2BA	2.566	330.457	2.566
New and modernized components of the design of a searchlight						
1	Flange (h = 3 mm)	1	D16T	2.303	831.265	2.303
2	Lug	2	D16T	0.027	9.869	0.054
3	Diffuser (of secondary optics)	57	Plexiglas or polymethyl methacrylate	0.012	2.715	0.684
4	Contact plate	114	Copper	0.8×10^{-5}	≈ 0.001	10^{-3}
5	Light-emitting plate		Alumina (Al$_2$O$_3$) and alumino-nitride (AlN) ceramics	0.02×10^{-5}	0.0005	≈ 10^{-5}
6	LED housing	57		0.41×10^{-5}	0.011	0.2×10^{-3}
7	Conductor of LED light source			3.5×10^{-3}	0.536	0.2
8	Base of LED light source		D16T	0.004×10^{-3}	1.273	0.257

Conclusions:

1. The indicator LEDs can be used in the headlight of a locomotive to provide the required lighting characteristics.
2. The indicator LEDs should be equipped with the original secondary optics.
3. The construction of a headlight with the LED light source should include the design activities, raising its vibration resistance.
4. It is possible to optimize the design of a headlight, taking into account all the regulatory requirements only if there is a parametric model.
5. The presented results play an important role in the design [20−25] of hyperspectral remote sensing equipment feeling strong vibrations loads in the derivation of Earth's orbit. Also, these results will be useful for creating transport systems of computer vision [26−29], optical devices [30−33], components, and devices of diffractive nanophotonics [34−40].

References

1. **Moiseev MA, Doskolovich LL, Kazanskiy NL.** Design of high-efficient freeform LED lens for illumination of elongated rectangular regions. Optics Express, 2011; 19(S3): A225-233.
2. **Aslanov ER, Doskolovich LL, Moiseev MA, Bezus EA, Kazanskiy NL.** Design of an optical element forming an axial line segment for efficient LED lighting systems. Optics Express, 2013; 21(23): 28651-28656.
3. **Abulkhanov SR.** Construction of authentic 3-D model of head-lamp of electric locomotive VL series. Vestnik Samara State University of Communications, 2012; 3(17): 81-86. [in Russian]
4. **Golub MA, Kazanskii NL, Sisakyan IN, Soifer VA.** Computational experiment with plane optical elements. Optoelectronics, Instrumentation and Data Processing, 1988; 1: 78-89.
5. **Golub MA, Kazanskii NL, Sisakyan IN, Soifer VA, Kharitonov SI.** Diffraction calculation for an optical element which focuses into a ring. Optoelectronics, Instrumentation and Data Processing, 1987; 6: 7-14.
6. **Kazanskiy NL, Kotlyar VV, Soifer VA.** Computer-aided design of diffractive optical elements. Optical Engineering, 1994; 33(10): 3156-3166.
7. **Kazanskiy NL, Soifer VA.** Diffraction investigation of geometric-optical focusators into segment. Optik International Journal for Light and Electron Optics, 1994; 96(4): 158-162.
8. **Doskolovich LL, Kazansky NL, Kharitonov SI, Soifer VA.** A method of designing diffractive optical elements focusing into plane areas. Journal of Modern Optics, 1996; 43(7): 1423-1433.
9. **Doskolovich LL, Kazanskiy NL, Bernard S.** Designing a mirror to form a line-shaped directivity diagram. Journal of Modern Optics, 2007; 54(4): 589-597.
10. **Doskolovich LL, Kazanskiy NL, Soifer VA, Kharitonov SI, Perlo P.** A DOE to form a line-shaped directivity diagram. Journal of Modern Optics, 2004; 51(13): 1999-2005.
11. **Doskolovich LL, Kazanskiy NL, Soifer VA, Perlo P, Repetto P.** Design of DOEs for wavelength division and focusing. Journal of Modern Optics, 2005; 52(6): 917-926. doi:10.1080/09500340512331313953.
12. **Doskolovich LL, Golub MA, Kazanskiy NL, Khramov AG, Pavelyev VS, Seraphimovich PG, Soifer VA, Volotovskiy SG.** Software on diffractive optics and computer generated holograms. Proceedings of SPIE, 1995; 2363: 278-284.

13. **Doskolovich LL, Kazanskiy NL, Soifer VA, Tzaregorodtzev AYe.** Analysis of quasiperiodic and geometric optical solutions of the problem of focusing into an axial segment. Optik - International Journal for Light and Electron Optics, 1995; 101(2): 37-41.

14. **Khonina SN, Kazanskiy NL, Volotovsky SG.** Influence of Vortex Transmission Phase Function on Intensity Distribution in the Focal Area of High-Aperture Focusing System. Optical Memory and Neural Networks (Information Optics), 2011; 20(1): 23–42. doi: 10.3103/S1060992X11010024.

15. **Golovashkin DL, Kasanskiy NL.** Solving Diffractive Optics Problem using Graphics Processing Units. Optical Memory and Neural Networks (Information Optics), 2011; 20(2): 85–89. doi: 10.3103/S1060992X11020019.

16. **Kazanskiy NL.** Research & Education Center of Diffractive Optics. Proceedings of SPIE, 2012; 8410: 84100R. doi:10.1117/12.923233.

17. **Kazanskiy N, Skidanov R.** Binary beam splitter. Applied Optics, 2012; 51(14): 2672-2677. doi: 10.1364/AO.51.002672.

18. **Doskolovich LL, Dmitriev AYu, Moiseev MA, Kazanskiy NL.** Analytical design of refractive optical elements generating one-parameter intensity distributions. J. Opt. Soc. Am. A, 2014; 31(11): 2538–2544. doi: 10.1364/JOSAA.31.002538.

19. **Abulkhanov SR, Gorjainov DS, Skuratov DL.** Optimization of strength characteristics of aircraft lighting devices by building their virtual models. Bulletin of Samara State Aerospace University, 2012; 5(36). Part 1: 72-78. [in Russian]

20. **Abulkhanov SR, Lopatin EV.** Vibration resistance of design of frontal lamp of electric locomotive VL series. Bulletin of Volga Transport, 2013; 6(42): 30-36. [in Russian]

21. **Karpeev SV, Pavelyev VS, Khonina SN, Kazanskiy NL, Gavrilov AV, Eropolov VA.** Fibre sensors based on transverse mode selection. Journal of Modern Optics, 2007; 54(6): 833-844. doi: 10.1080/09500340601066125.

22. **Kazanskiy NL, Kharitonov SI, Khonina SN, Volotovskiy SG, Strelkov YuS.** Simulation of hyperspectrometer on spectral linear variable filters. Computer Optics, 2014; 38(2): 256-270. [in Russian]

23. **Kazanskiy NL, Kharitonov SI, Karsakov AV, Khonina SN.** Modeling action of a hyperspectrometer based on the Offner scheme within geometric optics. Computer Optics, 2014; 38(2): 271-280. [in Russian]

24. **Kazanskiy NL, Kharitonov SI, Khonina SN.** Simulation of a hyperspectrometer based on linear spectral filters using vector Bessel beams. Computer Optics, 2014; 38(4): 770-776. [in Russian]

25. **Kazanskiy NL, Kharitonov SI, Doskolovich LL, Pavelyev AV.** Modeling the performance of a spaceborne hyperspectrometer based on the Offner scheme. Computer Optics, 2015; 39(1): 70-76. [in Russian]

26. **Kazanskiy NL, Popov SB.** Machine Vision System for Singularity Detection in Monitoring the Long Process. Optical Memory and Neural Networks (Information Optics), 2010; 19(1): 23-30. doi:10.3103/S1060992X10010042.

27. **Kazanskiy NL, Popov SB.** The distributed vision system of the registration of the railway train. Computer Optics, 2012; 36(3): 419-428. [in Russian]

28. **Kazanskii NL, Khonina SN, Skidanov RV, Morozov AA, Kharitonov SI, Volotovskiy SG.** Formation of images using multilevel diffractive lens. Computer Optics, 2014; 38(3): 425-434. [in Russian]

29. **Kazanskiy NL, Popov SB.** Integrated Design Technology for Computer Vision Systems in Railway Transportation. Pattern Recognition and Image Analysis, 2015; 25(2): 215-219. doi: 10.1134/S1054661815020133.

30. **Khonina SN, Kazanskii NL, Ustinov AV, Volotovskii SG.** The lensacon: nonparaxial effects. Journal of Optical Technology, 2011; 78(11): 724-729. doi: 10.1364/JOT.78.000724.

31. **Doskolovich LL, Kazanskiy NL, Khonina SN, Skidanov RV, Heikkila N, Siitonen S, Turunen J.** Design and investigation of color separation diffraction gratings. Applied Optics, 2007; 46(15): 2825-2830.

32. **Borodin SA, Volkov AV, Kazanskii NL.** Device for analyzing nanoroughness and contamination on a substrate from the dynamic state of a liquid drop deposited on its surface. Journal of Optical Technology, 2009; 767: 408-412.

33. **Khonina SN, Savelyev DA, Kazanskiy NL.** Vortex phase elements as detectors of polarization state. Optics Express, 2015; 23(14): 17845-17859. doi: 10.1364/OE.23.017845.

34. **Kazanskiy NL, Serafimovich PG, Khonina SN.** Harnessing the Guided-Mode Resonance to Design Nanooptical Transmission Spectral Filters. Optical Memory and Neural Networks (Information Optics), 2010; 19(4): 318-324. doi: 10.3103/S1060992X10040090.

35. **Bezus EA, Doskolovich LL, Kazanskiy NL.** Scattering suppression in plasmonic optics using a simple two-layer dielectric structure. Applied Physics Letters, 2011; 98(22): 221108. doi: 10.1063/1.3597620.

36. **Bezus EA, Doskolovich LL, Kazanskiy NL, Soifer VA.** Scattering in elements of plasmon optics suppressed by two-layer dielectric structures. Technical Physics Letters, 2011; 37(12): 1091-1095.

37. **Kazanskiy NL, Serafimovich PG, Khonina SN.** Use of photonic crystal cavities for temporal differentiation of optical signals. Optics Letters, 2013; 38(7): 1149-1151.

38. **Kazanskiy NL, Serafimovich PG.** Cloud Computing for Nanophotonic Simulations. Lecture Notes in Computer Science, 2013; 7715: 54-67.

39. **Bezus EA, Doskolovich LL, Kazanskiy NL.** Low-scattering surface plasmon refraction with isotropic materials. Optics Express, 2014; 22(11): 13547-13554. doi: 10.1364/OE.22.013547.

40. **Kazanskiy NL, Serafimovich PG.** Coupled-resonator optical wave-guides for temporal integration of optical signals. Optics Express, 2014; 22(11): 14004–14013. doi: 10.1364/OE.22.014004.

Correction of parameters of fiber-optical systems on the basis of the magneto tunable gradient elements

Leonovich G.I.,

Samara State Aerospace University

Karpeev S.V.,

Samara State Aerospace University
Institute of Image Processing Systems, Russian Academy of Sciences

Paranin V.D.

Samara State Aerospace University

Abstract. A method of controlling optical parameters of elements and structures formed inside step-index and gradient optic fibers on the basis of external magnetostrictive impact on physical and geometric parameters of light guides is proposed in the paper. The control is accomplished by the impact of a 3D-magnetic actuator on the magnetosensitive thin-film coating of optic fiber.

Keywords: gradient optic fibers, 3D-magnetic actuator, thin-film coating of optic fiber.

1. Introduction

The latest achievements in the area of fiber-optic technologies are widely used today to form high-speed stable data links [1] and intelligent sensor-based systems [2].

When high-speed fiber-optic data links are formed the impact of temperature and mechanical strain [3, 4] on the refracting index, ellipticity and length of optic fiber (OF) in the process of cabling should be taken into account and controlled. To avoid mechanical tension and strain of OF special cable structures are used for instance, wavy profile structures or those with modular stranding. Nevertheless, thermal effect still leads to local deformation of OF in all structures. As a result, the speed of information transfer may decrease by a factor of two or more. Additional noise, attenuation, modal dispersion [1, 5] and crosstalk appear in the cable, which also has a negative impact on the range and quality of communication, including that in the case

of information transfer from fiber-optic sensors [2]. Methods of controlling these phenomena focused on the use of mode filtration [5-10] are known, but those are rather complex and expensive technologies. The use of optic vortices to transmit information along fiber light guides [11, 12] or dispersion-free beams [13] is another way of correcting distortion, but these methods do not allow transmitting information to considerable distances.

Therefore, the search and application of efficient measures of on-line control of OF incorporated in fiber-optic systems, quick trimming and correction of parameter distortion caused by the impact of operational factors remain a pressing challenge that is not entirely solved today.

2. Physical foundations of the proposed solution

The method proposed is based on the combination of the force field forming unit with OF incorporated in its body and an optional sensitive film coating. This device represents a 3D-actuator for the variation of geometrical and related physical and optical OF parameters.

The actuator can be realized in the versions of control by temperature and direct mechanical impact, as well as indirect impact of force magnetic and/or electric field. From the point of view of energy costs, dynamic characteristics, hysteresis phenomena, dependence of the impact on the distance and possibility of constructing systems with fixed parameters control by the external magnetic field is the preferable option.

The main OF optical parameters in the context of the actuator's functional area are the distribution of the refracting index that determines the OF optical properties and the optical path length.

The effects of a control system based on a 3D-magnetic actuator (3DMA) realized within the limits of mechanical strain admissible for a specific type of OF are:

— general and local control of the OF optical path length;
— general and local control of the OF refracting index distribution;
— control of OF anisotropic properties, including ellipticity and birefringence;
— creation of simple and complex gradient structures with constant and variable refraction parameters;
— control of the spatial position of fiber ends and local areas of OF;
— control of intrafibrous Bragg grating parameters.

3. Realizable aspects of the proposed technology

Versions of structural arrangement of the control system for different formats and position of controlled elements are presented in fig. 1 and 2. The gradient magnetic field forming unit is responsible for the formation of a structure with OF local axial and radial non-uniformities (fig. 1). In the general case the unit contains a group of N operating solenoids and M permanent magnets wherein the appropriate OF areas with a magnetostrictive coating act as armature or magnets interacting with it. It is possible to use materials possessing magnetostrictive properties the use of which in many applications is limited by low sensitivity to the impinging magnetic field. A polymer

coating is used to produce microdisplacements of areas of optic fiber and permanent magnets are mounted on it.
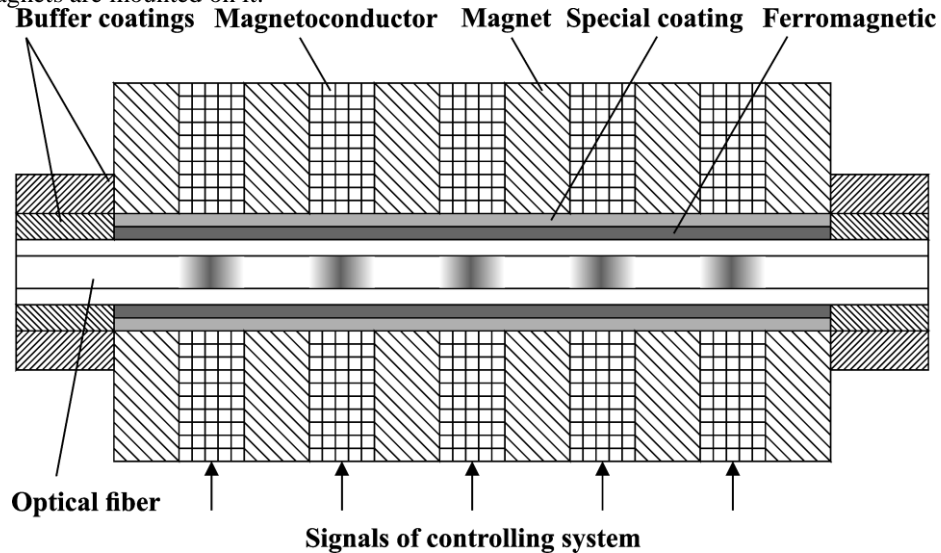
Fig. 1. – Scheme of a multiple module localized system for controlling the properties of an OF area

Fig. 2 presents a structure based on a set of actuators spaced along the OF length on permanent magnets with the function of fixed axial and radial local-integral extension and compression. It is intended to form a gradient structure in an OF specimen.
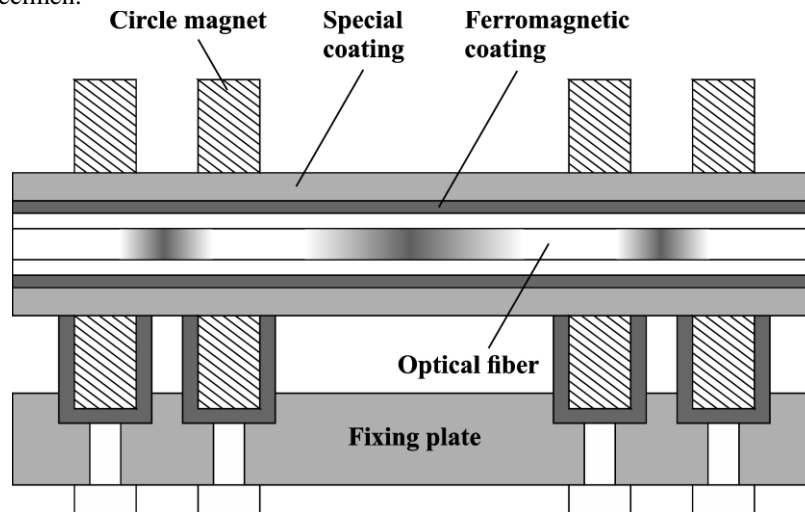
Fig. 2. – Scheme a fixed in-fiber optical structure based on a set of permanent magnet actuators spaced along the OF length

Local axial compression and extension in a device of this kind takes place due to the interaction of fixed or shifting permanent magnets. Local axial compression takes place in the OF area between permanent annular magnets 2 (+) and 3 (-), while local axial extension takes place in the area between the magnets 1 (-) and 2 (-), 3(+) and 4 (+). Axial and radial compression and extension is also caused by the interaction of annular and other magnets with a magnetosensitive coating deposited on the OF. The choice of the arrangement, material, selection and arrangement of the magnets are also determined by calculation according to the results of mathematic simulation.

The structures presented as examples can be used both for connected step-index profile OFs and for those with gradient variation of the refracting index.

There are two lines of possible usage for step-index profile OFs: first, to control OF parameters essential for the formation of high-speed data links- the refracting index, anisotropic and other properties mentioned above, and, second, to implement a new principle of creating a gradient structure in a step-index OF. In the case of radial extension or compression realized by the described actuator structure variation of the refracting index of the OF material is approximately proportional to the square of the radius. Consequently, this variation is expected to result in the origination of lenslike gradient medium, that is, in the formation of a new optical element- a gradient lens with a tuning option. A positive lens is formed in the case of radial extension and a negative one in the case of compression.

If OF with gradient variation of the refracting index is used the control of the external magnetic field takes place in the form of tuning or correction of the parameters of the available lenslike medium.

4. Conclusion

The prospects of the implementation of the proposed approach arise from the following factors:

- the possibility of creating a wide range of hybrid-gradient intrafibrous structures that combine the properties of controlled gradient OF medium and the properties of refractive, diffractive and nonlinear-optical elements (gradient lenses, integral-optic, phase and amplitude phase structures);
- the use of the mastered technologies of producing basic components (optical fiber, magnet actuators for microdisplacement of objects);
- the use of simple production equipment and unified techniques to produce elements;
- the simplicity of elements assembly and operation;
- high reliability of the components, resistance to external destabilizing factors.

References

1. **Kutluyarov RV, Sultanov AH, Bagmanov VH.** Reduction of WDM-transmission nonlinear impairments due to polarization mode dispersion. Computer Optics, 2014; 38(4): 737-742.

2. **Karpeev SV, Pavelyev VS, Khonina SN, Kazanskiy NL, Gavrilov AV, Eropolov VA.** Fiber sensors based on transverse mode selection. Journal of Modern Optics, 2007; 54(6): 833-844.

3. **Garitchev VP, Golub MA, Karpeev SV, Krivoshlykov SG, Petrov NI, Sissakian IN, Soifer VA, Haubenreisser W, Jahn JU, Willsch R.** Experimental investigation of mode coupling in a multimode graded-index fiber, caused by periodic microbends using computer-generated spatial filters. Optics Communication, 1985; 55(6): 403-405.

4. **Karpeev SV, Pavelyev VS, Khonina SN.** Investigation of dependence of mode intensity at the exit of the step-index optical fiber from its deformation. Computer Optics, 2003; 25: 95-99. [in Russian]

5. **Lyubopytov VS, Tlyavlin AZ, Sultanov AKh, Bagmanov VKh, Khonina SN, Karpeev SV, Kazanskiy NL.** Mathematical model of completely optical system for detection of mode propagation parameters in an optical fiber with few-mode operation for adaptive compensation of mode coupling. Computer Optics, 2013; 37(3): 352-359.

6. **Golub MA, Kazanskiy NL, Sissakian IN,Soifer VA, Karpeev SV, Mirzov AV,Uvarov GV.** Spatial phase filters matched to transver modes. Quantum Electronics, 1988; 18(3): 392-393.

7. **Karpeev SV, Pavelyev VS, Duparre M, Luedge B, Rockstuhl C, Schroeter S.** DOE-aided analysis and generation of transverse coherent light modes in a stepped-index optical fiber. Optical Memory and Neural Networks (Information Optics), 2003; 12(1): 27-34.

8. **Golub MA, Karpeev SV, Krivoshlykov SG, Prokhorov AM, Sisakyan IN, Soifer VA.** Spatial filter investigation of the distribution of power between transverse modes in a fiber waveguide. Quantum Electronics, 1984; 11(9): 1869-1871.

9. **Garitchev VP, Golub MA, Karpeev SV, Krivoshlykov SG, Sissakian IN, Soifer VA, Uvarov GV.** Application of the synthesized holograms for selective excitement of gradient optical fiber modes and investigation of their sensitivity to radial shift of an exciting bunch. Computer Optics, 1988; 3: 103-109. [in Russian]

10. **Karpeev SV, Pavelyev VS, Duparre M, Ludge B, Schroeter S.** Mode excitement of a step-index waveguide by means of binary phase DOE. Computer Optics, 2002; 24: 99-101. [in Russian]

11. **Karpeev SV, Khonina SN.** Experimental excitation and detection of angular harmonics in a step-index optical fiber. Optical Memory & Neural Networks (Information Optics), 2007; 16(4): 295-300. [in Russian]

12. **Khonina SN, Karpeev SV.** Excitation and detecting angular harmonics in fiber waveguide using DOE. Computer Optics, 2004; 26: 16-26. [in Russian]

13. **Borodin SA, Volkov AV, Kazanskiy NL, Pavelyev VS, Karpeev SV, Palagushkin AN, Prokopenko SA, Sergeev AP, Arlamenkov AN.** Numerical and experimental study of the dispersion-free multimode beams formed by means of DOE. Computer Optics, 2005; 27: 41-44. [in Russian]

Analysis of activity of the scientific journal *Computer Optics*

Kolomiets E.I.

Samara State Aerospace University

Abstract. The author analyzes the significance of the journal *Computer Optics* for the development of science in Russia. A particular attention is given to research areas covered and journal publications that attracted a special interest of the research community in the fields of diffractive optics and nanophotonics, optical information technology, pattern recognition, and image processing. The author gives credit to the efforts of the editorial staff that contributed to the Journal success and outlines prospects of the journal development.

Introduction

This year we celebrate the 40th anniversary of the Computer Science Faculty of Samara State Aerospace University (National Research University) (SSAU) and the 70th anniversary of the chief editor of the scientific journal *Computer Optics* Professor V.A. Soifer. *Computer Optics* is published jointly by the Image Processing Systems Institute of the RAS (IPSI RAS, scientific lieder of IPSI RAS is Prof. V.A. Soifer) and Computer Science Faculty of SSAU. This is a good occasion to look back at the journal accomplishments and give credit to the editorial staff for essential efforts they have contributed to the Journal success.

1. Background and prerequisites

Fundamental research findings jointly made at the turn of the 60-70s of the last century by the research teams from Moscow and Kuibyshev (presently Samara) headed by academician A.M. Prokhorov, professor I.N. Sisakyan, and professor V.A. Soifer enabled the design of new classes of optical elements [1 – 6], making it possible to address problems going beyond the scope of classical optics. The novel optical elements were given the name diffractive optical elements (DOEs), with elements intended for performing specific tasks termed as laser light focusators [1 –

3], modans [4], Bessel-optics elements [5], compensators/equalizers [6], and so on. Some of the above-listed terms, e.g. the term focusator proposed by academician A.M. Prokhorov, have been adopted not only in Russia but also internationally [7 – 10]. As the research community embraced the significance of the new findings, it became evident that we witness the emergence of a new field of research at the interface of information technology, laser physics, optics, and microelectronics, having become known as Diffractive Computer Optics. Thus, a demand arose for a scientific periodical that would promptly peer-review and publish articles dealing with the new, rapidly developing area. In May 1986, the decision of the kickoff meeting on *Computer Optics* (the city of Zvenigorod) to start the publication of a new journal was approved by the Russian science leadership. In 1987, the first issue of the international scientific collection *Computer Optics* with a subtitle Physical Principles was published.

Fig. 1. – Academician Alexander Mikhailovich Prokhorov (1916-2002)

2. Kick-start beginning

Among the co-founders of *Computer Optics*, there were the International Center for Scientific and Technical Information (ICSTI), Institute of General Physics of the USSR Academy of Sciences, Institute of Information Transmission Problems of the USSR Academy of Science, with the ICSTI also acting as a publisher. The publication was funded as part of the information support of the complex program of scientific and technical progress of member-states of the Council for Mutual Economic Assistance (CMEA). In the initial years, the collection of papers *Computer Optics* was edited by academicians Ye.P. Velikhov and A.M. Prokhorov. The first issues were compiled by I.N. Sisakyan, V.A. Soifer, R.V. Matveeva, S.A. Orekhov, A.M. Kostin, and V.A. Danilov, with the essential contribution made by scientists of Kuibyshev Aviation Institute (presently, SSAU).

In the Foreword to the very first issue, academician Ye.P. Velikhov, in particular, wrote [11], 'Truly revolutionary has been the role played by the computer in designing totally new classes of optical elements like light focusators, wavefront correctors, modal content analyzers, to name just a few. In computer optics, the computer serves a wide variety of functions from solving the inverse problem of diffraction and conducting numerical simulations to numerically controlling the automated machinery, interpreting and visualizing the experimental data, designing elements with optimal characteristics, to developing databanks, and so on'. The following words by Ye.P. Velikhov have recently become particularly relevant, '…computer optics is not just computers in optics, but optics in computers as well. A number of optical elements intended for information processing and capable of addressing a broad range of interesting problems have been already designed'. Actually, advanced components for diffractive nanophotonics, such as resonant diffraction gratings [12 – 14], nanocavities [15 – 18], and other devices [19] are able to perform analog operations of the differentiation and integration of optical signals and, when combined with diffractive optics elements such as beam splitters [20] and multi-purpose DOEs [21 – 22], form a basis for the development of analog optical computers [19]. Taking a retrospective view at the progress made on the way from the first diffraction grating to diffractive optics elements, Nobel Prize laureate A.M. Prokhorov noted [23], 'Flat optics took a drastic turn, essentially resulting in the advent of a new field of diffractive optics, when focusators of laser light were designed in 1980. The very first focusator was created jointly by researchers of the Institute of General Physics of the USSR Academy of Sciences and Kuibyshev Aviation Institute. Before long, mathematicians from the Moscow University became actively involved in the work. Over a short time span of less than 10 years, a variety of diffractive optics elements were designed and diffractive optics was formed as a new research area …'

Great contribution to the creation of initial issues of Computer Optics collection was made by Professor Iosif Norairovich Sisakyan [24]. In particular, the article entitled 'Computer Optics. Achievements and Challenges' written jointly by I.N. Sisakyan and V.A. Soifer [25] became a hit publication of the first issue, having determined the vector of development in the field for decades to come. Among the contributors to the first issue, there were leading soviet researchers active in computer optics in those years, such as A.M. Prokhorov, M.A. Golub, G.I. Greysukh, A.V. Goncharskiy, V.A. Danilov, N.L. Kazanskiy, B.E. Kinber, D.D. Klovsky, S.G. Kryvoshlykov, V.V. Popov, S.A. Stepanov, A.B. Shvartzburg, S.M. Shirokov, and others. A number of publications included in the first issue opened up new directions of computer/diffractive optics. For instance, synthesis of optical elements and systems intended to generate desired radiation directivity diagrams [26] has led to the design of various lighting devices which were proposed both in *Computer Optics* [27 – 31] and in leading international scientific journals [32 – 35]. Diffraction analysis of the focusing elements by means of numerical simulation [36] went on to be actively developed in follow-up publications [37 – 45]. Great interest was attracted by an article reporting on techniques for focusators design [46]. In the follow-up research, those techniques were essentially improved and extended onto new focal regions of interest [47 – 52]. An important research area concerned with generating a

diffraction microrelief of optical elements was first proposed in Ref. [53] and was further developed in numerous publications in Russian [54 – 60] and foreign [61 – 63] Editions.

The first issue of *Computer Optics* became internationally recognized, having attracted interest from "Pergamon Press" that published two volumes of the journal in English in the years 1989–1990 (Vol. 1, N 1, 1989; Vol. 2, N 1 & N 2, 1990) with world-wide distribution (with cities like Oxford, New York, Beijing, Frankfurt, San Paolo, Sidney, Tokyo, Toronto indicated on the journal cover). Volume I in English was compiled on the basis of the first Russian issue, and Volume II included papers from Russian issues 3 and 4.

Following I.N. Sisakyan's appointment to the position of director of Central Design Bureau of Unique Instrumentation (CDB UI) of the USSR Academy of Sciences, the list of co-founders changed. Since 1988 (issues 3 – 9), the ICSTI and the CDB UI of the USSR Academy of Sciences acted as the collection's co-founders. Especially noteworthy in issue 3 is a paper [64] devoted to the technological applications of focusators, which laid the basis for a new direction of diffractive optics that was thriving in the subsequent years [65 – 68]. This research topic was among others which allow a group of SSAU researchers (V.A. Soifer, V.P. Shorin, V.A. Barvinok, V.I. Mordasov, V.I. Bogdanovich and A.G. Zidulko) jointly with I.N. Sisakyan to receive the RF State Prize for outstanding achievements in science and technology in 1992.

Fig. 2. – Professor Iosif Norairovich Sisakyan (1938-1995)

3. Help from Samara

Collapse of the USSR followed by the disintegration of the CMA, temporarily brought the publication of *Computer Optics* to stop in 1992, which was associated with the termination of the Complex program of scientific & technical progress of the CMA member-states. Being the RAS establishment, the CDB UI was run on the self-financing basis, not having a financing from the state budget. With the collapse of the Soviet Union, the contract-based financing of scientific research was drastically decreased. In those circumstances, in 1992 the research group headed by Prof. V.A. Soifer had to take care of the financial back-up of the publication, with the SSAU having become a third cosponsor of the collection. 1992 saw the publication of a twin issue 10-11 and issue 12, with issue 13 published in 1993. Unfortunately, since those years were marked by the growth of publication and distribution costs significantly exceeding the financing of scientific research, Computer Optics was not published in 1994.

However, in 1995, thanks to the assistance of academician N.A. Kuznetsov, director of Institute for Information Transmission Problems of the Russian Academy of Sciences (IITP of the RAS), and Dr. N.S. Merzlyakov, the head of digital optics sector at the IITP of the RAS, the financing was obtained, which enabled the publication of a two-part twin issue 14-15. Alongside the ICSI, SSAU, and CDB UI of the RAS, the IITP of the RAS and Image Processing Systems Institute of the Russian Academy of Sciences (IPSI of the RAS, before 1993 known as Samara branch of CDB UI of the RAS) also acted as a cosponsor of twin issue 14-15 of *Computer Optics*. Twin 14-15 issue became the last to be compiled and edited with participation of I.N. Sisakyan, who soon untimely passed away.

Starting from issue 16 commemorating I.N. Sisakyan, the collection starts to be entirely published in Samara, with the ICSTI, SSAU, and IPSI of the RAS acting as cosponsors.

4. Journal

Even though *Computer Optics* is no longer published in English, it acquires ever growing recognition in the scientific community. On October 17, 2001 the collection was included into the list of RF Higher-Certifying-Commission-recommended scientific periodicals for publication of research papers relating to key findings of doctoral dissertations. The results published in *Computer Optics* later formed the basis of doctoral dissertations by V.M. Chernov, L.L. Doskolovich, A.I. Danilin, Ye.G. Ezhov, V.A. Fursov, D.L. Golovashkin, O.V. Goryachkin, N.Yu. Ilyasova, V.V. Ivakhnik, N.L. Kazanskiy, S.V. Karpeev, S.I. Kharitonov, S.N. Khonina, A.G. Khramov, A.A. Kovalev, V.A. Kolpakov, A.V. Kupriyanov, I.V. Minin, O.V. Minin, S.P. Murzin, V.V. Myasnikov, V.S. Pavelyev, A.G. Poleschuk, S.B. Popov, V.V. Sergeev, R.V. Skidanov, S.A. Stepanov, A.V. Volkov, and others.

Since 2007 the collection has been a quarterly scientific journal jointly published by the SSAU and IPSI of the RAS. The Editorial Board includes three academicians of the RAS (Yu.I. Zhuravlev, V.Ya. Panchenko and I.A. Scherbakov), three corresponding members of the RAS (S.Yu. Zheltov, B.V. Kryzhanovsky and V.A. Soifer), six Doctors of Science (N.L. Kazanskiy, V.V. Korlyar, V.S. Pavelyev,

V.V. Sergeev, S.N. Khonina, and V.M. Chernov), as well as scientists from Germany (professor Richard Kowarschik of Friedrich Shieller University, Jena), India (professor Kehar Singh), China (academician Jin Guofan of Tsinghua University, Beijing), and Finland (professor Jari Turunen of Joensuu University). On 22 March 2007, V.A. Soifer was appointed Editor-in-Chief of the journal of *Computer Optics* by Resolution N 2-8 of the RAS' Information Technologies and Computing Systems department. V.A. Soifer outlines [69] the Journal's strategic direction, the scope of research topics to be covered, also dealing with staffing the Editorial Board. The process of reviewing the submitted manuscripts on optical information technologies and diffractive nanophotonics is supervised by professor S.N. Khonina, the Editorial Board's secretary, on image processing and geo-information technologies – by V.M. Chernov, Doctor of Physics & Math. Credit for big work associated with preparation of the Journal for publication should be given to Ya.Ye. Takhtarov, issue editor, S.V. Smagin, M.A. Vakhe, and Yu.N. Litvinova. The Journal is published under financial support of the Samara Region government.

The scope of research topics covered by the Journal has been extended, embracing areas such as plasmonics and diffractive nanophotonics [70 – 79], geo-information technologies [80 – 84], computer vision [85 – 87], interpretation and understanding of nanoscale images [88 – 92], diffractive X-ray optics [93 – 94], optical computations [12 – 16], analysis of hyperspectral data [95 – 98], the development of Hyper-spectral instruments for Earth remote sensing [99 – 102], new types of diffraction conditioners beams with unique properties [103 – 105], sharp focusing [106 – 108]. Further contributing to the development of the above-mentioned new topics, the journal authors have published corresponding articles in the leading international journals [109 – 120]. Promptly responding to emerging research areas and following the cutting-edge scientific trends enables *Computer Optics* to be actively developing, winning the growing recognition in the research community. Online versions of the Journal articles are in open access at www.computeroptics.smr.ru, and can also be found on the scientific e-library website at eLIBRARY.RU. According to the e-library statistics, most widely cited are publications [55 – 56, 66, 121 – 127].

Conclusion

The fact that since 2012 *Computer Optics* has been abstracted and indexed in international databases of scientific publications, such as SCOPUS and Compendex, can be considered a significant success of the Journal, which is lacking the full-text English version. This enabled *Computer Optics* to be included in the list of scientific periodicals recommended by the Higher Certifying Commission of the RF Ministry of Science and Education for publication of key research findings of doctoral dissertations. Synergy of different topics covered by the Journal, which integrates achievements of diffractive optics, diffractive nanophotonics, and digital image processing, is critical for the progress of the world science, also forming the basis for further success of the scientific periodical. The goal of the current stage of the Journal development is its inclusion in the Web of Science Core Collection.

References

1. **Golub MA, Karpeev SV, Prokhorov AM, Sisakyan IN, Soifer VA.** Focusing light into a specified volume by computer synthesized holograms. Soviet Technical Physics Letters, 1981; **7**(10): 618-623.

2. **Golub MA, Degtyarova VP, Klimov AN, Popov VV, Prokhorov AM, Sisakyan IN, Soifer VA.** Machine synthesis of focusing elements for CO_2-laser. Soviet Technical Physics Letters, 1982; 8(8): 449-451. [in Russian]

3. **Danilov VA, Popov VV, Prokhorov AM, Sagatelyan DM, Sisakyan IN, Soifer VA.** Synthesis of optical elements, that create focal free-form line. Soviet Technical Physics Letters, 1982; 8(13): 810-815. [in Russian]

4. **Golub MA, Prokhorov AM, Sisakyan IN, Soifer VA.** Synthesis of spatial filters for investigation of the transverse mode composition of coherent radiation. Soviet Journal of Quantum Electronics, 1982; 12(9): 1866-1868.

5. **Bereznyi AE, Prokhorov AM, Sisakyan IN, Soifer VA.** Bessel-optics. Dokl. Akad. Nauk USSR, 1984; 274(3): 605-608. [in Russian]

6. **Golub MA, Kazanski NL, Sisakjan IN, Soifer VA.** Computer generated optical elements for optical testing. Proceedings of SPIE, 1990; 1319: 635-636.

7. **Golub MA, Sisakyan IN, Soifer VA.** Infra-red Radiation Focusators. Optics and Lasers in Engineering, 1991; 15(5): 297-309.

8. **Doskolovich LL, Kazanskiy NL, Kharitonov S.I, Usplenjev GV.** Focusators for laser-branding. Optics and Lasers in Engineering, 1991; 15(5): 311-322.

9. **Kazanskiy NL, Soifer VA.** Diffraction investigation of geometric-optical focusators into a segment. Optik – International Journal for Light and Electron Optics, 1994; 96(4): 158-162.

10. **Kazanskiy NL, Kharitonov SI, Soifer VA.** Application of a pseudogeometrical optical approach for calculation of the field formed by a focusator. Optics & Laser Technology, 1996; 28(4): 297-300.

11. **Velikhov EP.** Foreword. Computer Optics, 1989; 1(1): 1.

12. **Golovastikov NV, Bykov DA, Doskolovich LL, Soifer VA.** Temporal differentiation of optical signals in reflection using resonant gratings. Computer Optics, 2012; 36(2): 151-157. [in Russian]

13. **Golovastikov NV, Bykov DA, Doskolovich LL, Soifer VA.** Resonant diffraction gratings for differentiation of optical signals in reflection and transmission. Computer Optics, 2013; 37(2): 138-145. [in Russian]

14. **Golovastikov NV, Bykov DA, Doskolovich LL.** Spatial integration of optical beams using phase-shifted Bragg grating. Computer Optics, 2014; 38(3): 372-376. [in Russian]

15. **Kazanskiy NL, Serafimovich PG, Khonina SN.** Use of photonic crystal resonators for differentiation of optical impulses in time. Computer Optics, 2012; 36(4): 474-478. [in Russian]

16. **Kazanskiy NL, Serafimovich PG.** Using photonic crystal nanobeam cavities for integration of optical signal. Computer Optics, 2014; 38(2); 181-187. [in Russian]

17. **Kazanskiy NL, Serafimovich PG, Khonina SN.** Use of photonic crystal cavities for temporal differentiation of optical signals. Optics Letters, 2013; 38(7): 1149-1151.

18. **Kazanskiy NL, Serafimovich PG.** Coupled-resonator optical wave-guides for temporal integration of optical signals. Optics Express, 2014; 22(11): 14004–14013.

19. **Gavrilov AV, Soifer VA.** Prospects of optical analog computer development. Computer Optics, 2012; 36(2): 140-150. [in Russian]

20. **Kazanskiy NL, Skidanov RV.** Binary beam splitter. Applied Optics, 2012; 51(14): 2672-2677.

21. **Golub MA, Doskolovich LL, Kazanskiy NL, Kharitonov SI, Soifer VA.** Computer generated diffractive multi-focal lens. Journal of Modern Optics, 1992; 39(6): 1245-1251.
22. **Soifer VA, Doskolovich LL, Kazanskiy NL.** Multifocal diffractive elements. Optical Engineering, 1994; 33(11): 3610-3615.
23. **Prokhorov AM.** Foreword. Computer Optics, 1989; 1(1): 2.
24. **Soifer VA.** Computer Optics in the works by Professor I.N. Sisakyan. Computer Optics, 2002; 24: 5-10. [in Russian]
25. **Sisakyan IN, Soifer VA.** Computer Optics: achievements and problems. Computer Optics, 1989; 1(1): 3-12.
26. **Golub MA, Kazanskii NL, Prokhorov AM, Sisakyan IN, Soifer VA.** Synthesis of optical antennae. Computer Optics, 1989; 1(1): 25-28. [in Russian]
27. **Kazanskiy NL, Soifer VA, Kharitonov SI.** Modeling of lighting devices with DOE. Computer Optics, 1995; 14-15(2): 107-116. [in Russian]
28. **Doskolovich LL, Kazanskiy NL, Kharitonov SI.** Design of DOE-aided lighting devices. Computer Optics, 1998; 18: 91-96. [in Russian]
29. **Volkov AV, Kazanskiy NL, Usplenjev GV.** Experimental study of lighting devices based on diffractive optical elements. Computer Optics, 1999; 19: 137-142. [in Russian]
30. **Dmitriev AYu, Doskolovich DL, Doskolovich LL, Kazanskiy NL.** Analytic design of refractive optical elements generating one-parameter directivity diagram. Computer Optics, 2014; 38(2): 207-212. [in Russian]
31. **Doskolovich LL, Moiseev MA, Kazanskiy NL.** On using a supporting quadric method to design diffractive optical elements. Computer Optics, 2015; 39(3): 339-346. [in Russian]
32. **Doskolovich LL, Kazanskiy NL, Soifer VA, Kharitonov SI, Perlo P.** A DOE to form a line-shaped directivity diagram. Journal of Modern Optics, 2004; 51(13): 1999-2005.
33. **Doskolovich LL, Kazanskiy NL, Bernard S.** Designing a mirror to form a line-shaped directivity diagram. Journal of Modern Optics, 2007; 54(4): 589-597.
34. **Doskolovich LL, Dmitriev AYu, Moiseev MA, Kazanskiy NL.** Analytical design of refractive optical elements generating one-parameter intensity distributions. J. Opt. Soc. Am. A, 2014; 31(11): 2538-2544.
35. **Aslanov ER, Doskolovich LL, Moiseev MA, Bezus EA, Kazanskiy NL.** Design of an optical element forming an axial line segment for efficient LED lighting systems. Optics Express, 2013; 21(23): 28651-28656.
36. **Kazanskii NL.** Correction of focuser phase function by computer-experimental methods. Computer Optics, 1989; 1(1): 69-73.
37. **Golub MA, Kazanskii NL, Sisakyan IN, Soifer VA, Kharitonov SI.** Diffraction calculation for an optical element which focuses into a ring. Optoelectronics, Instrumentation and Data Processing, 1987; 6: 7-14.
38. **Golub MA, Kazanskii NL, Sisakyan IN, Soifer VA.** Computational experiment with plane optical elements. Optoelectronics, Instrumentation and Data Processing, 1988; 1: 78-89.
39. **Kazansky NL.** Numerical experiment with a Fresnel lens. Computer Optics, 1990; 2(1): 17-21.
40. **Kazanskiy NL, Kharitonov SI.** Transmission of space-limited broadband symmetrical radial pulses focused through a thin film. Computer Optics, 2012; 36(1): 4-13. [in Russian]
41. **Kazanskiy NL, Kharitonov SI, Khonina SN.** Joint solution of the Klein–Gordon and Maxwell's equations. Computer Optics, 2012; 36(4): 518-526. [in Russian]
42. **Kazanskiy NL, Kotlyar VV, Soifer VA.** Computer-aided design of diffractive optical elements. Optical Engineering, 1994; 33(10): 3156-3166.
43. **Doskolovich LL, Kazanskiy NL, Soifer VA.** Comparative analysis of different focusators focusing into segment. Optics and Laser Technology, 1995; 27(4): 207-213.

44. **Doskolovich LL, Kazanskiy NL, Soifer VA, Tzaregorodtzev AYe.** Analysis of quasiperiodic and geometric optical solutions of the problem of focusing into an axial segment. Optik – International Journal for Light and Electron Optics, 1995; 101(2): 37-41.

45. **Kazanskiy NL, Serafimovich PG.** Cloud Computing for Nanophotonic Simulations. Lecture Notes in Computer Science, 2013; 7715: 54-67.

46. **Danilov VA, Kinber BE, Shishlov AV.** Theory of coherent focusers. Computer Optics, 1989; 1(1): 29-37.

47. **Doskolovich LL, Golub MA, Kazanskiy NL, Khramov AG, Pavelyev VS, Seraphimovich PG, Soifer VA, Volotovskiy SG.** Software on diffractive optics and computer generated holograms. Proceedings of SPIE, 1995; 2363: 278-284.

48. **Doskolovich LL, Kazanskiy NL, Kharitonov SI, Soifer VA.** A method of designing diffractive optical elements focusing into plane areas. Journal of Modern Optics, 1996; 43(7): 1423-1433.

49. **Doskolovich LL, Kazanskiy NL, Perlo P, Repetto P, Soifer VA.** Direct two-dimensional calculation of binary DOEs using a non-binary series expansion approach. International Journal of Optoelectronics, 1996; 10(4): 243-249.

50. **Soifer VA, Kazanskiy NL, Kharitonov SI.** Synthesis of a binary DOE focusing into an arbitrary curve using the electromagnetic approximation. Optics and Lasers in Engineering, 1998; 29(4-5): 237-247.

51. **Doskolovich LL, Kazanskiy NL, Soifer VA, Perlo P, Repetto P.** Design of DOEs for wavelength division and focusing. Journal of Modern Optics, 2005; 52(6): 917-926.

52. **Bezus EA, Doskolovich LL, Kazanskiy NL.** Low-scattering surface plasmon refraction with isotropic materials.Optics Express, 2014; 22(11): 13547–13554.

53. **Popov VV.** Materials and methods for flat optical elements. Computer Optics, 1989; 1(1): 125-128.

54. **Volkov AV, Kazanskiy NL, Soifer VA, Solovyov VS.** Technology for forming continuous microrelief of diffractive optical elements. Computer Optics, 1997; 17: 91-93. [in Russian]

55. **Volkov AV, Kazanskiy NL, Rybakov OE.** Investigation of plasma etching technology for producing multilayer diffractive optical elements. Computer Optics 1998; 18: 127-130. [in Russian]

56. **Volkov AV, Kazanskiy NL, Rybakov OE.** Development of technology for creation of diffractive optical elements with submicron dimensions of the relief in the silicon wafer. Computer Optics, 1998; 18: 130-133. [in Russian]

57. **Volkov AV, Moiseev OYu, Poletaev SD, Chistyakov IV.** Application of thin molybdenum films in contact masks for manufacturing the micro-relief of diffractive optical elements. Computer Optics, 2014; 38(4): 757-762. [in Russian]

58. **Kazanskiy NL, Kolpakov VA, Kolpakov AI.** Anisotropic etching of SiO_2 in high-voltage gas-discharge plasmas. Russian Microelectronics, 2004; 33(3): 169-182.

59. **Abulkhanov SR, Kazanskii NL, Doskolovich LL, Kazakova OY.** Manufacture of diffractive optical elements by cutting on numerically controlled machine tools. Russian Engineering Research, 2011; 31(12): 1268-1272.

60. **Bezus EA, Doskolovich LL, Kazanskiy NL.** Interference pattern generation in evanescent electromagnetic waves for nanoscale lithography using waveguide diffraction gratings. Quantum Electronics, 2011; 41(8) 759-764.

61. **Volkov AV, Kazanskiy NL, Moiseev OJu, Soifer VA.** A method for the diffractive microrelief forming using the layered photoresist growth. Optics and Lasers in Engineering, 1998; 29(4-5): 281-288.

62. **Pavelyev VS, Borodin SA, Kazanskiy NL, Kostyuk GF, Volkov AV.** Formation of diffractive microrelief on diamond film surface Optics & Laser Technology, 2007; 39(6): 1234-1238.
63. **Kazanskiy NL, Kolpakov VA, Podlipnov VV.** Gas discharge devices generating the directed fluxes of off-electrode plasma. Vacuum, 2014; 101: 291-297.
64. **Sisakyan IN, Shorin VP, Soifer VA, Mordasov VI, Popov VV.** Technological capabilities of focusators in laser-induced material processing. Computer Optics, 1990; 2(1): 85-87.
65. **Doskolovich LL, Kazanskiy NL, Mordasov VI, Murzin SP, Kharitonov SI.** Investigation of the optical transmission control systems for high energy. Computer Optics, 2002; 23: 40-43. [in Russian]
66. **Kazanskiy NL, Murzin SP, Tregub VI.** Optical system for realization of selective laser sublimation of metal alloy components. Computer Optics, 2010; 34(4): 481-486. [in Russian]
67. **Murzin SP.** Method of composite nanomaterials synthesis under metal/oxide pulse-periodic laser treatment. Computer Optics, 2014; 38(3): 469-475. [in Russian]
68. **Kazanskiy NL, Murzin SP, Osetrov Ye L, Tregub VI.** Synthesis of nanoporous structures in metallic materials under laser action. Optics and Lasers in Engineering, 2011; 49(11): 1264-1267.
69. **Soifer VA.** Quo vadis. Computer Optics, 2014; 38(4): 589.
70. **Soifer VA.** Nanophotonics and diffractive optics. Computer Optics, 2008; 32(2): 110-118. [in Russian]
71. **Bezus EA, Doskolovich LL, Kadomin II, Kazanskiy NL, Civera P, Pizzi M.** Generating varying-period interference patterns of surface plasmons by diffraction gratings. Computer Optics, 2008; 32(3): 234-237. [in Russian]
72. **Bezus EA, Doskolovich LL, Kazanskiy NL, Soifer VA, Kharitonov SI, Pizzi M, Perlo P.** The design of diffractive optical elements to focus surface plasmons. Computer Optics, 2009; 33(2): 185-192. [in Russian]
73. **Soifer VA, Kotlyar VV, Doskolovich LL.** Diffractive optical elements in nanophotonic devices. Computer Optics, 2009; 33(4): 352-368. [in Russian]
74. **Kazanskiy NL, Serafimovich PG, Popov SB, Khonina SN.** Using guided-mode resonance to design nano-optical spectral transmission filters. Computer Optics, 2010; 34(2): 162-168. [in Russian]
75. **Kazanskiy NL, Serafimovich PG, Khonina SN.** Optical nanoresonator on a ridge of crossing photonic-crystal waveguides. Computer Optics, 2011; 35(4): 426-431. [in Russian]
76. **Egorov AV, Kazanskiy NL, Serafimovich PG.** The use of coupled photonic crystal cavities for increasing of sensor sensitivity. Computer Optics, 2015; 39(2): 158-162. [in Russian]
77. **Kazanskiy NL, Khonina SN, Kharitonov SI.** The perturbation theory for Schroedinger equation in the periodic environment in momentum representation. Computer Optics, 2012; 36(1): 21-26. [in Russian]
78. **Khonina SN, Volotovskiy SG, Kharitonov SI, Kazanskiy NL.** Calculation of the power spectrum of complex low-dimensional heterostructures in the electric field. Computer Optics, 2012; 36(1): 27-33. [in Russian]
79. **Kazanskiy NL, Serafimovich PG, Khonina SN.** Enhancement of spatial modal overlap for photonic crystal nanocavities. Computer Optics, 2012; 36(2): 199-204. [in Russian]
80. **Zherdev DA, Kazanskiy NL, Fursov VA, Kharitonov SI.** Electromagnetic field scattering simulation from anthropogenic objects on underlying surface. Computer Optics, 2013; 37(1): 91-98. [in Russian]

81. **Sergeyev VV, DenisovaAYu.** Iterational method for piecewise constant images restoration with an a priori knowledges of image objects boundaries. Computer Optics, 2013; 37(2): 239-243. [in Russian]

82. **Fursov VA, Goshin YeV.** Information technology for digital terrain model reconstruction from stereo images. Computer Optics, 2014; 38(2): 335-342. [in Russian]

83. **Zherdev DA, Kazanskiy NL, Fursov VA.** Object recognition by the radar signatures of electromagnetic field scattering on base of support subspaces method. Computer Optics, 2014; 38(3): 503-510. [in Russian]

84. **Zherdev DA, Kazanskiy NL, Fursov VA.** Object recognition in radar images using conjugation indices and support subspaces. Computer Optics, 2015; 39(2): 255-264. [in Russian]

85. **Kazansky NL, Popov SB.** A machine vision system for counting the number of gel particles in a polymer solution. Computer Optics, 2009; 33(3): 325-331. [in Russian]

86. **Kazanskiy NL, Popov SB.** The distributed vision system of the registration of the railway train. Computer Optics, 2012; 36(3): 419-428. [in Russian]

87. **Kazanskiy NL, Khonina SN, Skidanov RV, Morozov AA, Kharitonov SI, Volotovskiy SG.** Formation of images using multilevel diffractive lens. Computer Optics, 2014; 38(3): 425-434. [in Russian]

88. **Borodin SA, Volkov AV, Kazanskiy NL.** An automated device for assessing the substrate purity based on the dynamics of a surface fluid droplet. Computer Optics, 2005; 28: 69-75. [in Russian]

89. **Babin SV, Doskolovich LL, Kadomin II, Kadomina EA, Kazanskiy NL.** Characterization of a trapezoidal diffraction grating profile based on polynomial approximations of the reflected field. Computer Optics, 2009; 33(2): 156-161. [in Russian]

90. **Soifer VA, Kupriyanov AV.** Analysis and recognition of the nanoscale images: conventional approach and novel problem statement. Computer Optics, 2011; 35(2): 136-144. [in Russian]

91. **Kupriyanov AV.** Texture analysis and identification of the crystal lattice type in nanoscale images. Computer Optics, 2011; 35(2): 151-157. [in Russian]

92. **Kupriyanov AV.** Observability of a crystal lattice by multiple nodes in the images of their projections. Computer Optics, 2012; 36(4): 586-589. [in Russian]

93. **Kotlyar VV, Nalimov AG, Shanina MI, Soifer VA, O'Faolain L, Mineyev EV, Yakimchuk IV, Asadchikov VE.** Study of focusing properties of a zone plate for hard X-rays. Computer Optics, 2012; 36(1): 65-71. [in Russian]

94. **Nalimov AG, Kotlyar VV.** Use of combined zone plates as imaging optics for hard x-rays. Computer Optics, 2015; 39(1): 52-57. [in Russian]

95. **Zhuravel YN, Fedoseev AA.** The features of hyperspectral remote sensing data processing under environment monitoring tasks solution. Computer Optics, 2013; 37(4): 471-476. [in Russian]

96. **Zimichev EA, Kazanskiy NL, Serafimovich PG.** Spectral-spatial classification with k-means++ particional clustering. Computer Optics, 2014; 38(2): 281-287. [in Russian]

97. **Denisova AYu, Myasnikov VV.** Anomaly detection for hyperspectral imaginary. Computer Optics, 2014; 38(2): 287-296. [in Russian]

98. **Kazanskiy NL, Protsenko VI, Serafimovich PG.** Comparison of system performance for streaming data analysis in image processing tasks by sliding window. Computer Optics, 2014; 38(4): 804-810. [in Russian]

99. **Kazanskiy NL, Kharitonov SI, Khonina SN, Volotovskiy SG, Strelkov YuS.** Simulation of hyperspectrometer on spectral linear variable filters. Computer Optics, 2014; 38(2): 256-270. [in Russian]

100. **Kazanskiy NL, Kharitonov SI, Karsakov AV, Khonina SN.** Modeling action of a hyperspectrometer based on the offner scheme within geometric optics. Computer Optics, 2014; 38(2): 271-280. [in Russian]
101. **Kazanskiy NL, Kharitonov SI, Khonina SN.** Simulation of a hyperspectrometer based on linear spectral filters using vector Bessel beams. Computer Optics, 2014; 38(4): 770-776. [in Russian]
102. **Kazanskiy NL, Kharitonov SI, Doskolovich LL, Pavelyev AV.** Modeling the performance of a spaceborne hyperspectrometer based on the Offner scheme. Computer Optics, 2015; 39(1): 70-76. [in Russian]
103. **Kotlyar VV, Kovalev AA, Zaskanov SG.** Two-dimensional accelerating Bessel beams. Computer Optics, 2014; 38(3): 386-392. [in Russian]
104. **Kotlyar VV, Kovalev AA, Porfirev AP.** Hermite-gaussian laser beams with orbital angular momentum. Computer Optics, 2014; 38(4): 651-657. [in Russian]
105. **Kovalev AA, Kotlyar VV, Porfirev AP.** Generation of half-Pearcey laser beams by a spatial light modulator. Computer Optics, 2014; 38(4): 658-662. [in Russian]
106. **Stafeev SS, O'Faolain L, Shanina MI, Nalimov AG, Kotlyar VV.** Sharp focusing of a mixture of radially and linearly polarized beams using a binary microlens. Computer Optics, 2014; 38(4): 606-613.
107. **Degtyarev SA, Ustinov AV, Khonina SN.** Nanofocusing by sharp edges. Computer Optics, 2014; 38(4): 629-637. [in Russian]
108. **Savelyev DA, Khonina SN.** Numerical analysis of subwavelength focusing using a silicon cylinder. Computer Optics, 2014; 38(4): 638-642. [in Russian]
109. **Karpeev SV, Pavelyev VS, Khonina SN, Kazanskiy NL, Gavrilov AV, Eropolov VA.** Fiber sensors based on transverse mode selection. Journal of Modern Optics, 2007; 54(6): 833-844.
110. **Doskolovich LL, Kazanskiy NL, Khonina SN, Skidanov RV, Heikkila N, Siitonen S, Turunen J.** Design and investigation of color separation diffraction gratings. Applied Optics, 2007; 46(15): 2825-2830.
111. **Kazanskiy NL.** Research and Education Center of Diffractive Optics. Proceedings of SPIE, 2012; 8410: 84100R. doi: 10.1117/12.923233.
112. **Bykov DA, Doskolovich LL, Soifer VA, Kazanskiy NL.** Extraordinary Magneto-Optical Effect of a Change in the Phase of Diffraction Orders in Dielectric Diffraction Gratings. Journal of Experimental and Theoretical Physics, 2010; 111(6): 967-974. doi:10.1134/S1063776110120095.
113. **Kazanskiy NL, Popov SB.** Machine Vision System for Singularity Detection in Monitoring the Long Process. Optical Memory and Neural Networks (Information Optics), 2010; 19(1): 23-30. doi:10.3103/S1060992X10010042.
114. **Khonina SN, Kazanskiy NL, Volotovsky SG.** Influence of Vortex Transmission Phase Function on Intensity Distribution in the Focal Area of High-Aperture Focusing System. Optical Memory and Neural Networks (Information Optics), 2011; 20(1); 23-42. doi: 10.3103/S1060992X11010024.
115. **Khonina SN, Kazanskii NL, Ustinov AV, Volotovskii SG.** The lensacon: nonparaxial effects. Journal of Optical Technology, 2011; 78(11): 724-729. doi: 10.1364/JOT.78.000724.
116. **Golovashkin DL, Kasanskiy NL.** Solving Diffractive Optics Problem using Graphics Processing Units. Optical Memory and Neural Networks (Information Optics), 2011; 20(2): 85-89. doi:10.1134/S1063776110120095.
117. **Bezus EA, Doskolovich LL, Kazanskiy NL.** Scattering suppression in plasmonic optics using a simple two-layer dielectric structure. Applied Physics Letters, 2011; 98(22): 221108. doi: 10.1063/1.3597620.

118. **Bezus EA, Doskolovich LL, Kazanskiy NL, Soifer VA.** Scattering in elements of plasmon optics suppressed by two-layer dielectric structures. Technical Physics Letters, 2011; 37(12): 1091-1095. doi: 10.1134/S1063785011120030.

119. **Soifer VA.** Diffractive Nanophotonics and Advanced Information Technologies. Herald of the Russian Academy of Sciences, 2014; 84(1): 9-18.

120. **Khonina SN, Savelyev DA, Kazanskiy NL.** Vortex phase elements as detectors of polarization state. Optics Express, 2015; 23(14): 17845-17859. doi: 10.1364/OE.23.017845.

121. **Kazanskiy NL.** A research complex for solving problems of computer optics. Computer Optics, 2006; 29: 58-77. [in Russian]

122. **Kazanskiy NL, Murzin SP, Tregub VI, Mezhenin AV.** Application of a focusator radiation for generating nanoporous structures of crystalline materials. Computer Optics, 2007; 31(2): 48-51. [in Russian]

123. **Kazanskiy NL, Murzin SP, Mezhenin AV, Osetrov EL.** Laser radiation shaping for creation nanodimensional porous structures of materials. Computer Optics, 2008; 32(3): 246-248. [in Russian]

124. **Golub MA, Kazanskiy NL, Sisakyan IN, Soifer VA.** Standard wavefronts formation with the computer optics elements. Computer Optics, 1990; 7: 3-26. [in Russian]

125. **Kotlyar VV, Stafeev SS.** Modeling the sharp focus of radially polarized laser mode with conical and binary microaxicons. Computer Optics, 2009; 33(1): 52-60. [in Russian]

126. **Khonina SN, Volotovsky SG.** Controlling the contribution of the electric field components to the focus of a high-aperture lens using binary phase structures. Computer Optics, 2010; 34(1): 58-68. [in Russian]

127. **Zvekov AA, Kalenskii AV, Nikitin AP, Aduev BP.** Radiance distribution simulation in a transparent medium with Fresnel boundaries containing aluminum nanoparticles. Computer Optics, 2014; 38(4): 749-756. [in Russian]

Asymptotic research in computer optics

Kazanskiy N.L.

Image Processing Systems Institute, Russian Academy of Sciences,
Samara State Aerospace University

Abstract. I give an overview of the methods and possibilities of the asymptotic studies for solving the computer optics. I analyze the relevance of the use of the results in the design of diffractive optical elements for laser material processing. I discuss the prospects of the developed approaches for the study of the components of diffractive nanophotonics.

Introduction

Asymptotic methods have always been in the focus of scientists-opticians [1-3]. These methods have evident interest in recent years [4-11]. Scientists working in the field of diffractive computer optics, also actively used the opportunities provided by asymptotic methods [12-17]. Asymptotic methods are especially good in the study of such class of diffractive optical elements (DOEs), as focusators of laser radiation [14-17]. In the paper I give an overview of the methods and possibilities of the asymptotic studies for solving the computer optics. In particular, I analyze the relevance of the use of the results in the design of diffractive optical elements for laser material processing.

1. Focusators research

For creating a new focusator we have several important steps: obtaining a phase function; study of the phase function; choice of sampling parameters and method for manufacturing diffractive microrelief; calculation and production of focusator; experimental study of the microrelief and output parameters of focusator. To study the phase function of focusator scientists use analytical calculation of the diffraction patterns of the focused radiation. This calculation must take into account the finite size and specific physical parameters of created focusator [12-17]. Typically, the

geometric optics approximation is used to calculate the phase function of focusator. Diffractive analysis allows us to explore the limits of this approach. It allowed us to identify the initial values of the physical parameters under which the distortion of the focus area began. This analysis allows us to identify possible errors in the analytical solution of the inverse problem of the diffraction theory.

However, we can carry out diffractive analyzes only for simple phase functions, axially symmetric illuminating beams and focus areas - such as the ring [12], a set of points [18-20], longitudinal [21-24] or cross [15-17, 25-26] segments. In some cases, the analytical study can provide diffractive corrections to the phase function of focusator [14]. Unfortunately, in the framework of the analytical study, we cannot take into account the effect of sampling and quantization of the phase function focusator arising during the manufacture of the DOE. However asymptotic analysis is an important stage of research and complements the capabilities of the computational experiment [21-28].

Unfortunately, asymptotic methods do not allow us to analyze different methods for manufacturing micro-relief of diffractive optical elements [29-36]. Such a study is necessary to select the most appropriate technology for manufacturing DOEs intended for solving a particular problem.

As an example, I cite the results of the asymptotic study of the geometric-optical focusator, concentrated laser beam into the ring [12, 21]. Fig. 1 shows the results of the asymptotic calculation of the intensity distribution in the focal plane of the geometric-optical focusator into the ring with the following parameters: focal length f = 750 mm; focusator diameter $2R$ = 25.6 mm; the wavelength of focused beam λ = 0.6328 μm; focal ring diameter r_0 = 0.1 mm.
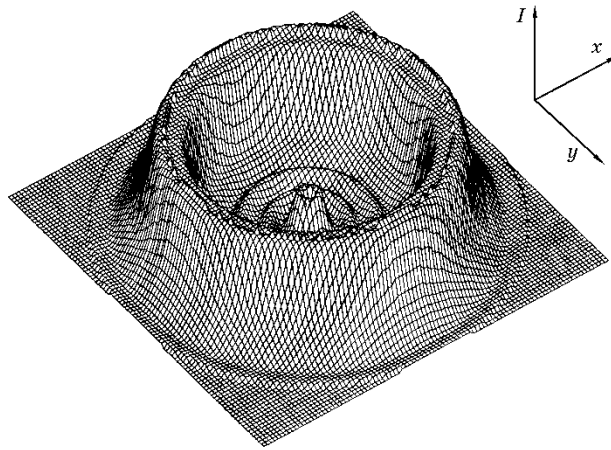
Fig. 1. – The intensity distribution I(x,y) in the focal plane of the focusator into the ring

Asymptotic calculation shows that the diffraction width of the focus ring is comparable to the radius of the ring for focusator with these parameters. As a result, the ring begins to merge with the central spot. The asymptotic calculation shows that such a draining does not occur when the radius of the focal ring in several (and furthermore many) times larger than 0.1 mm. So we clearly see the limitations of the

methods of geometrical optics in calculating the phase function of focusator. The results can also be used in the study of other types of DOEs [37-45] and to focus the surface electromagnetic waves [46-48].

2. Temperature calculation

Asymptotic analysis allows us to optimize the phase function of focusator for use in a specific laser processing technology of a given type of material [49-55]. Focusators have broad prospects for application in a variety of laser materials processing technologies [49-55]: hardening, cutting, welding, drilling, branding, etc. Therefore, the problem of investigating the temperature characteristics of the laser effects produced by focusators is very important. Known focusators form a predetermined intensity distribution in some areas. Laser technology requires forming a desired temperature distribution on the object surface intended for processing. In [26], we conducted an analysis of the temperature distribution formed by focusator into segment (focusator focuses laser light into a line segment located in the focal plane). Asymptotic approach allowed us to obtain a phase function of focusator focusing laser beam into the line segment with a predetermined temperature profile. For example, in [26] we calculated optical element for focusing the circular (and ring) beam into the line segment with a constant temperature distribution. Fig. 2 shows the simulation results for these focusators. Fig. 2a shows a normalized graph of the calculation of temperature distribution along the focal segment for thermal focusator focusing uniform beam of circular cross section of radius $R = 5$ mm with the following parameters: the wavelength of the focused radiation $\lambda = 1.06$ µm; focal length $f = 100$ mm; length of focal segment $2d = 2$ mm; $(4at_0)^{1/2} = 20$ µm (here a is thermal diffusivity, t_0 is the duration of the laser action).

Fig. 2b shows the calculated normalized graph of the temperature distribution along the focal segment for the heat focusator focusing uniform beam of annular cross section with radii $R_1=3$ mm and $R_2=5$ mm with the following parameters: the wavelength of the focused radiation $\lambda=1.06$ µm; focal length $f=400$ mm; length of focal segment $2d=8$ mm; $(4at_0)^{1/2} = 0.2$ mm (here used value for thermal diffusivity of the steel $a=12$ mm/s^2). We can interpret the data in Fig. 2 as a result of forming by the heat focusator a constant temperature profile on the steel surface by the end of the laser pulse duration $t_0 = 0.001$s. For investigated focusators standard deviation from the constant temperature is 8.8% (for the illuminating beam of circular cross-section, Fig. 2a) and 12.2% (for the illuminating beam of the annular cross-section, Fig. 2b). It is about two times better than using geometrical optics focusators.

3. Electromagnetic theory

In recent years, we are actively developing new asymptotic methods within the electromagnetic theory for calculating the field generated by DOE [56-65].

For example, in [57] we presented an asymptotic method for solving problems of diffraction on the diffractive microrelief. This method combines the geometric-optical approach and solution to the problem of diffraction by a periodic structure with a period comparable to the wavelength. We solved the problem of diffraction by a

153

standard quasi-periodic structure that combines the functions of a beam splitter and a diffraction lens. On the basis of the standard solution of the problem we got a simple expression for the field in a plane adjacent to the DOE. The resulting expression allows us to estimate the distribution of the field at the output of the DOE without resorting to complex computational methods.
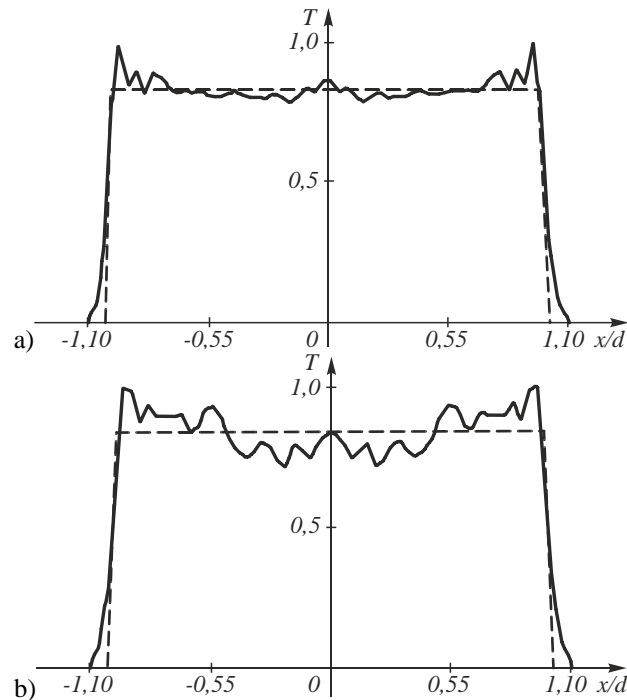
Fig. 2. – The temperature distribution T on the focal segment for thermal focusators: a) uniform illuminating beam with a circular cross-section; b) uniform illuminating beam with an annular cross-section

We have obtained the results of calculation for the intensity distributions of electromagnetic radiation in the focal plane of the focusator into ring for various combinations of system parameters. Calculation of the field in the focal region, we carried out on the basis of the distribution of the field at the output of the DOE calculated within the electromagnetic theory [57]. Further, the field in the focal plane, we calculated using the propagator, described in [58], on the base of the field at the output of the DOE.

Fig. 3 shows an example for calculation of fields generated by focusators into the ring for the values shown in Table. 1 (all dimensions are in microns). For small relationship σ/f (σ is parameter of an illuminating Gaussian beam, f is the focal length), the intensity distribution in the focal plane of focusator into the ring is close to the intensity distributions obtained [12, 21] in the framework of scalar approximation. In this case, the energy distribution has good axial symmetry. The

symmetry is improved in the case of increasing the focal length. The asymmetry in the energy distribution along the ring appears at the increase in the ratio σ/f. The presence of asymmetry is due to the following factors:

- presence of linear polarization of the incident wave destroys radial symmetry, since the electric fields from different points of the focusators come at different angles in different points of the focal plane;
- in the case of linear polarization of the incident wave the diffractive coefficient depends on the direction of the local grating, it appears with increasing ratio σ/f.

Table 1. The parameters of focusators

Parameter	Value (option 1), μm	Value (option 2), μm
Wavelength λ	1	0.1
Parameter of Gaussian beam σ	50	50
The distance from the optical element to the observation plane	1000	100
Focal length f	1000	100
Dimensions of the optical element	500×500	500×500

Uneven intensity of light in the observation plane of focusator into ring caused unevenness coefficient values in transmission (reflection) of the *E*- and the *H*-polarization depending on the current value of the period of the band structure (diffraction grating).

Conclusion

In recent years, scientists were actively developing asymptotic methods in the frame of the electromagnetic theory for calculation of the field formed by the DOEs [56-64]. We use this methods not only for the study of diffractive optical elements (in particular, of short-focus DOEs), but also for the study of nanophotonics components [66-74], for the design of equipment for hyperspectral remote sensing [75-79] and solving other urgent tasks of diffractive nanophotonics [80].

Acknowledgements
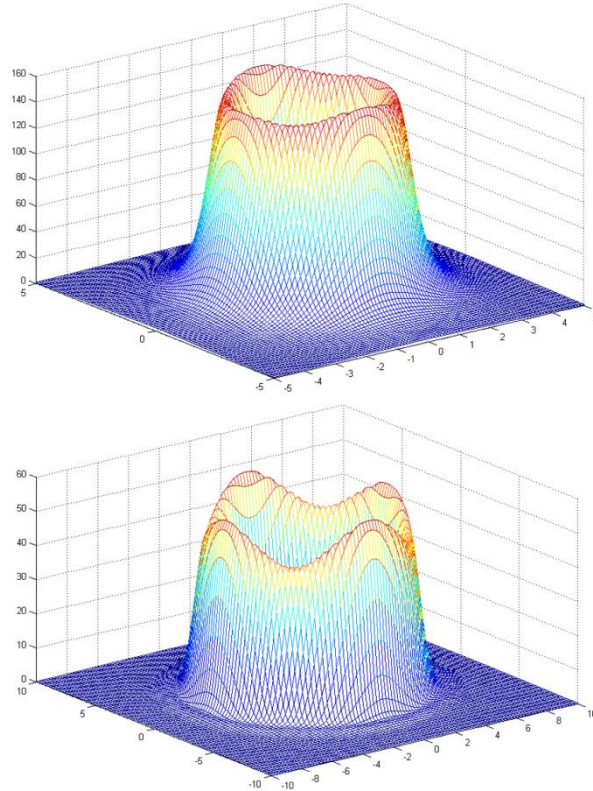
Fig. 3. – The calculated intensity distribution in the focal planes of focusators into the ring with the parameters given in the Table 1 (option 1 - the top; option 2 - the bottom)

References

1. **Walker J.** The Analytical Theory of Light. C. J. Clay and Sons, 1904. 432 p.
2. **Born M, Wolf E.** Principles of Optics 6 ed. New York: Pergamon, 1986.
3. **Babich VM, Buldyrev VS.** Asymptotic methods in short wave diffraction problems. Moscow: "Nauka" Publisher, 1972. 456 p. [in Russian]
4. **Heyman E, Felsen LB.** Gaussian beam and pulsed-beam dynamics: complex-source and complex-spectrum formulations within and beyond paraxial asymptotics. J. Opt. Soc. Am. A 2001; 18(7): 1588-1611.
5. **Ahrens CD, Ablowitz MJ, Docherty A, Sinkin OV, Grigoryan V, Menyuk CR.** Asymptotic analysis of collision-induced timing shifts in return-to-zero quasi-linear systems with predispersion and postdispersion compensation. Optics Letters, 2006; 31(1): 5-7.
6. **Simonov AN, Rombach MC.** Asymptotic behavior of the spatial frequency response of an optical system with defocus and spherical aberration. J. Opt. Soc. Am. A 2010; 27(12): 2563-2573.

7. **Zhu J, Chen Z, Tang S.** Leaky modes of optical waveguides with varied refractive index for microchip optical interconnect applications — asymptotic solutions. Microelectronics Reliability, 2008; 48(4): 555-562.

8. **Zhu J, Lu YY.** Asymptotic solutions of eigenmodes in slab waveguides terminated by perfectly matched layers. J. Opt. Soc. Amer. A 2013; 30(10): 2090-2095.

9. **Sheppard CJR.** Limitations of the paraxial Debye approximation. Optics Letters, 2013; 38(7): 1074-1076.

10. **Rawlins AD.** A note on uniform asymptotic wave diffraction by a wedge. Quarterly Journal of Mechanics and Applied Mathematics, 2014; 67(1): 43-56.

11. **Groth SP, Hewett DP, Langdon S.** Hybrid numerical-asymptotic approximation for high-frequency scattering by penetrable convex polygons. IMA Journal of Applied Mathematics (Institute of Mathematics and Its Applications), 2015; 80(2): 324-353.

12. **Golub MA, Kazanskiy NL, Sisakyan IN, Soifer VA, Kharitonov SI.** Diffraction calculation for an optical element which focuses into a ring. Optoelectronics, Instrumentation and Data Processing, 1987; 6: 7-14.

13. **Golub MA, Kazanskiy NL, Sisakyan IN, Soifer VA, Kharitonov SI.** Diffraction calculation of the field intensity near the focal line of a focuser. Optics and Spectroscopy, 1989; 67(6): 814-815.

14. **Golub MA, Doskolovich LL, Kazanskiy NL, Soifer VA, Kharitonov SI.** Diffraction approach to the synthesis of multifunctional phase elements. Optics and Spectroscopy, 1992; 73(1): 111-113.

15. **Kazanskiy NL, Soifer VA.** Diffraction investigation of geometric-optical focusators into segment. Optik – International Journal for Light and Electron Optics, 1994; 96(4): 158-162.

16. **Kazanskiy NL, Kharitonov SI, Soifer VA.** Application of a pseudogeometrical optical approach for calculation of the field formed by a focusator. Optics & Laser Technology, 1996; 28(4): 297-300.

17. **Kazanskiy NL.** Research & Education Center of Diffractive Optics. Proceedings of SPIE, 2012; 8410: 84100R. doi: 10.1117/12.923233.

18. **Golub MA, Doskolovich LL, Kazanskiy NL, Kharitonov SI, Soifer VA.** Computer generated diffractive multi-focal lens. Journal of Modern Optics, 1992; 39(6): 1245-1251.

19. **Doskolovich LL, Kazanskiy NL, Perlo P, Repetto P, Soifer VA.** Direct two-dimensional calculation of binary DOEs using a non-binary series expansion approach. International Journal of Optoelectronics, 1996; 10(4): 243-249.

20. **Kazanskiy N, Skidanov R.** Binary beam splitter. Applied Optics, 2012; 51(14): 2672-2677.

21. **Golub MA, Kazanskii NL, Sisakyan IN, Soifer VA.** Computational experiment with plane optical elements. Optoelectronics, Instrumentation and Data Processing, 1988; 1: 78-89.

22. **Kazanskiy NL.** Correction of focuser phase function by computer-experimental methods. Computer Optics, 1989; 1(1): 69-73.

23. **Kazanskiy NL, Kotlyar VV, Soifer VA.** Computer-aided design of diffractive optical elements. Optical Engineering, 1994; 33(10): 3156-3166.

24. **Doskolovich LL, Golub MA, Kazanskiy NL, Khramov AG, Pavelyev VS, Seraphimovich PG, Soifer VA, Volotovskiy SG.** Software on diffractive optics and computer generated holograms. Proceedings of SPIE, 1995; 2363: 278-284.

25. **Doskolovich LL, Kazanskiy NL, Soifer VA.** Comparative analysis of different focusators focusing into a segment. Optics and Laser Technology, 1995; 27(4): 207-213.

26. **Doskolovich LL, Kazanskiy NL, Soifer VA, Tzaregorodtzev AYe.** Analysis of quasiperiodic and geometric optical solutions of the problem of focusing into an axial segment. Optik – International Journal for Light and Electron Optics, 1995; 101(2): 37-41.

27. **Doskolovich LL, Kazanskiy NL, Kharitonov SI, Soifer VA.** A method of designing diffractive optical elements focusing into plane areas. Journal of Modern Optics, 1996; 43(7): 1423-1433.

28. **Golovashkin DL, Kasanskiy NL.** Solving Diffractive Optics Problem using Graphics Processing Units. Optical Memory and Neural Networks (Information Optics), 2011; 20(2): 85-89.

29. **Volkov AV, Kazanskiy NL, Moiseev OYu, Soifer VA.** A Method for the Diffractive Microrelief Forming Using the Layered Photoresist Growth. Optics and Lasers in Engineering, 1998; 29(4-5): 281-288.

30. **Kazanskiy NL, Kolpakov VA, Kolpakov AI.** Anisotropic Etching of SiO_2 in High-Voltage Gas-Discharge Plasmas. Russian Microelectronics, 2004; 33(3): 169-182.

31. **Pavelyev VS, Borodin SA, Kazanskiy NL, Kostyuk GF, Volkov AV.** Formation of diffractive microrelief on diamond film surface. Optics & Laser Technology, 2007; 39(6): 1234-1238.

32. **Bezus EA, Doskolovich LL, Kazanskiy NL.** Evanescent-wave interferometric nanoscale photolithography using guided-mode resonant gratings. Microelectronic Engineering, 2011; 88(2): 170-174.

33. **Bezus EA, Doskolovich LL, Kazanskiy NL.** Interference pattern formation in evanescent electromagnetic waves using waveguide diffraction gratings. Quantum Electronics, 2011; 41(8): 759-764.

34. **Abulkhanov SR, Kazanskiy NL, Doskolovich LL, Kazakova OY.** Manufacture of diffractive optical elements by cutting on numerically controlled machine tools. Russian Engineering Research, 2011; 31(12): 1268-1272.

35. **Kazanskiy NL, Kolpakov VA, Podlipnov VV.** Gas discharge devices generating the directed fluxes of off-electrode plasma. Vacuum, 2014; 101: 291-297.

36. **Volkov AV, Kazanskiy NL, Moiseev OYu, Poletayev SD.** Thermal Oxidative Degradation of Molybdenum Films under Laser Ablation. Technical Physics, 2015; 60(2): 265–269. doi: 10.1134/S1063784215020255.

37. **Doskolovich LL, Kazanskiy NL, Soifer VA, Kharitonov SI, Perlo P.** A DOE to form a line-shaped directivity diagram. Journal of Modern Optics, 2004; 51(13): 1999-2005.

38. **Doskolovich LL, Kazanskiy NL, Soifer VA, Perlo P, Repetto P.** Design of DOEs for wavelength division and focusing. Journal of Modern Optics, 2005; 52(6): 917-926.

39. **Doskolovich LL, Kazanskiy NL, Khonina SN, Skidanov RV, Heikkila N, Siitonen S, Turunen J.** Design and investigation of color separation diffraction gratings. Applied Optics, 2007; 46(15): 2825-2830.

40. **Karpeev SV, Pavelyev VS, Khonina SN, Kazanskiy NL, Gavrilov AV, Eropolov VA.** Fibre sensors based on transverse mode selection. Journal of Modern Optics, 2007; 54(6): 833-844. doi: 10.1080/09500340601066125.

41. **Borodin SA, Volkov AV, Kazanskiy NL.** Device for analyzing nanoroughness and contamination on a substrate from the dynamic state of a liquid drop deposited on its surface. Journal of Optical Technology, 2009; 76(7): 408-412.

42. **Kazanskiy NL, Popov SB.** Machine Vision System for Singularity Detection in Monitoring the Long Process. Optical Memory and Neural Networks (Information Optics), 2010; 19(1): 23-30.

43. **Khonina SN, Kazanskiy NL, Volotovsky SG.** Influence of Vortex Transmission Phase Function on Intensity Distribution in the Focal Area of High-Aperture Focusing System.

Optical Memory and Neural Networks (Information Optics), 2011; 20(1): 23-42. doi: 10.3103/S1060992X11010024.

44. **Aslanov ER, Doskolovich LL, Moiseev MA, Bezus EA, Kazanskiy NL.** Design of an optical element forming an axial line segment for efficient LED lighting systems. Optics Express, 2013; 21(23): 28651-28656.

45. **Kazanskiy NL, Khonina SN, Skidanov RV, Morozov AA, Kharitonov SI, Volotovskiy SG.** Formation of images using multilevel diffractive lens. Computer Optics, 2014; 38(3): 425-434. [in Russian].

46. **Bezus EA, Doskolovich LL, Kazanskiy NL.** Scattering suppression in plasmonic optics using a simple two-layer dielectric structure. Applied Physics Letters, 2011; 98(22): 221108. doi: 10.1063/1.3597620.

47. **Bezus EA, Doskolovich LL, Kazanskiy NL, Soifer VA.** Scattering in elements of plasmon optics suppressed by two-layer dielectric structures. Technical Physics Letters, 2011; 37(12): 1091-1095.

48. **Bezus EA, Doskolovich LL, Kazanskiy NL.** Low-scattering surface plasmon refraction with isotropic materials. Optics Express, 2014; 22(11): 13547-13554. doi: 10.1364/OE.22.013547.

49. **Doskolovich LL, Kazanskiy NL, Kharitonov SI, Usplenjev GV.** Focusators for laser-branding. Optics and Lasers in Engineering, 1991; 15(5): 311-322.

50. **Kazanskiy NL, Murzin SP, Tregub VI.** Optical system for realization of selective laser sublimation of metal alloy components. Computer Optics, 2010; 34(4): 481-486. [in Russian]

51. **Kazanskiy NL, Murzin SP, Osetrov YeL, Tregub VI.** Synthesis of nanoporous structures in metallic materials under laser action. Optics and Lasers in Engineering, 2011; 49(11): 1264-1267.

52. **Murzin SP, Tregub VI, Shokova EV, Tregub NV.** Thermocycling with pulse-periodic laser action for formation of nanoporous structure in metal material. Computer Optics, 2013; 37(1): 99-105. [in Russian]

53. **Murzin SP, Tregub VI, Melnikov AA, Tregub NV.** Application of radiation focusators for creation of nanoporous metal materials with high specific surface area by laser action. Computer Optics, 2013; 37(2): 226-233. [in Russian]

54. **Murzin SP.** Synthesis of metal materials nanoporous structures with cyclic elasto-plastic deformation under laser treatment using radiation focusators. Computer Optics, 2014; 38(2): 249-255. [in Russian]

55. **Murzin SP.** Method of composite nanomaterials synthesis under metal/oxide pulse-periodic laser treatment. Computer Optics, 2014; 38(3): 469-475. [in Russian]

56. **Soifer VA, Kazanskiy NL, Kharitonov SI.** Synthesis of a Binary DOE Focusing into an Arbitrary Curve, Using the Electromagnetic Approximation. Optics and Lasers in Engineering, 1998; 29(4-5): 237-247.

57. **Kharitonov SI, Doskolovich LL, Kazanskiy NL, Kalyaev ML.** The asymptotic method for calculation of the field of the optical elements having the band structure. Computer Optics, 2007; 31(4): 7-18. [in Russian]

58. **Kazanskiy NL, Kalyaev ML, Kharitonov SI.** Compact recording solutions of Maxwell's equations in the space-frequency representation. Antennas, 2007; 10: 13-21. [in Russian]

59. **Khonina SN, Kazanskiy NL, Ustinov AV, Volotovskii SG.** The lensacon: nonparaxial effects. Journal of Optical Technology, 2011; 78(11): 724-729.

60. **Doskolovich LL, Kazanskiy NL, Kharitonov SI.** Integral representations for solutions of Maxwell's equations for anisotropic media. Computer Optics, 2010; 34(1): 52-57. [in Russian]

61. **Kazanskiy NL, Kharitonov SI.** Transmission of the space-limited broadband symmetrical radial pulses focused through a thin film. Computer Optics, 2012; 36(1): 4-13. [in Russian]

62. **Kazanskiy NL, Khonina SN, Kharitonov SI.** The perturbation theory for Schrödinger equation in the periodic environment in momentum representation. Computer Optics, 2012; 36(1): 21-26. [in Russian]

63. **Khonina SN, Volotovsky SG, Kharitonov SI, Kazanskiy NL.** Calculation of the power spectrum of complex low-dimensional heterostructures in the presence of electric field. Computer Optics, 2012; 36(1): 27-33. [in Russian]

64. **Kazanskiy NL, Kharitonov SI, Khonina SN.** Joint solution of the Klein–Gordon and Maxwell's equations. Computer Optics, 2012; 36(4): 518-526. [in Russian]

65. **Zherdev DA, Kazanskiy NL, Fursov VA, Kharitonov SI.** Electromagnetic field scattering simulation from anthropogenic objects on underlying surface. Computer Optics, 2013; 37(1): 91-98. [in Russian]

66. **Bykov DA, Doskolovich LL, Soifer VA, Kazanskiy NL.** Extraordinary Magneto-Optical Effect of a Change in the Phase of Diffraction Orders in Dielectric Diffraction Gratings. Journal of Experimental and Theoretical Physics, 2010; 111(6): 967-974.

67. **Golovashkin DL, Kazanskiy NL.** Mesh Domain Decomposition in the Finite-Difference Solution of Maxwell's Equations. Optical Memory & Neural Networks (Information Optics), 2009; 18(3): 203-211.

68. **Kazanskiy NL, Serafimovich PG, Khonina SN.** Harnessing the Guided-Mode Resonance to Design Nanooptical Transmission Spectral Filters. Optical Memory and Neural Networks (Information Optics), 2010; 19(4): 318-324. doi: 10.3103/S1060992X10040090.

69. **Kazanskiy NL, Serafimovich PG.** Cloud Computing for Rigorous Coupled-Wave Analysis. Advances in Optical Technologies, 2012; Article ID 398341. doi: 10.1155/2012/398341.

70. **Kazanskiy NL, Serafimovich PG, Khonina SN.** Use of photonic crystal cavities for temporal differentiation of optical signals. Optics Letters, 2013; 38(7): 1149-1151. doi: 10.1364/OL.38.001149.

71. **Kazanskiy NL, Serafimovich PG.** Cloud Computing for Nanophotonic Simulations. Lecture Notes in Computer Science, 2013; 7715: 54-67.

72. **Kazanskiy NL, Serafimovich PG.** Coupled-resonator optical wave-guides for temporal integration of optical signals. Optics Express, 2014; 22(11): 14004-14013. doi: 10.1364/OE.22.014004.

73. **Khonina SN, Savelyev DA, Kazanskiy NL.** Vortex phase elements as detectors of polarization state. Optics Express, 2015; 23(14): 17845-17859. doi: 10.1364/OE.23.017845.

74. **Egorov AV, Kazanskiy NL, Serafimovich PG.** Using coupled photonic crystal cavities for increasing of sensor sensitivity. Computer Optics, 2015; 39(2): 158-162. [in Russian]

75. **Kazanskiy NL, Kharitonov SI, Khonina SN, Volotovskiy SG, Strelkov YuS.** Simulation of hyperspectrometer on spectral linear variable filters. Computer Optics, 2014; 38(2): 256-270. [in Russian]

76. **Kazanskiy NL, Kharitonov SI, Karsakov AV, Khonina SN.** Modeling action of a hyperspectrometer based on the Offner scheme within geometric optics. Computer Optics, 2014; 38(2): 271-280. [in Russian]

77. **Kazanskiy NL, Kharitonov SI, Khonina SN.** Simulation of a hyperspectrometer based on linear spectral filters using vector Bessel beams. Computer Optics, 2014; 38(4): 770-776. [in Russian]

78. **Doskolovich LL, Bezus EA, Bykov DA.** On the compensation of the diffraction orders overlap effect in the Offner spectrometer. Computer Optics, 2014; 38(4): 777-782. [in Russian]

79. **Kazanskiy NL, Kharitonov SI, Doskolovich LL, Pavelyev AV.** Modeling the performance of a spaceborne hyperspectrometer based on the Offner scheme. Computer Optics, 2015; 39(1). 70-76. [in Russian]

80. **Soifer VA.** Diffractive Nanophotonics and Advanced Information Technologies. Herald of the Russian Academy of Sciences, 2014; 84(1): 9-18. doi: 10.1134/S1019331614010067.

Modeling and identification of centered crystal lattices in three-dimensional space

Kirsh D.V.,

Samara State Aerospace University

Kupriyanov A.V.

Image Processing Systems Institute, Russian Academy of Sciences

Abstract. The paper offers a method that allows to model crystal lattices in three dimensional space. The method is based on a description of crystal lattices in the six-dimensional Euclidean space G6. Transformations of three basic translation vectors from centered types to primitive types have been derived. Using these transformations, the proposed method provides a uniform way to model both primitive and centered Bravais lattices. On a set of simulated lattices, the possibility of structural identification of primitive and centered crystal lattices has been investigated. The previously developed parametric identification method based on estimation of Wigner-Seitz cell volume has demonstrated the best result of separation of centered lattices from primitive ones. In addition, this method allowed to identify the type of centering for five out of seven centered Bravais lattices.

Keywords: crystal lattice, primitive lattice, centered lattice, Bravais unit cell, Wigner-Seitz cell, structural identification, similarity measure

1. Introduction

A three-dimensional crystal lattice is a mathematical model which does not only allow to describe a structure of any crystalline material, but also determines its basic physical and chemical properties.

The problem of structural identification of crystal lattices still remains one of the main problems related to X-ray diffraction analysis. In his paper, Kupriyanov [1] has proposed an efficient approach to its solution which consist of estimating a number of parameters in the lattices under investigation and their subsequent comparison with parameters of reference lattices. The lattices either previously investigated or derived by modeling can be used as samples. Thus, the accurate structural identification of crystal lattices requires a large database of predetermined reference parameters.

The analysis of existing methods to solve the problem of structural identification has shown that the methods are mainly studied for lattices of seven primitive types, while the centered lattices are completely ignored.

In this paper, we propose a modeling method for centered crystal lattices and investigate the possibility of structural identification of primitive and centered lattices by using the existing and developed parametric identification methods.

2. Modeling Method for Centered Crystal Lattices

A crystal lattice model used in previous researches was based on three translation vectors [2]. Its basic parameters are:

- three edge lengths l_1, l_2, l_3 and three angle values $\alpha_1, \alpha_2, \alpha_3$ of a unit cell (Fig. 1);
- a number of lattice points by each of the translation vectors N_1, N_2, N_3.
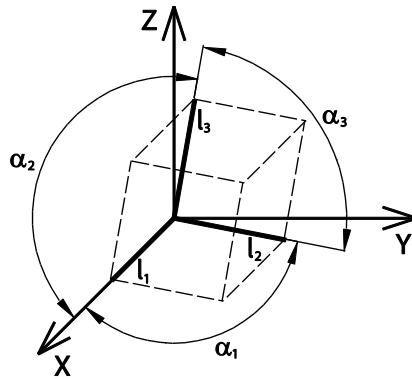
Fig. 1. – Unit cell model constructed on three basic translation vectors

This model has one significant disadvantage: it can only describe lattices of seven lattice systems – primitive Bravais lattices (index P). However, there are seven more centered Bravais lattices, which, in turn, are divided into the following three types [3]:

- body-centered (index I): one additional point at the center of the unit cell;
- base-centered (indices A, B, C): additional points at the centers of two parallel sides of the unit cell;
- face-centered (index F): additional points at the centers of each face of the unit cell.

Therefore, all crystal lattices can be assigned to one of the 14 Bravais lattice types (Fig. 2).
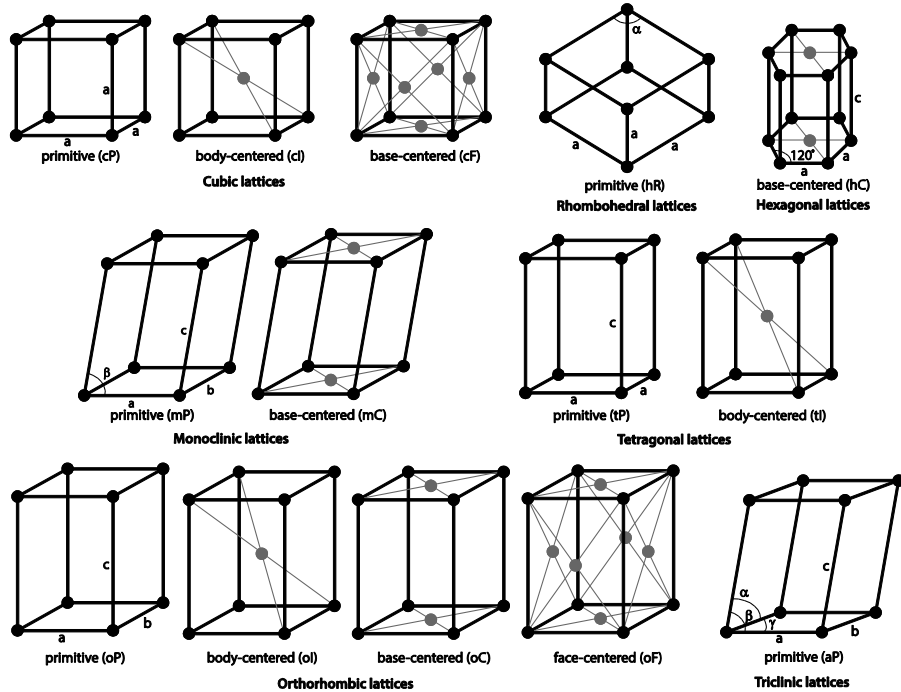
Fig. 2. – Primitive and centered types of Bravais lattices

To describe centered lattices, the used model has to be expanded by adding up to three translation vectors (Fig. 3). Doubling the number of parameters makes the model overly complicated.
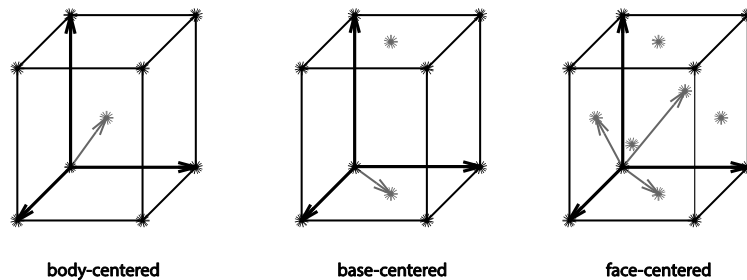
Fig. 3. – Choice of extra translation vectors within a centered lattice

An analogue of this model was suggested by Andrews and Bernstein [4]. It describes the lattice in the form of a six-dimensional vector $\bar{g}$ in the space G6. In addition, Andrews and Bernstein proved that each centered lattice $\bar{g}_T$ might be transformed to a primitive representation $\bar{g}_P$ by the following transformation:

164

$$\bar{g}_P = A \cdot \bar{g}_T. \tag{1}$$

Each centered type has its own general form of the transformation matrix A. By solving the system of linear equations (1) with respect to basic translation vectors $\bar{a}_1, \bar{a}_2, \bar{a}_3$, we deduced the following solutions:

$$\begin{cases} \bar{a}_{1P} = \bar{a}_{1I} \\ \bar{a}_{2P} = \bar{a}_{2I} \\ \bar{a}_{3P} = 0.5\bar{a}_{1I} + 0.5\bar{a}_{2I} + 0.5\bar{a}_{3I} \end{cases} ; \begin{cases} \bar{a}_{1P} = \bar{a}_{1C} \\ \bar{a}_{2P} = 0.5\bar{a}_{1C} + 0.5\bar{a}_{2C} \\ \bar{a}_{3P} = \bar{a}_{3C} \end{cases} ; \begin{cases} \bar{a}_{1P} = 0.5\bar{a}_{1F} + 0.5\bar{a}_{2F} \\ \bar{a}_{2P} = 0.5\bar{a}_{1F} + 0.5\bar{a}_{3F} \\ \bar{a}_{3P} = 0.5\bar{a}_{2F} + 0.5\bar{a}_{3F} \end{cases} . \tag{2}$$

In other words, the transformations (2) make a choice of three new translation vectors. These vectors also allow to simulate all lattice points, however their parameters correspond to a primitive lattice that can be allocated within a centered lattice (Fig. 4).

body-centered   base-centered   face-centered
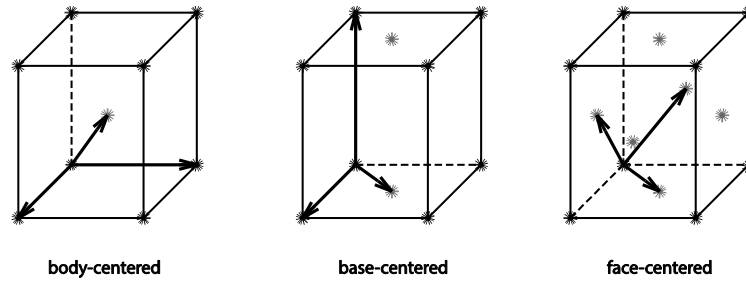
Fig. 4. – Selection of translation vectors of a primitive lattice within a centered lattice

This result gives a completely different look at the problem of modeling crystal lattices. On the one hand, if it is necessary to model a large set of random lattices, this set can be simulated by changing each parameter of a unit cell (lengths of the edges and values of the angles) independently in a specified range with a given partition. The resulting set of lattices will cover all primitive as well as centered lattices.

On the other hand, if the experiment requires a certain number of lattices for each type of centering, it would be possible to obtain a necessary number of lattices using the above transformations (2).

In the framework of new ideas, three basic translation vectors are to be sufficient to describe any crystal lattice in three-dimensional space. It is only needed to supplement them with the transformations (2) allowing to simulate a lattice of a particular centered type.

3. Methods of Crystal Lattice Parametric Identification

The basic methods among the existing crystal lattice parametric identification methods are the following:

- parametric identification method based on estimation of atomic packing factor [5];

165

- parametric identification method based on estimation of distances between isosurfaces [6].

In the parametric identification method based on estimation of atomic packing factor, each unit cell is represented as close packing of spheres (Fig. 5). The atomic packing factor can be calculated by dividing volume of atoms in unit cell by volume of unit cell.
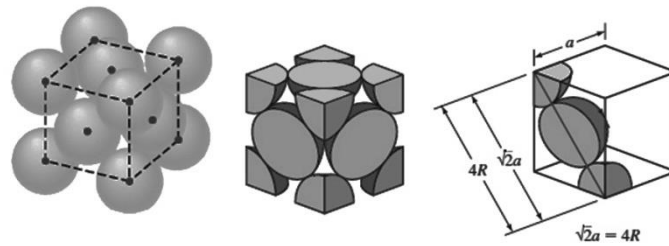
Fig. 5. – Close packing of spheres

In the parametric identification method based on estimation of distances between isosurfaces, a set of isosurfaces are constructed for each unit cell (Fig. 6). Then the root mean square distance and the Hausdorff distance between the isosurfaces are calculated.
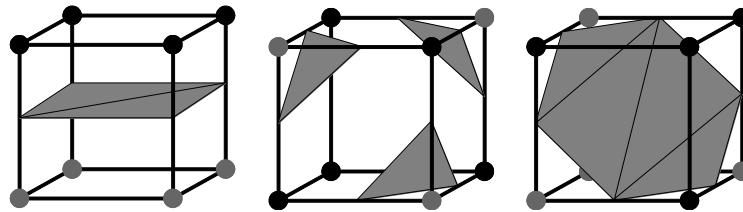
Fig. 6. – Types of isosurfaces constructed for a cubic lattice

The investigation of above two methods has shown that they have a number of disadvantages: a strong dependence of the crystal lattice identification accuracy from the type of the crystal system and a high sensitivity to distortions of coordinates of crystal lattice points. In order to eliminate these drawbacks, we have developed two new parametric identification methods.

The first of the developed method is based on estimation of Bravais unit cell parameters (lengths of three edges and values of three angles between the edges). By using the rotation of the analyzed lattice about coordinate axes, the proposed algorithm chooses three lattice points and calculates lengths of their radius vectors and angles between them. The radius vectors of the chosen points are non-coplanar and have minimum lengths [7].

The second of the developed method is based on estimation of Wigner-Seitz cell volume. The proposed algorithm uses Monte Carlo method to calculate the volume. It

166

constructs planes limiting Wigner-Seitz cell and scatters randomly a great number of points in the lattice area. The amount of points that fall into the limited area determines the Wigner-Seitz cell volume [8].

All the methods listed above use normalized similarity measures to compare estimated parameters with reference parameters. The similarity measures take the greatest value of unit when parameters completely coincide.

4. Identification of Centered Crystal Lattices

We conducted a series of computational experiments in order to investigate the possibility of separation centered lattices from primitive ones, as well as the possibility of delimiting types of centering.

Using the developed modeling method, crystal lattices of 11 Bravais types were simulated: monoclinic (mP, mC), orthorhombic (oP, oC, oI, oF), tetragonal (tP, tI) and cubic (cP, cI, cF). Triclinic, rhombohedral and hexagonal crystal systems were excluded from our consideration since all lattices of these systems are primitive. As simulation parameters we used the parameters of crystal lattices of natural minerals which have the unit cells similar in volume.

Then, the identification methods were used to estimate parameters of each crystal lattice and to calculate similarity measures between parameters of primitive and centered lattices. The results of computational experiments in the form of diagrams are presented below in Fig. 7 and Fig. 8.
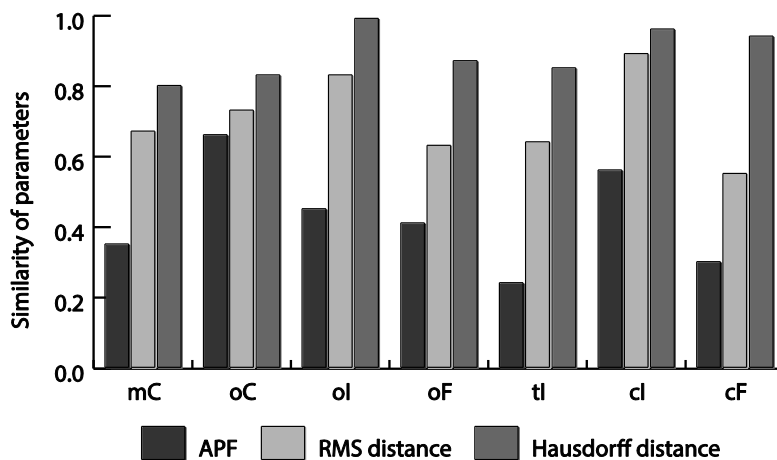
Fig. 7. – Similarity between centered and primitive Bravais lattices.
Comparing atomic packing factors and distances between isosurfaces

Fig. 7 shows that RMS and Hausdorff distances are weakly dependent on the type of centering. Moreover, for two centered lattices, the value of their similarity with primitive lattices was about 0.95. Thus, the identification method based on estimation of distances between isosurfaces is not applicable to separate centered lattices from primitive ones. The obtained result can be explained by the fact that this method

estimates the maximum and the average distances between lattice points, whereas the centering has the greatest influence on the minimum distance. A similar situation can be observed in Fig. 8 for the identification method based on estimation of Bravais unit cell parameters (edges and angles).
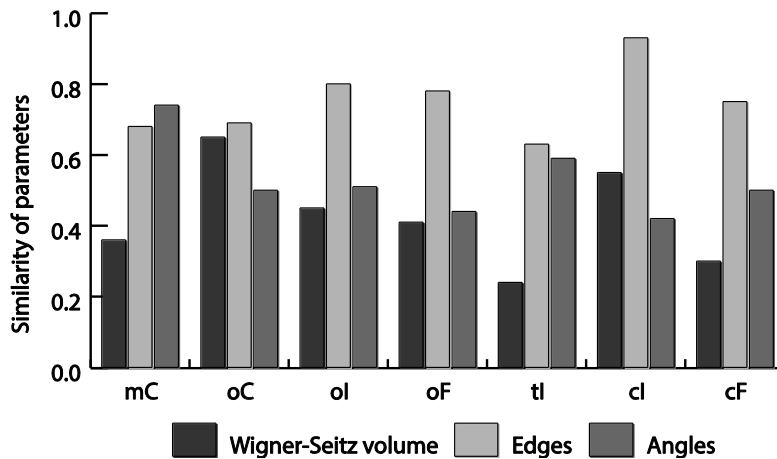
Fig. 8. – Similarity between centered and primitive Bravais lattices.
Comparing edges and angles of unit cell and Wigner-Seitz cell volumes

The identification methods based on estimation of atomic packing factor and Wigner-Seitz cell volume have demonstrated the best result among other identification methods. The maximum value of their similarity with the primitive types was 0.66 and the average value of difference between the centered types was 0.2. Therefore, these methods allow to identify the type of centering with high accuracy. However, for orthorhombic system, it proved to be impossible to separate body-centered lattices from base-centered lattices.

It should be noted that the parametric identification method based on estimation of Wigner-Seitz cell volume does not require any information about basic translation vectors of a unit cell. As a consequence, this method is more universal than the parametric identification method based on estimation of atomic packing factor. At the same time, the parametric identification method based on estimation of Wigner-Seitz cell volume has the highest computational complexity because of the Monte Carlo method taken as its basis.

5. Conclusion

The developed crystal lattice modeling method allows to simulate any primitive or centered lattice in three-dimensional space. Besides, by changing each parameter of a unit cell (lengths of the edges and values of the angles) independently, a large set of lattices can be simulated to cover all 14 types of Bravais lattices. This set is a necessary condition for correct structure identification of crystal lattices.

168

The performed investigation of possible identification of centered crystal lattices has demonstrated that the parametric identification method based on estimation of Wigner-Seitz cell volume allows to separate with the high accuracy the centered lattices from the primitive lattices. In addition, it can identify the type of centering for five out of seven centered Bravais lattices (mC, oF, tI, cI, cF).

As it has been shown in previous papers, the parametric identification method based on estimation of Bravais unit cell parameters provides the high accuracy of lattice system identification. However, the Bravais type is determined not only by the lattice system but also by the type of centering. Therefore, it is essential to use both developed methods for the most accurate structural identification of crystal lattices.

Acknowledgements

References

1. **Kharitonov SI, Volotovskiy SG, Khonina SN, Kazanskiy NL.** A differential method for calculating x-ray diffraction by crystals: the scalar theory. Computer Optics, 2015; 39(4): 469-479. [in Russian]
2. **Murzin SP.** Synthesis of metal materials nanoporous structures with cyclic elasto-plastic deformation under laser treatment using radiation focusators. Computer Optics, 2014; 38(2): 249-255. [in Russian]
3. **Volkov AV, Moiseev OYu, Poletaev SD, Chistyakov IV.** Application of thin molybdenum films in contact masks for manufacturing the micro-relief of diffractive optical elements. Computer Optics, 2014; 38(4): 757-762. [in Russian]
4. **Murzin SP, Balyakin VB, Melnikov AA, Vasiliev NN, Lichtner PI.** Determining ways of improving the tribological properties of the silicon carbide ceramic using a pulse-periodic laser treatment. Computer Optics, 2015; 39(1): 64-69. [in Russian]
5. **Murzin, S.P.** Method of composite nanomaterials synthesis under metal/oxide pulse-periodic laser treatment. Computer Optics, 2014; 38(3): 469-475. [in Russian]
6. **Kupriyanov AV, Soifer VA.** On the Observability of the Crystal Lattice with the Images of their Projections. Computer Optics, 2012; 36(2): 249-256. [in Russian]
7. **Kirsh DV.** Information System of Crystal Lattice Modeling in Three-Dimensional Space. SSAU Press, Samara, 2014. 448-452. [in Russian]
8. **Shaskolskaya MP.** Crystallography: Manual for Institutes of Higher Education. Higher School, Moscow, 1984. [in Russian]
9. **Andrews LC, Bernstei HJ.** Lattices and Reduced Cells as Points in 6-Space and Selection of Bravais Lattice Type by Projections. Foundations of Crystallography, 1988; 44(6): 1009-1018.
10. **Smith WF.** Foundations of Materials Science and Engineering. McGraw-Hill, New York, 2004.

11. **Patera J, Skala V.** Centered Cubic Lattice Method Comparison. Proceedings of Algoritmy, 2005; 309-319.
12. **Kupriyanov AV, Kirsh DV.** Estimation of the Crystal Lattice Similarity Measure by Three-Dimensional Coordinates of Lattice Nodes. Optical Memory and Neural Networks (Information Optics), 2015; 24(2): 145-151.
13. **Kirsh DV, Kupriyanov AV.** Crystal Lattice Identification by Coordinates of Their Nodes in Three Dimensional Space. Pattern Recognition and Image Analysis, 2015; 25(3): 456-460.

Spectrum of spatial frequency of terahertz vortex Bessel beams formed using phase plates with spiral zones

Zhabin V.N.,

Novosibirsk State University

Volodkin B.O.,

Samara State Aerospace University

Knyazev B.A.,

Budker Institute of Nuclear Physics & Novosibirsk State University

Mitkov M.S.,

Budker Institute of Nuclear Physics

Pavelyev V.S.,

Samara State Aerospace University,
Image Processing Systems Institute, Russian Academy of Sciences

Choporova Yu.Yu.

Budker Institute of Nuclear Physics & Novosibirsk State University

Abstract. This paper presents the first numerical and experimental investigation into the angular spectrum of terahertz Bessel beam with orbital angular momentum generated by a phase plate with spiral zones. The plate was exposed to a Gaussian beam of the Novosibirsk free electron laser. The Bessel beam formed was passed through a collecting lens. The distribution of the intensity of radiation with a wavelength of 141 microns before and after the focusing lens was recorded by a microbolometer array, which was moved along the optical axis by a motorized translation stage. The experimentally measured intensity distributions over the beam cross section recorded along the optical axis are in good agreement with numerical calculations.

1. Introduction

A plane electromagnetic wave is characterized by polarization in addition to the amplitude and wave vector. In a general case, an elliptical polarization can be split into the right and left circular polarizations corresponding to spin angular momentum (SAM) of the photon $\pm\hbar$. If the angular dependence of the wave function is $e^{il\phi}$, the photon has, in addition to the spin, the orbital angular momentum (OAM) $\pm l\hbar$, where l is any integer. Such beams have helical phase fronts with the number of intertwined helices depending on the magnitude of l [1].

In this work we investigated vortex Bessel beams, which are described by the following formula:

$$F(r,\phi,z,t) = J_l(\kappa r)e^{il\phi}e^{ik_z z}e^{-i\omega t}. \tag{1}$$

where $J_l(x)$ is the Bessel function of the first kind of the l th order, κ is the radial component of the wave vector.

In this paper we investigated the angular spectrum of Bessel beam formed by a phase diffractive element [2]. Actually, the spectrum is an expansion of the initial wave into plane waves, which enables better understanding of the structure and behavior of such beams. In particular, one can experimentally check whether a beam is a Bessel one. From the mathematical point of view, the angular spectrum is the Fourier transform. If done with a thin lens, it can be written as follows:

$$\frac{k}{f}i^{-l-1}e^{il\psi}\int_0^R rJ_l(\kappa r)J_l(\frac{k\rho r}{f})dr. \tag{2}$$

where R is the radius of the lens aperture; f is the focal distance; ρ and ψ are the polar coordinates in the focal plane. With an infinite lens aperture, the angular distribution takes the form of a thin ring described with the following formula:

$$\frac{i^{-l-1}}{\kappa}e^{il\psi}\delta(\rho-\rho_0),$$

where $\rho_0 = \dfrac{\kappa f}{k}$ is the radius of the ring. In case of finite lens aperture, the main ring smears, and there are a number of subordinate concentric rings near it.

2. Generation of Bessel beams

There are many ways to produce a vortex beam from a plane wave, e.g. with diffractive elements, which are particularly suitable for the terahertz range. They can

172

be forked diffraction gratings or a spiral Fresnel plate. The application of amplitude spiral Fresnel plate to formation of beams with a spatial singularity was proposed in [3]. The boundaries of the zones of the plate are described by the following formula:

$$l\varphi = (n + \frac{1}{2})\pi + \frac{kr^2}{2f},$$

where l is the topological charge of the beam; f is the focal distance of the plate; $n = 0, \pm1, \pm2, \ldots$ If $l = 0$, it is a conventional Fresnel zone plate.

The experiment was conducted with similar binary phase plates of 30 mm in diameter produced by reactive ion etching [4] on a high-resistivity silicon wafer but with a constant width of the zones, as shown in Fig. 1. The boundaries of the zones are described by the following formula:

$$\frac{l\varphi}{2\pi} = r + ln.$$
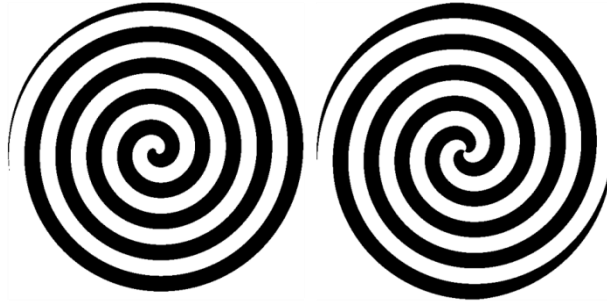
Fig. 1. – Phase plates with spiral zones to form beams with topological charge $l = \pm1$ (left) and $l = \pm2$ (right); the charge sign changes when the plate is rotated through an angle of 180º around the vertical axis. The phase shift between the black and the white areas is π

Hereinafter this phase plate with spiral zones is referred to as a spiral phase plate (SPP). It was confirmed experimentally (see below) that a plane wave incident on it forms a Bessel beam. If $l = 0$, it is a usual axicon.

The numerical modelling was performed in the approximation of the scalar diffraction theory. In the Fresnel approximation the Kirchhoff integral yields an expression of the following form:

$$E(x, y) = \frac{e^{ikz}}{i\lambda z} \int_s E(\xi, \eta) \exp\left[\frac{ik}{2z}\left((x - \xi)^2 + (y - \eta)^2\right)\right] d\xi d\eta.$$

This integral is a two-dimensional convolution of two functions and can be expressed using the Fourier transform,

$$E(x, y) = 2\pi \frac{e^{ikz}}{i\lambda z} \mathsf{F}_-\{\mathsf{F}_+[E(x, y)] \cdot \mathsf{F}_+[w(x, y)]\},$$

where $w(x, y) = \exp\left[\frac{ik}{2z}(x^2 + y^2)\right]$. This approach can significantly facilitate the numerical simulation of diffraction with the fast Fourier transform.

For numerical calculations it is necessary to turn from the continuous Fourier transform to the discrete Fourier transform (DFT), which can be done in accordance with the following formulas:

$$X_{mn} = \sum_{k=0}^{M-1}\sum_{l=0}^{N-1} x_{kl} e^{-\frac{2\pi i}{M}mk} e^{-\frac{2\pi i}{N}nl},$$

$$x_{kl} = \frac{1}{MN} \sum_{n=0}^{M-1}\sum_{m=0}^{N-1} X_{mn} e^{\frac{2\pi i}{M}mk} e^{\frac{2\pi i}{N}nl}.$$

3. Modeling and experimental verification

Computer program Huygens for OS Windows on x86-64 processors was designed for numerical simulation. The library FFTW was used to calculate fast Fourier transform. We carried out the numerical simulation by a scheme corresponding exactly to the experimental set-up shown in Fig. 2. The radiation source was the Novosibirsk free electron laser [5]. In this experiment it was tuned to a wavelength of 141 microns, the phase plates to generate beams with the topological charge were calculated for.
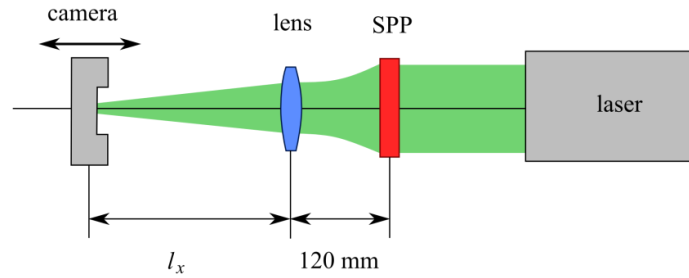
Fig. 2. – Schematic of the experiment. SPP is spiral phase plate

A series of numerical simulations was carried out. In the first numerical simulation, the diffraction of plane wave on a spiral phase plate was investigated, as well as diffraction of ideal Bessel beam on a circular aperture, the radius of which corresponded to the aperture of the plate. From the simulation results the corresponding parameters of the Bessel beam were found. For example, it was found that a plate with the index $l = 2$ is best matched by a Bessel beam with the radial

174

parameter $\kappa = 1.6\,\text{mm}^{-1}$. Fig. 3 presents the respective images. Hereinafter, the brightness corresponds to the intensity and the phase distribution is shown with color.
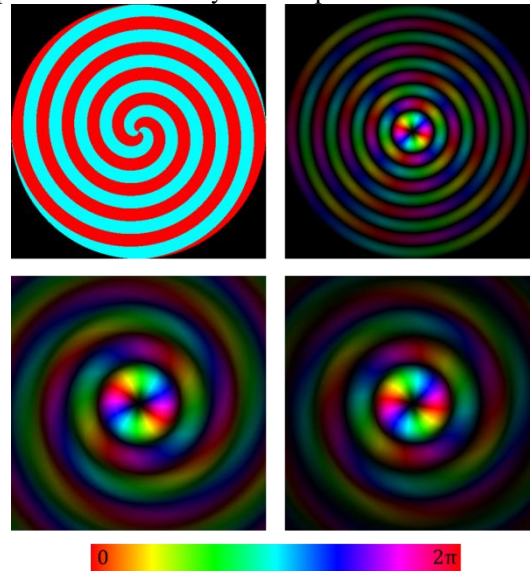
Fig. 3. – Comparison of plane wave diffraction on SPP (left) and Bessel beam diffraction on aperture (right)

The second simulation modeled images of ideal Bessel beam of finite radius and plane wave diffracted on a SPP in the Fourier plane of a converging lens with the focal length $f = 50\,\text{mm}$, which are shown at Fig. 4. A comparison with theoretical data shows the images in the Fourier plane to be in qualitative agreement with the theoretical predictions, i.e. there is a ring-shape spot. However, there is some difference, i.e. the ring shape is distorted into a fragment of a number of spirals when SPP was used. An analysis of distribution formed by a spiral phase plate is given in [6, 7].
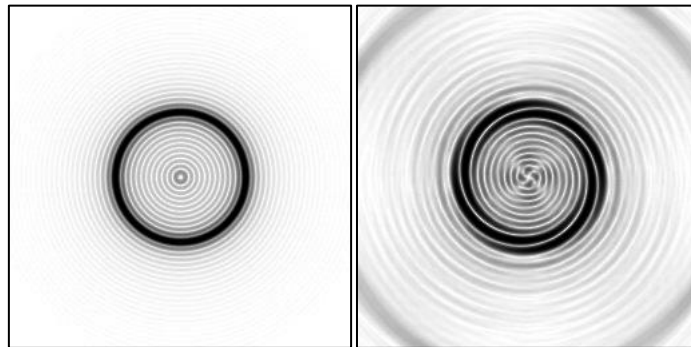
Fig. 4. – Images in Fourier plane of ideal Bessel beam (left), and plane wave diffracted on SPP with $l = 2$ (right)

In the real experiment, the spiral phase plates were exposed to a Gaussian beam of the Novosibirsk free electron laser I : $\exp(-2r^2 / w^2)$ with $w = 15.1$ mm. The radiation intensity distribution along the Bessel beam and in the area behind a TPX lens with a focal length of 50 mm or 100 mm was recorded with a microbolometer array (MBA) as a video at 20 frames per second. The MBA was moved along the optical axis by a motorized translation stage 300 mm long. The size of the sensitive elements (pixel) of the MBA was $51 \times 51 \,\mu m^2$, which is three times as small as the wavelength of the radiation used. The physical size of the matrix was $16.36 \times 12.24 \, mm^2$.

Then the experimental data were compared with the results of the numerical simulation. The calculated and experimentally measured intensity distributions are shown in Fig. 5. It is seen that the experiment and the numerical simulation yield a difference from the ring-shaped image as a spiral fragment. There is a visible substantial difference, the bright spot in the center of the image in the experiment, which indicates that after passing through the SPP some radiation retains the initial direction of the wave vector. As for the rest, the numerical simulation and the experiment are in qualitative agreement, including the observation of spiral fragment instead of ring as predicted by the theory for an ideal Bessel beam.
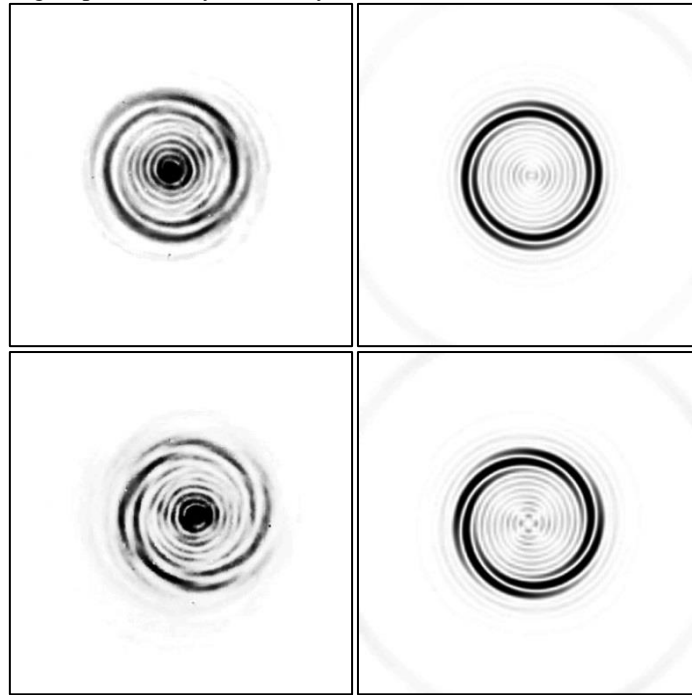
Fig. 5. – Distribution of radiation intensity in lens focal plane (inverted and gamma-corrected). Left: images recorded with MBA. Right: results of numerical modeling for SPP with $l = 1$ (top) and $l = 2$ (bottom) with lens with $f = 50$ mm

To explain the experimental results, we have carried out additional calculations in which we varied the structure of the plates. The results are presented in Fig. 6. To reveal weak higher-order angular spectrum components, we present images with a low contrast $\gamma = 0.15$ ($\gamma = 0.10$ for the amplitude plate). For both amplitude and phase binary plates, spiral-like distorted angular distributions were obtained similar to those shown in Fig. 5. For the plates with linearly growing phase within a zone (kinoform phase plate), the angular distribution is a ring which has to be a perfect Bessel beam. Technically valuable to investigate how the angular distribution changes, if besides the binary plates to use multilevel ones. The last two pictures clearly demonstrate that the three-level and four-level plates generate combination of practically perfect Bessel beam with weak components of higher orders. The latter can be easily removed using a simple system of optical filtering.
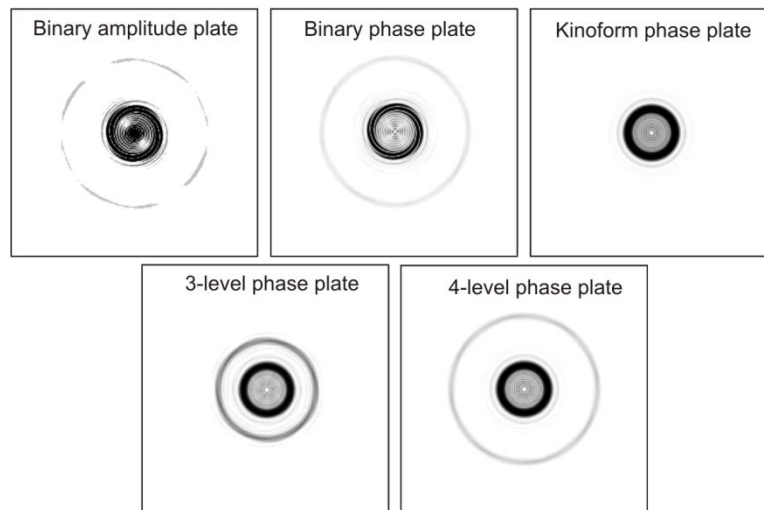
Fig. 6. – Distributions of radiation intensity in the lens focal plane ($f = 50$ mm) for vortex beams with $l = 2$ formed with the spiral plase plates of different structure

4. Conclusion

In summary, this study was the very first investigation into the angular distribution of Bessel beam formed by a spiral phase plate in the terahertz frequencies range, which showed good agreement between the results of computer simulation, the theory and the results of the optical experiments. It is shown that perfect Bessel beam can be achieved using multi-level phase spiral plates.

References

1. Twisted Photons. Applications of Light with Orbital Angular Momentum. Willey, 2011.
2. **Knyazev BA, Choporova YuYu, Pavelyev VS, Volodkin BO, Mitkov MS.** High-Power Terahertz Non-Diffractive Bessel Beams with Angular Orbital Momentum. Generation and Application. Sourse: <http://www.irmmw-thz2015.org/paper 3129943>.
3. **Heckenberg RN, McDuff R, Smith CP, White AG.** Generation of optical phase singularities by computer-generated holograms. Optics Letters, 1992; 17: 221-223,.
4. **Agafonov AN, Volodkin BO, Kaveev AK, Kachalov DG, Knyazev BA, Kropotov GI, Tukmakov KN, Pavelyev VS, Tsypishka DI, Choporova YuYu.** Binary DOE with elongated focal depth to focus terahertz free electron laser radiation (NOVOFEL). Computer Optics, 2015; 39(1): 58-63. [in Russian]
5. **Kulipanov GN, Bagryanskaya EG, Chesnokov EN, Choporova YuYu, Gerasimov VV, Getmanov YaV, Knyazev BA, Kubarev VV, Peltek SE, Popik VM, Salikova TV, Scheglov MA, Seredniakov SS, Shevchenko OA, Skrinsky AN, Veber SL, Vinokurov NA.** Novosibirsk free electron laser: Facility description and recent experiments. IEEE Transactions on Terahertz Science and Technology, 2015; 5(5): in print.
6. **Soifer VA.** Diffractive computer-based optics. Moscow: FIZMATLIT, 2007. 736 p. [in Russian]
7. **Gavrilov AV, Golovashkin DL, Doskolovich LL, Dyachenko PN, Khonina SN, Kotlyar VV, Kovalev AA, Nalimov AG, Nesterenko DV, Pavelyev VS, Shuyupova YO, Skidanov RV, Soifer VA.** In Diffracrive Nanophotonics. Edited by V.A. Soifer. CRC Press. Taylor&Francis Group. CISP. Boca Raton, 2014. 679 p.

Critical phenomena in a model
of fuel's heating in a porous medium

Shchepakina E.A.

Samara State Airspace University

Abstract. The autoignition of flammable liquid in an inert porous medium are studied. In this paper we concentrated on the critical case which is concerned with the phenomenon of delayed loss of stability in the dynamical model. The realizability conditions for the critical regime are obtained. It is shown that critical regime is modelled by a canard − a trajectory of slow–fast system, which first move near the stable part of the slow invariant manifold, then move near the unstable part of it.

Keywords: ignition, critical phenomenon, canard, invariant manifold, delayed loss of stability.

Introduction

This paper deals with the investigation of the critical conditions for autoignition of combustible fluids in porous insulation materials [1, 2]. This phenomenon is usually caused by a leaking of a combustible liquid into lagging material surrounding a hot pipework. Due to highly insulation environment heat losses are remarkable low and autoignition may occur as a result of exothermic oxidation reaction.

The investigation of the autoignition process has been carried out by many authors, see for instance [3–12] and references therein.

We shall study a process which may be defined as the autoignition in two-phase medium (combustible liquid and inert porous matrix). The possible depletion of oxygen or its diffusion into porous structure and transport of the liquid or its vapour within the insulation are all ignored, in order to focus attention on the competitive effects of the reactive term of the dispersed liquid and evaporative heat loss. The dimensionless model in this case has the form [1]

$$\frac{du}{dt} = QK_1 xe^{-1/u} - (u - u_a) - Q_c K_2 xe^{-\beta_e/u},$$

$$\frac{dx}{dt} = -K_2 xe^{-\beta_e/u} - K_1 xe^{-1/u}.$$

(1)

179

Here, u is a dimensionless temperature of the reactant phase; the dimensionless concentration x represents the mass fraction of combustible liquid present in the porous material; the dimensionless parameters Q and K_1 characterize the heat of reaction and the reaction frequency, respectively, for the exothermic oxidation reaction, while Q_c and K_2 are the similar terms for the endothermic evaporation reaction; β_e is the ratio of the enthalpy of vaporization to the activation energy of the oxidation reaction; u_a is ambient temperature.

Introducing the new variables θ and τ by

$$u = \theta + \beta^2, \quad t = \tau \exp(1/\beta), \quad \beta = u(0),$$

and taking into account

$$\exp\left(-\frac{1}{\beta(\theta\beta+1)}\right) = \exp\left(\frac{1}{1+\beta\theta}\right)\exp\left(-\frac{1}{\beta}\right),$$

leads (1) to the form

$$\dot{\theta} = \frac{QK_1 x}{\beta^2}\exp\left(\frac{\theta}{1+\beta\theta}\right) - \left(\theta - \frac{u_a - \beta}{\beta^2}\right)\exp\left(\frac{1}{\beta}\right)$$

$$- \frac{Q_c K_2 x}{\beta^2}\exp\left(\frac{1-\beta_e}{\beta}\right)\exp\left(\frac{\beta_e\theta}{1+\beta\theta}\right), \tag{2}$$

$$\dot{x} = -K_2 x \exp\left(\frac{1-\beta_e}{\beta}\right)\exp\left(\frac{\beta_e\theta}{1+\beta\theta}\right) - K_1 x \exp\left(\frac{\theta}{1+\beta\theta}\right).$$

We introduce the new parameters

$$\varepsilon = \exp\left(-\frac{1}{\beta}\right), \quad a = K_2 \exp\left(\frac{1-\beta_e}{\beta}\right), \quad \theta_a = \frac{u_a - \beta}{\beta^2},$$

$$\mu = \frac{QK_1}{\beta^2}\exp\left(-\frac{1}{\beta}\right), \quad \nu = \frac{Q_c K_2}{\beta^2}\exp\left(\frac{-\beta_e}{\beta}\right).$$

Due to the smallness of the parameter ε for typical combustible liquids, system (2) can be rewritten in the singularly perturbed form (see, for instance, [13−17]):

$$\varepsilon\dot{\theta} = \mu x \exp\left(\frac{\theta}{1+\beta\theta}\right) - (\theta - \theta_a) - \nu x \exp\left(\frac{\beta_e\theta}{1+\beta\theta}\right), \tag{3}$$

$$\dot{x} = -a x \exp\left(\frac{\beta_e\theta}{1+\beta\theta}\right) - K_1 x \exp\left(\frac{\theta}{1+\beta\theta}\right). \tag{4}$$

The chemically relevant phase space Ω of system (3), (4) is defined by $\Omega = \{x \geq 0, \theta \geq -1/\beta\}$.

In [2] system (1) was investigated numerically under quasi-steady-state assumption that corresponds to the assumption $\varepsilon = 0$ for system (3), (4). This approach allows determining the main types of chemical regimes of the investigated process. The quasi-steady-state assumption is widely used in the theory of combustion and gives good results

to draw conclusions about the qualitative behavior of the full system for sufficiently small ε. However, the critical phenomena are highly sensitive with respect to the parameters. Hence, this fact implies the considerable difficulties under the numerical calculations. Thus, detailed study of this mathematical object is possible with taking into account the small perturbations and using of asymptotic methods, for example, methods of the integral manifolds theory for singularly perturbed systems.

Criteria for the critical regimes

The trivial solution is the final steady state of the system. The degenerate equation

$$0 = \mu x \exp\left(\frac{\theta}{1+\beta\theta}\right) - (\theta - \theta_a) - \nu x \exp\left(\frac{\beta_e\theta}{1+\beta\theta}\right) = F(x,\theta) \text{ describes } the\ slow\ curve\ S \text{ of}$$

(3), (4) (see, for example, [17, 18]). The subset $S^s(S^u)$ of S with

$$\frac{\partial F(x,\theta)}{\partial\theta} < 0 \quad (>0)$$

is called the *stable* or *attractive* (*unstable* or *repulsive*) part of S. A point A on S in which $\partial F / \partial\theta = 0$ is called the *jump* or *turning point*. Stable and unstable parts of the slow curve are zeroth order approximations of corresponding stable and unstable slow invariant manifolds. The invariant manifolds lie in an ε-neighborhood of the slow curve, except near jump or turning points (see [17] and references therein).

The slow curve has an asymptote $\theta = \theta_\infty$, where

$$\theta_\infty = \frac{1}{\beta_e - 1 - \beta \ln(\mu/\nu)} \ln(\mu/\nu),$$

and intersects the axis $O\theta$ in the point with $\theta = \theta_0$. The shape of the curve S varies with the relation between values of the parameters, which leads to a change in qualitative behavior of the system. So, if we change the value of one parameter, with fixed values of the other parameters, we can change the type of chemical reaction. Following [2], we consider β_e as a control parameter. For $\theta_\infty = \theta_0$ we have $\beta_e = b_0$ where

$$b_0 = 1 + \frac{1+\beta\theta}{\theta_a} \ln(\mu/\nu).$$
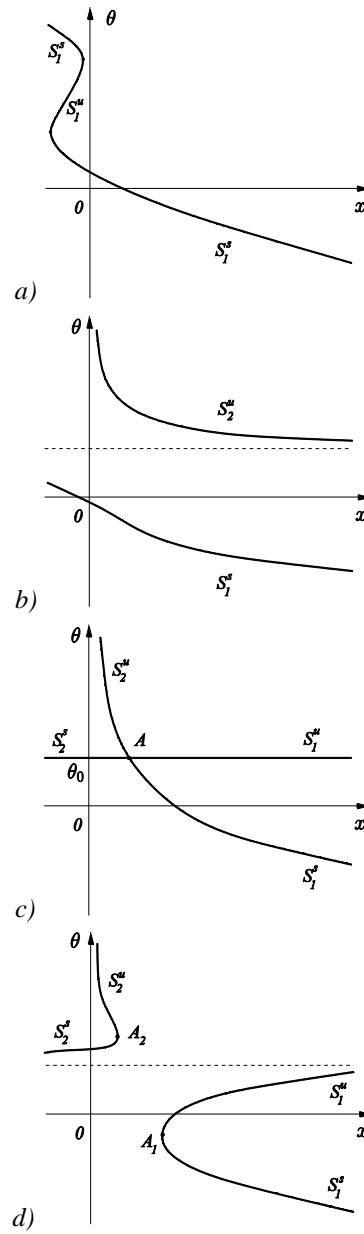
Fig. 1. – The slow curve of (3), (4) for $b_0 < 1$, $\beta > u_a$, and a) $\beta_e < b^T < b_0$; b) $b^T < \beta_e < b_0$; c) $\beta_e = b_0$; d) $\beta_e > b_0$
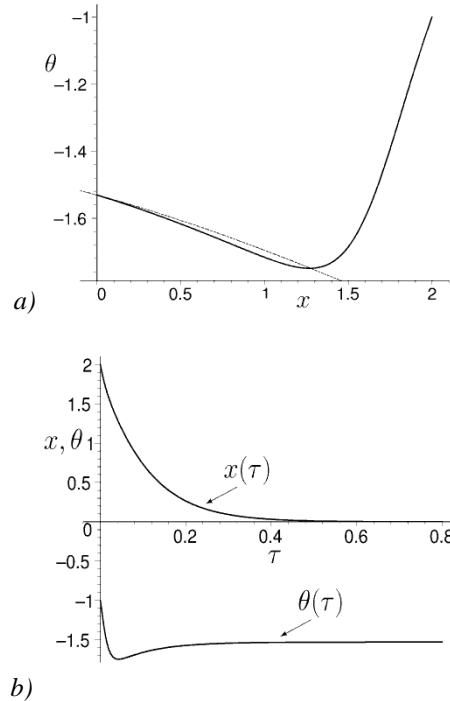
Fig. 2. – a) The trajectory (the solid line) and the slow curve (the dashed line) of (3), (4), and b) the x− and θ −components of the solution in the case of the slow regime: b=0.3685

Consider the case $\beta > u_a$ and $b_0 < 1$. For $\beta_e < b^T$ the lower branch of S can consist of two stable parts (S_1^s) and one unstable part (S_1^u), see Fig. 1a. These parts are divided by two turning points, which merge with one another and disappear at a value $\beta_e = b^T$ [2, 11], see Fig. 1b. In both cases the trajectories of system (3), (4) move along the stable part of the slow curve to the final steady state. These trajectories correspond to the slow regimes, which are safe, see Fig. 2.

For $\beta_e > b_0$ the upper and lower branches of S consist of stable (S_1^s and S_2^s) and unstable (S_1^u and S_2^u) parts, which are divided by the turning points A_1 and A_2, see Fig. 1d. And the system's trajectories starting at any point of the basin of attraction of S_2^s correspond to the slow regimes, see Fig. 3.

In other case, when the initial point is out of the basin of attraction of S_2^s, we can observe the thermal explosion (Fig. 4) or thermal explosion with delay [8, 18]. The thermal explosion with delay occurs when the initial point belongs to the basin of attraction of S_1^s and the system's trajectories having reached the jump point A_1 along S_1^s at the tempo of the slow variable jump into the explosive regime.

183

a)

b)
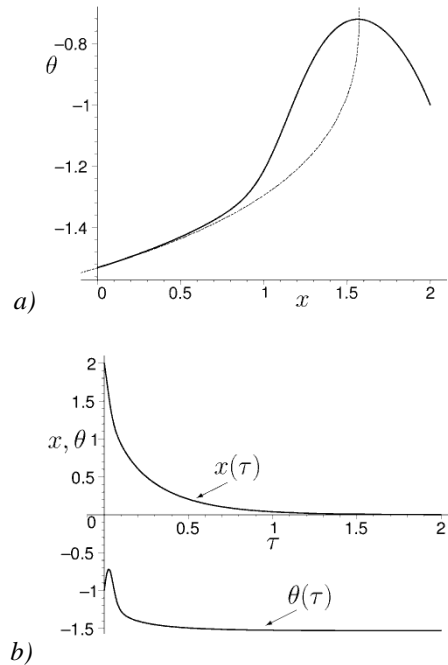
Fig. 3. – The case of the slow regime: b=1; the initial point belongs to the basin of attraction of S_2^s

For $\beta_e = b_0$ the point A_1 merges with A_2 to give one self–intersection point A of the slow curve, see Fig. 1*c*. As it was noted above, in ε-neighborhood of the subset S_1^s (S_2^u) there exists a stable (unstable) slow invariant manifold $S_{1,\varepsilon}^s$ ($S_{2,\varepsilon}^u$). For some value $\beta_e = b^* = b_0 + O(\varepsilon), (\varepsilon \to 0)$ [11], the stable and unstable slow invariant manifolds $S_{1,\varepsilon}^s$ and $S_{2,\varepsilon}^u$ are glued at the point A. As a result for $\beta_e = b^*$ system (3), (4) has a *canard* trajectory [17-22] which, at first, follows an attractive invariant manifold, and then a repulsive one. In both cases the distances travelled are $O(1)$ as $\varepsilon \to 0$, see Fig. 5.

This canard simulates the critical regime, separating slow chemical regimes from regimes with a self–acceleration in the case $b_0 < 1$.

If $\beta > u_a$, one can observe the similar transformation of the slow curve (and the qualitative behavior of the system) as shown in Fig. 1 but with a decreasing value of the parameter β_e ($b^T > b_0$ in this case).

For $b_0 > 1$ plots of the slow curve are mirror images with respect to the vertical axis of the graphs shown in Fig. 1, and for nonsignificant values of the initial concentration of a combustible liquid the thermal behavior of the chemical system is safe. Otherwise, the value $\beta_e = b^T$ determines the boundary of the safe region [2].

a)

b)
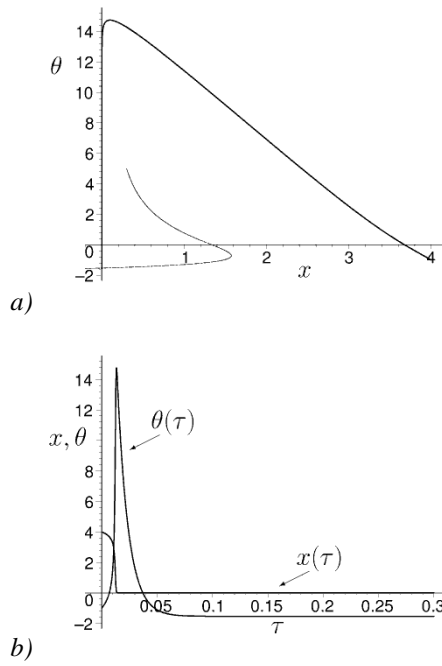
Fig. 4. – The case of thermal explosion: b=1; the initial point is out of the basin of attraction of S_2^s

Our goal is to reveal the sufficient conditions for realization of the critical regime for the case $b_0 < 1$. As it has been noted above, the main feature here consists in fact that during the critical regime the temperature attains a high value but without explosion. The interest in critical phenomena is occasioned by not only for reasons of safety, but in many cases the critical regime is the most effective in technological processes [6-9, 18, 20-22].

Realizability conditions for the critical regime

Using the method of integral manifolds and the canard techniques in [17,18] it is possible to find the critical value of the parameter $\beta_e = b^*$ and corresponding trajectory in the form of the asymptotic representation

$$\theta = \varphi(x, \varepsilon) = \varphi_0(x) + \varepsilon\varphi_1(x) + o(\varepsilon), \tag{5}$$

$$\beta_e = b^* = b_0 + \varepsilon b_1 + o(\varepsilon). \tag{6}$$

We write (3), (4) as

185

$$\varepsilon\theta'\left[ax\exp\left(\frac{\beta_e\theta}{1+\beta\theta}\right)+K_1x\exp\left(\frac{\theta}{1+\beta\theta}\right)\right]$$

$$=\theta-\theta_a+\nu x\exp\left(\frac{\beta_e\theta}{1+\beta\theta}\right)-\mu x\exp\left(\frac{\theta}{1+\beta\theta}\right),$$

or, taking into account (5), (6),

$$x\left(\varepsilon\varphi_0'+\varepsilon^2\varphi_1'\right)\left[K_1\exp\left(\frac{\varphi_0}{1+\beta\varphi_0}\right)\left(1+\varepsilon\frac{\varphi_1}{\left(1+\beta\varphi_0\right)^2}\right)\right.$$

$$\left.+a\exp\left(\frac{b_0\varphi_0}{1+\beta\varphi_0}\right)\left(1+\varepsilon\frac{\left(1+\beta\varphi_0\right)b_1\varphi_0+b_0\varphi_1}{\left(1+\beta\varphi_0\right)^2}\right)\right]$$

$$=\varphi_0+\varepsilon\varphi_1-\theta_a+\nu x\exp\left(\frac{b_0\varphi_0}{1+\beta\varphi_0}\right)\left(1+\varepsilon\frac{\left(1+\beta\varphi_0\right)b_1\varphi_0+b_0\varphi_1}{\left(1+\beta\varphi_0\right)^2}\right)$$

$$-\mu x\exp\left(\frac{\varphi_0}{1+\beta\varphi_0}\right)\left(1+\varepsilon\frac{\varphi_1}{\left(1+\beta\varphi_0\right)^2}\right)+o(\varepsilon). \tag{7}$$

a)

b)
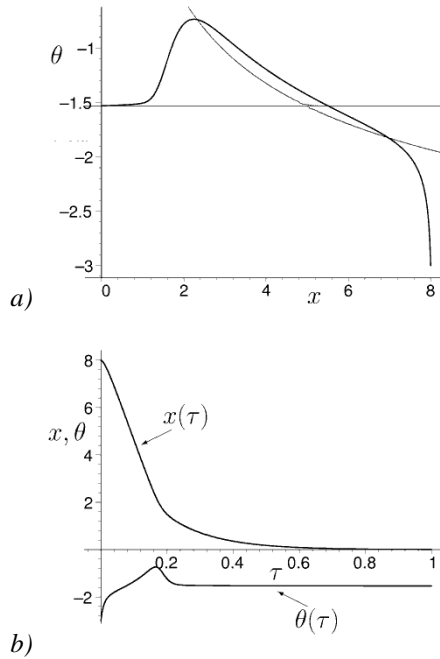
Fig. 5. – a) The trajectory (the solid line) and the slow curve (the dashed line) of (3), (4), and (b) the x− and θ −components of the solution in the case of critical regime: $b=b^*=0.56827$

Setting $\varepsilon=0$ in (7) we obtain the slow curve equation:

$$F(x,\varphi_0) = \mu x \exp\left(\frac{\varphi_0}{1+\beta\varphi_0}\right) - \varphi_0$$

$$+\theta_a - \nu x \exp\left(\frac{b_0\varphi_0}{1+\beta\varphi_0}\right) = 0. \tag{8}$$

Conditions for self-intersection of the slow curve in point $A\left(x_s, \varphi_0(x_s)\right)$

$$\left.\frac{\partial F}{\partial x}\right|_{(x_s,\varphi_0(x_s))} = \left.\frac{\partial F}{\partial \varphi_0}\right|_{(x_s,\varphi_0(x_s))} = 0 \tag{9}$$

give us the coordinates of the self-intersection point and the zeroth-order approximations for critical value b^*. Indeed, from (8), (9) we obtain

$$x_s = \frac{(1+\beta\theta_a)\theta_a}{\mu \exp\left[\theta_a / (1+\beta\theta_a)\right]\ln(\nu/\mu)}, \quad \varphi_0(x_s) = \theta_a \tag{10}$$

and

$$b_0 = 1 + \frac{1+\beta\theta_a}{\theta_a}\ln(\mu/\nu). \tag{11}$$

Equating the coefficients with ε^1 in (7) we get

$$x\varphi_0'\left[a\exp\left(\frac{b_0\varphi_0}{1+\beta\varphi_0}\right) + K_1\exp\left(\frac{\varphi_0}{1+\beta\varphi_0}\right)\right]$$

$$= \varphi_1\left\{1 + \frac{x}{(1+\beta\varphi_0)^2}\left[b_0\nu\exp\left(\frac{b_0\varphi_0}{1+\beta\varphi_0}\right) - \mu\exp\left(\frac{\varphi_0}{1+\beta\varphi_0}\right)\right]\right\} \tag{12}$$

$$+\nu x\exp\left(\frac{b_0\varphi_0}{1+\beta\varphi_0}\right)\frac{b_1\varphi_0}{(1+\beta\varphi_0)}.$$

From (9) we note that the expression in brackets in r.h.s. of (12) is equal to zero at point A. To avoid a discontinuity in function $\varphi_1(x)$ at x_s we put

$$\varphi_0'(x_s)\left[a\exp\left(\frac{b_0\varphi_0(x_s)}{1+\beta\varphi_0(x_s)}\right) + K_1\exp\left(\frac{\varphi_0(x_s)}{1+\beta\varphi_0(x_s)}\right)\right]$$

$$= \nu\exp\left(\frac{b_0\varphi_0(x_s)}{1+\beta\varphi_0(x_s)}\right)\frac{b_1\varphi_0(x_s)}{(1+\beta\varphi_0(x_s))}.$$

From this and (10) we get

$$b_1 = \frac{\varphi_0'(x_s)(1+\beta\theta_a)}{\nu\theta_a}\left[K_1\exp\left(\frac{(1-b_0)\theta_a}{1+\beta\theta_a}\right) + a\right]. \tag{13}$$

Note, that the value $\varphi_0'(x_s)$ can be found from equation (8) after double differentiation with respect to x, taking into account (9):

$$\varphi_0'(x_s) = 2\left[\frac{\mu(1+\beta\theta_a)}{\theta_a}\ln\frac{\nu}{\mu}\exp\left(\frac{\theta_a}{1+\beta\theta_a}\right)\right]^3$$
$$\times\left[2\beta(1+\beta\theta_a)-2-\frac{(1+\beta\theta_a)}{\theta_a}\ln\frac{\mu}{\nu}\right]. \tag{14}$$

Expressions (13) and (14) give us

$$b_1 = \frac{2\mu^3(1+\beta\theta_a)^4}{\theta_a^{\,4}}\ln^3\frac{\nu}{\mu}\exp\left(\frac{3\theta_a}{1+\beta\theta_a}\right)\left(\frac{K_1}{\mu}+\frac{a}{\nu}\right)$$
$$\times\left[2\beta(1+\beta\theta_a)-2+\frac{(1+\beta\theta_a)}{\theta_a}\ln\frac{\nu}{\mu}\right]. \tag{15}$$

Thus, the expressions (8), (11), (12), and (15) determine the first−order approximation for canard and corresponding critical value $\beta_e = b^*$.

It should be noted that it is not possible to explicitly solve equation (8) with respect to φ_0, while the critical value b^* has been found in the explicit form. However, one can use the implicit or parametric representation for slow invariant manifold [17] to obtain an approximation of the canard.

Conclusion

In this paper the model of autoignition of combustible fluids in an inert porous medium has been studied. The realizability conditions for the critical regime have been obtained as the explicit asymptotic expression for the control parameter. It was shown that the critical regime is modelled by the canard. This regime plays the role of a watershed between the safe processes and regimes with self-acceleration that leads to the explosion.

It should be noted that the critical regime is not a slow regime, since the temperature may attain a high value, and is not explosive, as the temperature increases at the tempo of the slow variable. Thus, for the examined model the new type of the safe regime has been revealed.

Acknowledgements

References

1. **McIntosh AC, Bains M, Crocombe W, Griffiths JF.** Autoignition of combustible fluids in porous insulation materials. Combust Flame, 1994; 99: 541-550.
2. **McIntosh AC, Griffiths JF.** On the thermal runaway of combustible fluids in lagging material. IMA Journal of Applied Mathematics, 1996; 55: 83-96.
3. **Spalding Von DB.** Combustion and mass transfer. Oxford, New York: Pergamon Press, 1979.
4. **Zeldovich YaB, Barenblatt GI, Librovich VB, Makhviladze GM.** The mathematical theory of combustion and explosions. New York: Consultants Bureau, 1985.
5. **Babushok VI, Goldshtein VM, Sobolev VA.** Critical condition for the thermal explosion with reactant consumption. Combustion Science and Technology, 1990; 70: 81-89.
6. **Gorelov GN, Sobolev VA.** Mathematical modeling of critical phenomena in thermal explosion theory. Combust Flame, 1991; 87: 203-210.
7. **Gorelov GN, Sobolev VA.** Duck−trajectories in a thermal explosion problem. Applied Mathematics Letters, 1992; 5(6): 3-6.
8. **Gol'dshtein V, Zinoviev A, Sobolev V, Shchepakina E.** Criterion for thermal explosion with reactant consumption in a dusty gas. Proceedings of the Royal Society of London A, 1996; 452: 2103-2119.
9. **Shchepakina E.** Black swans and canards in self−ignition problem. Nonlinear Analysis: Real Word Applications, 2003; 4: 45-50.
10. **Kuo K−K.** Principles of Combustion. New York: Wiley, 2005.
11. **Sobolev VA, Shchepakina EA.** Model reduction and critical phenomena in macrokinetics. Moscow: "Fizmatlit" Publisher, 2010. [in Russian]
12. **Sazhin S.** Droplets and sprays. London, New York, Heidelberg: Springer, 2014.
13. **Mishchenko EF, Rozov NKh.** Differential equations with small parameters and relaxation oscillations. New York: Plenum Press, 1980.
14. **O'Malley RE.** Singular perturbation methods for ordinary differential equations. Applied Mathematical Sciences, 1991; 89.
15. **Mishchenko EF, Kolesov YuS, Kolesov AYu, Rozov NKh.** Asymptotic methods in singularly perturbed systems. New York: Plenum Press, 1995.
16. **Vasilieva AB, Butuzov VF, Kalachev LV.** The boundary function method for singular perturbation problems. In: Series in Applied Mathematics. Philadelphia: SIAM, 1995; 14 p.
17. **Shchepakina E, Sobolev V, Mortell MP.** Singular perturbations. Introduction to system order reduction methods with applications. In: Lecture Notes in Mathematics. Cham − Heidelber − NewYork − Dordrecht − London: Springer, 2014; 2114 p.
18. **Shchepakina E, Sobolev V.** Black swans and canards in laser and combustion models. In: Mortell, M.P., O'Malley, R.E., Pokrovskii, A., Sobolev, V. (eds) Singular perturbation and hysteresis. Philadelphia: SIAM, 2005; 207-255.
19. **Benoit E, Callot JL, Diener F, Diener M.** Chasse au canard. Collectanea Mathematica, 1981-1982; 31-32(1-3): 37-119. [in French]
20. **Sobolev VA, Shchepakina EA.** Duck trajectories in a problem of combustion theory. Differential Equations, 1996; 32: 1177-1186.
21. **Shchepakina EA, Sobolev VA.** Integral manifolds, canards and black swans. Nonlinear Analysis: Theory, Methods & Applications - Series A, 2001; 44(7): 897-908.
22. **Gorelov GN, Shchepakina EA, Sobolev VA.** Canards and critical behavior in autocatalytic combustion models. Journal of Engineering Mathematics, 2006; 56: 143-160.

Mathematical Modeling

Canards and the effect of apparent disappearance

Sobolev V.A.

Samara State Airspace University

Abstract. The aim of the paper is to give examples of apparent disappearance phenomenon which is typical for microbiological systems. It is well known that canards play an important role in the theory of mixed−mode oscillations consisting of large amplitude, and followed by small amplitude oscillations. In a sense we consider limiting cases of mixed−mode oscillations, when large amplitude oscillations are followed by vanishingly small amplitude oscillations.

Keywords: apparent disappearance phenomenon, canard, invariant manifold

Introduction

The aim of the paper is to give illustrative examples of apparent disappearance phenomena which are typical for microbiological systems. Our interest in this topic was prompted by a recent trip to Israel made by the author several years ago. During the visit he was told about a group of Bedouins who, together with camels, were drowned in a flash flood in the desert. The following day he toured an old cemetery in Jerusalem that contained the remains of some English soldiers. The majority of the soldiers had died in a similar flash flooding event. In both cases, the victims had set up camp on a dry river bed. The river bed remained dry for long periods of time throughout the year. However, this normal state disappeared for a few hours when the catastrophic flooding occurred. Similar behaviour occurs in the illustrative model of a hydrodynamical system shown in the figure below, in which the lower reservoir is empty apart from a very short time interval where it is full.

The second reservoir also empties through a siphon. A small inflow causes the water level in the first reservoir to rise slowly until the U-turn in the siphon is reached. The water is then very quickly transferred to the lower reservoir due to the siphoning effect, filling it almost instantly. The second siphon then causes the lower reservoir to empty at an equally fast rate.

Strange as it may seen, the analogous situations appear in systems of diversified natures, such as in the case for ``predator-prey'' systems in microbiology. In this paper we discuss some examples and mathematical models of the apparent disappearance phenomenon in population dynamics.
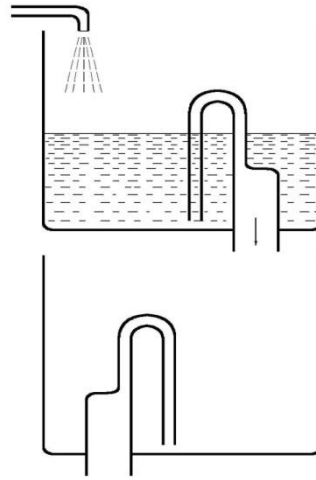
Fig. 1. – Cascade of two Tantal reservoirs

Canards

To offer a satisfactory mathematical explanation to the apparent disappearance phenomena we will use a technique of singularly perturbed differential equations. Below we will relate the apparent disappearance phenomena to the existence of special kinds of the so called canards or duck--trajectories. These terms have been introduced by French mathematicians [1]. In this section we recall, in a convenient form, the corresponding definitions (see, for example, [2]-[6]).

First we consider a two-dimensional autonomous system:

$$\frac{dx}{dt} = f(x, y), \quad \varepsilon \frac{dy}{dt} = g(x, y)y; \tag{1}$$

where x, y are scalar functions of time, ε is a small positive parameter, and f, g are sufficiently smooth scalar functions. The set of points

$$S = \{(x, y): y = 0\}$$

of the phase plane is both a slow curve of the system (1) and a one-dimensional slow invariant manifold. Part of S, all points of which satisfy the inequality

$$g(x, 0) < 0 \quad (g(x, 0) > 0),$$

is called attractive (repulsive). A point $x = A$ of S is called a turning point if it divides attractive and repulsive parts of S.

We assume that all points at which

$$g(x, 0) = 0,$$

in particular, the turning points, are isolated on S. Let, for simplicity,

$$f(A, 0) > 0, \text{ and } g(A, 0) < 0, \text{ for } x < A;$$

$$g(A, 0) > 0, \text{ for } > A.$$

Trajectories which at first pass along the attractive part of S and then continue for a while along the repulsive part of S are called canards or duck-trajectories. In the case that a turning point is unique, S is a canard and it is a longest canard.

Otherwise, this canard may be bounded by neighbouring turning points (or points at which $g(x, 0) = 0$).

In many papers devoted to canards this term is associated with periodic trajectories [1, 4, 6]. In the papers [7, 8] it was suggested a canard is a one-dimensional slow invariant manifold if it contains a stable slow invariant manifold and an unstable one, and a canard is obtained as a result of gluing stable (attractive) and unstable (repulsive) slow invariant manifolds at one point of the breakdown surface due to availability of an additional scalar parameter. This approach was proposed for the first time in [7, 8] and was then applied to construct canards in $\mathbb{R}^3$ [9]-[11], canards for PDE [8, 12] and canard travelling waves. Moreover, the use of additional functions instead of additional parameters allowed the construction of black swans [13]-[17], and canard cascades, and the solution of a number of applied problems [18]-[24].

We will introduce some types of canards [25], which are important in the context of this article. Trajectories which at first pass along a repulsive part of S and then continue for a while along an attractive part of S are called false canards.

In the above cases properties of attraction or repulsion can be viewed as exponential attraction and exponential repulsion by analogy with exponential stability. Using an analogy with the asymptotic stability, we introduce the following notion.

Trajectories which are canards but in which attraction and repulsion are not exponential are called feeble canards.

If on one side of the trajectory it looks like a canard, but on the other side it looks like a false canard, we'll say that this trajectory is a two−faced canard.

It is easy to extend these concepts to the case of vector variables x and y. If, in particular, x is a vector and y is a scalar, then we consider the subspace $y = 0$ as a slow manifold. If it contains repulsive and attractive parts, it is called a black swan (attractive/repulsive invariant manifold) [13]-[17].

It should be noted that attractive/repulsive invariant manifolds can be considered for the case of small ε just as for the case ε = 1. The essence of the effect of apparent disappearance is as follows: variable y has vanishingly small amplitude for most of the time. This is due to the fact that trajectories of the system under consideration asymptotically approach an attractive part of the curve (surface) y=0 and escape from it repulsive part with a substantial time delay.

Canards' role in modelling the apparent disappearance phenomenon

Consider the system

$$\frac{dx}{dt} = f(x, y), \quad \varepsilon \frac{dy}{dt} = y^p g(x, y); \tag{2}$$

where $p \geq 1$, $f(x, y)$ is positive for $y < 1$ and $f(x, y) < 0$ for $y > 1$, and moreover, that f increases to infinity when $x \to \infty$. Let also $g(x, 0)$ be negative for $x < 0$ and positive for $x > 0$. Then $y = 0$ is a canard; this canard is feeble if $p > 1$, and it is a

two−faced canard if $p = 2,4, \dots$. Suppose that this system has periodic solutions for any small $\varepsilon > 0$, and that the graph of this solution crosses the interval
$I = \{(x, 1): -\delta < x < 0\}$,
where δ is a positive constant. Then for small ε the qualitative features of this periodic orbit are predetermined, and may be divided in the six stages.

- S1 The trajectory falls down almost vertically, until it will be of order $\varepsilon \ln \varepsilon$.
- S2 It will continue approach zero moving simultaneously to the right until $x(t)$ becomes equal to 0. The rate of approaching zero by $y(t)$ is exponential, with an exponent ~ -1/ε, if $p = 1$ and convergence is polynomial if $p > 1$.
- S3 The trajectory will still follow very closely the x-axis, but $y(t)$ will increase until it becomes of order $\varepsilon \ln \varepsilon$; this stage is essentially symmetric with S2.
- S4 The trajectory will go up almost vertically, until $y(t) = 1$ ("symmetrically" to stage S1).
- S5 The solution will go up (rapidly), simultaneously drifting faster and faster to the left until $x(t)$ is equal to 0.
- S6 At the final stage the trajectory goes down and to the left until it cross again the interval. This stage is essentially symmetric with Stage S5.

(a)   (b)
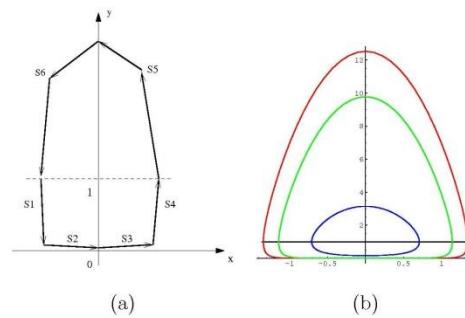
Fig. 2. – (a): Schematic representation of the structure of periodic trajectories of system (2); (b): Trajectories (4) for c=1 (blue), c=1.5 (green) and c=2 (red).

The dynamics of $y(t)$ exhibits the essential features of theapparent disappearance phenomenon, because all stages, except for S2 and S3, are fast. It is easy to give examples of equations (2) where this scenario happens, that is where the above mentioned periodic trajectories exist. For instance, if f is even in x:
$$f(x, y) = f(-x, y),$$
and g is odd:
$$g(x, y) = -g(-x, y),$$
then any solution is periodic. Figure 2(b), right graphs sample trajectories of an illustrative system
$$\frac{dx}{dt} = 1 - y, \quad \varepsilon \frac{dy}{dt} = xy; \tag{3}$$
Here the trajectories can be written explicitly as

193

$$x^2 + 2\varepsilon(y - \ln y) = c, \tag{4}$$

where $c > 0$ is a parameter.

The crucial question is the following: are there many real world phenomena which are consistent with this scheme, or with its suitable amendments?

The purpose of the paper is to demonstrate that the answer is in the affirmative.

Canards and marine phage population dynamics

The classic Lotka-Volterra Equations were suggested to model population dynamics of a predator--prey system. They are [26, 27]:

$$\frac{dx}{dt} = x(\alpha - \beta y), \quad \frac{dy}{dt} = (-\gamma + \delta x)y; \tag{5}$$

where x and y are functions of time representing the populations of the prey and predator respectively, and α, β, γ, and δ are positive constants which govern the strength of the interactions between the two species and amongst themselves. This system has a unique positive equilibrium $(\bar{x}, \bar{y})$ when $0 = x(\alpha - \beta y)$, $0 = (-\gamma + \delta x)y$; that
$\bar{x} = \gamma/\delta$, $\bar{y} = \alpha/\beta$.

Hoffmann [27] proposed that for the phage—bacteria interaction the equations be modified such that a power law applies to the Lotka-Volterra equations.

The modified Lotka-Volterra equations are therefore:

$$\frac{dB}{dt} = B(\alpha - \beta\Phi^p), \quad \frac{d\Phi}{dt} = \Phi^p(-\gamma + \delta B); \tag{6}$$

we will assume the inequality

$p > 1$.

Loosely speaking the equations (6) mean that the "effective size" of the phage population differs from its "physical size", and this effective size is proportional to the power p of the physical size. A naive explanation may be as follows: in the traditional Lotka-Volterra equations (5) and (6), it is assumed that the important meetings are when one predator meets one prey. With the power of two, which was among the best fits in the modified equations, we can hypothesize that unlike the traditional system, it is the meeting of two phages and one bacteria that are important. Correspondingly, the power Φ^p in (6) indicated that that are ``hunting−teams" of p phages which are effective. This sounds strange for a fractional Φ, but such ideas are not unusual in mathematics.

This system also has a unique positive equilibrium:

$$B_* = \frac{\gamma}{\delta}, \quad \Phi_* = (\alpha/\beta)^{\frac{1}{p}}. \tag{7}$$

Returning to equations (6), we can look for a constant of motion for the system. We do this by dividing the first equation (6) by the second to obtain

$$(-\gamma \log(B(t) + \delta B(t)) + (\alpha\Phi(t)^{1-p})/(p-1) + \beta\,\Phi(t)) = const.$$

for any positive solution
$(B(t), \Phi(t))$
of (5).

194

Thus,

$$W(B, \Phi) = \left(-\gamma \log\big(B(t) + \delta B(t)\big) + \frac{(\alpha \Phi(t)^{1-p})}{p-1} + \beta\, \Phi(t) \right) \qquad (8)$$

is a conserved quantity, in other   words, the first integral, for the motion of trajectories in this system. The value of the constant is determined by the initial conditions. Rewriting system (6) as

$$\frac{dB}{dt} = B\big(\alpha \Phi_*^p - \Phi^p\big), \quad \frac{d\Phi}{dt} = \Phi^p \gamma(-B_* + B), \qquad (9)$$

we can see the direction vector field in the strictly positive quadrant.

Since

$$p > 1, \qquad \lim W(B, \Phi) = \infty$$

as $B \to 0$, or $\Phi \to 0$, or $B \to \infty$, or $\Phi \to \infty$, the trajectories system could not expand to infinity.

Finally, since the restriction

$$W(B) = W(B, \Phi_*)$$

is strictly monotone for

$$0 < B < B_*,$$

we conclude that all trajectories of (6) are periodic, and they orbit anti−clockwise around the equilibrium

$$B_* = \frac{\gamma}{\delta}, \quad \Phi_* = (\alpha/\beta)^{\frac{1}{p}}.$$

Let us consider the modified Lotka-Volterra equations (6), when one of the variables (B or Φ) is significantly faster than the other. We can use singularly perturbed differential systems for modelling such phenomena. The biologically relevant case is "Fast Phages - Slow Bacteria", and the corresponding system is

$$\frac{dB}{dt} = B(\alpha - \beta \Phi^{p+1}), \quad \varepsilon \frac{d\Phi}{dt} = \Phi^{p+1}(-\gamma + \delta B),$$

with $p > 0$.

Proposition 1. *The trajectory $\Phi = 0$ is a feeble canard with the attractive part $B < \frac{\gamma}{\delta} = B_*$ and the repulsive part $B > \frac{\gamma}{\delta} = B_*$ for positive B and Φ.*

We can observe here the effect of apparent disappearance of phages: they almost disappear for most of the time; however the phages population "explodes" for some short time intervals, see Fig. 3. A curious point is that this feeble canard is two-faced if $p = 2, 4, 6, \dots$, but that is irrelevant because we are interested in the behavior of our system for positive values of Φ, only.
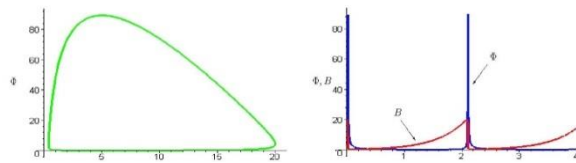
Fig. 3. – Fast phages and slow bacteria model for ε =0., α=2, β=0.1, γ=1, δ= 0.2

We consider also the "Fast Bacteria - Slow Phages" case with the corresponding equations

$$\varepsilon\frac{dB}{dt} = B(\alpha - \beta\Phi^{p+1}), \quad \frac{d\Phi}{dt} = \Phi^{p+1}(-\gamma + \delta B).$$

Note that this case is not interesting from the biological point of view.

Proposition 2. *The trajectory $B = 0$ is a canard with the attractive part $\Phi > \Phi_* = (\alpha/\beta)^{\frac{1}{p}}$ and the repulsive part $\Phi < \Phi_* = (\alpha/\beta)^{\frac{1}{p}}$.*

In this case we observe the effect of the apparent disappearance of bacteria, see Fig. 4.
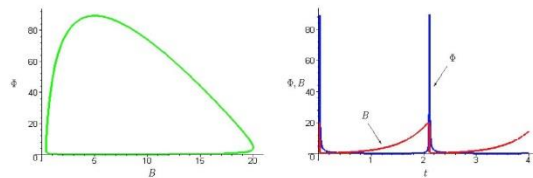
Fig. 4. – Fast bacteria and slow phages model for ε=0.2, α=2, β=0.1, γ=1, δ= 0.2.

Conclusion

The modification of the famous Lotka-Volterra equations is considered in the paper. This modification has been recently suggested to model the structure of marine phage populations, who are the most abundant biological entities in the biosphere. The paper attempts to realize the following intentions:

- to make some methodical remarks concerning this modification;
- to discuss new types of canards which arise naturally in this context;
- to present results of some numerical experiments.

Acknowledgements

References

1. **Benoit E, Callot JL, Diener F, Diener M.** Chasse au canard. Collectanea Mathematica, 1981-1982; 31-32(1-3): 37-119. [in French]
2. **Mishchenko EF, Rozov NKh.** Differential equations with small parameters and relaxation oscillations. New York: Plenum Press, 1980.
3. **O'Malley RE.** Singular perturbation methods for ordinary differential equations. Applied Mathematical Sciences, 1991; 89.
4. **Mishchenko EF, Kolesov YuS, Kolesov AYu, Rozov NKh.** Asymptotic methods in singularly perturbed systems. New York: Plenum Press, 1995.

5. **Vasilieva AB, Butuzov VF, Kalachev LV.** The boundary function method for singular perturbation problems. Series in Applied Mathematics, 1995; 14.
6. **Arnold VI, Afraimovich VS, Il'yashenko YuS, Shil'nikov LP.** Theory of Bifurcations. Dynamical Systems. Encyclopedia of Mathematical Sciences, 1994; 5.
7. **Gorelov GN, Sobolev VA.** Mathematical modeling of critical phenomena in thermal explosion theory. Combust Flame, 1991; 87: 203-210.
8. **Gorelov GN, Sobolev VA.** Duck−trajectories in a thermal explosion problem. Applied Mathematics Letters, 1992; 5(6): 3-6.
9. **Gol'dshtein V, Zinoviev A, Sobolev V, Shchepakina E.** Criterion for thermal explosion with reactant consumption in a dusty gas. Proceedings of the Royal Society of London A, 1996; 452: 2103-2119.
10. **Sobolev VA, Shchepakina EA.** Duck Trajectories in a problem of combustion theory. Differential Equations, 1996; 32: 1177-1186.
11. **Shchepakina EA.** Two forms of stability change for integral manifolds. Differential Equations, 2004; 40(5): 766-769.
12. **Gorelov GN, Shchepakina EA, Sobolev VA.** Canards and critical behavior in autocatalytic combustion models. Journal of Engineering Mathematics, 2006; 56: 143-160.
13. **Shchepakina E.** Black swans and canards in self−ignition problem. Nonlinear Analysis: Real Word Applications, 2003; 4: 45-50.
14. **Shchepakina E, Sobolev V, Mortell MP.** Singular perturbations. Introduction to system order reduction methods with applications. Lecture Notes in Mathematics, 2014; 2114.
15. **Shchepakina E, Sobolev V.** Black swans and canards in laser and combustion models. Singular perturbation and hysteresis, 2005; 207-255.
16. **Shchepakina E, Sobolev V.** Integral manifolds, canards and black swans. Nonlinear Analysis. Series A: Theory Methods, 2001; 44(7): 897-908.
17. **Shchepakina E.** Canards and black swans in model of a 3-D autocatalator. Journal of Physics: Conference Series, 2005; 22: 194-207.
18. **Sobolev VA, Shchepakina EA.** Model reduction and critical phenomena in macrokinetics. Moscow: "Fizmatlit" Publisher, 2010. [in Russian]
19. **Shchepakina E.** Critical conditions of self-ignition in dusty media. Journal of Advances in Chemical Physics, 2001; 20(7): 3-9.
20. **Shchepakina E.** Slow integral manifolds with stability change in the case of a fast vector variable. Differential Equations, 2002; 38(10): 1146-1152.
21. **Golodova E, Shchepakina E.** Maximal combustion temperature estimation. Journal of Physics: Conference Series, 2006; 55: 94-104.
22. **Golodova ES, Shchepakina EA.** Modeling of Safe Combustion at the Maximum Temperature. Mathematical Models and Computer Simulations, 2009; 1(2): 322-334.
23. **Shchepakina E, Korotkova O.** Condition for canard explosion in a semiconductor optical amplifier. Journal of the Optical Society of America B, 2011; 28(8): 1988-1993.
24. **Shchepakina E, Korotkova O.** Canard explosion in chemical and optical systems. Discrete and Continuous Dynamical Systems Series B, 2013; 18(2), 495-512.
25. **Gavin C, Pokrovskii A, Prentice M, Sobolev V.** Dynamics of a Lotka-Volterra type model with applications to marine phage population dynamics. Journal of Physics: Conference Series, 2006; 55: 80-93.
26. **Dancso A, Farkas H, Farkas M, Szabo G.** Investigation on a class of generalized two−dimensional Lotka-Volterra schemes. Acta Applicandae Mathematica, 1990; 23: 103-127.
27. **Hoffmann K H, Rodriguez−Brito B, Breitbart M, Bangor D, Angly F, Felts B, Nulton J, Rohwer F, Salamon P.** The structure of marine phage populations. Proceedings of ECOS, 2005; 5-9.

Numerical simulation of the resonance effect at Re-entry of a rigid body with low inertial and aerodynamic asymmetries into the atmosphere

Lyubimov V.V.

Samara State Aerospace University

Abstract. We consider a motion relative to centre of mass of a rigid body with low inertial and aerodynamic asymmetries at re-entry into the atmosphere. Numerical and mathematical simulation provide a means to study the resonance effect that results in changes of the direction of the rigid body rotation. It is shown that the realization of the effect in question is observed when selecting the initial conditions of the integration and defined values of the asymmetry parameters.

Keywords: resonance effect, numerical simulation, asymmetry, rigid body, atmosphere

1. Introductions

It is known [1]-[2] that the presence of the small asymmetry can lead to realization of the resonance that is observed in re-entry of a spacecraft viewed as a rigid body (RB) into the atmosphere. A continuous resonance leads to violation of the technological limitations on the RB's angle of attack or angular velocity. Besides the resonance itself, some secondary resonance effects can lead to violation of the technological limitations. The mentioned effects were found by Sadov Y.A. in dynamical systems with slow and fast variables [3]. The essence of these effects is: in the area close to the resonance, characteristic evolutions of slow variables of the system are observed, caused by this resonance. From the mathematical point of view, the secondary resonance effects are explained with presence of the resonant frequency mistuning in the denominators of averaging method's highest approximations that are received in the non-resonant case. Secondary resonance effects were studied particularly in the spherical rotation of the heavy asymmetrical rigid body [4]. Applying to the task of re-entry of an asymmetrical RB in the atmosphere, the mentioned resonance effects were studied in detail in the work [5]. In particular, it has been revealed that the secondary resonance effect itself can lead to the realization of

the RB's strong spin-up that was received earlier in the work [1]. In the following, using of traditional mathematical analysis methods allowed to extend the classification of the secondary resonance effects applying to the task of atmospheric re-entry of RB [6]. Other features of the task of atmospheric re-entry that affect the behaviour of the descent craft, are random character of the initial conditions on the separatrix (that lead or don't lead to the transfer into the resonance area) [7], and also the possibility of losing part of data on the craft's movement [8]. In the work [9], it is shown that the negative consequences of the resonance effects in respect to the task of atmospheric re-entry of the spacecraft with low mass and aerodynamic asymmetries can be solved with introducing the control over the amount of asymmetry. In the process of numerical simulation of movement of the RB with low mass and aerodynamic asymmetries, a secondary resonance effect has been considered, leading to changes in the direction of the craft's rotation [10]. Numerical simulation and analytical study of the similar resonance effect in the task of atmospheric re-entry of RB with low aerodynamic and inertial asymmetries are of practical interest.

2. Mathematical models

Initial non-linear equation of the asymmetrical RB's movement relating to the centre of mass in the atmosphere appear, for example, in the work [11]. However, the significant non-linearity of these equations and instability of frequencies of the system significantly complicate the application of such studies for detection and detailed study of secondary resonance effects. It is known that application of the integral manifold method [12] allow to decrease the order of differential equation system. For instance, in the work [13] it is shown that the application of one of the variants of integral manifold method makes it possible to receive from initial non-linear system of asymmetrical RB's movement relating to the centre of mass an equation system that is approximated to the non-linear. With allowance only for aerodynamic and inertial asymmetries, this system takes the following form:

$$\dot{\omega}_x = \varepsilon \frac{m^\Delta \sin^2 \alpha}{\bar{I}_x \omega_{1,2}^{-2}} \cos 2(\theta + \theta_3) \,, \tag{1}$$

$$\dot{\alpha} = -\varepsilon \frac{2m^\Delta \omega_a \omega_{1,2} \sin \alpha}{F_a} \cdot \left[\omega_x + \frac{\omega_{1,2}^2 \sin^2 \alpha}{2\omega_a} \right] \cos(2\theta + 2\theta_3) -$$

$$-\varepsilon \frac{2m^A \omega_a}{F_a} \cos(\theta + \theta_1) + \varepsilon^3 \frac{4m_{zn} \omega_a^2 SL}{IF_a} \frac{dq}{dt} \,, \tag{2}$$

$$\dot{\theta} = \omega_x - \omega_{1,2} \cos \alpha \,. \tag{3}$$

Here, ε is a small parameter that characterizes the value of RB's small inertial and aerodynamic asymmetries, and the slowness of changing the dynamic pressure q ($dq/dt = O(\varepsilon^3)$), ω_x is the RB's angular velocity relating to axis with least moment of inertia; α is the space angle of attack; $\omega = \sqrt{-m_{zn} qSLctg\alpha / I}$; S and L are

199

characteristic area and size of the RB; I_x and $I = I_y = I_z$ are the moments of RB's inertia relating to axes of XYZ body-fixed coordinate system; $\overline{I}_x = I_x / I$, $\theta = \varphi_n - \pi / 2$; φ is the aerodynamic roll angle; m^A and m^Δ are generalized parameters of aerodynamic in inertial asymmetries, $m^A = \sqrt{\left(m_1^A\right)^2 + \left(m_2^A\right)^2}$,

$$\omega_{1,2} = \frac{\overline{I}_x}{2}\omega_x \pm \omega_\alpha,$$

$$m_1^A = -\frac{\left(1+\overline{I}_x\right)\omega_x - 3\omega_{1,2}}{2\omega_a} * \frac{\omega^2}{m_{zn}}(m_y^\phi - C_x \overline{\Delta z})tg\alpha, \quad \sin\theta_1 = m_1^A / m^A,$$

$$m_2^A = -\frac{\left(1+\overline{I}_x\right)\omega_x - 3\omega_{1,2}}{2\omega_a} * \frac{\omega^2}{m_{zn}}(m_z^\phi + C_x \overline{\Delta y})tg\alpha, \quad \cos\theta_1 = -m_2^A / m^A, \quad \overline{m}^A = m^A / \omega^2,$$

$$m^\Delta = \sqrt{(\overline{I}_{yz})^2 + (\overline{\Delta I})^2}, \quad \sin 2\theta_3 = \overline{\Delta I} / m^\Delta, \quad \cos 2\theta_3 = -\overline{I}_{yz} / m^\Delta, \quad m_y^\phi, m_z^\phi -$$

aerodynamic shape asymmetry coefficients, $I = (I_y + I_z)/2$, $\Delta I = (I_z - I_y)/2$, $\overline{\Delta I} = \Delta I / I$, $\overline{I}_{yz} = I_{yz} / I$ - inertial (dynamic) asymmetry, m_{zn} - coefficient of restoring moment, $\omega_a = \sqrt{\overline{I}_x^2 \omega_x^2 / 4 + \omega^2}$, $\omega_x - \omega_{1,2}$ - resonant frequency mistuning, $F_a(\omega_x, \alpha, q)$ is the known function of the slow variables. Equation system (1)-(3) is solved together with three differential equations that describe change in characteristics of the RB's centre of mass movement [1]: airspeed, flight-path inclination angle and flight altitude. Mentioned three variables are considered as slow.

Equation system (1)-(3) takes into account the possibility of implementing the main resonance: $\omega_x - \omega_{1,2} \cong 0$. When passing through the main resonance, significant perturbations of movement parameters (compared to multiple resonances of higher orders) are observed [14]. By solving the equation $\omega_x - \omega_{1,2} = 0$, we find the resonance values of the angular velocity:

$$\omega_x^r = \pm \frac{\omega}{\sqrt{1 - \dfrac{I_x}{I}}}. \tag{4}$$

The sign in the expression (4) matches the sign of angular velocity ω_x. The equation system (1)-(3) contains in its right side the dependency on the phase of rapid movement θ, which complicates the analysis of non-resonant evolutions at secondary resonance effects. For further simplification of this system, we will use averaging method in non-resonant case [15].

System (1)-(3) applies to the class of systems with single rapid phase θ and several slow variables. It has a standard form for application of averaging method:

$$\dot{u} = \varepsilon U(u, \theta, \varepsilon), \tag{5}$$

$$\dot{\theta} = \omega(u). \tag{6}$$

Here $u = \{\omega_x, \alpha\}$ is the vector of slow variables, $\omega(u) = \omega_x - \omega_{1,2}$, $U(u, \theta, \varepsilon)$ is the vector function of right side of equations (1) and (2). Equations for centre of mass movement parameters do not depend on θ, so they are not taken into account in process of averaging.

System (1)-(3) is averaged on the non-resonant areas of movement under the rapid phase θ. Resulted averaging of equations for slow variables have the following form:

$$\frac{du^o}{dt} = \varepsilon A_1(u^o) + \varepsilon^2 A_2(u^o) + \varepsilon^3 A_3(u^o) + \dots, \tag{7}$$

where the functions A_i, $i=1,2,3,\dots$ are determined through standard averaging method [15].

After averaging the system (1)-(3) in non-resonant case we obtain: $A_1 = 0$, $A_2 = 0$ $A_3 \neq 0$. Hence, the evolution of slow variables ω_x, α, caused by the secondary resonance effects, is determined by the members of the third approximation of averaging method. The equations for slow variables ω_x, α, being averaged on non-resonant areas of movement and taking into account first three approaches of averaging method, are

$$\left\langle \frac{d\omega_x}{dt} \right\rangle = \varepsilon^3 \left\{ \frac{\overline{m}^A g_2 g_3}{\Delta^3} \frac{\partial}{\partial \alpha} (\overline{m}^A g_3 \frac{\partial \Delta}{\partial \alpha}) - \frac{\overline{m}^A g_3}{\Delta^2} \frac{\partial}{\partial \alpha} (\overline{m}^A g_3 \frac{\partial g_2}{\partial \alpha}) + \right.$$

$$\left. + \frac{3(\overline{m}^A g_3)^2}{\Delta^4} (\Delta \frac{\partial \Delta}{\partial \alpha} \frac{\partial g_2}{\partial \alpha} - g_2 \left(\frac{\partial \Delta}{\partial \alpha} \right)^2) \right\} \frac{m^\Delta \cos(2\theta_1 - 2\theta_2)}{8}, \tag{8}$$

Averaged equations (8) and (9) contain generalized parameters of asymmetry m^A, m^Δ, θ_1, θ_2 in numerator. The parameters m^A, m^Δ define the value of RB's asymmetry, and parameters θ_1, θ_2 characterize the location of asymmetry on the rigid body. From the equations (8)-(9) it appears the main resonance $\Delta = 0$ contributes to the realization of secondary resonance effects, for all the members of mentioned averaged equations contain frequency mistuning $\omega_x - \omega_{1,2}$ in their denominators. In particular, while approaching the resonance in the boundaries of non-resonant area, a decrease of $\omega_x - \omega_{1,2}$ value occurs, which leads to an increase of speed in averaged values of variables ω_x, α. Such behaviour of slow variables is typical for secondary resonance effects.

$$\left\langle \frac{d\alpha}{dt} \right\rangle = \varepsilon^3 \left\{ \frac{\overline{m}^A g_3 g_1}{\Delta^3} \left[\frac{\partial}{\partial\alpha}(\overline{m}^A g_3) \frac{\partial\Delta}{\partial\alpha} - \overline{m}^A g_3 \frac{\partial^2\Delta}{\partial\alpha^2} \right] - \right.$$

$$- \frac{\overline{m}^A g_3}{\Delta^3} \frac{\partial}{\partial\alpha}(\overline{m}^A g_3 \Delta) \frac{\partial g_1}{\partial\alpha} + \frac{g_1}{\Delta^2}\left[\frac{\partial}{\partial\alpha}(\overline{m}^A g_3) \right]^2 -$$

$$- \frac{\overline{m}^A g_2}{\Delta^3} \frac{\partial g_3}{\partial\omega_x} \left[\frac{\partial}{\partial\alpha}(\overline{m}^A g_3)\Delta + 2\overline{m}^A g_3 \frac{\partial\Delta}{\partial\alpha} \right] -$$

$$- \frac{(\overline{m}^A)^2 g_3}{\Delta^2} \frac{\partial g_1}{\partial\alpha} \frac{\partial g_3}{\partial\alpha} + \frac{(\overline{m}^A)^2 g_3^2}{2\Delta^4} \frac{\partial\Delta}{\partial\omega_x} \left[7 g_2 \frac{\partial\Delta}{\partial\alpha} - 4\Delta \frac{\partial g_2}{\partial\alpha} \right] +$$

$$+ \frac{(\overline{m}^A)^2 g_3^2}{2\Delta^4} \left[2\Delta^2 \frac{\partial^2 g_1}{\partial\alpha^2} - g_1 \left(\frac{\partial\Delta}{\partial\alpha} \right)^2 \right] \left. \right\} \frac{m^\Delta \cos(2\theta_1 - 2\theta_2)}{8} + \varepsilon^3 g_4 . \qquad (9)$$

Here $\quad g_1 = \dfrac{2\omega_a \omega_{1,2} \sin\alpha}{F_a}(\omega_x + \dfrac{\omega_{1,2}^2 \sin^2\alpha}{2\omega_a}) \quad , \quad g_2 = \dfrac{\omega_{1,2}^2 \sin^2\alpha}{\overline{I}_x} \quad , \quad g_3 = \dfrac{2\omega_a \omega^2}{F_a} \quad ,$

$g_4 = \dfrac{4 m_{zn} \omega_\alpha^2 SL}{I F_a} \dfrac{dq}{dt} .$

To analyse the secondary resonance effects, we also have to obtain the equation for the second derivative of the averaged angular velocity:

$$\left\langle \frac{d^2\omega_x}{dt^2} \right\rangle = \frac{\partial\langle\dot\omega_x\rangle}{\partial\omega_x}\left\langle \frac{d\omega_x}{dt} \right\rangle + \frac{\partial\langle\dot\omega_x\rangle}{\partial\alpha}\left\langle \frac{d\alpha}{dt} \right\rangle + \frac{\partial\langle\dot\omega_x\rangle}{\partial\omega}\frac{d\omega}{dt} . \qquad (10)$$

3. Numeric simulation with different initial conditions

The numerical integration of the equation system (1)-(3) (with allowance of the equation for derivative dq/dt) is implemented via four-staged Runge-Kutta method with adaptive stepsize. The secondary resonance effect is considered, when the angular velocity $\omega_x(t)$, changing from initial positive value, envelopes the $\omega_x^r(t)$ ascending curve and reaches significant values with further keeping its sign in the area of descending curve $\omega_x^r(t)$. At certain decrease of initial conditions of integration or decrease of asymmetry parameters, the situation of angular velocity behaviour changes dramatically. If in the area of ascending curve $\omega_x^r(t)$ the angular velocity $\omega_x(t)$ also increases, in the area of descending curve $\omega_x^r(t)$, the realization of continuous resonance occurs that can be followed with transition to the negative range of values $\omega_x(t)$. Let us assume that the time of integration is 300 s. We consider the influence of various initial condition of integration on the realization of the aforementioned resonance effects. Here, two cases shall be pointed.

202

Case 1. The resonance effect followed by change of rotation direction is observed in various values of initial angular velocity of the body. Let us assume that the condition $\omega_x(0) > \omega_x^r(0)$ has been met. In the first case, generalized parameters of asymmetry take the following values: $\bar{m}^A = 0.011$, $m^\Delta = 0.04$, $\theta_1 = \theta_2 = 0$. Initial values of the angle of attack: $\alpha(0) = 5$ grad, and initial value of aerodynamic roll angle is * $\varphi(0) = 0$.

In the process of numerical integration of equations (1)-(3), a narrow interval of positive values for initial angular velocity $\omega_x(0) \in [17,23]s^{-1}$, has been found. With boundary values of $\omega_x(0)$ within this interval, the resonance effect in question is observed. Let us have a more detailed review of these numerical results.

1. We assume that the initial value of angular velocity $\omega_x(0) = 23s^{-1}$. In the Fig.1, the upper curve describes the increase of angular velocity $\omega_x(t)$, and the curve with maximum is associated with the change of resonance values of angular velocity $\omega_x^r(t)$. At that, in the area of ascending branch of resonance curve $\omega_x^r(t)$, a monotonic non-resonance increase of $\omega_x(t)$ occurs. Further, the withdrawal from resonance values is observed, and angular velocity $\omega_x(t)$ is stabilized. From the Fig.1 it appears that the craft acquires the terminal positive angular velocity which exceeds the initial velocity $\omega_x(0)$ more than twice. Thus, with $\omega_x(0) = 23s^{-1}$, a slow increase of spacecraft angular velocity positive values is observed. The angle of attack also increases slowly from the initial value of 5 grad, but does not reach the value in 90 angle degree, typical for realization of main resonance. The direction of RB's rotation remains unchanged and positive. The increase of angular velocity $\omega_x(t)$ in the area of ascending branch of $\omega_x^r(t)$ curve is explained by positivity of the derivate (8). The change of signature of the $\omega_x(t)$ curve's convexity happens due to flip of the second derivate's sign (10). The increase of the $\omega_x(t)$ fluctuation area after passing the maximum of the resonance curve can be explained with the following: in the right side of the equation (8) there are terms directly proportional to sinα. After 220 seconds of flight, the angle of attack takes values from 40 to 50 grades, which leads to a certain perturbation on the angle of attack in the right side of the equation (8).
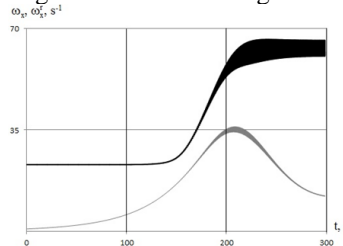
Fig. 1. – Change of angular velocity at $\omega_x(0) = 23s^{-1}$

2. Let the initial angular velocity be $\omega_x(0) = 20s^{-1}$. In this case value of the initial angular velocity is within the $\omega_x(0) = 17s^{-1}$ range. Also, from the Fig.2 it appears that the angular velocity $\omega_x(t)$ in the area of ascending curve $\omega_x^r(t)$ changes similarly to the previously considered variant. But in the area of the descending resonance curve, angular velocity $\omega_x(t)$ passes a bit lower than on the Fig.1. Also, after passing the maximum of the resonance curve, the fluctuation amplitude $\omega_x(t)$ increases significantly, which also promotes the angular velocity to reach its resonance values $\omega_x^r(t)$. In its turn, an increase of the resonance curve fluctuation area is observed. The expansion of the angular velocity fluctuation area occurs due to increase of angle of attack that reaches 75 grads on the 200th second. It should be noticed that the continuous resonance does not occur nevertheless.

3. Let the initial angular velocity be $\omega_x(0) = 17s^{-1}$. From the Fig.3 it appears that in the variant under consideration (similarly to the first one), a growth of non-resonance RB spin-up in the area of ascending resonance curve is realized.
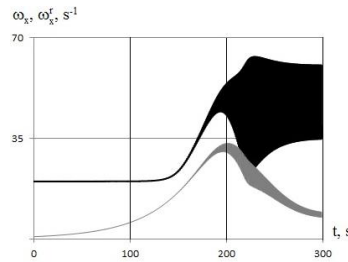
Fig. 2. – Change of angular velocity at $\omega_x(0) = 20s^{-1}$

Yet, the spin-up is slightly smaller than in variant 2, so the increase of amplitude $\omega_x(t)$ in the area of the curve maximum leads to meeting the resonance values $\omega_x^r(t)$. Further, the main resonance is realized, and the angle of attack quickly reaches 90 grades. After the resonance realization, angular velocity returns to the non-resonance movement in the negative range of its values.

Comparing the results of the Fig.1 and Fig.3, it may be noticed that with values of the initial angular velocity that are the boundaries of the $\omega_x(0) \in [17, 23]s^{-1}$ interval, in the process of evolution $\omega_x(t)$, opposite directions of the RB rotating motion are reached.

Case 2. Resonance effect followed by change of the rotation direction is also observed in various values of the initial angle of attack $\alpha(0)$. In the second case, generalized parameters of asymmetry take the following values: $\bar{m}^A = 0.011$, $m^\Delta = 0.002$, $\theta_1 = \theta_2 = 0$. Initial value of the angular velocity: $\omega_x(0) = 25s^{-1}$, and

initial value for the aerodynamic roll angle is $\varphi(0) = 0$. In the process of numerical integration of the equations (1)-(3), we found a narrow range of values for initial angle of attack $\alpha(0) \in [3; 5.7]$ grad, with boundary values of which, the studied resonance effect is observed. The results obtained in the second case are shown on the Fig. 4-6.

4. Let the initial value for the angle of attack be $\alpha(0) = 3$ grad. On the Fig.4, in the area of ascending branch of the resonance curve, a monotonic non-resonant increase $\omega_x(t)$ occurs, similar to variant 1 shown on Fig.1. Further, a withdrawal of $\omega_x(t)$ from resonance values $\omega_x^r(t)$ is also observed, and the angular velocity of the body is stabilized at $\omega_x(0) = 47s^{-1}$. Yet, different from variant 1, the angular speed changes in monotonic way throughout the whole integration interval. It occurs due to fact that the angle of attack at the slow increase from initial value of 5 grad reaches the value of 38 grad in the end of integration interval. As a result, no perturbations of angular velocity is observed taking place with angles of attack higher than 50 grades and more. The direction of the craft's rotation also remains positive throughout the whole integration interval. The increase of the angle velocity $\omega_x(t)$ in the area of ascending branch of the curve $\omega_x^r(t)$ is also explained by positivity of the derivative (8), and the change of the character of the $\omega_x(t)$ curve's convexity occurs due to flip of the second derivative's sign (10).
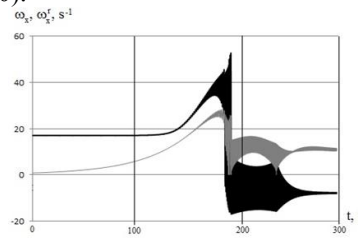
Fig. 3. – Change of angular velocity at $\omega_x(0) = 17s^{-1}$
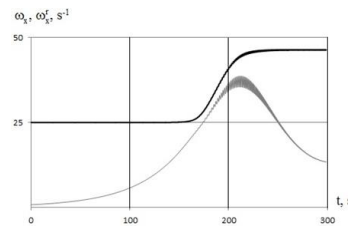
Fig. 4. – Change of angular velocity in the second case at α(0)=3 grad

5. Let us assume that the initial value for the angle of attack is α(0)=4.7 grad. Here, the value for the initial angle of attack is within the section of $\alpha(0) \in [3; 5.7]$ grad. At that, the angular velocity $\omega_x(t)$ in the area of ascending curve $\omega_x^r(t)$ changes

similarly to variant 4. Yet in the area of descending resonance curve, angular velocity $\omega_x(t)$ passes slightly lower than on the Fig.4. Compared to variant 2, in this variant the angular speed perturbation in the area of descending resonance curve is not significant. This is due to fact that the angle of attack in the considered area takes value of about 40 grades. Comparing to variant 4, a slightly increase takes place in the fluctuation are of the resonance curve. Also, in the area of maximum $\omega_x^r(t)$ on the curve $\omega_x(t)$, another inflexion point arrives. As a result, on the curve $\omega_x(t)$ there are two inflexion points, where the mentioned curve changes the character of the convexity twice. From the Fig.5 it appears that in the end of the integration interval, angular velocity $\omega_x(t)$ doesn't reach its resonance values $\omega_x^r(t)$.
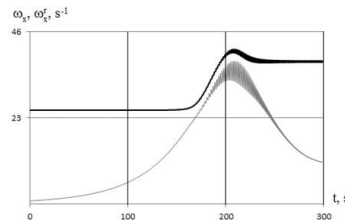
Fig. 5. – Change of angular velocity in the second case at α(0)=4.7 grad

6. Let the initial angle of attack be α(0)=5.7 grad. From the Fig.6 it appears that in the considered variant, similarly to variants 4 and 5, a growths of the non-resonant RB spin-up occurs in the area of the ascending resonance curve. Still, the mentioned spin-up is slightly lower than in the variant 5. As a result, the expansion of range of the resonance values leads angular velocity $\omega_x(t)$ to reaching the resonance values $\omega_x^r(t)$ Further, main resonance is realized, and angle of attack reaches 90 grades. After leaving the continuous resonance, RB's angular velocity $\omega_x(t)$ takes non-resonance values in the negative range. Comparing the results presented on Fig.4 and Fig.6, a conclusion can be made that with the initial values for angle of attack that are the boundaries of section $\alpha(0) \in [3; 5.7]$ grad, in the process of the evolution the angular velocity $\omega_x(t)$ reaches opposite values of the rotating motion.

4. Numerical simulation at different values of asymmetry parameters
We perform a numerical simulation that allow us to study the issue of the influence of different values of asymmetry parameters on the realization of the considered resonance effect. We conduct an individual analysis of influence of inertial and aerodynamic parameter values on the considered resonance effect. Hence, two cases are found.

Case 3. Realization of the resonance effect with changing the rotation direction occurs at different values of the generalized parameter of m^Δ inertial asymmetry. In the process of the RB rotating motion numerical simulation, a range of small values

was found for $m^{\Delta} \in [0.012, 0..040]$ parameter, for which three types of body's angular velocity evolution, similar to the first case, were revealed. Let us give them more detailed overview. At values of the parameters $m^{\Delta} = 0.040$, $\bar{m}^A = 0.011$, $\theta_1 = \theta_2 = 0$ and initial condition of integration $\omega_x(0) = 23 s^{-1}$, $\alpha(0) = 5$ grad, $\varphi(0) = 0$ we obtain the result shown in Fig.1. When integrating the system (1)-(3) with asymmetry parameter $m^{\Delta} = 0.012$ (all other parameters and initial conditions are the same as in variant 1), we obtain the result shown in Fig.7. This result confirms that with parameter value $m^{\Delta} = 0.012$ angular velocity changes the rotation direction.
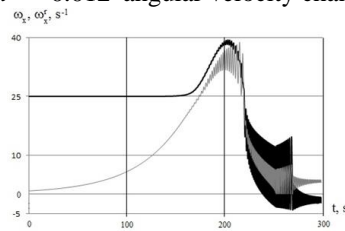
Fig. 6. – Change of angular velocity in the second case at α(0)=5.7 grad

In numerical simulation with parameter $m^{\Delta} = 0.013$ we obtain result that conforms the result on Fig.2 in the qualitative manner.

Case 4. Also, the realization of the resonance effect with change of the rotation direction occurs with different values of m^A aerodynamic asymmetry generalized parameter. In numerical simulation of RB rotating motion, a narrow range of small values for parameter $m^A \in [0.008, 0.011]$ was found. With three values from this range we obtain three types of spacecraft's angular speed evolution which are similar to the first case. Let us give them more detailed overview. The initial variant conforms the case shown on the Fig.1. Indeed, the parameters of the craft and initial
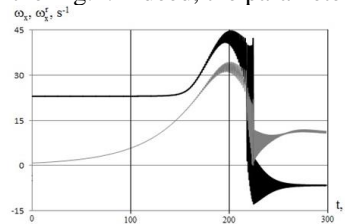
Fig. 7. – Change of angular velocity at $m^{\Delta} = 0.012$

data are identic to the variant 1: $m^A = 0.040$, $\bar{m}^A = 0.011$, $\theta_1 = \theta_2 = 0$, $\omega_x(0) = 23 c^{-1}$, $\alpha(0) = 5$ grad, $\varphi(0) = 0$. If the aerodynamic asymmetry parameter is considered equal to $m^A = 0.008$ (leaving other parameters and initial integration conditions unchanged), we obtain the result of integration presented on the Fig.8. This result is approximate to the results shown in Fig.3 and Fig.7. Here, the angular velocity $\omega_x(t)$

207

also transits to non-resonant negative range of its values after the realization of the continuous resonance and withdrawal from it. Numerical simulation of angular speed $\omega_x(t)$ at the parameter value $m^A = 0.0082$ allow us to obtain a result identical to the result of simulation shown on Fig.2.
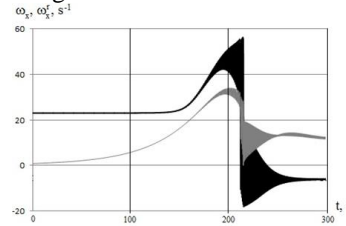
Fig. 8. – Change of angular velocity at $m^A = 0.008$

5. Conclusion

In this work, application of numerical simulation together with analytical research allows us to study in detail the new resonance effect observed in the process of movement in relation to centre of mass of the rigid body with low inertial and aerodynamic asymmetries at re-entry into the atmosphere. An unusual feature of the studied resonance effect is the following: while changing in the boundaries of the ascending branch of the resonance curve, angular velocity $\omega_x(t)$ in absolutely most cases "glides" with delay of relatively resonant curve $\omega_x^r(t)$ without reaching the resonant values. At the transition to the area of the descending part of the curve $\omega_x^r(t)$, two typical cases were peculiar to angular velocity $\omega_x(t)$ behaviour:

- angular velocity kept increasing the positive values (practically by the linear law) with further gradual non-linear transition to some large constant value;
- angular velocity reached resonant value, resonance realization occurred with further withdrawal from it and transition to non-resonant negative range of values.
  In numerical simulation, narrow intervals of initial integration conditions $\omega_x(0)$, $\alpha(0)$ and a small interval of asymmetry of m^Δ, $\bar{m}^A$ parameters values were found. Taking into account the values on the boundaries of intervals in the process of numerical integration led us to realization of the two described typical cases. While accounting intermediate values from aforementioned intervals in the process of numerical simulations, we found a number of cases where an increase of amplitudes of $\omega_x(t)$ and $\omega_x^r(t)$ oscillations was observed after passing the maximum by the resonance curve. At that, change of the $\omega_x(t)$ curve convexity character occurred.

The conducted numerical simulation and results of analytical research allow us to draw the following conclusions:

1. The values of initial integration conditions $\omega_x(0)$, $\alpha(0)$ and values of asymmetry parameters m^Δ, $\bar{m}^A$, $\theta_1 = \theta_2 = 0$ together have an effect on realization of the considered resonance event.

2. One may talk of a common pattern of influence by the values $\omega_x(0)$ and m^Δ, $\bar{m}^A$ on the realization of the found resonance effect that takes place in case when mentioned initial conditions and asymmetry parameters are chosen from the intervals found in this study.

3. The comparison of the numerical results obtained in process of integration of the approximated system (1)-(3) with the results of numerical integration of initial non-linear system has shown good qualitative agreement with these results.

4. The further study of the considered dynamical event of $\omega_x(t)$ sign flip is of practical interest, for instance in the process of movement of a RB with low inertial and aerodynamic asymmetries in the atmosphere.

References

1. **Yaroshevsky VA.** The movement of the body in an uncontrolled atmosphere. Moscow: Mechanical engineering, 1978; 168. [in Russian]

2. **Platus DH.** Roll Resonance Control of Angle of Attack for Re-entry Vehicle Drag Modulation. Journal of Guidance, Control, and Dynamics, 1981; 4(5): 632-636.

3. **Sadov YuA.** Secondary Resonance Effects in Mechanical Systems. Mechanics of Solids, 1990; 4: 20-24.

4. **Zabolotnov YuM, Lyubimov VV.** Secondary Resonance Effects in the Rotation of a Rigid Body about a Fixed Point. Mechanics of Solids, 2002; 1: 49-59.

5. **Zabolotnov YuM, Lyubimov VV.** Secondary Resonance Effect in the Motion of a Spacecraft in the Atmosphere. Cosmic Research, 1998; 36(2): 194-201.

6. **Lyubimov VV.** Asymptotic Analysis of the Secondary Resonance Effects in the Rotation of a Spacecraft with Small Asymmetry in the Atmosphere. Russian Aeronautics (Iz VUZ), 2014; 57(3): 245-252.

7. **Zabolotnov YuM.** Statistical Analysis of Movement of Light Capsule around of the Centre of Mass at Re-Entry into the Atmosphere. Cosmic Research, 2013; 51: 1-12.

8. **Sedelnikov AV.** The Usage of Fractal Quality for Microacceleration Data Recovery and for Measuring Equipment Efficiency Check. Microgravity Science and Technology, 2014; 26(5): 327-334.

9. **Lyubimov VV.** Dynamics and Control of Angular Acceleration of a Re-Entry Spacecraft with a Small Asymmetry in the Atmosphere in the Presence of the Secondary Resonance Effect. International Sibefian Conference on Control and Communications (SIBCON), 2015; 1-4.

10. **Lyubimov VV, Lashin VS.** Numerical simulation of resonance effect with the change of the direction of rotation at atmospheric descent asymmetric nanosatellite. Samara: SamNC RAN, 2015; 250-253. [in Russian]

11. **Belokonov VM, Belokonov IV, Zabolotnov YuM.** Fast calculation of the trajectories in the atmosphere reduce uncontrolled spacecraft with regard to their motion relative to the center of mass. Space activities, 1983; 21(4): 512-521. [in Russian]

12. **Strygin VV, Sobolev VA.** Separation of Motions by the Integral Manifolds Method. Moscow: Nauka, 1988. [in Russian]

13. **Zabolotnov YuM.** The method of investigation of resonant vibrational motion of a nonlinear system. Izvestiya RAN: Mechanics of Solids, 1999; 1: 33-45. [in Russian]
14. **Zabolotnov YuM.** The asymptotic analysis of quasi-linear equations of motion in the atmosphere the spacecraft with a small asymmetry and. Space Exploration, 1994; 32(2): 22-23. [in Russian]
15. **Moiseev NN.** Asymptotic Methods in Nonlinear Mechanics. Moscow: Nauka, 1986. [in Russia]

Numeric simulation of the interaction between subsonic flow and a deformable profile blade on the compressor experiment phase

Mekhonoshina E.V., Modorskii V.Ya., Petrov V.Yu.

Perm National Research Polytechnic University

Abstract. The article investigates the numeric simulation of two-way aeroelastic processes applied to the experimental phase of a compressor; physical, mathematical, rigid and grid models of the system "gas – rotor – stator" have been worked out; 2 FSI (two-way Fluid-Structure Interaction) calculations have been performed on the evaluation of the interaction between a gas-dynamic flow and a deformable rotor blade; the effect of voltage gain is found in a blade, in an aeroelastic state compared with the transient calculations of a stress-strain state.

Keywords: interdisciplinary calculation, experimental compressor stage

Introduction

During the operation of compressors diverse vibrations may come out together with increased dynamic loads on the bearings; they can initiate the decrease of operating characteristics [1].

Blade machines produce vibrations for different reasons. For example, there might be technological imbalances of shafts and other rotation parts, or imbalances by assembly – all lead to vibrations. It's also necessary to consider vibration processes in magnetic suspensions. Vibration processes in labyrinth seals and in a gas-dynamic tracks are also taken as key vibration factors [2, 3, 4, 5].

Moreover, the analysis of vibration and aerodynamics is carried out separately due to the complexity of the calculations. Nowadays the vibrations in compressors cannot be predicted as essential factors and are not taken into account.

1. Survey

The history of aeroelastic numeric calculations traces back to works related to an asymmetric flutter that occurred during the flight on the bomber built by Handley Page. In 1918 after the failure of the lower wing of the biplane Albatros D3 German

physicist Paul Richard Heinrich Blasius was the first to perform the analytical calculations of a flutter. First numeric calculation of the aerodynamic power acting on a harmonically vibrating thin plate in a two-dimensional flow was performed later in 1922 by W. Birnbaum in his thesis at Gottingen University [6, 7].

Since that time many researchers have referred to such issues of aeroelasticity. In 1972 A.S. Volmir described forced vibrations of the plate that was exposed to a periodically varying transverse load [8]. The issue of aerohydroelasticity and its component parts is thoroughly investigated in the following work [9]. The authors consider the tasks where the impact of environment on structures operation is necessary to consider and emphasize the always expanding scope of such tasks [9]. The main trend of the advance in technology is the increase of energy-and-mass characteristics; hence loads are increasing and the mass of structures reduces at the same time the stiffness of structures is coming down. In such a case unpredictable effects might occur, such as a "flutter". These kinds of issues are researched in the following works [2]. The authors take a gas-elastic approach to calculate vibration modes in power installations, give physical and mathematical models of a process, and suggest a unified algorithm and solution method [2]. Lots of model task solutions are given.

The researchers from the USA [10] did a review of associated numeric schemes. They took one of the approaches to study the issue of a flutter [10]. The scientists from three countries (ie. – China, Australia and USA), studied together the vibration of wind turbine blades [11]. In the calculations the authors paid attention to the interaction of gas flow and structure in the applied software ANSYS. The scientists stress that the effect of such an interaction is essential and it has to be considered [11]. The scientists from China write about the interaction of a gas-dynamic flow and structure with the profile NACA0012 [12]. Together with the idea of the following work [2] it's being suggested that the deformations change the flow field around the structure, while the change in the field of a gas-dynamic pressure flow affects the deformations as well [14].

As shown in [9] the solution of aeroelastic tasks requires theoretical methods of elasticity, aeromechanics and vibrations. It's necessary to simulate interdisciplinary physical phenomena in order to solve such tasks. It's complicated to calculate together aerodynamics and rigidity as we deal with different mathematical models, solution methods, the dynamics of calculated areas and approaches to discrete the equations.

There are two variants of associating the equations of rigid body dynamic deformation and the equations of gasdynamics: monolithic and consecutive [3]. By a monolithic approach we use numeric schemes which result in the formation and subsequent solution of a unified system of algebraic equations. A consecutive approach is used to solve associated interdisciplinary tasks based on a separate solution by the systems of equations for each subtask and requires the implementation of calculation data exchange between the subtasks over a set period of time [3, 13] with help of iteration procedures. Otherwise the synchronization is performed directly. Such an approach is implemented in well known commercial products, such as ANSYS, FlowVision, Abacus, CCM+, SolidWorks, LS-Dyna, Sysnoise NASTRAN, OpenFOAM and FEStudio [14].

2. Physical model

This work suggests a fully associated non-standardized solution scheme for an aeroelastic task applied to the simulation in the dynamical system "gas-rotor-stator interaction" on the example of a compressor experiment phase.

Two domains have been considered: inlet guide vane (IGV) and the rotor itself. The domain IGV is permanent, rotor domain is rotating with a constant angular rate. The interaction of a gas-dynamic flow and rotor blade deformation is being considered. Three-dimensional calculation model is given in the figure 1.
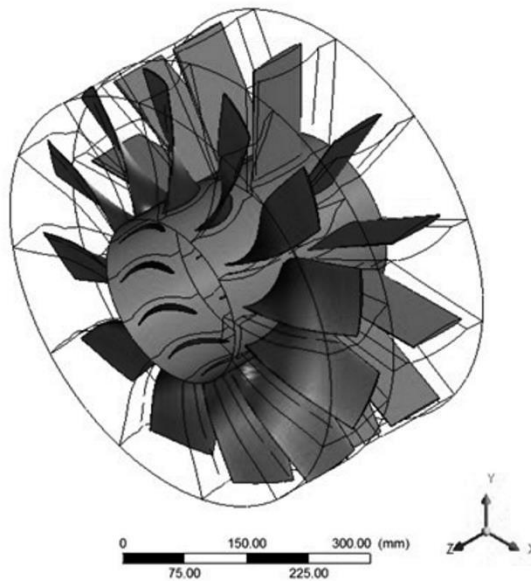
Fig. 1. – Three-dimensional calculation model of a compressor

We look at the sector that takes 1/12 of the structure. The sector is bounded by the planes on which symmetry conditions are written. We consider the flow of an ideal gas with the set properties; chemical processes are not considered; one-phase flow; the calculations are performed without taking into account gravitation; the walls of the structure neither absorb nor give off heat; the walls of the structure are rugged; the coefficients of heat capacity don't depend on the absolute temperature.

3. Mathematical model

Mathematical model is worked out based on the chosen physical model; mathematical model includes two submodels. The submodel of gasdynamics is based on the conservation laws of mass, momentum, energy, the equation of state of the ideal compressible gas and encloses with the initial and boundary conditions. Boundary conditions for gasdynamics are shown in the figure 2.

1 – stator domain, 2 - rotor domain, 3 – input, 4 – output; 5 – stator domain symmetry, 6 – rotor domain symmetry, 7 – interface between the domains, 8 – the interface "gas - structure" (movable grid of a rotor blade), 9 – movable grid of the gap in the rotor domain
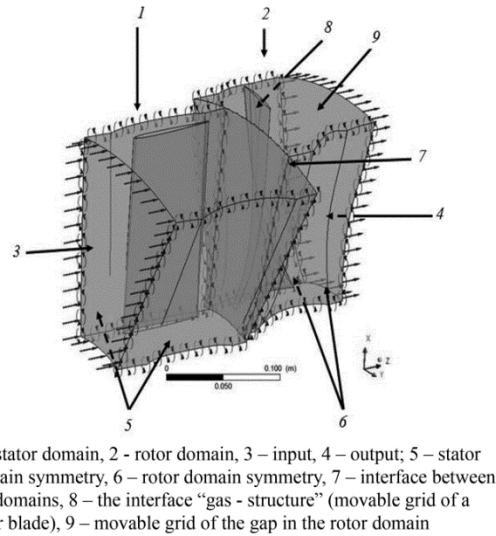
Fig. 2. – Boundary conditions for gas dynamic calculation

Mathematical model for the evaluation of a stress-strain state is written down as follows [15, 16]:

$$m\ddot{x} + c\dot{x} + kx = F(t);$$

(1)

Where m – mass matrix; c – damping matrix; k - rigidity matrix; $F(t)$ – load vector; x – displacement.

At each moment these equations can be considered as a set of static equations of equilibrium which take up the forces of inertia and damping as well. Time integration by the *Newmark* method is used to solve these equations [15, 16]. We calculate the increment between subsequent time points, integration step. Boundary conditions for the structure are shown in Figure 3.

1 - ban displacements normal to the surface of the blade lock, 2 – symmetry, 3 the interface "structure – gas"
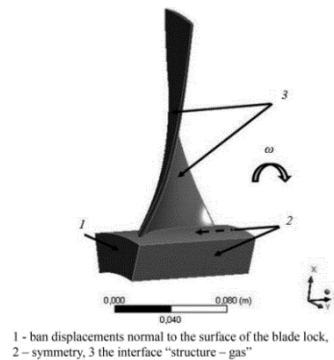
Fig. 3. – Boundary conditions for stress-strain state calculation

Afterwards we developed rigid body and grid models of the structure and gas dynamic part. The number of the elements of the grid model of a gas dynamic rotor track made up 56482 nodes and 51750 elements; of a gas dynamic stator track – 51863 nodes and 47490 elements; structures – 7728 nodes and 3378 elements.

4. Computational experiments

The solution is found by the iteration way. Two solvers – Transient Structural (transient mechanics, finite element approach) and CFX Transient (gas dynamics, finite volume approach) – are connected by data transfer. For the flow diagram of such a solution refer to the following work [11].

The calculations are performed in the system of the computer engineering analysis ANSYS 15.0 using the power of the high performance computing complex of PNRPU. The duration of the calculations averages 4 hours on 16 cores «IntelXeon E5-2680». We believe that the application of hybrid supercomputing systems with graphics accelerators has great potential [17].

5. Results

According to the results of the computational experiments we found that the dependence of the increment of displacements is specified by the aeroelasticity from rotation speed at the control point which is located on the upper edge of the blade. Figure 4 shows the diagram where in the vertical axis the difference of displacements is given received by the calculation 2FSI and transient calculations of a stress-strain state (calculated by the formula: $\Delta U = U_{2FSI} - U_{transient}$).
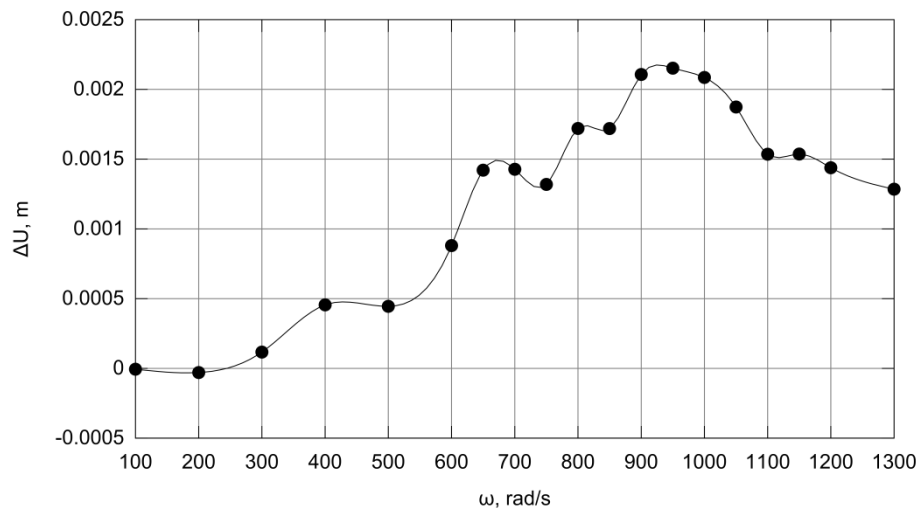
Fig. 4. – Aeroelasticity impact on the full movements at the control point on the upper edge of the blade

In the horizontal axis the rotation of rotor speed is given. For the analysis we selected the points which fit the period of time of the second peak occurrence by the calculations 2FSI. At the same time the critical frequency of the rotation of the

compressor model phase was determined by the Campbell diagram which made up 1013,8 rad/s that determines the increase of movements by the rotation at the speeds close to the critical speed.

In the computational experiment we received the dependence of the von Mises stress σ time by the transient calculations (without considering FSI) and by the calculations 2FSI for the rotor rotation speed ω=650 rad/s (see the figure 5).
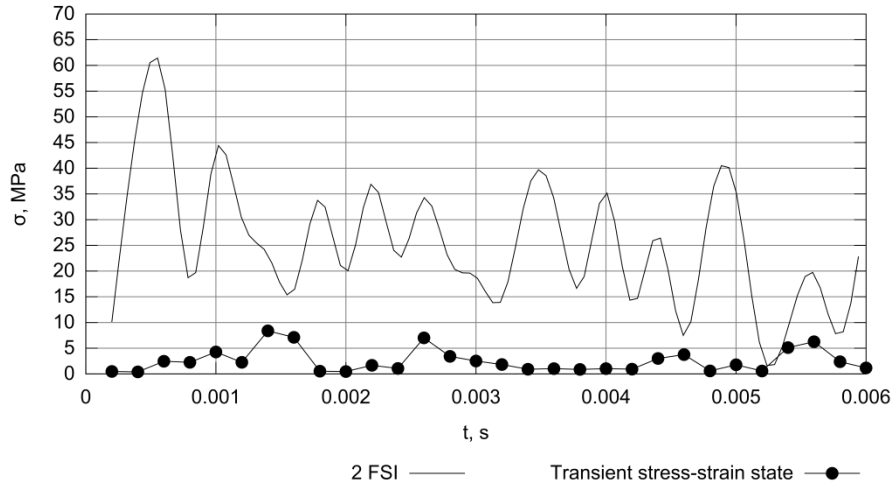
Fig. 5. – Von Mises stress (ω=650 c-1)

We carried out the analysis of these dependences by diverse speeds of rotor rotation. The following charts of the dependences Δσmax and Δσav from ω were worked out (figure 6a, 6b respectively), with $\Delta\sigma_{max} = \dfrac{\sigma_{max}^{FSI} - \sigma_{max}^{trans}}{\sigma_{max}^{trans}}$,

$$\Delta\sigma_{av} = \frac{\sigma_{av}^{FSI} - \sigma_{av}^{trans}}{\sigma_{av}^{trans}} \text{, where } \sigma_{av}^{FSI} = \frac{\sum_{1}^{N} \sigma^{FSI}}{N} \text{ , } \sigma_{av}^{trans} = \frac{\sum_{1}^{N} \sigma^{trans}}{N} \text{ .}$$

We can see that at the frequencies close to the critical ones there is the increase of von Mises stress related with aeroelastic effect.

Acknowledgements

a)

b)
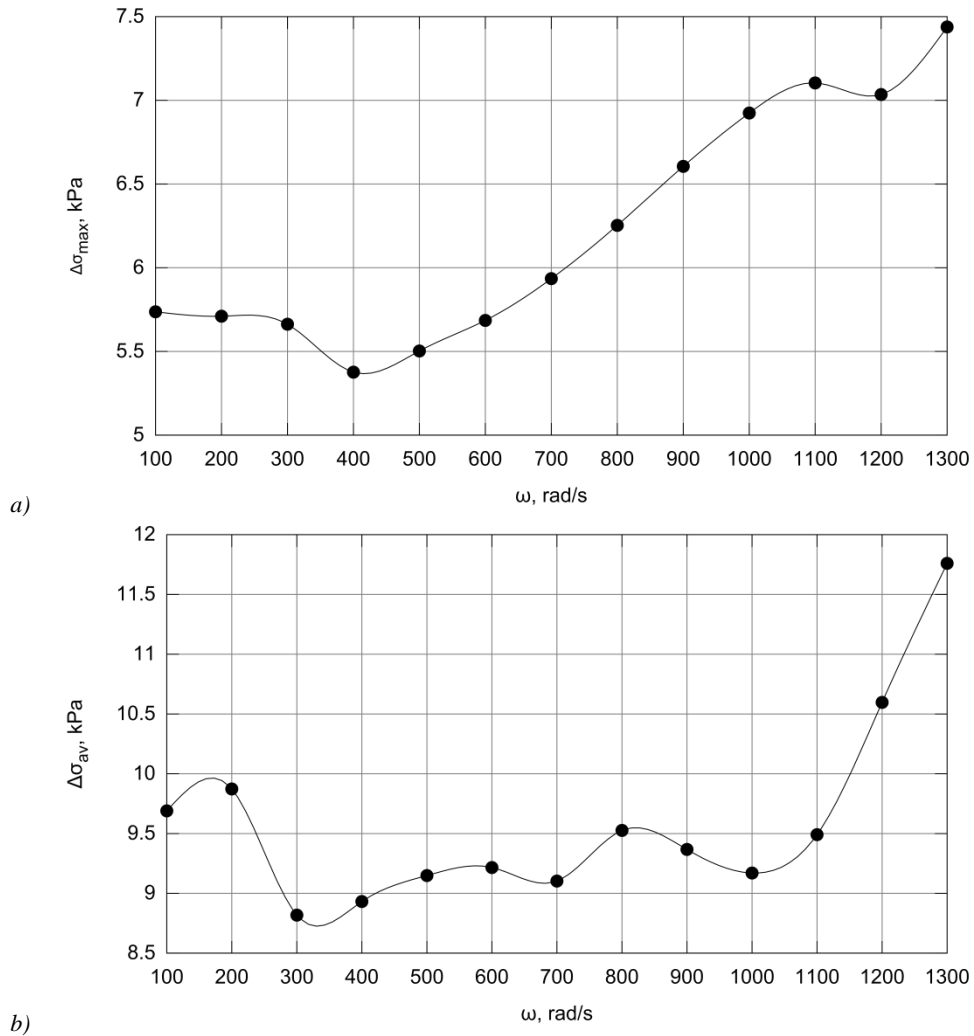
Fig. 6. – The increase of von Mises stress by considering aeroelastic effect: a – by maximum values; b – by average values

References

1. **Mekhonoshina EV, Modorsky VYa.** Development of a technique of numerical modeling of the aeroelastic work of Compressor. Scientific and technical bulletin of the Volga region, 2014; 5: 264-268. [in Russian]

2. **Modorsky VYa, Sokolkin YuV.** Gas-elastic processes in power installations. Ed by Sokolkin YuV. Moscow: Nauka, 2007. [in Russian]

3. **Kopysov SP, Tonkov LE, Chernova AA.** Bilateral binding when modeling interaction of a supersonic stream and deformable plate. Comparison of numerical schemes and results Experiment. Computational Continuum Mechanics, 2013; 6(1): 78-85. [in Russian]

4. **Amarantov GN, Egorov MYu, Egorov SM, Egorov DM, Nekrasov VI.** Numerical modeling of intra chamber processes at an exit to an operating mode of the rocket engine of solid fuel. Computational Continuum Mechanics, 2010; 3(3): 5-17. [in Russian]

5. **Ganeev MS, Moiseyev VE, Skvortsova ZV.** A nonlinear bend and stability of the ellipsoidal cover interacting from Liquid. Computational Continuum Mechanics, 2011; 4(3): 32-40. [in Russian]

6. **Arsentiev TP.** The Abstract of the thesis "Fluctuations of a wing in a supersonic stream of gas": PhD thesis abstract physical and mathematical science. SPb. University, St. Petersburg, 2009; Source: <http://www.dissercat.com/content/kolebaniya-kryla-v-sverkhzvukovom-potoke-gaza-0>

7. **Blasius H.** Über Schwingungserscheinungen an Einholmigen Unterflügeln. Zeitschrift für fFugtechnik und Motorluftschiffahrt, 1925; 16: 39-42.

8. **Volmir AS.** Nonlinear dynamics of plates and Covers. Ed by Kildibekov IG. Moscow: Nauka, 1972. [in Russian]

9. **Gorshkov AG, Morozov VI, Ponomarev AT, Shklyarchuk FN.** Aero hydroelasticity of designs. Moscow: Fizmatlit, 2000. [in Russian]

10. **Xiangying Ch, Ge-Cheng Zh, Ming-Ta Ya.** Numerical simulation of 3-D wing flutter with fully coupled fluid–structural interaction. Computers & Fluids, 2007; 36: 856–867.

11. **Jianping Z, Liang G, Helen W, Aixi Zh, Danmei H, Jianxing R.** The influence of wind shear on vibration of geometrically nonlinear wind turbine blade under fluid–structure interaction. Ocean Engineering, 2014; 84: 14-19.

12. **Hefeng D, Chenxi W, Shaobin L, Zhen SXi.** Numerical Research on Segmented Flexible Airfoils Considering Fluid-structure Interaction. Procedia Engineering, 2015; 99: 57-66.

13. **Farhat C, Lesoinne M.** Two efficient staggered algorithms for the serial and parallel solution of three-dimensional nonlinear transient aeroelastic problems. Computer Methods in Applied Mechanics and Engineering, 2000; 182(3-4): 499-515.

14. **Kopysov SP, Kuzmin IM, Rychkov VN, Tonkov LE.** The divided approach at the solution of the connected problems of FSI on hybrid computing systems. Works of the international scientific conference "Parallel computing technologies (PAVT '2015)". Yekaterinburg: UrFU of the first President of Russia B. N. Yeltsin, 2015; 415-419. [in Russian]

15. ANSYS Structural Analysis Guide, Release 15.0. Source: <http://www.ansys.com/>.

16. **Wang E, Nelson T.** Structural Dynamic Capabilities of ANSYS. Source: <http://easc.ansys.com/staticassets/ANSYS/staticassets/resourcelibrary/confpaper/2002-Int-ANSYS-Conf-200.PDF >.

17. **Golovashkin DL, Loganova LV.** Solution of difference equations difference scheme with cyclic boundary conditions on two-dimensional grid areas using multiple graphics computing devices. Computer Optics, 2012; 36(4):534-540.

Simulation of DTN nodes' mobility using least action principle for locations selection

Privalov A.Yu., Tsarev A.A.

Samara State Aerospace University

Abstract. Three modifications of mobility model of DTN's nodes are presented. These modifications are based on the Levy mobility model. Flight length of DTN nodes inside some locations (hot spots) is a random value with the Levy probability distribution function. Between locations the nodes can move differently. In the first modification nodes walk between different locations randomly; in the second modification nodes walk between locations using the least action principle; and in the third modification each node chooses the next location according to a limiting number of possible visits. These modifications are implemented in the Omnet++ simulation environment. This paper presents an experimental results of DTN nodes' movements modeling, and comparison of these results with real nodes movements data.

Keywords: mobility model, Levy probability distribution function, self-similarity, OMNET++.

1. Introduction

MANET is a continuously self-configuring, infrastructure-less network of mobile devices connected without wires. Each device can move independently in any direction, so it often breaks off and establish connection. Delay-Tolerant Networking (DTN) is an approach for constructing of network architecture for heterogeneous network that may lack continuous network connectivity. In this context, delay means time loosing occurred in transitive nodes or generated by low channel bandwidth.

For the aim of routing on the network layer, it used special protocols oriented on dynamic networks: reactive (AODV, DSR, etc.) and proactive (OLSR, etc.). Preferences for a particular type of protocols may be given only in view of real situation and velocity of subscribers. People often carries wireless devices, so understanding human mobility patterns contributes for more accurate performance modeling and for more predictable protocols used for these networks.

Widely used mobility models in research of the computer networking are random waypoint [1], random walk models [2], such as model of Brownian motion or

Markovian mobility [3]. These models are simple enough for theoretical treatment and, at the same time, are simple for emulating in the simulation environment in a scalable manner. However, the adequacy and accuracy of these mobility models is still the subject of research, and the problem of building adequate mobility models is very important and urgent.

In this paper we construct the modification of mobility model Truncated Levy Walk [4] and study the effectiveness of each movement simulation model.

2. Levy mobility model

To analyze the performance of mobile networks, as mentioned above, different mobility patterns are used. In the proposed mobility model, well-known Levy Mobility Model [7] plays an important role, so further we shortly remind a mathematical description of this model and an application to the people mobility.

Let a *flight* be the longest straight transition of node from one location to another without changing direction or pause. The path, built of successive movements will be called *route*.

To simulate the mobility on a confined area a truncated distribution (TLW – Truncated Levy Walk), based on a truncated Pareto distribution for the length of the movement and pause time interval is often used [5, 6]. This truncated distribution is used instead of simple Levy distribution, based on a normal distribution of Pareto. The Levy distribution itself with the normalizing factor c and the exponent α in terms of the Fourier transform looks as [5]:

$$f_X(x) = \frac{1}{2\pi} \int\limits_{-\infty}^{+\infty} \exp\left(-itx - |ct|^\alpha\right) dt . \tag{1}$$

In the model it is assumed that the node performs its flights based on a given distribution function for the length of Levy flight and for the duration of the pause following the jump, with coefficients c_α, α and c_β, β, respectively – these are parameters of the model. It needs to define these settings for simulations, because they will fit the artificial route closer to the real one in a statistical manner.

As shown in [5], the average speed of movement of people is not constant, and can be expressed by the following relationship between the duration of the flight and its length:

$$\Delta t_f = k l^{1-\rho}, \ \ 0 \le \rho \le 1, \tag{2}$$

where k and ρ some constants, l – flight length, Δt_f – time duration of flight.

2.1. Levy walks for short distances and flights between locations

Real traces are recorded using GPS sensors carried by the participants of the experiment. Some of these data is available in [8]. The data in these traces are a set of records "time – place position". As mentioned in [5, 6, 9], the processing of these data shows that the Levy mobility model describes well the movements of people only for short distances.

According to [9], we also call *waypoint* a circle of radius R = 5 m, in which a person holds on more than T = 30 sec. The position of a waypoint is a position of the center of this circle. Waypoints are determined from the real traces of people.

This "aggregating" procedure produces a consistent set of waypoints for a more precise definition of the relocation fact of one person. So all positions in the circle for the specified time threshold are took as a point at which person spent time. The radius and the threshold time are determined based on a typical user behavior. After that, there is determined the *visited location* – rectangular clusters combine similar points. Locations are transitive closure of points placed from each other at a distance of 100 m. These locations outline typical regions of the cluster of users. From real source traces, numerical estimates of the probability distribution function for the length between waypoints in the same location and pause time in them are obtained. Parameters c_α, α and c_β, β are determined from this distributions. These parameters will be used to simulate the users' movements within a single location.

Our mobility model (in all modifications), organized as follows: the movement of the node begins at a random location and hold on there according to the Levy mobility model until the next flight gets out the node of the location. After that, the cornering procedure tries to keep the node inside location by changing direction of the flight. This cornering procedure is carried out in a way saved flight length to not spoil it's probability distribution function. If this procedure failed, then node selects the next location.

In the first modification of the model next location is selected in a random manner and each location can be selected only once.

2.2. Levy mobility model with the LATP algorithm

These movements are fully consistent with the previous movements, in terms of generation regular flights and pauses, but differs in terms of the choice of another location.

Movements of people depend on the selection of the next waypoint. Many factors play a role in this choice. Everyone has different factors and personal situation, so it is almost impossible to get an algorithm that takes into account all of these factors. Work [9] shows the selection of the next location is strongly dependents on the current location. The principle of least action of Maupertuis in this case may provide some explanation: people tend to perform actions that require the least effort. Due to this it is possible to introduce an algorithm which reflects this trend to select the next location (out of the previously known set), depending on the distance to it. This algorithm is called Least Action Trip Planning (LATP).

We describe this algorithm below. While the current location is i, the set of all locations is V, then the probability of selecting the next location with number j is calculated as follows:

$$p_j = \frac{1/d_{ij}^a}{\sum_{k \in \{V - V'\}} 1/d_{ik}^a} \,, \tag{3}$$

where d_{ij} – the Euclidean distance from the location i to j, parameter a –a fixed real variable with values in the range $\left[0;+\infty\right]$, and V' – a set of locations from V, that have already visited.

2.3. Levy mobility model with the LATP algorithm and possible plural visits of location

This version is almost completely corresponds to the previous model, except for the possibility to choose of previously visited location. Experimental analysis of user-produced traces in [8] shown that people are also returning to the previously visited location. That was not considered in the model [9]. So, in our third modification, the number of visits of all previously defined locations obtained from real traces is used to provide simulation with this information. All traces are analyzed before simulation and compiled a histogram frequency of visits for each location.

3. Modeling

For experimental studies of these modifications of the mobility model, they have been implemented in the simulation environment OMNeT ++ using INET framework. The simulation results are artificially generated traces of human mobility. They pass through the same analysis as the real traces to obtain numerical estimates of the probability distribution function of the flight lengths and pauses. Below we present some results of experiments based on real traces of KAIST's and NCSU's campuses [8].

The simulation parameters are: c_{α}=0.5 and α=1.5 for the flight length, $c_{\beta}=0.1$ and β=0.5 for the pause time. Duration of simulation is 2 days of model time (or 172800 model seconds). The area of simulation is the same as for the original traces.

The results of the simulation of our first modification for the complementary cumulative distribution function can be seen on the Figure 1. By definition, cumulative distribution function has form:

$$\overline{F}\left(x\right)=P\left(X>x\right)=1-F\left(x\right).\tag{4}$$

Figure 1 shows that the general shape of the graphs are pretty close, which indicates the adequacy of this model, although at some distances quantitative differences are considerable (in our paper [4] one can find the results for this modification without cornering procedure). The initial parts of the graphs (up to 16 meters – a mark 4 on a logarithmic axis) correspond to movements inside a location according to the Levy mobility model. The rest of the charts – is mainly movements between locations.

a)

b)
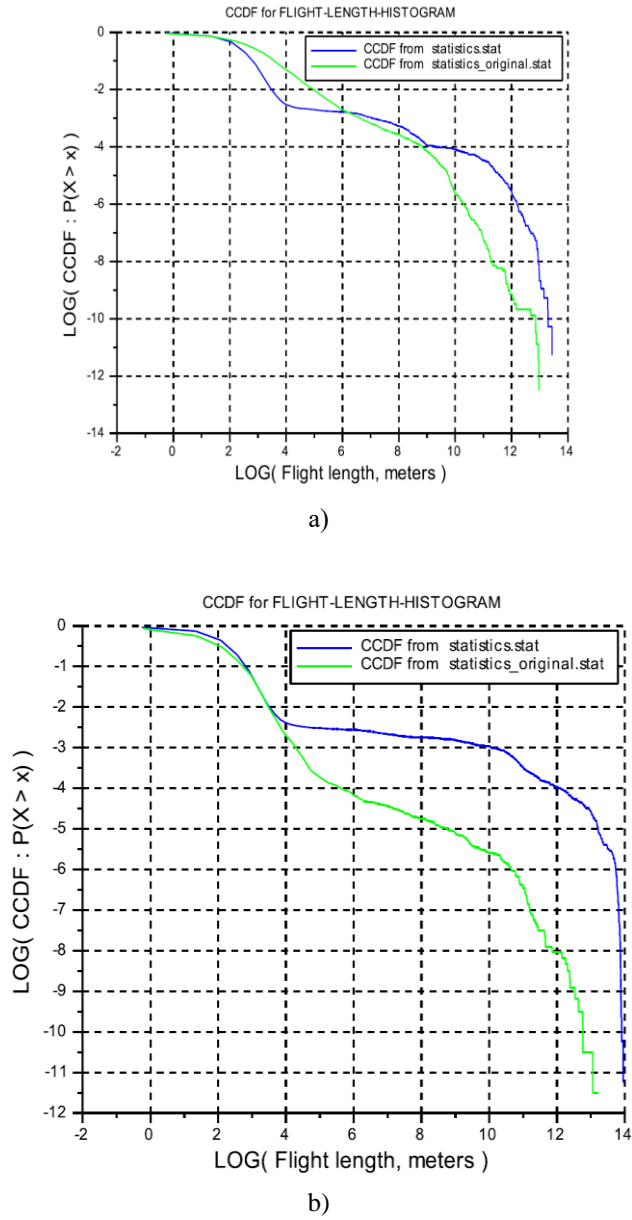
Fig. 1. – The CCDF (4) in the logarithmic coordinate axes for the real and the simulated traces on the KAIST's territory (a) and on the NCSU's territory (b)
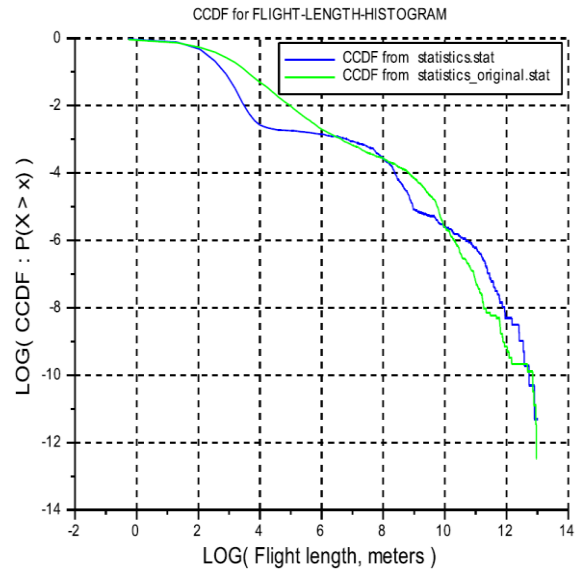
a)
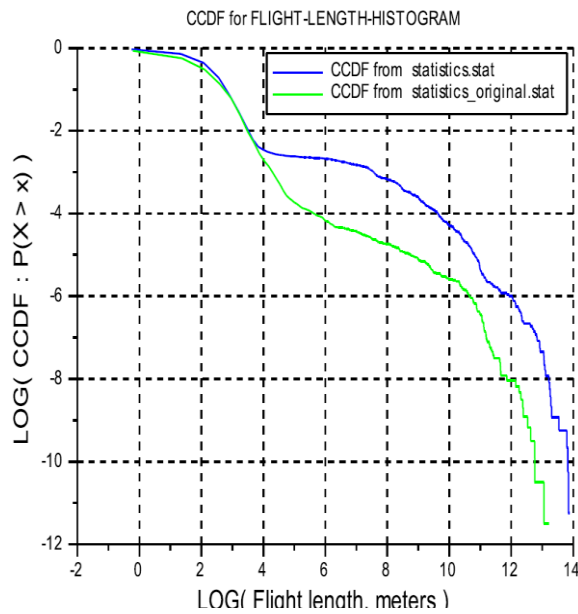
b)

Fig. 2. – The CCDF (4) in the logarithmic coordinate axes for the real and the simulated traces on the KASIT's territory (a) and on the NCSU's territory (b)
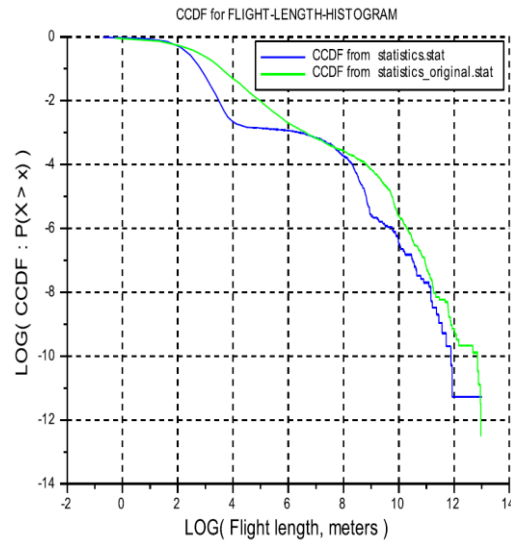
a)
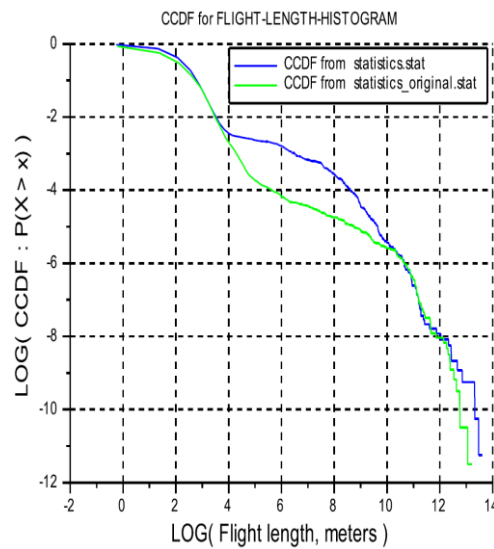
b)

Fig. 3. – The CCDF (4) in the logarithmic coordinate axes for the real and the simulated traces on the KAIST's territory (a) and on the NCSU's territory (b)

The results of the simulation of Levy mobility with LATP algorithm (our second modification) for complementary cumulative distribution function (4) are shown on Figure 2.

225

Figure 2 shows that the overall shape of the graphs became much closer than on Figure 1, which indicates that the second modification of the mobility model closer captures the statistical features. However quantitative differences remain. As you can see, part of the graph, which corresponds to movements between locations has been improved, and it indicates the advantages of the LATP algorithm.

The results of the simulation of Levy mobility model with LATP algorithm and possible plural visits of location (our third modification) are shown on Figure 3.

Figure 3 shows the shapes of the graphs even closer, compared with the previous model modifications. It indicates a best adequacy of this last model modification.

4. Conclusion

Three modification of mobility model of nodes are implemented: TLW mobility model using just information about crowd of people on the real terrain (visited locations), and then the same model with an LATP algorithm for selection of a next location, and the same model with the LATP algorithm with possible plural visits of location. The comparison of the simulation results with the real traces are presented.

Presented model with its all modifications are easy to implement and should be more efficient than other popular models (e.g. [6]). We plan to develop a better selection algorithm for the next location by using information about the history of the movements of a real people. As we hope, this will bring the simulation even closer to the real life.

References

1. **Bettstetter C, Resta G, Santi P.** The node distribution of the random waypoint mobility model for wireless ad hoc networks. IEEE Transactions on Mobile Computing, 2003; 2(3): 257-269.
2. **Camp T, Boleng J, Davies V.** A survey of mobility models for ad hoc network research. Wireless Communications and Mobile Computing, 2002; 2(5): 483-502.
3. **Bettstetter C.** Mobility modeling in wireless networks: Categorization, smooth movement, and border effects. Mobile Computing and Communications Review, 2001; 5(3): 55-66.
4. **Privalov AYu, Tsarev AA.** The DTN nodes' mobility model based on Levy distribution function. Advanced information technologies. Samara: Publisher Samara Scientific Center RAS, 2015; 2: 30-34.
5. **Rhee I, Shin M, Hong S, Lee K, Kim SJ, Chong S.** On the Levy-Walk Nature of Human Mobility. IEEE/ACM Transactions on Networking, 2011; 19(3): 630-643.
6. **Lee K, Hong S, Kim SJ, Rhee I, Chong S.** SLAW: Self-Similar Least-Action Human Walk. IEEE/ACM Transactions on Networking, 2012; 20(2): 515-529.
7. **Shlesinger MF, Zaslavsky GM, Klafter J.** Levy dynamics of enhanced diffusion: Application to turbulence. Physical Review Letters, 1987; 58: 1100-1103.
8. **Kotz D.** Community Resource for Archiving Wireless Data at Dartmouth. Dartmouth College. Source: <http://www.crawdad.org/index.html>.
9. **Lee K, Hong S, Kim SJ, Rhee I, Chong S.** Demystifying Levy Walk Patterns in Human Walks. NCSU/CSC: Technical Reports, 2008.

Mathematical Modeling

On some applications of one wave equation with variable coefficients

Senitskiy A.Yu., Evdokimova N.N.

Samara State Transport University

Abstract. In the present study we consider the cases of integrability of hyperbolic equation with variable coefficients. For this purpose, a Fourier transform is used in combination with a special representation of the transform in image space.

Various versions of closed solutions are formulated with the help of introduced arbitrary functions. The solutions obtained in the work are absent in the known reference manuals on differential equations, and the results obtained for continuously-heterogeneous anisotropic media with cylindrical or spherical symmetry at certain ratios of elastic constants of the material complement the well-known studies of wave processes in similar media [4,5] .

In this work the procedure of building the general solution of hyperbolic equations of general form is presented, which is very effective, along with the methods of transformation of equations which use the group analysis [1,2] and methods of factorization [3].

1. Construction of closed solutions

Let us consider the following differential equation in the area $\Omega : \{ t > 0, 1 < r < a \}$:

$$\frac{\partial^2 U(r,t)}{\partial r^2} - \frac{\partial^2 U(r,t)}{\partial t^2} + A(r)\frac{\partial U(r,t)}{\partial r} + B(r)U(r,t) = 0, \qquad (1)$$

where $A(r), B(r) \in C_{[1,a]}$.

We assume that function $U(r,t)$ satisfies Dirichlet conditions, therefore it can be represented by a Fourier integral, recorded as formulas:

227

$$\tilde{U}(r,p) = \frac{1}{\sqrt{2\pi}} \int\limits_{0}^{+\infty} U(r,t)e^{-ipt} dt; \tag{2}$$

$$U(r,p) = \frac{1}{\sqrt{2\pi}} \int\limits_{0}^{+\infty} \tilde{U}(r,t)e^{ipt} dp. \tag{3}$$

We apply transformation (2) to (1), assuming that $U(r,0) = \dfrac{\partial U(r,0)}{\partial t} = 0$. Then in the space of images we obtain the following equation:

$$\frac{\partial^2 \tilde{U}(r,p)}{\partial r^2} + A(r)\frac{\partial \tilde{U}(r,p)}{\partial r} + [B(r) + p^2]\tilde{U}(r,p) = 0. \tag{4}$$

The solution of the equation is represented in the form:
$$U(r,p) = \varphi(r) \cdot G(s), \; s = p\psi(r), \tag{5}$$

where $\varphi(r), \psi(r) \, u \, G(s)$ are twice continuously-differentiable functions of their arguments. As a result of setting (5) in (4), we obtain the differential relation

$$s^2 \left[\frac{d^2 G}{ds^2} + \frac{1}{(\psi')^2} G \right] + s \left[\frac{\psi''\psi}{(\psi')^2} + \frac{2\varphi'\psi}{\varphi\psi'} + \frac{A\psi}{\psi'} \right] \frac{dG}{ds} +$$

$$+ \frac{\psi^2}{\varphi\,(\psi')^2} [\varphi'' + A\varphi' + B\varphi] G = 0, \tag{6}$$

which can be satisfied in various ways. In works [6, 7] we obtained closed solutions of equation (1), containing the wave functions. Let us consider an alternative option of building the general solution of equation (1) that does not contain wave functions, assuming that $\psi'(r) = 1$, i.e.

$$\psi(r) = r. \tag{7}$$

Case1.

Suppose we have the following equations:

$$\frac{\psi''(r) \cdot \varphi(r)}{[\psi'(r)]^2} + 2\frac{\psi(r) \cdot \varphi'(r)}{\varphi(r)\psi'(r)} + \frac{A(r) \cdot \psi(r)}{\psi'(r)} = 0; \tag{8}$$

$$\frac{\psi^2(r)}{\varphi(r)[\psi'(r)]^2} [\varphi''(r) + A(r)\varphi'(r) + B(r)\varphi(r)] = -6; \tag{9}$$

In this case, equation (6) is converted to the following form

$$s^2 \frac{d^2 G(s)}{ds^2} + (s^2 - 6)G(s) = 0.$$

The general solution of the latter equation can be represented as follows [8]:

$$G(s) = C_1(p)\left\{ \frac{3}{s}\cos[s + C_2(p)] + (1 - \frac{3}{s^2})\sin[s + C_2(p)] \right\}. \tag{10}$$

228

Performing convertion equations (5), (10), we find

$$U(r,t) =$$
$$= \frac{\varphi(r)}{\sqrt{2\pi}} \int\limits_{0}^{+\infty} C_1(p) \left\{ \frac{3}{s} \cos[s + C_2(p)] + (1 - \frac{3}{s^2}) \sin[s + C_2(p)] \right\} e^{ipt} dp. \tag{11}$$

From (8) correlation we find

$$\varphi(r) = \exp[-\frac{1}{2} \int A(r)dr]. \tag{12}$$

Finally, from equation (9) we obtain

$$B(r) = \frac{1}{4} \left[2A'(r) + A^2(r) - \frac{24}{r^2} \right]. \tag{13}$$

Theorem I.

If the coefficients of equation (1) satisfy correlation (13), then expressions (11) and (12) are its general solution.

Case 2.

Suppose that condition (7) is met and following correlations are valid:

$$\frac{\psi''(r) \cdot \psi(r)}{[\psi'(r)]^2} + \frac{A(r) \cdot \psi(r)}{\psi'(r)} + 2 \frac{\psi(r) \cdot \varphi'(r)}{\varphi(r)\psi'(r)} = 1; \tag{14}$$

$$\frac{\psi^2(r)}{\varphi(r)[\psi'(r)]^2} \left[\varphi''(r) + A(r)\varphi'(r) + B(r)\varphi(r) \right] = -\nu^2; \tag{15}$$

where $\nu \in R$.

Then (6) is transformed into Bessel equation, i.e.

$$s^2 \frac{d^2 G(s)}{ds^2} + s \frac{dG(s)}{ds} + (s^2 - \nu^2)G(s) = 0.$$

Its solution is written as

$$G(s) = C_1(p)I_\nu(s) + C_2(p)Y_\nu(s). \tag{16}$$

Here $I_\nu(s), Y_\nu(s)$ - Bessel function of $"\nu"$ order of I and II kind.

Performing conversion of expression (5), taking into account (16), we determine $U(r,t)$.

We have

$$U(r,t) = \frac{\varphi(r)}{\sqrt{2\pi}} \int\limits_{0}^{+\infty} \left[C_1(p)I_\nu(s) + C_2(p)Y_\nu(s) \right] e^{ipt} dp. \tag{17}$$

Taking into consideration (7), from (14) we find function

$$\varphi(r) = r^{1/2} \exp[-\frac{1}{2} \int A(r)dr]. \tag{18}$$

Further, from (15) it follows that

$$B(r) = \frac{1}{4}\left[2A'(r) + A^2(r) + \frac{1-4\nu^2}{r^2}\right]. \tag{19}$$

Theorem II.

When condition (19) is met, expression (17) is a closed solution of equation (1).

2. Problem statement

The differential equation of motion of continuously-heterogeneous anisotropic elastic medium in the case of its axis-symmetric deformation, as well as the equations of state, connecting components of the stress tensor and the displacement vector, are recorded as follows [9].

$$\frac{\partial \sigma_{rr}^*}{\partial r^*} + \frac{n(\sigma_{rr}^* - \sigma_{\theta\theta}^*)}{r^*} - \rho_* \frac{\partial^2 U^*}{\partial t_*^2} = 0,$$

$$\sigma_{rr}^* = c_{11}^* \frac{\partial U^*}{\partial r^*} + n c_{12}^* \frac{U^*}{r^*}, \tag{20}$$

$$\sigma_{\theta\theta}^* = \sigma_{yy}^* = c_{12}^* \frac{\partial U^*}{\partial r^*} + \left[c_{22}^* + (n-1)c_{23}^*\right]\frac{U^*}{r^*}. \tag{21}$$

Here $\sigma_{rr}^*(r^*,t^*), \sigma_{yy}^*(r^*,t^*), \sigma_{\theta\theta}^*(r^*,t^*)$ are the relevant components of the normal stresses;

$U^*(r^*,t^*)$ are the radial component of the displacement vector;

$c_{ik}^*(r^*), \rho_*(r^*)$ are respectively elastic characteristics and density of heterogeneous anisotropic medium;

r^*, t^* are radial coordinate and time; $n = 1,2$ is value, corresponding to the cylindrical and spherical cavities.

After substitution of correlations (21) into (20) and introducing the dimensionless quantities by formulas

$$c_{ik} = \frac{c_{ik}^*}{a_{33}^*}, r = \frac{r^*}{a}, U = \frac{U^*}{a}, \rho = \frac{\rho^*}{\rho_0}, t = \frac{1}{a}\sqrt{\frac{a_{33}^*}{\rho_0}}t^*,$$

$$\sigma_{rr} = \frac{\sigma_{rr}^*}{a_{33}^*}, \sigma_{\theta\theta} = \frac{\sigma_{\theta\theta}^*}{a_{33}^*}, \sigma_{yy} = \frac{\sigma_{yy}^*}{a_{33}^*}.$$

Here a is the cavity radius; a_{33}^*, ρ^* are corresponding stiffness coefficients of density of homogeneous anisotropic medium. Equation (20) and correlation (21) in area $\Omega : \{t > 0, 1 < r < a\}$ are defined by the system of equations

230

$$\frac{\partial^2 U(r,t)}{\partial r^2} + A(r)\frac{\partial U(r,t)}{\partial r} +$$

$$+ B(r)U(r,t) - C(r)\frac{\partial^2 U(r,t)}{\partial t^2} = 0, \tag{22}$$

$$\sigma_{rr}(r,t) = c_{11}(r)\frac{\partial U(r,t)}{\partial r} + nc_{12}(r)\frac{U(r,t)}{r} = 0, \tag{23}$$

$$\sigma_{yy}(r,t) = \sigma_{\theta\theta}(r,t) = c_{12}(r)\frac{\partial U(r,t)}{\partial r} + \left[c_{22}(r) + (n-1)c_{23}(r)\right]\frac{U(r,t)}{r},$$

where

$$A(r) = \frac{1}{c_{11}}\left[\frac{dc_{11}(r)}{dr} + \frac{c_{11}(r)}{r}n\right] = \frac{d}{dr}\left[\ln(c_{11}r^n)\right], \tag{24}$$

$$B(r) = \frac{n}{c_{11}(r)r^2}\left[(n-1)(c_{12}(r) - c_{23}(r)) - c_{22}(r) + r\frac{dc_{12}(r)}{dr}\right],$$

$$C(r) = \frac{\rho(r)}{c_{11}(r)}.$$

If at t=0, the elastic medium is at standstill, then

$$U(r,0) = \frac{\partial U(r,0)}{\partial t} = 0, \ 1 \le r < \infty. \tag{25}$$

Note. Suppose $C(r) = \frac{\rho(r)}{c_{11}(r)} = 1$. This corresponds to a constant speed of propagation of elastic waves in anisotropic heterogeneous medium. Consequently, the differential equation (22) of hyperbolic type models wave processes propagating at finite speed.

Case 1[*].

From comparing the respective equations (24) and (13), it follows: Theorem III.

Expression (11) defines dynamic displacements, and by formulas (23) and heterogeneous anisotropic medium stress, if its elastic characteristics $c_{ik}(r)$ satisfy the functional equation

$$2\frac{d^2}{dr^2}\left[\ln(c_{11}r^n)\right] + \left\{\frac{d}{dr}\left[\ln(c_{11}r^n)\right]\right\}^2 - \frac{24}{r^2} =$$

$$= \frac{4n}{c_{11}r^2}\left[(n-1)(c_{12} - c_{23}) - c_{22} + r\frac{dc_{12}}{dr}\right]. \tag{26}$$

Let us consider as an example a heterogeneous anisotropic medium, the elastic characteristics of which are periodic functions of the radial coordinate, i.e.,

231

$$c_{11}(r) = a_{11} \sin mr, c_{12}(r) = a_{12} \sin mr,$$

$$c_{23}(r) = a_{23} \sin mr, c_{22}(r) = a_{22} r^2 (\sin mr + \frac{1}{\sin mr}). \tag{27}$$

After substitution of equations (27) in the criterion formula (26) and simple algebraic transformations, we obtain relations connecting the elastic constants of the material

$$a_{12} = \frac{a_{11}}{2}, a_{22} = \frac{m^2}{4n} a_{11}, a_{23} = \frac{n^2 + 24}{4n(n-1)} a_{11}. \tag{28}$$

Thus, in the case of a sinusoidal law of heterogeneity of elastic and inertial characteristics of the anisotropic material (27), solution (11) is valid only for a spherical cavity (n=2). At that the elastic constant is chosen arbitrarily.

Case 2^*.

Comparing the respective equations (24) and (19), it follows:
Theorem IV.

In order for expression (17) to represent a closed solution of the considered dynamic problem for an anisotropic heterogeneous medium, it is enough to meet the functional relation, connecting characteristics $c_{ik}(r)$

$$2 \frac{d^2}{dr^2} \left[\ln(c_{11} r^n) \right] + \left\{ \frac{d}{dr} \left[\ln(c_{11} r^n) \right] \right\}^2 + \frac{1 - 4v^2}{r^2} =$$

$$= \frac{4n}{c_{11} r^2} \left[(n-1)(c_{12} - c_{23}) - c_{22} + r \frac{dc_{12}}{dr} \right]. \tag{29}$$

Suppose that characteristics of material $c_{ik}(r)$ are changed by the power law

$$c_{11}(r) = a_{11} r^m, c_{12}(r) = a_{12} r^m, c_{23}(r) = a_{23} r^m, c_{22}(r) = a_{22} r^m. \tag{30}$$

Here m is an index of anisotropic medium heterogeneity;
$a_{ij}; i, j = 1,2,3$ are dimensionless constants of anisotropic material.

Then relation (29) takes the form

$$v^2 a_{11} = n \left[(n-1) a_{23} + a_{22} \right] - \left[n(n-1) + m \right] a_{12}. \tag{31}$$

From (31) it follows that three of the four parameters a_{ik} can be selected arbitrarily. If the elastic characteristics of the material change by the cosine law,

$$c_{11}(r) = a_{11} \cos mr, c_{12}(r) = a_{12} \cos mr,$$

$$c_{23}(r) = a_{23} \cos mr, c_{22}(r) = a_{22} r^2 (\cos mr + \frac{1}{\cos mr}), \tag{32}$$

the elastic constants a_{ik} of the material satisfy relations

$$a_{12} = \frac{a_{11}}{2}, a_{22} = \frac{m^2}{4n} a_{11}, a_{23} = \frac{1}{4} \left[1 - \frac{1 - 4v^2}{n(n-1)} \right] a_{11}.$$

232

Thus, in this case, only one elastic constant of the anisotropic material is arbitrary.

References
1. **Zaytsev VF, Polyanin AD.** Handbook on nonlinear differential equations. Moscow: Nauka, 1993; 462 p. [in Russian]
2. **Zaytsev VF.** Discrete-group analysis of ordinary differential equations. Differential equations, 1989; 25(3): 379-387. [in Russian]
3. **Berkovich LM.** Factorization and transformations of ordinary differential equations. Edited by N.K. Rozova. Saratov: Publishing House of Saratov University, 1989; 192 p. [in Russian]
4. **Petrashen GI.** Wave propagation in anisotropic elastic media. Leningrad: Nauka, 1980; 280 p. [in Russian]
5. **Green W.** Wave propagation in strongly anisotropic elastic materials. Arch.Mech.Stosow, 1978; 30(3): 297-307.
6. **Senitskiy AY.** On the integrability of the wave equation with variable coefficients. Proceedings of the higher educational institutions. Mathematics, 1998; 7: 39-46.
7. **Evdokimova NN, Senitskiy AY, Kharkovskiy SI.** The study of wave propagation in infinite anisotropic media. Int. scientific conference "Modern problems of mathematics, mechanics, computer science." Proceedings of the conference. Tula: TSU, 2007; 145-147.
8. **Kamke E.** Handbook on ordinary differential equations. Moscow: Nauka, 1965; 703 p. [in Russian]
9. **Lyav A.** Mathematical theory of elasticity. Moscow: ONTY, 1935; 674 p. [in Russian]

An adaptive mesh refinement in the finite volume method

Avdeev E.V., Fursov V.A.,

Samara State Aerospace University

Ovchinnikov V.A.

Laduga Automotive Engineering Ltd.

Abstract. In this paper we describe the method of adaptive mesh refinement, based on the estimation of eigenvalues of discretization matrix. This estimation based on Gershgorin Circle Theorem. This method can be used for unstructured meshes in two-dimensional problems as well as and in three-dimensional. The implementation of the grid adaptation algorithm was made within OpenFOAM open source library of continuum mechanics. This library consists of a set of modules for computational needs, modules written in C++. We give two numerical examples, which show the effectiveness of the proposed method of mesh adaptation.

1. Introduction

Finite volume method (FVM) is a mesh method based on differential equations approximation or on integral equations, which correspond to balance relations. An important property of finite-volume methods is that the balance principles, which are the basis for the mathematical modelling of continuum mechanical problems, per definition, also are fulfilled for the discrete equations conservativity [1].

In the FVM the computational domain is divided into a number of control volumes.

The values are calculated at cell centers. The values of fluxes on the cell interfaces are determined through interpolation of values at the cell centers. As a result we obtain the system of algebraic equations [2].

As in the finite element method, in finite volume method a mesh is constructed, which consists in a partition of the domain where the space variable lives. The elements of the mesh are called control volumes. The most compelling feature of the FVM is that the resulting solution satisfies the conservation of quantities such as mass, momentum, energy, and species. This is exactly satisfied for any control

234

volume as well as for the whole computational domain and for any number of control volumes.

One of the advantages of the finite volume method over finite difference methods is that it does not require a structured mesh. Finite volume methods are especially powerful on coarse nonuniform grids and in calculations where the mesh moves to track interfaces or shocks.

In general case it is impossible to know a priori how to design an optimal mesh, i.e. mesh with minimal number of cells still satisfying the defined tolerance of the computational error. For transient problems, where the flux is unsteady and the points of interest can reposition during the simulation, uniform mesh becomes ineffective and would need to be very fine to satisfy the error tolerance throughout the whole simulation. To solve this problem a scheme where the mesh self-adapts its structure upon some criteria can be used.

The refinement based commonly on the physical quantity gradient field (see [3] and [4]). Our algorithm based on discretization matrix eigenvalues estimation, which mark cells to be refined or likewise mark cells to be unrefined. This approach has a more effective use of cells and thereby lower computational cost.

2. Problem Formulation

Suppose that after equations have been discretized by FVM we obtain the system of algebraic equations, which can be written in matrix form as

$$Ax = b \tag{1}$$

where A − square $n \times n$ discretization matrix, $x - n \times 1$ column vector of unknown variable, $b - n \times 1$ right-hand column vector. The problem consists in finding vector x whose elements are the values of physical quantity in the cell centers.

It is known that the accuracy of the solution of the problem is largely connected with conditionality of the matrix A. Perform the following transformation with the expression (1).

$$0 = -Ax + b$$

$$x = (I - A)x + b , \tag{2}$$

Where I – is the identity matrix. Then rewrite the expression (2) taking into account that we use iterative method for solving, i.e.

$$x_{k+1} = (I - A)x_k + b \tag{3}$$

Note that error of the k-th and (k+1)-th iteration respectively can be written as follows:

$$e_k = x - x_k , \; e_{k+1} = x - x_{k+1} . \tag{4}$$

235

Subtract (3) from (2)

$$x - x_{k+1} = (I - A)(x - x_k)$$

or using (4)

$$e_{k+1} = (I - A)e_k$$

$$e_{k+1} = Me_k \tag{5}$$

Expression (5) shows that for the sequence error reduction at each iteration, it is necessary that for all eigenvalues of the matrix performs:

$$|\lambda(M)| < 1$$

Thus we see that the eigenvalues of the matrix $M = I - A$ depend on the matrix A elements and play an important role in achieving the required accuracy. In particular, they show whether the problem under these conditions converge, converge to the correct solution and how fast.

On other hand, it is known that the elements of matrix A and the right-hand side b are functions of the mesh spacing. Consequently, there is a relation between conditionality and mesh discretization step. Identification of this relations using approximated equations is not easy task. Moreover, in closed source software, this details are hidden. Therefore we construct procedures of direct analysis of matrix M to identify the relations of conditionality and solution accuracy with mesh and adaptive mesh refinement.

3. Adaptive mesh refinement algorithm

It is known that the solution of eigenvalues problem is significant and has high computational cost. Moreover, if the case is ill-conditioned, then small eigenvalues can be calculated with low accuracy. Therefore, we have sufficient interest to use simple estimates of eigenvalues, estimates which calculated by the matrix elements insensitive to its conditioning.

Gershgorin circles method [4] is a well-known method for the localization of eigenvalues. According to Gershgorin's Theorem every eigenvalues satisfies:

$$|\lambda - M_{ii}| \le \sum_{i \ne j} |M_{ij}| \tag{6}$$

where $i \in \{1, 2, ..., n\}$.

Let $d_i = \sum_{j \ne i} |M_{ij}|$. Then the set

$D_i = \{z \in \mathbb{C} : |z - M_{ii}| \le d_i\}$ is called the ith Gershgorin disc of the matrix M. This disc is the interior plus the boundary of a circle. The circle has a radius d_i and is centered at (the real part of M_{ii}, the imaginary part of M_{ii}).

Calculating of estimates of the eigenvalues based on equation (6) is the computationally simple task. However, sufficiently strong upper and lower estimations are possible only for diagonally dominant matrices:

$$\left| \mathrm{M}_{ii} \right| > \sum_{i \neq j} \left| \mathrm{M}_{ij} \right|.$$

If the matrix is not diagonally dominant, then lower and upper estimations of eigenvalues are undefined.

We offer to predict conditionality and mesh quality associated with conditionality through the right boundary of the Gershgorin circle:

$$\mathrm{F}_i = \left| m_{ii} \right| + \sum_{i \neq j} \left| m_{ij} \right|. \tag{7}$$

This boundary can be easily calculated. The maximum value, which calculated among the boundaries for all Gershgorin circles, defines an upper bound for the maximum eigenvalue of the matrix. Because of change of mesh all eigenvalues "shift" together with appropriate Gershgorin circles. There is reason that changes in the mesh, which lead to increase F_i in (7), may lead to increase small eigenvalues.

Based on these assumption we have the mesh adaptation algorithm, which based on the analysis of scalar field F_i $i \in \{1, 2, ..., n\}$, which formed by calculating the values of (7) for all mesh nodes. Then mesh adaptation was made based on this scalar field. The normalization of field F is performed before each iteration:

$$\mathrm{F}_i{}_{normalised} = \frac{\mathrm{F}_i}{\max(\mathrm{F}_i)} \tag{8}$$

Thus the values of the field F are within the semi-interval (0;1] and it let us to set in OpenFOAM to refine mesh for cells with F_i close to 1 and unrefined cells with F_i around 0. Values of field F decrease while refining mesh and increase while coursing mesh.

4. Computational examples and analysis

In order to illustrate feasibility and effectiveness of the algorithm, we use following two examples [5]. Both examples use modified laplacianFoam OpenFOAM solver called laplacianFoamF. New solver has ability to work with dynamic mesh, which allows to adapt mesh.

We compare AMR based on temperature scalar field T, i.e. based on temperature gradient minimization (AMR T) and AMR based on described above scalar field F (8) – (AMR F). For every example we tried to get about the same amount of cells.

Initial geometry of first example, as shown on Fig.1, thin square plate. The length along the x-axis and z-axis is 100 meters, along y-axis is 1 meter.
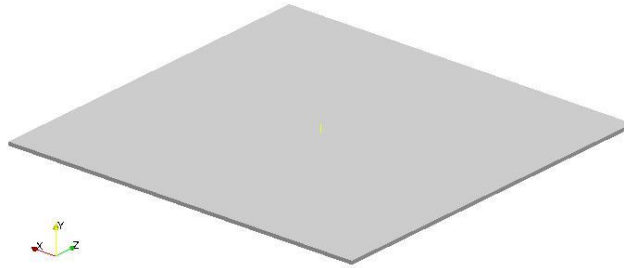
Fig. 1. – Geometry of first example case

Boundary conditions: on the surface *xy*, *z*=0: temperature *T* = 1°C; on other 5 surfaces: *grad(T)* = 10. These boundary conditions were chosen for ease of estimation error of the final result. In this case, the temperature decreases linearly from the heated surface.

We want to find out temperature distribution. The heat transfer expressed by Laplace equation:

$$\frac{\partial T}{\partial t} - \alpha \nabla^2 T = 0 \,, \tag{9}$$

where for the mathematical treatment is sufficient to consider the case $\alpha = 1$.

For comparison, residual plots for both AMR are given (see Fig.2). As you can see from Fig.2, in case with AMR *F* adaptation the residual converges little faster than that of the AMR *T* case.

In second example we show the work of the AMR F on a more complex geometry. Geometry and boundary conditions are showed on Fig.3.

As shown in Fig.3 one surface of flange has temperature $T_1 = 573°C$ and second has temperature $T_2 = 273°C$. On all other surfaces the temperature gradient is set to 0, that walls do not conduct heat (adiabatic walls).

During testing, we found that AMR based on scalar field F detects too large cells, but does not take into account the boundary conditions (see Fig. 4). This occurs due to the fact that the boundary conditions are contained in right-hand column vector *b* of Eq.1, but almost no effect on discretization matrix M.

AMR based on temperature gradient field *T* vice versa takes into account the boundary conditions, but skips "bad" cells.

Therefore for comparison was made third "hybrid" variant, which include first five iterations of AMR *F* and after that it continues with AMR *T*. For comparison, residual plots of three cases are given (see Fig. 6).

As can be seen from the figure, AMR *FT* has the best residual, AMR *F* and AMR *T* slightly worse.
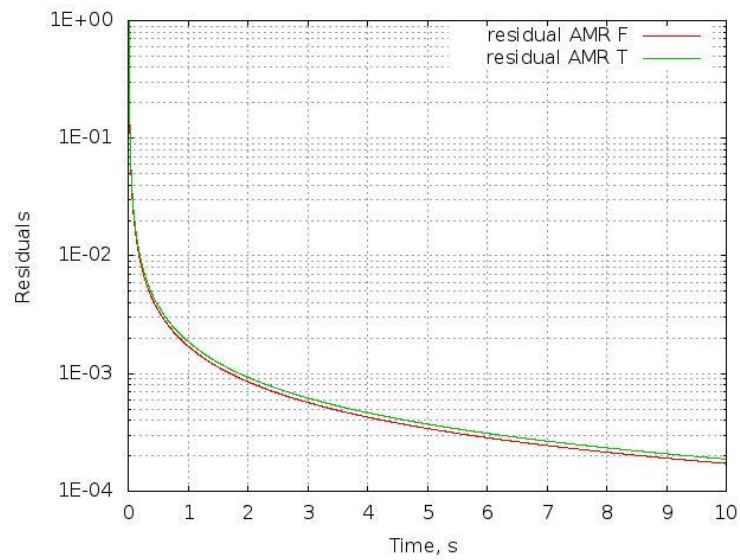
Fig. 2. – First example, AMR *F* and AMR *T* residuals
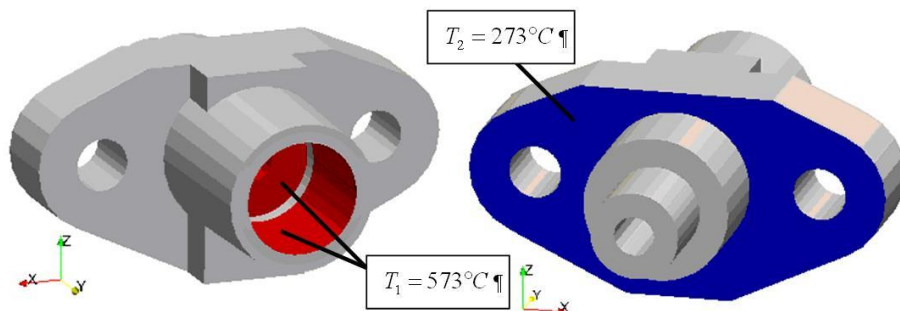
Fig. 3. – Second example, geometry and boundary conditions
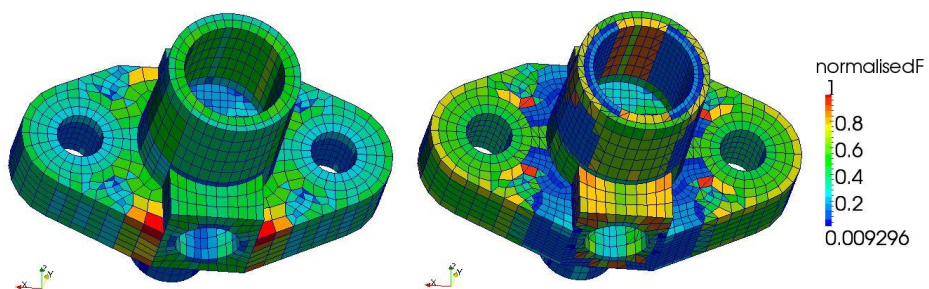
Fig. 4. – AMR *F* detects and refines too large cells
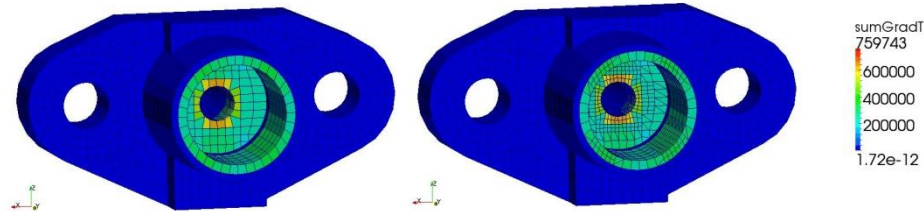
Fig. 5. – AMR *T* takes into account the boundary conditions
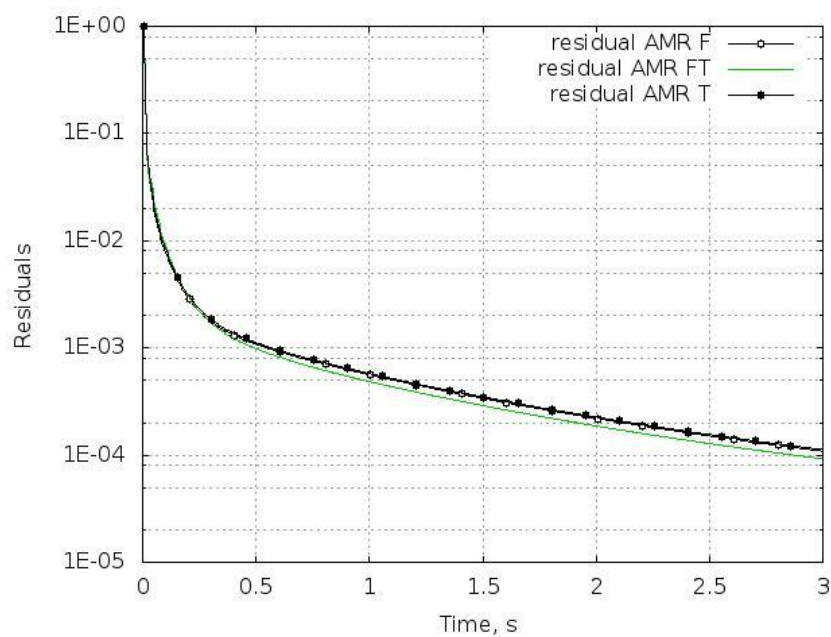
Fig. 6. – Comparison of AMR *F*, AMR *T* and AMR *FT*

5. Conclusion

In the proposed method mesh refinement based on discretization matrix conditioning. As can be seen from above two examples – the method does not provide a significant performance increase compared to AMR, based on temperature gradient minimization, but use AMR *T* not always convenient or possible. Such situations are possible in complex problems with dynamic geometry, multiphase flows, etc. Our proposed method allows to choose more suitable AMR settings than in case of AMR *T*.

Acknowledgements

References

1. **Versteeg HK, Malalasekera W.** An introduction to computational fluid dynamics. 2ed., Pearson Ed., 2007; 517 p.
2. **Joubarne E, Guibault F, Braun O, Avellan F.** Numerical capture of wind tip vortex improved by mesh adaptation. International Journal for Numerical Methods in Fluids, 2011; 67(1): 8-32.
3. **Escobar JA, Ramirez S, Jimenez RA, Giraldo AM, Silva C, Lopez OD, Ochoa N, Mahecha J, Leguizamon S.** Numerical simulation of NASA wing-trap model as a Colombian Contribution to the High-Lift Prediction workshop. 30th AIAA Applied Aerodynamics Conference Special Session: CFD High Lift Prediction Workshop Follow-on II, 2012.
4. **Brakken-Thal P.** Gershgorin's Theorem for Estimating Eigenvalues. Source: <http://buzzard.ups.edu/courses/2007spring/projects/brakkenthal-paper.pdf>.
5. Source: <https://github.com/j-avdeev/laplacianFoamF>.

Application of fast discrete wavelet transformation on the basis of spline wavelet for loosening correlation of sequence of data in mass service theory

Blatov I.A., Gerasimova U.A., Kartashevskiy I.V.

Povolzhskiy State University of Telecommunications and Informatics, Samara

Abstract. The task of loosening of correlation of sequence of strongly correlated random variables within the mass service theory is set. The algorithm of application of spline wavelet for loosening of correlation of sequence of strongly correlated random variables is described. Properties of the matrixes received as a result of application of transformation algorithm are studied. Results of numerical experiment studies are given.

Keywords: spline wavelets, decorrelation, fast discrete wavelet transformation

1. Introduction

Strong correlation of sequence of random variables can create considerable problems in the solution of mass service theory. Let $X = (x_0, \dots, x_n)^T$ be some vector with known correlation matrix A. It is required to analyze the traffic characterized by vector X taking into account it correlation properties.

The traffic as random process is known to have self-similar properties, which indirect sign is the existence of heavy residuals, i.e. big redundancy of the appropriate integral functions of distribution. Therefore in such situation the method of preliminary execution of some orthogonal transformation determined by matrix $T = (t_{ij})$, which purpose is elimination or lowering of correlation of basic data is often used. The application of up-to-date analysis from the mass service theory concerning vector $\tilde{X} = TX$, but not vector X, will proves to be more effective.

It is possible to eliminate correlation and to receive the best result by means of application of Karhunen-Loeva transformation. However creation of such basis is a very resource-capacious task. In this case matrix T consist of eigenvectors of matrix A. The resultant correlation matrix will be of a diagonal type. However this method has some drawbacks such as: absence of fast algorithms of computation; dependence

on the structure of matrix A. Therefore the task pf creation of more available bases in which the correlation can be, if not eliminated, but weakened essentially, is actual. In this report the spline wavelet is used.

1.1. Elaboration of the system of semiorthogonal spline wavelets

Let $[a, b]$ be a random interval, $m \geq 1$ be integer, n_0 be such an integer that $2^{n_0} < 2m + 1 < 2^{n_0+1}$ and k be such an integer that $2^k > 2m - 1$. Let us consider the family $\Delta = \{\Delta_n, n = n_0, n_0 + 1, \dots\}$ of partitions of the interval $[a, b]$ with the constant step $h = h_n = (b - a)/2^n$. Let us define $S(\Delta_n, m, k)$ as the combination of spline wavelets, where m is a power and k is a degree. On each partition, we consider a space of splines $L_n = S(\Delta_n, m - 1, 1)$. Then, for each $k \geq n_0$, space $S(\Delta_n, m - 1, 1)$ can be represented as direct sum $L_k = L_{n_0} \oplus W_{n_0+1} \oplus W_{n_0+2} \oplus \dots \oplus W_k$, where W_k denotes the orthogonal complement of L_{k-1} up to L_k space. The desired wavelet basis is the result of combination of the basis in L_{n_0} and all the bases in spaces $W_n, n_0 \leq n \leq k$.

Let $i \geq 0$ be a such a fixed integer that the interval $[x_i^{n-1}, x_{i+2m-1}^{n-1}]$ lies within $[a, b]$. Function is computes according to formula

$$\psi_{i,n}(x) = \sum_{j=2i}^{2i+3m-2} \alpha_j \phi_{j,n-1} \tag{1}$$

where $\phi_{j,n-1}$ normalized B-spline. The α_j -coefficients are defined according to $\left(\psi_{i,n}(x), \phi_{k,n-1}\right) = 0, k = i - m + 1, i - m + 2, \dots, i + 2m - 2$.

The combination of elaborated wavelet functions is resulted by shifting of the only function according to formula $\psi_{i,n}(x) = \psi_{0,n}(2^{n-n_0}x - i(b - a)/2^{n_0-1})$.
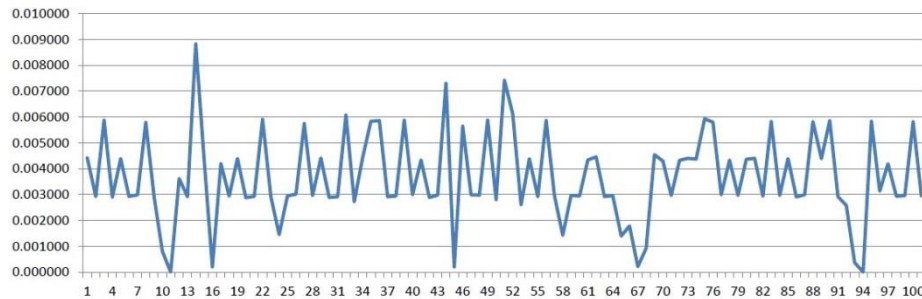
Fig. 1. – Sequence of experiment's data X

1.2. Fast discrete wavelet transformation in the space of spline wavelets on the finite interval

The direct transformation consist in the search of wavelet coefficients d_{0j} and c_{ij}.

$$\left\{d_{0j}, -m + 1 \leq j \leq 2^{n_0-1}\right\} \cup \bigcup_{i=1}^{k-n_0}\left\{c_{ij}, -m + 1 \leq j \leq 2^{n_0+i-1} - m\right\} \tag{2}$$

According to known function $f = \{f_{ij}\}, 0 \leq i \leq 2^k - 1, 1 \leq j \leq s$.

The inverse transformation consist in reconstruction of all values of function $f_{ij}, 0 \leq i \leq 2^k - 1, 1 \leq j \leq s$ by $\{f_{ij}\} \in \tilde{S}(\Delta_k, m - 1, 1)$ according to the known set of wavelet coefficients

$$f = \sum_{j=-m+1}^{2^{n_0}-1} d_{0j} \phi_{j,n_0} + \sum_{i=1}^{k-n_0} \sum_{j=-m+1}^{2^{n_0+i-1}-m} c_{ij} \psi_{j,n_0+1} \tag{3}$$

For more details on the a.m. items please consult [1].

2. Numerical experiment

We made an experiment on loosening of correlation of data represented by sequence Y consisting of 9999 random values, each represents the time of traffic processing in the system[1].

To the initial experiments data X we applied direct fast discrete transformation on the basis of the linear spline.

Fig. 2. – Sequence of data $\tilde{X}$(after direct transformation)

The correlation coefficients were calculated on the basis of the experimental data X (for more details see [3]):

$$R_k = \frac{V_k}{D} \tag{4}$$

where

$$V_k = \frac{1}{n-k} \sum_{i=1}^{n-k} (Y_k - X)(Y_{i+k} - X) \tag{5}$$

$$D = \frac{1}{n} \sum_{i=1}^{n} (Y_i - X)^2 \tag{6}$$

$$X = \frac{1}{n} \sum_{i=1}^{n} Y_i \tag{7}$$

---

[1] Problem definition about decorrelations and data for experiment were provided I.V. Kartashevsky
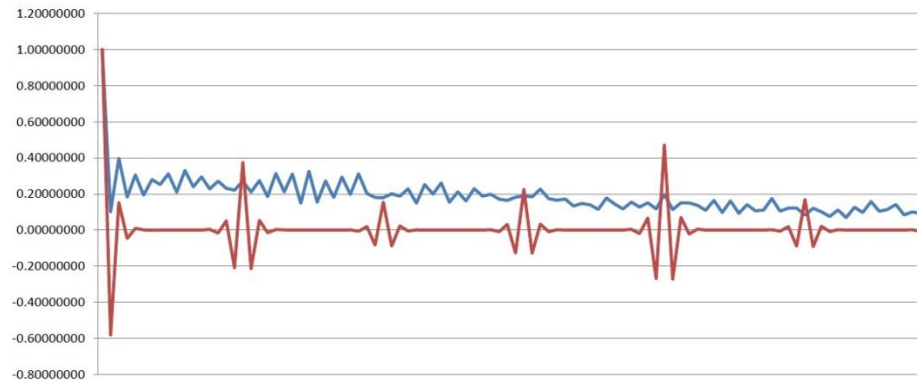
Fig. 3. – Correlation coefficients for experiment data and for transformed data

The sums of modules of correlation coefficients are calculated:

$$R_k : \sum_{i=0}^{k-1} |r_i| = 18.963$$

$$\tilde{R}_k : \sum_{i=0}^{k-1} |\tilde{r_i}| = 5.344$$

The correlation is seen to have reduced by more than by 3.5 times. The similar result was received for square and cubic splines.

3. Summary

In the conclusion we would like to stress that the application of fast discrete algorithm of wavelet transformation in the space of spline wavelet allows loosening the correlation of sequence of strongly correlated random variables. That is confirmed by the data obtained in the numerical experiments.

References

1. **Blatov IA, Rogova NV.** Fast wavelet-transform in the space of discrete polynomial semiorthogonal splines. Computational Mathematical and Mathematical Physics, 2013; 53(5): 727-736.
2. **Kartashevsky IV.** Application Lindley equation for correlation traffic processing. Journal Electrosvyaz, 2014; 12: 41-42.
3. **Kartashevsky IV.** Calculation of correlation coefficients of times intervals in sequence of events. Journal Electrosvyaz, 2012; 10: 37-39.
4. **Umnyashkin SV, Kochetkov ME.** Analysis of efficiency of using orthogonal transform for digital coding of correlation data. Electronic, 1998; 6:79-84.
5. **Myasnikov VV.** Effective algorithm of calculation of local discrete wavelet-transformation. Computer Optics, 2007; 31(4): 86-94. [in Russian]

Mathematical Modeling

Structure and algorithms of motion control system's software of the small spacecraft

Filatov A.V.,

Progress Space Rocket Centre, Samara

Tkachenko I.S., Tyugashev A.A., Sopchenko E.V.

Samara State Aerospace University

Abstract. The paper is devoted to some features and algorithms of AIST-2D experimental technological small spacecraft's Motion Control System Software. Special Flight Control Software is embedded in Motion Control System. There are several modes of software functioning depending on state of the spacecraft. There are descriptions of the basic software algorithms in the paper.

Keywords: Motion Control System, Flight Control Software, Real-Time Control Algorithm, Program Turn

1. Introduction

Software is a very important part of every modern space project. The errors and glitches of Flight Control Software could lead to critical consequences including losses of expensive spacecrafts. Onboard computational opportunities are the basis for successful execution of widespread spectrum of tasks in long space flights [1]. This issue is important even for micro- and nano- satellites which represent the very fast growing segment of the spacecrafts.

The Motion Control System (MCS) of the AIST-2D small spacecraft includes both hardware (sensors, devices and aggregates) and software [2].

The MCS should perform the following:

— quieting of the spacecraft after separation from the launch vehicle;
— orientation of the spacecraft with a given accuracy in the Orbital Coordinate System;
— orientation of the solar panels' surfaces towards the Sun with a given accuracy;
— self-diagnostic information's forming and transmission to Earth;

— form and send information about the spacecraft angular position to the Onboard Control System (OCS) upon request;
— support the mode without control pulses.

After the separation from the launch vehicle's upper stage or after the Undirected Flight Mode (UFM), the Mode of Compensation of the Initial Angular Velocity is being started by activation of Executive and Sensing Elements Complex (ESEC). When the angular velocity reaches the given value, Single-Axis Solar Orientation Mode will start automatically. This mode supported until the moment of request from the Onboard Control System to start Three-Axis Orientation in Orbital Coordinate System Mode. The switching between the MCS modes is possible by transmission of the special command messages. Timing Diagram of the MCS functioning is being presented in Fig. 1.

So, in accordance with its purpose, MCS supports the following set of modes:

— Compensation of the Initial Angular Velocity Mode (MCIAV);
— Single-Axis Solar Orientation Mode (MSASO);
— Three-Axis Orientation in Orbital Coordinate System Mode (MTAORS);
— MCS experiments Mode (MMET).
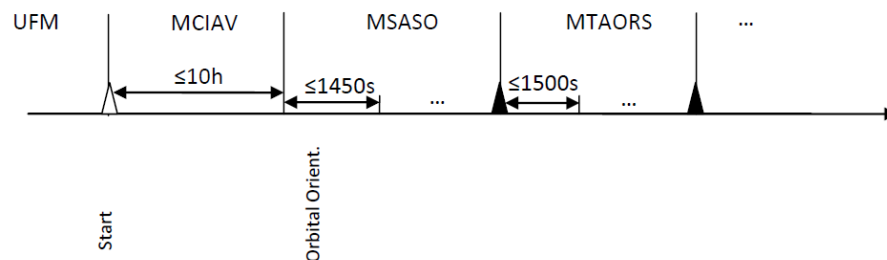
Fig. 1. – Motion Control System Functioning Timing Diagram

2. Modes Description

Compensation of the Initial Angular Velocity Mode starts after its activation and should compensate the angular velocity of the spacecraft. The mentioned angular velocity could be formed after the separation from the upper stage or during the Undirected Flight.

With decreasing kinetic moment of the apparatus to a predetermined value (corresponding to the angular velocity of 0.07 degrees per second), the MCS automatically activates (without control actions from the OCS) stabilization using the Reaction Wheels.

Next, on the time interval of 100 sec, the process of angular velocity damping process is being performed with the use of Reaction Wheels.

MCIAV ends automatically by the transition to Single-Axis Solar Orientation Mode.

Single-Axis Solar Orientation Mode designed to support orientation the surfaces of the solar panels towards the Sun with a given accuracy.

The Mode starts automatically after the end of the MCIAV or by the request from the OCS. The command message from OCS is being transmitted using the special channel of information exchange.

The first operations of the MSASO are activation of the Orbital Solar Sensors (OSS) and checking of the Sun's detection. If the Sun detection process completed successfully by at least the one OSS, the Program Turn into Solar Orientation will be activated.

If the Sun cannot be detected, the spacecraft begins the rotation to find the Sun.

The maximal duration of the Sun Search process depends on angular velocity and guaranteed review of the full sphere by the Sensor's Visual Field. Thus, the maximal duration of the search will not exceed 600 sec (excluding time of shadow).

The velocity of the search is 1 degree per second.

After the Program Turn, the stabilization in Solar Orientation begins. In this case, the combination of the axis of OYSCS with the direction vector to the Sun in Associated Coordinate System should be carried out.

The Mode continues until reception of command message from the OCS to change the MCS mode.

Three-Axis Orientation in Orbital Coordinate System Mode should support Spacecraft's orientation in the Orbital Coordinate System with the given accuracy and support the Program of Angle Motion Control. This Program implements the Time Control Method and starts upon request from OCS.

The Mode starts by the command message from OCS via information exchange channel.

The first actions of the Mode are the following. The Search of Earth (SOE) process starts and it checks if the Earth detected in the spacecraft's field of view. If there is no Earth in the field of view in initial position, the SOE should be executed by the spacecraft's rotation.

The maximal duration of the SOE process depends on angular velocity and guaranteed review of the full sphere by the Sensor's Visual Field. The maximal duration of the search is not exceeds 300 sec. The velocity of the search is 1 degree per second.

After the successful end of Earth's detection process, the pre-defined sequence of algorithm's segments will be implemented. After completion of the mentioned segments, the spacecraft will have the right orientation in Orbital Coordinate System and will be ready for implementation of Program of Angle Motion Control.

This Program can be initiated by the one of the following:

1. Array containing the time of turn's start and the quaternion defines the position of the Solar Coordinate System in the Orbital Coordinate System at the moment of the end of turn;
2. Array of the parameters (A_i, ω_i, φ_i) which define angle position of Solar Coordinate System relatively to Orbital Coordinate System, by the three channels. In this case, Program of Angle Motion Control is being formed by MCS in accordance with the

expression: $\psi_i = A_i \cdot \sin(\omega_i \cdot t + \varphi_i)$, considering correspondingly the angles of roll, yaw, pitch.

3. Array containing the polynomials of approximation – Program of Angle Motion Control for the each channel.

The Mode executes until receiving the command message from the OCS to change the mode of functioning.

MCS experiments Mode should support tests of the MCS equipment and checking of the experimental algorithms of the MCS functioning.

The Mode starts by the command message from the OCS to implement the tests or experiments. Which devices of MCS will be used, depends on the program of experiment.

The Mode is active until the command message from the OCS to change the mode of functioning.

To effective implementation of the all described modes of MCS functioning, the development of the AIST-2D software includes the following steps:

─ Development of the technical overviews of the software algorithms;
─ Programming;
─ Unit testing;
─ Integration testing using the emulator of Earth's Debug Testbed Complex;
─ Complex testing and debugging of the software using the Earth's Debug Testbed Complex.

All algorithms of the MCS's onboard software can be divided into the following categories:

System Algorithms:

─ Planning of the MCS functioning;
─ Collection of telemetry information and its output to OCS;
─ Forming of control information related to angle motion of the spacecraft;

Algorithms of the MCS Modes:

─ Solar System Coordinates Orientation of the spacecraft;
─ Orbital System Coordinates Orientation of the spacecraft;
─ MCS control in case of technical faults;
─ MCS tests and experiments;

Device control algorithms:

─ Fiber-optic gyroscopes control;
─ Reaction Wheels control;
─ Star trackers control;
─ Magnetic Executives control;
─ Magnetometers control ;
─ Optical Solar Sensors control;
─ Earth orientation devices control;

Algorithms of Stabilization:

─ Spacecraft Motion Control by Reaction Wheels;
─ Kinetic Moment Clear;
─ Program Turn;
─ Calculation of Control Parameters;
─ Program of Angle Motion Control Forming;
─ Algorithms of Orientation Detection;
─ Solar Orientation;

Algorithms of Control:

─ Control of Redundancy in case of technical faults;
─ Control of Stabilization using Reaction Wheels;
─ Control of Magnetic System;

Algorithms of Experiments:

─ Orientation Detection using Angle Velocity measurement and data from Star Trackers;
─ Orientation Detection in Inertial Coordinate System using Star Trackers.

3. Conclusion

Thus, algorithms and Flight Control software of AIST-2D small spacecraft's MCS provide:

1. Compensation of the angle velocity after the separation from the upper stage of the launch vehicle (duration of the compensation process not more than 3 hours when angle velocity less than 7 degrees per second and 2 hours 15 minutes when angle velocity less than 3 degrees per second);
2. Orientation in Orbital Coordinate System with the error less than (with probability P = 0,96):
   (a) by the angle position
      (i) not worse than 30 angle minutes (without additional navigation information);
      (ii) not worse than 30 angle minutes in of pitch and roll channels и 10 angle minutes in yaw channel (with usage navigation information);
   (b) by angle velocity - 0,005 degrees per second;
3. One-axis solar panels orientation towards the Sun with the error not exceeds (P = 0,96):
   (a) in angle position – 3 degrees;
   (b) in angle velocity - 0,5 degrees per seconds in all channels;
4. Maximal angle velocities of the spacecraft during Program Turn – 1 degree per second;
5. Maximal angle acceleration during Program Turn - 0,029 degrees per quadrate seconds;
6. Transition from Solar Orientation into Orbital Orientation and in reverse order:

250

(a) 10 minutes (using additional data about center of mass position);
(b) 25 minutes (without navigation information).
7. Reaching of maximal accuracy in Orbital Coordinate System for no more than 35 minutes from the moment of building of Orbital Orientation.

Acknowledgment

References

1. Journal Aircraft Engineering. Vol. 6: The results of science and technology VINITI. Moscow, 1998. [in Russian]
2. **Sevastyanov NN, Branets VN, Panchenko VA, Kazinskiy NV, Kondranin TV, Negodyaev SS.** The analysis of the modern opportunities of small Earth observation satellites' development. Proceedings of MIPT, 2009; 1(3). [in Russian]

Method of UNIT testing for algorithms of computing software modules

Kovartsev A.N., Popova-Kovartseva D.A., Gorshkova E.E.

Samara State Aerospace University

Abstract. The method of automating Unit testing processes for computing software modules is considered in the paper. Modern means of testing automation, which are analyzed in many scientific studies, specialize mainly in testing graphical user interfaces, web-interfaces, network communications, information systems, etc., which is the result of a huge demand in the market for software products within these spheres. Software modules of computing character are overshadowed by such products despite the fact that these modules have considerable scientific and practical value. They deal mostly with high tech spheres: aerospace cluster, energy industry, defense complex, etc. The article presents an original method of Unit testing for computing modules based on the algorithm of global search for infinite discontinuity points of testing function, which allows to find fatal errors in computing software modules, as well as incorrectness in implementation of algorithms for mathematical models. The universal method of Unit testing is offered within the class of computing modules, which helps to minimize the time for program debugging and to find fatal errors with less effort, as well as to organize total module testing for all modules of the program.

Keywords: Unit testing, testing automation, computing software modules, global optimization, fatal errors

Introduction

Developers of modern software (SW) face the challenge to carry out their projects within tight deadlines and with minimal resources consumption [1, 2], whereas software vendors strive to carry out testing appropriately, quickly, and thoroughly. Most types of work, used in software programming, are to be supported by automated means of testing.

Modern means of automated testing are constantly expanding at present and include testing of graphical user interfaces, checking requirement compatibility, download speed, code coverage, web-interface, network communications, information

systems, etc. This results from the huge demand in the market for software products within these spheres. Software modules of computing character are overshadowed by such products despite the fact that these modules have considerable scientific and practical value. They deal mostly with high tech spheres [3]: aerospace cluster, energy industry, defense complex, etc.

Testing is the method of providing the required level of SW quality. In the general sense, software testing is the process that allows to determine the correctness, completeness and quality of the developed software product. Unfortunately, it is impossible to determine unambiguously whether the analyzed program functions correctly or not, as well as to guarantee the absence of defects in a software product because human factor problems may appear at all SW lifecycle stages [4]. Therefore, all existing testing methods operate within private formal methods of testing organized for the analyzed product. The list of modern methods and approaches for solving the problem of program testing is extensive and diverse. On the one hand, this diversity is determined by the current practice of using a computer while solving a variety of problems and, accordingly, by the specific features of software products themselves.

The class of computing software modules (CSM), based on the use of mathematical models, has some specific features. Such programs, carried out on a computer, are sure to calculate any function that realizes the display output of input data. This implies that a computer by means of its resources finishes the definition of a partly determined function, which results in complete definition. Consequently, it is possible to estimate if the results of program execution are right or wrong only by comparing the specification of the expected function with the results of its calculation; this is carried out in the testing process. For the class of computing software modules, methods of Unit testing [20] and test tools based on models using formal methods [4,6] are more suitable.

Formal methods usually allow to solve a limited range of testing software tasks within a particular class, however, they are able to work effectively in industrial projects and require a minimum number of special skills and knowledge so that to be used [4]. Currently, within monitoring the formal properties of SW, methods of test construction are thoroughly developed on the basis of finite-state automation [7, 8]. For them, accuracy characteristics and evaluation of completeness of performed tests are known. In these techniques, computing route is analyzed not only for performing some formulae, but also for coordination with the specified automation model of the proper behavior. Nowadays these methods are rarely used, mainly for monitoring small critical applications [4]. Formal methods are rather "heavy-weight", they require well-qualified specialists, at least at the stage of software modeling. The weak point of formal methods is the need to construct the model itself on the parallel basis and to check its correctness.

The practice of industrial software production shows that the most effective strategy is to search and correct as many errors as possible at the earliest stage of software development. Methods of Unit testing are appropriate for this purpose. Unit testing consists in checking the software performance on a set of input and corresponding output data. This approach allows to reveal a significant number of errors and locate them quickly as it is easier to find an error within a module than to do it within the whole project. CSM can be easily interpreted with a vector

computable function $Z = f(X) = (f_1(X), f_2(X), \dots, (X))^T$, having a set of input parameters $X = (x_1, x_2, \dots, x_n)^T$ of the module and a set of calculated data $Z = (z_1, z_2, \dots, z_m)^T$.

The origin of errors for CSM is extensive and diverse. Errors occur when initial and boundary conditions, which characterize the value and location of external factors, are set incorrectly. They may be related with a set of limitations and assumptions resulting from the physical nature of the object and limiting the range of input parameters.

Among the errors of this kind for CSM, two most common groups can be distinguished: calculation errors and logical (algorithmic) errors. Calculation errors are mostly connected with incorrect recording or programming of mathematical expressions and manifest themselves as arithmetic error of division by 0, the square root of a negative number, as calculation of rational or transcendental functions, etc. They can only be detected while executing the program and lead to program stoppage.

Logical errors are connected with the distortion of problem solving algorithm and result from incorrect problem setting, wrong consideration of all conditions for solving the problem, incorrect management organization within CSM, and errors in the input of logical expressions. These errors are difficult to correct, corrections often being made with the help of formal methods [5].

Nevertheless, there is a universal method for detecting errors of calculating and partly logical character in computing software modules [3, 9]. This method is based on the fact that all computing modules, implemented as a program, "work" within integrity of used functions or mathematical models. Otherwise, the program can't be used. If we organize the search for infinite discontinuity of the function by some means, we will be able to detect all calculating errors of any origin mentioned above. Relatively "simple" methods of global optimization (GO) of multivariable functions are appropriate for this purpose[10].

In this paper we consider the improved algorithm of global search for points of discontinuity of the second type, intended for detecting error situations in the software modules of computing character. This algorithm is the basis of Unit testing for computing software modules.

1. Problem Statement

Let the area of error search in computing module be a unit cube (in general – hypercube) $\Pi = [0, 1] \times [0, 1] \times [0, 1]$, which is proportionally divided into eight smaller cubes.

Unit testing algorithm of computing modules, formally described by vector function $Z = f(X)$, can be put as the problem of global optimization

$$\max_X f_k^2(X), \quad k = 1, \dots, m, \tag{1}$$

which is aimed at detecting (or ensuring the absence of) discontinuity points of the second type in the examined function. The infinite discontinuity $\pm \infty$ is realized in numbers marked by code NaN on a computer; in fact we can specify the upper limit

of acceptable values $|f_k(X)| \leq M_{sup}^{(k)}$ or each calculating parameter of a module. To simplify the situation, we will further consider scalar function $f(X) = max f_i^2(X)$.

Among the well-known one-parameter methods of multiextremal optimization, R.G. Strongin statistic information method is the most effective [10]. The method is based on the use of approximate posterior probability distribution of global extremum location, which is formed in the process of function testing, which allows to realize a more balanced strategy to search for function global minimum. This strategy is so effective that it is often transferred from one-dimensional case to multivariable function optimization.

It is shown in the paper [10] that function extremum search is realized by maximizing a simple characteristic function:

$$R(i) = \mu(x_i - x_{i-1}) + \frac{(z_i - z_{i-1})^2}{\mu(x_i - x_{i-1})} - 2(z_i + z_{i-1}), \tag{2}$$

where μ – estimation of Lipschitz constant, which is calculated in the process of function extremum search:

$$\mu = \begin{cases} 1 & M = 0, \\ rM & M > 0, \end{cases} \qquad M = \max_i \frac{|z_i - z_{i-1}|}{(x_i - x_{i-1})},$$

where r – parameter.

The condition of Lipschitz for optimized function simplifies greatly the search for function extremum as the limitation of function growth degree allows to find local extremum vicinity quickly. However, while searching for a set of infinite discontinuity, areas of function monotony as well as extremum vicinity are equally useless. It is much more important to determine the criteria which will be responsive to the fast increase and decrease of function.

Nowadays, mathematical aspects of function behavior in vicinities of discontinuity points are not analyzed thoroughly, which complicates detecting function discontinuity presence while analyzing its behavior on local continuous sections. The paper [11] offers the characteristic function, created by analogy with (2), but it is more adapted to solve the task of search for infinite discontinuities points. The following characteristic function is offered to use:

$$R(i) = (d^2 f(X_i^c))^2 D_i^r, \tag{3}$$

where X_i^c – the centre of a cube, D_j – cube diagonal of search algorithm, r – scaling parameter.

The second differential of function can be calculated with the help of interpolation of initial function using Newton's first interpolation formula [12] for full factorial plan 3^n [13]. Then, using $P_{2,2,2}(X)$ it is easy to calculate $d^2 f(X) \approx d^2 P_{2,2,2}(X)$.

In search algorithm, there is a proportional division of search area into smaller parts: the unit interval – into 2 parts; square – into 4 parts, cube – into 8 parts, etc. Fig. 1 shows a diagram of search area division for two-dimensional case. We will consider the three-dimensional case further in order to present a good illustration.

255
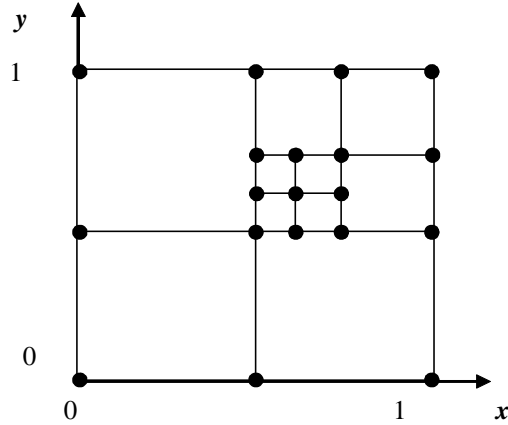
Fig. 1. – Diagram of Search Area Division

Construction of interpolating polynomial for multidimensional case can be realized as follows.

$$Z = \|z_{ijk}\| (i,j,k = 0,1,2)$$

is the matrix of testing function values at nodal points of full factorial plan 3^n. We introduce new variables $q = \frac{x_1 - x_1^{(0)}}{h}$; $p = \frac{x_2 - x_2^{(0)}}{h}$; $r = \frac{x_3 - x_3^{(0)}}{h}$. The starting point of interpolation grid is $X^{(0)} = (x_1^{(0)}, x_2^{(0)}, x_3^{(0)}$; h – the step of interpolation grid. Newton's interpolation polynomial is to be calculated in the form of matrix. Symbols of multidimensional matrix and content of main operations are borrowed from the paper [13]. To do this, we need to calculate the matrix of finite differences $\tilde{Z}$.

$$\tilde{Z} = \begin{Vmatrix} z_\alpha & \Delta_r^1 z_\alpha & \Delta_{rr}^2 z_\alpha & \Delta_q^1 z_\alpha & \Delta_{qr}^{1+1} z_\alpha & \Delta_{qrr}^{1+2} z_\alpha & \Delta_{qq}^2 z_\alpha & \Delta_{qqr}^{2+1} z_\alpha & \Delta_{qqrr}^{2+2} z_\alpha \\ \Delta_p^1 z_\alpha & \Delta_{pr}^{1+1} z_\alpha & \Delta_{prr}^{1+2} z_\alpha & \Delta_{qp}^{1+1} z_\alpha & \Delta_{qpr}^{1+1+1} z_\alpha & \Delta_{qprr}^{1+1+2} z_\alpha & \Delta_{qqp}^{2+1} z_\alpha & \Delta_{qqpr}^{2+1+1} z_\alpha & \Delta_{qqprr}^{2+1+2} z_\alpha \\ \Delta_{pp}^2 z_\alpha & \Delta_{ppr}^{2+1} z_\alpha & \Delta_{pprr}^{2+2} z_\alpha & \Delta_{qpp}^{1+2} z_\alpha & \Delta_{qppr}^{1+2+1} z_\alpha & \Delta_{qpprr}^{1+2+2} z_\alpha & \Delta_{qqpp}^{2+2} z_\alpha & \Delta_{qqppr}^{2+2+1} z_\alpha & \Delta_{qqpprr}^{2+2+2} z_\alpha \end{Vmatrix} \quad (4)$$

Here α= 000. We introduce a vector

$$Q = (1 \quad q \quad q(q-1)/2)';$$
$$P = (1 \quad p \quad p(p-1)/2)'; \quad (5)$$
$$R = (1 \quad r \quad r(r-1)/2)'.$$

Considering (λ, μ)-convoluted product of vectors Q, P, R with $\lambda = 0$, $\mu = 0$, we get the matrix of independent variables

$$\tilde{X} = QPR = \|q_i \cdot p_j \cdot r_k\| \quad (i,j,k = 0,1,2) \quad (6)$$

Thus, Newton's interpolation polynomial has the following matrix form

$$P_{2,2,2}(X) = {}^3(\tilde{Z}\ \tilde{X}) = \sum_{c_0, c_1, c_3 = 0}^{2} \tilde{Z}_{c_0 c_1 c_2} \cdot \tilde{X}_{c_0 c_1 c_2} , \quad (6)$$

where $c = (c_0, c_1, c_2)$ – Caylean summation index [14].

The elements of matrix (4) can be calculated using the definition of finite differences of corresponding orders.

To calculate partial derivatives we need vectors
$Q' = (0 \quad 1 \quad q - 0.5)'$; $P^i = (0 \ 1 \ p - 0.5)'$; $R' = (0 \quad 1 \quad r - 0.5)'$; $Q'' = P'' = R'' = (0 \quad 0 \quad 1)'$,
then

$$P'_{x_1}(X) =^3 (\breve{Z} (Q'PR)) \frac{1}{h}; \ P'_{x_2}(X) =^3 (\breve{Z} (QP'R)) \frac{1}{h}; \ P'_{x_3}(X) =^3 (\breve{Z} (QPR')) \frac{1}{h},$$

and the second derivatives:

$$P''_{x_1x_1}(X) =^3 (\breve{Z} (Q''PR)) \frac{1}{h^2}; \ P''_{x_2x_2}(X) =^3 (\breve{Z} (QP''R)) \frac{1}{h^2}; \ P''_{x_3x_3}(X) =^3 (\breve{Z} (QPR'')) \frac{1}{h^2}.$$

Now it is easy to calculate the value of the second differential in the centers of each eight cubes of original search area partition:

$$d^2 f(X_i^c) \approx (P''_{x_1x_1}(X_i^c) + P''_{x_2x_2}(X_i^c) + P''_{x_3x_3}(X_i^c) + 2(P''_{x_1x_2}(X_i^c) + P''_{x_1x_3}(X_i^c) + P''_{x_2x_3}(X_i^c)))h^2.$$

The value of characteristic function is calculated for each of new cubes, which are written onto the line ordered list in descending order of values. At each stage of search algorithm for discontinuity points of testing function, the first item on the list is chosen – a cube with maximum value of characteristic function, which is subjected to further division. The algorithm works till the condition of algorithm stoppage appears: $(\max|z_i| > M_{sup}) \vee (min_i h_i < \varepsilon)$. This condition of algorithm stoppage ensures the completion of its work if the value of testing function is outside function domain or the given density of viewing the original area of testing function is reached.

2. Examples of using the proposed method of Unit testing for computing modules
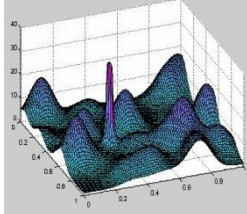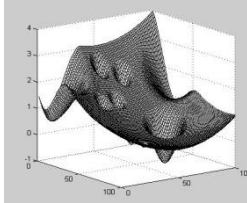
2.1. Method testing with model examples

The proposed testing method of CSM got its name as finite differences method (FDM) due to the use of finite differences of the function. The efficiency of its work can be evaluated by means of discontinuous function – Kovartsev's test [11], specially developed for this case, and a set of test functions generated by the GKLS generator [15]. The first test is characterized by a single discontinuity point (which is difficult to detect) added to linear combination of error functions. The second one is a continuous function with a large number of local extrema. Test functions are presented in Table 1.

In literature, the efficiency of search algorithms is usually evaluated using the operating characteristics machine [16]. Operating characteristic is the dependence of error detection probability P_{alg} on the amount of calls to the tested function N_f.

Since the second-order discontinuity points can be found by any of the global optimization algorithms, the efficiency of the proposed FDM algorithm was compared with the efficiency of direct GO method, for example, the modified bisection method (BM) [17].

Table 1. A set of test functions

№	Function	General view
1	Kovartsev test function: $f(x_1, x_2) = \sum_{i=0}^{19}(i+1)e^{-\frac{(x_1-a_{1i})^2+(x_2-a_{2i})^2}{0.01}} + 1/(1-e^{-\frac{(x_1-b_1)^2+(x_2-b_2)^2}{0.01}})$ $x_1, x_2 \in [0; 1]$ 20 local extrema. One second-order discontinuity point	
2	GKLS test functions. Continuous twice differentiable function. 10 local extrema. One global extremum. Points of discontinuity are not observed.	

The operating characteristics of FDM and BM methods are shown in Fig. 2. They are created for test function 1 which has a local discontinuity point of the second type (see Table 1). As we can see from fig. 2, the efficiency of the proposed algorithm is much greater than the efficiency of the bisection method. In Fig. 2 the solid line indicates operating characteristics of FDM algorithm, the dashed one indicates characteristics of BM algorithm. It happens because the bisection method is focused on the optimization of continuous functions, which leads to a more detailed analysis of the function areas when Lipschitz constant evaluation increases. This situation occurs every time when the function is calculated near the points of its discontinuity. By contrast, FDM method is oriented on looking for areas of rapid growth of the test function.

The situation changes if FDM method "works" with continuous function. Figure 3 shows the operating characteristics of these methods, created for continuous GKLS test function.

The figure illustrates the fact that the efficiency of FDM algorithm for continuous functions is much lower than the efficiency of BM algorithm. If we have continuous functions with no discontinuity points of the second type (test software module has no errors), the finite difference method is forced to examine thoroughly the space of the optimized variables.

2.2. Testing of software modules for calculating acoustic characteristics of gas pressure regulator

This part presents the results of Unit testing for computing models included in the program that realizes the optimization of gas pressure regulator (GPR) parameters with use of orifice plates [21].Significant changes in pressure during orificing and speed acceleration generate the noise which accompanies the work of these machines. This noise exceeds the established health standards. Rational choice of orifice flow area (and their quantity) can significantly reduce the noise level of this device [18].

258
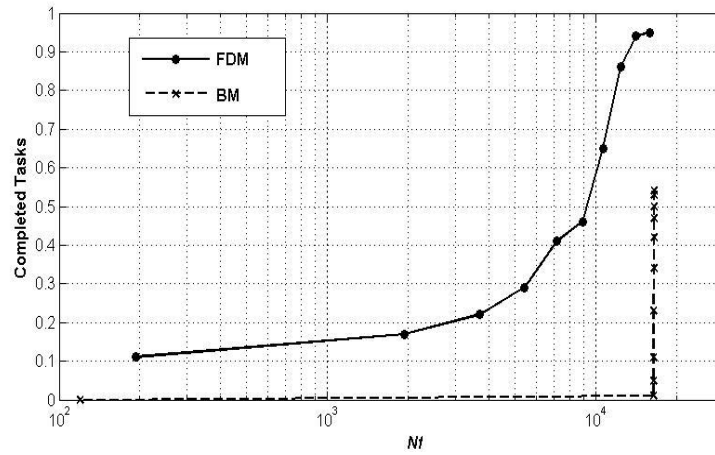
Fig. 2. – Operating characteristics of FDM and BM methods for function №1
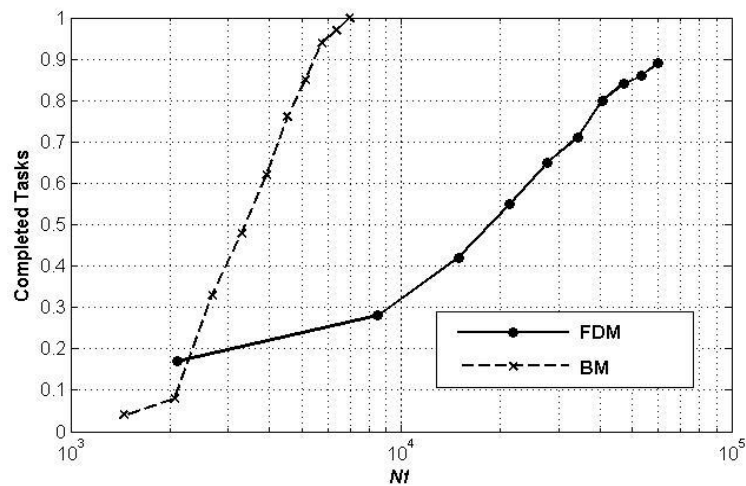
Fig. 3. – Operating characteristics of FDM and BM methods for function №2

Output parameters of GPR for the stationary case have been calculated by solving the system of nonlinear equations that describe gas motion in its specific sections: the valve mechanism and orifice package:

$$\begin{cases} G_x - G_1 = 0, \\ G_1 - G_2 = 0, \\ .... \\ G_{n-1} - G_n = 0, \end{cases} \qquad (7)$$

259

G_x- gas flow through the valve, G_i – gas flow through i-orifice plate. When the input parameters of module are given, for example, $p_i, p_{i+1}-$ pressure before and after orifice plate correspondingly; S_i – areas of i-orifice flow, etc. we can calculate gas mass flux through orifice and as a result – acoustic power generated by orifice plate [19].

We used a rather simple module for calculating the orifice flow capacity (C_{vi}) in order to calculate the gas mass flux through orifice. Testing the module by FDM method with approximately 200 calls to the module revealed methodological error in the algorithm model. It turned out that if $p_i \rightarrow p_{i+1} - C_{vi} \rightarrow \infty$, and $p_i < p_{i+1}$, flow capacity is indefinite (error code NaN occurs).

Certainly, it would be possible to require the calculation with this module $C_{vi}(p_i, p_{i+1})$ to be carried out only in accordance with the condition $p_i > p_{i+1}$, which is natural for this type of device. But how can it be realized when numerical method for solving systems of nonlinear equations (8) generates the values of independent variables at each iteration on its own, not taking into consideration the above mentioned circumstances? The easiest way to solve the problem is the artificial replacement of function infinite discontinuity $C_{vi}(p_i, p_{i+1})$ with a larger but finite discontinuity, and extension of definition by "penalty" value where it is indefinite. In this case, the algorithm for solving systems of nonlinear equations is to find solutions on its own, "starting with" "dysfunctional" combinations of independent variables.

High speed of detecting fallible combinations of FDM independent variables in this example can be explained by the fact that at the first stage of work, when the area of rapid function growth is not detected, FDM distributes test points of testing function in the search area. Since function $C_{vi}(p_i, p_{i+1})$ has significant areas of uncertainty, FDM finds them quickly.

Conclusion

The paper offers an original method of Unit testing for computing modules, based on the algorithm of global search for infinite discontinuity of the testing function, which allows to detect fatal errors in software computing modules, as well as incorrectness in implementation of mathematical models of algorithms.

The proposed scheme of accelerating algorithms for global optimization applied to the search for points of discontinuity of the second order has confirmed completely its viability with model and real examples. The basic idea of FDM algorithm is to introduce a new heuristic characteristic function to the classical algorithm of global optimization. The new function is based on the analysis of Strongin characteristic function and takes into account the problem matters being solved. FDM algorithm is the universal method of Unit testing for the class of computing modules. The application of this method leads to the reduction of time for debugging, helps to find fatal errors with less effort, and, as a result, to organize total testing of all program modules.

References

1. **Dastin E, Reshka D, Paul D.** Automatic software testing. Application, operation and maintenance. Moscow: Lori, 2003; 567 p. [in Russian]
2. **Lipaev VV.** Program testing. M.: Radio and connection, 1986; 296 p. [in Russian]

3. **Kovartsev AN.** Automation of software development and testing. Samara State Aerospace University, 1999; 148 p. [in Russian]
4. **Kuliamin VV.** Software verification methods. Source: <http://panda.ispras.ru/~kuliamin/docs/VerMethods-2008-ru.pdf >
5. **Kovartsev AN.** An efficient algorithm for testing the truth of assertions for real numbers expressed in relational signatures. Computer Optics, 2014; 38(3): 550-554. [in Russian]
6. **Heitmeyer C, Archer M, Bharadwaj R, Jeffords R.** Tools for constructing requirements specifications: The SCR toolset at the age of ten. Journal of Computer Systems Science and Engineering, 2005; 20(1): 19-35.
7. **Farchi E, Hartman F, Pinter SS.** Using a model-based test generator to test for standard conformance. IBM Systems Journal, 2002; 41(1): 89-110.
8. **Cavalli A, Gervy C, Prokopenko S.** New approaches for passive testing using an Extended Finite State Machine specification. Information and Software Technology, 2003; 45(12): 837-852.
9. **Kovartsev AN, Logvinov AL.** Efficiency improvement of testing algorithms for computing modules. Journal of Telecommunication systems, 2004; 4. [in Russian]
10. **Strongin RG.** Search for global optimum. Moscow: Znanie, 1990. [in Russian]
11. **Kovartsev AN, Popova-Kovartseva DA, Serpovskaya EE.** Testing mathematical models of computing algorithms based on global optimization method. Information technology and nanotechnologies. SSAU, 2015; 191-196. [in Russian]
12. **Kovartsev AN.** Computational mathematical. Samara: Ofort, 2011; 230 p. [in Russian]
13. **Ermakov SM, Zhigliavsky AA.** Mathematical theory of optimal experiment operation. Moscow: Nauka, 1987; 320 p. [in Russian]
14. **Sokolov NP.** Introduction to multidimensional matrix theory. Kiev: Nukova dumka, 1972; 177 p. [in Russian]
15. **Gaviano M, Kvasov DE, Lera D, Sergeyev YaD.** Software for generation of classes of test functions with known local and global minima for global optimization. ACM TOMS, 2003; 29(4): 469-480.
16. **Gergel VP, Strongin RG.** Absolute. Software system for global optimization method studying. Textbook. Nizhny Novgorod: Nizhegorodsky University Press, 1998; 141 p. [in Russian]
17. **Kovartsev AN, Popova-Kovartseva DA, Abolmasov PV.** Efficiency study of global parallel optimization for multivariable function. Vestnik NNGU, 2013; 3(1): 252-261. [in Russian]
18. **Igolkin AA, Kruchkova AN, Koh AI, Safin AI, Shakhmatov EV.** Pressure reducing valve noise reduction. Proceedings of the Nineteen International Congress on Sound and Vibration (ICSV 19). The international institute of Acoustics and Vibration, 2012, July 08-12.
19. **Istvan L, Beranek V, Beranek L.** Noise and vibration control engineering. Second edition. Principles and applications. Published by Wiley and Sons, Inc, 2006; 966 p.
20. **Meszaros, G.** xUnit test patterns: rafactoring test code. U.S. at Courier in Wesrford, Massachusetts, 2009; 835 p.
21. **Karczub DG, Catron FW, Allen C.** Blow-down valve noise and interactions with down stream orifice plates. Fagerlund Proceedings of IMECE'03. ASME International Mechanical Engineering Congress, 2003; 43-49.

The enhancement of the operating speed of the algorithm of adaptive compression of binary bitmap images

Borusyak A.V.

Research Institute of Applied Mathematics and Cybernetics Lobachevsky Nizhni Novgorod State University National Research University

Abstract. The paper deals with the problem of the enhancement of the operating speed of the algorithm of adaptive compression of binary bitmap images (BBI) on the basis of entropy coding using context simulation. The influence of the size of the maximal order context on the compression rate is considered. The enhancement of the speed of the algorithm depending on the number of the threads used is considered.

Keywords: compression, optimization, binary images, context-based modeling

1. Introduction

The development of specialized algorithms, targeted for a specific data type, remains relevant in many areas. These algorithms use the knowledge of the internal data structure to achieve a greater degree of compression. One of the important areas is the compression of monochrome black-and-white binary images (MBI). Among the most effective methods of compression of data with a certain structure and specificity there are contextual data compression techniques based on the PPM technique (Prediction by Partial Matching).

The PPM algorithm involves entropy coding using individual context models (CM) for each context, encountered in the stream of encoded data. Each CM includes the counters for all the characters, encountered after the corresponding context. At the same time, the implicit weighting of estimates is used for the application of the context models of several orders. The PPM model itself only predicts the value of a character, while the encoding itself is performed by an encoder using entropy coding algorithms, such as Huffman's algorithm and arithmetic encoding.

2. PCTB Algorithm

The MBI compression algorithm, named PCTB, based on the PPM context simulation technique [1], was developed and implemented. The distinctive feature of

262

this algorithm, as compared to the standard PPM algorithm, is the use of two-dimensional binary context of a specific shape and size, instead of standard one-dimensional context. The use of the property of the two-dimensionality of data in the process of image compression makes it possible to substantially improve the compression ratio, by taking into account the relationships between the neighboring pixels both in horizontal and vertical directions.

The algorithm uses a specific context shape and models of 31th, 11th, 7th, 4th and zeroth order. The B-tree storage structure is used for the efficient storage of context models in the memory.

The following techniques and methods are used in the algorithm: the proprietary algorithm of the estimation of the probability of escape, the method of exclusion of the last encountered symbol, the method of scaling the last encountered symbol using the chosen scaling factor, the modified method of information inheritance.

An arithmetic encoder is used as the entropy encoder. The decoding process is symmetric to the coding process.

The implementation of the algorithm has shown high efficiency in terms of the compression ratio (R_c), but the time expenditures were too high. The time, required for encoding, was reduced by 1.5-2 times by optimization of the computation [3]. However, even after the optimization, the process of encoding remains time-consuming. Moreover, for large images with low redundancy the context model tree grows too quickly, resulting in a high level of RAM consumption and frequent calls for the context model tree purge procedure. The context model tree purge procedure is required for the limitation of RAM consumption. At the same time, frequent calls for this procedure slow down the operating speed of the algorithm and reduce the R_c.

This paper deals with the problem of the reduction of the algorithm run-time and RAM consumption. To further enhance the operating speed of the algorithm, the methods of the parallelization and reduction of the size of maximal order context (MOC) are proposed.

3. Optimization of the time complexity of the algorithm

One way to enhance the speed of the algorithm is the optimization of existing computations. As part of the work [2], various approaches to the enhancement of the operating speed of the algorithm by means of the optimization of computations are proposed. The brief description of the proposed techniques is given below.

In order to optimize the computation function of a new MOC, the sequence order of the context pixels was changed from fixed, predetermined by a programmer, to serial row-major, from the leftmost pixel of the context, which is in line with the pixel to be encoded, to the rightmost, located as far as possible in vertical direction from the pixel to be encoded. This conversion made it possible to reduce the number of access operations to the image when calculating a new MOC from the value of the entire context to the value of the context in height. In the transition to a new line of the image, the fast computation was realized only for those context pixels that did not go beyond the boundaries of the image. A method of calculating lower order contexts, using the MOC calculated with the help of the predetermined mask, is proposed. A mask is a fixed list of serial numbers of MOC pixels, specified by a programmer.

263

In order to limit RAM consumption, the upper limit for the number of context models, stored in a context model tree, is introduced. When the predefined limit is exceeded, the tree of maximal order context models is purged completely.

A link to a parent context model was added to each context model, in order to accelerate the operation of identification of the parent context model, used in information inheritance and in the escape to the lower order contexts.

Initially, the algorithm used the AVL-tree structure to store the context models. Various options of the storage of the model tree were considered. As a result of the experimental testing, the B-tree turned out to be more efficient with respect to the operating speed, and it was taken as the basic structure for the storage of the context model tree.

The transition of the program to the Q_t 4.8.3 programming environment made it possible to improve efficiency and make the program structure more flexible.

The procedure of the updating of the percentage indicator of the encoding/decoding process was also optimized to improve efficiency.

The above approaches made it possible to reduce significantly, by 1.5-2 times, the time, required for encoding/decoding. The RAM consumption was also limited. Despite the fact that the acceleration proved to be essential, the algorithm still was significantly slower than its counterparts. Due to that, the work on the improvement of the algorithm performance was continued.

4. The dependence of the main compression parameters on the value of the context

One way to enhance the operating speed of programs is to identify the "hot spots of a program" or, in other words, the parts of the program code, consuming the most amount of computer resources. As a result of the research conducted by using a profiler, it was found, that most of the CPU time and RAM are consumed by the functions of calculating a new MOC and searching for a new CM in the CM tree. As noted above, these functions have already been optimized with respect to computation. However, it was noted, that MOC size has a strong influence on the operation of the said functions. Consequently, MOC size affects not only the compression ratio, but also the operating speed of the algorithm and the amount of memory consumed. It has been suggested, that in case of decrease in the MOC size to a certain level, R_c will be reduced slightly, but the compression rate will increase significantly. In view of this, the experiments were conducted to identify the dependence of R_c, compression time and RAM consumption on the MOC size. The results of this experiment are presented in Table 1. According to the experiments conducted, in case of the reduction of the size of the context to 15, the compression ratio is reduced slightly, while a significant decrease in the time required for compression and reduction of the amount of the RAM consumed are noted. The reduction of MOC size to less than 15 leads to a significant reduction in the compression ratio complete with less significant reduction in the RAM consumed and the time required for compression. In Tables 1-3, the rows correspond to the number of the compressed file, and the columns correspond to the size of the maximal order

context. At the same time, the reduction of MOC size to below 20 almost does not affect the level of RAM consumption.

Table 1. The dependence of the compression time (sec) on the context size

File\context	31	25	20	15	10	5	1
1	0.98	0.94	0.92	0.77	0.70	0.74	0.66
2	5.47	4.31	3.50	2.67	2.11	2.05	1.56
3	4.30	4.11	4.08	3.56	3.16	3.58	2.87
4	712.63	544.81	358.42	214.62	139.06	127.47	97.89
5	180.71	175.30	173.63	155.85	137.90	188.71	123.95

Table 2. The dependence of the compression ratio on the context size

File\context	31	25	20	15	10	5	1
1	113.46	111.58	107.17	99.73	94.28	78.17	36.94
2	5.26	5.15	5.04	4.83	4.57	4.11	3.78
3	62.34	61.20	59.98	58.07	55.32	49.03	17.92
4	2.69	2.66	2.66	2.54	2.28	1.72	0.99
5	55.57	53.29	51.90	50.34	45.93	37.23	15.30

Table 3. The dependence of RAM consumption (Mb) on the context size

File\context	31	25	20	15	10	5	1
1	16	15.4	14.3	14.2	15	14.2	14.3
2	38.6	26.5	19	15.2	15.2	15.2	14.7
3	18.2	17.3	17.1	17.3	17.3	17.2	17
4	621	259.7	103.5	103	104	103	103
5	189	188.7	188.4	188.4	189	188	188.7

5. Parallelization of the encoding algorithm

Modern computers are often equipped with processors, containing multiple cores, which enables parallel computing. This feature is currently often used to speed up the algorithms. In order to further enhance the coding/decoding speed, the possibility of encoding and decoding BBI through the parallelization of processing into multiple threads was implemented in the compression algorithm. The parallelization algorithm for the compression of indexed images [3] is used as the basis of the parallelization algorithm. The ability to split the image into *n* parts is implemented. Assume the vertical dimension (height) of the image for *H*, the horizontal dimension (width) for *W*. The image is divided as follows: if the number of parts is equal to 4, the image is divided along the lines, connecting the midpoints of the opposite sides. If $n \neq 4$, the vertical sides of the image are divided into *n-1* equal parts with the height equal to H/n, and one part with the height (*H-H/n*(n-1)*). After splitting the image into several parts, each part of the image is compressed as an individual image in a separate

thread. This approach makes it possible to use the capabilities of modern computers, evenly distributing the load on processor cores, while slightly reducing the compression efficiency. It is assumed that with this approach, the increase in the number of threads by n times will increase the compression rate to n times, provided that the number n is less than or equal to the nc number of the processor cores. At the same time, the rate will increase in proportion to the number of threads. If the n number is greater than the nc, the increase in the compression rate, approximately equal to the use of the nc threads, is expected. During the computation on a dual core PC1 (CPU – Core 2 Duo E7400 2.8 GHz) and a quad-PC2 (CPU – Core i5-3230M 2.6 GHz) the following results were obtained:

Table 4. Comparison of encoding time for the file PGS2 (32294x25003, colour depth – 1 bit, number of colours – 1) depending on the number of threads

Number of threads	Time PC1 (sec.)	Time PC2 (sec.)	R_c
1	90.496	69.405	71.99
2	53.228	50.701	71.90
4	51.012	43.992	71.76
8	50.451	39.094	71.53
16	50.029	37.565	71.14
32	49.764	36.769	70.52
64	51.106	37.564	69.54

Table 5. Comparison of encoding time for the file floor_plan (5000x3336, colour depth – 1 bit, number of colours – 1) depending on the number of threads

Number of threads	Time PC1 (sec.)	Time PC2 (sec.)	R_c
1	1.86	1.389	62.35
2	0.984	0.827	61.98
4	1.062	0.78	61.25
8	0.99	0.796	60.46
16	0.983	0.78	59.11
32	0.996	0.78	57.18
64	0.949	0.827	53.99

Where, in the first column of Tables 4 and 5 the number of threads used for image encoding is indicated. In the second and the third columns the corresponding encoding time in seconds is indicated for PC1 and PC2. The last column shows the Rc for this file, depending on the number of the threads used. This ratio depends on the number of threads, but doesn't depend on the computer used for encoding, so the two computers possess the same factors. It is seen from the experiments, that, as expected,

266

the optimal number of threads is equal to the number of cores in the system. Thus, the compression ratio reduces linearly, but very slightly, and at 64 threads, the losses less than 3% are observed, while at n-16 threads, the losses are less than 1%.

6. Conclusion

The problem of the enhancement of the operating speed of the algorithm of adaptive compression of binary bitmap images was considered. The experiments were conducted for the enhancement of the operating speed of the proposed algorithm by parallelizing the algorithm into several threads and reducing MOC size. Both approaches proved to be effective. The MOC size, the reduction to which greatly reduces the file encoding time and significantly reduces RAM consumption, while only slightly reducing the Rc, was identified. The experiments were conducted for parallelizing the algorithm into several threads. Using these two approaches together, it is possible to enhance the rate of compression to an average of 8 times on a computer with a 4-core processor, to reduce RAM consumption by 2 times, with the average Rc losses being less than 10%.

Acknowledgments

References

1. **Borusyak AV, Vasin YuG, Zherzdev SV.** Compression of Binary Graphics Using Context Simulation. Pattern Recognition and Image Analysis, 2013; 23(2): 207-210.
2. **Borusyak AV, Vasin YuG, Zherzdev SV.** Optimizing the computational complexity of the algorithm for adaptive compression of binary raster images. Proceedings of The 11-th International Conference "Pattern Recognition and Image Analysis: new information technologies", 2013; 1: 170-172.
3. **Borusyak AV, Vasin YuG.** Compression of indexed graphic images using context modeling. Vestnik of the Lobachevsky State University of Nizhni Novgorod, 2014; 4(1): 486-492.
4. **Vatolin D, Ratushnyak A, Smirnov M, Yurkin V.** Methods of data compression. Construction of archivers, image and video compression. Moscow: Dialog – MEPHI, 2003.
5. **Vasin YuG. Zherzdev SV.** Information Techniques for Hierarchical Image Coding. Pattern Recognition and Image Analysis, 2003, 13(3): 539-548.
6. Source <http://www.imagecompression.info/test_images>.

3D scene stereo reconstruction with the use of epipolar restrictions

Fursov V.A., Goshin Y.V.

Samara State Aerospace University,
Image Processing Systems Institute, Russian Academy of Sciences

Abstract. In the present paper a new approach to scene digital model reconstruction from pair of stereo images is considered. We propose to perform image matching with use of weight coefficient as a penalty function for the distance from the point to the correspondent epipolar line. Technology implementation for unknown camera parameters is also considered. In this case, identification of the fundamental matrix from corresponding points is performed on the initial stage. The main advantage of this technology is the absence of the image rectification stage which causes additional distortions due to image interpolation. There is an example of scene reconstruction from pair of test images and a digital model reconstruction from satellite images.

Keywords: stereo image processing, image matching, 3D reconstruction, projective geometry, epipolar geometry

1. Introduction

The main problem with 3D-scene reconstruction is image matching. Solving this problem presents some difficulties because projective distortions on stereo pairs are usually significantly different. To overcome these difficulties, an image preprocessing rectification technique is used. Rectification of stereo images is a transformation, in which corresponding points on stereo images are arranged in the same rows.

In [1], the theoretical basis for the method of projective rectification is provided, and the basic algorithm for rectification is introduced. The algorithm involves calculation of the fundamental matrix and projective transformation. The method of projective rectification is also covered in [2]. The idea of this method is to decompose the matrix of the projective transformation into several matrices. But a common disadvantage of projective rectification is its inapplicability in case when the epipoles are located on the images as it results in infinite resolution images. In addition, images can become very large, for example, when the epipole is close to the image.

In [3], polar rectification is introduced as an alternative method of rectification. The method consists in polar scanning of images around the epipoles. Operation of the proposed approach is illustrated on real pairs of images. This method has two main advantages: an opportunity to operate with epipoles on images and guaranteed minimum size of images without losing pixels.

Though it solves many problems of projective rectification mentioned above, polar rectification has a number of disadvantages too. For instance, it does not operate correctly when an epipole is located at infinity. In particular, there may be cases where one epipole is located at infinity, and another one is located on the image. In papers [4] and [5], the idea of polar rectification is extended for these cases.

The above methods of rectification do not take into account possible differences in the internal parameters of the camera, such as focal lengths. This problem is described in [6], in which an algorithm for rectification of heterogeneous and uncalibrated image pairs is proposed, in particular, for the pairs of images obtained from static and dynamic cameras of different focal lengths and/or different resolutions. Rectification is performed in two steps. The first step is the correction of heterogeneity (different scale) by the expansion, compression or shift of images. The second step is a standard rectification of images. This approach avoids image distortions associated with differences in scale (compression or tension as a result of rectification).

At the same time, necessity for conversions directly on an image is a common disadvantage of the rectification approach. The images and objects on them are distorted considerably, owing to polar transformation. Feature points detection is performed on the new interpolated image which causes additional errors. Although polar rectification is more universal than the projective one, it still impairs some problems connected with distortions of images during conversions.

An alternative technique of matching is an approach of scene elements tracing, in particular, using a method of optical flow [7], [8]. The method of an optical flow operates efficiently with a sequence of images, for example, with sequences of video frames. However, when the images are obtained from cameras which are located relatively far apart, losses of objects during the tracing are possible.

Earlier authors proposed a technology [9] in which a projective transform is constructed from reliable corresponding points in an informative areas of images. And then this transform is used to determine and adjust the corresponding points in uninformative areas. Number of correspondence points on images given by this technology is low and resulting 3D model is too rough.

The technology of 3D scene reconstruction proposed in this paper to a considerable degree allows to avoid the above mentioned disadvantages. The basic idea is to take into account epipolar restrictions in the course of points matching.

We consider the approach to the epipolar restrictions implementation in which the most similar image fragments are selected in the neighborhood of the epipolar line. Then, according to the given criterion, the best points with real coordinates belonging to the epipolar line are selected.

2. Problem definition

In order to solve the problem of image matching, the camera obscura model is used [9]. Let us consider the case when the parameters of the cameras, as well as their position and orientation are known. To characterize them, camera parameters matrices are defined:

$$\mathbf{K} = \begin{bmatrix} f & 0 & u_0 \\ 0 & f & v_0 \\ 0 & 0 & 1 \end{bmatrix}, \ \mathbf{K}' = \begin{bmatrix} f' & 0 & u_0' \\ 0 & f' & v_0' \\ 0 & 0 & 1 \end{bmatrix}, \tag{1}$$

where f and f' is focal length of the camera, (u_0, v_0), (u_0', v_0') are cameras' principal points location in the coordinate system associated with these cameras [10].

Let us introduce a global coordinate system and the coordinate systems of first and second cameras with their centers at points $\mathbf{c}$, $\mathbf{c}'$ in the global coordinate system. Neither of these two points, in general, coincides with the origin of the global coordinate system.

Suppose $\mathbf{M}$ is a coordinate vector of some point in the global coordinate system. Coordinate vectors of this point in the coordinate systems of the first and second cameras $\mathbf{m}$ and $\mathbf{m}'$ are defined as

$$\mathbf{m} = \mathbf{K}[\mathbf{R} \vdots \mathbf{t}]\mathbf{M}, \tag{2}$$

$$\mathbf{m}' = \mathbf{K}'[\mathbf{R}' \vdots \mathbf{t}']\mathbf{M}, \tag{3}$$

$\mathbf{R}$, $\mathbf{R}'$ are the matrices of 3×3-dimension, describing the rotation of the coordinate systems of the first and second cameras on the global coordinate system, and $\mathbf{t} = \begin{bmatrix} t_x, t_y, t_z \end{bmatrix}^T$, $\mathbf{t}' = \begin{bmatrix} t_x', t_y', t_z' \end{bmatrix}^T$ are coordinates of the origin of the global coordinate system in the coordinate systems of the first and second cameras respectively, defined as

$$\mathbf{t} = -\mathbf{R}\mathbf{c},$$

$$\mathbf{t}' = -\mathbf{R}'\mathbf{c}',$$

If projections $\mathbf{m}$ and $\mathbf{m}'$ (2), (3) on the first and second camera images are known, point $\mathbf{M}$ coordinates in three-dimensional space can be calculated as the intersection of rays $(\mathbf{c}, \mathbf{m})$ and $(\mathbf{c}', \mathbf{m}')$. Due to errors in the course of determining of the corresponding points coordinates, these rays will not probably cross. The errors occur in the internal and external calibration matrices and image distortions due to rectification. Therefore, some inaccurate estimates of the point coordinates are usually computed.

A detailed review of methods for image matching is given in [11]. It presents a classification of methods for stereo matching by the cost function, aggregation area, and a disparity map construction approach. The paper [12] describes stereo matching by use of so-called super pixels. Superpixel is a set of pixels that are homogeneous in their brightness and texture. In [13], the method of matching in a rectangular area, based on cross-correlation and the maximum-surface method is proposed. In [14] an intensity-based method that takes into account discontinues and occlusions are presented.

In our technology, rectified images are not generated. Matching points are searched directly on the epipolar lines belonging to the same plane. Then, for each pair of corresponding points, spatial coordinates of the scene are computed.

3. Points matching using weighting coefficients

We assume that the fundamental matrix is calculated with use of cameras parameters or estimated on the set of corresponding points (for example, with use of the 8-th point algorithm [15]). We will designate the points coordinates on the first image of stereo images as (u,v), and the corresponding points coordinates on the second stereo images as $(u+\Delta u, v+\Delta v)$, where Δu and Δv are relative shifts of the coordinates respectively. Let $I(u,v)$ and $I'(u+\Delta u, v+\Delta v)$ are values of the brightness distribution functions of these images. We will use Euclidean norm as a measure of proximity between values of brightness for point (u,v) and the corresponding point $(u+\Delta u, v+\Delta v)$:

$$e(u,v,\Delta u,\Delta v) = \|I(u,v) - I'(u+\Delta u, v+\Delta v)\|$$

The problem of the determination of shifts values is formulated as a problem of the following criterion minimization:

$$E(u_0, v_0, \Delta u, \Delta v) = \sum_{(u,v) \in D(u_0, v_0)} a(u,v) e(u,v,\Delta u,\Delta v)$$

where $D(u_0, v_0)$ is the area around point (u_0, v_0), and $a(u,v)$ is the weight function defined as multiplication of three weighting coefficients:

$$a(u,v) = w_c \cdot w_d \cdot w_f$$

where w_c, w_d are the coefficients which reduce projective distortions, and w_f is the coefficient providing the location of the point on the epipolar line. These coefficients depend on point coordinates (u,v) in area $D(u_0, v_0)$.

Coefficients w_d, w_c are determined similar to algorithm SimpleFlow [16] by the following equations:

$$w_d = \exp\left\{-\|(u_0, v_0) - (u,v)\|^2\right\}, \qquad (u,v) \in D(u_0, v_0),$$

$$w_c = \exp\left\{-\|I(u_0, v_0) - I'(u,v)\|^2\right\}, \quad (u,v) \in D$$

Coefficient w_d increases the weight of the points values depending on the proximity to the center of area $D(u_0, v_0)$. It reduces distortions influence, as the distance from the center to the edges of area increases.

Weighting coefficient w_c performs the same function; however, in this case, the values of the brightness distribution functions are used. This coefficient extends the effective area of the fragments comparison in case of sufficiently different intensity values in area $D(u_0, v_0)$.

Along with the weight coefficients w_d, w_c, which were considered in paper [16], we introduce weight coefficient w_f, which characterizes the distance from a point to an epipolar line. For each point (u_0, v_0) on the first image there is a corresponding epipolar line $l' : au' + bv' + c = 0$ on the second image:

$$(u, v) \rightarrow \begin{pmatrix} F_{11} & F_{12} & F_{13} \\ F_{21} & F_{22} & F_{23} \\ F_{31} & F_{32} & F_{33} \end{pmatrix} \begin{pmatrix} u \\ v \\ 1 \end{pmatrix} = \begin{pmatrix} a \\ b \\ c \end{pmatrix}$$

$$a = u_0 F_{11} + u_0 F_{12} + F_{13},$$
$$b = u_0 F_{21} + u_0 F_{22} + F_{23},$$
$$c = u_0 F_{31} + u_0 F_{32} + F_{33}.$$

Coefficient w_f is calculated as

$$w_f = \exp\left\{ -d\left((u', v'), l' \right) \right\}$$

where

$$d\left((u', v'), l' \right) = \left| \frac{au' + bv' + c}{\sqrt{a^2 + b^2}} \right|$$

is a distance from point $(u + \Delta u, v + \Delta v)$ on the second image to the epipolar line l'. This coefficient is used as penalty function for the distance from the point to the correspondent epipolar line.

4. Examples

4.1. Test scene reconstruction

We compared the algorithm of the corresponding points determination using the epipolar restrictions with similar SimpleFlow algorithm. For this experiment we use a set of test stereo images "Tsukuba" (Figure 1) in the daylight and in the flashlight. Figure 2 shows the results of the disparity map reconstruction using proposed method and SimpleFlow. For quantitative assessment of quality we use the number of the disparity map pixels, which are not occlusions and differ more than by 10\% from their exact values. The number of such pixels is given in Table 1. This table contains the results of processing by Simple Flow algorithm as well. The first number is the absolute number of pixels. The relative number of pixels (to total number of pixels) is given in brackets.

4.2. Digital terrain model reconstruction

Stereo images obtained from a spacecraft and shown in Figures 2a and 2b were used in the test. As parameters of the spacecraft at the moment of recording by an optical device are unknown, the problem of the fundamental matrix determination using the corresponding points of the stereo images shown in Figure 3 should be solved. Let us refer to this stage as preliminary comparison of the stereo images.

Fig. 1. – Scene stereo images: a) left view; b) right view

Table 1. Number of wrong correspondences

Images registration conditions	Proposed method	SimpleFlow
Daylight	19 191 (~8,3%)	21 187 (~9,1%)
Direct light	15 645 (~6,7%)	21 088 (~9,1%)

Fig. 2. – Disparity map: a) proposed method; b) SimpleFlow

Fig. 3. – Initial pair of stereoimages

Figure 4 (a) shows the fragment of one (left) image of a stereo pair with white lines illustrating the sizes and the directions of shifts between images (optical flow). Let us note that the relative number of chaotically directed white lines is rather great. When using a small number of the corresponding points these errors can lead to rough

273

errors when calculating a fundamental matrix. Therefore we form a system of linear equations and use conforming estimate method as it is described in [18], [19]. Thus, the fundamental matrix is obtained:
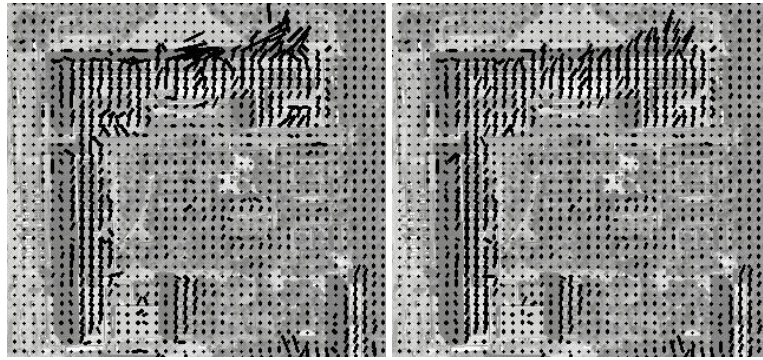
Fig. 4. – Images with the results of comparison of points: a) at a preliminary stage; b) taking into account epipolar restrictions

$$F = \begin{pmatrix} -6.73 \cdot 10^{-5} & -6.56 \cdot 10^{-5} & -5.94 \\ 1,22 \cdot 10^{-4} & 6.25 \cdot 10^{-6} & -0.65 \\ 5.98 & 0.62 & 1 \end{pmatrix}$$

After the fundamental matrix is determined, it is possible to find the corresponding points with using the epipolar restrictions. Figure 4 (b) gives a fragment of the same image with the black lines showing sizes and directions of shifts errors under the epipolar restrictions. It is easy to notice that the number of the chaotic black lines characterizing errors in this case is significantly lower.
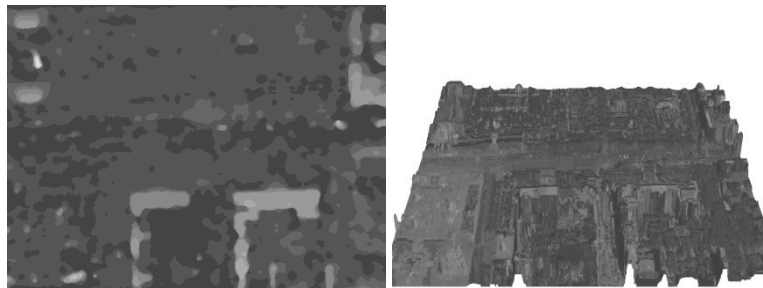
Fig. 5. – a) the disparity map, b) restored DTM

In Figures 5 the disparity map (a) and the restored digital terrain model (b) of the image segment, constructed with use of the corresponding points, are shown.

5. Conclusion

When the fundamental matrix is not known precisely, high quality of the reconstruction can be reached by the use of epipolar restrictions in the form of weight coefficient in the penalty function. These coefficients correspond to the distance from the point to the epipolar line. The results of the comparison with the most popular SimpleFlow algorithm demonstrate the prospects of the proposed approach.

Acknowledgements

References

1. **Hartley RI.** Theory and Practice of Projective Rectification. International Journal of Computer Vision, 1999; 35: 115-127.
2. **Monasse P, Morel JM., Tang Z.** Three-step image rectification. BMVC 2010-British Machine Vision Conference, 2010; 89.1-89.10.
3. **Pollefeys M.** A simple and efficient rectification method for general motion. The Proceedings of the 7th IEEE International Conference on Computer Vision, 1999; 1: 496-501.
4. **Häming K, Peters G.** Extension of the generalized image rectification. Catching the infinity cases. Proceedings 4th International Conference on Informatics in Control, Automation, and Robotics (ICINCO 2007), 2007; 2: 275-279.
5. **Oram D.** Rectification for any epipolar geometry. British Machine Vision Conference, 2001; 653-662.
6. **Kumar S, Micheloni C, Piciarelli C, Foresti GL.** Stereo rectification of uncalibrated and heterogeneous images. Pattern Recognition Letters, 2010; 31(11): 1445-1452.
7. **Fleet D, Weiss Y.** Optical flow estimation. Handbook of Mathematical Models in Computer Vision, 2006; 237-257.
8. **Barron JL, Fleet DJ, Beauchemin SS.** Performance of optical flow techniques. International Journal of Computer Vision, 1994; 12(1): 43-77.
9. **Goshin YeV, Kotov AP, Fursov VA.** Two-stage formation of a spatial transformation for image matching. Computer Optics, 2014; 38(4): 886-891. [in Russian]
10. **Forsyth D, Ponce J.** Computer Vision: A Modern Approach. Moscow: "Williams" Publisher, 2004. 928 p. [in Russian]
11. **Hartley R, Zisserman A.** Multiple view geometry in computer vision. Cambridge university press, 2003.
12. **Scharstein D, Szeliski R.** A taxonomy and evaluation of dense two-frame stereo correspondence algorithms. International journal of computer vision, 2002; 47(1-3): 7-42.
13. **Mičušík B, Košecká J.** Multi-view superpixel stereo in urban environments. International journal of computer vision, 2010; 89(1): 106-119.
14. **Sun C.** Fast stereo matching using rectangular subregioning and 3D maximum-surface techniques. International Journal of Computer Vision, 2002; 47(1-3): 99-117.
15. **Luo A, Burkhardt H.** An intensity-based cooperative bidirectional stereo matching with simultaneous detection of discontinuities and occlusions. International Journal of Computer Vision, 1995; 15(3): 171-188.
16. **Hartley R.** In defense of the eight-point algorithm. Pattern Analysis and Machine Intelligence, IEEE Transactions on, 1997; 19(6): 580-593.

17. **Tao M, Bai J, Kohli P, Paris S.** SimpleFlow: A Non-iterative, Sublinear Optical Flow Algorithm. Computer Graphics Forum, 2012; 31(2): 345-353.
18. **Fursov V, Goshin Ye.** Conformed Identification of the Fundamental Matrix in the Problem of a Scene Reconstruction, using Stereo Images Image Mining. Theory and Applications. Proceedings of IMTA-4, 2013; 29-37.

Computer-aided system of data protection by steganography methods

Kiseleva A.V., Kudrina M.A.

Samara State Aerospace University

Abstract. The article contains the description of the computer-aided system which allows to hide information by means of steganography methods. The system involves methods of hiding text information such as LSB, Koch-Zhao method, and method of Kutter-Jordan-Bossen, as well as the method of hiding color bmp images.

1. Introduction

Modern society faces an up-to-date problem concerning the means which help to protect confidential information when it is stored or sent. The steganography is one of ways of data protection.

Steganography involves hiding message in such a way that the casual observer would not be able to detect the hidden information.

Due to the increase of global computer networks role, the value of steganography becomes more and more important. Now steganography systems are actively used for the solution of the following main tasks [1]:

- protecting confidential information against unauthorized access;
- overcoming the monitoring and management systems of network resources;
- camouflaging the software;
- copyright protection of some types of intellectual property.

2. Theoretical part

The *steganography system* is a set of means and methods which are used for formation of the hidden channel of information transfer [2, 3]. The *embedded-message* or *payload* is something to be hidden in something else. Any type of information can be used as the embedded-message: texts, images, videos, etc.

The *carrier* or the *cover message* is the signal, stream, or data file that hides the embedded-message. The resulting signal, stream, or data file with the encoded payload is called the *package* or *stego-file*.

Computer steganography methods can be divided into two basic classes in accordance with the hiding principle: methods of direct replacement and spectral methods. Methods of direct replacement use redundancy of data environment and consist in the replacement of insignificant part of the cover message with bits of the embedded-message. Spectral methods of data hiding use spectral representations of the environment elements with the embedded-message within the environment structure.

LSB method

The method of replacement of *Least Significant Bits* (*LSB method*) is the most common nowadays. The method consists in replacing final bits in cover message bytes with bits of the embedded-message. The difference between empty and filled cover message has to be imperceptible for the human perception system [4]. The scheme of LSB method is shown in figure 1.

Method of Kutter-Jordan-Bossen

This method is based on the peculiarity of human visual system, which consists in low   susceptibility of a human to changes in brightness of blue color in comparison with red and green colors.
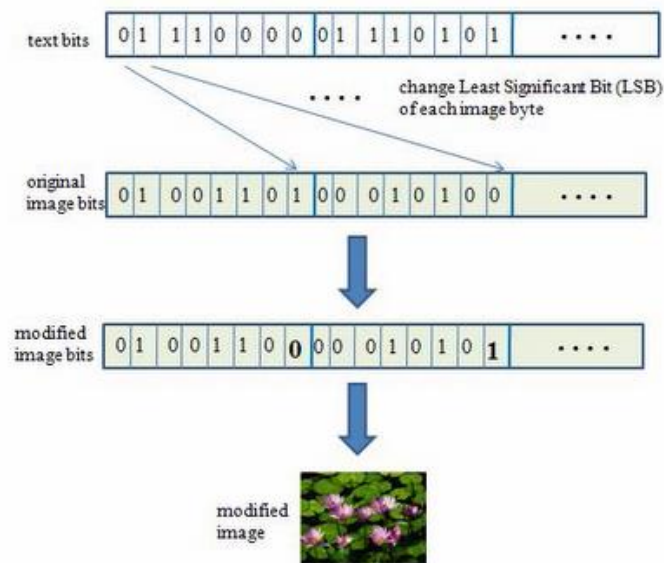
Fig. 1. – The scheme of LSB method

One bit of the embedded-message is written to one pixel of the cover message. The brightness of red and green components of pixel remains unchanged, but the brightness of blue component changes in accordance with the following formula [5]:

$$B_{x,y}^* = \begin{cases} B_{x,y} + \lambda Y_{x,y}, \text{if } m_i = 1, \\ B_{x,y} - \lambda Y_{x,y}, \text{if } m_i = 0, \end{cases} \qquad (1)$$

where $B_{x,y}$ – the brightness of blue component of the pixel with coordinates (x,y);

$B_{x,y}^*$ – the changed brightness of blue component of the pixel with coordinates (x,y);

$Y_{x,y}$ = 0.29890$R_{x,y}$+0.58662$G_{x,y}$+0.11448$B_{x,y}$ – pixel brightness;

$R_{x,y}$ – the brightness of red component of the pixel with coordinates (x,y);

$G_{x,y}$ – the brightness of green component of the pixel with coordinates (x,y);

m_i – i-bit of the embedded-message;

λ = 0.1 – the coefficient setting the energy of the built-in bit of data (it is set depending on the functional purpose and features of steganography system). When λ increases, the embedded-message becomes more apparent, but it is more resistant to distortions.

Since the recipient doesn't have the original image, it is impossible to find out whether the brightness of blue component increased or decreased. Therefore, in order to extract the information, brightness of blue component should be predicted [6]:

$$\overline{B}_{x,y} = \frac{\sum_{i=1}^{\sigma}(B_{x,y+i} + B_{x,y-i} + B_{x+i,y} + B_{x-i,y})}{4\sigma}, \qquad (2)$$

where σ = 1÷3 – the size of the area on which brightness will be predicted.

The following formula is used for extracting the embedded-message:

$$m_i = \begin{cases} 1, \text{if } B_{x,y}^* > \overline{B}_{x,y}, \\ 0, \text{if } B_{x,y}^* < \overline{B}_{x,y}. \end{cases}$$

Koch-Zhao method

Koch-Zhao method uses frequency characteristics of the cover message and consists in relative replacement of the discrete cosine transformation (DCT) coefficients. The image is divided into blocks with dimension 8×8 pixels and DCT is applied to each block. Each block is suitable for recording one information bit [7]. This method has high resistance to image distortion, even to its significant change, but it can't be used for hiding large volumes of data.

Hidden transmission of color images

24-bit bitmap-pictures are used as input images; each color contains 8 bits of information. The data are hidden by using LSB method. The essence of the algorithm is that the secret image is divided into three color primitives (tints of red, green and blue), and then each primitive is put into the least significant bits of one of image containers. Thus, after the data is hidden, each cover message will contain only one color component of the secret image [8-10].

Two most significant bits from each color primitive of the secret image are recorded to the least significant bits of the corresponding color of the corresponding carrier. In figure 2 you can see the illustration of the method of image hiding. Two least significant bits of other colors are nulled. This operation is repeated for each pixel.

To restore the secret image, you need to take the first pixel from each carrier. Two least significant bits of each color component of this pixel are becoming the most significant bits and corresponding color components are added. This operation is repeated for each pixel and secret image is restored.
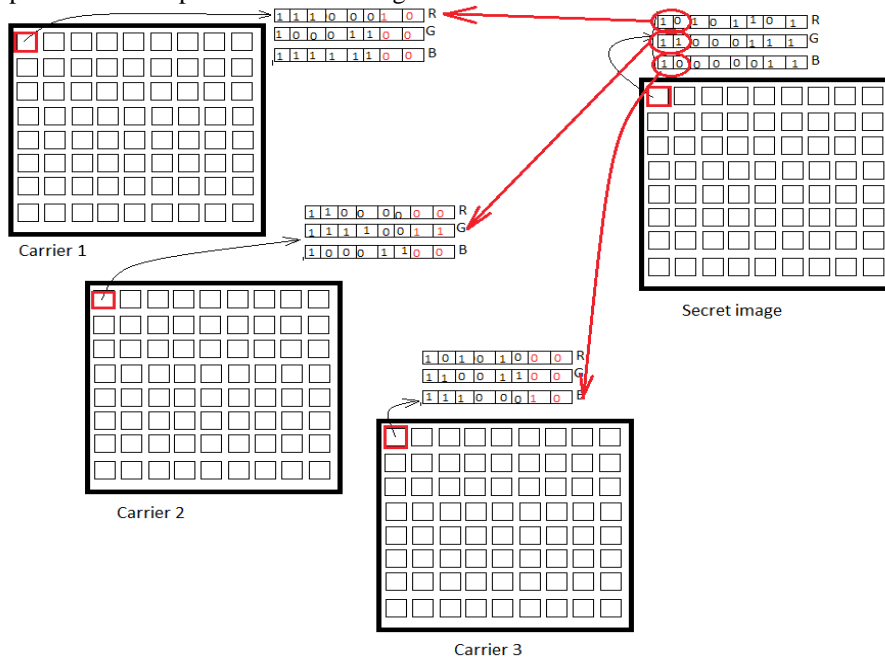
Fig. 2. – Illustration of the method of image hiding

3. Realization of the system

The researched carried out within the frame of bachelor's final qualifying work initiated the development of computer-aided system of data protection, which hides information using steganography methods. This system allows you to select a container for embedding information, to choose an embedding method, to create a stego-file and to extract secret information from the stego-file.

The system performs the following functions:

- embedding text information;
- embedding an image;
- extracting text information;
- extracting an image.

After the system starts, the window for embedding messages opens and the user can click "Load Container" in the menu and select a file to download. The selected image will be displayed on the screen. After that the user has to choose an embedding method, for example, LSB, and click on "Write" button to enter the secret message. After embedding, the user can save the filled cover message. For extraction of the embedded message, it is necessary to pass to "Read the message" tab. Click on "Read" button, select the file, and the secret message appears in the text field.

To hide an image, the user needs to go to the tab "Hide the picture" (see figure 3), to load three containers and the secret image. All images will be displayed in the form. The user needs to select the number of replaceable bits. It influences the quality of the stego-file and the extracted message.
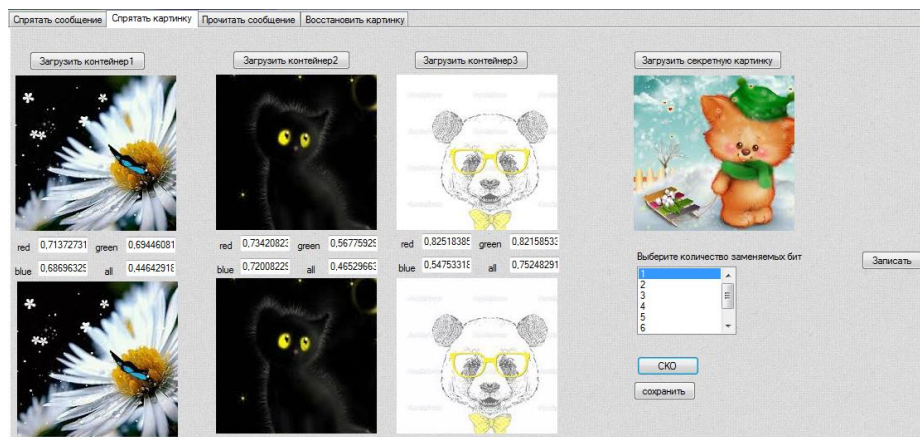
Fig. 3. – Embedding the image using 1 bit of container color

Select the number of replaceable bits which equals 1, press "Save" button and save all of the containers.

To restore the image, it is necessary to pass to tab «Restore image», to load containers and to press «Restore» button.

4. Experimental part

The carried out research demonstrated how the number of replaced bits in RGB components of the container pixels influences the quality of the restored image and container distortion.

Figures 4 - 6 illustrate results of LSB-algorithm with 1, 4 and 8 replaced bits.

It's clear that 1 bit replacement distorts the secret image considerably, but the change of the containers is invisible. When 4 bits are replaced, the secret message is distorted slightly, but embedding can be noticed in the containers. When 8 bits are replaced, the secret image can not be transmitted unnoticed because containers are RGB components of the secret image. Furthermore, when the amount of replaced bits

281

is the same (e.g., 4), the distortion can be seen better in the light container than in the dark one.
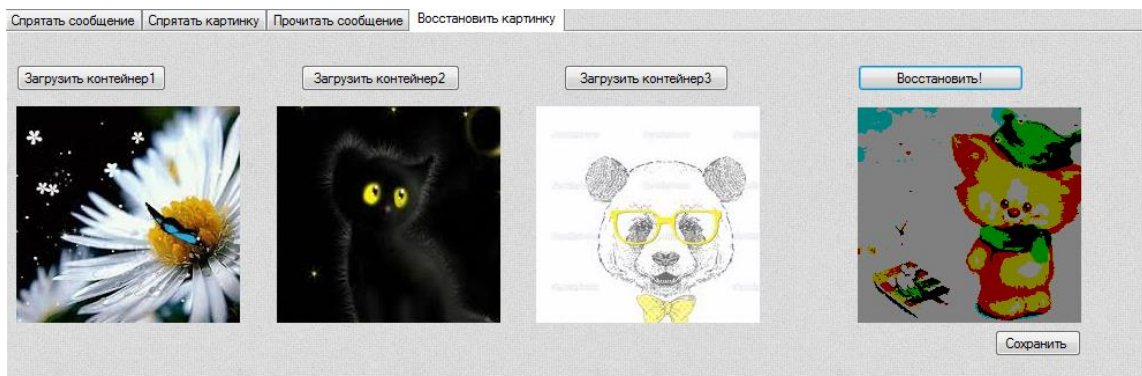
Fig. 4. – Restoring the image with 1 replaced bit
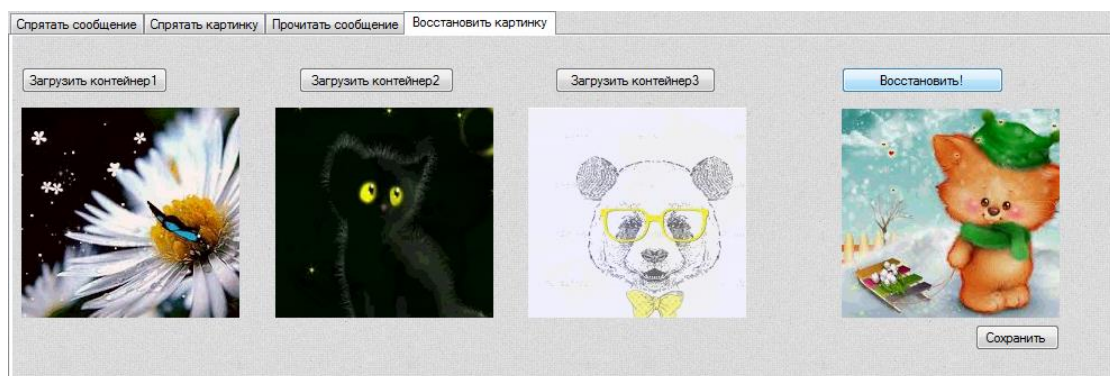
Fig. 5. – Restoring the image with 4 replaced bits
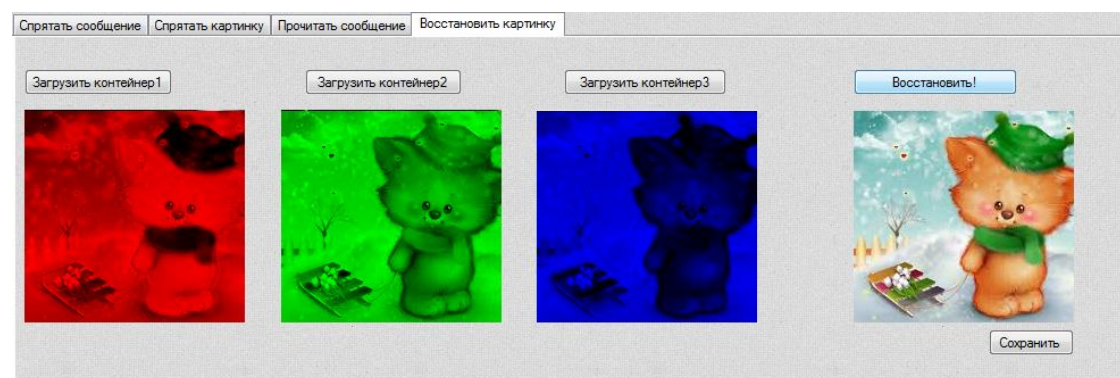
Fig. 6. – Restoring the image with 8 replaced bits

282

Figures 7-8 are dependency graphs which illustrate the relation between mean-square-error of RGB container distortion and the number of replaced bits in containers, presented for the dark and the light image containers respectively.
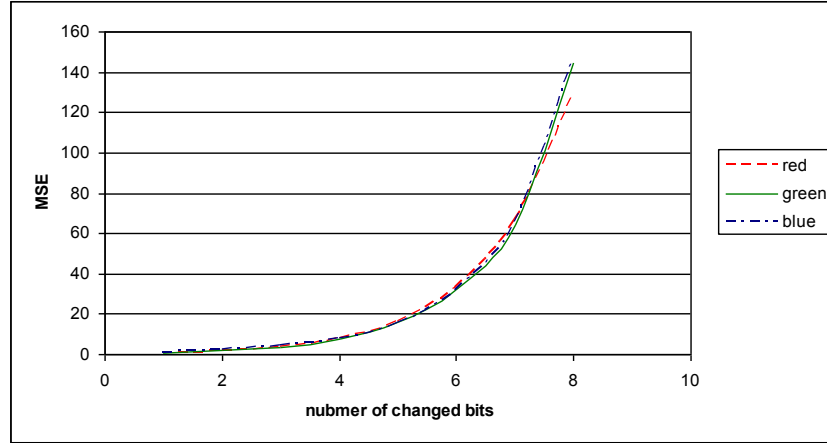
Fig. 7. – Dependency graphs of MSE distortion and the quantity of changed bits for the dark container
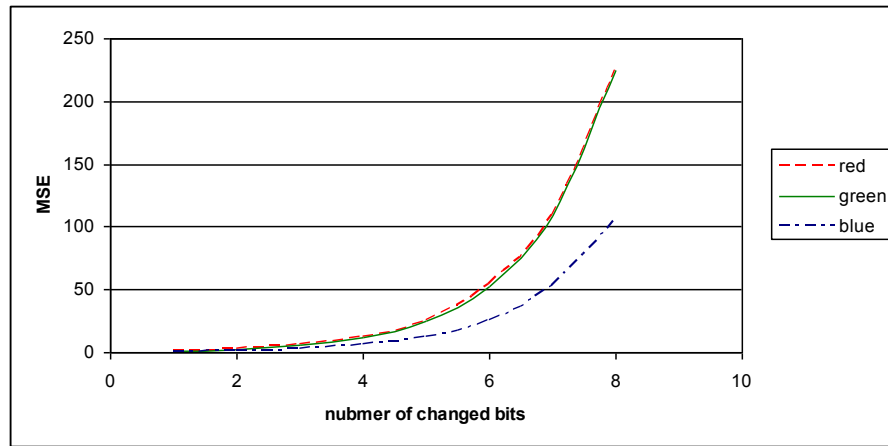
Fig. 8. – Dependency graphs of MSE distortion and the quantity of changed bits for the light container

Mean-square-error (MSE) is calculated using the following formula:

$$MSE = \sqrt{\frac{\sum\limits_{i=1}^{n}\sum\limits_{j=1}^{m}(x_{i,j} - x_{i,j}^{*})^2}{m \cdot n}}, \qquad (3)$$

where n – the length of the image;
m – the width of the image;

283

$x_{i,j}$ − the value of pixel color component of the original image;

$x_{i,j}^{*}$ − the value of pixel color component of the modified image.

The graphs show that the increase in the number of changed bits leads to MSE increase. In addition, it is evident that mean-square-error for the light image is larger than for the dark one.

Thus, it can be concluded that darker images serve better in the function of containers and the number of bits should be restricted to 3-4. Following these recommendations will help to achieve the best balance between the quality of the transmitted image and the degree of distortion of containers.

5. Conclusion

The researched carried out within the frame of bachelor's final qualifying work implied the study of steganography methods and the development of computer-aided system of data protection by means of the following steganography methods: LSB method, Koch-Zhao method, Kutter-Jordan-Bossen method and the method of color bmp images hiding.

References

1. Steganography yesterday, today and tomorrow. Source: <http://www.ess.ru/ sites/default /files/files/articles/1998/0405 /1998_0405_03.pdf >. [in Russian]
2. Basic principles of steganography. Source: <http://citforum.ru/internet/securities/ stegano.shtml>. [in Russian]
3. **Pfitzmann B.** Information hiding terminology. Lecture Notes in Computer Science, 1996; 1174: 347-350.
4. Replacement of the least significant bit, or LSB. Source: <http://www.nestego.ru/2012/07/lsb.html>. [in Russian]
5. Modification of Kutter-Jordan- Bossen method of information hiding. Source: <http: //www.amursu.ru/attachments/article/11563/11.pdf>. [in Russian]
6. Kutter-Jordan-Bossen method of steganography. Source: <http:// habrahabr.ru /post/115287/>. [in Russian]
7. Koch-Zhao method of steganography. Source: <http:// habrahabr.ru /post/216207/>. [in Russian]
8. Visual cryptography for color images. Source: <http://habrahabr.ru /post/121878/>. [in Russian]
9. **Dryuchenko MA, Sirota AA.** Steganography algorithm for information hiding based on spatial deformation of full-color image fragments. Computer Optics, 2014; 38(4): 833-842. [in Russian]
10. **Glumov N, Mitekin V.** A new semi-fragile watermarking algorithm for image authentication and information hiding. Computer Optics, 2011; 35(2): 262-267. [in Russian]

Development of parallel implementation for the dendritic crystallograms modeling algorithm

Paringer R.A., Kupriyanov A.V.

Samara State Aerospace University
Image Processing Systems Institute, Russian Academy of Sciences

Abstract. The paper considers a simulation algorithm for dendritic crystallogram images and offers its parallel implementation using MPI technology. As a basis we took an algorithm using an impurity-and-material-substance diffusion equation. The algorithm used as a guide was upgraded. An impurity redistribution method was changed, and the order of crystallization was updated that allowed to maintain the impurity volume during the crystal growth. A separation technique for algorithm stages was proposed on compute cores. An acceleration value of the proposed MPI-implementation has proven to be 20% more than the OpenMP analogue. The resulting implementation may be used to simulate large crystallograms in shared-memory systems.

1. Introduction

The analysis of medical crystallogram images is an important part of medical diagnostics. Medical crystallograms are the structures formed at crystallization of salts as a result of drying biological liquids (tears, blood, saliva, etc.). Automated processing of crystallogram images will enable to improve the quality of diagnostics and will reduce the time required for a diagnostic procedure [1-4].

It is necessary to simulate the image of the entire drop, therefore in order to speed up the computing it is proposed to use parallel computations, that widely used lately [5, 6]. There are several possible techniques to implement a parallel algorithm. Let us consider two of them: OpenMP and MPI [7]. The OpenMP technique is used for shared-memory systems, and the number of compute cores in such systems rarely exceeds 16, which imposes certain restrictions on the system scaling. The need for MPI implementation arises if you want to simulate a large crystallogram with a fine partition grid.
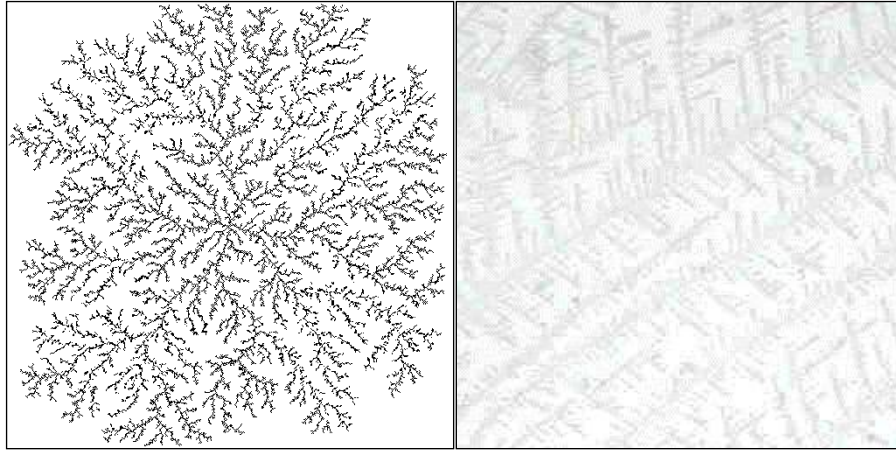
Fig. 1. – Crystallogram image. Simulated (left). Full-scale (right).

2. MPI implementation

The previously described model has been taken as a basis [8]. The OpenMP description of implementation of the simulation algorithm is presented in references below [9]. The model implementation includes consistent application of the following algorithms: diffusion, calculation of crystallization probability, check of material substance quantity, material substance redistribution, impurity redistribution, and crystal dissolution.

One of the model disadvantages is the fact that under certain simulation parameters the impurity conservation law was not executed. The impurity quantity was reduced. Therefore, we used the impurity wave redistribution: the entire impurity in a crystallized cell was redistributed to neighboring cells of different orders. To evaluate the possibility of performing such distribution we had to add the check of impurity quantity; it determines whether the remaining volume will be enough to store the impurity displaced during crystallization.

The second disadvantage is the fact that the crystal dissolution is performed after crystallization and, accordingly, after the check of the material substance quantity available for crystallization that lead to skipping some crystallization stages and to reducing the crystal growth. Therefore, we have changed the order of these actions. First, the crystals are dissolved, and then crystallization is performed, thus the amount of the material substance available for crystallization increases. This change did not lead to significant differences in a crystal shape, but it allowed to reduce the time of the crystal growth up to 2% of the total time. The obtained algorithm is schematically shown in Figure 2.
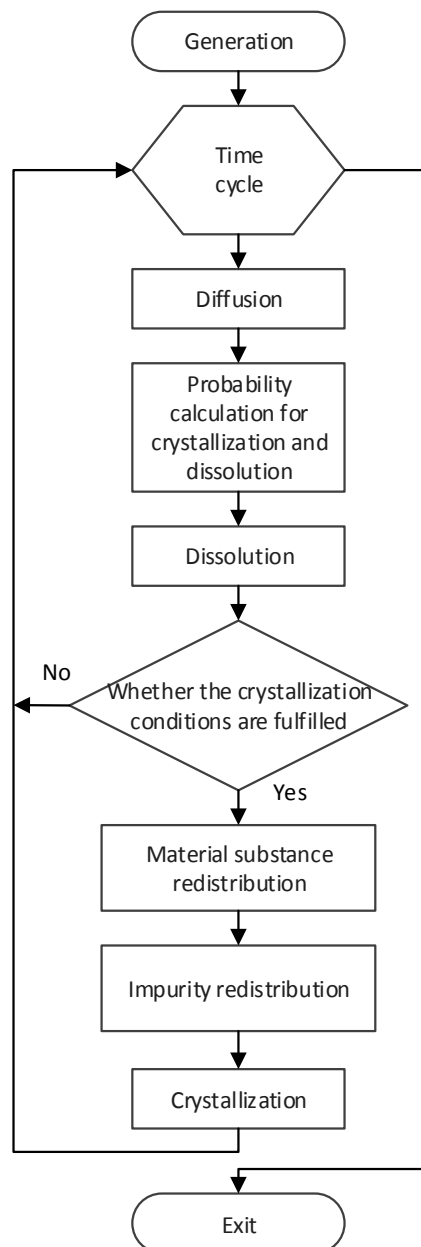
Fig. 2. – Crystallogram simulation algorithm

Table 1 shows the dependence of the relative operation time of algorithm stages on the image size. It should be noted that the longest time is taken by diffusion of the material substance, however since an explicit scheme is used, the diffusion algorithm may be split up at each stage.

Table 1. Dependence of a relative operation time of algorithm stages on the image size

Algorithm stage	Image size			
	512×512	1024×1024	2048×2048	4096×4096
Diffusion	0.27	0.32	0.30	0.33
Probability calculation	0.16	0.18	0.17	0.19
Dissolution	0.04	0.04	0.04	0.04
Crystallization condition test	0.09	0.08	0.08	0.08
Impurity redistribution	0.23	0.18	0.18	0.17
Material substance redistribution	0.15	0.14	0.15	0.14
Crystallization	0.06	0.06	0.06	0.06

The parallel implementation in MPI is carried out by the exchange of messages between compute cores. The acceleration takes place due to the fact that independent operations are also performed in parallel, but a part time is spent to transfer data between calculators. Therefore, the less operations of the message exchange, the greater the efficiency of the parallel program.

In the parallel implementation of the algorithm in each time cycle iteration (except the first one) the data are to be casted after the impurity redistribution, and the computing results are to be collected before the operation of material substance redistribution, but only if the crystallization conditions are satisfied. The "Material substance redistribution" and the "Impurity redistribution" methods, due to implementation features (i.e. use of wave redistribution), may not be efficiently parallelized using MPI, since it will require a large number of transmissions. Therefore, the "Material substance redistribution" and the "Impurity redistribution" methods are executed sequentially, but in different flows, since they use independent data.

Acceleration results of the obtained program implementation are shown in Table 2. The resulting acceleration values were 20% higher than in a similar paper using the OpenMP technology [8].

Table 2. Dependence of the acceleration on the number of cores and the image size

Image size	Number of compute cores						
	2	3	4	5	6	7	8
512×512	1.67	2.06	2.34	2.54	2.70	2.82	2.93
1024×1024	1.74	2.22	2.57	2.85	3.07	3.25	3.40
2048×2048	1.75	2.23	2.59	2.86	3.08	3.26	3.40
4096×4096	1.76	2.26	2.65	2.94	3.18	3.38	3.54

3. Conclusion

A parallel algorithm for the simulation of dendritic crystallograms was presented. It was described a modification of the existing sequential algorithm taking into account the chosen technology of parallelization. The resulting implementation turned out to be 20% faster than the OpenMP implementation. The developed algorithm can be used to simulate the high-resolution images crystallograms.

References

1. **Denisov AB.** Crystal structures of the oral fluid. Message 1. The estimation method of crystal figures obtained on drying mixed saliva. Dental forum, 2011; 37(1): 50-54.
2. **Shabalin VN, Shatokhina SN.** The morphology of human biological fluids. Chrysostom, 2001; 304 p.
3. **Volchetsky AL, Ruvinova LG, Spasennikov BA, Zenovsky VP.** Crystallization and crystallography: Biomedical aspects. Arkhangelsk: Pomorsky State University Publishing House, 1999; 190 p.
4. **Martusevitch AK.** The crystallographic analysis: general characteristics. The Vyatsk Medical Bulletin, 2002; 3: 59-61.
5. **Vorotnikova DG, Golovashkin DL.** Long vectors algorithms for solving grid equations of explicit difference schemes. Computer Optics, 2015; 39(1): 87-93. [in Russian]
6. **Zhdanov AI, Sidorov YV.** Parallel implementation of a randomized regularized Kaczmarz's algorithm. Computer Optics, 2015; 39(4): 536-541. [in Russian]
7. **Antonov AS.** MPI and OpenMP Multiprogramming technologies. Moscow State University Publishing House, 2012; 344 p.
8. **Baranov VG, Khramov AG.** Simulation of the growth process of dendritic crystal structures. Computer Optics, 2001; 21: 193-197. [in Russian]
9. **Khalirakhmanov DI, Mayakova SA.** Parallel algorithm of the growth simulation of dendritic crystal structures. Proceedings of the International Conference "Parallel Computing Technologies 2012", 2012; 704–710.

Researching methods of reconstruction of three-dimensional crystal lattice from images of projections

Shirokanev A.S.,

Samara State Aerospace University

Kirsh D.V., Kupriyanov A.V.

Samara State Aerospace University
Image Processing Systems Institute, Russian Academy of Sciences

Abstract. The paper presents the developed algorithms for the reconstruction of multiple crystal lattice sites. The study was conducted with a set of crystal lattices and the developed method of modeling a three-dimensional structure of ideal crystal lattice sites. The results of the reconstruction of three-dimensional structures of lattice sites are shown using different metrics comparison. Comparative characteristics of accuracy of the algorithms are given in the paper.

Introduction

Nowadays, a great number of publications are devoted to reconstruction methods for three-dimensional structures [1-5]. In particular, an important stage in the study of the atomic structure of the matter is the development of mathematical methods for the reconstruction of the spatial structure of the matter on two-dimensional images obtained by electron microscopy [6, 7]. The development of these methods is crucial in the study of materials with ordered structure, called crystals [8].

The purpose of the work is to develop algorithms for the reconstruction of the crystal lattice and research the developed algorithms using image comparison metrics.

Modeling an ideal crystal lattice

A model crystal lattice can be described by the Bravais lattice. A comprehensive description of the Bravais lattice is a unit cell, represented in the form of three non-

coplanar translation vectors [9]. The main parameters adopted in crystallography, are the length of the translation vectors: a, b, and c, and the angles between the vectors: α, β, and γ. Additionally, we define the starting and ending indices: I_0, J_0, K_0, I_1, J_1, and K_1 of sites on each axis as the input parameters for modeling a set of crystal lattices.

To construct a model of a crystal lattice, we need to know the translation vectors [10]. The developed method allows us to compute the translation vectors by the parameters adopted in crystallography. The method allows us to specify the range of angles, in which the model of the lattice would be correct.

Knowing the translation vectors, we can generate a set of points corresponding to the crystal lattice. We can do that by specifying the range of variation of integers: I_0, J_0, K_0 and I_1, J_1, K_1.

From the geometry of a unit cell, the corners α, β, and γ can take values from the ranges:

$$\alpha \in (0,\pi), \;\; \beta \in (0,\pi),$$

$$\gamma \in \{\varphi : \cos\varphi \in (\cos(\alpha+\beta),\cos(\alpha-\beta))\} \cap (0,\pi).$$

The limitation on the angle γ can be represented as (1).

$$\gamma \in \left[\min(a_1,a_2), \max(a_1,a_2) \right], \tag{1}$$

where $a_1 = \left(\{2\pi - (\alpha+\beta)\} \cup \{\alpha+\beta\} \right) \cap (0,\pi)$,

$a_2 = |\alpha - \beta|$.

The condition (1) limits the angle γ of the segment that allows us to generate a random lattice on the set parameters adopted in crystallography.

The developed method makes it possible to generate a three-dimensional set of sites representing a Bravais lattice [9]. In practice, the method is useful for studying a large set of crystal lattices. The set of sites is generated automatically. Lattices, which the algorithm works poorly with, are also detected automatically.

Algorithms of reconstruction of sets of sites of a crystal lattice.

Back-projection algorithm – the reverse process to the algorithm for projecting a three-dimensional image on a plane. The reconstruction algorithm receives image projections and their position in the space as input parameters. The result of the algorithm is a three-dimensional image, which is a set of points in the space or, to put it mathematically, a finite set of points in a three-dimensional space [11].

The main task of the reconstruction algorithms – to restore an image, approximating the "total picture".

Reconstruction algorithm based on grid partitioning of a line

The first back-projection algorithm based on grid partitioning of a straight line means that each line recoverable from a non-zero point of a preselected projection, is split into a grid. Grid points are projected onto the plane of the other projections. Then the number of projections, which the site falls in, are counted [11].

If a three-dimensional point is projected onto a plane (by ignoring one component of the radius vector), then it can be reconstructed ambiguously (along the line). In other words, the inverse operator of the projection should be replaced by a functional of the following form (2).

$$\varphi^{-1}(x) = A\left[\begin{pmatrix} 1 & 0 \\ 0 & 0 \\ 0 & 1 \end{pmatrix} x + \begin{pmatrix} 0 \\ C \\ 0 \end{pmatrix}\right], C \in \Re . \tag{2}$$

The basic logic of the algorithm can be described in the form of the equation (3).

$$S(x) = \left|\left\{ k : R_k(\varphi_k x) > 0 \wedge k = 1,...,i-1,i+1,...,n \right\}\right|, \tag{3}$$

where φ_k – projection operator, R_k – two-dimensional function (ray transform).

We get a lot of points on the line for each point with non-zero intensity, which lies on the main projection, using the inverse operator (2). The continuous line is limited to the grid. This means that the varied variable belongs to the multitude of $D_h^n \subset \Re_h^n$

Then the corresponding points are projected onto the planes of the other projections. In other words, the points of the line are substituted in the right side of formula (3).

The algorithm has a number of drawbacks. The sampling of the line leads directly to the non-accuracy of the algorithm, and decreasing the sampling step affects the speed of the algorithm.

Reconstruction algorithm based on minimizing distance

The second algorithm eliminates these disadvantages. The construction of the algorithm is based on solving the problem of minimizing the distance between the point with non-zero intensity that lies on some projection and the line projected on the plane of the projection from the line recoverable from a non-zero point of some main projection [11].

This algorithm works with three-dimensional geometry. That means that all points on the projections should be previously converted into three-dimensional space, and all normal of the projections for them must be found.

To find a recoverable point, one should carry out the following procedure:

1. Find the parameter using the formula (4).

$$t = \frac{(n, z_{on})(n, n_{on}) - (z_{on} - z, n_{on})}{\left(\|n_{on}\|^2 - (n, n_{on})^2 \right)}, \tag{4}$$

where n_{on} – normal to the plane of the main projection,

z_{on} – point on the main projection,

n – plane normal to the projection of interest,

z – point on the projection of interest.

2. Find point x using the formula (5).

$$x = n_{on}t + z_{on},$$ (5)

where n_{on} − normal to the plane of the support projections,

z_{on} − point on the main projection,

t − found by the formula (4).

3. Determine whether the point is recoverable. To do this, we use the condition (6).

$$d^2 = D_\gamma^2 - D^2 = (x-z, x-z) - (n,x)^2 < \varepsilon^2(h),$$ (6)

where x − recoverable point,

z − point lying on the projection of interest,

n − plane normal to the projection of interest.

The result of the algorithm is a set of three-dimensional points of a recoverable set of the crystal lattice.

The algorithm works with the points of non-zero intensity; that allows speeding up the recovery of the crystal lattice. Due to use of analytical computation of recoverable points, the algorithm has a higher accuracy than the first one.

The recovered set represents a certain distribution of probabilities. Thus the set can undergo further filtration to obtain the final estimate of the original set. In this work, the filter based on the clustering algorithm distinguishing a "cloud" of points was used.

Metrics of comparison of sets of spatial points

The metric called Hausdorff distance (or Hausdorff metric) is well-known among many comparison metrics of sets [12]. Let E and F − non-empty compact subsets of R^n. Hausdorff distance between E and F will be determined by the formula (7).

$$H(E, F) = \max\{d(E,F), d(F,E)\},$$ (7)

where $d(E, F) = \sup_{x \in X} \inf_{y \in Y} d(x, y)$.

To compute the Hausdorff metric for finite sets, it is sufficient to run a computation by the formula (8).

$$H(E, F) = \max\{\overline{d}(E,F), \overline{d}(F,E)\},$$ (8)

where $\overline{d}(E, F) = \max_{i:x_i \in E} \min_{j:y_j \in F} d(x_i, y_j)$.

Metric quaternion signals have been analyzed in addition to the Hausdorff metric [13]. The metric is based on finding polynomial coefficients, which are polynomial function of a hyper variable.

The coefficients of the polynomial a_m can be found by using the least squares method. By solving the problem of minimizing the total error of the approximation, we obtain a system of linear quaternion equations, which can be solved directly using the Gauss method or reduced to solving a system of equations with real coefficients [13].

293

A value that characterizes the measure of similarity between objects can be the result of a scalar multiplication of the coefficients of the polynomial of the reference and processed objects. It can be defined by the formula (9).

$$\eta = \sum_{m=0}^{M-1} a_m a_m^{*(\mathfrak{I})} . \tag{9}$$

Researching reconstruction algorithms

For the experiment, the set is projected onto the projection plane. Then the reconstruction algorithm is executed. The result set is compared to the reference using the metrics of comparison. By the results of the experiment, we can draw conclusions on the quality of the algorithm.

Let's define the "pseudo image" as the result of the back-projection algorithm. Each site of the recovered lattice has a pseudocolor, that is, a color corresponding to the number of projections, in which the site can be projected. [11]

Figure 1 shows the results of the reconstruction using the first and the second algorithms by the example of the triclinic lattice. The blue color indicates a site that enters the two projections of the three, and red – all three projections. The result recovered with the first algorithm contains errors related to splitting the line. The second algorithm recovers the lattice sites much better.
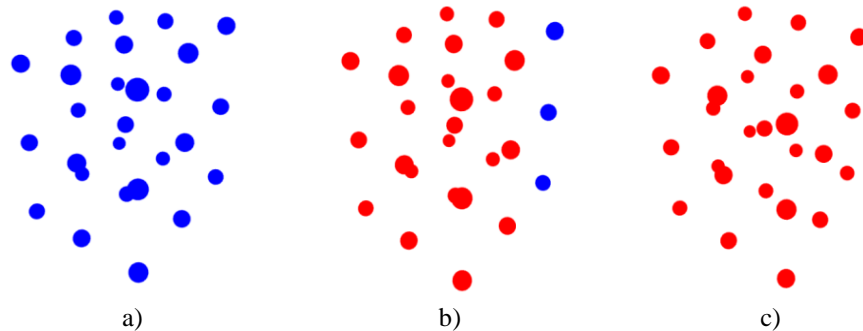
Fig. 1. – Comparing the work of the reconstruction algorithms: a) reference image; b) reconstructed image by the algorithm based on grid partitioning; c) reconstructed image by an algorithm based on minimizing the distance

Clustering-based filter applied to the result demonstrates good performance in examples with grids with frequent congestions (clouds) of sites. Figure 2 shows the result of the clustering algorithm by the example of the triclinic lattice.

a)   b)
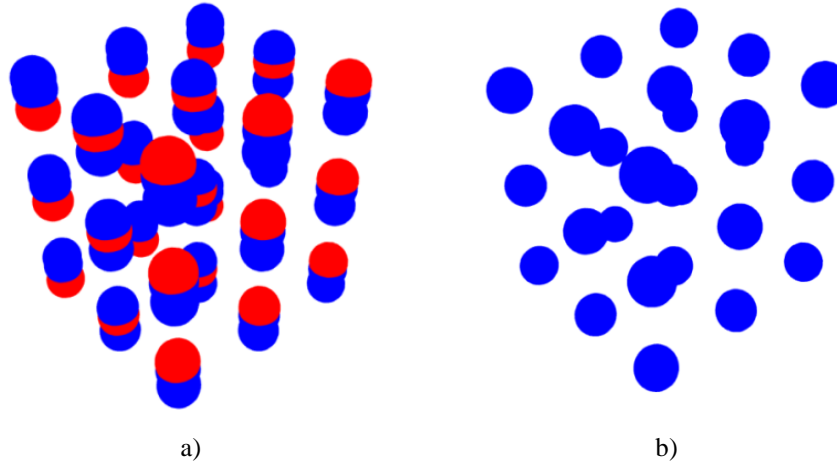
Fig. 2. – The result of processing the image by the filter based on the clustering algorithm: a) image reconstructed by the reconstruction algorithm; b) the processed image

The analysis of the first two algorithms on all crystal system arrays using both metrics discussed in this paper is presented in the form of quantitative results of recovering the structure of lattice sites by each algorithm (Table 1).

Table 1. Researching reconstruction algorithms

Crystal system primitive lattice	Hausdorff metric		Metric quaternion signals	
	The algorithm based on grid partition	The algorithm is based on finding the minimum distance	The algorithm based on grid partition	The algorithm is based on finding the minimum distance
Cubic	0.100	0.000	0.0007	0.0000
Tetragonal	0.100	0.000	0.0008	0.0000
Hexagonal	1.001	1.001	0.0008	0.0003
Trigonal	0.480	0.480	0.0007	0.0002
Orthorhombic	0.100	0.000	0.0010	0.0001
Monoclinic	1.870	0.751	0.0007	0.0003
Triclinic	0.110	0.107	0.0005	0.0002

Comparing the results of the first and second columns with the Hausdorff metric and the third and the fourth columns with the metric of quaternion signals of Table 1, we can be convinced that the second algorithm recovers the image more accurately than the first one. Both metrics generally show a lower value for the case of the second algorithm. This means that the image recovered by the second algorithm is more similar to the reference image.

295

The results of the research

The studies have shown that the algorithm based on the minimization of the distance more accurately reconstructs the lattice structure than the algorithm based on the partitioning grid line. The reconstruction algorithms can be used for recovering three-dimensional models of crystal lattices. Modifications in the recovery procedures in some cases can increase the accuracy of the reconstruction of the object. Thus, the algorithms that operate with sets of sites work better than the algorithms that resort to approximations.

Acknowledgements

References.

1. **Kharitonov SI, Volotovskiy SG, Khonina SN, Kazanskiy NL.** A differential method for calculating x-ray diffraction by crystals: scalar theory. Computer Optics, 2015; 39(4): 469-479. [in Russian]

2. **Kotov AP, Fursov VA, Goshin YeV.** Technology for fast 3d-scene reconstruction from stereo images. Computer Optics, 2015; 39(4): 600-605. [in Russian]

3. **Fursov VA, Goshin YeV.** Information technology for digital terrain model reconstruction from stereo images. Computer Optics, 2014; 38(2): 335-342. [in Russian]

4. **Bessmeltsev VP, Bulushev ED.** Fast image registration algorithm for automated inspection of laser micromachining. Computer Optics, 2014; 38(2): 343-350. [in Russian]

5. **Kudinov IA, Pavlov OV, Kholopov IS.** Implementation of an algorithm for determining the spatial coordinates and the angular orientation of an object based on reference marks, using information from a single camera. Computer Optics, 2015; 39(3): 413-419. [in Russian]

6. **Rad LB, Feng H, Ye J, Pease RFW.** Computational scanning electron microscopy. Proceedings of the 2013 international conference on frontiers of characterization and metrology for nanoelectronics, 2007; 512-517.

7. **Frank J.** Electron tomography. Albany: Springer Science+Business Media, 2006; 455 p.

8. **Kupriyanov AV, Soifer VA.** On the observability of the crystal lattice with the images of their projections. Computer Optics, 2012; 36(2): 249-256. [in Russian]

9. **Egorov-Tismenko YuK.** Crystallography and crystal chemistry. Moscow: KDU, 2005; 592 p. [in Russian]

10. **Kupriyanov AV, Kirsh DV.** Estimating the similarity measure of crystal lattices by coordinates of their nodes in three-dimensional space. Computer Optics, 2012; 36(4): 590-595. [in Russian]

11. **Shirokanev AS, Kupriyanov AV.** Development methods of reconstruction of three-dimensional crystal lattice from images of projections. Advanced Information

Technologies and Scientific Computing (PIT 2015), Proceedings of the International Scientific Conference. Samara Scientific Center of RAS, 2015; 2: 334-337. [in Russian]

12. **Kronover RM.** Fractals and chaos in dynamical systems. Fundamentals of the theory. Moscow: Postmarket, 2000; 92-94. [in Russian]

13. **Rozhentsov AA, Bayev AA, Naumov AS.** Estimation of parameters and recognition of images of three-dimensional objects with disordered readouts. Journal of Mari State Technical University. Radio engineering and information and communication systems, 2010; 2(1): 57-69. [in Russian]

Information-theoretic preprocessing method for computer vision systems

Tananykina L.V.

Research Institute of Applied Problems, Saint-Petersburg

Abstract. The aim of the research is finding an image obtaining method which is invariant to shooting conditions for further application of correlation-extremal matching method in technical vision systems. The method based on entropy analysis is offered. Some testings of the method were carried out; images obtained in different conditions were used. The tests showed that preprocessed images have more stable correlation coefficient than original images.

Keywords: image preprocessing, technical vision, correlation systems, entropy analysis

1. Introduction

Preprocessing methods are commonly used in present-day data analysis techniques. The main task in computer vision systems is obtaining images invariant to the capturing conditions or the physical nature of the sensor.

Main features which determine image internal structure are: bright points, lines, object edges, regions. In general they may be defined by brightness, color or texture contrast; and the direction (gradient) of the brightness difference (dark/light object on light/dark background) or of the color difference is also a-priori undefined.

It is difficult to use recognition procedures like correlation detector in case when images were captured at dissimilar conditions. But methods based on structural analysis are also insolvent in that case.

The information-theoretic image preprocessing method is offered for solving problems of comparison between images which differ in type of presentation or capturing conditions. The method effectiveness is demonstrated.

2. Image correlation analysis. Formulation of the problem

One of the typical objectives in technical vision is element-wise matching of two images of one object which were captured by different sensors or images captured by the same sensor but under different conditions or at different time. To make such a

comparison we should do mutual binding of the images and compensate shifts, rotations, geometric and brightness distortions etc.

The classic way of finding superimposition of the pair of functions (to match pair of functions) is to find meaning of value measured correlation between these functions, and find position of the maximum of the correlation function.

For example, we need to match aerial photograph and topographic map of the same area (figure 1).

a)

b)
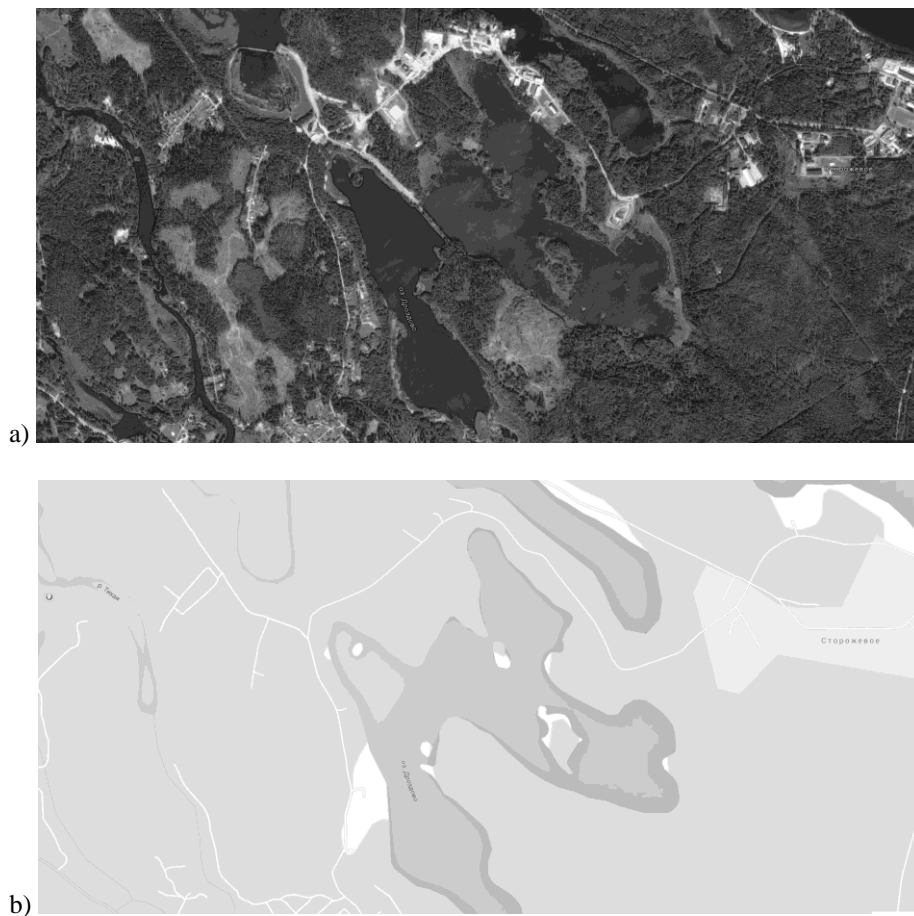
Fig. 1. – Images: a) aerial photograph; b) topographic map

Figure 2 shows the normalized cross-correlation function of the images.

The figure shows that the function has several peaks (two equal-amplitude maxima). The positions of both peaks are different from zero; although in this example images have zero shift. This example shows that the correlation-extreme method has serious limitations on the types of the compared images.

299
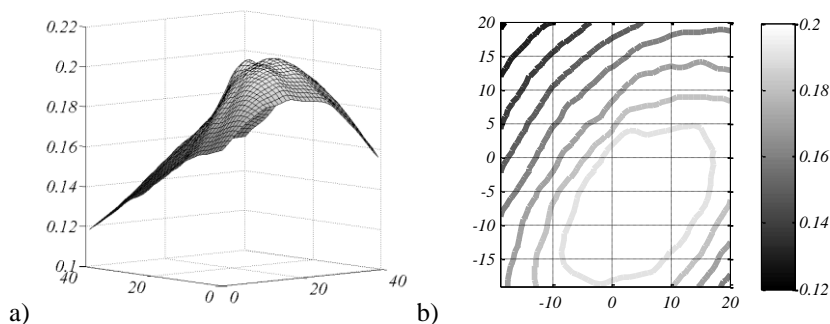
Fig. 2. – Normalized cross-correlation function of the images from fig.1

As usual, methods of structural analysis are used for image matching. For example, specific points are detected and compared. But even for shifted images of the same type specific points can be different. Consequently, some special points may not have a pair, or the specific points in the pair will have a slightly different spatial position. In the case of dissimilar images special points will be unique for each image.

There is one thing that we should take into consideration: correlation-extremal method gives more precise solution than structural methods. Besides, there are effective algorithms and hardware for image correlation analysis which are already used.

That's why it is of great interest to adapt correlation-extremal method for matching dissimilar images. It's offered to use preprocessing method based on entropy analysis. To be more correct it is offered to substitute image with its' local entropy map, because local entropy map is more resistant to the effects of the factors we studied (as will be shown below).

3. Image preprocessing method based on entropy analysis

The solution of the problem is achieved by using the method of image preprocessing based on by taking into account existing internal statistical relationships between image elements. This decision is based on the assumption that statistically interconnected elements in a changing conditions of image capturing are statistically related.

Information-theoretic methods are used for identification of internal statistical relations in any type of data. To adapt correlation-extremal method for matching dissimilar images it is proposed to do entropy analysis of the images, namely to calculate local entropy maps of the images.

The image is considered as a realization of random process. Local entropy (H_i) characterizes the degree of surprise happening of i-th event (occurrence). The less its' a-priori probability is, the greater its' local entropy.

Let's define what is implied under "event". An event (e) is a specific brightness of the pixel. To calculate the probability of event e ($p(e)$) we should count the number of

300

occurrences of the combination over the defined area $M \times N$ (or entire image) and divide by the total number of considered pixels.

The output image is formed by replacing each pixel with value, calculated according to the formula of local entropy (i.e. local entropy map is calculated):

$$Y(i, j) = -\sum_{m=-(M-1)/2}^{(M-1)/2} \sum_{n=-(N-1)/2}^{(N-1)/2} p(e_{i+m, j+n}) \cdot \log(p(e_{i+m, j+n})) . \qquad (1)$$

Figure 3 shows local entropy maps of images from fig.1.

a)

b)
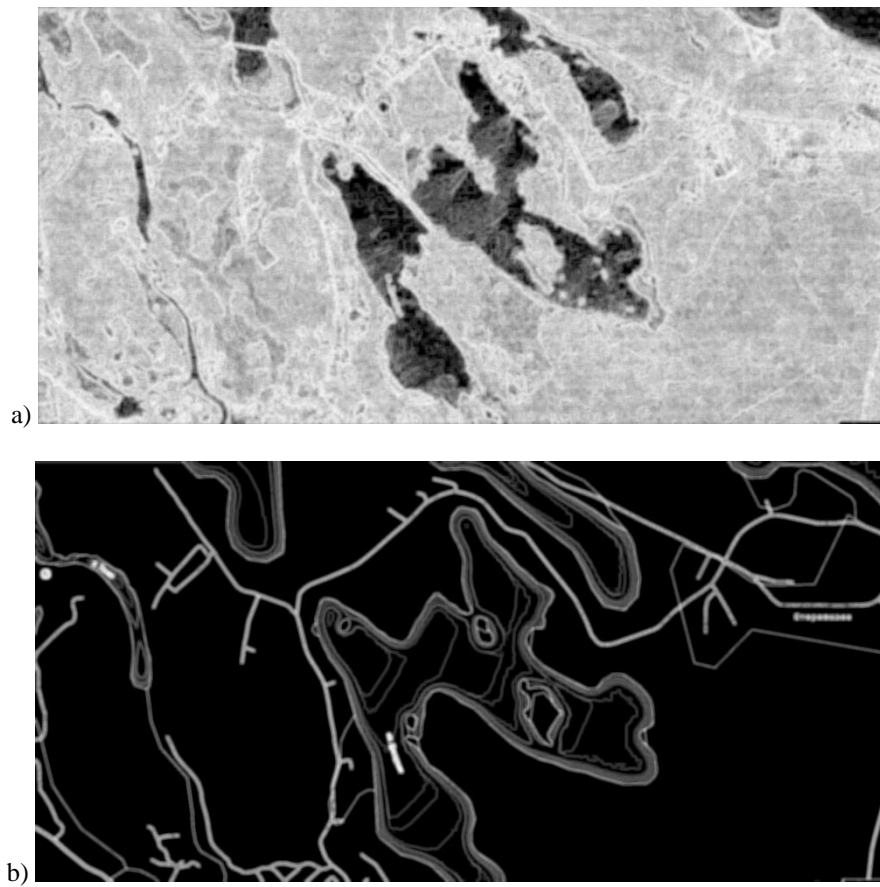
Fig. 3. – Local entropy maps: a) photo; b) map

Figure 4 shows normalized cross-correlation function of the local entropy. As we can see from the figure, the correlation function has a strongly marked maximum corresponding to zero shift.

301
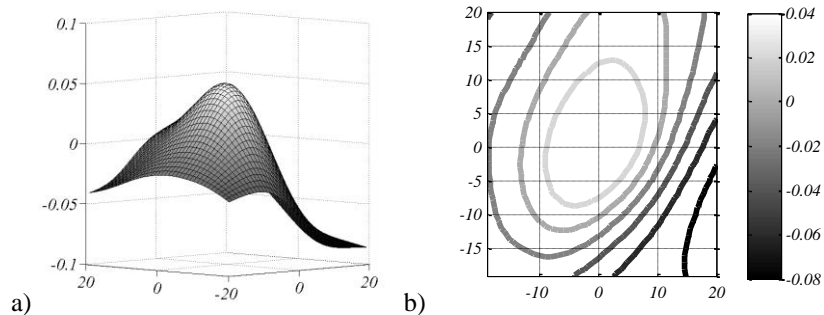
Fig. 4. – Normalized cross-correlation function of the images from fig.3

Similar results were obtained using other test images: maps and aerospace photographs, photographs in winter and in summer, optical and infrared photographs. Test images after preprocessing demonstrate greater correlation coefficient and smoother correlation function than original images.

Thus, the entropy preprocessing method can be recommended for application in the correlation-extreme image matching for two reasons:

— it increases the correlation between dissimilar images;
— correlation function of entropy maps is smoother than the correlation function of the original images, whereby it is possible to significantly reduce the amount of computation to find the extremum.

4. Conclusion

The advantages of the correlation analysis are: this technology has been worked out many times before; there are fast algorithms to calculate correlation and hardware-based solutions. Currently it is of great interest to develop simple and cheap correlation vision systems implemented as special processors.

The aim of this paper was to use correlation method for image matching but in difficult conditions. Information-theoretic preprocessing technology allows comparing images more effective and correct. Researches of the method based on local entropy have shown that dissimilar images of the same scene have greater correlation coefficient after preprocessing. Developed method allows matching the following types of images automatically:

— aerial photographs captured at different times;
— aerial photographs and topographic map;
— optical and infrared images.

Thus, the application of developed method will significantly expand the application area of the correlation-extreme image matching method in computer vision systems.

References

1. **Tsvetkov OV, Polivanayte LV, Kutsenko SA, Repina MV.** Simple highly informative image quality metrics in biomedical systems. Biotechnosphere, 2014; 1-2(31-32): 55-57.
2. **Syrjamkin VI.** Correlation-extremal radionavigation systems. Tomsk: Tomsky University Publisher, 2010.
3. **Pratt WK.** Digital image processing. New York: Wiley-Interscience, 1982.
4. **Kullback S.** Information theory and statistics. Gloucester: PeterSmith, 1978.

Research and development of the classification algorithm based on the method of reference planes

Goshin Ye.V., Loshkareva G.E.,

Samara State Aerospace University

Fursov V.A.

Samara State Aerospace University
Image Processing Systems Institute, Russian Academy of Sciences

Abstract. In this paper a classification algorithm for hyperspectral images based on the reference planes using the values of the contingency table is developed and researched. We propose a new procedure for generating the reference planes. The training vectors areformed with the use of vectors from other classes. The results of experiments on the test image are given.

1. Introduction

Thematic classification of hyperspectral images is gaining popularity. Studies in remote sensing are useful in many fields such as agriculture, mineralogy, physics, surveillance, forensics etc. Remote sensing of the Earth surface allows us to survey the productivity of the lands, forest fires, construction of roadsand various objects.

The most widely used algorithms of thematic classification for solving the above problems are based on methods of spectral angle and support vector machine (SVM). This paper presents a classification algorithm based on the method of reference planes using the values of the conjugacy indices.

2. Statement of the problem

The source data is a hyperspectral image obtained by remote sensing [1]. It is a data structure in which intensity values are stored with the coordinates X, Y, Z, which includes spatial coordinates (X, Y) and spectral coordinates (Z). The objective is to find the given object in this hyperspectral image.

It is assumed that each of spatial coordinates of the hyperspectral image belongsto one of K classes. Each class represents some object (for example, field of corn, field of wheat, roads, etc.).

3. Description of the classification algorithm

To describe the algorithm, consider the kth class. In this class we will choose the reference plane X_k [2] consisting of a pair of hypervectors. For selected reference plane k class index of conjugacy [3] with the vectors from other classes can be calculated with the following expression:

$$R_k(j) = \frac{\mathbf{x}_j^T \mathbf{Q}_k \mathbf{x}_j}{\mathbf{x}_j^T \mathbf{x}_j}$$

where $\mathbf{Q}_k = \mathbf{X}_k \left[\mathbf{X}_k^T \mathbf{X}_k \right]^{-1} \mathbf{X}_k^T$, $\mathbf{x}_j$ is vector j from the class $n \neq k$, $j = 1,…,N_n$. Thus, we have N_n values of conjugacy indices R_k. For these indices the root-mean-square (RMS) value can be calculated as following

$$\mathbf{R}_{mean}(n) = \sqrt{\frac{(R_j)^2}{N_n}}$$

where $n = (1,…,K) \setminus k$. Next, we do the same with the remaining classes. For all remaining $K-1$ values $\mathbf{R}_{mean}$, we calculate RMS value

$$\mathbf{R}(i) = \sqrt{\frac{(\mathbf{R}_{mean}(n))^2}{K-1}}$$

where $n = (1,…,K) \setminus k$, $i = 1,…,C_{N_n}^2$.

Further, we similarly define conjugacy indicesfor all planes X_k of kth class and calculate $C_{N_n}^2$ values of $\mathbf{R}(i)$, where $i = 1,…,C_{N_n}^2$. Then the minimum value $\mathbf{R}(i)$ is sought among them

$$R = \min_{i=1,C_{N_n}^2} \mathbf{R}(i).$$

The hyperplane which corresponds to the received minimum value $\mathbf{R}$ is stored. Let us denote it as $\mathbf{Y}_k$. Thus, we get the reference plane with the highest value of the conjugacy index with its class. This plane allows us to effectively recognize the chosen class. At the same time, it will be less responsive to vectorsof other classes. This allows us to enhance the effectivity of the hyperspectral images classification.

On recognition stage [4] it is necessary to choose the minimum threshold of conjugacy. It is performed by calculating the conjugacy indiceswith the reference plane $\mathbf{Y}_k$

$$R_Y(m) = \frac{\mathbf{x}_m^T \mathbf{Q}_Y \mathbf{x}_m}{\mathbf{x}_m^T \mathbf{x}_m},$$

where $\mathbf{Q}_Y = \mathbf{Y}_k \left[\mathbf{Y}_k^T \mathbf{Y}_k \right]^{-1} \mathbf{Y}_k^T$, $\mathbf{x}_m$ is vector m from class k, $m = 1,\ldots,N_k$, and N_k is the number of vectors in class k. The N_k values obtained from this procedure are sorted in ascending order. Then first (lowest) or N^{th} value from ordered sequence of R_Y is chosen.

4. The results of the experiment

The algorithm was tested on a Salinastest image from open dataset of hyperspectral image MultiSpec. This image was obtained within AVIRIS program (AirborneVisible/ InfraredImagingSpectrometer). The image size is 512×217 hyperpixels. Each hyperpixelhas 224 spectral bands. A sample of hyperspectral layer and classified test image are shown in figures 1a), 1b), respectively.

a)   b)
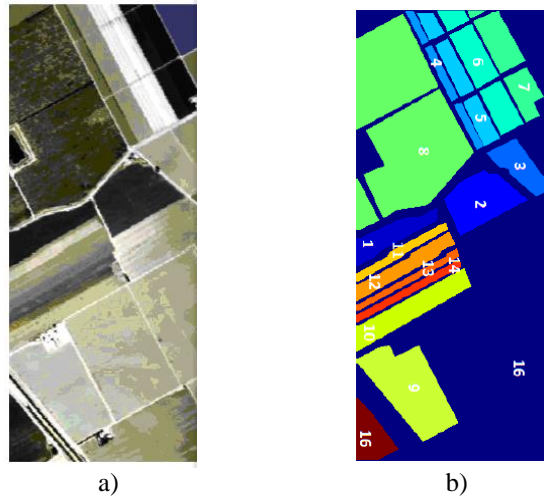
Fig. 1. – Salinas test image: a) hyperspectral layer with the use of artificial coloring; b) classified image

The algorithm was applied to detect the 4th, 5th, and 11th classes (the area with roughlyplowed fields, smooth ground, four-week lettuce, respectively). The figure shows the location of the fifth and eleventh class vectorswith skipping the 20% lowest conjugacy indices. The figuresshowsa few falsely recognized hyperpixels from other classes.

306
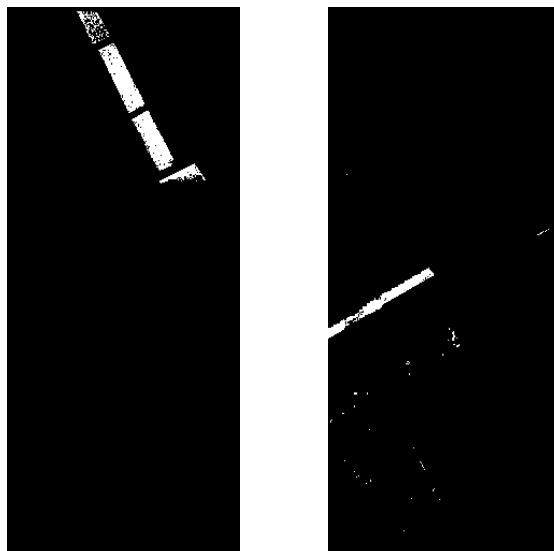
Fig. 2. –Location of 5 and 11 classes vectors respectively

a)   b)
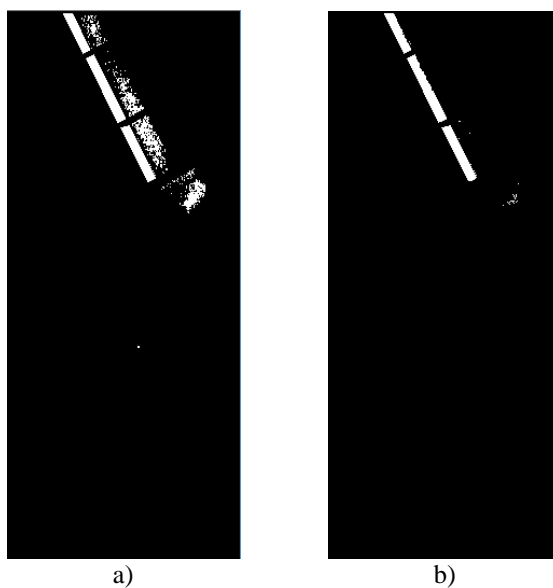
Fig. 3. – Location of the fourth class vectors: a) the 0% threshold; b) the 2% threshold

Figures 3a), 3b) shows an example of the recognition of the fourth class vectors with a different minimum conjugacy threshold. The figures show that the choice of the threshold strongly influences the number of recognition errors inother classes. The increase in the threshold enhances recognition quality in its class.

5. Conclusion

The choice of an appropriate reference plane in the proposed algorithm has a high computational complexity. Recognition quality depends on the choice of the minimum conjugacy threshold. A small value of the threshold increases the number of recognition errors associated with "wrong detection" from other classes. The increase in the threshold leads to thepoints loss in a recognized class.

References
1. **Lowengart RA.** Remote sensing. Models and methods for image processing. Moscow: Technosphere, 2010; 560 p.
2. **Zherdev DA, Kazanskiy NL, Fursov VA.** Object recognition by the radar signatures of electromagnetic field scattering on base of support subspaces method. Computer Optics, 2014; 38(3): 503-510. [in Russian]
3. **Fursov VA.** Training in Pattern Recognition from a Small Number. 15th International Conference on Pattern recognition, 2000; 2: 119-121.
4. **Fursov VA, Bibikov SA, Baida OA.** Thematic classification of hyperspectral images using conjugacy indicator. Computer Optics, 2014; 38(1): 154-157. [in Russian]

Analysis of the scientific and organizational results of the Image Processing Systems Institute of the RAS

Kolomiets E.I.

Samara State Aerospace University

Abstract. This work summarizes milestones of research activity of the Image Processing Systems Institute of the Russian Academy of Sciences. Key research achievements of the Institute's team are depicted, staff members who have made an essential contribution to the Institute's success are acknowledged, and research areas of the Institute has been working in are outlined.

Keywords: scientific results, research institute, computer optics, image processing, diffractive nanophotonics, research directions, Russian Academy of Sciences

Introduction

This year we celebrate the 40th anniversary of the Computer Science Faculty of Samara State Aerospace University (National Research University) (SSAU) and the 70th anniversary of corresponding member of the Russian Academy of Sciences (RAS) Professor Victor A. Soifer. Presidium of the USSR Academy of Sciences (USSR AS) organized Kuibyshev branch of the Central Design Bureau of Unique Instrumentation (KB CDB UI) of the USSR AS on the basis of the research group headed by Professor Victor Soifer in 1988. This research group worked at the Computer Science Faculty of the Kuibyshev Aviation Institute (now - Samara State Aerospace University). KB CDB UI of the RAS was reorganized into the Image Processing Systems Institute of the RAS (IPSI RAS) five years later. Prof. Victor Soifer was director of the Institute since 1988 until January 2015. Now he is scientific leader of IPSI RAS. 2015 is the last year of the IPSI RAS work as an independent institution. At the end of 2015 IPSI RAS will become part of the Federal Research Center "Crystallography and Photonics". Looking back at the milestones of the Institute history, I would like to summarize key achievements of the Institute's team over the years passed.

1. The origins

Late in the 70s of the last century, a research team at Kuibyshev Aviation Institute headed by professor V.A. Soifer actively collaborated with partners from the Institute of Information Transmission Problems of the RAS and P.N. Lebedev Physical Institute of the RAS. Those years were marked by obtaining basic research findings in areas such as digital image processing [1], focusing of light [2 – 5], generation of laser modes with desired transverse mode content [6 – 7], Bessel beams [8], and desired radiation directivity diagrams [9]; basics of computing experiment and asymptotic analysis in optics [10 – 13]. Following a host of articles jointly published in leading scientific Russian periodicals by V.A. Soifer, academician A.M. Prokhorov, professor I.N. Sisakyan, and their disciples [2 – 13], it became evident that at the interface of the research fields of cybernetics, quantum electronics, and microelectronics, a new research field was emerging, which became known as Computer, or Diffractive, Optics. In 1988, with the task to pursue research in the emerging area, the Kuibyshev branch of the Central Design Bureau of Unique Instrumentation of the USSR AS was established, with 60 people on the staff.

2. Kuibyshev branch of the CDB of unique instrumentation

The core of the KB CDB UI of the USSR Academy of Sciences was formed by young Candidates of Science: Ye.Yu. Arefiev, M.A. Golub, N.L. Kazanskiy, V.V. Kotlyar, O.V. Prisekina, and A.G. Khramov, with V.A. Soifer, Dr. of Eng., appointed director. Large organizational efforts associated with establishing the Branch were contributed by vice-director in charge of general issues Yu.N. Boyarkin and staff members L.P. Chepurnova, L.F. Egorova, Yu.A. Runkov, G.V. Uspleniev, Ye.D. Vasil'ev, D.M. Yakunenkova, and G.G Yamovich. The newly established KB CDB UI of the USSR Academy of Sciences was run as a self-sustained organization, with financing largely depending on the hunt for customers and commercial contracts for implementation of applied research projects. Notwithstanding the self-financing status, the basic research also stayed high on the list of priorities, which mainly became possible due to participation in the state-funded scientific & technical programs, such as 'Advanced Information Technologies', 'High Technologies', and 'Samara's Conversion'. In the arduous 90s, taking part in the above-mentioned programs enabled the KB's research team to obtain and publish a number of cutting-edge research findings in the field of laser technology [14 – 16] and generation of laser beams with novel properties [17 – 19]. With the KB's key researchers (V.A. Soifer, V.V. Kotlyar, M.A. Golub, N.L. Kazanskiy, L.L. Doskolovich, S.N. Khonina) steering a course toward extensively publishing in leading foreign journals from the very beginning, the scientific school soon acquired the international recognition, which brought along first foreign contracts, also enabling M.A. Golub and V.V. Kotlyar to defend dissertations for Advanced Doctor's Degrees with flying colors in Moscow. Scientific and practical significance of the results obtained by Samara research team in collaboration with colleagues from Moscow (V.P. Shorin, V.A. Soifer, I.N. Sisakyan, V.A. Barvinok) brought them the 1992 RF State Prize for achievements in science and technology.

3. IPSI of the RAS

Building on the success of the research team, V.A. Soifer – while enlisting the support of academicians S.V. Emelyanov, Yu.I. Zhuravlyev, and V.P. Shorin – initiated the adoption of RAS Presidium's Resolution N 21 of January 26, 1993 by which the Samara branch of the CDB UI of the RAS was reorganized into the Image Processing Systems Institute of the RAS. Divisions on pattern recognition and image analysis were organized in the newly established Institute. Unfortunately, the Institute continued to be run on the self-support basis, which survived till 1998.

Nowadays, the IPSI RAS has 44 budget-funded positions, with the general number of employees (including part-timers) having reached 100 people. The Institute boasts 16 holders of Dr. of Sc. degree and 19 holders of Candidates of Sc. degree on the staff. The researchers with Doctor's Degree are 50 year-old on average, with Candidate's Degree – 35 year-old. All in all, there are 63 young researchers under 35 (including part-time workers, graduate and postgraduate students). 48 per cent of the total wage fund accounts for the salary of young scientists (under 35).

During the challenging formative years, the IPSI RAS managed to survive, later growing into a successful research institution, which was largely due to close integration with a leading Russian university – S.P. Korolyov Samara State Aerospace University (National Research University), below referred to as SSAU. Just after the KB CDB UI of the USSR AS was established, a joint Scientific & Training Center (STC) 'Spectrum' was set up by the joint order N 167 (December 14, 1988) of the RSFSR Ministry of Higher Education and USSR AS. In the course of 25 years passed, the STC 'Spectrum' has been making rapid progress, making use of the opportunities offered by the RAS and federal programs aiming to promote the integration of basic research and higher education:

- 1997-2004: Participation, jointly with SSAU, in the federal program 'Integration of Basic Research and Higher Education';
- 2002-2012: Establishment and development of a Research & Education Center of Mathematical Principles of Diffractive Optics and Image Processing as part of the Russian-American program 'Basic Research and Higher Education';
- 2006-2007: Participation in the SSAU Innovative Education program;
- since 2009: Taking part in the program of development of SSAU as a National Research University;
- since 2013: Taking part in the "5-100" program for improving the SSAU competitiveness.

The partnership between the IPSI RAS and SSAU has provided a stable influx of aspiring young researchers and professionals. The fruits of the collaboration include the establishment of new University subdepartments and joint Centers for collective use of research equipment [20], with highly challenging competitions won by joined effort and collaborative projects being under way currently. Further integration with SSAU may prove to be one of the ways to preserve the IPSI RAS research team now that the RAS has been reformed since 2013.

4. Research achievements

The effectiveness of IPSI RAS' research activity can be evaluated in terms of the number of scientific articles published, the amount of grants won, and commercial contracts awarded.

Ever since its establishment, the number of publications by the Institute's researchers has exhibited a steady growth (Fig. 1). Noteworthy is not only the number of publications but also the journal titles where the articles have been published. Recent years have seen an increase in publications in the journals that have the Web-of-Science impact-factor exceeding 3: Physics Review Letters [21], Applied Physics Letters [22], Optics Express [23 – 26], and Optics Letters [27 – 30]. In 2013, the journal Nature Communications published an article by D.A. Bykov and L.L. Doskolovich prepared by an international team of researchers with the participation of Moscow State University's scientists [31]. The IPSI researchers published 81 scientific articles in 2013 and 136 scientific articles in 2014 in the Editions indexed in the international database SCOPUS.
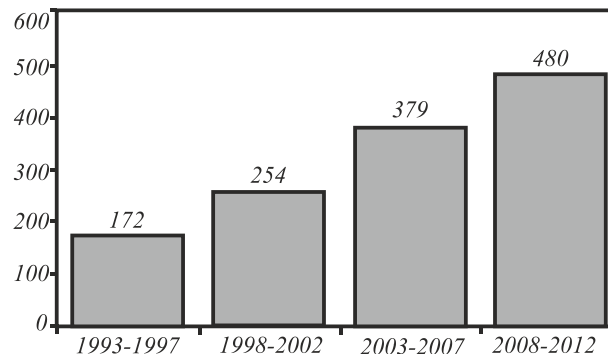
Fig. 1. – IPSI RAS: Publications dynamics

The interest in the research findings obtained by the IPSI RAS researchers is reflected in a high level of the articles' citation data. While Table 1 shows data according to the Russian Scientific Citation Index (RSCI), it should be noted that data on citations and Hirsh-indexes in Web of Science at V.A. Soifer, V.V. Kotlyar, and S.N. Khonina are not much different from those.

The research findings made by the IPSI scientists have also been summarized in a number of fundamental monographs published by recognized Publishing Houses around the world in the Russian, English [32-37], and Chinese languages [38]. Research topics covered by the monographs embrace all major IPSI's research areas - from diffractive nanophotonics to medical imagery processing.

The research achievements widely recognized in the research community have enabled the IPSI's RAS scientists to win a host of Russian Foundation for Basic Research (RFBR) grants and RF Presidential grants (Fig. 2). For instance, out of three RF Presidential grants for Young Doctors of Science awarded in the field of information and telecommunication technologies in 2003, two grants were awarded to the IPSI researchers (L.L. Doskolovich and S.N. Khonina). Three young researchers of the IPSI

RAS (D.A. Bykov, Ye.A. Bezus, A.V. Kuznetsov) get Russian President's Fellowships now. In 2014, three scientists of the IPSI RAS (L.L. Doskolovich, N.L. Kazanskiy, and R.V. Skidanov) won the Russian Science Foundation grants (2014-2016) for supporting research groups.

The bar charts in Fig. 3 present the number of Russian and international commercial contracts that IPSI RAS researchers have implemented over the last 15 years. Unfortunately, the world finance crisis has removed the international contracts from the agenda. However, thanks to active efforts undertaken at the domestic market the Institute landed two major Russian commercial contracts. One of them is to be implemented jointly with SSAU and aims to develop equipment for hyperspectral remote sensing [39 – 42] and tools for hyperspectral information processing [43 – 44] in the frame of the order of the space-missile center 'Progress' following RF Government's Resolution N 218. The other is concerned with the creation of compact vision systems for unmanned aircraft commissioned by the Research Institute for Applied Problems (Saint-Petersburg) [45 – 46].

Table 1. Citation indices of IPSI RAS leading researchers

N	Name	RSCI	Hirsh index
1	V. A. Soifer	4814	29
2	N. L. Kazanskiy	3036	26
3	V. V. Kotlyar	2805	24
4	S. N. Khonina	2775	24
5	L. L. Doskolovich	2045	21
6	R. V. Skidanov	1118	14
7	S. I. Kharitonov	931	14
8	A. V. Volkov	969	13
9	S. G. Volotovsky	449	13
10	V. S. Pavelyev	938	11
11	A.A. Kovalev	508	11
12	D. L. Golovashkin	647	10
13	V. V. Sergeev	827	9
14	N. I. Glumov	726	9
15	S. V. Karpeev	412	9
16	D. A. Bykov	277	9
17	Ye. A. Bezus	269	9
18	V. A. Kolpakov	291	8
19	A. V. Ustinov	282	8
20	O. Yu. Moiseev	254	8
21	P.G. Serafimovich	219	8
22	N. Yu. Ilyasova	672	7
23	A. G. Khramov	629	7
24	S.B. Popov	613	7
25	A.V. Kupriyanov	171	7
26	M. A. Moiseev	170	7
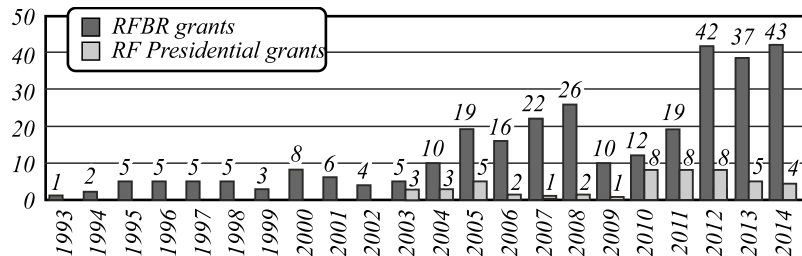
Fig. 2. – RFBR grants and RF President's grants
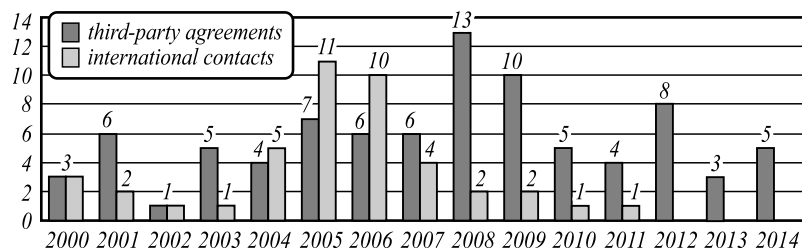
Fig. 3. – The bar chart shows successfully completed domestic and foreign commercial contracts

5. Modern day

Entering the RAS' division of Nano- and Information Technologies, the IPSI has been conducting research in the following fields, as approved by the RAS' Presidium Resolution N 37 of February 12, 2008:

— Computer/diffractive optics, nanophotonics, optical information technologies and systems;
— Systems for image analysis and pattern recognition;
— Geoinformation technologies.

In accordance with the Order of the Federal Agency of Scientific Organizations Professor N.L. Kazanskiy is temporarily working as acting director of the IPSI RAS since January 20, 2015. The IPSI RAS has four successful laboratories:

— Diffractive Optics (headed by Professor L.L. Doskolovich, Dr. of Phys. & Math);
— Laser Measurements (headed by Professor V.V. Kotlyar, Dr. of Phys. & Math);
— Micro- and Nanotechnologies (headed by Professor R.V. Skidanov, Dr. of Phys. & Math);
— Mathematical Methods of Image Processing (headed by Professor V.V. Sergeev, Dr. of Eng.).

The scientific leader of IPSI RAS V.A. Soifer makes a point of encouraging his research team to always be involved in the cutting-edge research, with new areas including such subjects as, understanding and analysis of nanoscale object images [47 –

314

48], intelligent analysis of the Earth's remote sensing data [49 – 50], optical computing [24, 28, 29], chip-aided nanophotonic data processing [51 – 52], and so on.

Research work concerned with further development of methods and technologies for diffractive optics and image processing has also been successfully continued. Topics that have been actively developed include methods for designing diffractive focusing elements [53 – 59], methods for synthesizing the diffractive microrelief on various optical materials [60 – 67], computer-aided simulation technologies [68-74], and asymptotic diffraction research methods [75]. Methods for designing optical antennae have been put in practice for designing lighting devices [76 – 79], multi-order [80 – 81] and spectral [82 – 83] optical elements. Facilities and techniques for conducting optical experiments have been persistently improved [83 – 85], with the range of industrial application of laser light focusers considerably expanded [86]. New optical devices and machine vision systems have been created [87 – 92], the dedicated software for diffractive optics purposes has been developed [93], and methods for image processing and recognition proposed [94 – 97].

Annually, a number of research findings by the IPSI RAS researchers have been included into the list of achievements of the Russian Academy of Sciences (see Table 2). Among topics worthy of noting here are sharp focusing of laser light [98 – 100], new types of diffraction conditioners beams with unique properties [101 – 102], hyper-resonant magnetooptic effects in periodic nanoheterostructrues [21, 31, 103], focusing of the surface electromagnetic waves [22 – 23, 58 – 59], nanolithography techniques based on evanescent electromagnetic waves [63 – 64], new methods for image processing [43 – 50, 91 – 92, 94 – 97, 104 – 106], and others.

Table 2. Number of IPSI RAS research findings included in the annual list of the Russian Academy of Sciences research achievements (RAS Reports)

2005	2006	2007	2008	2009	2010	2011	2012	2013	2014
1	1	1	4	7	5	9	3	4	3

As collaboration with SSAU, IPSI RAS publishes a journal of *Computer Optics*, which contains two major sections -- on optical technologies and image processing. The quarterly journal is peer-reviewed and indexed in international databases Scopus and Compendex. The most frequently cited journal articles [107 – 114] have been prepared mainly by the Institute's researchers. Now Computer Optics will be published every two months [115].

On a regular basis, the Institute hosts major regional international scientific conferences:

─ "The IV-th workshop on Computer Optics", (February 19-24, 1990, Togliatti);
─ 5th International Workshop on digital image processing and computer graphics "Image Processing and Computer Optics", (August 22-26, 1994. - Samara);
─ 5th international conference on "Pattern Recognition and Image Analysis" ("PRIA-2000", October 16-22, 2000, Samara);
─ International conference "Mathematical Modeling-2001", Chaired by academician A. A. Samarsky (June 13-16, 2001, Samara);

- Fourth international scientific and practical seminar and All-Russian youth school "High-performance parallel computing using clusters" (September 30 - October 2, 2004, Samara);
- Seminar on "Computer Optics and Image Processing" to mark the 30-th anniversary of SSAU's Technical Cybernetics subdepartment and 20-th anniversary of IPSI RAS (June 20, 2008, Samara);
- Third international conference on Physics of Metals and Mechanics of Materials, Nanostructures, and Deformation Processes (June 3-5, 2009, Samara);
- International conference with taught courses for young researchers "Advanced Technologies for Aviation and Space" ("PIT-2010", September 29 – October 1, 2010, Samara);
- Asia-Pacific Conference on Fundamental Problems of Opto- and Microelectronics (Москва-Самара, July 4-8, 2011, Moscow-Samara);
- 20th International Symposium "Nanostructures: Physics and Technology" (June 24-30, 2012, Nizhny Novgorod-Kazan-Saratov-Samara);
- 11th International conference "Pattern recognition and Image Analysis: New Information Technologies" ("PRIA-11-2013», September 23-28, 2013, Samara).

Active research activity, organizing and hosting big international scientific events have been attracting an interest that prominent Russian and foreign scientists take in IPSI RAS researchers' works (as illustrated by Figs. 4 – 9).

6. Public recognition

As recognition of the successful research and economic activities, many IPSI RAS workers have been awarded various state and public awards.

In 1993, V.A. Soifer and S.N. Khonina were awarded the First Prize of the German Society for Support of Applied Informatics for the best research paper in image processing and pattern recognition. IPSI RAS director, V.A. Soifer was awarded the Honor Order (1995), the Orders for 'Services to Motherland' of IV-th (2004) and III-rd (2010) degrees, RF Government's prizes for outstanding achievements in science and technology (2007) and in education (2010). In 2003, D.L. Golovashkin and V.S. Pavelyev were awarded the RF State Prize for Young Scientists. V.A. Soifer (2007), V.V. Kotlyar (2012), and S.N. Khonina (2014) were awarded the Governor's Prize of Samara region, 18 researchers (N.L. Kazanskiy, V.V. Kotlyar, V.V. Sergeev, 1998; V.M. Chernov, 1999; V.A. Soifer, V.A. Fursov, V.V. Kravchyuk, 2001; N.I. Glumov, N.Yu. Ilyasova, A.G. Khramov, 2003; A.V. Volkov, 2007; S.V. Karpeev, 2008; L.L. Doskolovich, 2009; S.N. Khonina, 2010; R.V. Skidanov, 2011; V.V. Myasnikov, 2012; S.I. Kharitonov, 2013; and S.B. Popov, 2014) become laureates of the Regional Prize in science and technology. V.A. Kolpakov (2011), D.A. Bykov and A.V. Gavrilov (2014) were awarded a RAS medal for young researchers, Ye.V. Byzov and S.V. Kravchenko were awarded a RAS medal for students in 2015. A.G. Khramov with colleagues from Samara Medical University was awarded the 2012 Gold medal of the International Inventions Exhibition in Geneva, Switzerland. V.A. Soifer was awarded the Scopus Award Russia 2014 and the title of "Honorary citizen of Samara Region".

Fig. 4. – Presiding over the international conference "Mathematical Modeling-2001" are our illustrious contemporaries, academicians A.A. Samarsky (left) and Yu.I. Zhuravlev

Fig. 5. – Vice-President of the International Commission in Optics (ICO), Prof. Jin Guofan of Tsinghua University delivers a lecture on "Binary Optics" at a seminar held at IPSI RAS on 8 September, 2006

Fig. 6. – Prof. R.V. Skidanov presents a diffractive optical element for laser micromanipulation to academician J.I. Alferov (center) and the corresponding member of the RAS V.A. Soifer

Fig. 7. – At the laboratory of Micro- and Nano-technologies (left to right): N.L. Kazanskiy, Yu.N. Boyarkin, academician Yu.V. Gulyaev, A.V. Volkov, SSAU Rector, Prof. Ye.V. Shakhmatov, academician G.V. Novozhilov, and the corresponding member of the RAS V.A. Soifer

Fig. 8. – Chief Academic Secretary of the RAS Presidium, academician I.A. Sokolov (left) is discussing problems of steganography at the laboratory of Mathematical Methods of Image Processing with N.L. Kazanskiy (center) and V.V. Sergeev
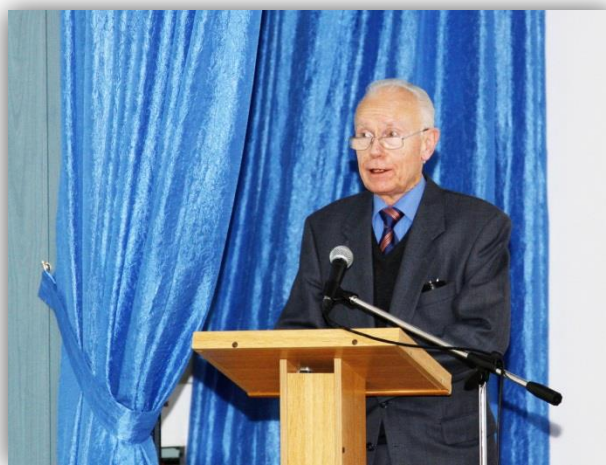
Fig. 9. – Professor Heinrich Niemann of the University of Erlangen-Nurenberg is greeting the IPSI RAS scientists at the 25th anniversary celebration session of the International conference "PRIA-11-2013" on September 26, 2013

7. Conclusion

IPSI RAS is now the largest Russian scientific team working in the field of image processing and diffractive computer optics. IPSI RAS results largely determine the success of Russia in these scientific areas. Summing up, I wish the IPSI RAS

researchers to stay in good health, showing inexhaustible energy, insatiable scientific curiosity and new creative accomplishments for the benefit of our Motherland and Russian science!

Acknowledgements

References

1. **Vittikh VA, Sergeyev VV, Soifer VA.** Image processing in automated systems for scientific research. Moscow: "Nauka" Publisher, 1982. [in Russian]

2. **Golub MA, Karpeev SV, Prokhorov AM, Sisakyan IN, Soifer VA.** Focusing light into a specified volume by computer synthesized holograms. Soviet Technical Physics Letters, 1981; 7(10): 618-623.

3. **Golub MA, Degtyarova VP, Klimov AN, Popov VV, Prokhorov AM, Sisakyan IN, Soifer VA.** Machine synthesis of focusing elements for CO_2-laser. Technical Physics Letters, 1982; 8(13): 449-451. [in Russian]

4. **Danilov VA, Popov VV, Prokhorov AM, Sagatelyan DM, Sisakian IN, Soifer VA.** Synthesis of optical elements that create focal free-form line. Technical Physics Letters, 1982; 8(13): 810-815. [in Russian]

5. **Goncharskii V, Danilov VA, Popov VV, Prokhorov AM, Sisakian IN, Soifer VA, Stepanov VV.** Solution of the inverse problem of laser-radiation focusing into an arbitrary curve. Doklady Akademii Nauk USSR, 1983; 273(3): 605-608. [in Russian]

6. **Golub MA, Prokhorov AM, Sisakyan IN, Soifer VA.** Synthesis of spatial filters for investigation of the transverse mode composition of coherent radiation. Soviet Journal of Quantum Electronics, 1982; 12(9): 1208-1209.

7. **Golub MA, Karpeev SV, Kazanskii NL, Mirzov AV, Sisakyan IN, Soifer VA, Uvarov GV.** Spatial phase filters matched to transverse modes. Soviet Journal of Quantum Electronics, 1988; 18(3): 392-393.

8. **Bereznyi E, Prokhorov AM, Sisakyan IN, Soifer VA.** Bessel-optics. Doklady Akademii Nauk USSR, 1984; 274(3): 605-608. [in Russian]

9. **Golub MA, Kazanskii NL, Prokhorov AM, Sisakyan IN., Soifer VA.** Synthesis of optical antennae. Computer Optics, 1989; 1(1): 25-28.

10. **Golub MA, Kazanskiy NL, Sisakyan IN, Soifer VA, Kharitonov SI.** Diffraction calculation for an optical element which focuses into a ring. Optoelectronics, Instrumentation and Data Processing, 1987; 6: 7-14.

11. **Sisakyan IN, Soifer VA.** Computer optics: achievements and problems. Computer Optics, 1989; 1(1): 3-12.

12. **Golub MA, Kazanskii NL, Sisakyan IN, Soifer VA.** Computational experiment with plane optical elements. Optoelectronics, Instrumentation and Data Processing, 1988; 1: 78-89.

13. **Kazanskii NL.** Correction of focuser phase function by computer-experimental methods. Computer Optics, 1989; 1(1): 69-73.

14. **Sisakyan N, Shorin VP, Soifer VA, Mordasov VI, Popov VV.** Technological capabilities of focusators in laser-induced material processing. Computer Optics, 1990; 2(1): 85-87.

15. **Golub MA, Sisakian IN, Soifer VA.** Infra-red Radiation Focusators. Optics and Lasers in Engineering, 1991; 15(5): 297-309.

16. **Doskolovich LL, Kazanskiy NL, Kharitonov SI, Usplenjev GV.** Focusators for laser-branding. Optics and Lasers in Engineering, 1991; 15(5): 311-322.

17. **Khonina SN, Kotlyar VV, Uspleniev GV, Shinkarev MV, Soifer VA.** The phase rotor filter. Journal of Modern Optics, 1992; 39(5): 1147-1154.

18. **Khonina SN, Kotlyar VV, Soifer VA, Shinkaryev MV, Uspleniev GV.** Trochoson. Optics Communications, 1992; 91(3-4): 158-162.

19. **Golub MA, Doskolovich LL, Kazanskiy NL, Kharitonov SI, Soifer VA.** Computer generated diffractive multi-focal lens. Journal of Modern Optics, 1992; 39(6): 1245-1251.

20. **Kazanskiy NL.** Research & Education Center of Diffractive Optics. Proceedings of SPIE, 2012; 8410: 84100R. doi: 10.1117/12.923233. 2012.

21. **Belotelov VI, Doskolovich LL, Zvezdin AK.** Extraordinary magneto-optical effects and transmission through metal-dielectric plasmonic systems. Physical Review Letters, 2007; 98(7): 077401.

22. **Bezus EA, Doskolovich LL, Kazanskiy NL.** Scattering suppression in plasmonic optics using a simple two-layer dielectric structure. Applied Physics Letters, 2011; 98(22): 221108. doi: 10.1063/1.3597620.

23. **Bezus EA, Doskolovich LL, Kazanskiy NL.** Low-scattering surface plasmon refraction with isotropic materials. Optics Express, 2014; 22(11): 13547-13554. doi: 10.1364/OE.22.013547.

24. **Kazanskiy NL, Serafimovich PG.** Coupled-resonator optical wave-guides for temporal integration of optical signals. Optics Express, 2014; 22(11): 14004-14013. doi: 10.1364/OE.22.014004.

25. **Aslanov ER, Doskolovich LL, Moiseev MA, Bezus EA, Kazanskiy NL.** Design of an optical element forming an axial line segment for efficient LED lighting systems. Optics Express, 2013; 21(23): 28651-28656.

26. **Khonina SN, Savelyev DA, Kazanskiy NL.** Vortex phase elements as detectors of polarization state. Optics Express, 2015; 23(14): 17845-17859. doi: 10.1364/OE.23.017845.

27. **Kotlyar VV, Kovalev AA, Soifer VA.** Asymmetric Bessel modes. Optics Letters, 2014; 39(8): 2395-2398.

28. **Bykov DA, Doskolovich LL, Soifer VA.** Temporal differentiation of optical signals using resonant gratings. Optics Letters, 2011; 36(17): 3509-3511.

29. **Kazanskiy NL, Serafimovich PG, Khonina SN.** Use of photonic crystal cavities for temporal differentiation of optical signals. Optics Letters, 2013; 38(7): 1149-1151. doi: 10.1364/OL.38.001149.

30. **Golovastikov NV, Bykov DA, Doskolovich LL.** Spatiotemporal pulse shaping using resonant diffraction gratings. Optics Letters, 2015; 40(15): 3492-3495. doi: 10.1364/OL.40.003492.

31. **Belotelov VI, Kreilkamp LE, Akimov IA, Kalish AN, Bykov DA, Kasture S, Yallapragada VJ, Gopal AV, Grishin AM, Khartsev SI, Nur-E-Alam M, Vasiliev M, Doskolovich LL, Yakovlev DR, Alameh K, Zvezdin AK, Bayer M.** Plasmon-mediated magneto-optical transparency. Nature Communications, 2013; 4. doi: 10.1038/ncomms3128.

32. **Soifer VA, Golub MA.** Laser Beam Mode Selection by Computer Generated Holograms. Boca Raton: CRC Press Inc, 1994.

33. **Soifer VA, Kotlyar VV, Doskolovich LL.** Iterative methods for diffractive optical elements computation. London: Taylor and Francis Ltd, 1997.

34. **Soifer VA, Kotlyar VV, Kazanskiy NL, Doskolovich LL, Kharitonov SI, Khonina SN, Pavelyev VS, Skidanov RV, Volkov AV, Golovashkin DL, Solovyev VS, Usplenyev GV.** Methods for computer design of diffractive optical elements. Edited by Soifer VA. New York: John Wiley & Sons, Inc, 2002.

35. **Myasnikov VV, Popov SB, Sergeyev VV, Soifer VA.** Computer Image Processing. Part I: Basic concepts and theory. Edited by Soifer VA. VDM Verlag, 2009.

36. **Chernov AV, Chernov VM, Chicheva MA, Fursov VA, Gashnikov MV, Glumov NI, Ilyasova NYu, Khramov AG, Korepanov AO, Kupriyanov AV, Myasnikov EV, Myasnikov VV, Popov SB, Sergeyev VV, Soifer VA.** Computer Image Processing. Part II: Methods and algorithms. Edited by Soifer VA. VDM Verlag; 2009.

37. **Golovashkin DL, Doskolovich LL, Kazanskiy NL, Khonina SN, Kotlyar VV, Pavelyev VS, Skidanov RV, Soifer VA. Computer design of diffractive optics. Edited by Soifer VA.** Cambridge International Science Publishing Ltd. & Woodhead Pub. Ltd., 2012.

38. **Doskolovich LL, Golovashkin DL, Kazanskiy NL, Khonina SN, Kotlyar VV, Pavelyev VS, Skidanov RV, Soifer VA, Solovyev VS, Usplenyev GV, Volkov AV.** Methods for Computer Design of Diffractive Optical Elements. Edited by Soifer VA. Tianjin: Tianjin Science & Technology Press, 2007. [in Chinese]

39. **Kazanskiy NL, Kharitonov SI, Khonina SN, Volotovskiy SG, Strelkov YuS.** Simulation of hyperspectrometer on spectral linear variable filters. Computer Optics, 2014; 38(2): 256-270. [in Russian]

40. **Kazanskiy NL, Kharitonov SI, Karsakov AV, Khonina SN.** Modeling action of a hyperspectrometer based on the offner scheme within geometric optics. Computer Optics, 2014; 38(2): 271-280. [in Russian]

41. **Kazanskiy NL, Kharitonov SI, Khonina SN.** Simulation of a hyperspectrometer based on linear spectral filters using vector Bessel beams. Computer Optics, 2014; 38(4): 770-776. [in Russian]

42. **Kazanskiy NL, Kharitonov SI, Doskolovich LL, Pavelyev AV.** Modeling the performance of a spaceborne hyperspectrometer based on the Offner scheme. Computer Optics, 2015; 39(1). 70-76. [in Russian]

43. **Denisova AYu, Myasnikov VV.** Anomaly detection for hyperspectral imaginary. Computer Optics, 2014; 38(2): 287-296. [in Russian]

44. **Gashnikov MV, Glumov NI.** Hierarchical compression for hyperspectral image storage. Computer Optics, 2014; 38(3): 482-488. [in Russian]

45. **Kazanskiy NL, Khonina SN, Skidanov RV, Morozov AA, Kharitonov SI, Volotovskiy SG.** Formation of images using multilevel diffractive lens. Computer Optics, 2014; 38(3): 425-434. [in Russian]

46. **Zherdev DA, Kazanskiy NL, Fursov VA, Kharitonov SI.** Electromagnetic field scattering simulation from anthropogenic objects on underlying surface. Computer Optics, 2013; 37(1): 91-98. [in Russian]

47. **Borodin SA, Volkov AV, Kazanskiy NL.** Device for analyzing nanoroughness and contamination on a substrate from the dynamic state of a liquid drop deposited on its surface. Journal of Optical Technology, 2009; 76(7): 408-412.

48. **Soifer VA, Kupriyanov AV.** Analysis and recognition of the nanoscale images: conventional approach and novel problem statement. Computer Optics, 2011; 35(2): 136-144. [in Russian]

49. **Gashnikov MV, Glumov NI, Sergeev VV.** A hierarchical compression method for space images. Automation and Remote Control, 2010; 71(3): 501-513.

50. **Zherdev DA, Kazanskiy NL, Fursov VA.** Object recognition in radar images using conjugation indices and support subspaces. Computer Optics, 2015; 39(2): 255-264. [in Russian]

51. **Kazanskiy NL, Serafimovich PG, Khonina SN.** Harnessing the Guided-Mode Resonance to Design Nanooptical Transmission Spectral Filters. Optical Memory and Neural Networks (Information Optics), 2010; 19(4): 318-324. doi: 10.3103/S1060992X10040090.

52. **Soifer VA.** Diffractive Nanophotonics and Advanced Information Technologies. Herald of the Russian Academy of Sciences, 2014; 84(1): 9-18. doi: 10.1134/S1019331614010067.

53. **Kazanskiy NL, Kotlyar VV, Soifer VA.** Computer-aided design of diffractive optical elements. Optical Engineering, 1994; 33(10): 3156-3166.

54. **Doskolovich LL, Kazanskiy NL, Soifer VA.** Comparative analysis of different focusators focusing into a segment. Optics and Laser Technology, 1995; 27(4): 207-213.

55. **Doskolovich LL, Kazanskiy NL, Soifer VA, Tzaregorodtzev AYe.** Analysis of quasiperiodic and geometric optical solutions of the problem of focusing into an axial segment. Optik – International Journal for Light and Electron Optics, 1995; 101(2): 37-41.

56. **Doskolovich LL, Kazanskiy NL, Kharitonov SI, Soifer VA.** A method of designing diffractive optical elements focusing into plane areas. Journal of Modern Optics, 1996; 43(7): 1423-1433.

57. **Soifer VA, Kazanskiy NL, Kharitonov SI.** Synthesis of a Binary DOE Focusing into an Arbitrary Curve, Using the Electromagnetic Approximation. Optics and Lasers in Engineering, 1998; 29(4-5): 237-247.

58. **Bezus EA, Doskolovich LL, Kazanskiy NL, Soifer VA, Kharitonov SI.** Design of diffractive lenses for focusing surface plasmons. Journal of Optics, 2010; 12(1): 015001.

59. **Bezus EA, Doskolovich LL, Kazanskiy NL, Soifer VA.** Scattering in elements of plasmon optics suppressed by two-layer dielectric structures. Technical Physics Letters, 2011; 37(12): 1091-1095.

60. **Volkov AV, Kazanskiy NL, Moiseev OYu, Soifer VA.** A Method for the Diffractive Microrelief Forming Using the Layered Photoresist Growth. Optics and Lasers in Engineering, 1998; 29(4-5): 281-288.

61. **Kazanskiy NL, Kolpakov VA, Kolpakov AI.** Anisotropic Etching of SiO_2 in High-Voltage Gas-Discharge Plasmas. Russian Microelectronics, 2004; 33(3): 169-182.

62. **Pavelyev VS, Borodin SA, Kazanskiy NL, Kostyuk GF, Volkov AV.** Formation of diffractive microrelief on diamond film surface. Optics & Laser Technology, 2007; 39(6): 1234-1238.

63. **Bezus EA, Doskolovich LL, Kazanskiy NL.** Evanescent-wave interferometric nanoscale photolithography using guided-mode resonant gratings. Microelectronic Engineering, 2011; 88(2): 170-174.

64. **Bezus EA, Doskolovich LL, Kazanskiy NL.** Interference pattern formation in evanescent electromagnetic waves using waveguide diffraction gratings. Quantum Electronics, 2011; 41(8): 759-764.

65. **Abulkhanov SR, Kazanskiy NL, Doskolovich LL, Kazakova OY.** Manufacture of diffractive optical elements by cutting on numerically controlled machine tools. Russian Engineering Research, 2011; 31(12): 1268-1272.

66. **Kazanskiy NL, Kolpakov VA, Podlipnov VV.** Gas discharge devices generating the directed fluxes of off-electrode plasma. Vacuum, 2014; 101: 291-297.

67. **Volkov AV, Kazanskiy NL, Moiseev OYu, Poletayev SD.** Thermal Oxidative Degradation of Molybdenum Films under Laser Ablation. Technical Physics, 2015; 60(2): 265–269. doi: 10.1134/S1063784215020255.

68. **Kazanskiy NL, Soifer VA.** Diffraction investigation of geometric-optical focusators into segment. Optik – International Journal for Light and Electron Optics, 1994; 96(4): 158-162.

69. **Golovashkin DL, Kazanskiy NL.** Mesh Domain Decomposition in the Finite-Difference Solution of Maxwell's Equations. Optical Memory & Neural Networks (Information Optics), 2009; 18(3): 203-211.

70. **Khonina SN, Kazanskiy NL, Volotovsky SG.** Influence of Vortex Transmission Phase Function on Intensity Distribution in the Focal Area of High-Aperture Focusing System. Optical Memory and Neural Networks (Information Optics), 2011; 20(1): 23-42. doi: 10.3103/S1060992X11010024.

71. **Golovashkin DL, Kasanskiy NL.** Solving Diffractive Optics Problem using Graphics Processing Units. Optical Memory and Neural Networks (Information Optics), 2011; 20(2): 85-89.

72. **Khonina SN, Kazanskiy NL, Ustinov AV, Volotovskii SG.** The lensacon: nonparaxial effects. Journal of Optical Technology, 2011; 78(11): 724-729.

73. **Kazanskiy NL, Serafimovich PG.** Cloud Computing for Rigorous Coupled-Wave Analysis. Advances in Optical Technologies, 2012. doi: 10.1155/2012/398341.

74. **Kazanskiy NL, Serafimovich PG.** Cloud Computing for Nanophotonic Simulations. Lecture Notes in Computer Science, 2013; 7715: 54-67.

75. **Kazanskiy NL, Kharitonov SI, Soifer VA.** Application of a pseudogeometrical optical approach for calculation of the field formed by a focusator. Optics & Laser Technology, 1996; 28(4): 297-300.

76. **Doskolovich LL, Kazanskiy NL, Soifer VA, Kharitonov SI, Perlo P.** A DOE to form a line-shaped directivity diagram. Journal of Modern Optics, 2004; 51(13): 1999-2005.

77. **Doskolovich LL, Kazanskiy NL, Kharitonov SI, Perlo P, Bernard S.** Designing reflectors to generate a line-shaped directivity diagram. Journal of Modern Optics, 2005; 52(11): 1529-1536.

78. **Doskolovich LL, Kazanskiy NL, Bernard S.** Designing a mirror to form a line-shaped directivity diagram. Journal of Modern Optics, 2007; 54(4): 589-597.

79. **Doskolovich LL, Dmitriev AYu, Moiseev MA, Kazanskiy NL.** Analytical design of refractive optical elements generating one-parameter intensity distributions. Journal of the Optical Society of America A, 2014; 31(11): 2538–2544. doi: 10.1364/JOSAA.31.002538.

80. **Soifer VA, Doskolovich LL, Kazanskiy NL.** Multifocal diffractive elements. Optical Engineering, 1994; 33(11): 3610-3615.

81. **Doskolovich LL, Kazanskiy NL, Perlo P, Repetto P, Soifer VA.** Direct two-dimensional calculation of binary DOEs using a non-binary series expansion approach. International Journal of Optoelectronics, 1996; 10(4): 243-249.

82. **Doskolovich LL, Kazanskiy NL, Soifer VA, Perlo P, Repetto P.** Design of DOEs for wavelength division and focusing. Journal of Modern Optics, 2005; 52(6): 917-926.

83. **Doskolovich LL, Kazanskiy NL, Khonina SN, Skidanov RV, Heikkila N, Siitonen S, Turunen J.** Design and investigation of color separation diffraction gratings. Applied Optics, 2007; 46(15): 2825-2830.

84. **Kazanskiy N, Skidanov R.** Binary beam splitter. Applied Optics, 2012; 51(14): 2672-2677.

85. **Bezus EA, Morozov AA, Volodkin BO, Tukmakov KN, Alferov SV, Doskolovich LL.** Formation of High-Frequency Two-Dimensional Interference Patterns of Surface Plasmon Polaritons. Journal of Experimental and Theoretical Physics Letters, 2013; 98(6): 317-320.

86. **Kazanskiy NL, Murzin SP, Osetrov YeL, Tregub VI.** Synthesis of nanoporous structures in metallic materials under laser action. Optics and Lasers in Engineering, 2011; 49(11): 1264-1267.

87. **Karpeev SV, Pavelyev VS, Khonina SN, Kazanskiy NL, Gavrilov AV, Eropolov VA.** Fibre sensors based on transverse mode selection. Journal of Modern Optics, 2007; 54(6): 833-844. doi:10.1080/09500340601066125.

88. **Egorov AV, Kazanskiy NL, Serafimovich PG.** The use coupled photonic crystal cavities for increasing of sensor sensitivity. Computer Optics, 2015; 39(2): 158-162.

89. **Kazanskiy NL, Popov SB.** Machine Vision System for Singularity Detection in Monitoring the Long Process. Optical Memory and Neural Networks (Information Optics), 2010; 19(1): 23-30.

90. **Kazanskiy NL, Murzin SP, Tregub VI.** Optical system for realization of selective laser sublimation of metal alloy components. Computer Optics, 2010; 34(4): 481-486. [in Russian]

91. **Kazanskiy NL, Popov SB.** The distributed vision system of the registration of the railway train. Computer Optics, 2012; 36(3): 419-428. [in Russian]

92. **Kazanskiy NL, Popov SB.** Integrated Design Technology for Computer Vision Systems in Railway Transportation. Pattern Recognition and Image Analysis, 2015; 25(2): 215-219. doi: 10.1134/S1054661815020133.

93. **Doskolovich LL, Golub MA, Kazanskiy NL, Khramov AG, Pavelyev VS, Seraphimovich PG, Soifer VA, Volotovskiy SG.** Software on diffractive optics and computer generated holograms. Proceedings of SPIE, 1995; 2363: 278-284.

94. **Chernov VM.** Fast algorithm for "error-free" convolution computation using Mersenne-Lucas codes. Chaos, Solitons & Fractals, 2006; 29(2): 372-380.

95. **Myasnikov VV.** Constructing efficient linear local features in image processing and analysis problems. Automation and Remote Control, 2010; 71(3): 514-527.

96. **Kuznetsov AV, Myasnikov VV.** A comparison of algorithms for supervised classification using hyperspectral data. Computer Optics, 2014; 38(3): 494-502. [in Russian]

97. **Kazanskiy NL, Protsenko VI, Serafimovich PG.** Comparison of system performance for streaming data analysis in image processing tasks by sliding window. Computer Optics, 2014; 38(4): 804-810. [in Russian]

98. **Stafeev SS, O'Faolain L, Shanina MI, Nalimov AG, Kotlyar VV.** Sharp focusing of a mixture of radially and linearly polarized beams using a binary microlens. Computer Optics, 2014; 38(4): 606-613. [in Russian]

99. **Degtyarev SA, Ustinov AV, Khonina SN.** Nanofocusing by sharp edges. Computer Optics, 2014; 38(4): 629-637. [in Russian]

100. **Khonina SN, Kazanskiy NL, Volotovsky SG.** Vortex phase transmission function as a factor to reduce the focal spot of high-aperture focusing system. Journal of Modern Optics, 2011; 58(9): 748-760. doi: 10.1080/09500340.2011.568710.

101. **Kotlyar VV, Kovalev AA, Zaskanov SG.** Two-dimensional accelerating Bessel beams. Computer Optics, 2014; 38(3): 386-392. [in Russian]

102. **Kotlyar VV, Kovalev AA, Porfirev AP.** Hermite-gaussian laser beams with orbital angular momentum. Computer Optics, 2014; 38(4): 651-657. [in Russian]

103. **Bykov DA, Doskolovich LL, Soifer VA, Kazanskiy NL.** Extraordinary Magneto-Optical Effect of a Change in the Phase of Diffraction Orders in Dielectric Diffraction Gratings. Journal of Experimental and Theoretical Physics, 2010; 111(6): 967-974.

104. **Zimichev EA, Kazanskiy NL, Serafimovich PG.** Spectral-spatial classification with k-means particional clustering. Computer Optics, 2014; 38(2): 281-287. [in Russian]

105. **Zherdev DA, Kazanskiy NL, Fursov VA.** Object recognition by the radar signatures of electromagnetic field scattering on base of support subspaces method. Computer Optics, 2014; 38(3): 503-510.

106. **Ilyasova NYu, Kupriyanov AV, Paringer RA.** Formation features for improving the quality of medical diagnosis based on the discriminant analysis methods. Computer Optics, 2014; 38(4): 851-855. [in Russian]

107. **Volkov AV, Kazanskiy NL, Rybakov OE.** Investigation of plasma etching technology for producing multilayer diffractive optical elements. Computer Optics, 1998; 18: 127-130. [in Russian]

108. **Volkov AV, Kazanskiy NL, Rybakov OE.** Development of technology for creation of diffractive optical elements with submicron dimensions of the relief in the silicon wafer. Computer Optics, 1998; 18: 130-133. [in Russian]

109. **Kazanskiy NL.** A research complex for solving problems of computer optics. Computer Optics, 2006; 29: 58-77. [in Russian]

110. **Kazanskiy NL, Murzin SP, Tregub VI, Mezhenin AV.** Application of a focusator radiation for generating nanoporous structures of crystalline materials. Computer Optics, 2007; 31(2): 48-51. [in Russian]

111. **Kazanskiy NL, Murzin SP, Mezhenin AV, Osetrov EL.** Laser radiation shaping for creation nanodimensional porous structures of materials. Computer Optics, 2008; 32(3): 246-248. [in Russian]

112. **Kotlyar VV, Stafeev SS.** Modeling the sharp focus of radially polarized laser mode with conical and binary microaxicons. Computer Optics, 2009; 33(1): 52-60. [in Russian]

113. **Khonina SN, Volotovsky SG.** Controlling the contribution of the electric field components to the focus of a high-aperture lens using binary phase structures. Computer Optics, 2010; 34(1): 58-68. [in Russian]

114. **Zvekov AA, Kalenskii AV, Nikitin AP, Aduev BP.** Radiance distribution simulation in a transparent medium with Fresnel boundaries containing aluminum nanoparticles. Computer Optics, 2014; 38(4): 749-756. [in Russian]

115. **Soifer VA.** Quo vadis. Computer Optics, 2014; 38(4): 589.

Challenges of data access in economic research based on Big Data technology

Chumak V.G., Ramzaev V.M., Khaimovich I.N.

International Market Institute Samara

Abstract. At present the world faces exponential increase of amount and variety of data. The data received as a result of research is used in joint projects of different countries by applying specialized up-to-date tools including Big Data. The present article indicates both the development of method application and data analysis facility, and data management in financial collective areas, it points out unprecedented rapid expansion of spectrum of tasks which require the solution based on data received, accumulation of solving similar tasks experience and making it possible to use it in many disciplines. The article gives applicability of economic data collections in Russia.

Let us consider the problems to access to financial data in Russia. There are two problems here: where to take them from and for which purpose to use. Intensive data use for solving financial tasks has just began in Russia, but in other countries, for instance in the USA it has been already used actively. The projects which are implemented in other countries are worth considering.

On November 11, 2014 in the United States National Institute of Standards and Technology has issued requirements for the financial data collection to use this data intensively in risk analysis and for financial markets development forecasting [1-13]. These requirements, made by NIST standard for Big Data, describe the use of intensive data in the financial sector, description of current solutions, as well as define the objectives and problems of the use of Big Data for financial data.

According to the requirements for financial data which are contained in Big Data, the following information is included:

— bank concerning commercial, retail, credit cards, consumer crediting, corporate banking services, banking operation, trade financing and global payments;
— data in the area of valuable securities and investments, such as retail brokerage services, services to individuals, asset management, institutional brokerage, investment banking, trust banking, safe custody and clearing services;
— data in the area of insurance including personal property accident insurance and collective property accident insurance.

Also these requirements contain one of the approaches to develop an efficient strategy for the financial services industry. When working with large collections of data in Big Data the organization must perform the following steps to define initial status for working with big data on the Internet within cloud systems of the public and private financial institutions offering financial services inside the United States; Great Britain, the EU and China.

In accordance with this strategy, every financial data should include description of people (resources), processes (time / cost / return on investment), technology (various operating systems, platforms), and statutory regulation (depending on the different and several controlling bodies).

Further these data must be identified, analyzed, evaluated, reviewed, tested and revised to in the processes of:

1. project initiation;
2. risk assessment;
3. analysis of the impact on business;
4. development and testing the strategies ensuring the business continuity;
5. emergency response;
6. development and implementation the plans ensuring continuity of financial projects;
7. carrying out of trainings.

Currently big data with hadoop methodology in cloud technology on the Internet is used as a part of hybrid systems as a tool for carrying out of the risk and fraud analysis, apart from assistance in process structuring ("know your customer"). These are three areas, where intensive data from Big Data has given good account.

At the same time, the traditional client/server/data bank/RDBM - systems are used for handling, processing, storage and archival subdivision of financial data. Recently, the financial community has approved the initiative for the presentation of the financial statements in xbrl (Extensible Business Reporting Language) as of 13th of May, 2013.

Currently, areas of concern associated with the use of intensive data storage on the Internet under the control of Big Data, include the aggregation and storage of data (confidential and other) from a number of sources that could create administrative and managerial problems concerning the following issues:

• access control;
• management/administration;

- data ownership.

However, based on the current analysis, these problems are well known and are being solved at the moment, for example, in R&D (research and development).

Russia does not practice the data exchanging (information received from the Sberbank) to predict changes in financial markets and to analyze the risks in the banking sector, so it is possible to use the American standard, provided that the necessary modifications must be made to adapt to the financial markets of Russia.

Based on these requirements the US and EU carry out their projects in the area of intensive financial data usage by the following organizations:

1. The IFRS, Securities and Markets Working Group, www.xbrl-eu.org is a group of organizations which deals with the issues of security and financial data usage in market sphere.
2. PCAOB http://www.pcaob.org is a nonprofit corporation created by Congress to oversee the audits of joint stock companies in order to protect the interests of investors and further the public interest in the preparation of informative, accurate and independent audit reports.
3. http://www.ey.com/GL/en/Industries/Financial-Services/Insurance - the organization monitors the major regulatory changes in the financial documents, analyzes the behavior of emerging markets, estimate the existing economic uncertainty, predicts consumer expectations.
4. http://www.treasury.gov/resource-center/fin-mkts/Pages/default.aspx is the website of the Treasury Department which is responsible for a wide range of activities such as advising the President on economic and financial issues, encouraging sustainable economic growth, and fostering improved governance in financial institutions. The Department of the Treasury operates and maintains systems that are critical to the nation's financial infrastructure, such as the production of coin and currency, the disbursement of payments to the American public, revenue collection, and the borrowing of funds necessary to run the federal government.
5. CFTC http://www.cftc.org is an organization which deals with insurance and financial issues.
6. SEC http://www.sec.gov is US Securities and Exchange Commission which protects investors, maintains fair, orderly, and efficient markets.
7. FDIC http://www.fdic.gov is the Federal Deposit Insurance Corporation.
8. COSO http://www.coso.org is the Committee of Sponsoring Organizations of the Treadway Commission (COSO) which is dedicated to providing thought leadership through the development of frameworks and guidance on enterprise risk management, internal control and fraud deterrence.
9. isc2 International Information Systems Security Certification Consortium, Inc.: http://www.isc2.org is a consortium which carries out wide ranging studies in the field of business management and financial flows taking into account financial risks analysis for the enterprises.
10. ISACA Information Systems Audit and Control Association: http://www.isca.org is an association which makes financial analytics.

329

These organizations carry out projects in the US and the EU on the stress testing practices of financial markets, i.e. they assess the stability of financial institutions toward adverse changes on the market and also they assess the systemic risk within the EU system according to special standardized procedures, road map, and generate key proposals of exercises. Also they create aggregate statistical data on the banking sector in EU, credit risk, operational risk, market risk, and supervisory actions and measures starting from 2007 to 2013 in the form of documents posted on the website https://www.eba.europa.eu/supervisory-convergence/supervisory-disclosure/aggregate-statistical-data.

For instance, there is some data related to credit risk in EU banks, which is brought according to stress tests on a real time basis in the form of final tables (see fig. 1).

Table Data related to Credit Risk

Data related to Credit Risk*			2010	2011	2012	2013
Credit Institutions: Own Funds Requirements	Own Funds Requirements Credit Risk % of Total Own Funds Requirements		90,02 %	89,07 %	90,81%	90,45%
Credit Institutions: Distribution by Approach	% Number	Standardised Approach (SA)	91,97 %	92,23 %	92,35%	91,42%
		Foundation IRB Approach (FIRB)	7,63 %	7,37 %	7,38%	8,42%
		Advanced IRB Approach (AIRB)	0,39 %	0,40 %	0,27%	0,15%
	Own Funds Requirements % of Own Funds Requirements Credit Risk**	Standardised Approach (SA)	68,77 %	69,40 %	71,52%	69,92%
		Foundation IRB Approach (FIRB)	18,76 %	18,27 %	15,07%	16,29%
		Advanced IRB Approach (AIRB)	12,47 %	12,34 %	13,41%	13,79%
Credit Institutions: Distribution by IRB Exposure Class	Exposures % of Risk Weighted Assets	Central Governments & Central Banks	2,85 %	1,30 %	2,09%	1,13%
		Institutions	17,53 %	21,22 %	21,02%	16,62%
		Corporate	37,64 %	39,70 %	37,37%	42,78%
		Retail	19,90 %	14,15 %	14,55%	17,69%
		Equity	6,43 %	7,43 %	7,53%	8,17%
		Securitisation positions	2,13 %	1,63 %	1,07%	1,05%
		Other Non Credit Obligation Assets	0,12 %	0,06 %	0,01%	0,17%

[data as per 31.12.]

* Data provided by the OeNB.
** If an institution uses more than one approach, it will be counted accordingly.

Fig. 1. – An example of credit risks assessment in EU as of 2013, carried out according to intensive data collection

Also these organizations conduct the registry of EU credit institutions. It does not contain any data on Russian financial market and credit institutions, but this data can be useful for investment projects of joint financing, as for example in rocket and space branch in the design and One of the largest financial projects in the USA with data-intensive in Big Data is the project of prediction of systemic risks of crediting in banking system [14-16]. The initial data for this project in the USA are contained in the documents on joint credits, posted on the website http://www.sec.gov/.

In Russia and in the regions the prediction of systemic risks of crediting (MIDAS)in today's complicated economic conditions is extremely vital. It is possible to define the goals of such project:

1) To define the most important financial institutions in case of loss of liquidity when the economic system evolves into an uncontrollable state;

2) To define the companies which most likely depend on credit resources (including external credit);

3) To define the effects of changes in the parameters and indicators of the financial system (the key rate, the change in exchange rates, changes in the value of bonds, etc.);

4) To conduct stress tests to define stability of entire system on the whole.

The initial data for these projects may be: requirements of SEC regulator (the analogue is former Federal Commission for Securities Market, now it is Central Bank

of Russian Federation), which oblige the issuers of securities to disclose their reporting data. This reporting data is made with application of GAAP standard, which is quite similar to IFRS and it allows to tell about the definite structure of data, which easily fits into the system of intensive processing of data. In Russia the requirement of Central Bank of Russian Federation to disclose the reporting data is applied to the issuers of securities, crediting institutions etc.

Using intensive financial data may take place, for example, according to the following algorithm: 1) forming a graph of joint crediting; 2) analysis of critical hubs; 3) visualization of corporate relations with other companies and key personalities.

Based on initial data the graph of joint crediting is formed. The graph nodes are the organizations. Two nodes are linked together by the edge if the relevant organizations present a joint credit (may be with other organizations). Edge has a weight depending on the amount of joint credits (the sum of money) the couple of organizations have. For each graph node normalized centrality of proper vector (the centrality is a measure of the graph node importance) is calculated. By such centrality measure, the contribution to the node importance is provided by the important nodes, which are connected. Nodes with the highest level of centrality with high probability are extreme hubs for the network of joint crediting. Extreme hubs then are the subject to a more detailed analysis:

- Relations with other companies (affiliated companies, competitors, credited parties etc.);
- management (taken positions and dates for each person, control over other companies);
- aggregated financial data (borrowing, investment etc.).

As the result America succeeded in creation relational graph of certain banks with other companies and banks, as well as in distinguishing key ventures in banking system. The examples of relations with other companies and key people for Citigroup are shown in figures 2 and 3.
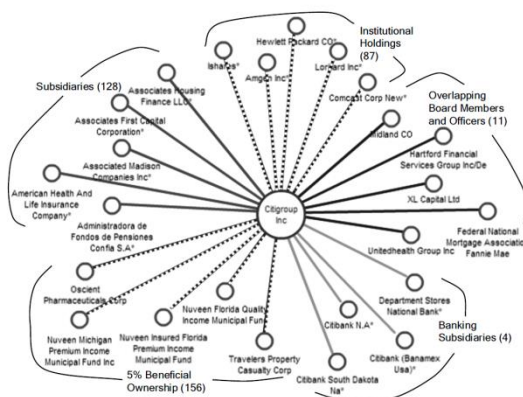
Fig. 2. – The example of connection between the Citigroup bank with other banks
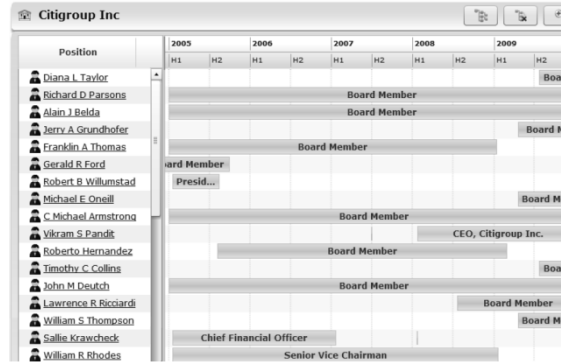
Fig. 3. – The defining of the key people for Citigroup bank within the MIDAS project

As a result, it can be concluded that the intensive use of financial data with the use of Big Data in Russia will allow us to solve problems of joint crediting in the banking sector and to predict the risks in time and develop coordinated management decisions before the crisis. Correct and timely decisions will avoid synergistic effects on the financial market and make the market more predictable and stable.

You can also use the BIG DATA technology in public and municipal administration of the territory on the basis of competitiveness. Competitiveness is an essential characteristic of social and economic systems, including territories. For several years a research on competitiveness of areas, such as region, urban districts, including small and single-industry towns, municipal districts and rural settlements was carried out.

Our approach is based on an understanding of competitiveness as the ability to compete in the competition for scarce resources [17,18].

The basis of the methodology that we developed is the economical and mathematical model of the additive type to assess the territory competitiveness state:

$$
\begin{cases}
KS = (\xi_1 GF + \xi_2 PRF + \xi_3 EF + \xi_4 PPF + \xi_5 APF + \xi_6 SF + \\
\quad + \xi_7 FEF + \xi_8 IfF + \xi_9 UVF + \xi_{10} IF + \xi_{11} InF + \xi_{12} DF) \\
0 \le \xi_i \le 1,\ i = \overline{1,\,12} \\
\sum\limits_{i=1}^{12} \xi_i = 1 \\
0 \le GF \le 1;\ 0 \le PRF \le 3;\ -2 \le EF \le 1;\ -3 \le PPF \le 12;\ 0 \le APF \le 6;\ -3 \le SF \le 29; \\
\le 0 FEF \le 11;\ -2 \le IfF \le 13;\ 0 \le UVF \le 1;\ 0 \le IF \le 2;\ 0 \le InF \le 3;\ 0 \le DF \le 5
\end{cases}
$$

where *KS* – competitiveness; *GF* – geographic factor; *PRF* – natural-recourse factor; *EF* – ecological factor; *PPF* – industrial production factor; *APF* – agricultural production factor; *SF* – social factor; *FEF* – financial and economic factor; *IfF* – infrastructural factor; *UVF* – factor of coordination level with higher public authorities; *IF* – innovative factor; *InF* – investment factor; *DF* – spiritual factor; ξ – coefficient of factor importance (is defined from the experts opinion).

The study highlighted 12 factors of competitiveness specific to the current level of socio-economic development of territories. Each factor has its own importance, which determines its weight, contribution to the total value of competitiveness. Importance of factors is different for different types of territories, reflecting the differentiation in the current state of development.

As for the management decision making, realizability and visibility of information are important, we propose a multi-dimensional visualizing results of the analysis and evaluation of competitiveness. By selecting the dimensions of the space it is possible to illustrate the level and the contribution of different factors of competitiveness to management purposes.

Moreover, it is obvious that a sustainable competitive economic development cannot be endless. For example, according to one theory it is limited by energy and natural resources of the planet, and we are already coming to the point of maximum use. There are other theories, according to which the development curve is approaching to the saturation range.

Despite this, competition or rivalry is still the most important factor which is stimulating the development and qualitative growth of socio-economic systems. Accordingly, the application of the above mentioned state models for the management, in practice based on extensive direct addition of factors components, has its limitations. In the area close to saturation, such models are characterized by large inaccuracy or are inadequate.

In consideration of the foregoing, we propose a more precise methodology for the control of competitive development, which is based on correlations of competitiveness factors that allow defining control vectors using key target parameters. Part of this approach is similar to the method of evaluation of a synergistic effect. However, the latter is quite complicated in terms of numerical values.

During research 6 groups of correlated factors were revealed.

From a practical standpoint, the factor grouping allows the most effectively control the competitiveness, as the maximum increase of the level of competitive development can only be obtained through co-regulatory factors within groups.

Analyzing the correlations it was found that the only factor that correlated with all the others is an investment. Therefore, the target function of management in terms of increase of competitiveness is supplemented by model of control action, which is defined as a limited resource investment:

$$
\left\{
\begin{array}{l}
\Delta_{KS} = 0,058(GF + \Delta GF(L)) \times 0,072(PRF + \Delta PRF(L)) \times 0,064(EF + \Delta EF(L)) \times \\
\times 0,11(PPF + \Delta PPF(L)) \times 0,075(APF + \Delta APF(L)) \times 0,115(SF + \Delta SF(L)) \times \\
\times 0,113(FEF + \Delta FEF(L)) \times 0,076(IfF + \Delta IfF(L)) \times 0,057(UVF + \Delta UVF(L)) \times \\
\times 0,101(IF + \Delta IF(L)) \times 0,104(InF + \Delta InF(L)) \times 0,055(DF + \Delta DF(L)) \to \max \\
\Delta \ldots F = \ldots F(L_m(\bar{\phi})) - (\ldots F) \\
L_m(\bar{\phi}) = \sum_{n=1}^{N} \sum_{m=1}^{M} \dfrac{PV_n^{\inf}}{(1+r^{\inf})^n} \cdot \dfrac{1}{IR} \cdot \phi_{im} \\
m = \overline{1,\ 12} \\
i = \overline{1,\ 12} \\
0 \le GF \le 1,\ 0 \le PRF \le 3,\ -2 \le EF \le 1,\ -3 \le PPF \le 12,\ 0 \le APF \le 6,\ -3 \le SF \le 29, \\
0 \le FEF \le 1,\ -2 \le IfF \le 13,\ 0 \le UVF \le 1,\ 0 \le IF \le 2,\ 0 \le InF \le 3,\ 0 \le DF \le 5
\end{array}
\right.
$$

where ΔF is a change of discounted effects of each factor of competitiveness in municipal entity.

The models which take into account the correlation interaction, are effectively used for the selection of investment projects of territorial development, including the competitive distribution, because they are focused not only on account of direct financial results, but also correlated indirect effects of competitiveness increase and its individual factors. For example, environmental, social and others.

Moreover the development of a modern economy is inherently unstable - a sharp acceleration is followed by the deceleration and vice versa.

For example, the GDP decline of the European economy was 6% in 2008-2009, 1.5% in 2011, 0.2% in 2012. In 2013, the EU GDP is forecasted to grow by 0.6%, in 2014 - by 1.2%. The budget deficit of the euro zone has fallen from 4.2% of GDP in 2011 and to 3.7% in 2012. Further decline in the deficit to 2.8% of GDP in 2013 is expected to happen. At the same time the government debt increased to 91% of GDP in 2012 from 87% in 2011. The unemployment rate is from 4 to 27% in different EU countries.

The Russian economy as less stable showed more prominent changes. GDP growth for the period of 2001-2008 was 6.6%. In 2009-2011 there was a drop to 0.2%, and again growth in 2012 to 3.4%. The size of the public debt amounted to minus 9.5% of GDP in 2011 and 3% in 2012. The budget deficit of 4% in 2010, gave way to a surplus of 0.8% in 2011. However, they could not retain positive dynamics and 2012 was with a deficit of 0.02%.

Moreover, these processes occur in a highly intense competitive environment. Therefore, it is obvious that in such a situation those territories, clusters, companies win which are highly sensitive systems - react to changes dynamically and increase their competitive state. Under these conditions, traditional static linear models cannot provide a solution to control tasks, as:

— They are situational and are applicable in short time intervals, it does not allow carrying out long-term and strategic management;
— They ignore the rate of control response;
— Modern complex multidimensional communication and processes are non-linear.

334

The most effective management of competitiveness in these environments is possible on the basis of dynamic models that have just begun to be used in modern economics.

Thus, we formulate the concept of competitiveness as a dynamic characteristics, defines the application response to any changes in the external socio-economic environment.

Due to the limited volume, we will give the results of dynamic modeling on the example of the social and economic systems of industrial clusters.

Under the proposed new approach, the identified factors of competitiveness, taking into account their mutual correlations, are structured into three dominants: production, labor and capital. In the process of modeling it is necessary to allocate the cluster formation of the overall economic system of the region, i.e., define their boundaries.

Analyzing territorial cluster formation from a position of control, 2 key types are allocated:

1) Functional or managed cluster is that:

— generates as a result of deliberate external influence in strategically important sectors of the state and in the implementation of strategic plans;
— uses the financial, economic and political support of the state;
— as a rule, has a nuclear structure.

2) Self-organizing and entrepreneurial cluster is that:

— is not a product of government agencies;
— generates spontaneously, on the initiative of the business and on the basis of economic relations;
— is not under control and does not have the institutional partners to ensure its survival;
— as a rule, has a matrix structure.

Since the cluster is an open dynamic system, its boundaries are unclear, which led to the use of fuzzy logic and fuzzy sets. Thus the degree of membership is determined by the elements of the system on the basis of necessary and sufficient conditions for the existence of the cluster. The use of fuzzy logic allows to find the area of the intersection of clusters, which are special areas of innovation activity and may provide a breakthrough in the development of cluster systems.

Dynamic models of functional competitiveness and business clusters have a certain look.

Next, the starting point for the management of competitiveness of regional industry clusters of Samara region is determined. For this objective function state model is supplemented by complex of parameters CL that we have developed. The complex CL-parameters includes:
1) Type the cluster according to the criterion of control;
2) Type of cluster development dynamics;
3) The type of the cluster structure;

4) Enterprises producing key products - the leaders of the cluster.

As a result the system characteristics of industrial clusters in the region were formed, on the basis of which it is possible to assess the necessity and the degree of control action and apply the appropriate management models

$$\frac{\partial u_i}{\partial t} = c_i u_i + \sum_{j \neq i}^{n} d_{ij} u_j - \sum_{j \neq i}^{n} b_{ij} u_i u_j + D_i \Delta u_i \quad i = \overline{1,n} \ ,$$

where members of the coefficients *dij* describe the dependence of production in the *i* element from production in the other elements of the cluster; members with the coefficients *bij* take into account the competition among manufacturers.

Dynamic modeling of territorial social and economic systems allowed directly:

— to determine the stationary states of the system, being the target results of management;
— to evaluate state variables of the system when one or another of its parameters is changed, i.e., to trace the impact of management;
— to assess the degree of approximation of the actual system state to the predefined target values and choose the most effective motion path in these conditions.

Despite the apparent complexity of the models, the use of application software at the user level allows to simply interpret the results and formulate management decisions.

To bring the territorial system, for example, the industrial cluster to the area of sustainable development of competitiveness, it is necessary to make adjustment of parameters of the cluster system. It was found that some of the parameters are rather inert. These include: the duration of the production cycle, the pace of staff rotation, tax liabilities and etc. Others have higher dynamics. These are extensive labour capacity, number of employed in production, the unit value of manufactured goods, and others. The most effective control parameters are nonlinear, namely intensive labor productivity growth is achieved through innovation and introduction of new technologies, as well as the employee displacement as a result of intense productivity growth.

The use of dynamic models allow to determine the best configuration of controlled parameters, to assess desired degree of the impact, target results and the speed of their achievements, all of which gives competitive advantage in managing the social and economic system.

To develop the models which predict the competitiveness of the territories it is vital to use large amounts of streaming data on a real time basis. The purpose of this research is to develop models and methods for making management decisions on the basis of forecasting the competitiveness of the territories. The objectives of this study are: to identify factors of competitiveness, to develop a model of competitiveness of the territories using expert estimates, to form information on experts with help of BIG DATA technology. The results of the study include management decision making models of competitiveness of the territories using expert assessments and BIG DATA technology. Practical results include improving the quality and timeliness of decision making on territory management on the basis of forecasting models of the area.

References

1. DRAFT NIST Big Data Interoperability Framework. Use Cases and General Requirements. National Institute of Standards and Technology, 2014; 4.
2. Big Data is a Big Deal. The White House, Office of Science and Technology Policy. Source: <http://www.whitehouse.gov/blog/2012/03/29/big-data-big-deal>.
3. **Shantenu Jha, Judy Qiu, Andre Luckow, Pradeep Mantha, and Geoffrey C. Fox**. A Tale of Two Data-Intensive Approaches: Applications, Architectures and Infrastructure. 3rd International IEEE Congress on Big Data Application and Experience Track, 2014.
4. **Judy Qiu, Shantenu Jha, Andre Luckow, and Geoffrey C.Fox**. Towards HPC-ABDS: An Initial High-Performance Big Data Stack, 2014.
5. **Geoffrey Fox, Judy Qiu, and Shantenu Jha.** High Performance High Functionality Big Data Software Stack. Big Data and Extreme-scale Computing (BDEC), 2014.
6. Source: <http://www.exascale.org/bdec/sites/www.exascale.org.bdec/files/whitepapers/fox.pdf.>.
7. **Geoffrey C.Fox, Shantenu Jha, Judy Qiu, and Andre Luckow.** Towards an Understanding of Facets and Exemplars of Big Data Applications, 2014. Source: <http://grids.ucs.indiana.edu/ptliupages/publications/OgrePaperv9.pdf>.
8. **Geoffrey Fox and Wo Chang.** Big Data Use Cases and Requirements, 2014. Source: <http://grids.ucs.indiana.edu/ptliupages/publications/NISTUseCase.pdf>.
9. **Geoffrey Fox.** INFO 590 Indiana University Online Class. Big Data Open Source Software and Project, 2014.
10. Source: <wttp://www.whitehouse.gov/mgi>.
11. Source: <http://www.whitehouse.gov/open>.
12. NIST Integrated Knowledge EditorialNet (NIKE). Source: <http://xpdb.nist.gov/nike/term.pl>.
13. Source: <https://rd-alliance.org/group/metadata-standards-directory-working-group.html>.
14. **Balakrishnan S, Chu V, Hernandez MA, Ho H, Krishnamurthy R, Liu S, Pieper J, Pierce JS, Popa L, Robson C, Shi L, Stanoi IR, Ting EL, Vaithyanathan S, Yang H.** Midas: Integrating PublicFinancial Data. SIGMOD, 2010; 1187-1190.
15. **Arasu A, Re C, Suciu D.** Large-Scale Deduplication with Using Dedupalog. ICDE, 2009; 952-963.
16. **Chiticariu L, Li Y, Raghavan S, Reiss F.** Enterprise Information Extraction: Recent Developments and Open Challenges. SIGMOD, 2010; 1257-1258.
17. **Ramzaev VM, Khaimovich IN, Chumak PV.** Management of investment projects during energy modernization of enterprises in the region. Economic sciences, 2013; 4(101): 109-113.
18. **Ramzaev VM, Khaimovich IN, Chumak PV.** Models and methods to manage energy efficiency in the organizations taking into account the limitation of investment resources. Modern problems of science and education4. Source: <http://www.science-education.ru/110-9960>.

Philosophic aspects of developing new knowledge under data intellectual analysis (Big Data)

Bodrov A.A., Ramzaev V.M.

International Market Institute Samara

Abstract. Based on interdisciplinary analysis, the paper considers the process of forming new philosophy of knowledge, which is currently emerging owing to the use of information technologies and, above all, the Big Data techniques. Examined are also transformations of ontological and gnoseological paradigms of the scientific cognition contemporary system. Offered are new conceptions enabling comprehensive interpretation of diversity of natural and social factors influencing the human being as the processes owner, use of unobvious correlations in philosophic and social-economic practice. Access to these conceptions actualizes appropriateness of analysis with the aid of Big Data in the most significant spheres of the people's biosocial activity.

Keywords: Big Data technologies, spheres of bio-sociological human activities, ontological reality development, epistemological potential, virtual setting.

Ontological manifestations of reality in the XXI-st century are notable for extreme diversity, which often complicates its perception and disorients the people misleading them as to trueness of objective reality manifestation.

Under these conditions, virtualization becomes inherent not only to the social-and-economic reality (which has been covered by the researchers quite a lot), but also the problem-bearing science field embracing ontological and gnoseological components, undergoing major transformations requiring philosophic and general-scientific comprehension.

In our opinion, the Big Data techniques can provide assistance to the human beings; these techniques make it possible to process and use huge information volumes, promote taking managerial decisions in all life spheres, change the world perception due to reality digital analysis as well as its ontological fundamentals, thus actualizing the necessity of revision of philosophic and general-scientific reality principles; it is equally true with regard to seemingly established 'material-spiritual'

dilemma. Indeed, being part of the contemporary social-cultural system, Big Data actively impact all the present-day society's spheres [May14], transforming them in the human state of awareness, which enables reconsideration of the classical philosophic dilemma 'substance-spirit' offering instead a much more topical one: 'material-informational'.

Such dynamically changing conditions and a huge information flow strongly force the human beings to mediate upon the pattern of behavior in the information space, handling this space and comprehending the development in general; primarily comprehension is critical with regard to social development and its representation: either by real transformation of the substantive being or by interactive manipulations embodied only in the virtual medium (which actually stands for digital medium) being of high relevance to the human beings.

Speaking about the philosophic aspects of practical implementation of the Big Data techniques potential, it is immediately advisable to single out two main aspects of their possible application – ontological and gnoseological, mentioning in this connection that Big Data represent not just another manifestation of the information space, but a new philosophy enabling reception of knowledge on the basis of large-scale data flow analysis.

In the ontological aspect, willingness to substitute real processes by virtual interactions becomes quite evident. Thus and so, excessive information does not always play a positive role, because in practice it can facilitate taking erroneous decisions, while in the philosophic sense it leads to emerging of virtual worlds (potential possibility of detalization of which is represented by Big Data), which ultimately facilitates deviation of the people from substantial reality. However, by changing perception of reality in its ontological manifestations the Big Data techniques enable large-scale visualization of social and natural processes in the interactive format, thus detailing the visualized objective reality while producing all sorts of models including economic ones. Undoubtedly, it leads to consolidation of perceptions of the objective reality's interactive nature.

In the context of the narrative it should be noted that the temporal presentation of classical science are subject to revision, but rather, a fundamentally new in-depth analysis on the basis of the potential detected by the use of Big Data technology.

It is worth noticing the increase in the variability of conceptual reality, multidimensionality of its capabilities, out of reach for philosophical and general scientific analysis without relying on the potential of Big Data.

In its ontological essence of Big Data technology actually form a fundamentally new coordinate system and the nature of modern society, which displaces an established understanding of the world. However, previous performance and characteristics of bio- and geo- systems do not disappear, but they are forced out by much more detailed new systems, capable of providing virtually sensory reflection of reality. The line between the virtual and sensual at the same time is disappearing; putting the person in a confusion asking a quite simple question: whether he has a true reality? One of its most important, as we can say "classic" characteristics is time, which has an ability that is worth noting separately, to accelerate and decelerate in a social sense, depending on the degree of saturation by socially significant events.

Each event, which is considered through the prism of Big Data, can be become an important, vital, revolving. Therefore, it should be stated clearly that now we face unprecedented acceleration of social time.

Thanks to Big Data technologies the primacy of permanently accelerating time makes the search for the cause of human reality a luxury, revealing the danger that the reality is transformed into an impersonal "white" space.

Knowledge of individual industries are integrated into a single system that visibly indicates the formation of integral knowledge, integrated in all its branches and directions and is able to respond to requests quickly, comprehensively and accurately, leading the search for the causes outside of the Big Data technology. And if earlier the reality had quite a limited number of variations of its epistemological perspectives, now the Big Data let you create countless variations of the potential realities represented in the digitized space-time models.

The Big Data techniques gnoseological potential deserves special attention; it can embrace all the scientific investigations stages – from research problem statement up to extension of the research outcomes [Sad14].

Special emphasis shall be made on the possibility of introducing changes in the key cognition methods with the aid of Big Data, which would help overcome crisis in many humanities, thus producing absolutely new scientific theories under the use of enormous array of diverse information. Attempts to use this approach with regard to analyzing the world history are undertaken at the Moscow State University. Detalization of the history-related reality turns out to be so multidimensional and thorough that within the framework of the interactive history visualization 'ChronoZoom' project it is entirely possible to pool together information on social events of the past, climate, geographical changes and genealogical data of individuals [Ber14]. However, addressing mainly the historical process formal detalization the philosophy of history is almost completely ignored.

Spreading of the Big Data possibilities in the gnoseological sphere makes it quite realistic to reconsider and expand the coherence notion as one of the criteria of scientific truth, practical realization of which implies correlation of each new scientific statement with the previously made statements within the framework of the given theoretical system. Application of the Big Data potential in this direction is practically inexhaustible.

The Big Data universal nature makes it possible to interpret the respective techniques in a broad spectrum of their potential capacity, which is extremely topical for the gnoseological sphere. That sort of consideration enables presentation of the Big Data simultaneously as a tool of scientific hypotheses publication, elicitation of facts and regularities in combination with their novelty validation as well as a tool of disseminating the research results.

Analysis of the potential of Big Data, an updated process of implementation of these technologies in the industrial and scientific practice, convinced us visibly of the need to use the axiological approach to the perception of the likely impact of technology on society beginning of XXI century. The background, providing the possibility of problematization of the process of interest is fairly simple to identify. In our opinion, it is in the situation, where the inner content perfectly correlates with the

biblical mythology that characterizes God as the omniscient beginning. It is the characteristics that will interest us, first of all, due to the fact that Big Data technology allows us to thoroughly detail the reality of man in elevating the status of being omniscient, thanks to the fundamental possibility of cloning able to create their own kind artificially.

This significant increase in the person's status really increases the potential impact on the environment, and the creatures of their own kind, setting at the same time before the man an extremely significant problem. They are defined by the opposite way; oriented meaningful vectors directed both from the surrounding reality, the perception of which is now more mediated by Big Data, and from the man as a creature possessing sufficient capacity to transform the world on your own.

Detailing these problem areas, we believe that it is important to note a number of highlights: gaining the ability to smallest, and probably the most precise detail of reality with the help of Big Data, including in terms of its potential development, will a man be able to "face the truth" if the forecast is extremely unfavorable, will he have the will and reason to overcome the uncertainty of the future and detailed Big Data problems, as all predictions based on Big Data, may affect his immediate personal interests, which a priori cannot be taken impartially? In the perspective it should also be determined who will have access to this kind of analysis and prediction, primarily of negative character, because one of the fundamental characteristics of scientific knowledge is accessibility to all, and it is closely associated with humanity, while the negative information is able to deprive the community from the balance, therefore, access to it should be limited.

Such-like reasoning touches not only philosophic spheres, but also the real economy sector, where balanced solutions are of great demand, where increase in goods and services sales volume is critical, i.e., what is meant here is managing the consumer behavior and primarily – forecasting for at least the short-term perspective the customers' preferences (as a special case).

Complexity of such forecasts is quite evident and seemingly formidable, which is largely determined by a huge diversity of all sorts of factors influencing the human beings as acting parties.

In terms of the sociocentrism principles, it is necessary to integrate the human being into the geosocial space from the standpoint of the XXI century science – in the status of collective subject with the purpose of establishing correlation between the individual and group conduct causality and primarily as to individual motivations (both deliberate and unconscious), which are often conditioned by geomagnetic processes of the surrounding media. That sort of task is extremely topical not only from the scientific point of view, but also in view of the complex optimization of all the social-economic system interrelations, specifically pertaining to their management. The abovementioned task can be successfully settled under application of large-scale diverse information field (of social and nature-specific kind) – by using the Big Data mechanisms.

This being so, it is quite possible to reveal and fully utilize (both in philosophic and social-and-economic practices) correlations that are not always evident. In such a way, the Big Data approaches – owing to analyzing huge information volumes –

341

make it possible to establish dependence of the social-and-economic manifestations of the people's life activities on the macro- and mega-processes proceeding in the geo- and helio-systems, thus demonstrating the possibility of perceiving the people's economic activity as a kind of derivative with respect to a number of factors, of which attention should be paid primarily to the non-cyclic factors emerging in the Sun; the 28-day cycle of the Moon's activity; annual, seasonal and daily solar cycle; the 11-year cycle of Sun's activity linked to periodicity in the motions of the Sun's spots. The potential of such information – as indicators in the economic simulation approaches – is at present far from being properly studied, although the abovementioned phenomena have been long known in natural science. By way of giving an example, the 11-year cycle of the solar activity was discovered by G. Schwabe as early as in mid of the XIX-th century. Dwelling on the relations between the people and the space global entity, the Russian cosmist K.E. Tsiolkovsky wrote: 'Everything is generated by the Universe. It is the beginning of all things, everything depends on it ... The most intelligent creature fulfills only the will of the Universe. This will, depending on the senses cannot be the sole source of acts: the Universe can always intervene, distort, disrupt, and not allow fulfilling the will of one mind. We say all depends on us, but we ourselves are the creation of the Universe. Therefore, it is better think and say that it all depends on the Universe. We believe, but the Universe manages it as it wants, without ceremony it destroys our plans, and even destroy the entire planet with its intelligent beings. If we succeed and fulfill our will, it is only because the Universe allowed this to us. It always has at its disposal many ways and causes to retard our activity and manifest another, a higher will, although our will is just the will of the Universe'. [Tsi28] Close interrelation of the mankind and our planet's biogeosphere was pointed out by V.I. Vernadsky paying attention to the fact that 'the man and the mankind are first of all, and most closely, linked with the living matter populating our planet. By no real physical process can they be separated from it… The man as any other living natural (or real) body is inseparably linked to a certain geological envelope of our planet, with the biosphere, noticeably differing from its other envelopes. The structure of the biosphere is defined by its peculiar state of organization. Being an isolated part of the whole, the biosphere occupies a regularly fixed place within the planet'. [Ver97]

Indeed, influence of such geo- and helio-factors on different aspects of human activities turns out to be quite evident. At the same time, the opportunity of integrating the given natural-science facts and figures into a unified system directly influencing the bio-social activity of human beings appears only today – owing to the analytical potential of the newest technologies and approaches under consideration, which enable detection and full-scale consideration of the unobvious correlations in the information-specific flows.

Eventually, within the framework of economy-specific simulation the human being can be represented not from the standpoint of his isolation or even opposition to the natural processes of terrestrial and space scales, but rather in terms of his biosocial essence being thus characterized as an element of reality subject to quite evident social-and-economic impact as well as influenced by global processes of space level, reducible to specific indicators, which – based on Big Data techniques – can be

successfully interpreted and used as individual cases while taking managerial decisions owing to correlation of the space-specific (biological) elements and social (economic) elements in the human conduct.

This bio-social human activity in the information interfacing system is manifested in various spheres that can be thoroughly studied with the aid of Big Data techniques – from the standpoint of possible impacting them with the aim of optimizing the process of managerial decision making and achieving the biggest possible economic effect.

In this context, we consider it quite reasonable to undertake intellectual analysis of a number of significant human bio-social activity spheres with the aid of Big Data techniques. These spheres could include environmental-geographical realm; approaching this realm would enable interpretation of the human social-economic activity as a derivative of the processes taking place in the geo- and helio-systems.

Analysis of spirituality and world outlook as manifestations of the people's activities will facilitate defining the influence of spiritual, religious and other forms of irrational perceptions on the social-and-economic sides of the people's life activities; it will also enable influence on the world outlook guidelines including (as individual case) new scientific achievements as related to collective consciousness.

In the sphere of educational preferences, the biggest interest is in the changes of educational priorities – with the view of determining policy in this sphere. The present-day demographic situation makes it necessary to turn to the family and marriage in order to detect tendencies of changes in perceiving the matrimonial relations and family values as well as views on different marriage forms.

Given all the complexity and manifoldness of financial process in the contemporary economy, the researchers are focused on the investment sphere, which implies addressing motivations and directions of the population's investment activity (forecasting possible alternatives of investing the available capital, revealing dependence of the lead-time on investment upon economic, social and natural trends).

Determining the marketing strategy – based on the Big Data approaches – actualizes significance of the consumption sphere from the point of view of producers with regard to manufacturing different product groups and taking possible corrective measures. Of no less importance is significance of politics – from the point of view of analyzing passionate manifestations of communities' activities and associated possibility of constructive impact on the public consciousness with the purpose of optimizing management and preventing conflicts and eliminating social tensions.

Deviant activities and social concerns cannon be always clearly institutionalized. Despite this fact, analysis with the aid of Big Data can be quite successfully applied to this sphere, in this case, it will be possible to reveal the causes and conditions determining realization of individual's deviant inclinations, which would facilitate prevention of similar actions and ensure development of technologies of eliminating social concerns at the personal and public levels.

Against the described background, Big Data techniques perform as a kind of tool of regular recreation of the interactive reality and manipulation in the virtual environment, thus making it possible to transform in a very profound manner the perception of the information-related aspect of manifoldness of societal relations

determining (in more precise terms – computing with the aid of large-scale data volume) the leitmotiv that directs specific phenomenon's or process's development vector. 'Webbed' in such a manner informational or digital reality, would enable appropriate decisions, thus submerging the person into the world of models and essential schemes, in which alteration of a given value can lead to a chain reaction and change the character of the whole 'reality' based on Big Data. Under these conditions, each indicator's value in the reality's 'digital vision' structure becomes more significant, otherwise interpretation of the situation will turn wrong and the respective decision – erroneous. Against this background, it is important to succeed in selecting from the variety of the Big Data-offered facts and figures those values that directly or indirectly affect the situation, simultaneously differentiating between data of primary and secondary importance, removing unnecessary information. This being so, it is appropriate to put the question of false knowledge occurrence, in which event the antecedent knowledge could be unnecessarily doubled and even cancelled; this would lead to impossibility of collecting qualitatively new knowledge as the next step in decision making and consequently – to failure of developing the Big Data-based reality.

It is possible to state formation of a new guideline, the principles of which significantly reduce topicality of the conventional question 'Why?' (which has been shaping the baseline of philosophical and scientific research for a long period) thus substituting this question for the questions 'How?' and 'What?', which are much more significant and meet the interests of the present-day society. At first sight, it might look as escaping causality, consequently – loss of scientific approach, rationality and feasibility.

In our opinion though, attentive consideration of the issue makes it possible to emphasize that deviation from searching for causality makes up merely outward appearances, because in reality the search for causality transforms and gives way to the use of huge data field, which combined with knowledgeable and correct problem setting and use of IT assures the XXI-century science transition to a qualitatively new level and in the practical sphere – enables weighed decisions and efficient economic modeling. In this connection, quantitative indicators will no longer act as transcendental quantities, they become immanent indicators of social-and-economic reality, being converted effectively into the cognition tool, into the tool of influence and perception, thus absolutizing the cause-and-effect relation, on the one hand, but remove them from the field of vision and make them unobvious, on the other hand.

As a result of using the Big Data techniques in the contemporary social-and-economic conditions, opportunity is generated as to assigning a new status to the information – as a virtually inexhaustible economic resource, the significance of which leaves no doubts in society, while its infiniteness and universal nature are ensured by the possibility of practically endless number of interpretations. In these circumstances, it is extremely important to mention that – as distinct from other economic resources (the volume and quality of which facilitate taking this or that decision) – the information is not 'depreciated', it is never unfit for use, but owing to the abovementioned capacities and in the course of interpretational possibilities with the aid of Big Data can be incorporated into new information flows. Alongside with

344

that, the information volume grows from year to year evidently demonstrating its inexhaustibility.

All that provides an opportunity of stating the fact that information is in the process of being converted into a multidimensional tool (of analysis, management and forecasting) affecting not only the up-to-the-minute interests and needs of the people, but requiring a deep philosophical comprehension – due to its orientation towards principal transformation of in-depth fundamentals of both gnoseological and (unconditionally) ontological planes, in any possible manifestations. Such processes require all-round analysis and development of distinctive and absolutely new theoretical platform, which in short-term perspective means raising the philosophy to a qualitatively new level linked to transformation of the whole problem-bearing research field, consequently providing for elaboration of new ontological principles and new methodology of comprehending the human's knowledge and existence.

References

1. **Berezin SB.** Cloud technologies in the natural sciences and humanities / S.B. Berezin, Big Data in the National Economy. Moscow, 2014. URL: http://istina.msu.ru/conferences/presentations/8469122/
2. **Mayer-Schonberger V, Cukier K.** Big Data: A Revolution That Will Transform How We Live, Work and Think / Viktor Mayer-Schonberger, Kenneth Cukier. Trans. from English by Inna Gaydyuk. M.: Mann, Ivanov and Ferber, 2014; 232 p.
3. **Sadovnichy VA.** Intelligent System of Scientific-and-Technical Information Thematic Study (ISTINA) / S.A. Afonin and colleagues. Under the editorship of Academician V.A. Sadovnichy. M.: Moscow University Publishers, 2014; 262 p.
4. **Tsiolkovsky KE.** The Will of the Universe. The Unknown Intelligence. M.: AVT, 1928; 23 p.
5. **Vernadsky VI.** Scientific Thought as a Planetary Phenomenon./ Trans. from Russian by B.A.Starostin. M.: Nongovernmental Ecological V.I.Vernadsky Foundation, 1997; 265 p.

The Big Data mining to improve medical diagnostics quality

Ilyasova N.Yu., Kupriyanov A.V.

Samara State Aerospace University,
Image Processing Systems Institute, Russian Academy of Sciences

Abstract. The paper offers a method of the big data mining to solve problems of identification of cause-and-effect relationships in changing diagnostic information on medical images with different kinds of diseases. As integrated indices of the fundus vessels and coronary heart blood vessels we have used a global set of geometric features which is supposed to be a rather complete characteristic of diagnostic images and allows to make a successful diagnosis of vascular malformations. To evaluate informativity of vascular diagnostic features based on a classification efficiency criterion and in order to form new features required to improve a diagnostics quality a method of discriminative analysis of sample data has been considered. A filtration method of invalid data is proposed using a clustering algorithm to improve a performance quality of the developed algorithm of the discriminative analysis of feature vectors.

Keywords: human vascular system, image processing, diagnostic features, discriminative analysis

1. Introduction

The very large data ('big data') mining is a key problem of modern information technologies. In accordance with the Forecast of the Scientific and Technology Development of the Russian Federation for the period until 2030 approved by the Chairman of the Government of the Russian Federation Dmitry A. Medvedev promising research areas include the "Technologies of data processing and analysis" including methods and techniques of collection, processing, analysis and storage of very large volumes of information. The purpose of the paper is to develop methods and algorithms of the bid data mining to solve problems of identification of cause-and-effect relationships in changing diagnostic information on medical images with different kinds of diseases. It is offered to use a single approach to the analysis of different image classes based on evaluation of combined geometric parameters of selected areas of interest which are considered to be a basic feature set for further diagnostic analysis [1-2]. In order to identify images based on the big data mining

using methods of the discriminative analysis a technique of efficient feature space formation has been developed [3-5]. As integrated indices of the fundus vessels and coronary heart blood vessels it is proposed to use the global set of geometric features which allow to make the successful diagnosis of vascular malformations [6-7]. Based on the specified methods new distributed technologies and software are developed to provide the remote image processing, analysis and understanding which are intended for implementation in automated telemedicine systems. The methods being developed are aimed at improvement of the medical diagnostics quality due to obtaining objective numerical estimates of biomedicine image parameters using large volumes of accessible information.

2. Diagnostic Image Mining Information Technology

The diagnostic image mining information technology includes a method of formation of the efficient feature space to classify a predefined image set.

A highlighting technique of diagnostically significant information on blood vessel images is based on a new generalized mathematical model of blood vessels for two classes of diagnostic images, i.e. the fundus blood-vessel system and coronary blood vessels, characterized by a set of geometric parameters [6-8].

A geometric approach to formation of diagnostic features, which, unlike traditional abstract spectral-and-correlation features are well accustomed and understandable by medical professionals, demonstrate a good visual effect and take into account an object's specific character, allows to finally increase a diagnostics efficiency.

In order to select the most successful features we use their correlation with results of expert evaluations, as well as a dispersion analysis of learning samples or the diagnostic error analysis using particular characteristics. The effectiveness of different features is evaluated for automated diagnosis problems and proper recommendations are articulated on how to use different groups of features in medical practice.

The diagnostic image mining information technology includes the following advanced techniques and algorithms:

— the technique and the algorithm of increasing a degree of the feature informativity based on the discriminative analysis and formation of an optimal learning sample to learn a disease diagnosis expert system;
— an estimation method of a class separatability which is not influenced by distribution of objects through classes and is independent from a used classifier;
— the algorithm of decrease of feature space dimensions and formation of new informative features that maximize a separatability criterion based on methods of the discriminative analysis and allow to increase a diagnosis accuracy of a pathology degree;
— a technique of optimum learning sample formation to learn a diagnostic system based on exemption of anomalous observations that will also enable to increase a disease diagnosis accuracy.

Problem-oriented and distributed software solutions of the analysis of medical and diagnostic images are developed to detect pathological changes including software

tools for quantitative estimates of the pathology degree based on expert findings and the proposed methods of classification. They are intended to ensure the user with an opportunity to manage a decision-making and analysis process [9]. Automated systems of the quantitative feature analysis make it possible to standardize a diagnosing process, considerably reduce an examination time and decrease its cost. The systems allow to carry out the analysis of subclinical morphological changes of pathomorphological components, computerize diagnosis stages and make a quantitative monitoring of pathological changes in diagnostic images. The peculiarity is the use of expert system components, i.e. a database of diagnostic features, the correlative, discriminative and cluster analysis of the feature space, and a prognosis of the pathology degree based on expert estimates.

A system of classification and diagnostic researches [1] provides tools for the correlative and discriminative analysis to form the informative feature space, resources to form an optimal feature sample based on the criterion of separation efficiency by pathology groups, and facilities for the cluster analysis to filtrate the learning sample in order to eliminate invalid data and to obtain standard feature values in accordance with pathology groups. The data mining system allows the user to obtain a proper pathology degree, standard feature values for each degree of disease pathology and a predicted disease development, and will provide proper diagnostic decisions.

3. The Discriminative Analysis to Form the Informative Feature Space

Proper researches have been performed together with medical professionals from the Medical and Stomatological University (Moscow), Ophthalmology Academic Department, based on a digital image analysis of the fundus. Diagnostics techniques for ophthalmic diseases have been developed based on evaluation of global vascular characteristics (features). The paper considers geometric characteristics proposed in [6-10]. These characteristics involve the following: the mean diameter, straightness, beads-looking shape, amplitude of thickness variations, frequency of thickness variations, thickness tortuosity, amplitude of path variations, frequency of path variations and path tortuosity, which correspond to diagnostic features of the fundus vessels. If two or more classes available (in our case there are 5 classes including a normal feature and 4 degrees of diabetic retinopathy and diabetes), the objective of feature selection is to select those features which are the most efficient in accordance with the class separability [5,8]. In the discriminative analysis the class separability criteria are formed using scatter matrixes inside classes and scatter matrixes between classes [11,12].

The scatter matrix inside classes demonstrates a variety of objects with respect to mean vectors of classes: $\mathbf{W} = \sum_{k=1}^{g} (\mathbf{X}_k - \bar{\mathbf{x}}_k)(\mathbf{X}_k - \bar{\mathbf{x}}_k)'$, where k − class data will correspond to the mean vector $\bar{\mathbf{x}}_k = [\bar{x}_{1k}\bar{x}_{21k}\dots\bar{x}_{pk}]$, and g − is a total number of classes.

Elements of the scatter matrix between classes B is counted by the formula: $b_{ij} = \sum_{k=1}^{g} n_k \left(\bar{x}_{ik} - \bar{x}_i\right)\left(\bar{x}_{jk} - \bar{x}_j\right), i, j = \overline{1, p}$, $\bar{x}_i = \left(1/n\right)\sum_{k=1}^{g} n_k \bar{x}_{ik}$ − is a mean feature

348

value of i - feature in all classes, n_k – is a number of objects in k - class, $\overline{x}_{ik} = 1/n_k \sum_{m=1}^{n_k} \overline{x}_{ikm}$ – is the mean feature value in class k, and x_{ikm} – is a value of i - feature for m -object in k - class. The matrixes W and B contain all basic information about interrelationships inside and between classes. In order to obtain the class separability criterion some number is to be associated to these matrixes. This number should be increased with the increase of scattering between classes or with the decrease of scattering inside classes. For this purpose the following criterion is more frequently used [11]: $J_1 = tr(\mathbf{T^{-1}B})$, where $\mathbf{T} = \mathbf{B} + \mathbf{W}$. The greater the value of the criterion - the more separability of classes. The following algorithm presented in Figure 1 has been developed to form new features.
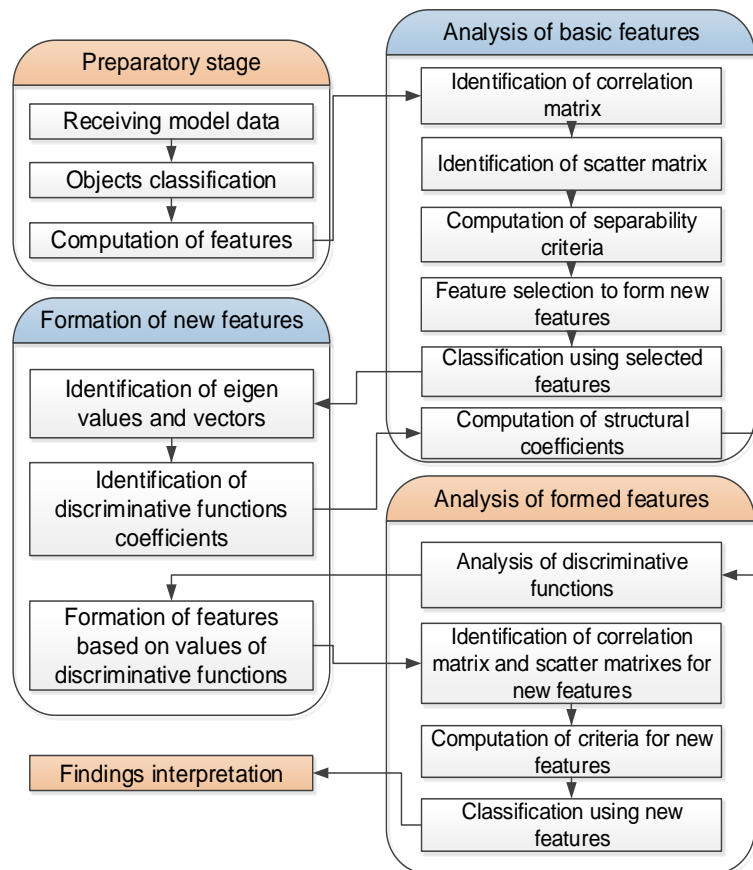
Fig. 1. – Algorithm of the discriminative feature analysis

4. Experimental Studies

A number of studies of vascular malformations have been undertaken for diabetic retinopathy (DR) of 151 patients suffered with diabetes (D) based on the digital image analysis of the fundus. After processing of images the sample amounted to 8175 measurements including 1490 arteriols of the 1st-order, 2345 arteriols of the 2nd-order, 1960 venules of the 1st-order, and 2380 venules of the 2nd-order. Medical professionals separately consider venules and arteriolas of the 1st and 2nd order (GROUP 1 – GROUP 4) since different tendencies of vessel changes can be observed in these GROUPS at different pathology stages. Figure 2 shows some examples of diagnostic images of the fundus for different stages of diabetes (1D, 4D) and a measurement sketch of the vascular system that gives an order of the vessel examination accepted by ophthalmologists.
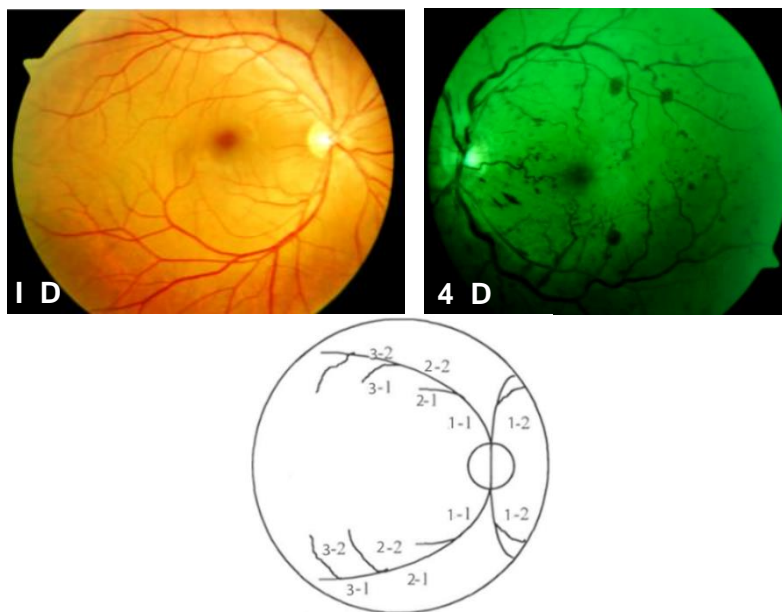
Fig. 2. – Examples of diagnostic images of the fundus for different stages of diabetes (1 D, 4 D) and a measurement sketch of the vascular system

At the examination of features it was concluded that there are two high-correlated characteristic groups. The first group includes those features which describe path parameters (e.g. the path straightness and tortuosity), and the second group includes the features characterizing a vessel radius function (e.g. the radius tortuosity and a beads-factor). Figure 3 gives values of the separability criteria of single features for each of the four GROUPS (venules and arteriols of the 1st and 2nd orders).
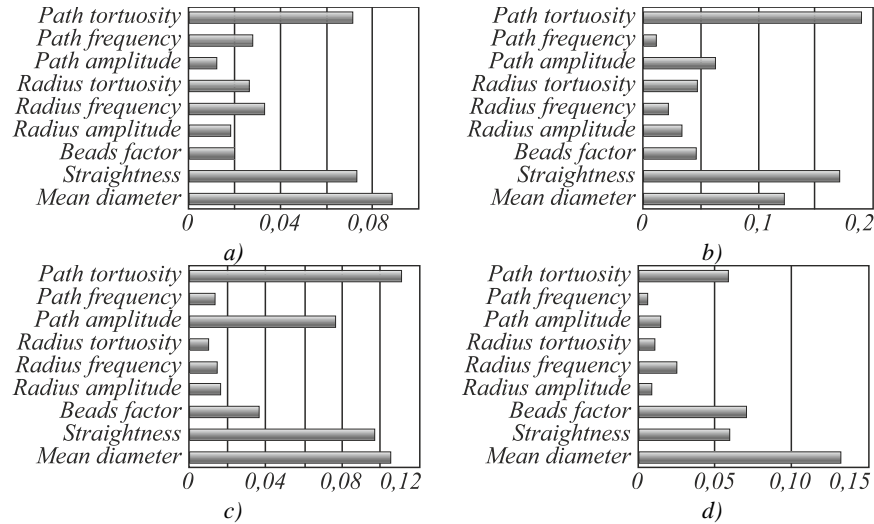
Fig. 3. – Values of feature separability criteria for each of the four GROUPS of vessels before filtration: a) and b) arteriols of the 1st and 2nd orders, and c) and d) venules of the 1st and 2nd orders

Figure 3 shows that maximum feature values belong to the vessel features which are not particularly significant for medical professionals in diagnosing. Besides, in proper pathological conditions each group may have vessels which do not comply with the given pathology (for instance, the norm feature). It may be thus concluded that the sample may contain some noisy data.

In order to eliminate noise in the sample it is proposed to filter down an original sample using the clustering approach of k-means. Each GROUP was divided into 5 clusters in accordance with original clusters inside each of the GROUPS. Feature vectors which were not included into a correct cluster were removed from the sample. Values of individual separability criteria for features inside the GROUPS after filtration are given in Figure 4.

Analyzing Figure 4 we may conclude that in the sample obtained after filtration the features with the greatest separability criterion are the characteristics which are considered by medical professionals as specifically diagnostically significant in visual diagnosing of pathology that corresponds to an information letter [13]. The discriminative analysis algorithm has been applied for original and filtered samples. In order to form new features we have completely enumerated original features to search a combination of new features that has maximized the separability criterion. The result was that we have obtained a set of four features for all GROUPS of either sample.

The classification error was evaluated for the GROUPS obtained thereby. The error was estimated by means of the U-approach [11]. Two samples were formed, i.e. the learning and test samples. The classifier was tuned using the learning sample based on the SVM approach (Support Vector Machines), and the test sample was thereby classified. Objects of the learning sample which are not contained within the test

sample are only used for the classifier synthesis. There are many opportunities to implement the U-approach. In order to evaluate probability of the classification error in researches a one-object-elimination method was used. The findings are illustrated in Table 1 where criterion values before the discriminative analysis are presented for the combination of original sample quads with the best separability values inside the GROUPS.
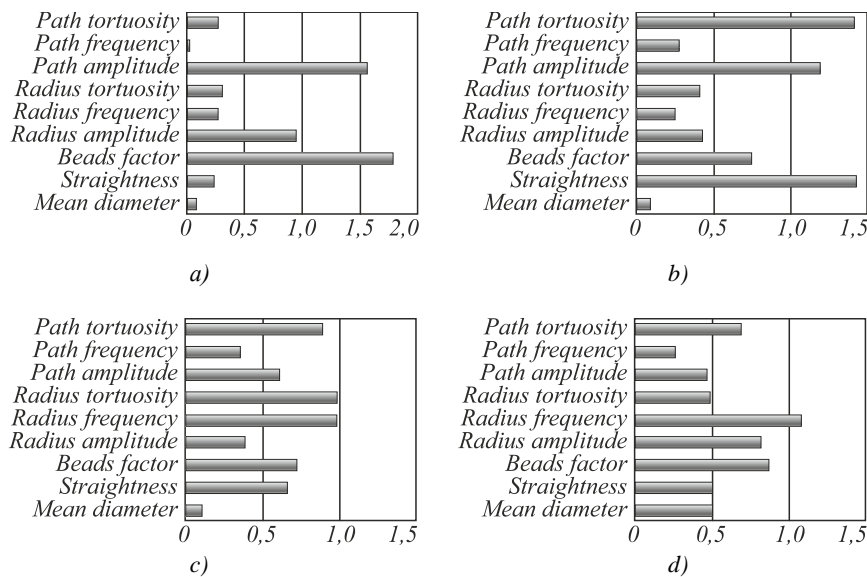
Fig. 4. – Values of feature separability criteria for four GROUPS of vessels after filtration: a) and b) arteriols of the 1st and 2nd orders, and c) and d) venules of the 1st and 2nd orders

Analyzing the obtained findings it may be concluded that filtration allows not only to increase feature separability criteria and decrease the classification error, but also to identify diagnostically significant features. Researches made on four GROUPS of blood vessels have shown that it is important for each GROUP to have its own set of diagnostic features that is proved by clinical research studies of medical practitioners. For example, the mean diameter of the blood vessel acts differently for venules and arteriols under pathological changes. The research results have showed that the application of the proposed feature formation technique allowed not only to eliminate invalid data, but also led to a reduction in errors of classification. This resulted to the increase of the separability criterion by 39% for GROUP 1, by 42% - for GROUP 2, by 24% - for GROUP 3 and by 39% - for GROUP 4. Besides, we have obtained some additional information based on the used features such as their informativity and have identified relationships between some features.

352

Table 1. Findings of the feature space discriminative analysis

Group		Original sample			Filtered sample		
		J	Increasing criterion	Error	J	Increasing criterion	Error
Arteriols of the 1st order	befor	0.21	40%	0.185	1.69	9%	0.071
	after	0.31		0.104	1.85		0.024
Arteriols of the 2nd order	befor	0.35	19%	0.144	2.48	6%	0.083
	after	0.42		0.090	2.62		0.028
Venules of the 1st order	befor	0.29	50%	0.128	2.07	17%	0.045
	after	0.44		0.096	2.41		0.035
Venules of the 2nd order	befor	0.28	27%	0.162	2.21	12%	0.072
	after	0.36		0.113	2.47		0.023

5. Conclusion

A new technology has been developed for the data mining to identify cause-and-effect relationships of changing diagnostic information on medical images with different kinds of diseases including the filtration of invalid data and the discriminative analysis based on maximizing the separability criterion.

The algorithm based on the selection of features with the biggest separability criterion and on a complete enumeration followed by new features maximizing this criterion has been developed. Separability criteria are formed using the scattering matrixes between and inside classes. As a result of the discriminative analysis the best features have been defined for each group of vessels based on the separability criterion. It is shown that each of the four GROUPS of vessels has efficiently used its own set of global geometric features that has been proved by clinical researches. The classification error was calculated for each group of vessels before and after the algorithm performance. It is shown that the proposed technology of the feature space analysis by groups, including the algorithm of filtration of sampled data and the algorithm of formation of the efficient feature space, allowed to increase the classification efficiency of vessels by "normal-feature" classes and different degrees of "pathology". The classification error was hereby reduced to 2.3%-3.5% for different pathology GROUPS.

Acknowledgements

References

1. **Ilyasova NYu.** Diagnostic   computer complex for vascular fundus image analysis, Biotehnosfera, 2014; 33(3): 20-24. [in Russian]
2. **Ilyasova NYu.** Methods for digital analysis of human vascular system. Literature review. Computer Optics, 2013; 37(4): 517-541. [in Russian]
3. **Simcher, VM.** Methods of multivariate statistical analysis. M.: Finance and statistics, 2008. [in Russian]
4. **Mookiaha MRK, Acharyaa UR, Lima CM, Petznickb A, Jasjit S.** Data mining technique for automated diagnosis of glaucoma using higher order spectra and wavelet energy features. Knowledge-Based Systems, 2012; 33: 73-82.
5. **Ilyasova NYu, Kupriyanov AV, Paringer RA.** Formation features for improving the quality of medical diagnosis based on the discriminant analysis methods. Computer Optics, 2014; 38(4): 851-855. [in Russian]
6. **Ilyasova NYu.** Estimating the geometric features of a 3D vascular structure. Computer Optics, 2014; 38(3): 529-538. [in Russian]
7. **Ilyasova NYu.** Methods to Evaluate the Three-Dimensional Features of Blood Vessels. Optical Memory and Neural Networks (Information Optics), 2015; 24 (1): 36-41.
8. **Ilyasova NYu, Kupriyanov AV, Khramov AG.** Information technologies of image analysis in medical diagnostics. M: Radio and Communication, 2012. [in Russian]
9. **Ilyasova N.** Computer Systems for Geometrical Analysis of Blood Vessels Diagnostic Images. Optical Memory and Neural Networks (Information Optics), 2014; 23 (4): 278-286.
10. **Ilyasova NYu, Kupriyanov AV, Ananin MA.** Measurement of the biomechanical vessels parameter for the diagnostics of the early stages of the retina vascular pathology. Computer Optics, 2005; 27: 165-169. [in Russian]
11. **Fukunaga K.** Introduction to statistical pattern recognition. New York and London: Academic Press, 1972.
12. **Kim JA, Myuller ChU, Klekka WR.** Factor, discriminant and cluster analysis. M.: Finance and Statistics, 1989. [in Russian]
13. **Moshetova LK, Yushchuk ND, Tsyganov DI, Sister VG, Branchevsky SL, Ilyasova NYu, Pavlova Y.** Method for digital image processing fundus. Information letter, 2004; 1.

Modern aspects in development of branch applications on the basis of Big Data: possibilities, prospects and limitations

Ramzaev M.V.

International Market Institute, Samara

Abstract. Storage, processing and intellectual analysis technologies of Big Data receives extended popularity throughout the world. The areas of implementation are also expanding, opening up new possibilities for solution to a variety of problems. However, it is important to consider the risks and limitations in implementation of such technologies and conduct detailed studies into revealing such issues. Therefore, it is necessary to form new analytical algorithms for Big Data, considering combination of wide use possibilities and limitations within rapidly changing conditions. One of the prospective areas for the comprehensive application of Big Data technologies is the State government. Having conducted the study into potentials of such technologies it's possible to formulate generalized methodological approach to working with them, which will allow resolving a number of current problems in real time.

In today's world more and more spheres of human activity are covered by various types of information technologies and their various field applications. Despite the fact that the existing mechanisms of data storage and processing are actively improving, the relevance of development and innovation in the software sector is one of the most important challenges for the economies of countries around the world. The most advanced, discussed and, according to researchers, promising in this field directions are the processing, storage and intelligent analysis of Big Data using cloud technology.

These technologies are already widely used in many fields of science and life. For example, marketing, energy, industry, oil and gas, public and municipal administration, housing and utilities (smart city), banking and insurance activities, bio

- and nanotechnology, GIS technology, the aerospace industry, the safety of various areas of life, health, etc.

The use of Big data technologies in Russia according to the analytical Agency CNews Analytics and Oracle is gradually increasing [1]. However, at the moment there is some skepticism about such trends, which can considerably limit the spread and application of these technologies. According to the international expert community, one of the most problematic issues of implementation and spreading of Big Data Analytics is currently the confidentiality of personal information.

Every year the number of companies which provide access to a variety of databases, as well as provide services for the analysis increases. For example, according to the analytical Agency Mind Commerce market size of Big Data in the U.S. in 2013 amounted to $ 20 billion, and in 2014 already 29 billion, which means that growth was 45%. This is an important sign of the framing trends and tendencies in the IT sector.

You can also give an example of a study made by Terradata on the subject of practical use of Big Data technologies. The study is based on survey data 316 of managers engaged in information technologies and data processing in leading companies. The results showed that the vast majority of respondents stated a high proportion of their investments in big data analytics, and high rates of return.

 About a fifth (21%) of respondents support the idea that technology is big data Analytics are a key activity to identify and create specific competitive advantages, and 38% include these technologies in line of five priorities.

However, the study showed that Big Data is promising and effective from side of innovation capacity in three key areas: the creation of new models of business activity (54%), search and formation of a new product or service (52%), selling data to third-party commercial organizations.

However, according to the results of the study there are a number of obstacles on the implementation of IT technologies in the current activities of the company, behavior models and strategy.

Thus, according to survey, one of the key tasks in the field of corporate culture is encouraging the use of data and experiments in working with them [2].

In this regard, due to the lack of a regulatory framework for activities in the field of storage, transfer to third parties and Big data Analytics, it is logical to assume that there will be a growing risk of wrong use of arrays of information.

However, the law existing in Russia [3] imposes a number of limitations and identifies new opportunities in the BIG DATA analysis.

Although now you can get "personal portraits" of any particular person based on the mappings of IP addresses. And it's not just bank accounts and property register list, but also the possibility to calculate the algorithms of the codes needed to control them.

However, one of the most soft elements of personal data is personal health information. The current trend toward cloud storage also provokes risk increase of information leak.

On the one hand, the organization of the process of collecting and analyzing all available and incoming real-time information about the medical data of millions of

patients around the world can have a significant positive impact on the health sector as a whole. That is true about defining the most effective drugs, schemes and methods of treatment, species diagnostics and other medical interventions. On the other hand, the patient is one of the most weak points in this chain. Patients have no influence on health information processing. He has the right only not to personalize the data and remain anonymous. However, anonymity in this case is a relative term, the guarantee of which is impossible to provide to full extent.

Close to medicine–genetics area recently experiences some difficulties in storing and processing of information, the volume of which is growing rapidly. According to rough estimates of experts, the scale of genetic data is comparable to the scale of the data in astronomy and physics, and in some ways even surpasses them. Therefore, it is logical to assume that further research in this area will soon need a completely new analytical and computational tool is capable of delivering results based on such a large streaming data. Of course, this will require substantial funding, but the scientific and practical relevance of this topic will allow access to all necessary means and resources, both financial and intellectual. However, in this scientific field, there are also certain potential risks from a wider and deeper implementation and application of Big Data technologies, but they are long-lasting and today represent a much smaller threat than potential usefulness.

But experts have other concerns too. They are connected primarily with the fact that almost any analytical agency will be able in real time to segment the society on different sets of criteria that, on one hand, will allow to predict public reactions within each segment, on the other hand simplifies the process of manipulating them for personal gain. Moreover, the prices of all these analytical services in the near future will only become more accessible because of the growing number of proposals. Due to the Economist Intelligence Unit agency survey, which surveys have identified the priorities for the development of Big Data for several years ahead, one of the most dramatically developing areas is human resource management [4]. Thus, it is believed that the mechanisms of active control in society have long been used, for example, in the United States. The expert community believes that the commercial interest of companies to this subject over the next three years will increase by almost 2 times in comparison with 2014.

Another aspect of the complexities of Big data usage, as Professor of Berkeley University Michael Jordan says, is associated with a qualitative segmentation of information and its analysis. The increase in the number of data, the increasing number of data sets and the increasing level of accessibility to them forms specialists trend of inflated expectations, which shows the history of the development of scientific disciplines that often leads to contradictions and unreliability of the results afterwards. In this regard, it is important to pay attention to the study of not only research and development opportunities of Big Data, but also to the research of the risks of negative consequences, constraints, and adapting. For example, if the user for several months studied the information about TV sets and then bought it on-line then he will no longer be an effective consumer for targeted marketing that will haunt him for another few months and more in the Internet and mobile devices. Hardly anyone will buy a TV every time you see an advertising banner in the corner of your screen.

There is also significant potential from the use of Big Data technologies in industrial production. Especially it concerns the production of large objects, parts produced and supplied by many suppliers. We are talking about millions of parts and thousands of manufacturers. So in Russia and in the world exist and work quite effectively standards of quality and technological features, on the other hand, the existing mechanisms do not allow to lead full adaptation of innovative design in real time in different areas of production and objects.

However, the development of Big Data technologies and their attendant widespread adoption of the Internet of things, allows not only to account for all the standards and requirements in the design of any component or construction, but also to optimize the production and bring to a new level control over each part, each node and object in General.

Such approach makes possible to create new mechanisms of standardization of the quality of production, which will run in real time. That is, in case of identifying any inefficient work of a particular piece, which is provided with a sensor, the data will automatically be transferred to the computer not only of the owner of the object itself, but to all project agencies and designer.

Thus, the use and implementation of Big data technologies in industrial production will reveal the rejection and its causes in the shortest possible time, and will also make it possible to significantly improve the predicting risks system associated with quality problems, use and operating characteristics of parts, components and objects in each case.

At the same time, technology in the world of Big Data are applied directly in the production process. Such innovations will allow, for example, to identify the optimal values of components in compositions of various metals, which, in its turn, will impact on the economy, on the accuracy of risk calculation and lifetime of the final products of production.

In modern terms, such global innovation is possible only in case of effective and constructive cooperation between large companies and corporations, bringing together the experience and tools involved in the creation of new technologies that will be useful to all partners. This also applies to the IT sector, and technologies of collection, processing and analysis of Big Data, as to extend the scope of their application is appropriate with the scale of funding and potential profit.

Another important field of application of Big data technologies is the Banking sector. On the one hand, existing in large banking institutions, the mechanisms for collecting, analyzing and processing Big data to solve a wide range of existing problems, on the other hand, current economic conditions and technology development of electronic fraud make Big Data a new vector of innovation in the work of the serious financial structures of the world level. First of all, the Bank needs to know and understand its customer. And it's not just his average annual income and the property which he owns. In particular, it its a detailed expenses structure with regard to the season of year and time of day. The Bank, as a credit institution must not only guess the possible customer need for money but has to some extent to form this need in order to be able to offer its products on the terms that will be acceptable here and now, in real time. These are the conditions of the market today. At the same time,

the Bank should partner with its customer and take care of the security. Widely implement of Big data technologies will be possible to warn the client at the time of any transaction, if the payment recipient for example showed himself earlier as unfair. Or, identifying special features of the movement of any client's funds in his account, to start negotiations with him about possible difficulties when repaying them next payment of the loan, for example. That is, to solve the customer's problem with him, without waiting for the consequences of those difficulties, which could result with significant debts.

Overall, it should be noted that the banking and financial sector nowadays are one of the most interesting directions in the search for practical applications of the use of Big Data technologies.

First of all, the reason for such trend is a direct customer economic benefit. It should be noted that previously the average growth in this sector was about 80% per year. Now competition among banks is already underway for each client, in addition to this is the need for a deeper and wider analysis of the current situation for each existing customer, the decision to change the bank is not a rare thing now.

Any miscalculation in individual work with consumers can lead to the situation when within an hour is not understood by the employees of one Bank, the client will become a client of another Bank. Therefore, the internal Bank study on prediction of customer care becomes a very urgent and necessary from the point of view of efficiency and appropriateness of current activities in general.

To create more definite personal portraits are used social networks, search engines, existing statistical data and data submitted by the clients themselves. Information about the state of the financial and banking sector in general is collected from data provided by the Central Bank and state statistical reports. Although, almost all of the specialists working with these sources note that the quality and the list of such data and the speed of changes arthe essential problems in the development of IT applications innovation in the financial sector in Russia.

Competition in the banking sector has led to the situation that market participants are directly interested in the development of new outlets and applications of Big Data technologies in their work because it depends primarily on their profits. In particular, technologies of big data analysis help to rebuild the geographic locations of Bank branches, taking into consideration the passability. This allows to reduce their number and to calculate the necessary and sufficient space and staff for each object separately.

Interesting developments on framing personal practical recommendations for optimizing the client's expenditure, part of which indicates the amount of savings per month. For sure it can be taken or left behind, but the potential for success lies in those elements of expenditure that is least painful for each individual client. This calculation can be particularly effective if the person specifies, for example, the subject for whose benefit saving are held and ongoing savings. This approach largely corresponds to the concept of working with clients based primarily on exactly the formation of a trusting relationship between the Bank and the customer.

However, now relevant are the issues of innovative projects financing and start-up companies, particularly in the area of small business. All this is now starting to be addressed through non-banking technologies on the basis of the Croud and the Croud

Sourcing Funding. Now there are many forms of this kind of financing – from philanthropy to the acquisition of a stake in the project, indicating a wide distribution of these phenomena in the world.

In this area a variety of approaches in handling and use of big data can be used in identifying the most relevant and popular areas of business to create a startup project for a specific target audience and on stage to test the idea of its potential popularity and consumer demand. In this connection it is useful to optimize the search of potential Internet investors in accordance with their personal content. That is, to propose to the users mainly the ideas that are most likely to interest them. Thus, we are talking about target management not only the realization of a particular innovative project or business idea, but also the process of developing this new product, search for optimal forms of financing and search of investors.

However, with the development of computer technology and the widespreading use of electronic payments, real time data (database, updated in real time) of any Bank is a threat to all clients, because such information when released into the hands of fraudsters, makes possible to deal with all customer accounts without their knowledge. Of course, the security services of major financial institutions are constantly monitoring these risks and try to prevent them, but without continuous improvement it is the computer protection mechanisms with the use of Big data technologies it will be extremely difficult. Don't forget that fraudsters often use innovative technology and are no less competent than those who protect them.

In the context of the possible application areas of Big Data technologies is increasingly seen public administration, including social services, and housing, security, economics and much more.

As for the security sector one of the most interesting experience is the one of Pakistan, there was created one of the world's largest database storage and processing of data of citizens, including their biometrics NADRA (National Database & Registration Authority), the national Agency for managing databases and registrations of citizens [5]. The main strategic goal of establishing such a system and the organization of the information base is the fight against corruption, combating terrorism, optimization of the process of reforms, as well as improving the efficiency of working with natural disasters. In general, the expert community agrees that this initiative is implemented successfully and today is a unique implementation model of IT innovation and Big Data technologies in public administration. At the same time, the NADRA today – is an independent and financially independent organization, which increased its income by 3 times over the last 5 years.

Considering the peculiarities of application of modern technologies of Big data in public administration, it seems appropriate to adapt a number of existing models and mechanisms in this category for new software and hardware capabilities. Information technology today is one of the prior directions of development in public administration on the Federal, regional and municipal levels. Thus, it seems logical the use of the concept of regional competitiveness, as a base for recording and processing of streaming data. Existing mathematical models for calculating the level of marketability of the territory is able to show results to quite a sufficient degree of

accuracy in the presence of true meanings of the required performance criteria in real time.

Developed additively weighed mathematical model of management of development of competitiveness of the territory has the following form [6]:

$$KS = (\xi_1 * GF + \xi_2 * PRF + \xi_3 * EF + \xi_4 * PPF + \xi_5 * APF + \xi_6 * SF + \xi_7 * FEF + \zeta_8$$

$$* IfF + \zeta_9 * RF + \zeta_{10} * IF + \xi_{11} * InF + + \xi_{12} * DF) \rightarrow \max,$$

where KS - marketability of municipal area; ξ - coefficient of importance of group of factors (is defined by expert questioning); GF - geography factor; PRF - nature and resource factor; EF - ecological factor; PPF - industry production factor; APF - argo-industrial factor; SF - social factor; FEF - economy and finance; IfF - infrastructure factor; RF - municipal area development factor; IF - innovation factor; InF - investment factor; DF - spiritual factor.

Each of the factors of this model is a separate function that takes into account a number of indicators of regional and municipal competitiveness. Factors of importance in the present formula are constant, which are usually defined by analysis of the views of the expert community. However, with the use of Big data technologies, they can be calculated almost in real time.

To do this we need to create queries criteria in the Internet space to identify the expert community on this or that factor, and then by personal content to determine the importance of a necessary factor in the opinion of the user with the desired characteristics. In this context, it is logical to establish and run the search algorithm of significant correlations excluding the binding to the experts. Thus, it is possible to detect a peak of the correlation values of certain ratios of opinions of experts and Internet content in general. Based on the results of this analysis are generated coefficients of significance and the calculation of the model. At the same time, while analyzing the streaming information in real time you can predict the occurrence of previously unforeseen factors and conditions for change of the model of competitiveness or the occurrence of critical values of significance of a factor (which may be indicative of the likelihood other emergency outbreaks of epidemics, the occurrence of environmental disasters, social disturbances, etc...).

Thus, on the basis of the study of the potential of Big Data technologies in state and municipal management, you can generate a generalized methodological approach in the use and implementation of these IT innovations. This approach consists of four main blocks, which are characterized by a certain kind of task.

The first block is the analysis and identification of certain types of relationships of current indicators of the competitiveness of the territory for now and over past periods. This will help to identify risk trends and growth of potentials of socio-economic modus The second part is the analysis of factors of competitiveness and identifying those which can be managed in real time. The third block is predicting, which with use modern software and hardware working with stream data becomes more accurate and almost continuous. The fourth block is a simulation of possible situations. In this aspect it is relevant to consider different urgency forecasts and to rank from the point of view of optimism and dark scenario, as a result getting one

real-time integrated programme for the formation of certain decisions that will be the most effective in each particular case.

However, the analysis shows that the widespread adoption and use of Big Data Analytics in public administration (including real time administration) has a number of limitations and problems. First, is the difficulty in framing databases themselves or data sets on socio-economic indicators of particular territories. Second, the problem of the formation of streaming data: collection and analysis of information in real time, which reduces any algorithms of risk identification and optimal decisions in specific situations. Third, an integral part of the use of IT innovation is a competence of the staff, where there is a need for state service staff but also to form a scientific school, specializing in this area that it is extremely difficult for countries with low and medium level of development, as well as having an extensive territory. Number four is that Big data technologies generally do not give accurate guidance that can be adapted in a logical algorithm, they give a set of results, connection of which with the request is not always visible. This means that in reality you can only talk about the calculation of the probability of occurrence of certain situations or critical values of certain indicators, which in its turn means that the prediction based on Big Data Analytics is just about the forecast probabilities.

However, this does not mean that such approaches to public management are not effective. On the contrary, this suggests that there must be a more balanced approach to the means of storing, processing and analyzing Big data in general, taking into consideration data security issues, and the likelihood of their inaccuracies, as well as to approach the analysis from the point of view of logical connection. Fifth, the system of state and municipal management is structurally in legislative frameworks, and the management of it in real time is difficult. Many of key decisions often require certain regulatory changes, which take time. However, the application of Big data technologies in the public sector can increase the accuracy of forecasts in general, so in some cases there is an opportunity to identify in advance the values that need to be adjusted in the future and to prepare appropriate legislative framework.

Now the practitioners and scientists work with the technology for collecting, analyzing, and processing large amounts of data to active discussions on the subject of new opportunities and fields of application. Today it becomes clear that the terminology criterion value of the volume of data goes by the wayside, as almost all streaming data to date are great. Another issue is that the potential of Big Data gets its bloom just by investing respective resources. Thus, the main motor of these technologies today is business that focuses mainly on the profit from the invested funds. This means that the research in the field of technologies of work with streaming large amounts of data will be held and already held in the format of sectional or thematic research aimed at solving specific tasks oriented on obtaining profit. Success cannot be achieved without considering and analyzing all available information and all available data, it can be assumed that this area of it innovation itself can be considered as micro industry, which may find applications in most sectors of the economy and state institutions in general. This means that the need in the educational mechanisms and, consequently, highly qualified specialists will grow. There is a strong likelihood that investments in education on the subject have

practicability and huge potential in terms of payback period as a separate line. However, the demand for such specialists today has no geographical or linguistic boundaries throughout the world, and their significance in the promotion and development of technologies for working with stream data is huge. Obviously, there are a number of tasks of the global level of significance, which nowadays have not been resolved partially because of lack of data, information and mechanisms of work. Environmental issues, and forecasting and prevention of natural disasters, research in genetics and space and global security concerns are in the list. However, as described above, you should carefully consider the possible problems and threats when trying the widespread implementation of Big Data technologies, particularly in the commercialization of search process for applications.

References

1. Research of Oracle и CNews Analytics: Big Data came to Russia: https://www.oracle.com/ru/corporate/pressrelease/study-of-oracle-and-cnews-analytics-20150226.html/
2. http://ko.com.ua/teradata_bolshie_dannye_sozdayut_potencial_rosta_112145.
3. Federal Law from 27.07.2006 N 152-FZ "About personal data" (edited 21.07.2014).
4. Analytical survey of Big Data market / http://www.eiu.com/home.aspx/
5. National Database & Registration Authority / https://www.nadra.gov.pk/
6. **Ramzaev M.** Management of marketability of municipal area development (on the basis of Samara region small towns). Samara: Economic Science, 2009; 3.

Development of the requirements template for the information support system in the context of developing new materials involving Big Data

Grechnikov F.V., Khaimovich A.I.

Samara State Aerospace University

Abstract. We consider a concept of databases for the numerical and physical experiments in the information management system used for new materials development. For this purpose, brief analysis of information systems and databases for large-scale experiments has been performed. Special features and general approach to the templates of the functional requirements are suggested.

One of the major issues tackled by the leading engineering departments and individual production engineers developing products for the aerospace branch with the use of new materials involves making all the strength calculations (structural analysis) with regard of such materials under consideration of mechanical, thermophysical and other features at the macro-level. At the micro-level though (the microstructure field) materials pertain to anisotropy of structure due to availability of heterogeneous phase composition, point-type and other localized defects, non-uniformity of crystal composition, foreign inclusions, etc. These localized defects as well as external micro-mechanical damages of the parts' surface give rise to crack formation and development, which in their turn lead to off-design cases and breakdowns of parts in the process of their operational use and maintenance. It is especially true with regard to composite materials with mechanical alloying, compounds of the 'binding-reinforcing fiber' type and others. Well-known are cases (e.g., at the AIRBUS and BOEING companies), when compound parts were withdrawn from manufacturing final products due to the mentioned reasons.

The material's life cycle consists of several stages:

1. development of the material's new composition;
2. optimization of its properties;
3. designing and developing products made of the material;
4. testing and certification;
5. production;
6. operation including repair and recovery;
7. disposal.

The innovations infrastructure in developing new materials is shown in Fig. 1 [1]. Designing of new materials requires creation of the existing materials' database: mathematical models of the materials, experimental data as to materials in form of photographic images and data based on vibroacoustic emission as well as digital data on the processes of generating the products' samples made of the respective materials.
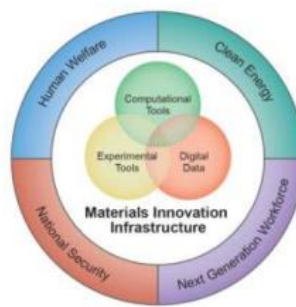
Fig. 1. – Innovations infrastructure in developing new materials [1]

Integration of the following methods is adapted in development of the materials database:

1. Tools of computer-based simulation (physical models of nano- and micro-level, numerical models and systems of simulation-type modeling of the macro-level continuum mechanics)
2. Toolware and experimental analysis methods
3. Digital data exchange and digital information storage formats

To enable works as to designing new material, it is necessary to create integrated medium in the BIG DATA system; the reason for that is that this database shall integrate sound data, experimental data photographs and existing materials mathematical models.

The input data (material database) for analysis are as below:

1. Results of simulation-type modeling of the structure – software modeling the material's structure (phase constitution, interrelationship, parts by volume, three-dimensional distribution and phases positioning)
2. Full-scale experiment results (standard tests) – microstructure pieces and material's submicrostructure obtained by means of light and electronic microscopy, results of the X-ray-structural analysis (describing material's structure and structural imperfections), and other analysis types. Final models as to the material's structure obtained as a result of the full-scale experiment data capture (development of special-purpose technique and software is required) linked to the models of P.1
3. Mechanical and other properties of the material (based on the experiment outcome, P. 2) – in strict compliance with the models of the structure.

The output information in the system of modeling new materials shall be viewed as the damage evaluation service based on the neural network. Principle of the service performance: on the basis of numerous selections of fragments of structures with defects as well as other parameters characterizing the material's macro- and micro-condition, the part's geometry parameters, operation conditions and calculated or experimentally obtained variants of damage or pathology development, training of the network is conducted. Flowsheet of the services' performance with regard to diagnostics and damage evaluation is presented in Fig. 2.
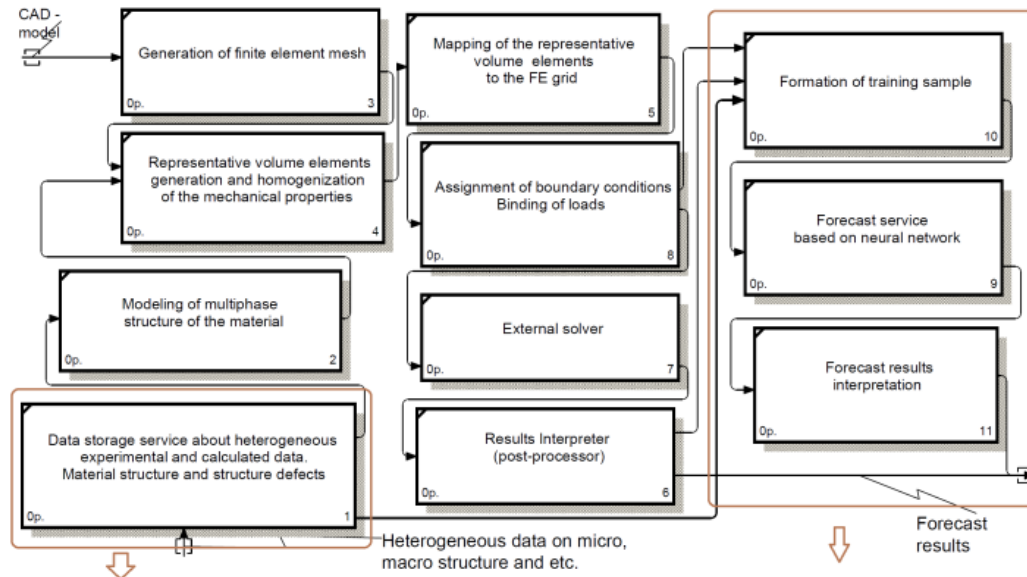
Fig. 2. – Flowsheet of the services performance with regard to diagnostics and damage evaluation. Arrows indicate the forecast service blocks.

The forecast is made in the following way: selected parameters are delivered at the input, which is similar to the elements of the training set of selected stuff. Selected parameters are obtained for the part material under testing, which in its turn has been selected from the industrial lot of the parts. For the required (possibly critical) working conditions, the grid generates a forecast of material's response.

In the event of unfavorable forecast, series of refined calculations and experiments are made, expert opinion is given as to ultimate solution and corrective actions are undertaken, which prevent failure of the product.

Training and clarification of the grid-related forecast is undertaken periodically by virtue of increase of the training set in size.

Some stages while creating new materials are implemented with the aid of hardware and special-purpose software. This being so, each stage can be implemented within special application package, which implies access to the complete package on the part of the material scientists. Moreover, scientific applications often require special skills for their installation, adjustment and startup, which the majority of researchers lack.

It is proposed to develop methods of producing cloud-based system of information support aimed at developing new materials, which would enable integration of the complete set of software tools into a unified medium and provide the researchers with the opportunity of operating it with the help of user-friendly web-interface having Internet access via web-browser. The web-interface as well as the computer modeling with the aid of application packages will be implemented in the cloud medium.

Start of computations in the cloud is proposed in the following way. In the cloud web-interface of the system, the user is expected to chose the system-supported application package from the list and assign the set of package- and task-specific input parameters (including the number of cores and RAM necessary for making relevant calculations) and in case of necessity – to indicate the file or directory with initial mega-data way, which is equally necessary to computations. After initiating the task start from the web-interface, the system will check availability of all the obligatory data and correctness of their input. In the event of successful check and availability of uncommitted resources, the system initiates startup of the corresponding number of virtual machines with preinstalled application software required for making calculations set by the user. After finalizing the calculations, the system will preserve results via the user-set way in the cloud storage.

The system based on the developed techniques will also enable storage of various information on properties of already known materials, experimental data linked to previously conducted tests as well as performance search by these data with the purpose of forecasting properties of new materials without undertaking any complementary full-scale experiments.

In the USA and Europe, this direction is marked by similar works within the framework of developing material genome under the use of the Big Data approach. In Russia, elaboration of methods with the aim of further creation on their basis a portal for researchers in the field of material science is just at the initial stage.

June 24, 2011, the US President announced the Materials Genome Initiative – in order to double the speed, at which development and production of new materials is

done. Acceleration of developing advanced materials is of fundamental importance for achieving global competitiveness (http://www.whitehouse.gov/sites/default /files/microsites/ostp/materials_genome_initiative-final.pdf).

New materials are of composite nature – they have multi-component and multi-phase structure: without adequate simulation modeling, information resource and data exchange development of new-generation materials (given the existing empirical approach) is either impossible of too time-consuming due to their complexity. The Materials Genome Initiative is aimed at promoting development of new materials; it accelerates the process and makes it more cost efficient. December 4, 2014, strategic plan of the Initiative was published (http://www.nist.gov/mpi/uploacl/MGI-StrateQicPlan-2014.pdf) NSTC (National Science and Technology Council). The subcommittee for genome includes NIST, Department of Energy, Department of Defense, NSF, NASA, NIH, USGS, DARPA in coordination with the infrastructure of Nanotechnologies Knowledge.

In much the same way that the Human Genome Project accelerated development of biological sciences owing to identification and decoding of basic construction blocks of human genetic code, the Materials Genome Initiative (MGI) will accelerate understanding of the material science fundamentals, providing information ensuring creation of new products and processes. MGI will require unprecedented level of cooperation of participants including government, industry, academic entities, professional communities, national laboratories, thus resulting in rebirth of the respective American industrial sectors. In order to integrate results of experiments, numerical methods (finite elements method, etc.), theoretical approach, the strategic plan envisages creation of a network of the MGI (Material Genome Initiative) resources – with the purpose of developing reliable techniques of precise simulation modeling, improving tools of performing and processing experiments' outcomes. Directional effect of these integrated data – discovery of new materials, development of analytical information for increasing value of the obtained experimental and computation data. Other objectives of the plan, linked to intensive data processing, include creation of means for materials' information-specific infrastructure implementation as well as development of the first rate techniques of maintaining proper storages of databases as per materials.

In order to start a dialogue within the framework of the MSE community (Engineering of Development and Study of Materials), the National Institute for Standards and Technologies (NIST, USA) conducted a workshop on materials' digital data in May 2012 under the aegis of MGI (Materials Genome Initiative). The workshop determined a number of issues that have to be settled in the process of creating data-specific strategy for materials; these include: schemes/ontologies of materials, standards of presenting data and metadata, data repositories/data achieves, data quality, incentives for joint use of data, intellectual systems and tools for data search [2].

The European Union is involved in elaborating standards of data exchange as for engineering materials within the framework of the European Committee for Standardization [3]. These standards mainly emphasize engineering materials for the aerospace branch. The European Commission finances activity of the expert group

called Integrated Computational Materials Engineering (ICMEg); the Group has been established as an entity for integrated materials computation engineering – with the purpose of developing standards and protocols required for supporting digital data exchange on materials [4].

In Russia, it is necessary to launch developments as to creating genome of materials under utilization of the Big Data technology. For this, it is necessary to form requirements with regard to large-volume digital data covering the stage of collecting and processing of experiments' outcomes as for mechanical properties studies (in dynamics, for example) or microstructure fragments, stage of the numerical simulation modeling of the process of materials' responses – with the view of further use of the collected experimental data for shaping an integrated model of materials-specific knowledge. The integrated knowledge model includes information required for concluding forecast related to the materials' response (including those with noncritical defects) – in the course of maintenance or in the technological process. Testing of the end-to-end information support and shaping the list of requirements as to materials' genome (for the damage evaluation case) could be performed as shown in Table 1.

Table 1. Application examples (use cases) of the materials information support services as per damage evaluation

Experimental data on pathology (defects, heterogeneities) in the material's structure	Simulation model of the material's response (computational model). Technology of identifying imperfections by indirect information	Response prediction model
Unstructured data storage on microstructure of material with micro-cracks	Modeling of crack development in CAE – system with preparing finite element pattern on the basis of selected micro-structure fragments with the aid of cloud service	Forecast (training) model of material's strength variation on the basis of neural networks
Fragment (sample) of vibroacoustic emission signal in the event of critical material load (e.g., in static test, deviation of the operational conditions and geometry from nominal ones (mechanical treatment, sheet pressworking, etc. for the know and new materials))	Spectral analysis technology as per emergencies identification on the basis of identifying emission parameters	Forecast (training) system of monitoring materials' responses in emergencies

369

Currently, there are precedents in Russia of global distributed information systems supporting experiments operating large data volumes. For illustrative purposes, one can mention the Central Information-Computer Complex of the Joint Institute for Nuclear Research (JINR) (in the town of Dubna), which develops as a multifunctional center for storing, processing and analyzing data and which is designed for providing a broad spectrum of opportunities to users on the basis of components integrated into it: grid-infrastructure of Tier-1 and Tier-2 – with the purpose of supporting experiments on LHC (ATLAS, ALICE, CMS, LHCb), FAIR (CBM, PANDA) and large-scale experiments; general-purpose computation cluster; cloud computation infrastructure; computation heterogenic cluster HybriLIT; training-and-research entity for distributed and parallel calculations [5].

Based on the experience of designing projects information support systems ATLAS, CMS of the JINR employees [6-10], it is possible to define a number of requirements concerning the databases conceptual structure with regard to information support of experiments within the genome of material project.

For full CMS databases' structure and hierarchy see Table 2, Appendix A [6].

Conclusion

High competition under the global market conditions requires continuous improvement of consumer properties in the output products', the major part of which depends on materials used in manufacturing. In this regard, rapid development of new materials with required properties is critically important; moreover, it is important often not just for individual companies but for branches of nation's economy. Development of methods of organizing interrelations of heterogeneous virtual services and applications in Big Data will enable a system of digital support of new materials development in Russia. The distributed system will make it possible to integrate on a uniform (from the uses' point of view) platform the whole set of diversified data required by the material scientists – with the purpose of forecasting defects development in the process of creating new materials.

Worthwhile mentioning is availability of commercial software in form of interfaced modules, designed for solving adjoint problems of the structural analysis, in which the composite material microstructure's influence on the developed structure is taken into account, e.g., Digimat, MultiMech. However, there is no available forecast service (e.g., solution on the neural networks basis). This enables rapid forecast solution on the basis of pre-conducted experiments and calculations with the aid of Big Data.

Recommendations on the information services assisting experiments have been validated and are more evident. For the dynamically resizable data, nested and user-defined arbitrary structure (multimedia, for example) NoSQL warehouses are preferable. Thus, the usage of the object model is recommended for distributed databases with a large number of complex relationships: cross-reference links, many-to-many relationships between objects.

A flexible object database can be a better choice for Configuration, but DB Conditions, Component and Event Data tag databases with slowly changing structures and simple relationship can use RDBMS for their implementation.

Appendix A

The Configuration DB will support only the data that is directly required to start and support the DAQ (Data AcQuisition) system in an efficient operating condition. This database should be elastic because not only data but the structures of data can vary. This means that the Configuration DB must be developed in close collaboration with the DAQ group.

Table 2. CMS databases structure

Database level	Database purpose
Equipment management database	Holds structured data about all detectors parts as equipment elements.
Construction database	Holds all information about relations between different equipment elements.
Conditions database	Holds all information about detector conditions (data on operating conditions).
Configuration database	Holds all information required to bring the detector in any running mode.

Typical use cases of DBs for physical experiments [6].

Configuration database	**Purpose:** to store the parameters describing the topology of the DAQ system, hardware and software components, and run parameters.
	Contents: nominal configuration of detectors, front-end electronics, and data acquisition/ hardware and software components, run parameters
	Consumers: setup of the configurations of detectors, front-end electronics/ data acquisition at run start through appropriate interfaces/ online computing farm at start-up and possibly during operation

| **Conditions database** | **Purpose:** to store, retrieve, and manipulate condition data. Conditions data keeps the state of the detector at the time when events are collected. A subset of the data will be used both for online computing (FLES) and for offline computing. |

Contents: nominal detector geometry/ nominal configuration of detectors, front-end electronics, and DAQ system/alignment parameters and calibration data/ control data from online monitoring / control system data needed for analysis / Parameter degrees of freedom: run/run campaign (e.g., nominal settings), real time (e.g., control data),version (e.g., alignment and calibration parameters)

Consumers: online computing farm at start-up and possibly during operation / offline computing farm

| **Geometry database** | **Purpose:** the object and detector geometry (or description) database provides primary numbers used in building the offline description and tracking its evolution through time and software version. |

Contents: characteristics of detector and electronics components /software version, etc.

Consumers: physicists for data simulation/reconstruction/analyses, /calibration/alignment software

| **Tag Event database** | **Purpose:** to store, retrieve, and manipulate event data from every stages of data processing (Raw, Event Summary Data, Analysis Object Data, etc.). |

Contents: tag event data in different formats /tag event metadata. Parameter degrees of freedom: version of format/ real time

Consumers: physicists for offline analysis, /algorithms

Component database	**Purpose:** manage properties of detector and electronics components obtained in a QA process after and during mass fabrication. This includes both mechanical/engineering production data and electronics data (calibrations, chip thresholds, etc.) which are generally kept completely separately.

Contents: tag event data in different formats /tag event metadata. Parameter degrees of freedom: version of format/ real time.

Consumers: physicists for offline analysis /algorithms.

The analysis of databases of physical experiments, such as ATLAS and CMS, shows that they have similar use cases and close structure of corresponding databases. Below the typical use cases for Configuration (Fig. 3), Conditions (Fig. 4), Component and Event (tag) (Fig. 5), Geometry (Fig. 6) databases is presents [6-10].
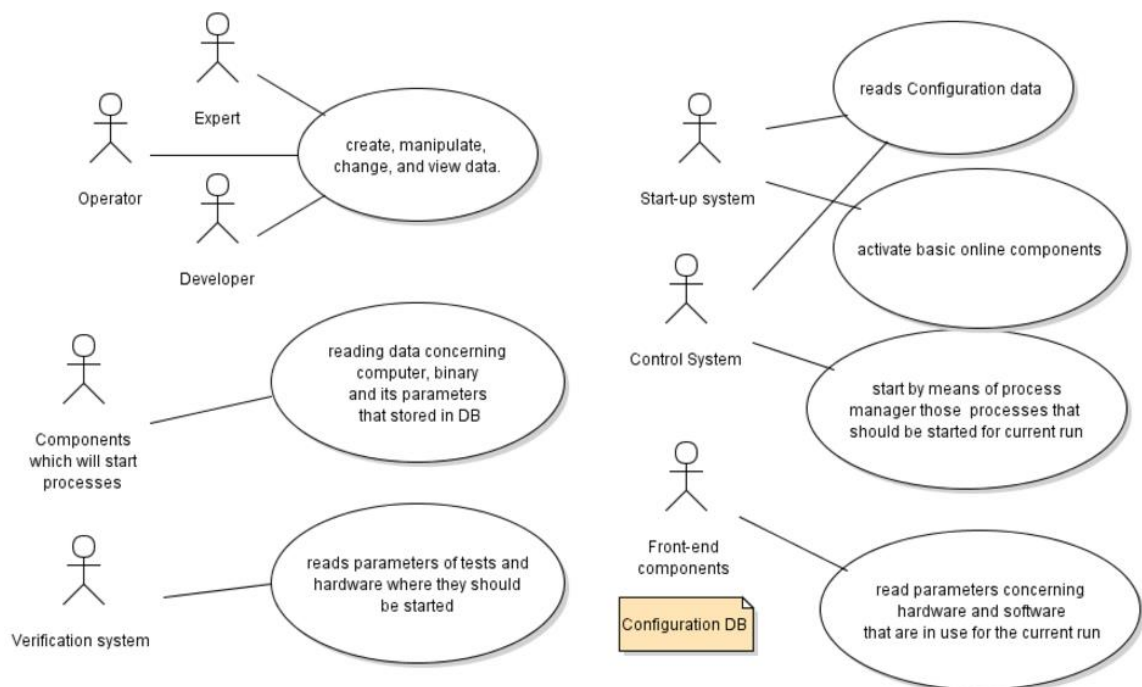
Fig. 3. – Use cases for Configuration DB
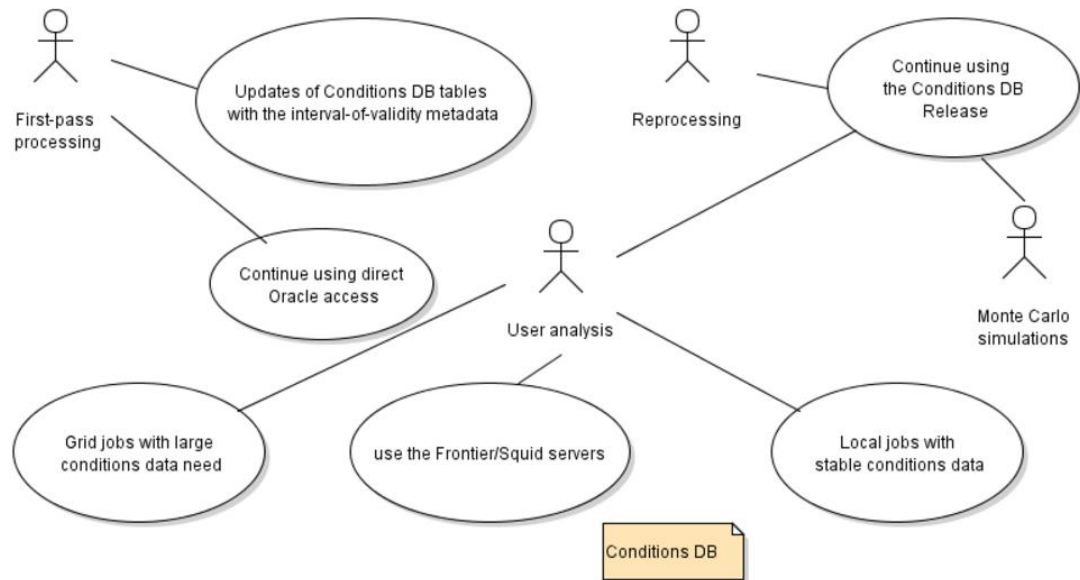
Fig. 4. – Use cases for Condition DB
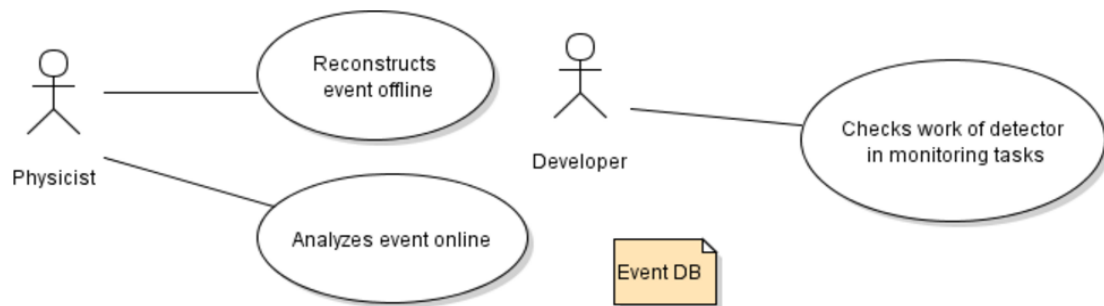
Fig. 5. – Use cases for Event DB
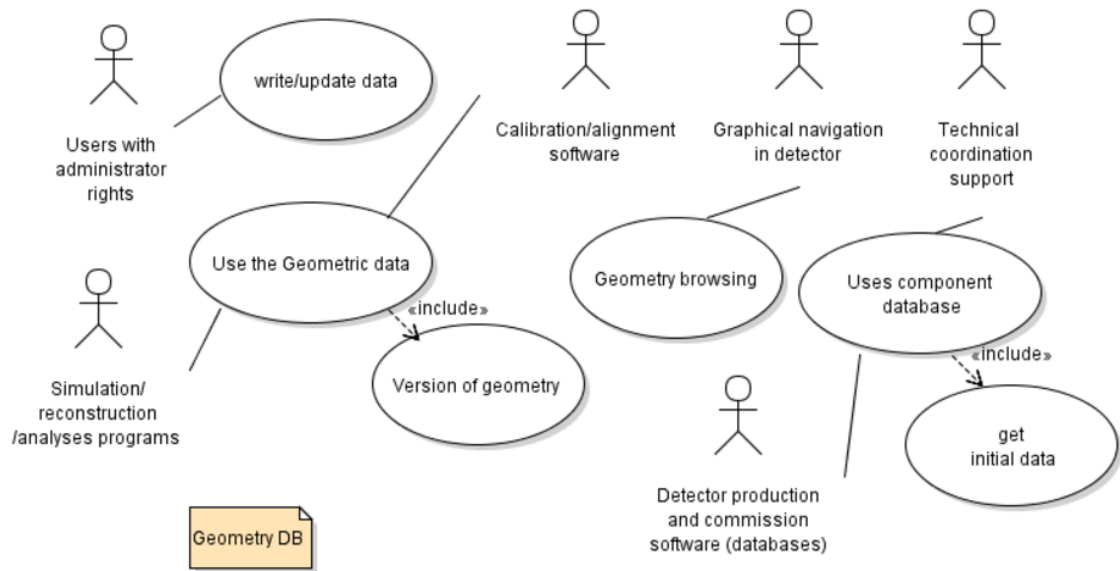
Fig. 6. – Use cases for Geometry DB

References

1. Materials Genome Initiative National Science and Technology Council Committee on Technology Subcommittee on the Materials Genome Initiative http://ssau.ru/files/science/conferences/itnt2015/itnt_2015_46.pdf

2. **Ward CH, Warren JA, Hanisch RJ.** Making materials science and engineering data more valuable research products, 2014. http://www.immijournal.com/content/3/1/22

3. **Austin T, Bullough C, Gagliardi D, Leal D, Loveday M.** Prenormative research into standard messaging formats for engineering materials data. Int J Dig Curation, 2013; 8: 5-13. doi:10.2218/ijdc.v8i1.245.

4. **Schmitz GJ, Prahl U.** ICMEg, the integrated computational materials engineering expert group a new European coordination action. Integr Mater Manuf Innov, 2014; 3:2. doi:10.1186/2193.

5. Joint Institute for Nuclear Research, 2014. Annual Report, 2015; 14.

6. **Akishina EP et al.** Conceptual Considerations for CBM Databases. Communications of the Joint Institute for Nuclear Research, 2014. E10-2014-103: 25.

7. **Gallas EJ et al.** An integrated overview of metadata in ATLAS. CHEP 2009 Conference, Prague, Czech Republic, J March 23, 2009.

8. **Miotto GL, Aleksandrov I, Amorim A, Avolio G et. al.** Configuration and control of the ATLAS trigger and data acquisition. Nuclear Instruments and Methods in Physics Research Section, 2010, A, 623(1): 549:551.

9. **Almeida J, Dobson M, Kazarov A et. al.** The ATLAS DAQ system online configurations database service challenge. J. Phys. Conf. Ser., 2008; 119(2): 022004.

10. **Vaniachine AV, von der Schmitt JG.** Development, deployment and operations of ATLAS databases. J. Phys. Conf. Ser., 2008; 119(2): 072031.

Automated detection system of insider attacks using fuzzy logic

Dodonov M.V., Dodonova N.L.

Samara State Aerospace University

Abstract. In this paper we design an insider threat monitoring system in the corporate information system. In the proposed system, fuzzy logic and the information about the current users' activity are used for effectively identifying the insider attacks.

Keywords: fuzzy logic, insider attacks, detection system.

In the modern corporate information systems (CIS) there is a huge amount of data, some part of which is classified as confidential. The confidential data play an important role in running of a successful commercial activity of a company. The theft of such information could lead to huge losses or bankruptcy of the company. From the standpoint of the data security, for the CIS there are two basic kinds of threats: the external threats and the internal ones. Now there is a sufficient number of decisions to protect the CIS from the external threats, whereas the techniques and methods for the CIS protection against the internal attacks are not yet sufficiently developed.

The systematic illegal activities of the CIS's own employees, who are called by the insiders, are now becoming the most common methods of the identity theft. By an insider we mean an employee who due to their official position has access to confidential information and use it in their own interests, perhaps going against the interests of the company.

Several types of potential insiders can be distinguished depending on the capabilities of the employee's access to an confidential information: top-rank authorities, privileged users, network engineers, maintenance staff of the CIS; employees who have access to the workstations (AWP) of the CIS, etc. This paper deals with one of the approaches for the protection of confidential information from the insiders in the CIS.

At present time, companies use various formal, technical and non-formal methods of information protection. In the paper we are focusing on the using of formal methods, and, more precisely, we will consider the possibilities of the software tools to detect the insider attacks. Usually companies bring out random monitoring of users with help

of remote desktop, URL filtering and systems traffic counting. But one should remember that there is a probability that a responsible person may be in a collusion with a traced person and implement data theft. Therefore, an effective protection against an insider must be higher than the privileged users and the network engineers.

Along with trust to employees, a monitoring of the suspicious and the dangerous activities that can sometimes occur at user's workstations should not be neglected. For example, following issues have been increased greatly: the internal network traffic, the number of requests to the corporate database, the amount of printer toner or paper. These and many other events should be recorded and resolved, because behind them an attack or preparing for an attack on sensitive data can be hidden.

There are many scenarios that resolve the problem of information leakage (files, facts, databases, hard copies, etc.). The entry-level products allow us to track the leak channels, collect statistics of employees' requests to the objects of the confidential information, and close the ports and writer-reader systems. Higher-end solutions are based on applying broad range solutions that include, along with the above, network traffic analysis, monitoring of user operations with confidential information, etc.

A special feature of these complexes is the ability to lock access to the CIS device as well as the possibility of logging the users' activity with the help of monitoring agents. The main shortage of these systems is that they do not answer the question how to search for an insider. Moreover, these systems demand support and maintenance of highly qualified specialists, which cannot be afforded by a small-scale company. During the work of tracking programs large amount of data are being collected about user activity in the CIS. These data, together with additional information about employees, can be used for online monitoring of insider's attacks. At present time security specialist had to track individually accumulated data of used documents by employees and classification levels.

In this paper we propose appliance of an developed automated system that performs the following functions for the detection of the insider attacks:

- an gathering information from monitoring agents and stores it in a centralized database;
- an maintaining a database of user activity and additional information about them;
- an automatic calculation of the possible insider attacks using rules of fuzzy inference;
- an ability to add and edit linguistic variables;
- an ability to change the rules in the knowledge base;
- an ability to view the list of potential insiders among employees.

In the proposed system, a fuzzy logic deduction is use as the method of evaluation of an insider activity. It should be noted that the fuzzy logic is currently widely used for solving of various problems. Let us assume that there is an opportunity to gather an information about an employee that characterizes its activity related to the access to a confidential information. By the values of these characteristics it is possible to draw conclusions about the safety of employee's activities. Such conclusions may be based on different mathematical models.

377

The input data for the system is the information from the logs of the monitoring program agents performing control over usage of peripheral devices and other user activity. The output result data will be a list of employees indicating implement level of actions to insiders ones. The General scheme of the system can be seen in figure 1.
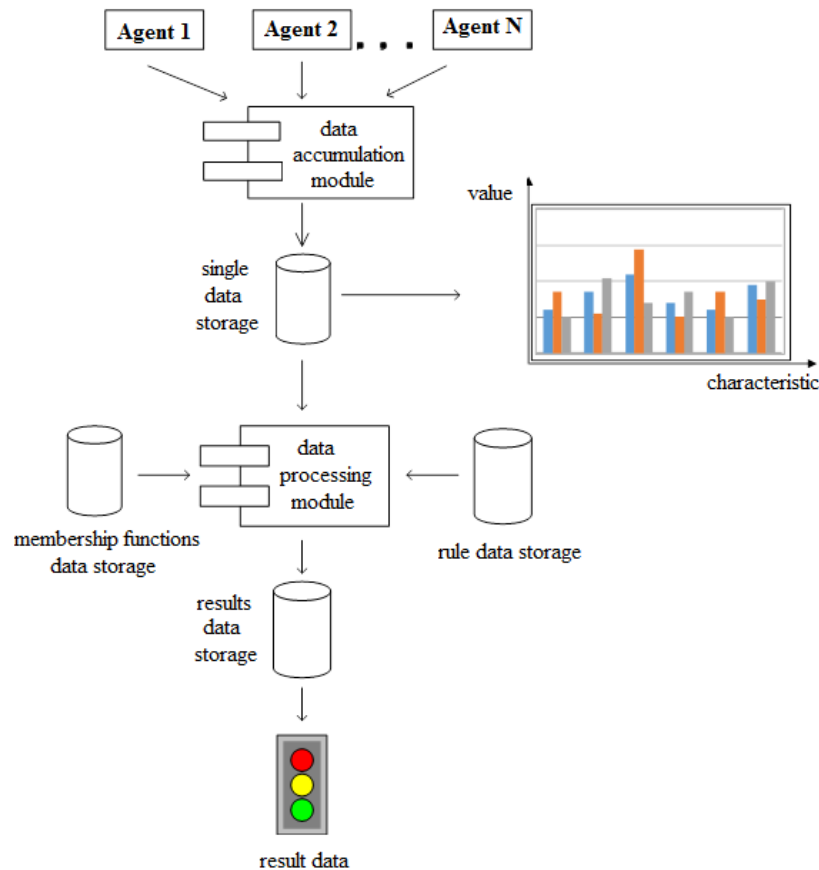
Fig. 1. – General scheme of the system

All information about employees' activities flows into one databank through the accumulation module data. Following information is being collected into this data-bank with specific time interval (year, quarter, month, day, hour, etc.). In other words, data collection module receives information from monitoring program agents and distributes by employees activity characteristics (working hours, number of sent data, etc.). Whereas the units of measurement will be also incommensurable, so usage of fuzzy logical inference allows to obtain the desired result.

   A single data storage was created to keep an information about the current activity of a company's employees (figure 2). The entity "Parameter_Value" keeps the relevant

data collected by the software agents during the certain period of time. The data accumulation module processes the received information and keeps it in convenient form for further processing.

The data processing module based on the fuzzy inference with help the given by experts the membership functions and the rule base draws the conclusions on the activity of each employee and writes the results into the data storage.

Let us consider algorithm of data processing module in more detail. Let *X* will be some employee of the organization, which can be characterized by a set of characteristics ($V\_1,\ V\_2,\ ...\ V\_n$). These characteristics take into account the work position of the employee, term of employment, his credentials, access and activity with confidential information, etc.

The assessment of individual activity from the viewpoint of the damage to the corporate security, can be described in terms of a natural language: "safe" and "likely safe" and "possibly dangerous", etc. Thus, the activity of the employee is set by the values of linguistic variables stored in the entity "Parameter".
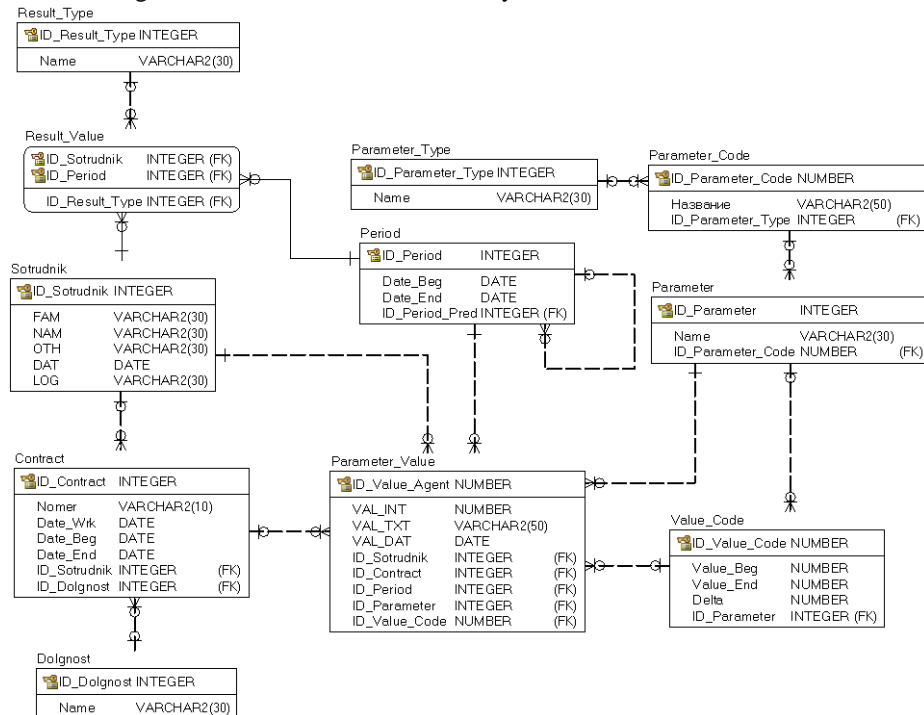
Fig. 2. – ER diagram (single data storage)

We will use the fuzzy inference procedure (figure 3) for evaluation of an individual activity. We input employee's information in the form of set of its characteristics (the values of the linguistic variables), then the output is an information about the extent of his belonging to the insider status.

The procedure is based on the algorithm Mamdani-Zadeh of the fuzzy inference. The construction of membership functions and the compilation of the rule base are carried out by an expert (or group of the experts) and are easily adjusted depending on the circumstances. The rule base can be stored in a separate database schema and it is constantly updated.
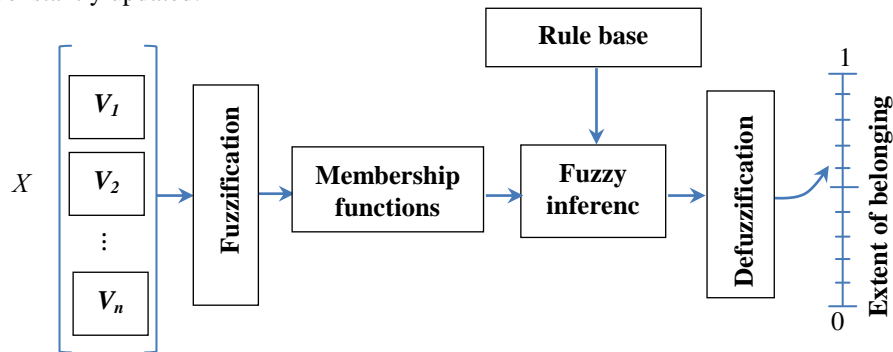
Fig. 3. – Procedure of fuzzy inference

The results of the analysis of activity of employees can be viewed in appropriate form of the system. Appropriate forms were developed for entering new characteristics and editing present ones of employees' activity (entity "Parameter", "Parameter_Code" and "Parameter_Type", see figure 2), membership functions, and rules of the knowledge base. Appropriate databases were developed for membership functions and rules of the knowledge base. This approach enables to take into account the peculiarities of the different companies' activities. Set of characteristics by themselves, characteristic sets, membership functions and rules in the knowledge base can be issues of sharing and discussions by the specialists.

This system will allow in real time to assess the state of data security in the CIS and the activities of employees working with sensitive data. In the case of appearing of the insider attacks marks, the system will automatically block the action of a potential insider and inform the corporate management about the danger. It should be noted that the system does not require maintenance by highly qualified specialists because it was created and customized by the expert for the specific company. Hence database of membership functions and rules of the knowledge base can be used independently from the highly skilled professionals.

References
1. **Zimmermann HJ.** Fuzzy Set Theory and its Applications. 3rd ed., Dordrecht: Kluwer Academic Publishers, 1996.
2. **Cappelli DM, Moore AP and Trzeciak RF.** The CERT Guide to Insider Threats: How to Prevent, Detect, and Respond to Information Technology Crimes (Theft, Sabotage, Fraud). Pearson Education, 2012.
3. CERT Insider Threat Center. Pattern-Based Design of Insider Threat Programs (CMU/SEI-2014-TN-024). Software Engineering Institute, Carnegie Mellon University, 2014.

Developing methods and algorithms for a decision-making intellectual support in personnel management systems

Danilenko A.N.

Samara State Aerospace University

Abstract. This paper proposes methods and algorithms for an intellectual support of decision-making management based on neuro-fuzzy networks. The algorithm for automatic generation of knowledge base is developed in accordance with the criteria of completeness and minimality. Reducing space is made on the basis of expert estimates.

1. Introduction

The management of modern enterprises demands more efficiency from their leaders. In the period of rapid changes in the market, a shorter rotation cycle of products and services, variability in consumer demand completeness and relevance of the knowledge base for strategic decision-making is quite important, as well as monitoring their implementation. In this regard, leaders have to make many decisions, based on the results of processing large amounts of data that must be carried out in a short time. At the same time, it is necessary to develop the systems of intellectual support of the managerial decision-making process based on modern information technologies.

The technologies of personnel decision-making are based on psycho-diagnostic data in a varying degree today: individual performance received by the diagnosis of individual employees or candidates for vacancies that allow determining the degree of the testee's compliance with the requirements of the profession or occupation. The possibilities of psycho-diagnostic analysis is expanding even more if a diagnostic system includes criteria oriented tests that detect the level of expertise and skills – in this way, diagnostic measurements test evaluate not only personal but also professional qualities of the testee.

The task of predicting the features of human behavior on the basis of psycho-diagnostics includes the following subtasks: diagnosis and interpretations of the data and predictions of certain events based on certain models. In this regard, there is a need to develop systems of decision-making intellectual support of managerial, which allow not only assigning data or conclusions of a certain probability, but also converting this probability as data processing and new revenues [1]. None of the existing software on the market meets these requirements. The methods and the algorithms proposed in this paper to some extent overcome the disadvantages mentioned above [2].

2. Methods and algorithms

The task of making decisions about the advisability of hiring can be attributed generally to the problem of classification, namely the assignment of the applicant to one of the classes: the candidate is fully compliant with the profession, basically meet the requirements for profession, partially compliant, is not compliant. Because of the large number of parameters affecting each other, there is a multifactorial uncertainty and therefore it becomes impossible to determine the type of the objective function to determine the degree of influence of each factor on the classification result. The application of data factor analysis at the same time does not give the desired results, and does not reduce the dimension of the space of classification. Therefore there is a need for the method of expert estimates. This helps reduce feature space, but does not solve the problem of uncertainty. To solve this problem, in this paper we propose to use the device of neural networks [3].

Since the information according we make a decision about aptitude of a candidate is the result of various psychological tests, classified data are inaccurate or insufficiently specific. Mathematical tools for solving this type of problems are fuzzy logics and the theory of fuzzy sets [4]. When solving the problem of classification fuzzy neural networks to conventional neural networks are preferred in the presence of the intersection of classes, as the behavior of such networks may be described on the basis of fuzzy rules, and thus the notation is set in these rules. For today there are two main groups of methods of knowledge acquiring: direct (interviews, literature study and others) and indirect (analysis of a training set of examples, observation of an expert and others). Numerous studies have shown that decision-making under uncertainty, that is when dealing with semi structured, incomplete or unclear information, the methods of the second group are more preferable.

At present there are many different methods of solving the problem of classification, but initially the number of classes is set by the user, based on an approximate idea of the nature of a future decision. Virtually unknown methods, in which in addition to solving the problem of classification the assessment of the significance of signs was carried out. For problems with a small number of examples (less than 20) and 2-3 attributes according to the classification methods of calculation can be carried out manually. For the problems with large dimension, these methods are not suitable [5].

In this case, the number of examples and the number of features is large enough, that requires the development of methods and algorithms for automatic generation of

382

a fuzzy rule base which is founded on quantitative assessments of classified attributes with the issuance of the result in the form of a set of production rules of the kind "IF – THEN".

2.1. Knowledge Base

In this paper we initially assume that the fuzzy–"IF – THEN"– rules specified by the experts are already represented in the linguistic form or in the form of a clear clustering correct input-output data sets. This knowledge base is examined for completeness and the minimum number of rules in the paper. Based on these results the methods and the algorithms for the automatic generation of a knowledge base have been developed [6].

For using this knowledge base in this paper in the problem of classification we modify the method of Abe and Lanused in to solve the problem of approximating functions. In our case, each subject is characterized by one-dimensional output y and m-dimensional input vector x, where x-the test results of the test for a particular factor and y-class accessories test (the candidate is fully compliant with the profession, basically meet the requirements for profession, partially compliant, is not compliant).

Write down the problem in general terms. The definition of a domain y is divided into n intervals and is determined by the degree of meeting the candidate the requirements of profession.

$$[y_0, y_1], (y_1, y_2], ... [y_{n-1}, y_n],$$

where $y_0=M_1$, $y_n=M_2$. Let us call i interval $(y_{i-1}, y_i]$ an output interval i. Using the specified output data, for which the outputs are in the output interval i, it is needed to recursively define the scope of the input values corresponding to this input interval. Namely, first of all, we must find the areas of activation which determine the input area corresponding to the output interval i by calculating maximum and minimum values of the input data. This must be done for each output interval. If the activation area of the output interval i overlaps the activation area of the output interval j, then the overlap area is defined as prohibition. If the input data for the output intervals and/or located inside the prohibition area, then one or two additional activation areas are determined. In future, if such additional areas of activation also overlap, the prohibition area is also determined for them. This process is shown in Figure 1, it is repeated as long as the problem of the overlay areas is resolved [7].

Fuzzy rules are defined on the basis of the activation area or a reason the basis of activation and the corresponding prohibition areas (if generated). Consider the algorithm by which fuzzy input data membership degree to the appropriate output intervals are calculated, followed by reduction to the clear value. This approach allows creating the initial rule base and optimizing it in the course of working with data. In the automatically generated basis of production rules its completeness and consistency is controlled, which leads to improvement of mechanisms of fuzzy logical deduction. Structuring the knowledge base to enhance the quality and effectiveness of decision-making and namely to increase the speed of training network and its accuracy.
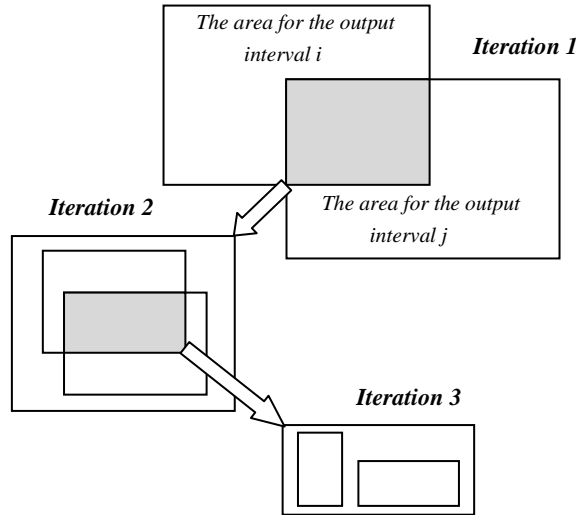
Fig.1. – Recursive Identification of the Areasof Activation and Prohibition

The contents of the generated knowledge base is supplied to the neural network as a training sample. Network input vector consists of the test results of a particular testee, and the class of the candidate belonging to a particular profession is the output of the network.

For implementation of the intellectual support of the decision-making system the model of a hybrid neuro-fuzzy classifier and a fuzzy multilayer perceptron is developed [8].

2.2. Hybrid neuro classifier

The hybrid neuro classifier consists of four layers. Elements of the first layer implement the operation of fuzzification that is form of membership of the input variables to certain fuzzy sets A_{ij}:

$$\mu_{A_{ji}}(x'_j) = \exp\left[-\frac{1}{2}\left(\frac{x'_j - c_{ij}}{\sigma_{ij}}\right)^2\right],$$

wherec_{ij}, σ_{ij}-the parameters of the membership function of bell type.

The initial values of these parameters are set so that the membership function satisfies the property of completeness, normality and convexity. The values c_{ij} should be uniformly distributed in the area of input vectors x. Values of these parameters are corrected during the training of the network based on the gradient method.

Each element of the second layer is neuron "I". They carry out the aggregation of the truth prerequisites degrees of each rule in the base in accordance with the operation of the T-norm by the formulas:

384

$$\alpha_1 = \min\{A_{11}(x_1), A_{12}(x_2), ..., A_{1n}(x_n)\}$$

$$\ldots \qquad\qquad\qquad\qquad\qquad\qquad ;$$

$$\alpha_n = \min\{A_{n1}(x_1), A_{n2}(x_2), ..., A_{nn}(x_n)\}$$

Elements of the third layer normalize and calculate the following values:

$$\beta_1 = \frac{\alpha_1}{\alpha_1 + \alpha_2 + ... + \alpha_n} ... \beta_n = \frac{\alpha_n}{\alpha_1 + \alpha_2 + ... + \alpha_n} ;$$

The elements of the fourth layer calculate the values of conclusions for each rule:

$$y_1' = B_1^{-1}(\alpha_1) = a_1 + \frac{1}{b_1} \ln \frac{1 - \alpha_1}{\alpha_1}$$

$$\ldots \qquad\qquad\qquad\qquad\qquad ,$$

$$y_n' = B_n^{-1}(\alpha_n) = a_n + \frac{1}{b_n} \ln \frac{1 - \alpha_n}{\alpha_n}$$

where a_i, b_i – the nonlinear parameters of membership functions $\mu_{B_i}(y)$ of the fuzzy sets of conclusions of the rules.

Fuzzy network outputs are calculated as follows: $y_i' = \beta_i B_i^{-1}(\alpha_i)$. These outputs are interpreted as membership degrees of the presented object to the corresponding class [9].

2.3. Fuzzy multilayer perceptron

The fuzzy multilayer perceptron consists of two parts: the "fuzzy layer" neurons and the actual multilayer perceptron. The activation function of the "fuzzy layer" neurons of such a network are radial basis functions (in the form of Gaussian function), modeling membership functions. These neurons are used to determine the degree of membership of the input vector components (which may be fuzzy). In the neurons outputs of this layer the coefficients are formed in the required for the furture recognition form. The outputs of the "fuzzy layer" are used as the inputs to the traditional multilayer perceptron [10].

If the input of the network is supplied by $x = [x_1, x_2, ..., x_m]^T$, then the output "of fuzzy layer" is formed vector of degrees of x belonging to specific centers (radial basis functions):

$$\mu(x) = [\mu_1(x), \mu_2(x), ..., \mu_m(x)]^T .$$

Specific components of the vector are calculated in such a way as to satisfy the condition of normalization

$$\sum_{i=1}^{L} \mu_1(x^{(k)}) = 1 ,$$

for each vector x^k, $k = 1...K$, where K – the number of vectors in the training set.

The model of the fuzzy multi-layer perceptron contains the following operators:

1. the operator forming the membership degrees of the input variables to certain fuzzy sets:

$$\mu_1(x^{(k)}) = 0.5 + \frac{\exp(f(p_2 - p_1)/p_{med}) - \exp(-f)}{2(\exp(f) - \exp(-f))}$$

$$\mu_2(x^{(k)}) = 1 - \mu_1(x^{(k)})$$

where f – the constant selected experimentally ($f>0$); p_2– the distance from the vector $x^{(k)}$ to the center of the class 2; p_2– the distance from the vector $x^{(k)}$ to the center of the class 1 in accordance with a selected metric (e.g., Euclidean); p_{med} – the distance between the centers of the classes 1 и 2;

2. the operator of logical product conditions for aggregation of the fuzzy rules relative to the classified image.

The outputs of the fuzzy multilayer perceptron are interpreted as membership degrees of the presented object of the appropriate class.

2.4. Research of constructing networks' quality

In these neuro-fuzzy networks is used the algorithm of Tsukomoto, and as a training algorithm is realized Backpropagation. The result of research of constructing networks' quality as a universal classifier revealed the influence of the parameters of a hybrid neuro-fuzzy classifier (the volume of training sample, the step of network training, the type of the fuzzification function and the defuzzification method) and the fuzzy multilayer perceptron (volume of training sample, step training network, the type of the fuzzification function and the number of neurons in the hidden layer) on the rate of learning [11]. These results can be summarized as follows:

1. Training sample high dimension does not lead to an improvement in quality of training of the neural network, but only causes its insensitivity to redundant data. For this task, the optimum is reached when the amount of training sample is 100 examples. However, if the number of training examples is limited, it is necessary to train the network to use the sample of 33 examples.
2. Quick network training increases the risk of deviations from the solutions followed by oscillations around it. Low values of the learning step eliminate this problem, leading to a slowdown in the process of network training. For this problem, in both networks 0.45 step is optimal.
3. Training of hybrid neuro-fuzzy classifier with Gaussian function is faster than modifying it with a triangular function. However, in the latter case, the network training algorithm is greatly simplified due to a simpler form of the fuzzification function, so that the system behaves more predictably. Training of the fuzzy multilayer perceptron with the hyperbolic tangent function is faster than it can be modified by the logistic fuzzification function. However, if the duration of the network training is not essential, it is advisable to use the fuzzy multilayer

perceptron with the logistic fuzzification function because in this case the system behaves more predictably.

4. With the increase in the number of neurons in the hidden layer the fuzzy multilayer perceptron is trained quickly to the set acceptable error threshold. In this problem with the optimal number of neurons step should be chosen from 35 to 40.

5. The view of the defuzzification method does not affect the standard deviation and the training rate of the hybrid neuro- fuzzy classifier.

6. The hybrid neuro-fuzzy classifier training algorithm has a fast the network and good interpretability of the gained knowledge.

7. The fuzzy multilayer perceptron naturally behaves at all the stage of the network training.

Next, a comparative analysis of the constructed fuzzy-neural classifiers is presented (table 1). To solve the original problem of classification of candidates for a specific position on the basis of their professional competence it is advisable to use the hybrid neuro- the fuzzy classifier, because it has a fast network training algorithm and good interpretability of the acquired knowledge, which is useful for solving applied problems.

The upgraded structure of the hybrid neuro-fuzzy classifier and its training algorithm allow using the network to solve the problem of predicting, e.g., predicting the success of a professional. The ordinary approach in this case demands a plurality of measuring of individual parameters, the dynamics of which would allow building the trend, but in the actual practice of personnel management it is impossible. However, the neural network proposed above is able to maintain these forecasts, after training on a variety of examples.

Table 1. ResultsoftheClassifying Properties ofNetworks

Network	Fuzzification Function	Defuzzification Method	Classification Error, %
The Hybrid Neuro Classifier	Gaussian	minimal deviation	6
		SD	1
		maximum deviation	7
	Triangular	minimal deviation	12
		SD	3
		maximum deviation	7
The Fuzzy Multilayer Perceptron	Logistic	-	4
	Hyperbolic tangent	-	17

3. Conclusions

Thus, in this paper we have proposed the method and the algorithm for automatic generation of knowledge in accordance with the requirements of the subject area, the

neuro-fuzzy network model for solving the problem of the support of decision-making in personnel management systems based on psycho-diagnostics has been developed.

The practical value of the paper is the development of algorithms and automated software system of decision-making in personnel management systems, which allows solving the following problems:

1. support of decision-making about the compliance of the candidate with the requirements of the profession;
2. rotation of employees and the redistribution of functional responsibilities within the team of the enterprise;
3. multifactorial diagnosis of professionally important qualities of the person on the basis of an interactive list of requirements for the profession;
4. predicting professional success.

References

1. **Gorunescu F, Belciug S, Gorunescu M and Badea R.** Intelligent decision-making for liver fibrosis stadialization based on tandem feature selection and evolutionary-driven neural network. Expert Systems with Applications, 2012; 39: 12824-12832.
2. **Huang H, Pasquier M and Quek C.** Decision support system based on hierarchical co-evolutionary fuzzy approach: a case study in detecting gamma ray signals. Expert Systems with Applications, 2011; 38: 10719-10729.
3. **Cruz-Ramirez M, Hervas-Martinez C, Fernandez JC, Briceno J and de la Mata M.** Predicting patient survival after liver transplantation using evolutionary multi-objective artificial neural networks. Artificial Intelligence in Medicine, 2013; 58: 37-49.
4. **Madaeni MM, Kurdian AR.** Fuzzy modelling and hybrid genetic algorithm optimization of virus removal from water using microfiltration membrane. Chemical Engineering Research and Design, 2011; 89(4): 456-470.
5. **Golmohammadi D.** Neural network application for fuzzy multi-criteria decision making problems. Int. J. Production Economics, 2011; 131: 490-504.
6. **Konysheva L, Nazarov D.** Basic theory of fuzzy sets. Piter: 2011; 192 p.
7. **Novak V, Perfilieva I and Mochkorzh I.** Mathematical Principles of Fuzzy Logic. Trans. from English ed. Averkina. M.:Fizmatlit, 2006; 252 p.
8. **Yarushkina N.** Basic theory of fuzzy and hybrid systems. Finance and Statistics, 2009; 320 p.
9. **Borisov VV, Kruglov VV and Fedulov AS.**Fuzzy Models and Networks.Hotline-Telec, 2007; 284 p.
10. **Osovsky S.** Neural networks for information processing. Finance and Statistics, 2002; 344 p.
11. **Kruglov VV, Borisov VV.** Artificial neural networks. Theory and practice. Hotline-Telec, 2002; 382 p.

Software testing based on global search of several variables functions discontinuity

Kovartsev A.N., Popova-Kovartseva D.A., Gorshkova E.E.

Samara State Aerospace University

Abstract. Testing of software products (SP) is one of the most important stages of SP lifecycles, when it can be found not only the errors, connected to computational algorithm coding process, but also those ones input at the stages of mathematical model (MM) development. The idea of the proposed software testing algorithm, directed on detection of fatal errors in MM, is based on a global search of several variables functions discontinuity. Moreover, a heuristic characteristic function, that takes into account the peculiarities of the problem, is used, which can significantly increase the efficiency of the error situations search algorithm.

Keywords: Global search algorithm, discontinuity point, mathematical model, software module, optimization function.

1. Introduction

Modern mathematical models (MM) allow to obtain extensive and highly accurate information about the processes occurring in nature and in technology by calculation. Computational experiments carried out with the mathematical model implemented as a computer program provides research shortening and its cost reduction. MM used in the calculations are finally realized in the form of software products (SP). Errors (including computational by nature errors) committed during the development of a mathematical model are directly inherited into correspondent SP [1, 2]. In this connection, it is appropriate to combine the troubleshooting procedures in mathematical models with the process of testing the respective SP.

If we consider a class of programs that are based on numerical analysis and computational mathematics, i.e., programs that implement some of mathematical models, the most difficult identifiable errors will be fatal computational errors such as "division by zero", resulting in exponent overflow and program execution failure [3]. Testing of these programs is a challenging task since the area of erroneous combinations of input data in this case is small, and the probability of accidental

exposure in this area of one of the test data set points, implemented, for example, by means of stochastic methods of testing, is negligible.

At the same time, order loss or overflow errors can be efficiently traced when viewed from the perspective of solving the problem of search of second order discontinuity points and use of algorithms for global optimization (GO) of several variables functions [4].

2. Problem statement and basic definitions

Formally, the computer module can be interpreted as a vector function $Y = F(X) = (f_1(X), f_2(X), \dots, f_m(X))^T$, that acts from set of current module inputs $X = (x_1, x_2, \dots, x_n)$ to set of calculated values $Y = (y_1, y_2, \dots, y_m)^T$.

The module domain will be described as the Cartesian product of the domains of each parameter $\Omega_X = \Omega_{X1} \times \dots \times \Omega_{Xn}$, where Ω_{Xn} – the domain of the *n*-th module parameter. By analogy, the set of admissible values of the function $F(X)$ is presented by $\Omega_F = \Omega_{Y1} \times \dots \times \Omega_{Ym}$, where Ω_{Ym} - the range of the *m*-th component of the vector function.

We will define the area of error situations as the set $\Omega_E \subset \Omega_X$, wherein when $X = \Omega_E$ there is a fatal computing error in a software module $F(X)$. In this case, if $f_i(X) = \pm\infty$ then the function has a second-order discontinuity.

The measure of error situations is zero ($\mu(\Omega_E) = 0$) for second-order discontinuity points, which creates serious difficulties in finding errors of this type. These errors are classified as "rare" in [3]. A comprehensive test focused on detecting "rare" errors may require a huge number of function tests, almost exhaustive search of all values of the module source data. This approach could not be implemented within a reasonable time.

The idea of the method of the second order discontinuity points searching [3] is based on the assumption that the second-order discontinuity points for mathematical functions could be found by solving one of optimization problems:

$$\max_X f_k(X) \quad (\min_X f_k(X)), \qquad k = \overline{1, m} \tag{1}$$

Indeed, the function value at the second-order discontinuity point is designated as $\pm\infty$. It could be associated for the computer with a large maximum positive or negative number, for example, $\pm M_{sup}$, the global extreme of the function in the broadest sense of the word. Applying the methods of global optimization, we are sure to discover function second-order discontinuity points.

3. An optimization approach for solving the problem of finding the second-order discontinuity points

The most effective method among the well-known one-parameter methods of multiextremal optimization is information-statistical method of R.G. Strongin [5]. This method is based on the use of the approximate posterior probability distribution of the global extremum location, which is formed during a function testing that implements a more balanced strategy for function global minimum search. This

390

strategy is so effective that it is often transferred from one-dimensional case to the case of several variables functions optimization.

To simplify the situation, we will consider the scalar function $f(X) = \max \left| f_i(X) \right|$.

For optimizable function we assume it to be a Lipschitz function with constant K, that means the condition $\left| f(x') - f(x'') \right| \le K \left| x' - x'' \right|$ is fulfilled.

In [5] it is shown that the function extremum search is realized by maximizing of a fairly simple characteristic function:

$$R(i) = m(x_i - x_{i-1}) + \frac{(y_i - y_{i-1})^2}{m(x_i - x_{i-1})} - 2(y_i + y_{i-1}), \tag{2}$$

where m - the Lipschitz constant estimate, which is calculated during the function extremum search:

$$m = \begin{cases} 1 & M = 0, \\ rM & M > 0, \end{cases} \qquad M = \max_i \frac{\left| y_i - y_{i-1} \right|}{(x_i - x_{i-1})},$$

where r – parameter.

To solve the problem of finding of several variables functions discontinuity irreparable points, we will choose the characteristic function similar to (2).

From the point of solving the problem of finding of second-order discontinuity points the Strongin method didn't manage to be effective because this method successful for Lipschitz functions, that are continuous by definition, loses its properties being applied to a class of discontinuous functions.

Let us analyze the characteristic function (2), which was deduced during information-statistical approach.

For simplicity, we assume $r = 1$. Formula (2) is presented in the following form:

$$R(i) = m\Delta x_i + \frac{\Delta y_i^2}{m\Delta x_i} - 2(y_i + y_{i-1}), \ \Delta x_i = (x_i - x_{i-1}), \ \Delta y_i = (y_i - y_{i-1}).$$

Providing that

$$m = \max_i \frac{\left| \Delta y_i \right|}{\Delta x_i} \approx \max_i \left| f'(x_i) \right| = \max_i \left| f_i' \right|,$$

we have

$$R(i) = \max \left| f_i' \right| \Delta x_i + \frac{f_i'^2}{\max \left| f_i' \right|} \Delta x_i - 2(y_i + y_{i-1}).$$

Using the first two terms of the Taylor expansion of optimizable function at the point x_{i-1} ($y_i \approx y_{i-1} + f_i' \Delta x_i$), we obtain

$$R(i) = \frac{(\max \left| f_i' \right| - f_i')^2}{\max \left| f_i' \right|} \Delta x_i - 4 y_{i-1}.$$

Hense,

$$R(i) \approx \frac{(\max\left|f_i'\right| - f_i')^2}{\max\left|f_i'\right|}\Delta x_i - 4y_{i-1}. \tag{3}$$

Analysis of the formula (3) shows that the characteristic function "inclined" to post test points in the vicinity of local minima of a function to be optimized, while tending towards the global minimum, or in uncertainty intervals, the dimensions of which are large compared to other intervals of the function.

We modify the characteristic function (3), based on the following assumptions.

Firstly, the algorithm of second-order discontinuity points search, in principle, should not rely on local extrema of the function, it should react to a rapid increase or decrease in the function growth rate.

Secondly, the function itself does not contain any information about its future behavior. The first-order derivative shows the function growth rate, while the second-order derivative - acceleration of this growth. It is obvious that the second-order derivative is more informative in this sense, therefore, we will choose $(f_i'')^2$ as the first component of the characteristic function. Squaring the second-order derivative is due to the fact that we don't need information about the sign of the function curvature at the point of discontinuity.

As a measure of uncertainty of partial interval, by analogy with the Strongin method, we will choose the length of the interval, improved by certain adjustment parameter r. On this basis we can choose the function $R(i) = (f''(x_i))^2(\Delta x_i)^r$ as the characteristic function of the irreparable discontinuity points search method. In a multidimensional case, for example for a function of 2 variables, the second-order differential could be used instead of the second-order derivative, and a characteristic function could be represented in the form:
$$R_{(i)} = (d^2 f(X_i))^2(\Delta_{x1}\Delta_{x2})^r. \tag{4}$$

4. Second-order discontinuity points search algorithm

Let us choose a unit square $\varPi = [0, 1] \times [0, 1]$, which is proportionally divided into four smaller squares during the fission process, as the errors searching range in computing module.

To calculate the second differential of the function by its values, calculated at the nodal points of the grid, it is easy to build a complete second-order polynomial $P_{2,2}(X)$, then $d^2 f(X) \approx d^2 P_{2,2}(X)$.

Summarizing the results, it is possible to construct an algorithm of finite-differences method (FDM) of second-order discontinuity points search:

Step 1. Regular full interpolation grid $\{X_{ij}\}$ $i,j = 0,1,2$ is formed for the current square Q_k. Values of the function at the vertices of the square and in the center were known while building on the previous step of the algorithm. We should only calculate the function values at the midpoints of the edges of a square. As a result, we have $Z^{(k)} = \left\|z_{i,j}^{(k)}\right\|$, $i,j = 0,1,2$. A source square Q_k, bounded by regular interpolation grid

nodes $\{X_{ij}\}$ $i, j = 1, 2, 3,$ is   divided   into   four   new   squares

$Q_k = Q_{k+1} \cup Q_{k+2} \cup Q_{k+3} \cup Q_{k+4}$.

Step 2. Using the matrix $z^{(k)}$ an interpolation polynomial $P_{2,2}^{(k)}(X)$ is constructed

for Q_k. In the centers X_{k+l}^c of the squares $Q_{k+l}, l = 1, 2, 3, 4$, the characteristic

function is calculated $R(k+l) = (d^2 P_{2,2}^{(k)}(X_{k+l}^c))^2 (h_k)^{2r}$. Here h_k - the length of the

squares side Q_{k+l} .

Step 3. Calculated values of the characteristic function are entered in the list R
in descending order of the function values, i.e. ($\forall i\ R(i) \geq R(i+1)$).

Step 4. As a "decisive" item from the list R we choose one with a maximum
characteristic, i.e., R (1). Thus, it is deleted from the list R.

Step 5. If algorithm stop condition is not fulfilled

($(\max\limits_{i} \left| z_i \right| > M_{\sup}) \vee (\min\limits_{i} h_i < \varepsilon)$), then go to step 1.

Stop condition of the algorithm described in step 5 contributes a conclusion of
its work, if the test function is outside the domain of the function, which is tantamount
to the appearance of the error.

5. Computational experiments

Test functions shown in Table 1 were considered to evaluate the effectiveness of
the FDM algorithm. The first two test functions were constructed of known functions
by their modifications. For example, the known modification of Rastrigin test
function [6], which has 625 local minimum and one global in the unit square, has
been converted into a function having a large number of local extrema and one "slit-
shaped" second-order discontinuity.
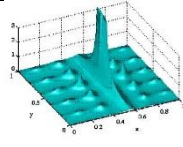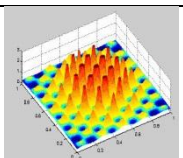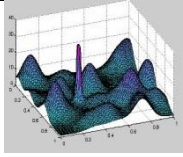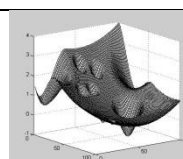
The second test function was constructed using division of one by Griewank
function, which gave rise to a large number of second-order discontinuity points. The
third Kovartsev test function was formed by the addition of a single second-order
discontinuity point to a linear combination of error functions generating smooth
function with more than 20 local extrema.

In literature the efficiency of search algorithms is typically evaluated using the
operating characteristics machine [7]. Operating characteristic is a dependence of an
error P_{alg} detection probability on the number of iterations of the algorithm. In our
case it depends on the amount of calls to the tested function N_f.

Since the second-order discontinuity points can be found in any of the global
optimization algorithms the efficiency of the proposed algorithm FDM was compared
with the efficiency of direct method GO, for example, the modified bisection method
(BM) [8].

Operating characteristics of FDM and BM methods built for test functions 1-3
(table 1) are presented in figure 1. Operating characteristics of the FDM algorithm are
denoted by solid line in the figure 1, operating characteristics of the BM algorithm -
by dashed line.

Table 1. A set of test functions

Function	General view
Modified Rastrigin function: $f(x_1, x_2) = 1/(10\sin^2(\pi z_1)$ $+ (z_1 - 1)^2(1 + 10\sin^2(\pi z_2))$ $+ (z_2 - 1)^2),$ $z_1 = 1 - (11 - 20(x_1 - a + 0.55))/4;$ $z_2 = 1 - (11 - 20(x_2 - b + 0.55))/4;$ $x_1, x_2 \in [0; 1].$ A set of local extrema. "Slit-shaped" second-order discontinuity.	
Modified Griewank function: $f(x_1, x_2) = 1/((x_1^2 + x_2^2)/400$ $- \cos(x_1)\cos(x_2/\sqrt{2}) + 1)$ $x_1, x_2 \in [0; 1].$ A set of second-order discontinuity points.	
Test Kovartsev function: $f(x_1, x_2) = \sum_{i=0}^{19}(i+1)e^{-\frac{(x_1 - a_{1i})^2 + (x_2 - a_{2i})^2}{0.01}}$ $+ 1/(1 - e^{-\frac{(x_1 - b_1)^2 + (x_2 - b_2)^2}{0.01}})$ $x_1, x_2 \in [0; 1].$ 20 local extrema. One second-order discontinuity point.	
GKLS test functions. Continuous twice differentiable function. 10 local extrema. One global extremum. No points of discontinuity is observed.	

As we can see from the graphs, the efficiency of the proposed FDM algorithm is much greater than the efficiency of the bisection method for functions #1 and #3. It happens as bisection method is focused on the optimization of continuous functions conceptually, which forces it to make more detailed "view" of the function areas with Lipschitz constant evaluation increase. This situation arises whenever the function is calculated at points of its discontinuity. FDM method conversely is looking for areas of rapid growth of the test function.

Function 2 (Griewank) has so many points of irreparable discontinuity that their detection is easily implemented with the same efficiency using FDM and BM methods. According to Fig. 1, the BM method has a slight advantage over the FDM method. The significant advantage of FDM over BM was recorded for all other functions.

Figure 2 shows the operating characteristics of these methods, built for continuous GKLS test function.
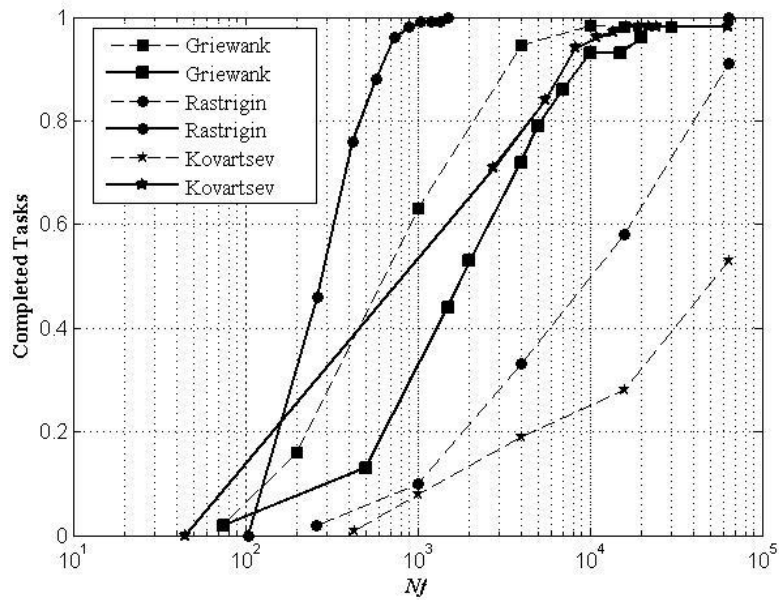
Fig. 1. – Operating characteristics of FDM and BM algorithm
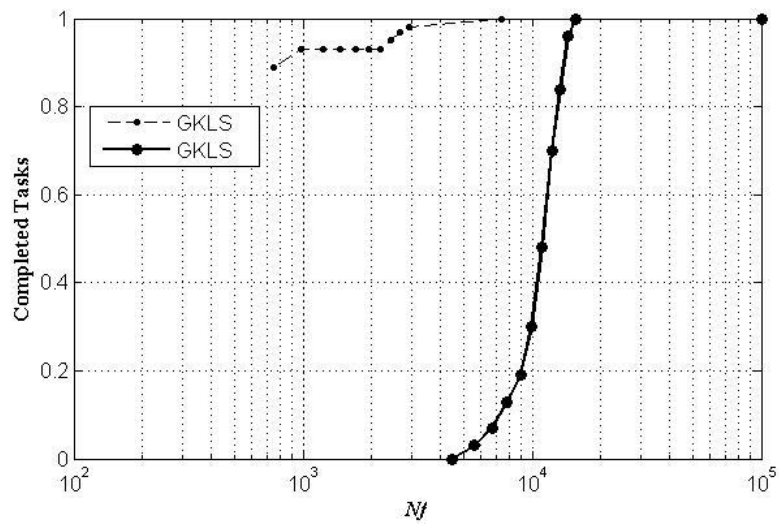
Fig. 2. – Operating characteristics of algorithms for continuous functions

It is clear from the figure, the efficiency of FDM algorithm for continuous functions is much lower than efficiency of BM algorithm. The finite difference method is forced to examine more carefully the space of the optimized variables in

case of continuous functions when there are no second-order discontinuity points (test software module has no errors). In this connection, there is an idea to use the FDM and BM algorithms for computational modules testing in a combined form and stop the calculation when either the FDM finds an error or BM stops.

Conclusion

The algorithm of global search of second-order discontinuity points, designed to detect fatal errors in mathematical models of computational algorithms, is considered in this paper. The basic idea of the algorithm is the addition of a heuristic original characteristic function to a classical algorithm of global optimization, where the first is based on the analysis of the characteristic Strongin function and considers the peculiarities of the problem. It has significantly increased the efficiency of the error search algorithm. This result allows us to hope on the organization of the error search for the functions of large dimensions. In the future, we plan to develop FDM algorithm using modern supercomputer technologys.

Acknowledgements

References

1. **Lipaev VV.** Program testing. M.: Radio and connection, 1986; 296 p. [in Russian]
2. **Kotliarov VP, Kolikova TV.** Basis of software testing. M.: BINOM, 2006; 285 p. [in Russian]
3. **Kovartsev AN.** Automation of software development and testing. Samara State Aerospace University, 1999; 150 p. [in Russian]
4. **Kovartsev AN, Popova-Kovartseva DA.** On efficiency of parallel algorithms for global optimization of functions of several variables. Computer Optics, 2011; 35(2): 256-261. [in Russian]
5. **Strongin RG.** Global optimum search. M.: Znanie, 1990. [in Russian]
6. **Abakarov ASh, Sushkov YuA.** Adaptation of random search using autocatalytic curve. SPb.: SPbGU, 2005; 67-75. [in Russian]
7. **Gergel VP, Strongin RG.** Absolute. Software system for global optimization method studying. Textbook. Nizhegorodsky University Press, 1998; 141 p. [in Russian]
8. **Kovartsev AN, Popova-Kovartseva DA, Abolmasov PV.** Efficiency study of global parallel optimization for multivariable function. Vestnik NNGU, 2013; 3(1): 252-261. [in Russian]

Technique of measurement of ultra-low resistance of current conductive junction of rail lines as the problem of states object identification

Tarasov E.M., Isaicheva A.G.

Samara State Transport University

Abstract. Systems of railway automation and remote control play an important role in transportation process ensuring the safety of train traffic, so it is necessary to eliminate failure and malfunctions of all its components and devices. Article deals with the principle of measuring of current conductive junctions rail lines, which allows to carry out the measurement and calculation of the resistance in a wide range of variation (from tens micro-ohm to unit ohm). The presented mathematical models of informative signs can be in automated complexes of diagnostic resistance of current conductive junctions' rail trunk lines, industrial railways, tram road and underground rail.

Keywords: Rail lines, return tractional network ,connection of joints, resistance of current conductive junctions, automated complexes of diagnostic

Automation and remote control devices are the main technical means ensuring automatic regulation and safety movement of trains, in which the sensitive element of the primary sensor of information on the state of control areas are rail lines. On electrified rail ways as return used the rail lines mainly consisting of rail links of length of 25 meters, at fish joints interconnected with tighten bolts and to equalize the resistance of junctions, apply copper connections of joints, cut set 70 mm^2. In terms of circulation in the area of heavy trains is getting loosening of tightening bolts, a partial or complete break of connections of joints that leads to fluctuations in electrical joint resistance and it adversely effects the stability work of the track - classifiers of rails lines states. By taking the normal traffic control course into accounting it is necessary to minimize eliminate faults and malfunctions operated devices of automation and remote control, it becomes apparent the important condition to provide control of the electrical resistance of current conductive junctions (CCJ). This requirement is particularly important of diagnosis of CCJ failures, which make up 15% of the total flow of failures of systems of automation and remote control.

Based on the resistance of the operated current conductive junction is within 60 - 300 × 10^{-6} Ohm, manual measurements require time, provide low accuracy and are not in heavy traffic. At the same time the resistance of the connection of joints can grow from 60× 10^{-6} to 0.4 Ohm and reaches the latest comes the effect of break the rail line to the signal current, which leads to the appearance of information on the refusal of automation and remote control system [1, 2].

In this regard, the development of control device value of resistance current conductive junctions is an urgent problem and requires the development of new principles of measurement of resistance junctions distributed in the area of control.

Nowadays it is apparent impossibility of direct remote sensing resistance current conductive junctions because of the low resistance value (tens micro-Ohm), their distribution and the large number - 200 current conductive junctions in the control area of 2500 m.

Indirect measurement of resistance current conductive junctions must be carried out in the operation of systems of interval train control when the rail line (the sensitive element of the state sensor of rail lines) receives only the voltage source survey to determine their status: available, busy or faulty.

The technique of indirect measurement of resistance junctions in the low value in complex of control devices of rail lines state is that the first phase is to realize training of the decision function of calculator resistance CCJ on the training set of known resistance, characterized by a set of primary informative features predetermined coordinates and discrete number of resistance junctions in the range of possible values, in a second phase using a pre-trained decision function of calculating coordinates and resistance junction decision device at each time moment reliably detects the calculation results belonging to the concrete coordinate and resistance. And, in the regard, the determination of the resistance current conductive junctions, mainly due to the decision of problems of selection of informative features related to resistance CCJ and the synthesis of the rules as a base which will be the assignment the result of the calculation to the coordinate location of the junction and its resistance.

As for the defition of the resistance junction and its coordinates, as informative signs, conveniently use the input and outpt power rail quadripole characteristics, depending on the condition of rail line of control area, including the resistance value CCJ, especially the amplitude and phase of the voltage and current at the input rail line as well as the amplitude and phase voltages at the output of the rail lines. Then, a multitude of images generated at these signs, take the form:

$$m_j = \left\{ U_{1_j}, \varphi_{1_j}, I_{1_j}, \psi_{1_j}, U_{2_j}, \varphi_{2_j} \right\}, \quad j = 1, 2, ..., n, \tag{1}$$

It is necessary take into account that the elementary quadripole rail line [A_{rl}] contains a link of rail line with distributed parameters and elements of the current conductive junctions with lumped parameters which resistance must be measured. Therefore, portions of the rail line in equivalent circuit (Figure 1) [1], it is necessary to replace the cascade connection quadripole link of rail line [A_r] and the quadripole current conductive junction [A_j], like
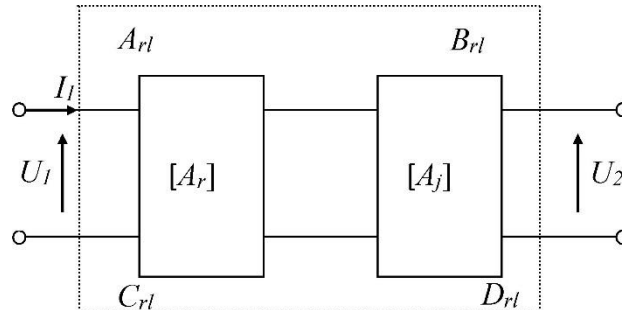
Fig. 1. The equivalent circuit rail quadripole current conductive junctions: U_1, U_2 - a complex value of the input and the output voltage of the elementary portion of the rail line; I_1- complex current value at its output

Parameters of the generalized quadripole rail line, control section, formed by n-cascade-connected quadripole link rail line and current conductive junction, defined by the expression

$$A_{rl} = \overset{n}{\underset{i,j=1}{X}} A_{ij}^r A_{ji}^l ,$$

where A_{ij}^r - quadripole rail link matrix; A_{ji}^l - quadripole current conductive junction matrix; n-the number of rail links.

The rail line presents in the form of a cascade-connected n-quadripole rail lines with uniform distributed parameters and lumped current conductive junction which allows investigate the effect of measured parameter - current conductive junction on informative signs in the changing disturbances in the form of fluctuations resistance in the insulation of rail lines in a wide range.

Rail links, due to contact with the earth and the electromagnetic mutual effect are described by the equations of lines with distributed parameters [1], where

$$A = D = \mathrm{ch}\gamma\ell, \ B = Z_w \mathrm{sh}\mathrm{g}1 , \ C = \mathrm{sh}\gamma1 / Z_w ,$$

$$\gamma = \alpha + j\beta = \sqrt{(r + j\omega L)(g + j\omega C)} , \ Z_w = \sqrt{\frac{r + j\omega L}{g + j\omega C}} . \qquad (2)$$

Rail quadripole matrix $[A_r]$ taking into account (2) and a current conductive junction $[A_j]$ take the form:

$$[A_r] = \begin{bmatrix} A_r & B_r \\ C_r & D_r \end{bmatrix}, \quad [A_j] = \begin{bmatrix} A_j & B_j \\ C_j & D_j \end{bmatrix}. \qquad (3)$$

In this case, the generalized matrix of the rail line portion control, as shown in Figure 1, is represented as:

$$\begin{cases} A_{rl} = \text{ch}\gamma l \cdot A_j + Z_w \text{sh}\gamma l \cdot C_j \\ B_{rl} = \text{ch}\gamma l \cdot B_j + Z_w \text{sh}\gamma l \cdot D_j \\ C_{rl} = \dfrac{1}{Z_w} \text{sh}\gamma l \cdot A_j + \text{ch}\gamma l \cdot C_j \\ D_{rl} = \dfrac{1}{Z_w} \text{sh}\gamma l \cdot B_j + \text{ch}\gamma l \cdot D_j \end{cases} \tag{4}$$

Mathematical models of informative features (1) with regard to (2) and (4):

$$U_1 = \frac{E A_{rl} Z_n + B_{rl}}{(C_{rl} Z_n + D_{rl}) Z_o + A_{rl} Z_n + B_{rl}}$$

$$I_1 = \frac{E(C_{rl} Z_n + D_{rl})}{(C_{rl} Z_n + D_{rl}) Z_o + A_{rl} Z_n + B_{rl}}$$

$$U_2 = \frac{E Z_n}{(C_{rl} Z_n + D_{rl}) Z_o + A_{rl} Z_n + B_{rl}}$$

where E - source of interrogating signal of rail lines; Z_n, Z_o - load resistance and limiter of the input current quadripole rail, respectively.

A crucial function of the calculator resistance CCJ $Z_i(X)$ conveniently represented in the form of a polynomial of the form [3],

$$Z_i(X) = C_1 x_1 + C_2 x_2 + \ldots + C_m x_m + C_{m+1} = C_o^T X + C_{m+1}, \tag{5}$$

where $x_1, x_2, \ldots x_m$ informative signs, X - vector of informative signs, $C_0 = (C_1, C_2, \cdot \ldots, C_m)^T$ transposed vector of coefficients.

In the process of constructing the decision function calculator in form (5), the main problem is to find the weight coefficients of polynomial, meet requirements the training calculator resistance current conductive junction for identifying discrete number resistance junctions in the range of possible value.

One way to solve this problem – the use of teaching methods [3, 4]. Training calculator (determination of the coefficients of the polynomial calculator) can be achieved by solving the system of equations of condition [5] using the methods of interpolation theory. For this entire system of equations must be written in matrix form as $XC = Z$ [6], where $C = K^{-1} X^T Z$, where X^T - transposed matrix X; K^{-1} - inverse matrix product, $K = X^T X$, which is equal to $K^{-1} = (X^T X)^{-1}$.

The result is a single data recovery, mathematical modeling function having the minimum error in determining the resistance CCJ.

Obviously, the resulting polynomial must have tolerance "field" data not falling into the learning procedure function calculator, which can be verified on the control sample of experimental data. If the error of calculation of resistance decision function in the space of the "field" of data is significant and the results fall into the adjacent discrete resistances, then obviously you need to complicate the decision function and repeat the process of training calculator.

Considered the principle of measuring resistance current conductive junctions rail lines is implement, allows take the measurement and the calculation of the resistance in a wide range of variations (from tens micro-Ohm to units Ohm) and can be used in automated diagnostic complexes resistance current conductive junctions rail trunk lines, industrial railways, tram road and underground line.

The relative error of indirect measurement research of resistance current conductive junctions of training calculator is showed that the value of the relative error depends on the complexity of features and the number of signs in the functions of the calculator. So computer simulation resistance CCJ measurement restored function calculator is showed that the maximum relative error is observed in the determination of the resistance CCJ in the low resistance values $\delta(Z_{i\,max}) = 3.94\%$, located closer to the source of the interrogation signal rail lines, and the minimum error $\delta(Z_{imax}) = 0.869\%$ CCJ located at the output of the control.

Reference

1. **Bryleev AM, Kravtsov Y, Shishlyakov AV.** The theory, structure and operation of track circuits. M.: Transport, 1978; 344 p. [in Russian]
2. **Dimitrenko IE.** Technical diagnostics and auto control systems of railway automation and remote control. M.: Transport, 1986; 144 p. [in Russian]
3. **Tu J, Gonzales R.** Principles of recognition. M.: Mir, 1978; 412 p. [in Russian]
4. RF Patent №2173276 method for controlling the state of the rail line. EM Tarasov, Belonogov AS. Stated. 31.05.99. Publ. BI 2001, 25, V61L MCI 23/16.
5. **Tarasov EM.** The principle of separation of space images into classes decisive functions. Bulletin of Samara Scientific Center of Russian Academy of Sciences, Special Issue, Samara, 2003; 78-83.
6. **Tarasov EM.** Methods of determining the coefficients of the polynomial decision function. Vestnik Samara Municipal Institute of Management, Samara, 2012; 3(22): 48-56.
7. **Tarasov EM, Yakobchuk AI.** Generalized structure of the device monitoring and diagnostics. Vestnik Samara Municipal Institute of Management, Samara, 2011; 2(17): 164-170.

The concept of "range" used in experimental calculations

Yablokova L.V.

Samara State Aerospace University

Abstract. In article considered the concept of range, as main design tool and implementation of algorithms of processing of the big data sets used in experimental calculations of mathematical physics.

Wise use of modern computer technology is unthinkable without the skillful use of the approximate and numerical analysis. This explains the extremely increased interest in methods for approximate computation and analysis of experimental data containing a big volume of information. Like no other branch of science, numerical methods, as the main tool of mathematical physics, is closely intertwined with many software applications, as a means or an object of research. At the same time the problems solved by modern science and modern technology, much more complex, and the way to solve them is not limited to general questions. Numerical methods and algorithms for processing big data sets, as a means to successfully meet the new challenges, are utilized in areas such as numerical solution of Maxwell's equations and d'Alambert's equation. As a rule, that to create complex mathematical computer model from the specialist require not only an impeccable mathematical background, but a basic knowledge of modern, high-performance algorithms, as well as effective methods for their use for big data. Currently, the bulk of the library for scientific calculations includes the implementation of the set of basic algorithms. However, manual implementation of simple variants of the basic algorithms it allows for better understanding and, consequently, more efficient using and configuring more advanced version of the library. Another important fact to re-implement the basic algorithms, is the fact that we are often faced with new computing environments with their new properties, which cannot be well involved in older implementations.

Realizing basis versions of algorithms, more fitted to specific objectives, and, not based on system subprograms, specialist's researchers can achieve bigger portability and more long save relevance, applied in the course of the decision, algorithms and data structures. Besides, despite the enhancements which are built in program libraries for scientific computations, the mechanisms used to sharing of programs aren't always rather powerful that library functions could be adjusted easily for effective

implementation within a specific objective. For example, the imperative programming paradigm with which use codes of the print_array programs (Fig. 1) and print_array_1 (Fig. 2) bringing array contents to the console provides to the developer of means of the description of sequence of commands and logical transitions which the computer is going to execute. It is very similar to the orders expressed by an imperative mood in natural languages, and the basic syntax concept supporting this paradigm is the operator. Within this it is quite enough simple, provided in examples, tasks, language tools, means supported by the selected coding style and the used idioms for implementation of the decision. But similar approach can be hardly conceptually widespread on more complex problems where the abstractions used in design process shall be already higher level.

```
program print_array
  implicit none
  integer, parameter :: n = 10
  integer :: i, arr(n) = (/1, 2, 3, 4, 5, 6, 7, 8, 9, 10/)
  do i = 1, n
    print *, arr(i)
  end do
end program
```

Fig. 1. – The output to console with using a subscript operator

```
program print_array_1
  implicit none
  integer, target :: i, arr(10) = (/(i, i = 1,10)/)
  integer, pointer :: p_arr(:)
  p_arr => arr(:)
  print "(i4)", (p_arr(i), i = 1, size(p_arr))
end program
```

Fig. 2. – The output to console with using a pointer

Provision of the most effective implementation of the specific algorithm directed on operation with a big data set will allow to use it for the solution of complex challenges of computing character and repeatedly. In an example of print_array_2 (Fig. 3), procedural and operator programming style which is development of an imperative paradigm is applied and allows to use concept the range for implementation of subprograms.

We will assume that there is a sequence which elements shall be processed by any algorithm. In the course of such processing there is an appeal to all elements of sequence, beginning from the first and finishing last. The similar situation meets in implementation process of algorithms so often that for processed elements of sequence there is a special notation: the range. For example, the range [first, last) consists of all elements from first to last, but not including the last. Such asymmetric form of record is used to focus attention that [first, last) is a half-open interval which includes all elements, since first, but not last. The range [first, last) is admissible if to all its elements, excepting last, it is possible to get access and if the element facing last is achievable from first namely if sequentially being moved, since first, on all line

403

items of the range a finite number of times it is possible to get to a line item the previous last. For example, the range [0, *N*) is valid. The empty range [0,0) also is valid, and here the range [*N*-1,0) is invalid as the element in a line item of *N*-1 appears after an element in a line item 0. Therefore it doesn't make sense to speak about elements in line items from *N*-1 to 0 as about tolerance range.

```fortran
program print_array_2
  implicit none
  integer, parameter :: n = 100000
  integer :: arr(n)
  ! .....
  ! array initialization
  ! .....
  call print(loc(arr(1)), loc(arr(n)))
end program
subroutine print(first, last)
  integer :: first, last, val
  pointer(first, val)
  do while(first <= last)
    print *, val
    first = first + sizeof(integer)
  end do
end subroutine
```

Fig. 3. – The output to console with using the range concept

Generally, the ranges satisfy the following properties:

1. id range.
2. For any element in *i* line items, the range [*i, i*) is a valIf [*i, N*) is a valid range, then [*i*+1, *N*) is also a valid range.
3. If [*i, N*) is a valid range, and an element in a line item of *k* is achievable from an element in *i* line item, and the element in a line item of *N*-1 is achievable from an element in *k* line items, the ranges [*i, k*) and [*k, N*) are both valid ranges.
4. If both ranges [*i, k*) and [*k, N*) are both valid ranges, the range [*i, N*) is also a valid range.

From the fundamental point of view the ranges are defined thus because their asymmetric form helps to avoid errors, the so-called, lost unit, i.e. the quantity of elements in the range [*i, N*) is equal to *N-i*, namely it is exactly so much, how many it is expected.

Using the concept of the range it is possible to pass to other more general concept of interval function. The concept of interval function provides possibility of creation of algorithms capable to process any data structures of the elements supporting concept of one-dimensional sequence, for example one-dimensional arrays in the FORTRAN and similar languages. Besides, writing of a code of the program with use of interval functions requires smaller efforts, and decisions with their application usually look more visually and logically.

References

1. **Artemov IL.** Fortran: the basics of programming. M.: Dialog-MIFI, 2007.
2. **Golub J, Van Lone C.** Matrix calculations: Trans. from English. M.: Mir, 1999.
3. **Demmel J.** Computational linear algebra. Theory and Applications. Trans. from English. M.: Mir, 2001.
4. **Podbelsky VV, Fomin SS.** The course Programming in C: Proc. Allowance. M.: DMK Press, 2013.
5. **Vorotnikova DG, Golovashkin DL.** Long vectors algorithms for solving grid equations of explicit difference schemes. Computer Optics, 2015; 39(1): 87-93.
6. **Kazanskiy NL, Protsenko VI, Serafimovich PG.** Comparison of system performance for streaming data analysis in image processing tasks by sliding window. Computer Optics. 2014; 38(4): 804-810.

Recovery of directed graphs from the matrix of peaks neighborhood

Kotenko A.P.,

Samara State Aerospace University

Dokuchaev A.V.

Samara State Technical University

Abstract. The properties of the graph problem of optimal investment of additional resources available to reduce the critical path network project are considered. It was proposed the algorithm in graph structure of the project on a given matrix of precedence works. The specified method of minimizing the required number of fictitious works to simplify the graph of the project is indicated.

1. Statement of the problem

Continued [1-4] to study the problem of network planning and management for the connected project $P = \{a(i)\}_{i=1}^{k \geq 1}$ with the jobs

$a(i): i \neq j \iff a(i) \neq a(j)$

which has the sets of predecessors $s(a(i)) \subset P$ and execution time

$t(a(i),x(i)): P \times U(X) \to \Re^+$

by additional resources $x(i) \in U(X)$ of the partition

$$U(X) \overset{def}{=} \{x(i)\}_{i=1}^k : \ X = \bigcup_{i=1}^k x(i), \ x(i) \underset{i \neq j}{\cap} x(j) = \varnothing \ \}.$$

Here $s(a(i))$ is own (may be empty) subset of project jobs P, which must be completed before starting job $a(i)$.

Resource X can be a real number with a non-negative partitioning $0 \leq \sum_{i=1}^{k} x(i) \leq X$ *(or* $1 < \prod_{i=1}^{k} x(i) \leq X$), or the set of discrete elements $X = \{y_t\}_{t=1}^{L \geq 1}$ with arbitrary partition into subsets $U(X) \subseteq 2^x$.

Let optimize the resource allocation $\{x(i)\}_{i=1}^{k}$ for minimizing the total time of the project P: $\sum_{i=1}^{k} t(a(i), x(i)) \to \min$

2. Reduce the list of predecessors

We describe the relation S of precedence $a_i S a_j$ of the project jobs $a_i, a_j \in P$ by the matrix of precedence $S = \|s(i,j)\|_{i,j=1}^{k}$:

$$s(i,j) \stackrel{def}{=} \chi(a(i), s(a(j))),$$

with the characteristic function

$$\chi(a(i), s(a(j))) \stackrel{def}{=} \begin{cases} 1 \leftarrow a(i) \in s(a(j)), \\ 0 \leftarrow a(i) \notin s(a(j)). \end{cases}$$

Thus, the unit *1* in the *i-th* row of the matrix S indicates preceding the job $a(i)$ of the respective columns. Then the transposed matrix S^T describes the inverse relation S^{*-1} following $a_j S^{-1} a_i$ project job: unity *1* in the *i-th* row of the matrix S^T indicates preceding job $a(i)$ by the job of relevant columns. Obviously, the relations S and S^T are transitive ($S^2 \subseteq S$, $(S^{-1})^2 \subseteq S^{-1}$) through the finiteness of the set of project jobs and has the inclusions

$$\varnothing = S^{k-1} \subseteq S^{k-2} \subseteq ... \subseteq S^3 \subseteq S^2 \subseteq S$$

$$\varnothing = (S^{-1})^{k-1} \subseteq (S^{-1})^{k-2} \subseteq ... \subseteq (S^{-1})^3 \subseteq (S^{-1})^2 \subseteq S^{-1}.$$

We call the job $a(i) \in P$ immediate predecessor of the job $a(j) \in P$, if $\chi(a(i), s(a(j)))=1$ and no other job such as $a(l) \in P$: $\chi(a(i), s(a(l)))=\chi(a(l), s(a(j)))=1$.

Otherwise, the preceding (following) will be called indirect.

With the immediate predecessors lists $\{s*(a(i))\}_{i=1}^{k}$ we define the relation $S*$ of immediate precedence by $k \times k$-matrix of direct precedence $S* = \|s*(i,j)\|_{i,j=1}^{k}$:

$$s*(i,j) \stackrel{def}{=} \chi(a(i), s*(a(j))).$$

Let the transposed matrix $S*^T$ defines the inverse relation $S*^{-1}$ of immediately following project jobs. Wherein the relations $S*$ and $S*^{-1}$ are generally transitive as

$$S* = S - \bigcup_{t=2}^{k-1} S^t \quad \text{and} \quad S*^{-1} = S^{-1} - \bigcup_{t=2}^{k-1} (S^{-1})^t.$$

We shorten the list of precedence $\{s(a(i))\}_{i=1}^k$ to the list of direct precedence $\{s*(a(i))\}_{i=1}^k$ and by permutation of rows and columns of the matrix S for correct precedence order of the project jobs:

$$\chi(a(j), s*(a(i)))\big|_{i<j} = 0 .$$

In the future, we consider the original numbering of project jobs $\{a(i)\}_{i=1}^k$ is correct, and the original list of predecessors $\{s(a(i))\}_{i=1}^k$ is shorthand. Let matrix A of direct precedence of the properly ordered jobs

$S=(A[i_1 \times j_1], A[i_2 \times j_2], ..., A[i_r \times j_r])$, $2 \leq r \leq k-1$, $i_1=j_1=i_2$, $j_2=i_3$,   ..., $j_{r-1}=i_r=j_r$,

$$\sum_{t=2}^{r} i_t = \sum_{t=1}^{r-1} j_t = k ,$$

be upper triangular and block-chained with zeros on the main diagonal and has continuous chain $i_t \times j_t$-blocks $A[i_t \times j_t]$, $1 \leq t \leq r$, of which the first block and the last block are zero and square

$A[i_1 \times j_1]=0, A[i_r \times j_r]=0$.

Let the remaining blocks are non-zero: $A[i_t \times j_t] \neq 0, 2 \leq t \leq r-1$.

Example 1.

The matrix of direct precedence of properly ordered 9 project jobs $\{a(i)\}_{i=1}^9 = P$ may take the form

	$a(1)$	$a(2)$	$a(3)$	$a(4)$	$a(5)$	$a(6)$	$a(7)$	$a(8)$	$a(9)$	
$a(1)$ $a(2)$	$A[i_1 \times j_1]$		$A[i_2 \times j_2]$			0		0		$\}i_2$
$a(3)$ $a(4)$ $a(5)$	0		0			$A[i_3 \times j_3]$		0		$\}i_3$
$a(6)$ $a(7)$	0		0			0		$A[i_4 \times j_4]$		$\}i_4$
$a(8)$ $a(9)$	0		0			0		$A[i_5 \times j_5]$		$\}i_5$
	$\underbrace{\quad}_{j_1}$		$\underbrace{\quad}_{j_2}$			$\underbrace{\quad}_{j_3}$		$\underbrace{\quad}_{j_4}$		

3. Project's graph

We construct a directed graph $G(V,R)$ of the project P. At first we define the set of vertices V as follows.

Case 1. If block $A[i_t \times j_t]$, $2 \leq t \leq r-1$, consists only of units, then exists a general conclusion

$v_\kappa(a(\alpha(1)))=v_\kappa(a(\alpha(2)))=...=v_\kappa(a(\alpha(i_t)))$

and common origins

$v_н(a(\beta(1)))=v_н(a(\beta(2)))=...=v_н(a(\beta(j_t)))$

408

of the project jobs $a(\alpha(1)),a(\alpha(2)),...,a(\alpha(i_t)),a(\beta(1)),a(\beta(2)),...,a(\beta(j_t)) \in P$ with numbers

$$1 \leq \sum_{s=1}^{t-1} i_s = \alpha(1) < \alpha(2) < ... < \alpha(i_t) < \beta(1) < \beta(2) < ... < \beta(j_t) = \sum_{s=t+1}^{r} j_s .$$

Wherein

$$\alpha(1) = \sum_{s=1}^{t-1} i_s , \quad \alpha(s+1) = \alpha(s)+1, \quad 1 \leq s \leq i_t-1; \quad \beta(1) = \alpha(i_t)+1, \quad \beta(s+1) = \beta(s)+1, \quad 1 \leq s \leq j_t-1,$$

$$\beta(j_t) = \sum_{s=1}^{t} i_s + j_t .$$

We may add vertex $v(\alpha(1),\alpha(2),...,\alpha(i_t);\beta(1),\beta(2),...,\beta(j_t)) \in V$ to connect said project jobs (Fig. 1). In this way,
$v(\alpha(1),\alpha(2),...,\alpha(i_t);\beta(1),\beta(2),...,\beta(j_t))=$
$=v_\kappa(a(\alpha(1)))=v_\kappa(a(\alpha(2)))=...=v_\kappa(a(\alpha(i_t)))=v_H(a(\beta(1)))=v_H(a(\beta(2)))=...=v_H(a(\beta(j_t))).$

$a(\alpha(1))$ $a(\beta(1))$

$a(\alpha(2))$ $a(\beta(2))$

...   ...

                                            $a(\beta(j_t))$

$a(\alpha(i_t))$ $v(\alpha(1),...,\alpha(i_t);\beta(1),...,\beta(j_t))$
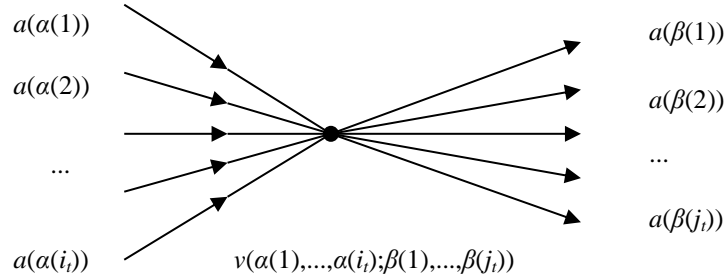
Fig. 1. – Top, obtained by combining inbound and outbound directed arcs

One can consider each added vertex $v(\alpha(1),...,\alpha(i_t);\beta(1),...,\beta(j_t))$ as notation of the complete bipartite graph $K(i_t,j_t)$, $1 \leq i_t \leq k-1$, $1 \leq j_t \leq k-1$, with the part $K(1,i_t)$ powered of i_t and the part $K(j_t,1)$ powered of j_t, having single $i_t \times j_t$-, $1 \times i_t$- and $j_t \times 1$-neighborhood matrix peaks co-responsible. Shares of $K(1,i_t)$ and $K(j_t,1)$ describe the overall time of completion

$$K(1,i_t) = \{v_\kappa(a(\alpha(s)))\}_{s=1}^{i_t}$$

and common moments of the beginning

$$K(j_t,1) = \{v_H(a(\beta(s)))\}_{s=1}^{j_t}$$

of the relevant design jobs. See. Fig. 2.

$a(\alpha(1))$ $a(\beta(1))$

$a(\alpha(2))$ $a(\beta(2))$

...   ...

$a(\alpha(i_t))$ $a(\beta(j_t))$
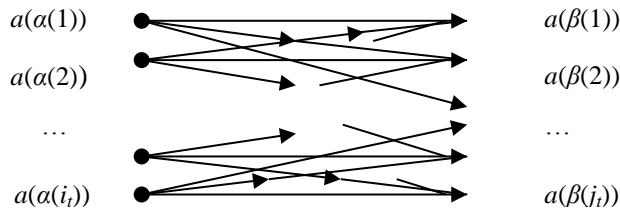
Fig. 2. – Key added in the form of the vertices bipartite graph

409

Obviously that the resulting subgraph $G(A[i_t \times j_t])$, which connects the project jobs

$$\{a(\alpha(u))\}_{u=1}^{i_t} \cup \{a(\beta(u))\}_{u=1}^{j_t},$$

is planar, and the number of options for passing full paths through project P unit block $A[i_t \times j_t]$ is equal to $i_t \times j_t$.

Case 2. If among the elements of the block $A[i_t \times j_t]$, $2 \leq t \leq r-1$, there are zeros, then relevant bipartite graph $K(i_t, j_t)$ is not complete and must be added by the fictional jobs, unlike the embodiment of Fig. 1 it can not to connect a it incoming and jt outgoing directed arcs by one vertex.

Example 2.

Consider the 2×2-blocked 5×9-matrix of the immediate preceding project jobs $\{a(i)\}_{i=6}^{14}$ by the jobs $\{a(i)\}_{i=1}^{5}$:

$$A[5 \times 9] = \begin{pmatrix} 1 & 1 & 1 & 1 & 1 & 1 & 1 & 1 & 1 \\ 1 & 1 & 1 & 1 & 1 & 1 & 1 & 1 & 1 \\ 1 & 1 & 1 & 1 & 1 & 1 & 1 & 1 & 1 \\ 1 & 1 & 1 & 1 & 0 & 0 & 0 & 0 & 0 \\ 1 & 1 & 1 & 1 & 0 & 0 & 0 & 0 & 0 \end{pmatrix}.$$

Combining events (Fig. 3)

$v_K(a(1)) = v_K(a(2)) = v_K(a(3)) = v_H(a(10)) = v_H(a(11)) = v_H(a(12)) = v_H(a(13)) = v_H(a(14))$,
$v_K(a(4)) = v_K(a(5)) = v_H(a(6)) = v_H(a(7)) = v_H(a(8)) = v_H(a(9))$,

introduce the additional (fictional) job b(1) to save the immediate preceding of the jobs $\{a(i)\}_{i=6}^{9}$ by the jobs $\{a(i)\}_{i=4}^{5}$, and the preceding of the jobs $\{a(i)\}_{i=10}^{14}$ by the jobs $\{a(i)\}_{i=1}^{3}$, and non-immediate preceding of the jobs $\{a(i)\}_{i=6}^{9}$ by the jobs $\{a(i)\}_{i=1}^{3}$.

Fig. 3. – A graph constructed according to Example 2

410

The permutation of the project jobs $\{a(i)\}_{i=6}^{9}$ and $\{a(i)\}_{i=10}^{14}$ and the addition of the fictional job $b(1)$ between $a(5)$ and $a(10)$ does not change the other blocks of the matrix of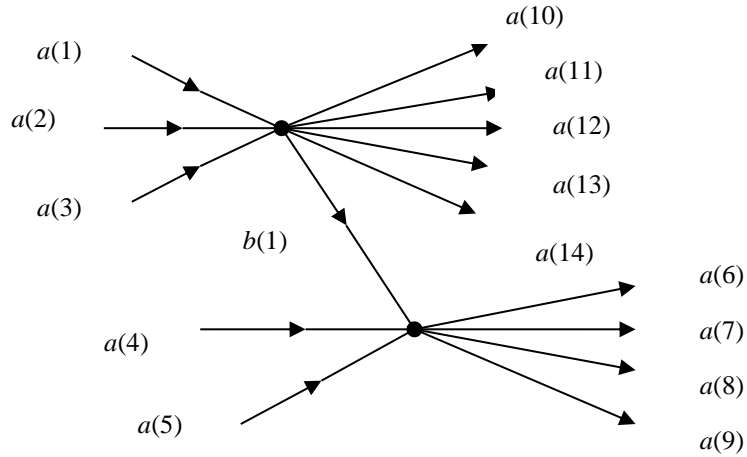 directly precedence S, setting the proper ordering of a united set of jobs $b(1) \cup \{a(i)\}_{i=1}^{14}$ and turning the block $A[5 \times 9]$ to the 2×2-blocked 6×10-submatrix

	$b(1)$	$a(10)$	$a(11)$	$a(12)$	$a(13)$	$a(14)$	$a(6)$	$a(7)$	$a(8)$	$a(9)$
$a(1)$	1	1	1	1	1	1	0	0	0	0
$a(2)$	1	1	1	1	1	1	0	0	0	0
$a(3)$	1	1	1	1	1	1	0	0	0	0
$a(4)$	0	0	0	0	0	0	1	1	1	1
$a(5)$	0	0	0	0	0	0	1	1	1	1
$b(1)$	0	0	0	0	0	0	1	1	1	1

with two 3×6- and 3×4- unit blocks in broken chain of non-zero blocks above the main diagonal of the matrix S.

Example 3.

Note that the permutation of the project jobs $\{a(i)\}_{i=1}^{5}$, as well as $\{a(i)\}_{i=6}^{14}$, does not change the accuracy of ordering. For example, a permutation of the jobs $\{a(i)\}_{i=6}^{14}$ of the Example 2 can get another 2×2-blocked 5×9-matrix of directly preceding of the jobs $\{a(i)\}_{i=6}^{14}$ by the jobs $\{a(i)\}_{i=1}^{5}$

$$
A[5 \times 9] = \begin{pmatrix} 1 & 1 & 1 & 1 & 1 & 1 & 1 & 1 & 1 \\ 1 & 1 & 1 & 1 & 1 & 1 & 1 & 1 & 1 \\ 1 & 1 & 1 & 1 & 1 & 1 & 1 & 1 & 1 \\ 0 & 0 & 0 & 0 & 1 & 1 & 1 & 1 & 1 \\ 0 & 0 & 0 & 0 & 1 & 1 & 1 & 1 & 1 \end{pmatrix},
$$

which, after the union of events (Fig. 4)
$v_K(a(1))=v_K(a(2))=v_K(a(3))=v_H(a(6))=v_H(a(7))=v_H(a(8))=v_H(a(9))$,
$v_K(a(4))=v_K(a(5))=v_H(a(10))=v_H(a(11))=v_H(a(12))=v_H(a(13))=v_H(a(14))$
and after the introduction of additional (fictional) job $b(1)$, stored directly preceding of the jobs $\{a(i)\}_{i=6}^{9}$ by the jobs $\{a(i)\}_{i=1}^{3}$, the jobs $\{a(i)\}_{i=10}^{14}$ by the jobs $\{a(i)\}_{i=4}^{5}$ and non-directly preceding and the jobs $\{a(i)\}_{i=10}^{14}$ by the jobs $\{a(i)\}_{i=1}^{3}$ corresponds to the following sub-boxes (Fig. 4).

Adding of the fictional job $b(1)$ between $a(5)$ and $a(6)$ does not modify other blocks of the matrix of direct precedence S, establishing the correct sequencing united plurality of the jobs $b(1) \cup \{a(i)\}_{i=1}^{14}$ and turning the block $A[5 \times 9]$ to 2×2-blocked 6×10-submatrix

	$b(1)$	$a(6)$	$a(7)$	$a(8)$	$a(9)$	$a(10)$	$a(11)$	$a(12)$	$a(13)$	$a(14)$
$a(1)$	1	1	1	1	1	0	0	0	0	0
$a(2)$	1	1	1	1	1	0	0	0	0	0
$a(3)$	1	1	1	1	1	0	0	0	0	0
$a(4)$	0	0	0	0	0	1	1	1	1	1
$a(5)$	0	0	0	0	0	1	1	1	1	1
$b(1)$	0	0	0	0	0	1	1	1	1	1

with two 3×5-unit blocks in broken chain of the non-zero blocks above the main diagonal of the matrix S.
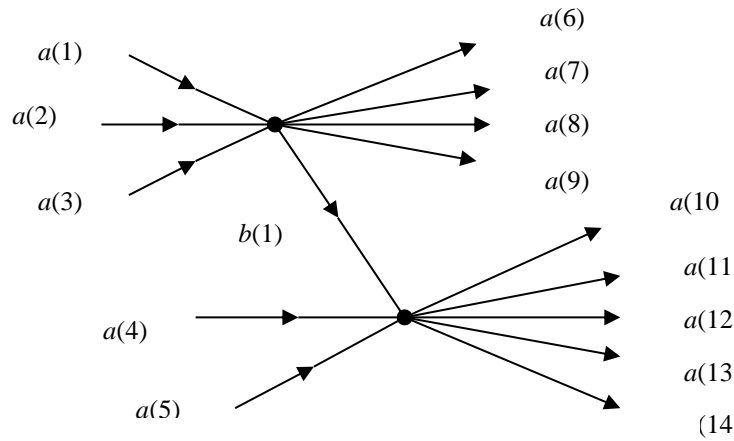
Fig. 4. – A graph constructed according to Example 3

4. Algorithm of adding of the fictional jobs

We give universal algorithm for adding the required number of fictional jobs $a(i) \notin P$, $i \geq k+1$.

Consider the non-zero non-trivial block $A[i \times j]$ of the rows $B \overset{def}{=} \{a(u)\}_{u=l}^{l+i}$ and the columns $C \overset{def}{=} \{a(u)\}_{u=l+i+1}^{l+i+j}$, $l = \sum_{u=1}^{t-1} i_u$, $1 \leq i = i_t$, $1 \leq j = j_t$, $2 \leq t \leq r-1$, of the project jobs in the continuous chain $\{A[i_t \times j_t]\}_{t=1}^{r}$ blocked chained matrix of directly precedence S. We consider the set of previous project jobs B as the factor-set of the relationship of equality of the rows of the matrix $A[i \times j]$. Then the relationship of direct sequence $s*–1$ determines the one-to-one mapping

s*^-1$:$ 2^C→2^C

on the set of all subsets of C. At the closure D of the image $s*^{-1}(2^C)$ of her step-intersection subsets ∩ build the oriented tree of the relation

$\forall D_1, D_2 \in D \ (D_1 \rightarrow D_2 \overset{def}{\Leftrightarrow} D_2 \subset D_1)$,

excluding the empty set $\varnothing$. Arcs of this tree are the desired fictional jobs you needed to build the subgraph $G(A[i\times j])$, binding the project jobs $B\cup C$. Therefore, it completed the construction of sub-graph for non-trivial block in the Case 2.

As is a tree, the subgraph $G(A[i\times j])$ is planar, and the number of passing ways of the project P through the block $A[i\times j]$ is equal to $i\times j$.

Thus, the total number M of the full paths of the project P is

$$M = \prod_{t=1}^{r-1} i_t = \prod_{t=2}^{r} j_t .$$

5. Completion of construction of the project's graph

Now from the resulting subgraphs $\{G(A[i_t \times j_t])\}_{t=2}^{r-1}$ we may form the graph $G(V,R)$ of the project P. For this the initial vertex of starting jobs the initial vertex of the whole project, and the finishing jobs must be joined to the ending vertex of the project. Then all the end vertices of the block $A[i_1\times j_1]$ will be the initial vertex of the block $A[i_2\times j_2]$, and then to the endpoints of the block $A[i_{r-1}\times j_{r-1}]$, which became the initial vertex of the block $A[i_r\times j_r]$.

This shows that, in any case, at least with the addition of some fictional jobs, the project's graph will be built.

Reference
1. **Dokuchaev AV, Kotenko AP.** Optimization of additional resources in network planning. Vestnik of Samara State Technical University. Series Sci. science, 2010; 1(20). [In Russian]
2. **Dokuchaev AV, Kotenko AP.** Transition to the direct precedence matrix for network project graph construction. Abstracts of VIII Conf. "Math. Simulation and Boundary Value Probl.", 2011; part 2. [in Russian]
3. **Dokuchaev AV, Kotenko AP.** Network project graph construction on the basis of jobs precedence table. Groups and Graphs, Algorithms and Automata-2015. Abstracts of the International Conf. Yekaterinburg: UrFU Publishing house, 2015.
4. **Dokuchaev AV, Kotenko AP.** Necessary conditions to complement the graph of project by fictitious arcs. Information Technology and Nanotechnology-2015. Abstracts of the International Conf. Samara: SSAU, 2015. [in Russian]

GPU implementation of Jacobi method for data arrays that exceed GPU-dedicated memory size

Kochurov A.V., Vorotnikova D.G., Golovashkin D.L.

Image Processing Systems Institute, Russian Academy of Sciences,
Samara State Aerospace University

Abstract. The paper proposes a method to extend the dimension of grids that GPU-aided implicit finite difference method is capable to work with. The approach is based on the pyramid method. A predictive mathematical model for computation duration is proposed. This model allows to find optimal algorithm parameters. The paper provides computation experiment results that has shown the model to be accurate enough to predict optimal algorithm parameters

Issues related to general-purpose computing on graphics processing units (GPU) and particularly GPU-aided finite-difference method implementations are discussed in a number of publications, such as [1, 2].

A major drawback of the methods discussed is the requirement for the video memory capacity to be big enough to contain the entire grid domain. Known open-source libraries that solve such problems, such as OpenCurrent (https://code.google.com/p/opencurrent/), have the same limitation. Note that modern GPUs do not provide memory upgrade capability. Besides, the video memory is much smaller that RAM.

Meanwhile, practical large-scale tasks require the grid domains as large as thousands of nodes in a single direction. Such problems may arise in many areas where partial differential equations (PDE) are applied, such as designing micron-size optical elements with nanoscale features [3], simulating light propagation with FDTD, seismic wave modelling, etc. There's clearly a need for PDE solving methods that do not require the entire grid to fit into the GPU memory.

There are few known approaches for explicit finite difference method that allow to apply GPU for such problems, such as: using multiple GPU or GPU-aided computing cluster [4]; algorithmic tricks allowing to reduce GPU-memory requirements by storing the main data array in RAM and dynamically copying the necessary data to

GPU memory just before computations. The generalized version of the last algorithm was explored by the authors last year [5] and has shown interesting results.

And even though the explicit finite difference method is suitable for many applications, the implicit finite difference method provides unconditional convergence in many cases or at least faster convergence.

The most time-consuming operation in the implicit finite difference method is solution of a system of linear equations of a form Ax=b, with the dimension of the variables vector x corresponding to the number of nodes in a grid domain. This fact leads to the memory requirements for the problem being as high as for explicit finite difference method.

The aim of this work is to show that large-scale problems may be solved efficiently by means of explicit finite difference method with the aid of GPU on existing hardware by cost of slightly worse performance.

Though the Jacobi method is considered to be too primitive and criticised for its slow convergence in some cases, but being simple and well-studied it is still used and investigated by many researchers, especially in a context of general-purpose GPU computing [5].

Jacobi Method

In this work the Jacobi method is applied to a finite difference approach for a stationary heat equation $\dfrac{\partial^2 U}{\partial x^2} + \dfrac{\partial^2 U}{\partial y^2} = \dfrac{-f(x,y)}{D}$, where $f\,(x,\,y)$ is a heat source density function, D is a thermal diffusivity, $U\,(x,\,y)$ is a temperature distribution in space defined in a square area $x \in (0,\,X)$, $y \in (0,\,X)$, with boundary conditions of a form $U(0,\,y) = U(X,\,y) = U(x,0) = U(x,\,X) = 0$.

The implicit finite difference approximation for this equation is as follows:

$$u_{i+1,j} + u_{i-1,j} + u_{i,j+1} + u_{i,j-1} - 4u_{i,j} = \frac{-h^2}{D} f_{i,j},$$

where $u_{i,j}$ is a sampled temperature distribution, $f_{i,j}$ is a sampled heat source density, h is a grid interval length, N is a grid size.

In order to find $u_{i,j}$ it is necessary to solve a system of linear equations $A_x = b$, where x is a vector representation of matrix U, i.e. $x_k = u_{1,k}$, for $k = 1,..,N, x_k = u_{2,k-N}$, for $k = N+1,...,2N$, etc., b is a vector representation of $\dfrac{-h^2}{D} f$ matrix and A matrix has the following form:

$$A = \begin{pmatrix} T & -I & & & \\ -I & \cdot & \cdot & & \\ & \cdot & \cdot & \cdot & \\ & & \cdot & \cdot & -I \\ & & & -I & T \end{pmatrix} \quad T = \begin{pmatrix} 4 & -1 & & & \\ -1 & \cdot & \cdot & & \\ & \cdot & \cdot & \cdot & \\ & & \cdot & \cdot & -1 \\ & & & -1 & 4 \end{pmatrix}.$$

415

Obviously the diagonal of A matrix contains only non-zero elements. Then the Jacobi method iteration for this system takes a form:

$$x_i^{k+1} = \frac{1}{a_{i,i}} \left(- \sum_{j \neq i} a_{i,j} x_j^k + b_i \right),$$ (1)

where $i = 1,..,N, \quad k = 0,1,..,N, \quad x_i^k$ is approximation of the solution at k-th iteration, x_i^0 is an initial approximation of the solution.

Taking into account that A has only five non-zero diagonals there are only four summands under the sum sign in Eq.1.

Replacing x_i back with corresponding $u_{i,i}$ turns the Jacobi iteration into the following form: $u_{i,j}^{k+1} = \frac{1}{4} \left(u_{i+1,j}^k + u_{i-1,j}^k + u_{i,j+1}^k + u_{i,j-1}^k + \frac{h^2}{D} f_{i,j} \right).$

The same idea of Jacobi iteration could be also applied to the stationary 3D heat equation $\frac{\partial^2 U}{\partial x^2} + \frac{\partial^2 U}{\partial y^2} + \frac{\partial^2 U}{\partial z^2} = \frac{-f(x,y,z)}{D}$. The Jacobi iteration for this equation is very similar to the one for 2D heat equation:

$$u_{i,j}^{k+1} = \frac{1}{6} \left(u_{i+1,j,k}^t + u_{i-1,j,k}^t + u_{i,j+1,k}^t + u_{i,j-1,k}^t + u_{i,j,k-1}^t + u_{i,j,k+1}^t + \frac{h^2}{D} f_{i,j,k} \right).$$ (2)

The Eq. 2 describes the basic iteration of Jacobi method. In order to perform a single iteration it is necessary to store matrices u^t, u^{t+1} and f. The required videomemory size limits the dimension of problems that GPU might solve. However as the Eq. 3 is almost identical to the iteration of a regular explicit finite-difference method for a non-stationary heat equation, the previously used pyramid method may also be used for this iteration [5].

This method assumes RAM as a main storage for data arrays while the grid is tiled into intersected blocks which are processed sequentially, each of them is copied to videomemory from RAM, a computing CUDA-kernel is invoked at GPU few times to perform a few time-steps of finite-difference method and then the resulting data is copied back to RAM. The number of time-steps performed in a row for a single block is called 'the pyramid height' n. The intersection between neighbouring tiles has 2n grid nodes in width. Obviously the values that fall into this intersection will be computed independently in both tiles.

The pyramid height is a parameter of decomposition. If it is too small then the algorithm will spend too much time on data transfers. If the pyramid height is too large then the intersection between tiles will lead to an excessive amount of duplicating computations. It seems reasonable to choose the pyramid height that would lead to minimal overall execution time.

As it has been shown (see Eq. 3, page 752 of [5]), the run time in a case of 1D tiling could be estimated as $\tau \approx K(I-1)^3 \frac{R-n}{R-2n} \left(\frac{2}{n} \tau_c + \tau_a \right)$, where τ is an overall execution time, K is the number of time steps, n is pyramid height, N is grid size in

one dimension (the grid is assumed to have equal size in all dimensions), R is a tile-basement width, τ c is an average data-transfer duration per a single value from RAM to GPU memory, τ a is an average duration of computing a single value. The last two constants could be measured empirically by performing computations for a small-dimension problems and measuring results with a tool like NVidia Visual Profiler.

Taking into account that the Jacobi iteration employs 3 matrices (u^t, u^{t+1} and f) instead of 2 used in explicit finite-difference method, the estimation should be modified as follows:

$$\tau \approx K(I-1)^3 \frac{R-n}{R-2n}\left(\frac{3}{n}\tau_c + \tau_a\right).$$

Finding an optimal pyramid height n is a non-linear optimisation problem. As the number of possible n values doesn't exceed $R/2$, this problem could be solved fast enough by bruteforcing all the possible $R/2$ values. However it is possible to find minimum with algebraic solution but brute-force is much simpler in practice. The computational complexity of this brute-force is $O(R)$, with R in practice being in range from 10 to 500. Thus the computation of an optimal pyramid height would not exceed few milliseconds which is absolutely minor in comparison with the total computation duration (minutes and hours).

A significant difference between the Jacobi iteration and the explicit finite-difference iteration should be mentioned: for a non-stationary heat equation there was a fixed number of time-steps (iterations) K, while Jacobi method termination condition has a form of $\left\|u^{k+1} - u^k\right\| < \varepsilon$. It means that the number of Jacobi method iterations is not predefined.

Practically the optimal pyramid height is a relatively small number (hundreds) while the number of iterations for Jacobi method to reach a reasonable error is an order of magnitude higher. The authors propose to limit the value of n to a reasonable maximal number (e.g. 100) and to check the termination condition every n iterations (see line 2 of the algorithm 1).

Algorithm 1. Piramid method for Jacobi

1. $u := u_0$

2. $n := min(maxPyramidHeight;\ optimalPyramidHeight)$

3. $blocks := buildPyramids(n;\ N)$

4. $repeat$

5. $u_n := zeroMatrix(N)$

6. $for\ i = 1 : size(blocks)do$

7. $u_{gpu} = copyRamToGpu(u(addGhostZone(blocks(i); n)))$

8. $f_{gpu} = copyRamToGpu(f(addGhostZone(blocks(i); n)))$

9. $for\ i = 1 : n\ do$

10. $tmp_{gpu} := JacobiKernel(u_{gpu}; f_{gpu})$

11. $swap\left(tmp_{gpu}; u_{gpu}\right)$

12. *endfor*

13. $u_n\left(blocks(i)\right) := copyGpuToRam\left(u_{gpu}\right)$

14. *endfor*

15. $swap\left(u; u_n\right)$

16. *until* $\left\| u_n - u \right\|_\infty < \varepsilon$

Proposed algorithm 1 uses three temporary GPU arrays of size $R \times N \times N$. JacobiKernel is a GPU kernel that performs Jacobi iteration at a given data arrays. All other operations are performed at CPU and all other variables are stored in RAM.

The main kernel JacobiKernel is a typical implementation of iterative stencil loop (ISL), its algorithm is listed in algorithm 2. Each GPU thread executing this kernel processes $R - 2$ values. This kernel has high theoretical occupancy on the hardware authors use and tends to be arithmetic-bound according to NVidia Visual Profiler data.

Results

Authors have developed a program for above-described algorithm and performed few series of experiments with different data sets. The experiments were carried out on a node of K100 cluster 1 equipped with $3 \times$ NVidia Tesla C2050 GPU (448 CUDA cores, 2.5 GB of memory), 96 GB RAM and $2 \times$ 6-core CPU Xeon X5670. The testing stand was running CentOS 5.5, CUDA toolkit 6.5 was used.

According to the results in Table 1, the pyramid method gives a significant performance benefit over pure-CPU performance even though the GPU-dedicated memory doesn't allow to fit u and f matrices at once.

Table 1.   Results of the Pyramid method for Jacobi

Grid size N	Data size, GB	# iterations	Method duration, sec	
			CPU, 12 treads	Pyramid method
800	5.7	8300	9687	1353
900	8.1	11200	20003	2671
1000	11.2	12300	33543	4218

The pyramid method allows to apply GPU for explicit finite-difference method for stationary PDEs with a grid size exceeding the available GPU-dedicated memory size. At the same time its performance is significantly better than that of pure-CPU implementation (the speedup is about 7–8 times).

Acknowledgments

This work has been supported by the grants of Russian Foundation of Basic Research 14-07-00291, 14-01-31305 and 14-07-31178.

References

1. **Golovashkin DL, Vorotnikova DG, Kochurov AV and Malisheva SA.** Solving finite-difference equations for diffractive optics problems using graphics processing units. Opt. Eng., 2013; 52 (9): 091719. doi: 10.1117/1.OE.52.9.091719.
2. **Yakimov PYu.** Preprocessing of digital images in systems of location and recognition of road signs. Computer Optics, 2013; 37(3): 401-405. [in Russian]
3. **Pavelyev VS, Karpeev SV, Dyachenko PN, Miklyaev YV.** Fabrication of three-dimensional photonics crystals by interference lithography with low light absorption. J. Modern Optics, 2009; 9 (56): 1133–1136.
4. **Micikevicius P.** Multi-GPU Programming for Finite Difference Codes on Regular Grids, Stanford AHPCRC/iCME Colloquium Series, 2012 http://www.stanford.edu/dept/ICME /docs/seminars/Micikevicius-2012-01-23.pdf
5. **Golovashkin DL, Kochurov AV.** Solution of difference equations on GPU. Pyramids method. Computational Technologies, 2012; 17(3): 39-52. [In Russian]

The Big Data methodology in computer vision systems

Popov S.B.

Samara State Aerospace University,
Image Processing Systems Institute, Russian Academy of Sciences

Abstract. I consider the advantages of using the big data methodology in the computer vision systems. It is noted that this solution provides transparent increasing the functionality of CVS and improvement its quality, the formation of new intellectual properties of the system based on the possibilities of a posteriori multivariate iterative processing of stored video in the background. The basic principles of such intelligent vision systems have been successfully used to create a distributed vision system of railway tanks registration.

Keywords: big data, information technologies, computer vision system, image processing, multimodal processing

1. Introduction

The emergence and development of new approaches and technologies in processing and analysis of big data has led to a shift in the methodology of formation of new knowledge. Some researchers polemically declare the end of science, since the scientific discoveries and insights can come from an exhaustive search of all possible models of any scientific phenomenon with subsequent clustering. It certainly is hyperbole, but there is a definite impact on modern information technologies. Transfer of big data technology to another subject domain does not involve simple copying a selected set of methods. It is important to understand how the basic principles of a new methodology allow to move to a qualitatively new level of target technology. Concrete solutions depend strongly on the specific application domain and its level of hardware and algorithmic advances.

In this work we are primarily interested in the impact of data science approaches to design solutions in the domain of computer vision.

2. The Big Data methodology

What is the main difference between the new approaches from the traditional data processing technologies?

New data, computational capabilities, and methods create opportunities and challenges [1]:

— Integrate statistics/machine learning to assess many models and calibrate them against "all" relevant data.
— Integrate data movement, management, workflow, and computation to accelerate data-driven applications.
— New computer facilities enable on-demand computing and high-speed analysis of large quantities of data.

Many models. Traditional research approaches are based on the initial formation of a certain model, then the accumulation and processing of data with subsequent estimation of the parameters of such pre-formed model. In the process of discovery of new knowledge big data technologies integrate simulation, experiment, and informatics. This integrated research solves the problem of finding the model or a set of models most appropriate to some experimental data. Moreover, this methodology is aimed at finding the most interesting (i.e., unexpected and effective) and robust models.

Data-driven applications. The relatively simple principles are at the core of big data processing technology: "Divide and Conquer" – distributed architecture of data storage system and total parallel processing at the lowest level; "Treat where Store" – data are not moved during processing, the data processing tasks are delivered and run on computing resources of distributed storage systems; "Data Are Forever" – data are not deleted or modified during processing, the results simply are saved in situ.

New computer facilities. The widespread introduction of parallelism even in commodity computers discovers new ability for developers of modern algorithms allowing to implement a multi variance and competitive methods of processing. Easy deployment of distributed systems allows transparently to increase intellectual capabilities of target systems.

Seeing computer vision tasks, the most interesting is real-time big data processing. Real-time big data analytics is an iterative process involving multiple tools and systems. It's helpful to divide the process into five phases [2]: data distillation, model development, validation and deployment, real-time scoring, and model refresh. At each phase, the terms "real time" and "big data" are context dependent.

1. Data distillation – This phase includes extracting data features, combining different data sources, filtering for domains of interest, selecting relevant features and outcomes for modeling, and exporting sets of distilled data to a local data store.

2. Model development – Processes in this phase include feature selection, sampling and aggregation; variable transformation; model estimation; model refinement; and model benchmarking. The goal at this phase is creating a predictive model that is powerful, robust, comprehensible and implementable.

3. Validation and deployment – The goal at this phase is testing the model to make sure that it works in the real world. The validation process involves re-extracting fresh data, running it against the model, and comparing results with outcomes run on data that's been withheld as a validation set. If the model works, it can be deployed into a production environment.

421

4. Real-time scoring – At this phase the generated decisions are scoring by consumers or by external control system.

5. Model refresh – Data is always changing, so there needs to be a way to refresh the data and refresh the model built on the original data. The existing programs are used to refresh the models in accordance with the newly accumulated data. It is also recommended simple exploratory data analysis, along with periodic (weekly, daily, or hourly) model refreshes.

Big Data methodology is the iterative process. Models should not be created once, then deployed and left in place unchanged. Instead, through feedback, refinement and redeployment, a model should continually adapt to conditions, allowing both the model and the work behind it to provide value to the organization for as long as the solution is needed [2].

3. Revised data processing technology in the computer vision

Turning to the problems of developing computer vision systems (CVS), it should be noted that the traditional approach of using sequential processing steps performed by the separate frames of video data largely exhausted the resources to increase processing accuracy and the ability to adapt as conditions of surveillance change.

It is necessary to use some principles of big data technology. With regard to the field of computer vision the most suitable solution are the following:

− Total parallelization of the processing and distribution of data.
− Multivariance and competitive data models and methods of their processing.
− Continuous scoring of competitive solutions, both in the process of forming solutions and to adapt to changing surveillance conditions.

The implementation of these solutions leads to the multimodal approach proposed in this work. In this case, this term is broadly interpreted. First of all, the principle of multimodal processing means the simultaneous use of a family of algorithms at the critical stages, each of which is built on a fundamentally different approach. At the same time, multimodality is a coordinated use of video data from different points of view, with different spatial resolutions, a simultaneous use of multiple consecutive frames and additional a priori information about objects of interest.

The results of such versatile processing are analyzed together. This achieves the variability of approaches to solving complex problems, a significant increase in the stability of technology in general with significant changes in observation conditions and parameters of controlled or analyzed objects in video streams.

At a time when for a particular purpose computer vision requires a complex multi-step process, to take a final decision on choosing the best one in a separate step is not possible.

The effectiveness of a multimodal approach is best manifested in computer vision applications in the presence of well-defined criteria for achieving the goal of processing. Since in this case the final decision stage can be implemented as a procedure of joint analysis of the whole set of variants generated by the multivariate multistage process.

A good example of the effective use of multimodal processing is the problem of recognizing the numbers of cars trains. It is noted that similar systems for recognition of train car number should be adapted for work under the following challenges: presence of various digit outlines, variety of color combinations of digits and background, distortions of numbers due to line of sight being non perpendicular to the surface where the number is located (this is especially common for tank cars), various kinds of contamination of the object's surface, and the necessity to operate in both artificial and natural lighting, with the latter accompanied by significant changes in illumination conditions during the day.

The first design decision is the choice of distributed architecture for computer vision system. Distributed modular software allows transparent mapping onto the distributed computation system with a variable number of computers and makes it possible to scale the system towards both a higher quantity of video streams being processed and time reduce of video data processing.

Multimodal processing uses as the base the multistage recognition technology developed for vision system of the railway train registration [3]. Revised technology is as follows: at each stage of processing it is used the previously formed set of algorithms that implement a completely different approaches; each algorithm from the working set is applied to each frame of a video stream of the current wagon. More than one result is obtained at all stages. The results lists are generated. All results are ordered on the basis of relevant metrics. Thus a decision tree, corresponding to one wagon video stream processing, is obtained. When forming the recognition result, code protection of numbering system of train wagons and containers is used and it takes into account the characteristics of validity of recognition formed for each digit. These characteristics are accounted with weights that correspond to algorithms used in previous steps of the process of obtaining a fragment of number. The final scoring is provided by the operator who is responsible for confirmation or adjustment of the final results within the system. It provides additional opportunities for improving the operational quality of recognition technology. With correct result available, it makes sense the posterior multivariate processing of archived video data in the background iterative mode. In this way the quality of generated results may be estimated and parameters of processing algorithms may be selected.

The using structured lighting [4] makes it possible to expand the spectrum of algorithms of fast symbol localization by using the alternative method of delineation of areas with no symbols, which uses the analysis of luminous line geometry of structured lighting for recognition of structural elements of train wagons and containers. Acquired data on the positions of the retaining bands on tank cars and stiffening plates on train cars and containers may be used for the identification of the type of the currently processed train car, tank, or container and therefore obtaining additional information on typical car number locations for them. It is a clear manifestation of the proposed multimodal processing principle.

Allocation of special computational capacity for data storage makes it possible to extend the set of goals of posterior video data processing. This procedure makes it possible to analyze and reveal additional information on the data located in the system, retrieve specific frames of interest for further viewing, interpretation, etc., and

generate an annotated list of detected abnormalities of the observation process [5], ensuring fast access to them for the operator. The indicated opportunities make it possible to use the system for security control. Further analysis of this information allows CVS developers to improve processing and recognition algorithms.

The implementation of this approach involves the development of modifications of the basic algorithms of fast localization of the alphanumeric information in multiple video streams, enabling to form an ordered list of results; the formation of a representative set of recognition algorithms; the implementation of tasks of analysis of the obtained list and selection of the most reliable results.

The distributed architecture of the system ensures further increase in real time video stream processing rate due to scalability of computations [6] within hardware–software platforms of distributed multiprocessor computation systems, in particular using CUDA technology within NVIDIA data processing acceleration hardware.

Distributed video data archive storage on several servers is based on the cascade principle [7]: the working storage with which the video server interacts and the set of archive storages, each one containing video data for a specific period of time. As the working storage is filled, the data are transferred to a first level archive, where space is cleared beforehand by transferring existing data to a second level archive. The same procedure is performed throughout the whole cascade of archives. The most outdated information is deleted at the bottom level.

The presence of the distributed archive storage needed for the implementation of the first three phases of the process of real-time big data analytics and subsequent model refresh.

5. Conclusion

The use of new technologies has a cumulative effect. Their implementation opens new opportunities and challenges. The use of distributed software architecture in CVS design considerably facilitates the transfer to advanced technologies based on cloud computing. When complimented by an extended stock list of high resolution IP cameras with possibility for wireless connection to the communication network, it makes it possible to efficiently use three most promising technologies, which are now showing an explosive growth of interest, namely computer vision, cloud computing, and wireless data transfer. Integration of these three technologies significantly expands the CVS application market due to a higher quality of services, a significant reduction in time and complexity and, therefore, implementation costs, and minimization of cost of ownership.

the Presidium of the RAS program # 6 "Problems of creation of high-performance, distributed and cloud systems and technologies" 2015.

References

1. **Foster I.** Taming Big Data: Accelerating Discovery via Outsourcing and Automation. Keynote Lecture, the International Winter School on Big Data Tarragona. Spain, January 26-30, 2015.
2. **Barlow M.** Real-Time Big Data Analytics: Emerging Architecture. O'Reilly Media, 2013; 30 p.
3. **Kazanskiy NL, Popov SB.** The distributed vision system of the registration of the railway train. Computer Optics, 2012; 36(3): 419-428. [in Russian]
4. **Popov SB.** The intellectual lighting for optical information-measuring systems. Proc. SPIE 9533, Optical Technologies for Telecommunications 2014, 2015; 95330 p.
5. **Kazanskiy NL, Popov SB.** Machine Vision System for Singularity Detection in Monitoring the Long Process. Optical Memory and Neural Networks (Information Optics), 2010; 19(1): 23-30.
6. **Kazanskiy NL, Popov SB.** Distributed storage and parallel processing for large-size optical images. Proc. SPIE 8410, Optical Technologies for Telecommunications 2011, 2012; 84100I.
7. **Kazanskiy NL, Popov SB.** Integrated Design Technology for Computer Vision Systems in Railway Transportation. Pattern Recognition and Image Analysis, 2015; 25(2): 215-219.